Dissertation zur Erlangung des Doktorgrades
der Fakultät für Chemie und Pharmazie
der Ludwig-Maximilians-Universität München

Studies Towards the Gas-Phase Detection of Hazardous Materials by Vapor Pressure Measurements with the Transpiration Method in Combination with Vacuum Outlet GC/MS

Martin Andreas Christian Härtel

aus

Rosenheim, Deutschland

2017

Erklärung

Diese Dissertation wurde im Sinne von § 7 der Promotionsordnung vom 28. November 2011 von Herrn Prof. Dr. Thomas M. Klapötke betreut.

Eidesstattliche Versicherung

Diese Dissertation wurde eigenständig und ohne unerlaubte Hilfe erarbeitet.

München, 24.10.2017

_____

(Martin Härtel)

Dissertation eingereicht am: 21. April 2017

1. Gutachter: Prof. Dr. Thomas M. Klapötke

2. Gutachter: Prof. Dr. Konstantin L. Karaghiosoff

Mündliche Prüfung am: 08. Juni 2017

With respect to the sensitive information about explosives provided in this thesis the public version contains selected blackened sections, tables and figures. A non-blackened version of this thesis is available for legitimate purposes upon request from

Prof. Dr. Thomas Klapötke (tmk@cup.uni-muenchen.de)

Martin Härtel (dr.martin.haertel@gmail.com)

Diese Arbeit widme ich einem Chemiker und einem Zöllner: meinen Großvätern Martin und Engelbert.

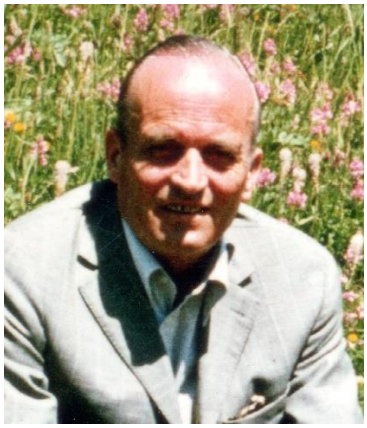

Martin L. Härtel
Diplom-Chemiker

* 01.07.1919
† 01.04.1981

Engelbert H. F. Spielmann
Zolloberamtsrat, ständiger Diakon,
Träger des Bundesverdienstkreuzes
* 02.11.1921
† 08.10.2011

Wer nicht will, der findet Gründe.
Wer will, der sucht Wege.

Danke!

Ich bedanke mich bei meinem Doktorvater **Herrn Prof. Dr. Thomas Klapötke** für die Aufnahme in seinen Lehrstuhl und die Betreuung meiner Dissertation. Ich wusste den maximalen Freiraum zur Selbstentfaltung in der Gewissheit, dass Sie bei Problemen immer für mich da sind, stets zu schätzen. Sie haben mir viel Verantwortung übergeben und mir das komplette ChemAir Budget zur Anschaffung eines GC/MS-Systems und aller Komponenten für die Dampfdruckmessungen in Eigenregie überlassen. Ich weiß diese einmalige Gelegenheit, ihr Vertrauen in meine Fähigkeiten und ihre Geduld bei der Etablierung des VO-GC/MS-Aufbaus und Transpirationsexperiments sehr zu schätzen. Es ist alles andere als selbstverständlich, dass Sie meine Finanzierung nach offizieller Beendigung des Projekts übernommen haben. Dafür und für vieles Anderes, das hier nicht genannt wurde, möchte ich mich bei Ihnen von Herzen bedanken.

Ich bedanke mich bei den weiteren Mitgliedern meiner **Prüfungskommission** (Prof. Dr. Karaghiosoff, PD Dr. Peter Boeker, Prof. Dr. Oliver Trapp, Prof. Dr. Andreas Kornath und Prof. Dr. Jürgen Evers) für das Lesen und Korrigieren meiner Dissertation und die aktive Teilnahme an meiner Verteidigung.

Dem **Bundesministerium für Bildung und Forschung** möchte ich für die Finanzierung eines Großteils meiner Dissertation danken. (BMBF Förderkennzeichen 13N12583)

Wenn Herr Prof. Klapötke mein Doktorvater ist, dann ist **Herr Prof. Sergey Verevkin** von der Universität Rostock mein Doktoronkel. Er hat mich gleich zu Beginn der Dissertation bei der Wahl der richtigen Messmethode kompetent beraten und mich zu zwei Forschungsaufenthalten in seiner Forschungsgruppe eingeladen um die Transpirationsmethode zu erlernen. Vor Ort wurde ich von **Dr. Ksenia Zaitseva** und **Dr. Aleksandra Russo** intensiv betreut. Seine rechte Hand, **Dr. Dmitry Zaitsau**, hat mir im persönlichen Gespräch und in unzählbaren E-Mails die mathematischen Hintergründe der Transpirationsmethode erläutert. Prof. Verevkin hat mit mir unzählige Stunden telefoniert um meine Messungen zu diskutieren, so manchen Unfug aus meinem Kopf zu vertreiben und dabei stets die Geduld bewahrt. Ich weiß es sehr zu schätzen, dass Sie bei zwei Publikationen die Federführung übernommen und diese auf ein für mich unerreichbares Niveau gehoben haben. Herr Prof. Verevkin, ich bedanke mich für Alles, was Sie und Ihre Gruppe für mich getan haben! Die Aufenthalte bei Ihnen in Rostock werden mir für immer in sehr schöner Erinnerung bleiben.

Ohne meinen Projektkoordinator **PD Dr. Peter Boeker** von der Universität Bonn hätte sich das GC/MS-System wohl nie zum VO-GC/MS System weiter entwickelt. Ich bedanke mich bei Ihnen und **Herrn Dr. Leppert** für den exzessiven Wissenstransfer in einer Vielzahl von E-Mails und angenehmen Telefonaten.

Ich möchte mich beim gesamten **ChemAir-Konsortium,** allen **asoziierten Partnern** und **VDI-Betreuerinnen** (siehe Kapitel 1.3) für die nette Aufnahme und die gute Zusammenarbeit bedanken. Ich vermisse schon jetzt das Fachsimpeln auf den Verbundtreffen und hoffe darauf, dass wir in neuen Projekten wieder zusammen finden. Insbesondere **Herrn Dr. Michael Hill** möchte ich für den Hinweis auf die frei werdende Stelle bei meinem neuen Arbeitgeber, dem Referat 65 der Bundespolizei in Lübeck, danken. Ich weiß es sehr zu schätzen, dass ich nah an meinem Promotionsthema und persönlichen Interessen weiterarbeiten kann. Herrn **Polizeidirektor Rainer Weinzierl** und dem gesamten **Referat 65 des Bundespolizeipräsidiums** in Lübeck danke ich für die herzliche Aufnahme. Ich freue mich schon auf die weitere Zusammenarbeit.

Bei **Regierungsdirektor Dr. Manfred Metzulat** möchte ich mich herzlich für die zwei-monatige Aufnahme in der Schule ABC-Abwehr und gesetzliche Schulaufgaben der **Bundeswehr** in Sonthofen bedanken. Ich habe die Zusammenarbeit in einem mehr als angenehmen Umfeld mit Retrocharme und dennoch hochmodernen Analyseinstrumenten sehr genossen. Trotz Ausmusterung kann ich jetzt sagen, dass ich für zwei Monate in einer der schönsten Kasernen Deutschlands gelebt habe und mit dem berüchtigten Kampfstoff VX unter Ihrer Aufsicht und Verantwortung arbeiten durfte. Insbesondere bei Herrn **Major Marc André Althoff** möchte ich mich für die fruchtbare Zusammenarbeit im Rahmen des Projekts zur Dampfdruckbestimmung von Amiton und seinen Derivaten bedanken.

Bei Herrn **Prof. Dr. Konstantin Karaghiosoff** möchte ich mich für seinen unermüdlichen Einsatz bei den XRD- und NMR-Messungen bedanken. Es war mir ein stetes Vergnügen mit Dir zusammen arbeiten zu dürfen und ich werde die gemeinsamen Mittagessen vermissen. Ich hoffe du hältst dein Wort und besuchst mich in Lübeck. Darüber würde ich mich sehr freuen.

Bei Herrn **Dr. Jörg Stierstorfer** möchte ich mich für seine Unterstützung über den gesamten Zeitraum meiner Dissertation als direkten Ansprechpartner bedanken. Du standst mir immer mit Rat und Tat zur Verfügung und hast nichts unversucht gelassen um mir meine Arbeit zur erleichtern. Du hast viele Verbesserungen der Arbeitsbedingungen in der Gruppe in die Wege geleitet und stets dafür gesorgt, dass der Spaß bei uns nicht zu kurz kommt!

Herrn **Dr. Burkhardt Krumm** danke ich für die Wahrung der Sicherheit im Arbeitskreis.

Besonderer Dank gilt auch **Frau Irene Scheckenbach** für die Übernahme der Verwaltungsaufgaben im Rahmen des BMBF-Projekts, welches mehr Bürokratie mit sich brachte als bei den Amerikanern.

Bei meinen Bachelorstudenten **Leopold Zehetner** und **Mathias Mallmann**, meinem F-Praktikanten **Max Born**, meiner Masterstudentin **Kathrin Grieger** und meiner Erasmus-Studentin und Nachfolgerin **Greta Bikelytė** bedanke ich mich für die aktive experimentelle Mitarbeit an dieser Dissertation. Ohne euch wäre diese Arbeit in diesem Umfang nicht möglich gewesen! Greta gilt besonderer Dank für das Korrekturlesen meiner Arbeit.

Bei den **Dres. Davin Piercey, Marcos Kettner, Anian Nieder, Camilla Evangelisti, Vera Hartdegen** und **Andreas Preimesser** möchte ich mich für den herzlichen Empfang und die Hilfe beim Start in der Gruppe bedanken. Auch bei allen weiteren **Alumni**, **Laborkollegen**, **AK-Mitgliedern, Kommilitonen** und **Universitäts-Mitarbeitern** möchte ich mich für die angenehme Arbeitsatmosphäre, die unzähligen Abende im Vereinsheim, Kochrunden, Grillfeste, Doktor- und Weihnachtsfeiern bedanken. Insbesondere dem **Glasbläser Rudolph Klinger** danke ich für das Anfertigen und kontinuierliche Reparieren meiner Saturatoren ohne welche meine Dissertation nicht möglich gewesen wäre.

Den Dank gegenüber meinen Eltern **Reinhold** und **Gabriela Härtel** kann ich nicht in Worte fassen. Ihr habt mich bedingungslos nie im Stich gelassen und mir meine komplette Ausbildung inclusive Studium finanziert. Ohne euch wäre diese Arbeit nicht möglich gewesen. Auch meinen Geschwistern **Madeleine** und **Michael** danke ich für den familiären Rückhalt während meiner gesamten Dissertation. Es war immer schön zu Hause nach Westerham zurück zu kehren und Zeit mit euch zu verbringen.

Im ersten Jahr meiner Promotion durfte ich einen ganz besonderen Menschen kennen lernen: **Katharina Banzhaf**. Es würde den Rahmen sprengen dir für Alles zu danken was du in den letzten Jahren für mich getan hast. Ich möchte nur ein paar Sachen erwähnen. Ohne dich hätte ich immer noch keine Brille, eine Schilddrüsenunterfunktion und wäre dadurch eine blinde Schlaftablette. Ohne dich hätte ich niemals in meiner Promotionszeit Prag, Kairo, die Pyramiden von Gizeh, den Nil von Luxor bis Assuan, Aachen, Maastricht, Brüssel, Wien, Rom, London, Stonehenge, Edinburgh, die schottischen

Highlands, Dublin, die Klippen von Moher, New York, Miami, Tübingen, den Pretzgenmarkt und viele andere Orte bereist. Deine Familie hat mich herzlich aufgenommen und ich habe jede unserer Fluchten aus dem Alltag genossen. Du musstest Zeiten ertragen in denen meine Stimmung extrem direkt proportional zum Bestimmtheitsmaß R^2 meiner Kalibriergeraden und Messergebnisse war. Ohne deinen Vorschlag nach Sonthofen zu gehen wären die Abzugsumbauarbeiten zur Prokrastination im Home-Office verkommen und die für mich wichtigsten Ergebnisse meiner Dissertation nicht zu Stande gekommen. Ich bin dankbar für jeden einzelnen Moment den ich mit dir verbringen durfte und hoffe dass noch viele weitere schöne Erlebnisse in Bonn und Lübeck hinzukommen!

Ich möchte mich auch bei meiner erweiterten Familie für die vielen schönen Momente und die Unterstützung bedanken. Insbesondere auch bei meinen Großeltern **Martin** und **Bertha Härtel** sowie **Engelbert, Anneliese** und **Käthe Spielmann**. Meiner Großtante **Dr. med. Annemarie Kloß**, einer Pionierin der automatisierten medizinischen Laboranalytik, danke ich für die großzügige finanzielle Unterstützung meines Studiums. Meiner Freundin **Katharina und ihren Eltern**, meinem Cousin **Johann Gillich,** meinem Bruder **Michael** und unserer **Kim** möchte ich für die tatkräftige Unterstützung bei meinem Umzug nach Lübeck danken. Ohne euch wäre dieser Kraftakt nicht möglich gewesen!

Bei meiner gymnasialen Chemie-LK-Leiterin **Angelika Leonhard** möchte ich mich dafür bedanken, dass Sie mir den Spaß an der Chemie vorgelebt hat und auf diese Weise daran beteiligt war mich auf den von mir eingeschlagenen Weg zu führen.

Ich möchte mich bei allen **Freunden** bedanken die Verständnis dafür hatten, dass mein Privatleben in der Regel zweitrangig war und Freundschaft nicht über die Frequenz des persönlichen Kontakts definieren. Ich weiß jeden von euch zu schätzen, hoffe ich finde wieder mehr Zeit für euch und dass der ein oder andere mich im hohen Norden besucht! Insbesondere möchte ich mich bei Chemieingenieur **Karl Nilsson** für das Asyl in seinem Refugium der Ruhe vor dem Stress des akademischen und familiären Alltags bedanken.

Bei der Firma **Shimadzu**, insbesondere bei **Dr. Jürgen Truckenbrodt**, **Carsten Zeidler** und **Barbara Ressler** möchte ich mich für die gute Zusammenarbeit im Rahmen der Methodenoptimierung, gemeinsamen Publikation und für die Gelegenheit der VO-GC/MS Geräteinstallation im Referat 65 der Bundespolizei Lübeck bedanken. Es ist schön, dass es noch Firmen gibt, die ein Herz für akademische Einrichtungen haben und auch nach dem Gerätekauf Unterstützung leisten ohne dafür die Hand auf zu halten.

Ich bin mir sicher, dass ich etliche Personen vergessen habe und möchte mich dafür entschuldigen. Als Wiedergutmachung biete ich ein Bier in Lübeck an. Meldet euch einfach bei mir. Vielen Dank dafür, dass ihr mich auf meinem Weg begleitet habt!

Martin

Table of Contents

1	**Detection of Explosives in the Context of Aviation**	1
1.1	Detection of Explosives in General	2
1.1.1	Olfactory Detection by Animals	2
1.1.2	Mass Spectroscopy	3
1.1.3	Ion Mobility Spectroscopy	6
1.2	Challenges in Explosive Detection	8
1.2.1	Low Vapor Pressures	8
1.2.2	Limited Sample Size	9
1.2.3	Deliberate Concealment	9
1.2.4	Interferences	9
1.3	Project ChemAir	9
1.3.1	Low Thermal Mass Flow-Field Thermogradient Gas Chromatography	11
1.3.2	Time of Flight Mass Spectroscopy with variable Ionization Energy	14
1.4	Facit	16
2	**Objectives of this Work**	20
3	**Deductive Summary of Results**	22
4	**The ChemAir Substance Repertoire**	30
4.1	The case of Anders Behring Breivik	30
4.2	Components of an Explosive Device	32
4.2.1	Primary Explosive	33
4.2.2	Booster Explosive	33
4.2.3	Secondary Explosives	33
4.2.4	Explosive Additives	33
4.3	Properties of Explosives	33
4.4	Availability of Starting Materials	35
4.5	Selection of Analytes for the ChemAir Substance Repertoire	36
4.6	Analytical Characterization of the ChemAir Substance Repertoire Analytes	38
4.6.1	Hexamethylene Triperoxide Diamine HMTD **01**	45
4.6.2	The Peroxides TATP **02** and DADP **03**	47
4.6.3	Ethyl Nitrate $EtONO_2$ **04**	48
4.6.4	D-Mannitol Hexanitrate MHN **05**	50
4.6.5	Ethyleneglycol Dinitrate EGDN **06**	51
4.6.6	Glyceryl Trinitrate GTN **07**	51
4.6.7	*meso*-Erythritol Tetranitrate ETN **08**	54
4.6.8	Pentaerythritol Tetranitrate PETN **09**	55
4.6.9	2-Diazonium-4,6-dinitrophenolate DDNP **10**	56
4.6.9.1	DDNP Precursor Picramic Acid	57
4.6.10	Picric Acid PA **11**	58
4.6.11	The Mononitrotoluenes 2-MNT **12**, 3-MNT **13** and 4-MNT **14**	59
4.6.12	The Dinitrotoluenes 2,4-DNT **15** and 2,6-DNT **16**	60
4.6.13	2,4,6-Trinitrotoluene **17**	61
4.6.14	Hexanitrostilbene **18**	62
4.6.15	RDX **19**	63
4.6.16	HMX **20**	64

4.6.17	CL-20 **21**	65
4.6.18	TETRYL **22**	66
4.6.19	FOX-7 **23**	67
4.6.20	Uronium Nitrate **24**	69
4.6.21	Urotropine Dinitrate **25**	70
4.6.22	2,3-Dimethyl-2,3-dinitrobutane **26**	72
4.6.23	Nitromethane **27**	73
4.6.24	Ammonium Nitrate **28**	74
4.6.25	Origin and Purity of commercially available materials	75
5	**Vacuum Outlet GC/MS for Detection and Quantification of Explosives**	83
5.1	Optimization for Quantification Applications	84
5.2	Calculation of the Flow in a Series of Capillaries	90
5.3	Experimental Verification of the Split-Flow	93
5.4	Analysis of Explosives	97
5.5	VO-GC/MS Limits of Detection of Explosives	105
5.6	Facit	112
5.7	APPENDIX 1 – Estimation of Air Concentration of Explosives	116
5.8	APPENDIX 2: EI-Mass Spectra measured by VO-GC/MS	119
6	**The Determination of Vapor Pressures with the Transpiration Method Experiment**	122
6.1	The Experimental Setup	122
6.2	Mathematical Evaluation of the Transpiration Method Experiment Results	126
6.3	Critical Discussion of Pressure-Correction for V_{amb}	133
6.4	Uncertainty Estimations for the Transpiration Method Experiment	134
6.4.1	Uncertainty of the Vapor Pressure p_{sat}	134
6.4.2	Uncertainty of Phase Transition Enthalpy $\Delta^{g}_{l/cr}H^{\circ}_{m}$ at T_{avg}	135
6.4.3	Uncertainty of Phase Transition Enthalpy $\Delta^{g}_{l/cr}H^{\circ}_{m}$ at T_{ref} = 298.15 K	136
6.5	Practical Advices for the Transpiration Method Experiment	137
6.5.1	Calibration of the Gas Chromatograph	137
6.5.2	Filling of the Saturator	139
6.5.3	Measuring a Datapoint with the Transpiration Method Experiment	140
6.6	Validation of the Experimental Results	142
6.7	Variables and Constants in order of Appearance	143
7	**Measurement of Vapor Pressures with the Transpiration Method**	145
7.1	Measurements of Reference Compounds	150
7.1.1	Naphthalene	151
7.1.2	Anthracene	154
7.1.3	iso-amyl acetate	158
7.1.4	n-Hexanol	161
7.1.5	n-Octanol	164
7.1.6	Purity of used Chemicals	167
7.1.7	Compilation of Heat Capacities and Heat Capacity Differences	167
7.2	Measurement of the Peroxides TATP **02** and DADP **03**	170
7.3	Measurement of the Nitrate Esters EGDN **06**, GTN **07** and ETN **08**	184
7.4	Measurement of the Mononitrotoluenes 2-MNT **12**, 3-MNT **13** and 4-MNT **14**	222
7.5	Measurement of 2,4-Dinitrotoluene **15**, 2,6-Dinitrotoluene **16** and 2,4,6-Trinitrotoluene **17**	238
7.6	Measurement of Measurement of 1-Nitronaphthalene and 2-Methyl-1-nitronaphthalene	253
7.7	Measurement of 2-Nitropropane, 2-Methyl-2-nitropropane and DMDNB **26**	261

7.8	Measurement of Amitone and Seven Related Derivatives	289
7.9	Measurement of Vapor Pressures with the Transpiration Method : Facit	334
8	**Evaluation of the Suitability of Isothermal Thermogravimetric Analysis for the Measurement of Vapor Pressures**	337
8.1	The isothermal TGA Experiment	339
8.1.1	Measurement of Phenanthrene	340
8.1.2	Measurement of Hexadecane	341
8.1.3	Measurement of Dibutyl Phthalate	342
8.1.4	Measurement of DMDNB **26**	343
8.1.5	Measurement of 2-MNT **12**	344
8.1.6	Measurement of 3-MNT **13**	345
8.1.7	Measurement of 4-MNT **14**	346
8.1.8	Measurement of 2,4-DNT **15**	348
8.1.9	Measurement of 2,6-DNT **16**	349
8.1.10	Measurement of TNT **17**	350
8.2	Facit	351
9	**Investigation on the Sodium and Potassium Tetrasalts of 1,1,2,2-Tetranitraminoethane**	354
	Curriculum Vitae	

1 Detection of Explosives in the Context of Aviation

The airport of Frankfurt am Main is the 12th biggest airport worldwide.[1] In 2014 59.571.802 passengers and 2.083.495 tons of freight were processed.[2] Since the 9/11 hijacking of four passenger airliners (Boeing 757/767), which were crashed into the World Trade Center and the Pentagon, the world-wide security standards in aviation were increased drastically.

This and other incidents lead to innovations like reinforced, locked cockpit doors and strict rules on liquids in cabin luggage. The November 2015 Paris attacks[3] demonstrated that a terrorist managed to infiltrate Europe hiding in the wave of refugees using fake documents. This revealed a lack of inspections at intra-european border crossings and the failure of detection by security agencies. In response to this, border inspections were increased in Belgium and 19 electronic gates were installed at the Brussels airport. [4] In December 2015 the European Union published a new aviation strategy which supports the use of new high-tech systems in favor of manual security checks. State of the art explosive detectors were installed across Europe.[5] These developments were initiated prior to recent terror attacks. Yet any terroristic incident catalyzes the decisions of raising the security level in aviation and the development of new technologies for the detection of explosives.[6]

The common basic standards on aviation security in the European Union are detailed in the commission implanting regulation (EU) 2015/1998.[7] With respect to this the following must be realized at any European airport:

On persons other than passengers, items carried by persons other than passengers, passengers, cabin luggage, hold baggage, cargo and mail at least one of the following security check methods must be performed:

- hand search
- x-ray equipment
- explosive detection systems (EDS) equipment
- explosive detection dogs (for cabin luggage only in combination with hand search)
- explosive trace detection (ETD) equipment
- walk-through metal detection equipment (WTMD, passengers only)
- security scanners which do not use ionizing radiation (passengers only)
- ETD equipment combined with hand held metal detection (HHMD) equipment (passengers only)
- visual check (cargo and mail only)
- metal detection equipment (cargo and mail only)

The process of checking has to be continued until the screener personal can determine whether the person carries or the object contains prohibited items (including explosives and firearms). When the screener is not satisfied, the item or person has to be rejected. A hand search must be performed on vehicles that enter secured airport areas. It can be supported by explosive detection dogs and ETD equipment.

In 2014 at the airport of Frankfurt 163210 passengers and 5708 tons of mail and cargo (averaged over the year) need to be checked each day in the fashion specified by regulation (EU) 2015/1998.[2, 7] Individual peak days with high traffic might even boost the requirements for security scans with a high throughput that can only be fulfilled with the continuous development of new high-tech methods.

Abraham David Sofaer, formerly a legal adviser to the US department of state, stated: **“The most effective measures for preventing acts of terror are usually technological.”**[8]

In context of the situation and challenges stated above the European Commision launched, in the framework of the Horizon2020 funding program, a research project for the assessment of the effectiveness, the efficiency and the cost of the combination of methods and techniques for countering improvised explosive devices (IED) possibly containing home-made explosives.[9] In this call the "European Network on the Detection of Explosives" was mentioned. The German Federal Ministry of Education and Research (BMBF) launched a security research program funding innovations that improve the civil security.[10] In July 2011 the BMBF called for projects to be funded in the field of "Security in Aviation".[11] One of the projects that were funded was the project "ChemAir", which was concerned with the development of a technology for the near real-time detection of airborne hazardous materials.[12] Project ChemAir was focused on the development of a gas-phase detection method for airborne hazardous materials by high volume air sampling, thermodesorption, gas chromatography and final detection by mass spectroscopy. This work was carried out in the framework of project "ChemAir", which will be elucidated in detail in the later course of this chapter.

1.1 Detection of Explosives in General

In the following technical solutions for the trace detection of explosives will be elucidated. There is a multitude of approaches for the detection of explosives including animal olfaction, gas chromatography, mass spectrometry, ion mobility spectrometry, vibrational spectroscopy (RAMAN/IR), Terahertz spectroscopy, conductive polymers, fluorescent polymers, nanomaterials, microcantilever and electronic nose approaches. All these techniques have been reviewed [13] excellently on a regular basis. Several books [14] that deal with the detection of explosives and terrorism in general can be recommended.

In the next sections the gold standard of explosive trace detection, explosive detection dogs, will be elucidated along with the two closely related technical approached of explosive trace detection by mass and ion mobility spectroscopy. Both techniques can be hyphenated with gas chromatography. Details on gas chromatographic analysis of explosives for detection purposes can be found in section 5.

1.1.1 Olfactory Detection by Animals

The nose of a trained explosive detection dog (EDD) is still the benchmark method for vapor detection of explosives. They were used since the beginning of World War II.[15] The limit of detection for the fragrance n-amyl acetate has been determined to be 1.14 and 1.90 ppt for two EDD tested.[16] Therefore EDD are the gold standard for the judgement of newly developed methods.[13h] The basic principle of EDD-"detection" is the sampling of vapors in the air by sniffing it into the nose of the EDD, where they are dissolved in the nasal mucus and interact with receptors that communicate with and are evaluated by the brain.[15] The canine olfactory system is quite complex and involves multiple organs that each produce their own receptors. [15, 17]

Not every dog is suitable for being trained to an EDD. German Shepherd Dogs are one of the preferred races. The dogs are trained by exposing them to specific compounds and rewarding a specified reaction upon recognizing the compound. The reaction of the dog can be a passive one like sitting down. EDD can be trained to a wide repertoire of compounds including traditional and improvised explosives as well as taggants.[16] It is of special importance to avoid contamination of the training equipment with smelling objects like adhesive tape. For this purpose special training samples have been developed that contain the analyte on a metal sponge.[18] The feasibility of remote-guided EDD that receive their voice commands and transmit a video signal via wireless equipment has been demonstrated.[19]

The advantages of EDD are a small number of false positives, high mobility, efficient sampling and the ease of detecting the source of the vapor.[13d] The disadvantages are, in contrast to electronic

detection solutions, that the EDD may be bored, distracted or even be repelled by uncomfortably smelling substances. Human errors including inattention from dog handlers cannot be excluded.

Other animals that were tested for olfactory detection of explosives are bees[20], rats[21], moths[22], pigs[23], mice[13i] and gerbils[13i]. The airport of Frankfurt has a team with 8 EDD. A young dog costs 2000 €, a fully trained dog 10000-15000 € including the training of the dog handler. It may be used 4 hours per day with 30 minutes of work and at least 20 minutes of break alternating. Each EDD has an individual dog handler that may handle two dogs and gets a salary of 40000-50000 € per year.

1.1.2 Mass Spectroscopy

Mass spectroscopy analyzes molecules by their mass to charge (*m*/*z*) ratio after ionization. The analysis can be divided in:

Sample Inlet → Ionization → Ion separation (based on m/z) → Ion detection

The initial step of the analysis is the conversion of neutral analyte molecules into charged ions. The sample inlet can be the eluent of a gas chromatograph (GC) or high performance liquid chromatograph (HPLC), direct heating of the compound on a filament or direct ionization of the analyte under atmospheric conditions using a noble gas ion plasma or (matrix-assisted) laser radiation amongst other methods.

Various types of ion sources exist, including electron impact ionization (EI), chemical ionization (CI) and electrospray ionization (ESI). In case of electron impact ionization electrons are extracted from a heated filament and accelerated by application of a potential until they reach an energy of 10-300 eV and collide with the analyte generating radical cations $M^{+\cdot}$. Usually an electron energy of 70 eV is used since a massive database generated by the American National Institute of Standards and Technologies (NIST) exists. It contains mass spectra of 242.446 compounds (NIST14 v2.2g)[24] that can be used for qualitative comparison and identification of unknown analytes. 70 eV EI is, in comparison to other methods, a relatively harsh condition that generates molecular fragments of molecules resulting in a characteristic fragment pattern. Whilst EI is usually combined with gas chromatography, it can also be coupled to liquid chromatography using an EI-LC-MS interface with supersonic molecular beam technology.[25] This combines the advantages of the database compatibility of EI ionization with the mild analytical conditions of LC in comparison to the thermal stress induced to the analyte by gas chromatography.

For other ionization techniques no commercial databases exist. This can be compensated by the generation of private libraries if the ionization process is reproducible.

A more mild technology is chemical ionization (CI). It generates less fragments and the peak corresponding to the unfragmented molecule is usually dominating the mass spectrum. For this type of ionization a reactant gas is ionized using electron ionization. The resulting radical cations can abstract protons from neutral reactant gas molecules. This can be exemplified for methane: $CH_4^{+\cdot} + CH_4 \rightarrow CH_5^+ + CH_3^{\cdot}$. CH_5^+ is a strong acid that protonates the analyte resulting in $[M+H]^+$ ions. In case of nitrate esters NO^+ and NO_2^+ adducts were observed in this work for CI with isobutane. Further suitable reactant gas ions are ammonia and other alkanes. In case of GC/MS applications it is possible to switch between EI and CI without manual modification of the instrument.[26]

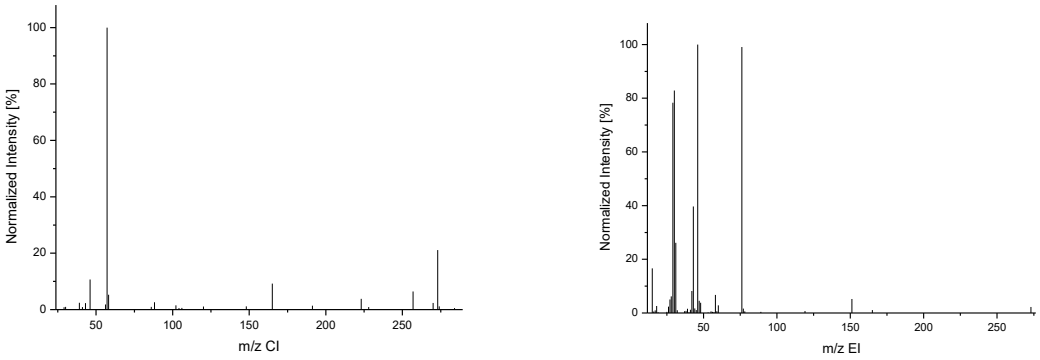

*Figure 1 – Mass Spectra of glyceryl trinitrate (GTN, **07**) under chemical ionization (CI, isobutane) and electron impact (EI, 70 eV) conditions.*

Figure 1 demonstrates the difference of CI and EI ionization mass spectra of glyceryl trinitrate. For EI (70 eV) the nitronium cation (NO_2^+, 100 % relative intensity, *m/z* 46), the $N_2O_3^+$ cation (99.11 % *m/z* 76) and the nitrosonium cation (NO^+, 82.88 %, *m/z* 30) dominate the spectrum. In case of CI (isobutane) the NO_2^+ adduct $C_3H_5N_4O_{11}$ (*m/z* 273) can be found with 21.09 % relative intensity. In the EI spectrum it is found with 2.24 % relative intensity.

Electrospray Ionization (ESI) is most frequently used in combination with high performance liquid chromatography (HPLC) since the liquid eluent can be ionized directly without removal of the solvent. The solvent is sprayed from a quartz/metal capillary. Between the capillary and a counter electrode a high voltage of 1-5 kV is applied. This generates ionized drops that get smaller by evaporation of the solvent and Coulomb explosions. ESI results in quasimolecular ions of positive (e.g., $(M+H^+)$) or negative charge (e.g., $(M+H^-)$). Cluster ions ($2M+H^+$) and adducts with the eluent (e.g., $(M+Na)^+$, $(M+Cl^-)$) can be formed. The formation of adducts can be promoted by addition of ionization dopants to the LC mobile phases (e.g., formic acid, ammonium acetate). With respect to the formation of adduct ions ESI should be considered more sensitive to matrix effects than EI.

Once the ions are generated by a method of choice, they are separated by *m/z* using different analyzers that include sector field analyzers, quadrupols, ion traps, ion cyclotron resonance, orbitraps and time of flight analyzers. More sophisticated analyzers can be realized by combination of several analyzers like tandem mass spectrometers, which contain a triple quadrupole setup (amongst other variants). In the first quadrupole an ion is selected and then fragmented in the second quadrupole by collision induced dissociation with a collision gas. The resulting fragment ions are analyzed with the third quadrupole. This is advantageous for structure elucidation of molecules and increasing the sensitivity and selectivity of the mass spectrometer.

The most comprehensive analyzer principle is time of flight. Figure 2 is a schematic illustration of the functional principle of a reflectron TOF setup. Ions are generated in an ion source and accelerated by an ion optic system towards a reflectron. Using electric fields the reflectron deaccelerates the ions and inverts their direction of movement towards the detector. The time of flight from ion source to detector is a function of *m/z*, the voltages applied and the length of the setup. Ions with a higher *m/z* ratio will arrive later at the detector.

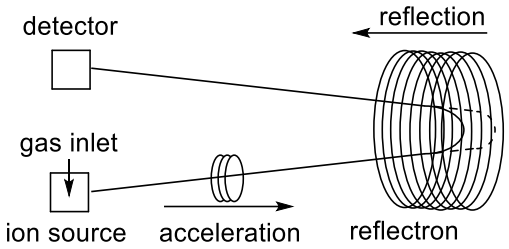

Figure 2 – Schematic illustration of the functional principle a reflectron TOF setup. Dashed line indicates the trajectory of a heavier ion. The system is evacuated to an ultra high vacuum level.

The major advantage of TOF is its sensitivity in comparison to the most commonly used quadrupole solutions. Quadrupoles use a sequential mass filter. Only ions of the same *m*/*z* ratio can pass at a time, the dwell time (time period where the detector accumulates the ion signal) per ion is dependent on the overall mass range. In a TOF-MS all ions are extracted from the ion source at the same time, hence the sensitivity is not dependent on the mass range.

This can be compensated by single ion monitoring methods (SIM) in which solely one or selected ions are monitored. Due to the pulsed ionization for TOF analyzers a direct comparison is not possible, but time of flight mass spectroscopy offers the advantage that each ion is detected with the same high sensitivity generating a full-scan spectrum with a sensitivity that is similar to that of quadrupole setups using SIM-methods.

For the detection of the ions various detectors like Faraday cups, secondary electron multipliers, post acceleration detectors (conversion dynode) and microchannelplate array detectors (TOF only) are used.

Recent advances in explosive detection include efforts for removing the necessity of analyte preconcentration, improving sample introduction methods, miniaturization and reduction of the cost for MS-based detector systems.[13d]

Atmospheric pressure chemical ionization (APCI) addresses some of these problems. A sample solution is sprayed into a corona discharge where the analytes are ionized to $(M+H)^+$ and $(M-H)^-$ quasimolecular ions. A possible ionization mechanism is similar to chemical ionization with the solvent vapour serving as reactant gas. Recent applications of sophisticated APCI applications have been reported by *Song* and *Cooks*[27] and by *Takada et al.[28]* for the detection of nitroaromatic compounds.

In case of desorption electrospray ionization (DESI) the analyte is bombarded in its ambient matrix with a mist of electrically charged droplets. The resulting ions are transported in the mass spectrometer using the detector vacuum.[29] This technique has been used for the detection of RDX **19** (500 pg), PETN **09** (50 ng) and TNT **17** (5 ng) on human skin.[30]

Direct analysis in real time (DART) is a technique that is similar to DESI. An electrical potential applied to the carrier gas creates metastable plasma ions that ionize the analytes in their ambient environment.[29] The technique has been used for the detection of various explosives on clothing, in water and on other surfaces.[30-31]

Desorption corona beam ionization (DCBI) is similar to DART but a small visible corona beam is generated. This technique has been demonstrated by *Wang et al.[32]* for the detection of TNT **17**. The startup NovionX has miniaturized a DCBI ion source (cf. Figure 3) using the plasma ionization of Argon or Helium. The plasma is generated using solid state radio-frequency technology. The technique has been demonstrated for the ionization of HMTD **01** and can be used to identify Theobromine and Caffeine directly in raw cocoa.[33]

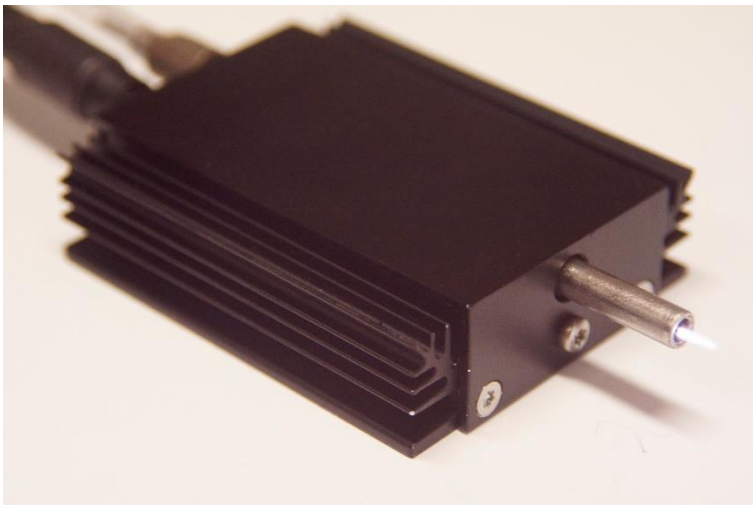

Figure 3 – The NovionX DCBI ion source operated with Argon.

The use of DESI with a portable mass spectrometer has been demonstrated to result in a RDX **19** detection limit of less than 1 ng on a paper surface.[34] Another miniaturized DESI setup has been demonstrated to be capable to detect TNT **17**, HMX **20** and TETRYL **22** on surfaces in µg cm^{-1} concentration levels. A miniaturized APCI setup was demonstrated to have low detection limits for RDX **19** (1 ng) and PETN **09** (250 pg).

Selective APCI using nitrate reactant ions generated from air was demonstrated for the detection of RDX **19** vapors without preconcentration in a sub-ppt level within 1-2 seconds. [35]

A multitude of further examples for the application of mass spectroscopy in explosive detection can be found in the reviews given.[13d, 13f, 13h, 13i]

The Spanish project SEDET[36] is a commercially available solution for the gas-phase detection of explosives. The sampling of air is performed with a vacuum cleaner type device. A TENAX-absorbent coated metal grid is introduced into the air suction stream of the sample collecting device. The nozzle can be placed under the tarpaulin of a truck to extract the air from the inside of the trailer. The next step is thermal desorption of the analytes. The analytes are ionized using electrospray ionization. The ions are separated by a differential mobility analyzer (DMA). The DMA is highly related to IMS technology (see section 1.1.3). The main difference between DMA and IMS is that the DMA separates ions in space whilst an IMS device separates them in time. The SEDET team states a sensitivity gain of two orders of magnitude in favor of the DMA device when compared with IMS. [36a, 37] The further ion separation and detection is carried out using a triple quadrupole mass spectrometer. The final device contains a cleaning unit for regeneration of the adsorbers by heating. The “minimal signal” sensitivity of the system for various explosives was stated without giving details about the determination: RDX **19** 0.12 ppq, PETN **09** 1.1 ppq, TNT **17** 132 ppq, EGDN **06** 1.508.000 ppq. The project team states that the concentration of explosives under real conditions is lowered by a factor of 100000 in comparison to saturation concentrations from vapor pressures. The system is stated to be capable to detect any explosive with a vapor pressure higher or equal to that of TNT **17** with 100 % probability.[36a, 37]

1.1.3 Ion Mobility Spectroscopy

Ion mobility spectroscopy (IMS) is the most applied technology for explosive trace detection. A critical review of ion mobility spectrometry for the detection of explosives and explosive related compounds is provided by *Ewing et al.*[13e]. *Steinfeld* and *Wormhoudt*[13i] describe ion mobility spectrometers to be “in some sense a time of flight mass spectrometer that operates at atmospheric pressure.” Sometimes IMS is referred to as “the small man’s mass spectrometer” in a humorous fashion with

respect to the lower cost for IMS equipment in comparison to mass spectrometers. The functional principle of IMS is based on the different mobility of accelerated ions in a drift gas. IMS and mass spectrometers (MS) have two components in common: ion source and detector. A large variety of MS ion sources (atmospheric pressure) and detectors is compatible with IMS devices. The ion sources of the most commercially available IMS devices rely on the β^-decay of ^{63}Ni and ^{241}Am.[38] The difference of IMS and MS is the analyzer. In contrast to the ultrahigh vacuum analyzers for MS, a drift tube is used for IMS. The separation of ions in the drift tube is based on their different mobility in a drift gas flow under simultaneous application of an electric field. The electrical acceleration of the ions is directed against the flow of the drift gas. (cf. Figure 4)

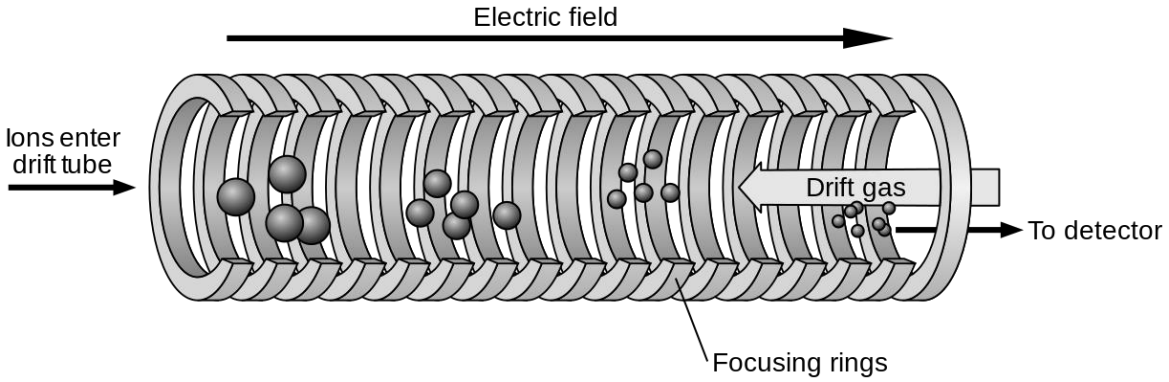

Figure 4 – Schematic illustration of the functional principle of an Ion Mobility Spectrometer.[39]

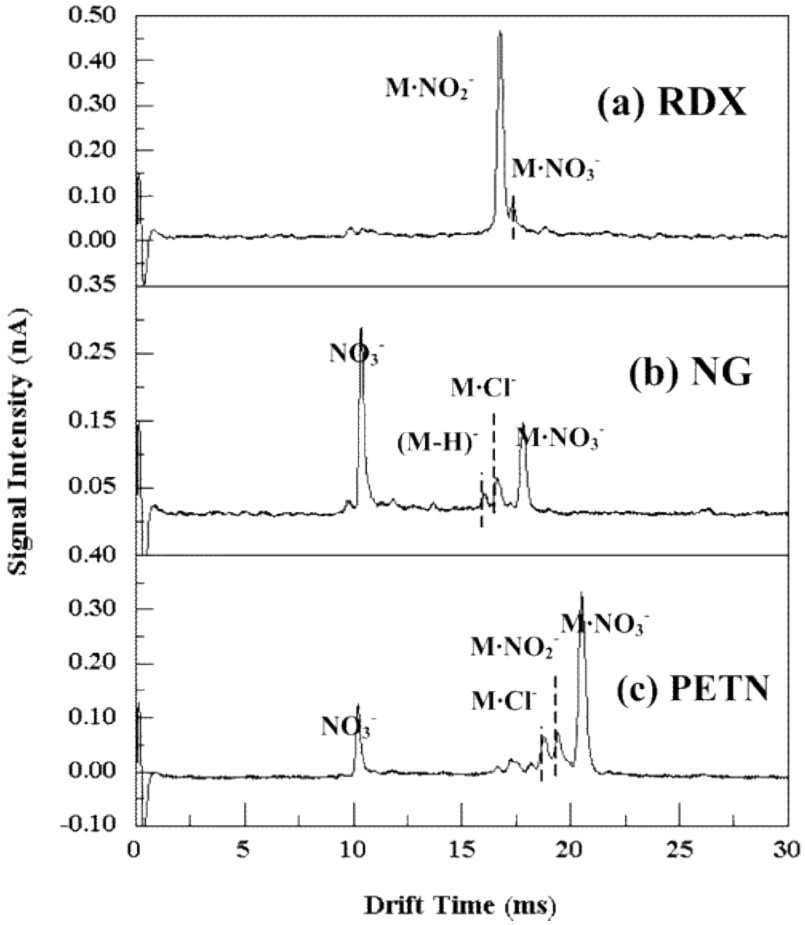

*Figure 5 - SESI-IMS spectra of 50 mg L^{-1} (a) RDX **19** (b) GTN **07**, and (c) PETN **09** in methanol–water. All spectra were run at 125 °C. Reprinted with permission from [40] Copyright 2004 American Chemical Society.*

The drift time depends on the charge, dimensions and mass of the ion. This enables the separation of different ions in the drift tube. In contrast to the high information output of mass spectrometers with unique *m/z* values and fragmentation patterns for each analyte, the output of an IMS device is limited to a plot of ion detector signal intensity versus drift time. (cf. Figure 5)

One analyte is often detected in form of different adduct and quasimolecular ions (e.g., $(M\text{-}H)^-$, $(M+NO_2)^-$, $(M+NO_3)^-$, $(M+Cl)^-$)[40]. Usually the relative mobility of the species observed is used for the identification of a compound since it is less dependent on operating conditions and allows the use of internal standard calibrants.[13g] Quadrupole ion trap mobility spectroscopy is a more sophisticated advancement of IMS with lower detection limits.[41] A limit of detection of 5.30 µg L^{-1} for RDX **19** was reported using secondary electrospray ionization with a nitrate dopant. For an application of positive corona discharge IMS limits of detection for various explosives were reported (RDX **19** 1 ng, HMX **20** 10 ng, PETN **09** 40 mg, TNT **17** 1000 ng). A multitude of further academic publications about the application of IMS for the detection of explosives using IMS is provided in the reviews given.[13d-i]

IMS is the explosive detection technology with the most applications in licensed explosive trace detector devices. Two of these devices used will be presented in the following. The Thermo Fisher EGIS Defender[42] hyphenates high speed gas chromatography with micro differential IMS (HSGC-DMS). The system is capable of detecting nanogram amounts of explosives (RDX **19**, TATP **02**, peroxides, nitrate esters, …) and narcotics in seconds.[13f] The ionscan 500 DT device is based on dual IMS and can detect explosives (RDX **19**, PETN **09**, GTN **07**, TNT **17**, HMX **20**, TATP **02**,…) in picogram amounts and narcotics in subnanogram amounts. Both devices use swipe samples.

1.2 Challenges in Explosive Detection

Steinfeld and *Wormhoudt* elucidate in their review [13i] four problems associated with explosive detection:

- low vapor pressures
- limited sample size
- deliberate concealment
- interferences

Each point will be detailed in the following. Further potential problems in explosive detection have been reported by *Oxley* [13c].

1.2.1 Low Vapor Pressures

The literature data on the vapor pressure of explosives has been reviewed by *Östmark et al.*[43] and *Ewing et al.*[44]. A comparison of measurement results from this work with the results stated by both reviews is given in section 7.9. In section 5.5 the vapor pressure limitation for detectability of explosives by the VO-GC/MS setup that was optimized in this work is elucidated. With respect to their enthalpy of vaporization or sublimation, the vapor pressure of explosives can be increased drastically by raising the temperature. According to *Steinfeldt* and *Wormhoudt*[13i] the vapor pressure of RDX **19** increases from 0.0084 ppb_v to 2.1×10^3 ppb_v. by raising the temperature from 300 K to 400 K. Since the vapor pressure is directly proportional to the concentration of the analyte in saturation equilibrium (cf. chapter 5.5) both parameters are increased by six orders of magnitude. This phenomenon is exploited by various instrumental explosive detection approaches. It was demonstrated that in case of the plastic explosives formulation C4, the vapor pressure of RDX **19** is reduced by two orders of magnitude. C4 is a solid solution of RDX **19** containing a plasticizer, a polyisobutylene polymer and mineral oil. Commercially available plastic explosives containing explosives with low volatility must contain an

explosive detection aid agent (so-called taggant). Compounds that can be used are EGDN **04**, DMDNB **26**, 2-MNT **12** and 4-MNT **14**.[45]

1.2.2 Limited Sample Size

The saturation concentration of explosives that is directly proportional to vapor pressures is not realistic. Diffusion processes lower the concentration by several orders of magnitude (cf. section 5.7).[46] In project SEDET it was stated that the room temperature concentrations of explosives concealed with cardboard boxes are lowered by a factor of 100.000 after 15 minutes. A study remarked that total sample weights of explosives, obtained from high-volume air sampling, could be in the 0.01-0.001 pg range. Fingerprints could be another source of traces of explosives. A study of calibrated fingerprints after Handling Semtex (plastic explosive formulation containing RDX **19**) revealed that the first fingerprint contains 3.0 – 4.5 mg, the tenth about 100 ng and the fiftieth 3 to 76 ng of RDX **19**. The RDX **19** particle size is in the 30-350 µm range. [13i, 47]

1.2.3 Deliberate Concealment

Some explosives themselves already require a confinement for their proper detonation. In case of a metal confinement, the resulting detonation-accelerated metal shrapnels increase the damage caused by the explosive device drastically. A proper concealment also reduces the gas phase concentration of an explosive depending on the materials used for concealment. It may be the case that only the traces left behind during the bomb preparation may be available for detection. Traces released into the gas phase may be absorbed by other surfaces. *Stott et al.*[48] state that with respect to the attenuation of vapors that "only the most volatile species can be detectable under real world conditions".[48] *Kolla* [13a] estimates that the concentration of an explosive gets decreased by a factor of 1000 when it is wrapped in foil.

1.2.4 Interferences

In explosive detection two possible sources of false positives exist. On the one hand, trace amounts of explosives can be present in absence of an explosive device. The other source is the presence of allowed substances that trigger the explosive detector. Only few examples of large field tests are published. In October 1988 a GC-based detection system with thermal decomposition and a nitrogen monoxide chemoluminescence detector was tested on over 2000 volunteers. The false positive rate was less than 0.15 %.[13i] A tandem mass spectrometer (MS/MS) device was tested on over 20000 cargo containers and vehicles. For a TNT threshold of 50 pg 0.13 % of false alerts were observed.[48] Literature reviews are not in agreement about the suitability of technical approaches (MS, IMS) for explosives detection in terms of selectivity.[13a, 13i]

1.3 Project ChemAir

In July 2011 the German Ministry of Education and Research (BMBF) called for projects to be funded in the field of "Security in Aviation".[11] One of the projects that were funded was the project "ChemAir", which was concerned with the development of a technology for the near real-time detection of airborne hazardous materials.[12] The research consortium included different academic workgroups, companies and official institutions:

- **University of Bonn**: Project Coordinator Dr. Peter Boeker and Dr. Jan Leppert. Development of a fast method for gas chromatography and a micro enrichment unit.
- **University of Munich**: Prof. Dr. Thomas M. Klapötke, Dr. Jörg Stierstorfer, Martin Härtel. Selection, synthesis and characterization of explosives.
- **five Technologies** (Munich): Project Coordinator Dr. Gerhard Horner and Dr. Pierre Schanen. Enhancement of selectivity for the detection of trace components by variation of the ionization energy of the mass-spectroscopic detector.

- **Inspire Analytical Systems** (Oberursel): Dr. Martin Schmäh, Dr. Florian Werunsky. Development of a sample transfer system and a reference gas generator.
- **Bundeswehr Research Institute for Protective Technologies and CBRN Protection (WIS)** (Munster): Dr. Joachim Ringer, Julia Rothe. Characterization of a time of flight mass spectrometer and method development for fast gas chromatography.
- **German Federal Police (Referat 61 – Research and Testing)**: Rainer Weinzierl, Dr. Michael Hill. Scientific mentoring in terms of the explosive detection application. Certification of explosive trace detectors.
- **Lufthansa Cargo**: Burkhardt Berndt. Associated partner and potential user of the developed technology.
- **Fraport AG**: Mark Zwirner. Associated partner and potential user of the developed technology.

Members of the research consortium that were present at the final project meeting on May 18th 2016 are depicted in Figure 6. The project was carried out from 03/01/2016 till 06/31/2016. It was funded by the German Ministry of Education and Research and monitored by the Verein Deutscher Ingenieure (VDI, Dr. Sandra Muhle, Svenja Wargers).

Figure 6 – The ChemAir research consortium. From left to right: Julia Rothe (German Bundeswehr, WIS Munster), Dr. Florian Werunsky (Inspire Analytical Systems), Dr. Michael Hill (German Federal Police), Dr. Sandra Muhle (VDI), Svenja Wargers (VDI), Dr. Gerhard Horner (five Technologies), Dr. Jan Leppert (University of Bonn), Dr. Peter Boeker (University of Bonn), Kai-Benjamin Schütt, Burkhardt Berndt (Fraport AG), Martin Härtel (University of Munich) and Kathrin Grieger (University of Munich).

The target of project ChemAir was the development of a detection system for airborne hazardous materials based on the following technologies that are directly compared with project SEDET. (cf. section 1.1.3)

Table 1 – Comparison of Technologies planned to be used in project ChemAir and used in project SEDET.

Detection Step	**ChemAir**	**SEDET**
Sample Collection	high volume air sampling with an absorbent coated filter.	
Analyte Desorption	thermal desorption	
Post Desorption Enrichment	Peltier Cooling Trap	none
Analyte Separation	LTM-FF-TG-GC*	Drift Mobility Analyzer
Analyte Ionization	Electron Impact Ionization (12-70 eV)	Electrospray Ionization
MS Analyzer	Time of Flight	Triple-Quadrupole

* Low Thermal Mass Flowfield Thermogradient Gas Chromatography

Table 1 compares the technologies planned to be used in project ChemAir and used in project SEDET. It is obvious that both projects are similar since they use high volume air sampling in combination with thermal desorption and mass-spectroscopic analyte detection. The major difference is the analyte processing after desorption. In project SEDET the analytes are directly ionized using electrospray ionization, separated by a drift mobility analyzer and detected by a triple-quadrupol mass spectrometer. In project ChemAir it was planned to enrich the analytes after thermal desorption using a capillary cooling trap with a doubletube isolator. The cooling trap can be cooled by a Stirling Peltier-element cooler to -95 °C. After the enrichment the capillary can be used as a resistive heating element to redesorb the analytes. The redesorbed analytes are separated using low thermal mass flowfield thermal gradient gas chromatography. The technology is capable of separating explosives within one minute (including the cooling of the GC "oven"). The final detection is carried out with a Markes International Select-eV time of flight mass spectrometer, which has the unique feature to switch the electron impact ionization energy within milliseconds from 12-70 eV without reducing the electron current. In this fashion false positives can be reduced by using low and high ionization energy mass spectra for the identification of the analyte. In project ChemAir a prototype that combines all components could not be demonstrated with respect to the limited project time. The individual results of all project participants are available online.[12] In the following the LTM-FF-TG-GC analyte separation setup by *Boeker* and *Leppert* and the variable ionization energy electron impact ion source by five technologies will be presented in detail.

1.3.1 Low Thermal Mass Flow-Field Thermogradient Gas Chromatography

Low Thermal Mass Flow-Field Thermogradient Gas Chromatography (in the following referred to as LTM-FF-TG-GC, cf. Figure 7 right) is a technique that was developed by *Boeker* and *Leppert* [49] in the framework of project ChemAir. This innovational technique was patented [50] and has excited the separation science community [51].

The advantages of a negative temperature gradient along the column of a gas chromatograph have been known and researched for decades with the first concepts going back to the 1950s. The application of a negative temperature gradient to the GC column results in two major advantages. Whilst the tail of a chromatographic peak is moving faster in a hotter zone, the front of the peak is moving slower in a colder zone along the separation column. This results in a focusing of the peak, which increases the peak capacity of the system and improves the limits of detection, which are often defined in terms of signal to noise ratio. (cf. Figure 7 left) The second advantage of this method is the reduction of thermal stress to the analyte in comparison to classical gas chromatography since short columns can be used and each peak travels with the gradient that is raised continuously during the analysis. With this each substance can exit the analytical column at its optimum elution temperature.

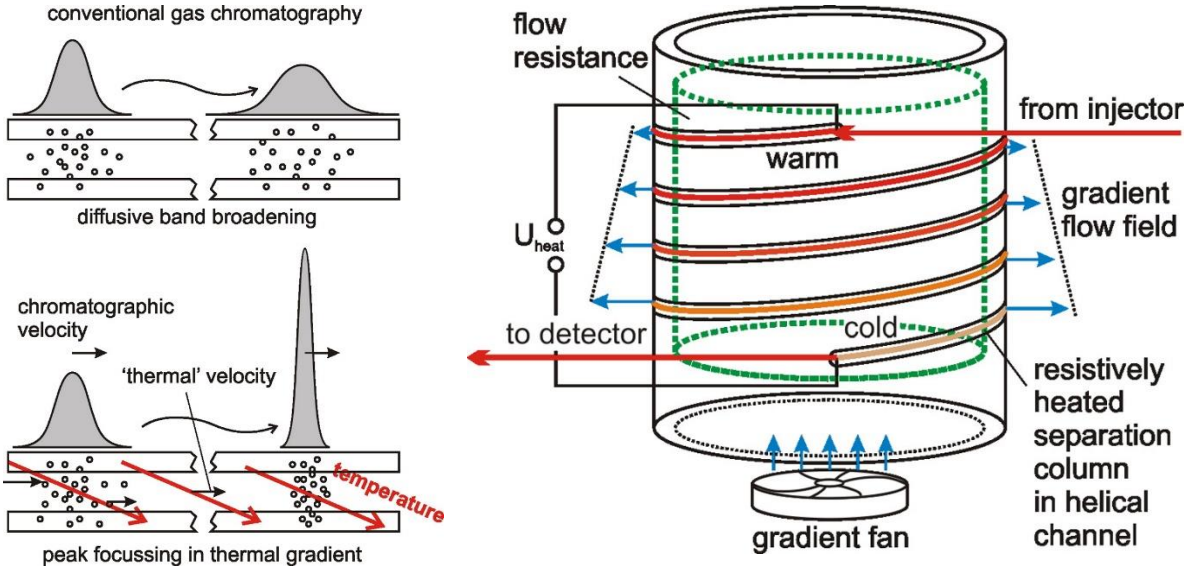

Figure 7 - Peak-focussing effect of a negative temperature gradient along the the column of a gas-chromatography column. Right: Schematic Illustration of the functional principle of Boeker and Lepperts LTM-FF-TG-GC setup. Reprinted with permission from [49] Copyright 2015 American Chemical Society.

This is of special interest for thermolabile analytes like explosives. There have been various technical approaches for the realization of a negative temperature gradient along the analytical column of a gas chromatograph. *Boeker* and *Leppert* [49] list numerous preceding publications about the realization of a negative temperature gradient along a GC column, including the wrapping of a heating wire with decreasing wrapping intensity, the manual application of conductive paint on a chromatography column with decreasing paint thickness or a sheath around the column to transfer cold gas along the resistively heated column. All those techniques are laborious and relatively expensive. The quick exchange of the analytical column is not possible.

Boeker and *Leppert* [49] have managed to establish a convenient, effective and affordable setup for negative thermal gradient gas chromatography. The chromatographic column is embedded in a resistively heated metal capillary. This allows the use and quick exchange of standard GC columns. The heated capillary is placed in a channel that is cut into a piece of pipe. The pipe is closed at one end and packed with porous material. At the other end of the pipe a gradient fan blows air into the pipe. The flow resistance caused by the porous material is proportional to the distance of the fan. This results in a gradual lowering of the airflow through the cut out channel towards the closed end of the pipe. The forced convection resulting from the spatial airflow gradient over the heated capillary generates the thermal gradient along the analytical column. A photograph of a prototype setup and a thermal image visualizing the thermogradient effect are provided in Figure 8.

The technique is compatible with autosamplers and has been successfully interfaced to a Markes International Select-eV TOF-MS. Using the low-thermal mass technology regarding the restively heated capillary around the column the GC/MS analysis can be completed within less than a minute, including the cooling of the capillary to starting conditions. With conventional GC ovens solely the cooling from 280 °C to 40 °C takes about five minutes. Figure 9 shows a LTM-FF-TG-GC/TOF-MS a chromatogram of 15 explosives and explosive-related compounds. The analysis is completed within 37 seconds with a medium peak width of 86 ms and a peak capacity of 105. With respect to the low peak width the system is only compatible with detectors that have a fast data acquisition rate above 150 Hz. This requirement is fulfilled by the Markes International select-eV TOF-MS which will be presented in the next section.

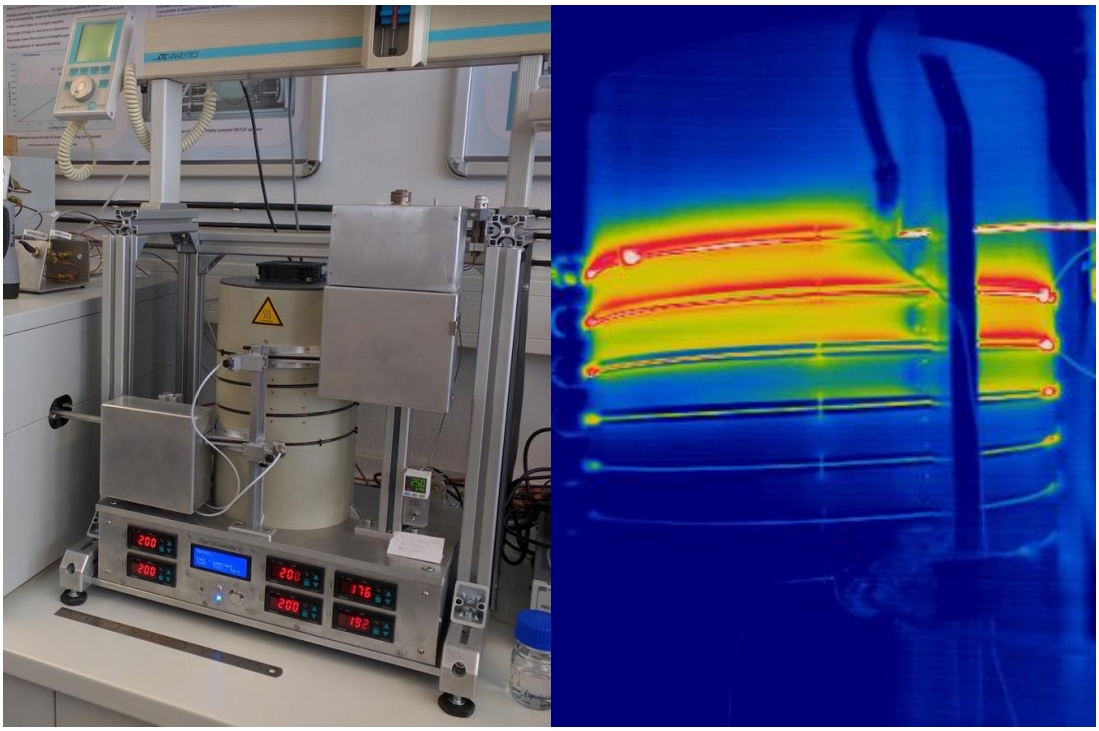

Figure 8: left: photograph of the LTM-FF-TG-GC setup in prototype state, right: thermal image visualizing the thermogradient.

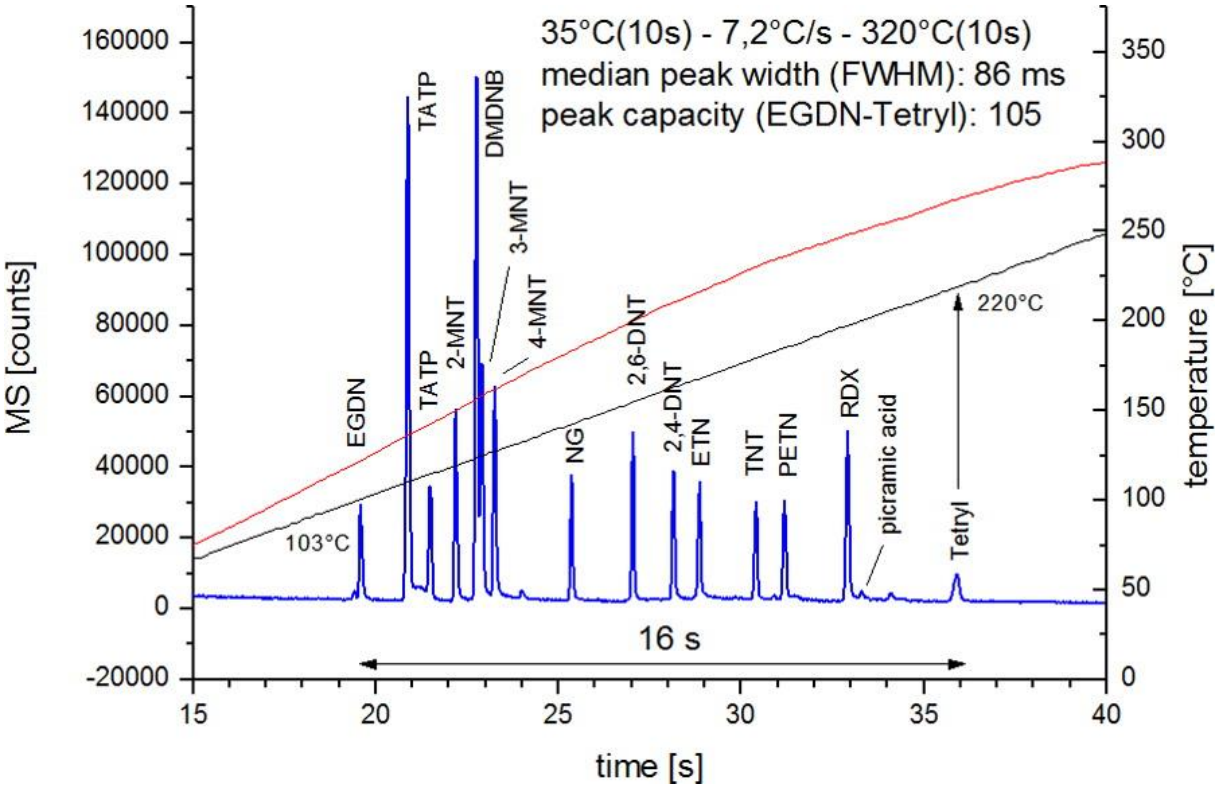

Figure 9 – LTM-FF-TG-GC/TOF-MS chromatogram of explosives and explosive-related compounds. Red: Temperature at the start of the analytical column. Black: Temperature at the end of the analytical column. Reprinted with permission from [49] Copyright 2015 American Chemical Society.

1.3.2 Time of Flight Mass Spectroscopy with variable Ionization Energy

Electron Impact ionization is one of the most frequently used types of ionization in hyphenation with gas chromatography since it requires no reactant gas like chemical ionization and, with respect to its reproducibility, large commercial databases of EI mass spectra with an ionization energy of 70 eV are available. (cf. section 1.1.2)

For electron impact ionization a filament is heated. The thermally emitted electrons are detracted from the filament by application of an electrical potential. If a potential of 70 V is applied, the electrons will have an energy of 70eV upon reaching the ion source. There they generate analyte molecule radical cations by collision with the analytes and cause fragmentation of the molecules.

For most molecules the ionization cross-section, the probability of ionization, reaches a maximum between 30 and 200 eV ionization energy. For this reason ionization energies below 30 eV were not taken into consideration for soft ionization techniques. The second, more severe problem is the 3-dimensional potential distribution between filament and ion source. Figure 10 illustrates this problem. At workpoint 1 only a raise of filament temperature can increase the ion current density, this is the case at the standard ionization energy of 70 eV. If the potential difference is decreased below 20 V the ion current density is reduced drastically. The thermally emitted electrons are building a space charge, which shields the ion source potential from the filament. A large fraction of thermally emitted electrons are either readsorbed by the filament or scattered into undesired directions lowering the electron current density. Five technologies have solved this problem by acceleration of the electrons to remove them from the filament followed by deacceleration to the desired electron energy. This is realized using electron optic components.

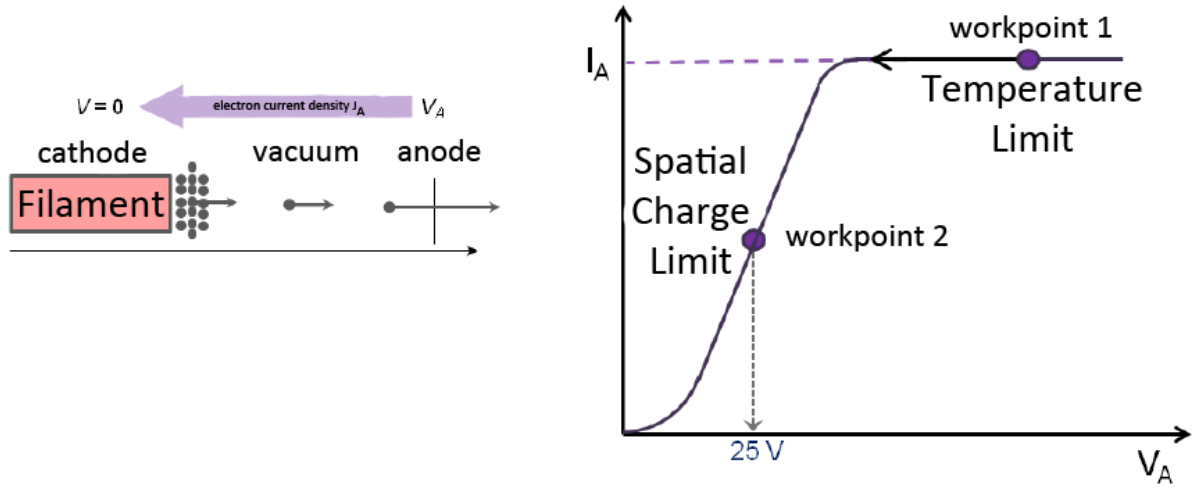

Figure 10 – Electron current density I_A as a function of ionization energy.

Within project ChemAir five technologies advanced this socalled “select-eV” technology to “Tandem Ionisation”. It is possible to switch from 12 eV to 70 eV ionization energy within milliseconds. With this technology two GC/MS chromatograms at different ionization energies can be recorded simultaneously. This is demonstrated for Caryophyllene in Figure 11. The chromatographic peak is recorded with mass spectra at 12 eV and 70 eV ionization energy.

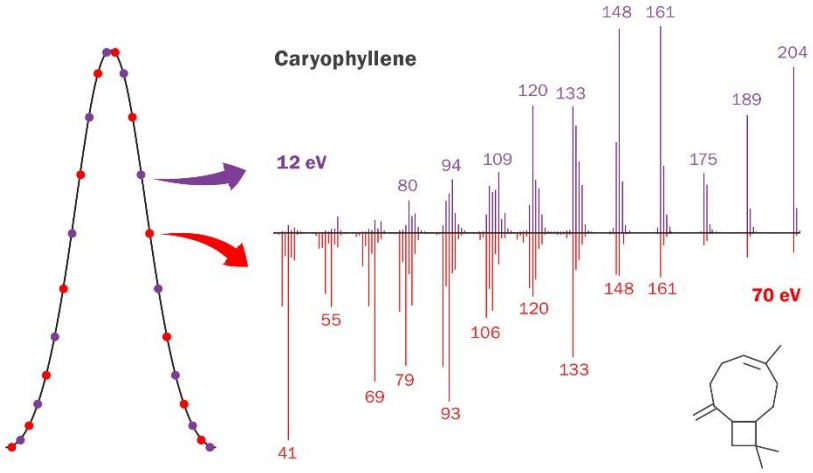

Figure 11 – Illustration of the effects „Tandem Ionization" allowing the simultaneous recording of a chromatographic peak at 12 and 70 eV ionization energy.

Lower ionization energies cause less and different fragmentation of the analyte molecule and can enhance the intensity of the molecular ion peak. The database comparison of mass spectra at two different ionization energies is a promising concept for the reduction of false positives. (cf. section 1.2.4)

Figure 12 shows two mass spectra of TNT **17** using an ionization energy of 12 and 70 eV. It is obvious that with 12 eV the fragmentation of the analyte is reduced in comparison to 70 eV. At 12 eV the relative intensity of the $M^{\cdot+}$ fragment peak m/z 210 is significantly higher when compared with the 70 eV mass spectrum of TNT **17**. A second point that should be noted is the different absolute intensity of the most intense peak m/z 210. At 70 eV its intensity is about 1.4×10^7 counts. At 12 eV the intensity is reduced to about 4×10^6 counts. The loss of sensitivity of one order of magnitude cannot be avoided since it is caused mainly by the reduction of the ionization cross section of the molecule.

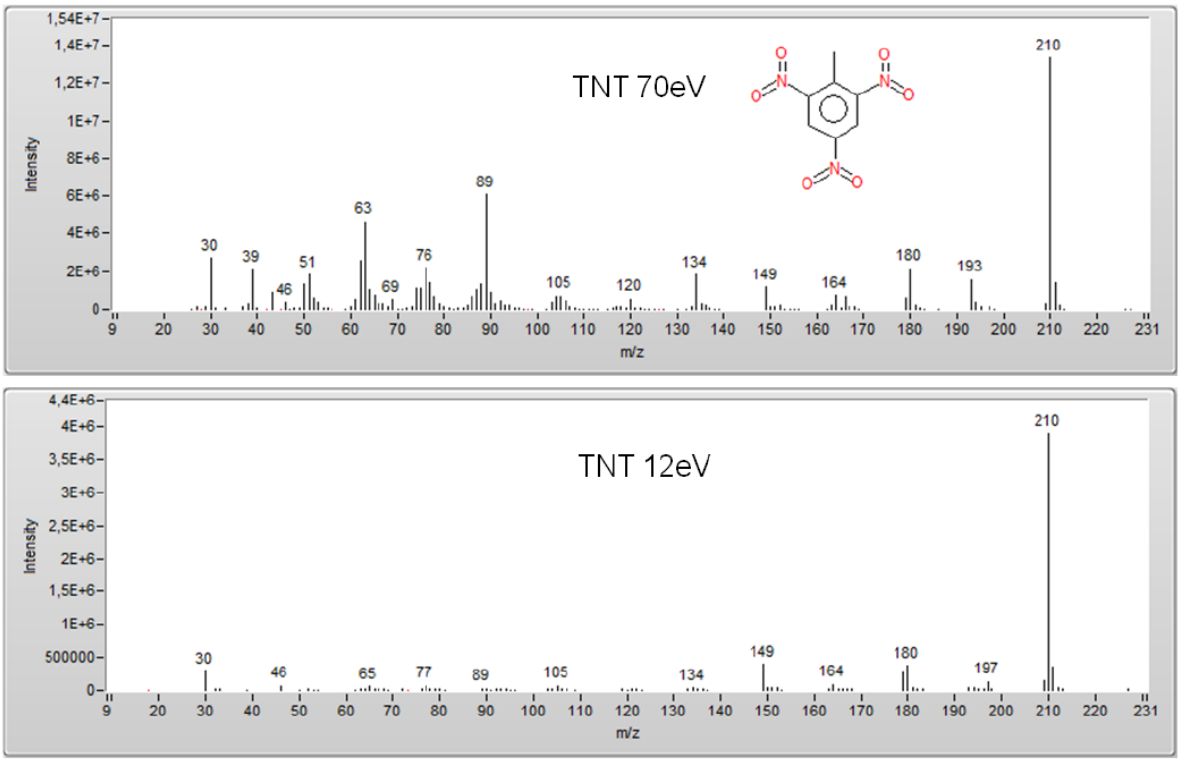

Figure 12 – Mass spectra of TNT 17 using 12 eV and 70 eV ionization energy.

1.4 Facit

In project ChemAir single components for the construction of an explosive detection apparatus could be constructed including a high volume air sampling unit, an infrared-based thermodesorption unit, a Peltier-element cooled capillary microenrichment unit, the LTM-FF-TG-GC technology for analyte separation and the "select-eV/Tandem Ionization" TOF-MS detector by five technologies. Further information about the single components can be found in the final reports of the project partners.[12] The LTM-FF-TG-GC was successfully interfaced to the TOF-MS detector. With respect to the limited project time, the other components were not interfaced for the construction of a complete explosive detection device. The established LTM-FF-TG-GC/TOF-MS device is a powerful component for future explosive detection devices with respect to the short cycle of analysis (< 1 min), the suitability for thermolabile analytes and the potential reduction of false positive by fast switching of the ionization energy. With respect to this it should be continued to complete this setup to a high performance explosive detection system. A detailed publication about the Limits of Detection (LOD) for the explosives using LTM-FF-TG-GC/TOF-MS in comparion with VO-GC/MS (cf. section 5) using split-injections of analyte solutions will be published soon in a cooperation of the project participants from the universities of Bonn and Munich. Single field tests using improvised air sampling and thermo-desorption equipment were carried out, but cannot replace extensive field measurements of the complete detection setup since the concentration of possibly concealed explosives in a real environment is more or less unknown and the limits of detection might be increased by the loss of analyte during the air sampling and the transfer to the detector. The selectivity of the method in terms of false positive rates must be evaluated carefully. To quote the Bundeswehr trace detection expert Joachim Ringer: "A multitude of nice trace detector systems exist. The real challenge is the loss-less sampling and transfer of the analytes to the detector." Project ChemAir produced fruitful, commercialized results and work should not be stopped at this point since a powerful next-generation detector system might be lost.

Literature References

1. https://www.panynj.gov/airports/pdf-traffic/ATR_2015.pdf.
2. http://www.fraport.de/content/fraport/de/misc/binaer/presse/publikationen/2015/zahlen--daten--fakten-2015/jcr:content.file/zahlen-daten-fakten-2015.pdf.
3. https://en.wikipedia.org/wiki/November_2015_Paris_attacks.
4. https://sputniknews.com/europe/201601141033143474-airport-security-gates-terrorism/.
5. https://www.aerotime.aero/en/airports/airports-news/other/20608-more-than-50-eu-airports-deploy-itemiser-4dx-explosives-trace-detectors.
6. https://www.ict.org.il/UserFiles/ICT-trends-aviation-terror-aug-16.pdf.
7. http://data.europa.eu/eli/reg_impl/2015/1998/oj.
8. Rouhi, A. M., Government, Industry Efforts Yield Array Of Tools To Combat Terrorism. *Chemical & Engineering News Archive* **1995,** *73* (30), 10-19.
9. http://ec.europa.eu/research/participants/portal/desktop/en/opportunities/h2020/topics/sec-11-fct-2016.html.
10. http://www.sifo.de/.
11. https://www.bmbf.de/foerderungen/bekanntmachung-662.html.
12. http://www.sifo.de/de/bewilligte-projekte-aus-der-bekanntmachung-sicherheit-im-luftverkehr-1761.html.
13. (a) Kolla, P., Detecting Hidden Explosives. *Analytical Chemistry* **1995,** *67* (5), 184A-189A; (b) Nyden, M. R.; Justice, N. I. o.; Laboratory, L. E. S., *A technical assessment of portable explosives vapor detection devices*. U.S. Dept. of Justice, Office of Justice Programs, National Institute of Justice: 1990; (c) Oxley, J., Explosives detection: potential problems. *SPIE Proceedings* **1995,** *2511*, 217-226; (d) Lefferts, M. J.; Castell, M. R., Vapour sensing of explosive materials. *Analytical Methods* **2015,** *7* (21), 9005-9017; (e) Ewing, R. G.; Atkinson, D. A.; Eiceman, G. A.; Ewing, G. J., A critical review of ion mobility

spectrometry for the detection of explosives and explosive related compounds. *Talanta* **2001,** *54* (3), 515-529; (f) Caygill, J. S.; Davis, F.; Higson, S. P. J., Current trends in explosive detection techniques. *Talanta* **2012,** *88*, 14-29; (g) Moore, D. S., Instrumentation for trace detection of high explosives. *Review of Scientific Instruments* **2004,** *75* (8), 2499-2512; (h) Moore, D. S., Recent Advances in Trace Explosives Detection Instrumentation. *Sensing and Imaging: An International Journal* **2007,** *8* (1), 9-38; (i) Steinfeld, J. I.; Wormhoudt, J., EXPLOSIVES DETECTION: A Challenge for Physical Chemistry. *Annual Review of Physical Chemistry* **1998,** *49* (1), 203-232.

14. (a) https://fas.org/irp/threat/terrorism/guide.pdf; (b) Apih, T.; Rameev, B.; Mozzhukhin, G.; Barras, J., *Magnetic Resonance Detection of Explosives and Illicit Materials*. Springer Netherlands: 2013; (c) Krausa, M., *Vapour and Trace Detection of Explosives for Anti-Terrorism Purposes*. Springer Netherlands: 2004; (d) Marshall, M.; Oxley, J. C., *Aspects of Explosives Detection*. Elsevier Science: 2011; (e) Schubert, H.; Kuznetsov, A., *Detection of Explosives and Landmines: Methods and Field Experience : [proceedings of the NATO Advanced Research Workshop on ... St. Petersburg, Russia, 9-14 September 2001]*. Springer Netherlands: 2002; (f) Schubert, H.; Kuznetsov, A., *Detection and Disposal of Improvised Explosives*. Springer Netherlands: 2006; (g) Schubert, H.; Kuznetsov, A., *Detection of Bulk Explosives Advanced Techniques against Terrorism: Proceedings of the NATO Advanced Research Workshop on Detection of Bulk Explosives Advanced Techniques against Terrorism St. Petersburg, Russia 16–21 June 2003*. Springer Netherlands: 2004; (h) Fraissard, J.; Lapina, O., *Explosives Detection using Magnetic and Nuclear Resonance Techniques*. Springer Netherlands: 2009; (i) Council, N. R.; Studies, D. E. L.; Technology, B. C. S.; Techniques, C. R. E. P. S. E. D., *Existing and Potential Standoff Explosives Detection Techniques*. National Academies Press: 2004; (j) Yinon, J., *Advances in Analysis and Detection of Explosives: Proceedings of the 4th International Symposium on Analysis and Detection of Explosives, September 7–10, 1992, Jerusalem, Israel*. Springer Netherlands: 2013; (k) Woodfin, R. L., *Trace Chemical Sensing of Explosives*. Wiley: 2006.

15. Furton, K. G.; Myers, L. J., The scientific foundation and efficacy of the use of canines as chemical detectors for explosives1. *Talanta* **2001,** *54* (3), 487-500.

16. Walker, D. B.; Walker, J. C.; Cavnar, P. J.; Taylor, J. L.; Pickel, D. H.; Hall, S. B.; Suarez, J. C., Naturalistic quantification of canine olfactory sensitivity. *Appl. Anim. Behav. Sci.* **2006,** *97* (2–4), 241-254.

17. Quignon, P.; Rimbault, M.; Robin, S.; Galibert, F., Genetics of canine olfaction and receptor diversity. *Mammalian Genome* **2012,** *23* (1), 132-143.

18. http://explotech.de/de/produkte/empk.html.

19. http://www.explotech.de/de/leistungen/fadi.html.

20. Shaw, J. A.; Seldomridge, N. L.; Dunkle, D. L.; Nugent, P. W.; Spangler, L. H.; Bromenshenk, J. J.; Henderson, C. B.; Churnside, J. H.; Wilson, J. J., Polarization lidar measurements of honey bees in flight for locating land mines. *Opt. Express* **2005,** *13* (15), 5853-5863.

21. Otto, J.; Brown, M. F.; Long Iii, W., Training rats to search and alert on contraband odors. *Appl. Anim. Behav. Sci.* **2002,** *77* (3), 217-232.

22. King, T. L.; Horine, F. M.; Daly, K. C.; Smith, B. H., Explosives detection with hard-wired moths. *IEEE Transactions on Instrumentation and Measurement* **2004,** *53* (4), 1113-1118.

23. Corcelli, A.; Lobasso, S.; Lopalco, P.; Dibattista, M.; Araneda, R.; Peterlin, Z.; Firestein, S., Detection of explosives by olfactory sensory neurons. *Journal of Hazardous Materials* **2010,** *175* (1–3), 1096-1100.

24. https://www.nist.gov/srd/nist-standard-reference-database-1a-v14.

25. Granot, O.; Amirav, A., LC–MS with electron ionization of cold molecules in supersonic molecular beams. *International Journal of Mass Spectrometry* **2005,** *244* (1), 15-28.

26. https://www.shimadzu.de/ci-und-cinci-messung.

27. Song, Y.; Cooks, R. G., Atmospheric pressure ion/molecule reactions for the selective detection of nitroaromatic explosives using acetonitrile and air as reagents. *Rapid Communications in Mass Spectrometry* **2006,** *20* (20), 3130-3138.

28. Takada, Y.; Nagano, H.; Suga, M.; Hashimoto, Y.; Yamada, M.; Sakairi, M.; Kusumoto, K.; Ota, T.; Nakamura, J., Detection of Military Explosives by Atmospheric Pressure Chemical Ionization Mass

Spectrometry with Counter-Flow Introduction. *Propellants, Explosives, Pyrotechnics* **2002,** *27* (4), 224-228.
29. Cooks, R. G.; Ouyang, Z.; Takats, Z.; Wiseman, J. M., Ambient Mass Spectrometry. *Science* **2006,** *311* (5767), 1566-1570.
30. Justes, D. R.; Talaty, N.; Cotte-Rodriguez, I.; Cooks, R. G., Detection of explosives on skin using ambient ionization mass spectrometry. *Chemical Communications* **2007,** (21), 2142-2144.
31. Nilles, J. M.; Connell, T. R.; Stokes, S. T.; Dupont Durst, H., Explosives Detection Using Direct Analysis in Real Time (DART) Mass Spectrometry. *Propellants, Explosives, Pyrotechnics* **2010,** *35* (5), 446-451.
32. Wang, H.; Sun, W.; Zhang, J.; Yang, X.; Lin, T.; Ding, L., Desorption corona beam ionization source for mass spectrometry. *Analyst* **2010,** *135* (4), 688-695.
33. http://www.novionx.de/.
34. Mulligan, C. C.; Talaty, N.; Cooks, R. G., Desorption electrospray ionization with a portable mass spectrometer: in situ analysis of ambient surfaces. *Chemical Communications* **2006,** (16), 1709-1711.
35. Ewing, R. G.; Atkinson, D. A.; Clowers, B. H., Direct Real-Time Detection of RDX Vapors Under Ambient Conditions. *Analytical Chemistry* **2013,** *85* (1), 389-397.
36. (a) http://www.sedet.com/descargas/SEDET_EUCDE%20II.pdf; (b) http://www.sedet.com/Technology.html.
37. Rus, J.; Moro, D.; Sillero, J. A.; Royuela, J.; Casado, A.; Estevez-Molinero, F.; Fernández de la Mora, J., IMS–MS studies based on coupling a differential mobility analyzer (DMA) to commercial API–MS systems. *International Journal of Mass Spectrometry* **2010,** *298* (1–3), 30-40.
38. Ewing, R. G.; Waltman, M. J., Mechanisms for negative reactant ion formation in an atmospheric pressure corona discharge. *International Journal for Ion Mobility Spectrometry* **2009,** *12* (2), 65-72.
39. https://upload.wikimedia.org/wikipedia/commons/thumb/6/66/Ion_mobility_spectrometry_diagram.svg/1267px-Ion_mobility_spectrometry_diagram.svg.png Picture was created by Jeff Dahl. No changes were made. Licensed under CC BY-SA 3.0 by the Wikimedia Foundation.
40. Tam, M.; Hill, H. H., Secondary Electrospray Ionization-Ion Mobility Spectrometry for Explosive Vapor Detection. *Analytical Chemistry* **2004,** *76* (10), 2741-2747.
41. March, R. E., An Introduction to Quadrupole Ion Trap Mass Spectrometry. *Journal of Mass Spectrometry* **1997,** *32* (4), 351-369.
42. https://fscimage.fishersci.com/images/D00700~.pdf.
43. Östmark, H.; Wallin, S.; Ang, H. G., Vapor Pressure of Explosives: A Critical Review. *Propellants, Explosives, Pyrotechnics* **2012,** *37* (1), 12-23.
44. Ewing, R. G.; Waltman, M. J.; Atkinson, D. A.; Grate, J. W.; Hotchkiss, P. J., The vapor pressures of explosives. *TrAC Trends in Analytical Chemistry* **2013,** *42*, 35-48.
45. Groom, C. R.; Bruno, I. J.; Lightfoot, M. P.; Ward, S. C., The Cambridge Structural Database. *Acta Crystallographica Section B* **2016,** *72* (2), 171-179.
46. (a) Dravnicks, A. *Bomb Detection System Study*; IIT Research Institute: Chicago, Illinois, 1965; (b) Dravnicks, A.; Brabets, R.; Stanley, T. A. *Evaluating Sensitivity Requirements of Explosive Vapor Detector Systems*; IIT Research Institute Technology Center: Chicago Illinois, 1972.
47. Liu, B. Y. H.; Yoo, S. H.; Davies, J. P.; Gresham, G. L.; Hallowell, S. F., Development of particle standards for testing explosive detection systems: characterization of the adhesion forces between composition 4 particles and polyethylene. *SPIE Proceedings 2276*, 34-44.
48. Stott, W. R.; Davidson, R. S., High-throughput real-time chemical contraband detection. *SPIE Proceedings* **1994,** *2092*, 53-63.
49. Boeker, P.; Leppert, J., Flow Field Thermal Gradient Gas Chromatography. *Analytical Chemistry* **2015,** *87* (17), 9033-9041.
50. Boeker, P. Patent DE102014004286B3: Strömungsfeld induzierte Temperatur-Gradienten-Gaschromatographie (flow field induced thermal gradient gas chromatography); DE102014004286B3, 26.03.14.

51. (a) Sandra, P. Go with the Flow (Field). The Analytical Scientist 2015, 1115, 32–33. https://theanalyticalscientist.com/issues/1115/landmark-literature-2015-part3/; (b) Boeker, P. Beginner's Luck and Hyper-Fast GC. The Analytical Scientist 2016, 0916, 38–42. https://theanalyticalscientist.com/issues/0916/beginners-luck-and-hyper-fast-gc/.
52. de Zeeuw, J.; Reese, S.; Cochran, J.; Grossman, S.; Kane, T.; English, C., Simplifying the setup for vacuum-outlet GC: Using a restriction inside the injection port. *Journal of Separation Science* **2009,** *32* (11), 1849-1857.
53. Verevkin, S. P.; Ralys, R. V.; Zaitsau, D. H.; Emel'yanenko, V. N.; Schick, C., Express thermo-gravimetric method for the vaporization enthalpies appraisal for very low volatile molecular and ionic compounds. *Thermochimica Acta* **2012,** *538*, 55-62.

2 Objectives of this Work

This work was carried out in the framework of project ChemAir, which was concerned with the near real-time detection of airborne hazardous materials. The technical approach was high volume air sampling followed by thermodesorption, analyte separation by gas chromatography and detection by mass spectroscopy. The project is detailed in section 1.3. In the following the objectives of this work in the context of project ChemAir will be elucidated and the related results will be summarized.

- **I: Analysis of Relevance**: Which analytes shall be included in the repertoire of analytes for project ChemAir? The focus should be on home-made explosives with a healthy balance of primary and secondary explosives.
- **II: Synthesis and Characterization**: The analytes selected in the analysis of relevance have to be synthesized unless they are commercially available. This includes the development of small-scale syntheses for high-purity samples. All analytes need to be fully characterized with standard analytical methods (NMR, IR, RAMAN, MS, EA, DTA, DSC, XRD, pycnometry). The materials also have to be characterized in terms of sensitivity towards external stimuli (impact, friction, electrostatic discharge). Energetic performance parameters are calculated using the EXPLO5 v6.03 computer code based on heat of formation (calculated on a CBS-4M level using Gaussian09) and room temperature density.
- **III: Reference Material Distribution**: All compounds included in the ChemAir analyte repertoire have to be provided in high purity to the project partners as solutions or pure compounds.
- **IV: Vapor Pressure Measurements**: Since project ChemAir is concerned with the gas phase of explosives, the most important physico-chemical parameter is the vapor pressure. It is directly linked to the gas-phase concentration of an explosive in saturation equilibrium concentrations:

$$c_{sat} = \frac{p_{sat} \times M}{R \times T} \quad (1)$$

c_{sat}: saturation concentration [mg L^{-1}], R: ideal gas constant (8.3145 J mol^{-1} K^{-1}), T: temperature [K]

Vapor pressures of explosives have been excessively reviewed [1], yet the data available was obtained with a multitude of different methods by different experimentators. The oldest experiments taken into account date back more than 100 years ago. In many cases, no sufficient information about the experimental details including substance purity and original p_{sat}-T-data is given. In many cases the experimental data reported for one compound are in disagreement.

For these reasons we decided to establish the so-called **transpiration method** at our research group in the framework of this thesis to measure reliable data for the ChemAir analytes.

- **V: Establishment of the Transpiration Method**: The basic principle of the transpiration method is the saturation of a well-defined carrier gas stream with the analyte of choice at a specified temperature. The analyte is recondensed from the carrier gas stream in a cooling trap. Based on the validity of the Ideal Gas Law and Dalton's Law of partial pressures the vapor pressure of the analyte can be calculated:

$$p_{sat}(T_{exp}) = \frac{m_a \mathrm{R} T_{amb}}{\mathrm{M} V_{amb}} \quad (2)$$

p_{sat}: vapor pressure of the analyte [Pa], T_{exp}: temperature of the saturator [K], m_a: mass of analyte [kg], T_{amb}: ambient temperature [K], V_{amb}: volume of carrier gas at ambient conditions [m^3], M: molecular weight of the analyte [kg mol^{-1}], R: universal gas constant: 8.3145 J mol^{-1} K^{-1}

The method was adapted from the research group of Prof. Verevkin (University of Rostock) and is suitable for compounds with medium to low volatility. In this work its suitability for the

measurement of the vapor pressure of explosives is tested. One of the most challenging tasks in this experiment is the precise quantification of the analyte in microgram amounts. Considering the strong emphasis of project ChemAir on gas-chromatographic methods we decided to use vacuum outlet GC/MS as established by *de Zeeuw et al.* [2] for the quantification of the analytes.

- **VI: Establishment of vacuum-outlet GC/MS**: The gas-chromatographic analysis of explosives is a delicate task considering the conflict of the thermolability of this analyte class with the standard operation temperatures of a gas chromatograph (40 – 280 °C). Vacuum outlet GC/MS as established by *de Zeeuw et al.* [2] is a suitable approach since the elution temperatures of the analytes are lowered by exploiting the MS detector vacuum. This is realized by installing a restriction capillary in front of a wide-bore, short analytical column. The method should be established using a Shimadzu GCMS-QP2010 SE equipped with an ATAS OPTIC 4 Injector. Due to various advantages[2] the restriction capillary should be positioned inside the injector.
- **VII: Benchmarking of vacuum-outlet GC/MS**: Since this method is relatively new, one of the main goals in this work was the evaluation of vacuum-outlet GC/MS for the detection and quantification of explosives. For qualitative analysis it should be investigated which compounds can be detected by this method. If a compound can be detected, its limit of detection (LOD) and limit of quantification (LOQ) should be determined and compared with the LTM-FF-TG-GC/MS developed by *Boeker and Leppert*. (cf. section 1.3.1) For the transpiration method experiments it is necessary to evaluate the suitability of the method for internal standard quantification with high precision.
- **VIII: Estimation of Air Concentration of Explosives**: The saturation equilibrium concentration of explosives is unrealistically high for real detection scenarios. Based on a diffusion model the real concentration of unconfined explosives needs to be estimated since it dictates the volume of air that needs to be sampled for the gas-phase detection of explosives.
- **IX: Benchmarking of isothermal TGA**: Isothermal thermogravimetric analysis is a quick method for the determination of enthalpies of sublimation and vaporization[3]. The obtained pressure analog values are claimed to be convertible to real vapor pressure values by calibration of the TGA instrument with a substance with well-known vaporization behavior. In this work the method shall be benchmarked with well-characterized medium to low-volatile analytes.

Literature References

1. (a) Östmark, H.; Wallin, S.; Ang, H. G., Vapor Pressure of Explosives: A Critical Review. *Propellants, Explosives, Pyrotechnics* **2012,** *37* (1), 12-23; (b) Ewing, R. G.; Waltman, M. J.; Atkinson, D. A.; Grate, J. W.; Hotchkiss, P. J., The vapor pressures of explosives. *TrAC Trends in Analytical Chemistry* **2013,** *42*, 35-48.
2. de Zeeuw, J.; Reese, S.; Cochran, J.; Grossman, S.; Kane, T.; English, C., Simplifying the setup for vacuum-outlet GC: Using a restriction inside the injection port. *Journal of Separation Science* **2009,** *32* (11), 1849-1857.
3. Verevkin, S. P.; Ralys, R. V.; Zaitsau, D. H.; Emel'yanenko, V. N.; Schick, C., Express thermo-gravimetric method for the vaporization enthalpies appraisal for very low volatile molecular and ionic compounds. *Thermochimica Acta* **2012,** *538*, 55-62.

3 Deductive Summary of Results

The objectives of this work were stated in section 2. For each objective the related results will be summarized in the following.

I: Analysis of Relevance: The ChemAir substance repertoire is presented in section 4. Based on the case of the bomb attack on the Norwegian government district by Anders Behring Breivik (section 4.1), the components of an explosive device (section 4.2), the properties of explosives (section 4.3) and the availability of starting materials to civil persons (section 4.4) analytes for the ChemAir substance repertoire were chosen. The substance repertoire (section 4.5) includes 28 analytes (cf. Figure 1) which contain primary and secondary explosives and explosive related compounds like detection-aid agents (taggants).

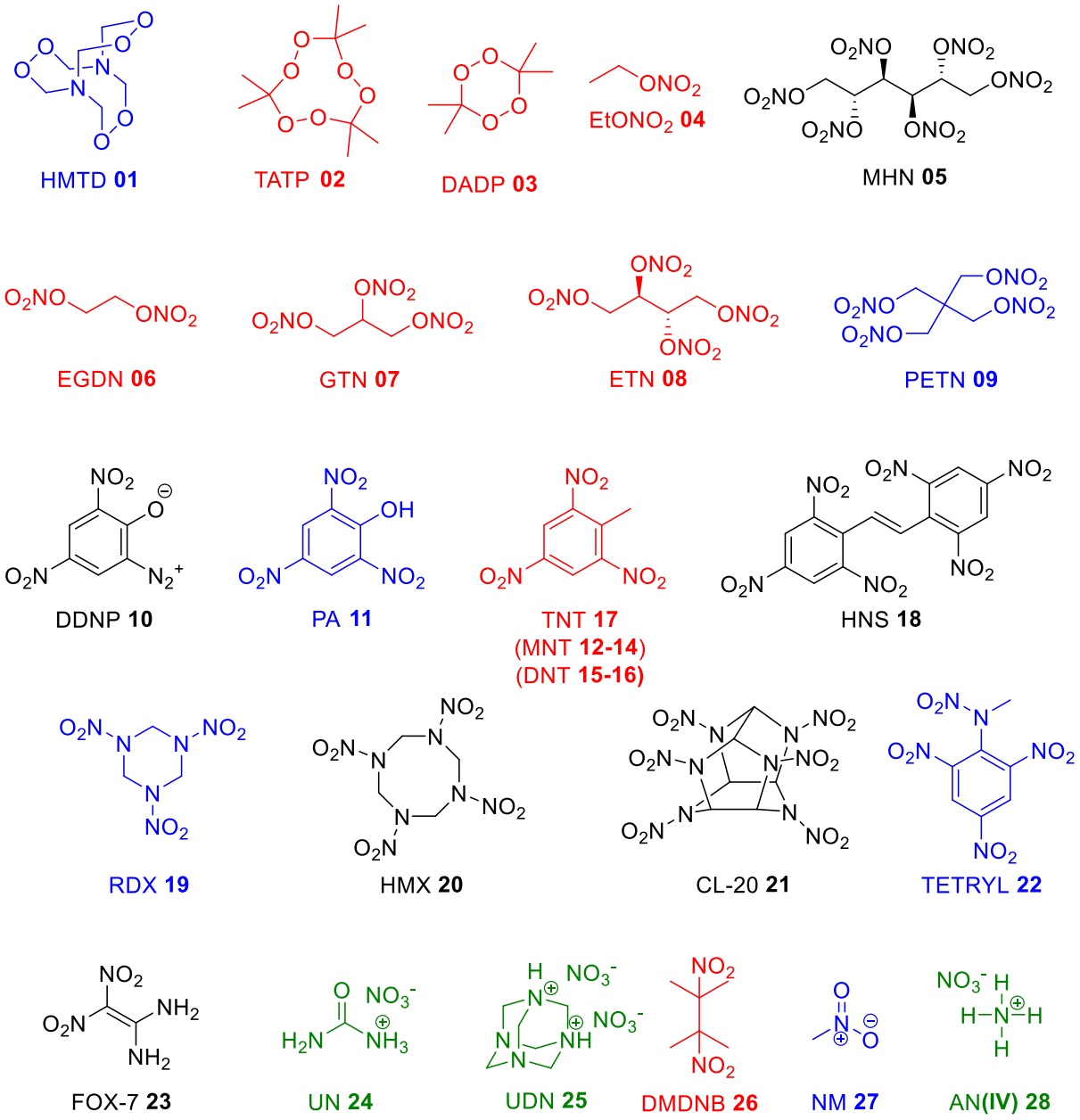

Figure 1 – The structures of the explosives that were included in the ChemAir substance repertoire. For VO-GC/MS (cf. section 5): black: substance not detectable, blue: substance detectable but not quantifiable, red: substance detectable and quantifiable, green: decomposition products of salts can be detected)

II: Synthesis and Characterization: All compounds were characterized using the methods detailed in the objective. The results are summarized in section 4.6. The relevant energetic and physico-chemical properties are summarized (cf. section 4.6 Table 3). For the detection of explosives by mass spectroscopy the corresponding spectra are essential for the establishment of a database. The commercial NIST-database [1] contains 70 eV electron impact ionization mass spectra of the majority of the ChemAir substance repertoire. In section 4.6 Table 4 the 70 eV EI-mass spectra of all analytes are detailed and can be used for the establishment and improvement of a database. The fragments that correspond most probably to the nitrosonium cation NO^+ (m/z 30), the nitronium cation NO_2^+ (m/z 46) and the $N_2O_3^+$ cation (m/z 76) can be observed in the EI mass spectra of the majority of the ChemAir analytes.

For each analyte important aspects are elucidated. 15 of the 28 analytes were synthesized in this work and a small-scale high purity synthesis is detailed. The crystal structure of ETN **08** was elucidated in this work simultaneously to the work by *Manner et al.* [2]. The crystal structures of MHN **05** and UDN **25** were elucidated for the first time. (cf. Figure 2)

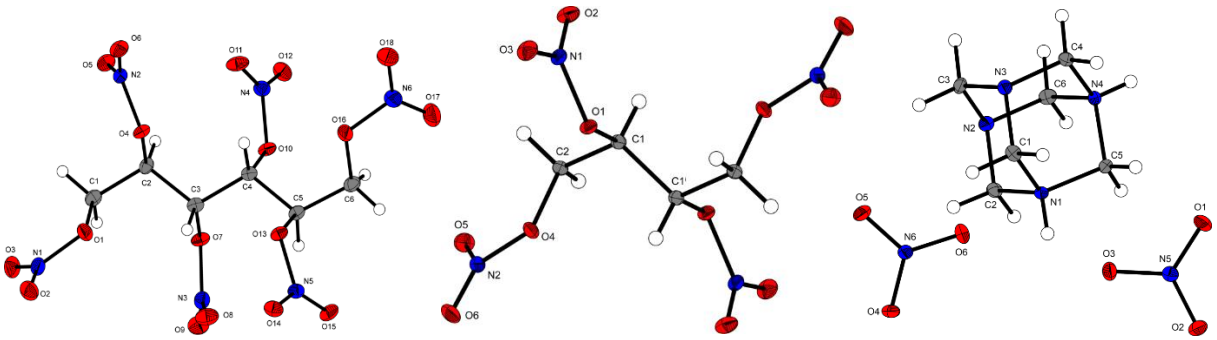

Figure 2 – The crystal structures of MHN 05, ETN 08 and UDN 25. Thermal ellipsoids are drawn at the 50% probability level, and H atoms are shown as spheres of arbitrary radii.

III: Reference Material Distribution: All project partners were supplied with high purity samples of the complete ChemAir substance repertoire over the total project duration.

IV: Vapor Pressure Measurements & **V: Establishment of the Transpiration Method**: The transpiration method experiment was successfully established at the workgroup of Prof. Klapötke in this work. The method was adapted from the research group of Prof. Sergey Verevkin from the University of Rostock. With preliminary measurements of the reference compounds *iso*-amyl acetate, *n*-hexanol, *n*-octanol, naphthalene and anthracene (section 7.1) it was demonstrated that the method was applied correctly for analytes with high, medium and low volatility. With these reference measurements in hands new analytes with unknown vapor pressure and literature-data in conflict could be investigated.

These measurements included the peroxides DADP **02** and TATP **03** (section 7.3), the nitrate esters EGDN **06**, GTN **07** and ETN **08** (section 7.4), the nitrotoluenes 2-MNT **12**, 3-MNT **13**, 4-MNT **14** (section 7.4), 2,4-DNT **15**, 2,6-DNT **16** and TNT **17** (section 7.5), the nitronaphthalenes 1-nitronaphthalene and 2-methyl-1-nitronaphthalene (section 7.6), the nitroalkanes 2-nitropropane, 2-methyl-2-nitropropane and DMDNB **26** (section 7.7) and the organothiophosphate Amitone with seven related isomers (section 7.8).

With the measurements of the peroxides TATP **02** and DADP **03** (cf. section 7.2) it could be demonstrated that the transpiration method is suitable for the measurement of solids that are highly sensitive towards impact and friction. The results obtained for DADP **03** are in acceptable agreement with literature values. For TATP **02** the literature values spread tremendously with enthalpies of

sublimation $\Delta_{cr}^{g}\boldsymbol{H}_{m}^{\circ}$(298.15K) ranging from 68.0 ± 6.3 kJ mol^{-1} to 103.4 ± 6.4 kJ mol^{-1}. A possible explanation for this is the rich polymorphism [3] of TATP **02**.

The measurement of the nitrate esters EGDN **06**, GTN **07** and ETN **08** (cf. section 7.3) demonstrated that the introduction of a methylene nitrato ($CHONO_2$) unit reduces the vapor pressure at 298 K by two orders of magnitude. This allows to predict that the vapor pressure of MHN **05** is lowered by a factor of ≈10^4 in comparison to ETN **08**. This work includes the first investigation of the vapor pressure of ETN **08** with a well-established method. Despite the instability of the molecule at ambient conditions it could be demonstrated that the obtained enthalpies of sublimation and vaporization are in agreement with the enthalpy of fusion published by *Oxley et al.* [4].

The measurement of the mononitrotoluene isomers **12**-**14** (cf. section 7.4) allowed the derivation of benchmark thermodynamic properties for each isomer. 2-MNT **12** and 4-MNT **12** are detection aid agents for commercial plastic explosive formulations.[5] The enthalpies of sublimation and vaporization obtained in this work are in agreement with literature values for the enthalpy of sublimation. The results obtained in this work are in high agreement with the evaluation of own and literature data by the *Clarke-Glew* equation[6] over a broad temperature range. The fitting coefficients of this data treatment allow the precise calculation of the vaporization behavior of these analytes in the ambient temperature regime.

The results of the measurement of the nitroalkanes 2-nitropropane, 2-methyl-2-nitropropane and DMDNB **26** (cf. section 7.7) were verified with a multitude of (semi)-empirical methods. Amongst other validation approaches it could be demonstrated that the obtained enthalpies of volatilization and formation are in agreement with gas-phase calculations of the heat of formation on a G-4 level. The conflict of literature values for the enthalpy of sublimation of the important detection-aid agent [5] DMDNB **26** could be resolved.

The measurement of Amiton and seven related organo(thio)phosphate isomers was a collaboration project with Dr. Manfred Metzulat and Major Marc André Althoff from the CBRN Defence, Safety and Environmental Protection School of the German Bundeswehr. The vaporization behavior of the pesticide Amitone (included in Schedule 2 of the Chemical Weapons Convention) and seven related isomers was studied. The influence of variation (sulfur/oxygen) of the chalcogen coordination at the (thio)phosphate-unit and chain-length elongation by methylene units on the enthalpy of vaporization was investigated. All results obtained are consistent with each other. It could be demonstrated that the results derived from the transpiration experiment are in good agreement with literature values.

Table 1 – Comparison of vapor pressures at $\boldsymbol{p_{sat}}$ at T = 298.15 K of values stated in the reviews by Östmark et al. [7] and Ewing et al. [8] with the values obtained by the transpiration method in this work.

analyte	I p_{sat}(298 K) **Ewing et al.** [8]	II p_{sat}(298 K) **Östmark et al.** [7]	III p_{sat}(298 K) **this work**	p_{sat}(298 K) **I/III**	p_{sat}(298 K) **II/III**
	[Pa]	[Pa]	[Pa]	%	%
TATP **02**	6.39E+00	6.20E+00	6.73E+00	5.00	7.86
DADP **03**	2.47E+01	1.77E+01	2.66E+01	7.06	33.34
EGDN **06**	1.03E+01	1.01E+01	1.21E+01	14.59	16.26
GTN **07**	6.54E-02	6.41E-02	8.22E-02	20.49	21.97
4-MNT **14**	6.56E+00	6.52E+00	5.57E+00	-17.70	-16.97
2.4-DNT **15**	4.16E-02	3.51E-02	4.03E-02	-3.34	13.01
2.6-DNT **16**	9.05E-02	8.27E-02	9.29E-02	2.60	11.00
TNT **17**	9.27E-04	7.34E-04	9.03E-04	-2.67	18.76

The results obtained with the transpiration method in this work are compared with the results of the literature analysis by Östmark et al. [7] and *Ewing et al.* [8] (cf. Table 1)

The deviation of the results measured in this work for p_{sat}(298.15 K) in comparison with the results by *Östmark et al.* [7] ranges from -16.97 % to 33.34 %, whilst for the results by *Ewing et al.* [8] it ranges from -17.70 % to 20.49 %. *Ewing et al.* [8] selected less sets of data for his recommended values at 298.15 K more carefully than *Östmark et al.* [7]. It can be concluded that the precision of the vapor pressure at 298.15 K by comparison of literature values with own experimental results is about ± 20%. This is sufficient for the estimation of the air concentration of hazardous materials, which might be influenced by numerous other parameters like confinement, air humidity, surface, etc. (cf. section 1.2)

VI: Establishment of vacuum-outlet GC/MS: For the transpiration method experiment it is necessary to quantify the analyte with high precision. (cf. equation (2), section 2) Low-volatile analytes must be quantified in microgram amounts. The quantification of the analyte is the most challenging part of the transpiration experiment. Since project ChemAir relied on gas chromatography a GC/MS device was acquired for the quantification of the analytes. The gas-chromatographic analysis of thermolabile, heavily volatile analytes like explosives is a special challenge since it requires the transfer of the analytes into the gaseous states at operating temperatures of 30 – 280 °C. Yet the elution temperature of the analytes must remain below their temperature of decomposition, which should be avoided until the final detection. The residence time of the analyte in hotter zones should be minimized.

The problem was solved by the application of vacuum outlet GC/MS (VO-GC/MS) as established by *de Zeeuw et al.* [9] (cf. chapter 5): A short analytical column with high diameter (6 m length, 0.53 mm inner diameter) is connected to the ultra-high vacuum of the MS-detector. A restriction (1 cm length, 0.050 mm inner diameter) is placed in front of the column. This results in the gradual expansion of the detector vacuum and lowers the elution temperatures of the analytes. If the restriction is placed in the isothermal injector of the gas chromatograph the flow-control system can be operated in constant pressure mode since the influence of the oven temperature on the total flow is negligible as demonstrated by flow-calculations based on the *Hagen-Poiseuille* equation [10] that were performed in this work. (cf. section 5.2) Further advantages of placing the restriction inside the injector is the self-sealing of the column connection at high temperatures and the inert-gas environment of the column-restriction-connection. Since the used Atas Optic 4 Injector has an inner diameter of 5 mm, the column-connectors that were described in the literature could not be used due to their dimensions.

The problem was solved by the use of a micro-union column connector (3.5 mm diameter) and custom stainless steel liners (4 mm inner diameter). The optimization for quantification applications included the use of silanized glass wool in the liner and the use of a single-ion monitoring (SIM) method. (cf. section 5.1) The use of glass-wool improved the reproducibility absolute peak areas. The use of the SIM-method enabled the application of higher data acquisition rates (10 Hz) for the mass spectrometer, which allowed the precise recording of chromatographic peaks. In combination with an internal standard method the reproducibility of the quantification could be optimized to < 1.00 % standard deviation. It could be demonstrated that split-injections were still possible with the micro-union positioned inside the injector. (cf. section 5.3)

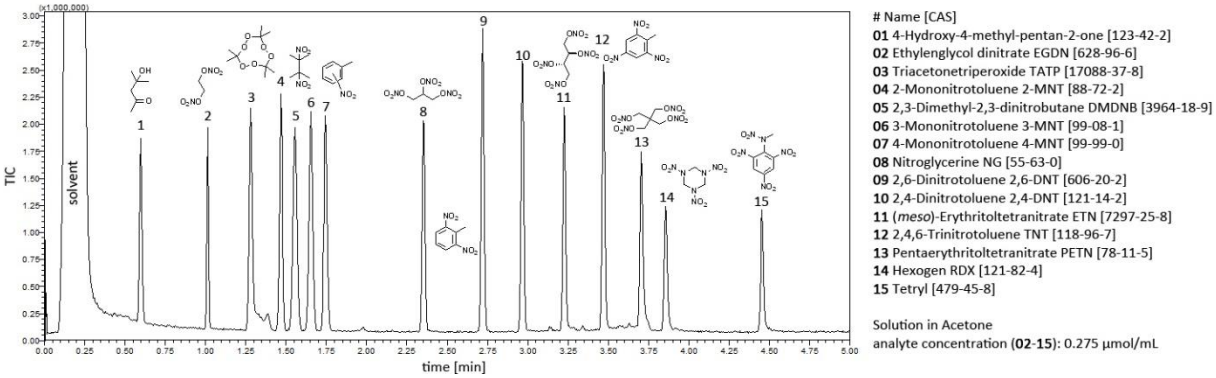

Figure 3 – VO-GC/MS-Chromatogram of mixture of explosives.

The optimized method was tested with all 28 analytes of the ChemAir substance repertoire. (cf. Figure 1, Figure 3) All substances besides MHN **05**, DDNP **10**, HNS **18**, HMX **20**, CL-20 **21** and FOX-7 **23** could be detected. For the ionic substances UN **24**, UDN **25** and AN **28** thermal decomposition products of the salts (nitrogen oxides, neutral compounds) could be detected. The peroxides TATP **02**, DADP **03**, the nitrate esters EGDN **06**, GTN **07**, ETN **08**, the nitrotoluenes **12** – **17** and DMDNB **26** could be quantified with the necessary precision (reproducibility: <1.00 % standard deviation) for the transpiration method experiment. In the other cases the analytes can be detected but not quantified due to their thermolability.

HNS **22** (p_{sat}(298 K): 6.19E-16 Pa, Pa T_{dec}: 338.9 °C) could not be detected by VO-GC/MS. HNS **22** is the most thermostable substance investigated and thermal degradation can be excluded as reason for its non-detectability. In terms of vapor pressure the limit seems to be around that of RDX **19** (p_{sat}(298 K): 4.40E-07 Pa). (cf. section 5.4, section 7 Figure 1).

VII: Benchmarking of vacuum-outlet GC/MS: For the analytes detailed in Table 2 the limit of detection was determined according to DIN 32645:2008 (α = β = 0.01, k = 3) in both SIM and SCAN mode with an optimized GC/MS method (oven temperature program, injector temperature 175 °C). (cf. section 5.5)

The LOD-values were calculated as the mass of analyte transferred on the GC-column in a split injection. Additionally the air concentration of the analyte was calculated under saturation conditions (c_{sat}) based on the vapor pressure of the analyte (equation (1), section 2). The concentration under diffusion conditions (c_{dif}) was calculated for each analyte. Based on both concentrations, the necessary volume for high volume air sampling for reaching the limit of detection (V_{sat}, V_{dif}) was calculated.

In terms of the availability of the analytes for gas phase detection with the VO-GC/MS setup presented in this work, ETN **08** and RDX **19** are the most interesting analytes. ETN **08** has the highest LOD values (SIM: 1201 pg, SCAN: 1190 pg). RDX **19** has the lowest vapor pressure at 298.15 K (4.40×10^{-7} Pa) in combination with medium LOD values (SIM: 110 pg, SCAN: 247 pg). Despite the lower limits of detection the volume of air that needs to be sampled for the successful detection of the explosive is higher for RDX **19**, since the concentrations c_{sat} and c_{dif} are both directly proportional to the vapor pressure of the analyte. Therefore RDX **19** is the benchmark analyte for the dectability of the explosives in this study. Since saturation conditions do not occur in a real detection scenario, the volume for

Table 2 – Calculation of necessary enrichment volume for successful detection of the explosive.

Mode / **Analyte**	**LOD**[a] SIM [pg]	**LOD**[b] SCAN [pg]	p_{sat}[c] [Pa]	c_{sat}[d] [ng L^{-1}]	c_{dif}[e] [ng L^{-1}]	V_{sat}[f] SIM [L]	V_{sat}[g] SCAN [L]	V_{dif}[h] SIM [L]	V_{dif}[i] SCAN [L]
EGDN **06**	2.76	18.5	1.02E+01	6.26E+05	4.36E+00	4.41E-09	2.96E-08	6.34E-04	4.25E-03
TATP **02**	7.43	90.8	6.20E+00	5.56E+05	2.84E+00	1.34E-08	1.63E-07	2.61E-03	3.20E-02
2-MNT **12**	9.36	16.4	1.92E+01	1.06E+06	6.97E+00	8.82E-09	1.55E-08	1.34E-03	2.35E-03
DMDNB **26**	9.23	39.9	2.20E-01	1.56E+04	8.84E-02	5.90E-07	2.55E-06	1.04E-01	4.52E-01
3-MNT **13**	8.29	21.1	1.17E+01	6.47E+05	4.20E+00	1.28E-08	3.26E-08	1.98E-03	5.03E-03
4-MNT **14**	27.9	25.9	6.52E+00	3.60E+05	2.49E+00	7.74E-08	7.19E-08	1.12E-02	1.04E-02
GTN **17**	25.8	46.0	6.41E-02	5.87E+03	3.13E-02	4.39E-06	7.83E-06	8.25E-01	1.47E+00
2,6-DNT **16**	15.1	49.6	8.27E-02	6.08E+03	3.88E-02	2.49E-06	8.16E-06	3.89E-01	1.28E+00
2,4-DNT **15**	34.9	26.7	3.51E-02	2.58E+03	1.62E-02	1.35E-05	1.04E-05	2.15E+00	1.64E+00
ETN **08**	1201	1190	6.00E-04	7.31E+01	3.87E-04	1.64E-02	1.63E-02	3.10E+03	3.08E+03
TNT **17**	164	349	7.33E-04	6.72E+01	3.91E-04	2.44E-03	5.20E-03	4.20E+02	8.93E+02
PETN **09**	170	385	1.55E-06	1.98E-01	9.78E-07	8.60E-01	1.95E+00	1.74E+05	3.94E+05
RDX **19**	110	247	4.40E-07	3.94E-02	2.21E-07	2.79E+00	6.27E+00	4.98E+05	1.12E+06

[a] Limit of detection according to DIN 32645:2008 (α = β = 0.01, k = 3) in SIM mode. [b] Limit of detection in SCAN mode. [c] Vapor pressure at 298.15 K [7] (**13**, **08**: results from transpiration experiment in this work), [d] Saturation concentration at 298.15 K, [e] Diffusion controlled concentration at 298.15 K according to section 5.7 with 200 cm² of exposed explosive surface, [f] Minimum volume of air that needs to be enriched with 100 % efficiency under saturation conditions for successful detection of analyte in SIM mode [g] see f but SCAN mode [h] see f but diffusion-controlled conditions [i] see h but SCAN mode.

diffusion conditions V_{dif} is more relevant. In SIM mode 498 m³ of air need to be sampled for the successful detection of RDX **19**. In SCAN mode 1120 m³ litres of air must be sampled. Typical vacuum cleaners work with suction flow rates of 4 m³ min^{-1}. That means for the air enrichment of RDX **19** 124 (SIM) and 279 (SCAN) minutes are necessary. For PETN **09** these times reduce to 43 (SIM) and 98 (SCAN) minutes. For all other analytes the sampling time necessary for the enrichment of an amount of sample above the limit of detection is below one minute. (cf. section 5.6 Table 24) The values stated for V_{dif} in this work are estimates and further transport barriers like foil wrapped around the explosive, which additionally lower the air concentration of the analyte are neglected. The next right step would the development of a sampling prototype and real-environment measurements to evaluate the validity of the estimates given in this work.

VIII: Estimation of Air Concentration of Explosives: The concentration of an explosive under saturation conditions will not be reached in a real detection scenario. For the estimation of the air concentration of an explosive in this work a diffusion-based model, stated by *Dravnieks et al.* [11], was used. Based on the vapor pressure, the density and the melting point of the solid or the boiling point of the liquid, the concentration of the explosive was calculated under the assumption of a 2 mm non-turbulent air layer surrounding the explosive and an unconcealed surface of 200 cm². Example calculations for the liquid EGDN **06** and the solid TATP **02** are detailed in section 5.7.

IX: Benchmarking of isothermal TGA: Isothermal thermogravimetric analysis (TGA), as established by *Verevkin et al.* [12], was benchmarked with the following compounds: Phenanthrene, Hexadecane, dibutyl phthalate and the nitrotoluenes **12**-**17**. For all compounds besides **12** – **14** the enthalpy of vaporization could be determined with ± 2 kJ mol^{-1} uncertainty agreement to literature values, as claimed by *Verevkin et al.* [12]. For solid DMDNB **26** the enthalpy of sublimation could be determined correctly aswell. For various reasons detailed in section 8.1, it was concluded that the isothermal TGA experiment for the determination of the enthalpies of vaporization and sublimation is a quick (<24 h), fully automated method. Yet it should not be used without an additional well-established method for the validation of the results obtained.

All objectives that were defined for this work in project ChemAir could be fulfilled. Additionally, the **tetrasodium and tetrapotassium salts of 1,1,2,2-tetranitraminoethane** were studied. The sodium salt $Na_4TNAE{\cdot}H_2O$ **A** and $K_4TNAE{\cdot}2\ H_2O$ **B** were synthesized and reported with their crystal structures at 173 K for the first time. Whereas sodium salt cannot be dehydrated, the dihydrated potassium salt can be dehydrated at 160 °C to K_4TNAE **C**. This is in accordance with the results of differential thermal analysis, as an endotherm corresponding to a loss of water was absent in the thermogram of **A** but present in that of **B**.

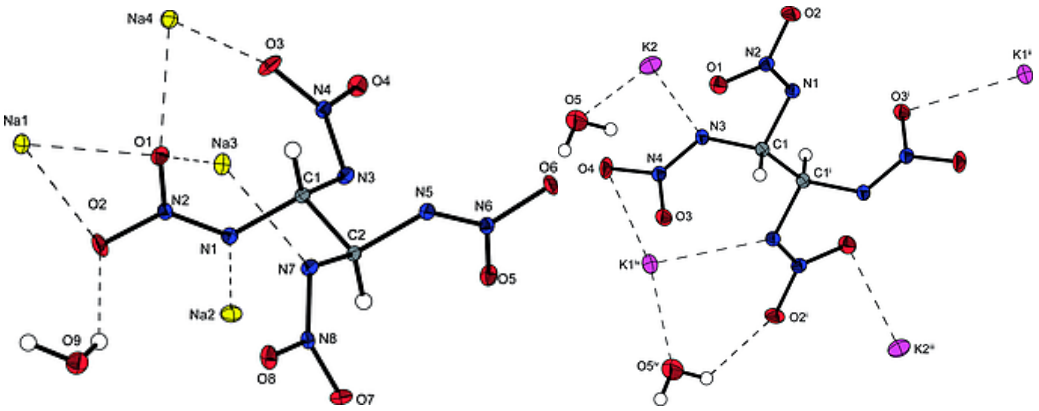

*Figure 4 - The crystal structures of $Na_4TNAE{\cdot}H_2O$ **A** and $K_4TNAE{\cdot}2\ H_2O$ **B**. Thermal ellipsoids are drawn at the 50% probability level, and H atoms are shown as spheres of arbitrary radii.*

The loss of two equivalents of water could be demonstrated by thermogravimetric analysis of **B**. Anhydrous K_4TNAE (**C**) was outperformed by the military explosive RDX and high performance explosive CL-20 in the smalls scale reactivity test (SSRT). The EC_{50} value aquatic bacteria of K_4TNAE (**C**) (>15.07 $g{\cdot}L^{-1}$) is more than 60 times higher than that of RDX **19** (0.24 $g{\cdot}L^{-1}$). Because of these results anionic nitramines were demonstrated to be a useful tool for the stabilization of energetic materials and might be suitable explosophores for high energy density materials with decreased toxicity in comparison to the widely used military explosive RDX **19**.

Literature References

1. https://www.nist.gov/srd/nist-standard-reference-database-1a-v14.
2. Manner, V. W.; Tappan, B. C.; Scott, B. L.; Preston, D. N.; Brown, G. W., Crystal Structure, Packing Analysis, and Structural-Sensitivity Correlations of Erythritol Tetranitrate. *Crystal Growth & Design* **2014,** *14* (11), 6154-6160.
3. Reany, O.; Kapon, M.; Botoshansky, M.; Keinan, E., Rich Polymorphism in Triacetone-Triperoxide. *Crystal Growth & Design* **2009,** *9* (8), 3661-3670.
4. (a) Oxley, J. C.; Smith, J. L.; Brady, J. E.; Brown, A. C., Characterization and Analysis of Tetranitrate Esters. *Propellants, Explosives, Pyrotechnics* **2012,** *37* (1), 24-39; (b) Oxley, J. C.; Smith, J. L.; Brady, J. E.; Brown, A. C., Erratum: Characterization and Analysis of Tetranitrate Esters. *Propellants, Explosives, Pyrotechnics* **2012,** *37* (6), 735-735.
5. http://www.mcgill.ca/iasl/files/iasl/montreal1991.pdf.
6. Clarke, E. C. W.; Glew, D. N., Evaluation of thermodynamic functions from equilibrium constants. *Transactions of the Faraday Society* **1966,** *62* (0), 539-547.
7. Östmark, H.; Wallin, S.; Ang, H. G., Vapor Pressure of Explosives: A Critical Review. *Propellants, Explosives, Pyrotechnics* **2012,** *37* (1), 12-23.
8. Ewing, R. G.; Waltman, M. J.; Atkinson, D. A.; Grate, J. W.; Hotchkiss, P. J., The vapor pressures of explosives. *TrAC Trends in Analytical Chemistry* **2013,** *42*, 35-48.
9. de Zeeuw, J.; Reese, S.; Cochran, J.; Grossman, S.; Kane, T.; English, C., Simplifying the setup for vacuum-outlet GC: Using a restriction inside the injection port. *Journal of Separation Science* **2009,** *32* (11), 1849-1857.
10. Boeker, P.; Leppert, J.; Mysliwietz, B.; Lammers, P. S., Comprehensive Theory of the Deans' Switch As a Variable Flow Splitter: Fluid Mechanics, Mass Balance, and System Behavior. *Analytical Chemistry* **2013,** *85* (19), 9021-9030.
11. Dravnicks, A.; Brabets, R.; Stanley, T. A. *Evaluating Sensitivity Requirements of Explosive Vapor Detector Systems*; IIT Research Institute Technology Center: Chicago Illinois, 1972.
12. Verevkin, S. P.; Ralys, R. V.; Zaitsau, D. H.; Emel'yanenko, V. N.; Schick, C., Express thermo-gravimetric method for the vaporization enthalpies appraisal for very low volatile molecular and ionic compounds. *Thermochimica Acta* **2012,** *538*, 55-62.

4 The ChemAir Substance Repertoire

In the initial phase of the explosive gas phase detection project ChemAir (cf. section 1.3) a suitable repertoire of analytes for the testing the device to be developed had to be chosen. In the preliminary phase of the project proposal a focus on components used in improvised explosive devices was agreed upon. Improvised explosives are synthesized from freely available starting materials. It is reasonable that the technical details of terroristic attacks involving explosives are restricted from public access since it would be negligent to publish construction manuals of improvised explosive devices from freely available chemicals. However, it should not be ignored that suitable procedures are available in the internet. It is hard to evaluate from public information about terroristic attacks which explosives were used. This is more than reasonable, but complicates the choice of suitable analytes since the German Federal Police, associated partner in project ChemAir, was not authorized to provide the required informations.

With respect to this, it was necessary to gather the informations required from public sources. One of the most important sources of information was the case of the Norwegian homicidal maniac Anders Behring Breivik, which will be elucidated in the following section to demonstrate the modus operandi of a terrorist in a one-man-operation bomb attack scenario.

4.1 The case of Anders Behring Breivik

Anders Behring Breivik assaulted the government district of Oslo on 07/22/2011 with an improvised explosive device killing 8 people and severely damaging several official buildings. (see Figure 1)

Figure 1 - The building housing the Office of the Prime Minister and Ministry of Justice and the Police with blown-out windows shortly after the explosion. The bomb van had been placed behind the people shown.[1]

The case of Breivik is of special interest since the attack was carried out in a one-man-operation by a citizen without initial professional chemical education and access to explosives including precursors that are only accessible for agricultural purposes. The preparation for his attack was documented meticulously in lab journal quality in Breivik's so-called manifest "2083 – A European Declaration of

Indepence", which is provided online [2] by the Federation of American Scientists. Based on this first-hand information the case will be elucidated in the following.

In April 2011 Breivik lives with his mother to save money. His main source of funds for his further course of action are 10 credit cards with a total credit limit of 29.000 €. Initially he rents a small transporter and contacts the landlord of a farm to rent it from May 2011.

On the 27th of April 2011 he orders approximately two tons of nitrogen fertilizer containing ammonium nitrate. This fertilizer was more specifically CAN 27-0-0, a formulation from calcium nitrate, ammonium nitrate and dolomite mineral ($CaMg(CO_3)_2$) with a nitrogen content of 27% that results usually from an ammonium nitrate weight proportion of 75 %. For the commercial application of the fertilizer he previously registered an agricultural company that pretends to be specialized in the cultivation of crop plants.

On the 3rd of May he begins to install a laboratory fume hood in the shed of his property. After this he starts with the synthesis of explosives. He already bought the necessary chemicals and additives in December 2010. The acquired chemicals are listed in Table 1 with their amounts, sources, prices and camouflage purposes.

Table 1 – Chemicals acquired by Breivik including sources, amounts, costs and camouflage purposes.

chemical	source	amount	cost [€]	camouflage purpose
S_8	ebay.co.uk [UK]	0.5 kg	20	pigment
$NaNO_2$	keten.pl [PL]	0.3 kg	10	food additive
$NaNO_3$	drugstore	3 kg	500	food additive
H_2SO_4 (30%)	car supply store	25 L	130	car battery
acetylsalicylic acid	pharmacy	3800 Tabletten	1140	medication
Al (400 mesh)	keten.pl [PL]	150 kg	2000	boat paint
microballoons	seasea.no	60 kg	770	boat construction

Especially the efforts for the acquisition of acetylsalicylic acid are worth to mention. Breivik frequented 20 pharmacies four times with periodic distances of two weeks to acquire in each store 2-3 packages with 20 pills of Aspirine. According to his statement, the content of acetylsalicylic acid was 440 mg per pill, which corresponds to a total amount of 1672 g.

Some of the chemicals had to be further processed prior to use as explosive precursor. Ammonium nitrate fertilizer granulate is rendered inert against uptake of fuel, which is essential for the use in explosive formulations. Breivik solved this problem by grinding the granules in household blenders. According to his statement, this technique was already used by the Red Army Fraction (RAF).

The concentration of the commercially available sulfuric acid (30 %) was increased to 80-90 % by boiling it down outside the shed of the farm. Breivik observed strong evolution of fumes during this process. With respect to this he carried out this step during the night. He states a final concentration of >90% in the final product.

The acetylsalicylic acid had to be extracted from the Aspirine pills. After a multitude of failures Breivik found a suitable solution: The tablets are initially grinded and the resulting powder is suspended in ethanol at 60-70 °C. The dissolved acetyl salicylic acid is separated from the filler material by filtration and the acid is reprecipitated by addition of ice water.

When all starting materials were available Breivik started with the synthesis of explosive materials:

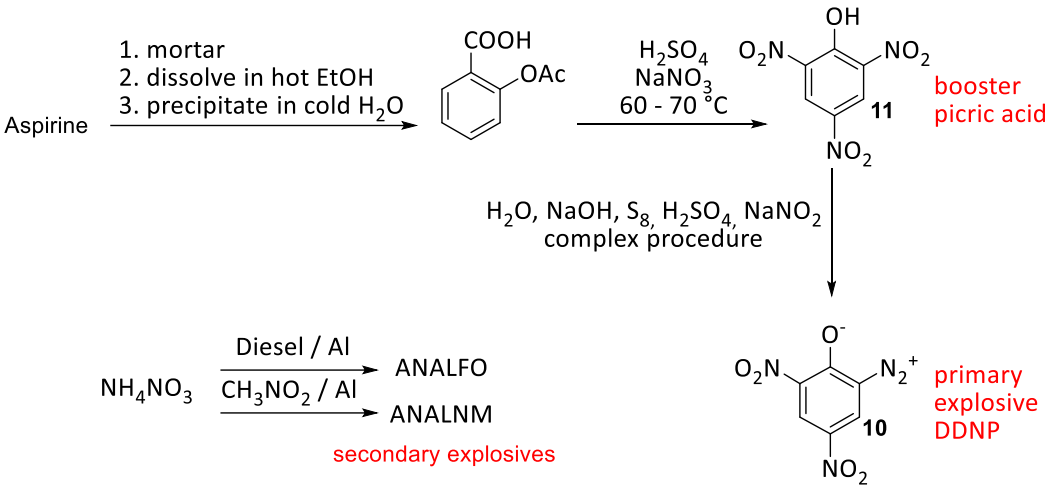

Figure 2 – Synthesis of components for an Improvised Explosive Device.

The components of an explosive device and their interaction are elucidated in section 4.2. Breivik used in his improvised explosive device the primary explosive DDNP **10**. With **10** he initiated the booster picric acid **11**. For the inner charge he used a mixture of ammonium nitrate, aluminium and nitromethane (ANALNM). For the main charge he used a mixture of ammonium nitrate, aluminium and fuel oil (ANALFO).

The synthesis of primary explosive **10** and booster **11** started from acetylsalicylic acid, which was extracted from Aspirine as described above. Subsequent nitration with sulfuric acid and sodium nitrate yields picric acid **11** that can be reduced to the non-isolated intermediate picramic acid (2-amino-4,6-dinitrophenol) with dihydrogensulfide generated from sodium hydroxide, sulfur and sulfuric acid. Subsequent diazotation with sodium nitrite under acidic conditions yields **10**. For the manufacturing of ANALNM CAN 27-0-0 fertilizer was grinded with household blenders. 38 kg of the grinded fertilizer were mixed subsequently with 6 L of nitromethane, 6 kg Aluminium (400 mesh) and 1.2 kg of micro balloons. Breivik acquired the nitromethane as model car fuel (30 % nitromethane, 18 % oil, 52 % methanol). He enriched the nitromethane content by open boiling to >50 %. In Germany pure nitromethane is freely available as fuel for model cars.[3]

For his improvised explosive device Breivik used the primary explosive DDNP **10**, the booster picric acid **11**, 40 kg ANALNM as inner charge and 900 kg ANALFO as main charge. The primary explosive was transported separately, integrated at the target location and initiated with a match cord. The improvised explosive device was initiated in a rented Volkswagen Crafter transporter. The further course of this tragic day in Norwegian history should be known from the media. The case of Breivik demonstrates the dangerous potential of improvised explosive devices that can be constructed by a single person without drawing the attention of security offices. All explosives involved were integrated in the ChemAir substance repertoire since their detection at vulnerable infrastructures is highly desirable.

4.2 Components of an Explosive Device

An explosive device includes the following components:

4.2.1 Primary Explosive

An explosive that is sensitive to external stimuli and is initiated by spark, impact, heat sources or even laser excitation. A characteristic property of a primary explosive is the so-called deflagration-detonation-transition (DDT). Initially the explosive deflagrates (combustion under autooxidation) upon heating. The accelerating deflagration exceeds the speed of sound and transfers into a detonation

process. In the framework of the detonation a detonation front is formed, which propagates through the explosive material. The detonation front can reach speeds of 3000 to 10000 m s^{-1} (depending on the used explosive) and can be transferred to booster and secondary explosives. A primary explosive must be highly brisant and possess a high ignition detonation velocity. Important primary explosives are: mercury fulminate, led azide, silver azide, lead styphnate, DDNP **10** and the heavy metal salts of 5-nitrotetrazole.

4.2.2 Booster Explosive

A booster explosive is a secondary explosive which ensures the initiation of the explosive device. Some secondary explosives are too insensitive for direct initiation with primary explosives. These explosives are so-called tertiary explosives. The primary explosive initiates the booster. During the propagation of the detonation front through the booster it gets amplified and is then capable to initiate the tertiary explosive main charge. Commonly used booster explosives are RDX **19,** PETN **09** and Tetryl **22**.

4.2.3 Secondary Explosives

Secondary explosives are the main source of blasting force of an explosive device. The major mass fraction of an explosive device is the secondary explosive. In contrast to primary explosives it should solely deflagrate without detonating upon heating for security reasons. Important secondary explosives are pure substances like RDX **19**, HMX **20**, TNT **17**, FOX-7 **23** but also compound mixtures like ammonium nitrate **28** and fuel (Diesel) oil (ANFO).

4.2.4 Explosive Additives

Explosive additives are components of secondary explosive formulations that can enhance the energetic performance or improve the mechanical properties. Aluminium can be added to ANFO (see Section 4.1) to obtain ANALFO and increase the performance. For a better detonation behavior microballoons can be added to ANFO or ANALFO. Those are little hollow glass beads. The pressure of the detonation front compresses the gas volume inside the microballoon and heats it up. This results in better detonation characteristics of the mixture as it facilitates the initiation of the detonation of the mixture.

4.3 Properties of Explosives

One of the essential questions for the choice of suitable molecules for project ChemAir is: “What is an explosive?” At first glance the answer is simple: A substance whose detonation can be initiated by external stimuli or primary explosives. Is it possible to predict that property from a chemical structure?

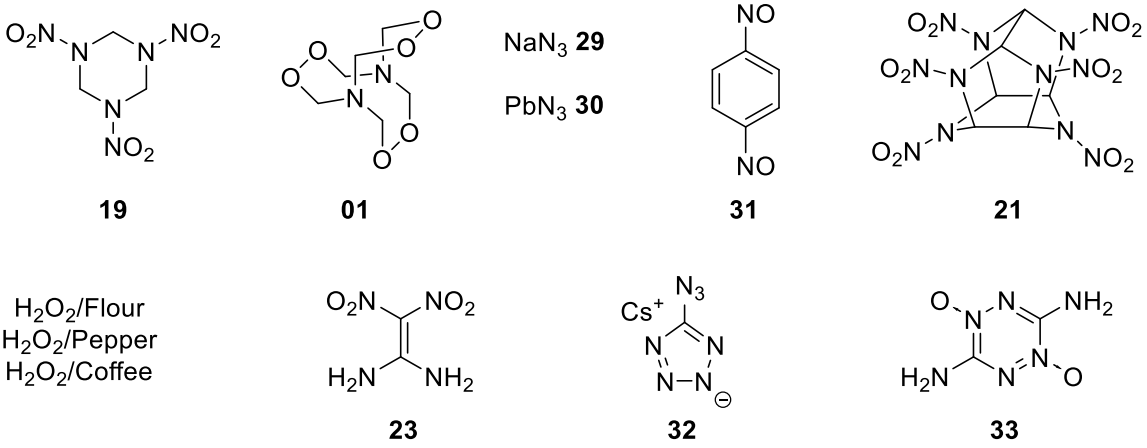

Figure 3 – Selected Molecules and Mixtures of Compounds. Which ones are explosives?

Figure 3 shows a selection of 12 different molecules or mixtures of compounds. All are primary or secondary explosives. Basically explosives can be divided into two classes of substances. Those that

derive their blasting force from their auto oxidation to CO and CO_2. On the other hand there are explosives that derive their power from high endothermic enthalpies of formation. A good example for an auto-oxidation explosive is FOX-7 **23**. With an exothermic heat of formation of -130 kJ mol^{-1} it derives its energetic performance solely from autooxidation.[4] The capability of a substance to auto-oxidize itself can be estimated from its sum formula $C_aH_bN_cO_d$ and its molecular weight *M* [g mol^{-1}] by the oxygen balance Ω_{CO2}. The postulated products of combustion are CO_2, H_2O and N_2:

$$\Omega_{CO2}[\%] = (d - 2a - 0.5b)\frac{1600}{M} \quad (1)$$

FOX-7 **23** has an oxygen balance Ω_{CO2} of -21.71 %. RDX **19** has the same empirical sum formula "$CH_2N_2O_2$" and oxygen balance but is a more powerful explosive with an endothermic heat of formation of +87 kJ mol^{-1}. (cf. Table 3) Therefore RDX **19** can be regarded as a hybrid material of autooxidation explosive and endothermic compound. One of these hybrid materials is CL-20 **21**, which has a better oxygen balance (-10.95 %) and a high heat of formation (+365 kJ mol^{-1}) caused by the ringstrain of the wurtzitane cage backbone. CL-20 **21** is presumably the most powerful secondary explosive in use currently.

Amongst the compounds in Figure 3 are some representatives of explosives that rely exclusively on their endothermicity. Cesium 5-azidotetrazolate **32** is an extremely sensitive primary explosive that detonates upon its crystallization from solution once the crystals reach a critical size. Since the salt contains no oxygen the energy released during the detonation is derived from the high heat of formation of the compound. Further representatives of this compound class are sodium azide **29** and lead azide **30**. Sodium azide **29** is an insensitive material which was used until the 1990s as gas-generating component in airbags. It can solely be initiated with another primary explosive. In contrast to this lead azide **30** is a sensitive primary explosive. This is caused by the higher covalent bond character in lead azide in comparison to sodium azide **29**. A higher degree of covalency results in a reduction of the mesomeric stabilization of the azide anion, which causes the higher sensitivity of lead azide **30**. A further reason for this difference might be the difference of electrochemical standard potentials since Pb^{2+} is more reductive than Na^+. Endothermicity is found in molecules with ring or cage strain or containing alkyne-, azo-, azol-, azine- or azido units.

An exotic explosive is 1,4-dinitrosobenzene **31**. With an oxygen balance of -141.60 % it is definitely not an auto-oxidation explosive. Even explosive experts are surprised that it can be detonated in a steel pipe of one inch diameter.[5]

When it comes to energetic mixtures of compounds there are almost no boundaries for creativity. This is demonstrated by hydrogen peroxide mixtures with flour, coffee or pepper. These mixtures are extremely sensitive towards external stimuli and are used against the intervention forces in areas of conflict.

As demonstrated it is not trivial to estimate the detonation initiability of a molecule. For the reason of completeness the Berthelot-Rot product B_R as a clear definition is mentioned:

$$B_R\ [\mathrm{kJ\ m^{-3}}] = \rho_0^2 V_0 Q_v$$

ρ_0 : densitiy [kg m^{-3}], V_0: volume of gaseous products [m^3 kg^{-1}], Q_v: heat of detonation [kJ kg^{-1}]

By definition compounds with a B_R-value ≥ 1193 kJ kg^{-1} are capable of detonation. This B_R-value corresponds to the "Oppauer Salt" (55 % ammonium nitrate, 45 % ammonium sulfate), whose detonation in the framework of an explosive catastrophe in a fertilizer factory killed more than 1000 people.

The volume of gaseous products, the heat of detonation and the heat of formation are parameters that require computer-assisted calculations or complex measurements. The oxygen balance Ω_{CO2} is a more accessible parameter for the assessment of the detonation capability of a C,H,N,O compound or mixture: a value above -100 % is an indicator for a compound with detonation capability. A second important indicator is the appearance of energetic molecular structure units (so-called explosophores). The most important explosophores are depicted in Figure 4. They can appear in *N*-oxidized form. Especially the repeated appearance of these motifs or their combination increases the probability that the substance or compound mixture is capable of detonation.

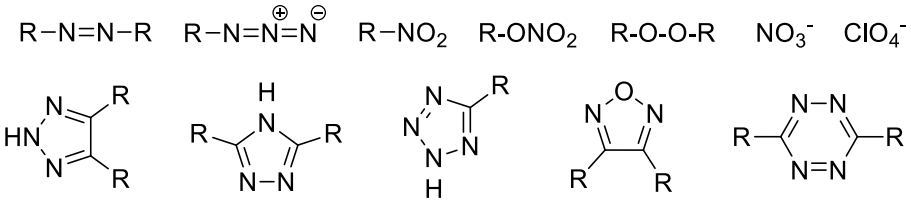

Figure 4 – Important explosophores: azo-, azido-, nitro- and nitrato-groups, peroxides, nitrates, perchlorates, 1,2,3-triazoles, 1,2,4-triaztoles, tetrazoles, furazanes, 1,2,4,5-tetrazines.

4.4 Availability of Starting Materials

[redacted]

[redacted]

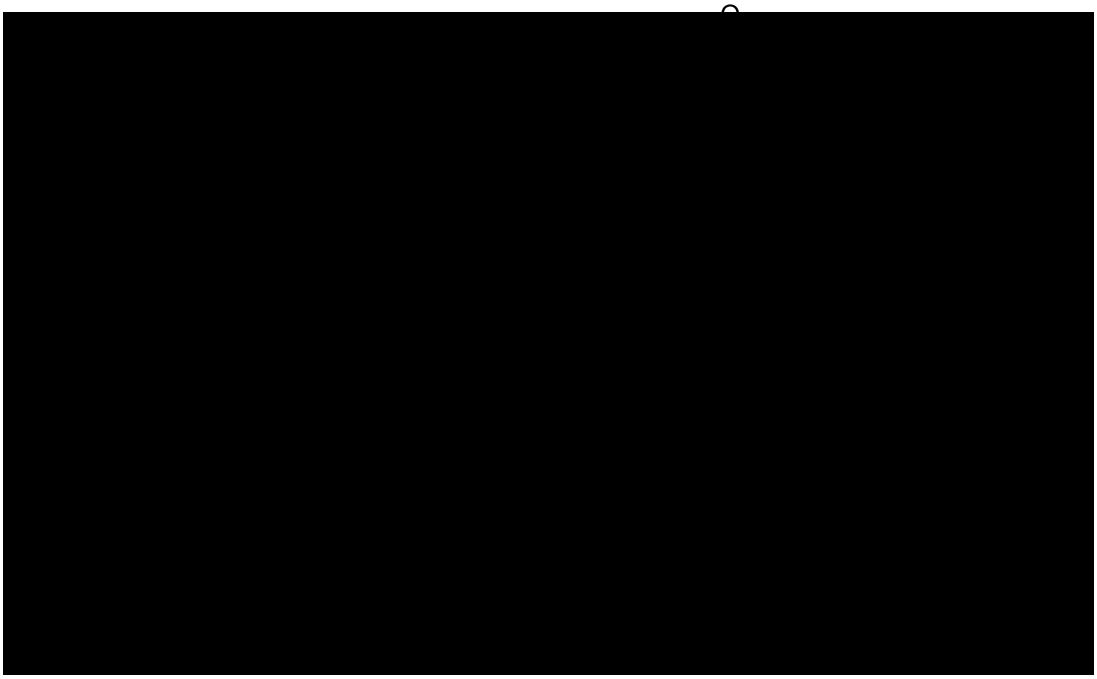

[redacted]

4.5 Selection of Analytes for the ChemAir Substance Repertoire

Using the case study of Breivik (section 1.1) and the concepts detailed in sections 4.2 – 4.4 the substances depicted in Figure 6 were chosen. The main focus was set on components of improvised explosive devices that can be synthesized from freely available chemicals. These include: The peroxides HMTD **01**, TATP **02** and DADP **03**, the nitrate esters ethyl nitrate **04**, D-mannitol-hexanitrate **05**, ethylene glycol dinitrate **06**, glyceryl trinitrate **07** and *meso*-erythritol tetranitrate **08,** the nitroaromatic compounds DDNP **10** and picric acid **11**, the nitramine RDX **19**, the ionic compounds uronium nitrate **24**, urotropine dinitrate **25**, ammonium nitrate **28** and the freely available nitromethane **27**. With respect to possible proliferation scenarios the military explosives PETN **09**, TNT **17**, HMX **20**, CL-20 **21**, TETRYL **22** and FOX-7 **23** were chosen to expand the ChemAir substance repertoire. The nitrotoluene derivates and TNT **17** precursors 2-, 3- and 4 nitrotoluene (**12**-**14**), 2,4- and 2,6-dinitrotoluene (**15**,**16**) as well as 2,3-dimethyl-2,3-dinitrobutane **26** were chosen to include compounds with similar retention indices to generate the gas-chromatographic challenge of isomer separation. Additionally EGDN **06**, 2- and 4-nitrotoluene (**12**, **14**) and DMDNB **26** are important explosive detection aid agents, so-called taggants that need to be incorporated in commercial explosive formulations, according to the 1991 Montreal Convention on the Marking of Plastic

Explosives [10]. Hexanitrostilbene was included since it is a highly thermostable explosive with low volatility. [11] With these compounds the ChemAir substance repertoire includes a healthy balance of 15 explosives with misuse potential in improvised explosive devices, 7 explosives with proliferation risk from the military and civil sector as well as all four taggants for the marking of plastic explosives.

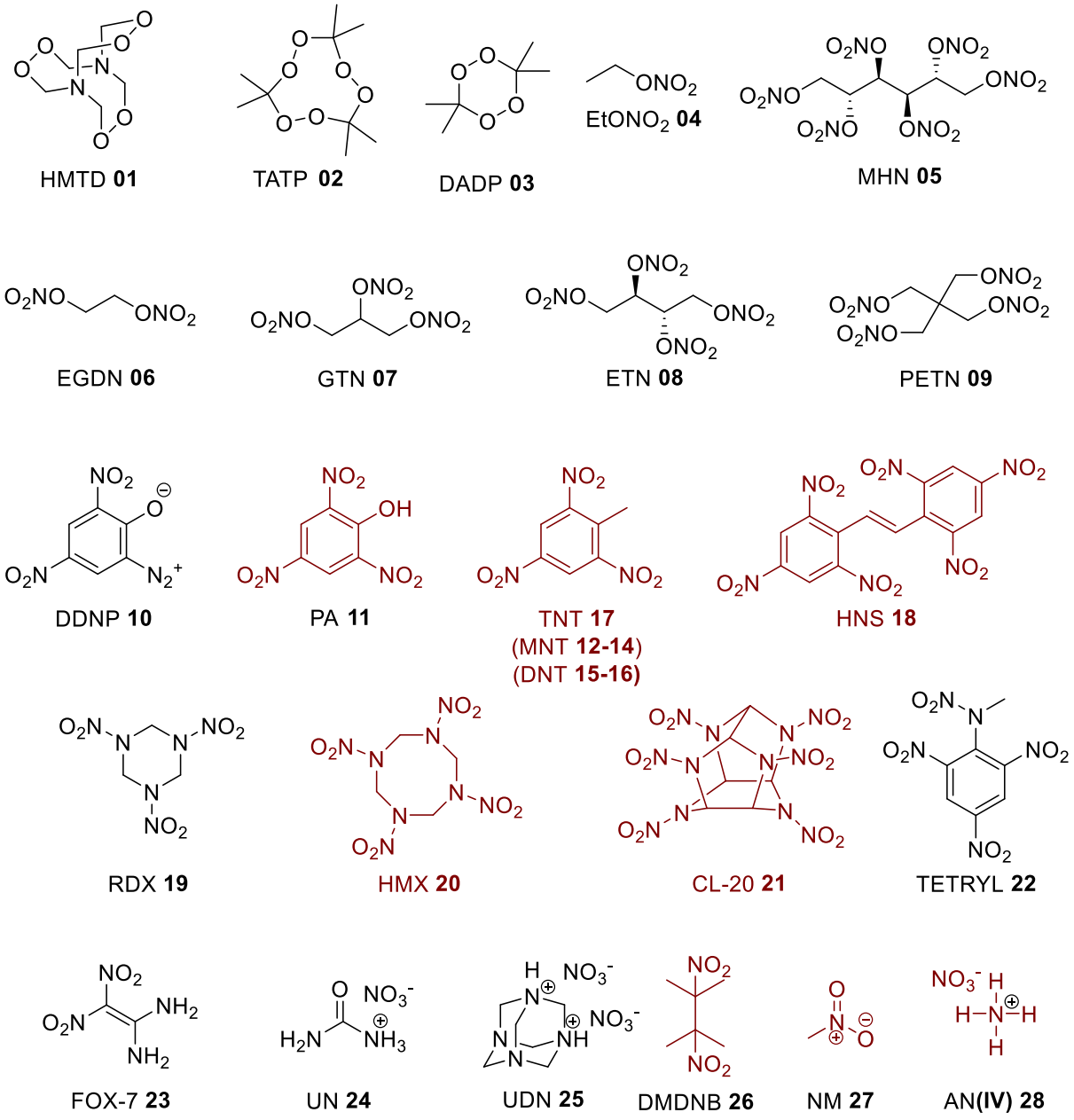

Figure 6 – The structures of the explosives that were included in the ChemAir substance repertoire. (black: substance was synthesized in this work, red: substance was acquired commercially).

4.6 Analytical Characterization of the ChemAir Substance Repertoire Analytes

In order to generate reliable analytical data from one source all substances were fully characterized in classical chemical fashion including ^{1}H, ^{13}C, $^{14/15}$ N-NMR-, IR- RAMAN- and mass-spectroscopy, elemental analysis, thermal analysis by DTA or DSC and gas-pycnometric density determination. In some cases not all analytical techniques could be applied for the reasons stated in the analytical section. For the calculation of the energetic performance parameters the heat of formation of all compounds was calculated using the CBS-4M Method in the Gaussian09 [12] software. Room temperature densities were taken from pycnometric measurements or from X-Ray diffraction (XRD) data.

Table 3 gives selected energetic and physico-chemical properties of the analytes of the ChemAir substance repertoire. (cf. Figure 6)

Densities derived from XRD at the temperature T were adjusted to room temperature with the following equation:

$$\rho_{298K} = \rho_T / (1+\alpha_v(298-T_0)); \alpha_v = 1.5 \cdot 10^{-4}\ K^{-1} \quad (2)$$

The impact and friction sensitivities were determined and carried out according to STANAG 4489 [13] and 4487 [14] modified instructions [15] using a BAM (Bundesanstalt für Materialforschung) drophammer and a BAM friction tester. [16]

The energetic properties of peroxides **2** and **3** and of the nitrate esters **4**-**9** are discussed in the corresponding publications. (cf. chapter 7.2, 7.3)

Mass spectra are important signatures of an explosives for its detection. (cf. section 1.1.2, 1.3.2) The mass spectra of each compound **01**-**28** were recorded on a JEOL JMS 700 mass spectrometer in DEI- or EI- mode with an ionization energy of 70eV. For DEI the sample is heated on a filament in the ion source. For EI the sample is placed in a crucible and volatized by the detector vacuum. Additionally CI spectra are available in some cases. In the following all mass spectra that were recorded are presented in a table.

All reagents and solvents were used as received (Sigma-Aldrich, Fluka, Acros Organics, ACBR). NMR spectra were measured with JEOL (270, 400 MHz) and Bruker (400 MHz) NMR spectrometers. The chemical shift of the solvent peaks were adjusted according to literature values [17]. Multiplets are referred to as m (multiplet), s (singulet), d (doublet), t(triplet), q(quartett), abq (AB-Quartett) and their combinations. Infrared spectra were measured with a Perkin-Elmer FT-IR Spektrum BXII instrument equipped with a Smith Dura SampIIR II ATR unit. Transmittance values are described as “strong” (s), “medium” (m), and “weak” (w). DEI, EI and CI- mass spectra were measured with a JEOL MStation JMS 700 instrument. Elemental analyses (EA) were performed with a Netsch STA 429 simultaneous thermal analyzer. Sensitivity data were determined using a BAM drophammer and a BAM friction tester. The electrostatic sensitivity tests were carried out using an Electric Spark Tester ESD 2010 EN (OZM Research) operating with the “Winspark 1.15” software package. Melting and decomposition points were measured with a *Linseis PT-10 DSC* or an OZM DTA apparatus using heating rates of 5 °C min^{-1}. Temperatures of phase-change, melting and decomposition are given in the order of beginning, onset, maximum, offset and end point. The literature reference for the original synthesis each analyte is given.

CAUTION! The majority of the described compounds are energetic materials with sensitivity to various stimuli. While we encountered no issues in the handling of these materials, proper protective measures (face shield, ear protection, body armor, Kevlar gloves, and earthened equipment) should be used during the handling of explosive compounds including vapor pressure measurements.

Table 3 – Selected energetic and physico-chemical properties of the analytes of the ChemAir substance repertoire. (cf. Figure 6)

	HMTD 01	**TATP 02**	**DADP 03**	**$EtONO_2$ 04**	**MHN 05**	**EGDN 06**	**GTN 07**	**ETN 08**	**PETN 09**	**DDNP 10**	**PA 11**	**2-MNT 12**	**3-MNT 13**	**4-MNT 14**
CAS #[a]	283-66-9	17088-37-8	1073-91-2	625-58-1	15825-70-4	628-96-6	55-63-0	7297-25-8	78-11-5	05.03.4682	88-89-1	88-72-2	99-08-1	99-99-0
Formula[b]	$C_6H_{12}N_2O_6$	$C_9H_{18}O_6$	$C_6H_{12}O_4$	$C_2H_5NO_3$	$C_6H_8N_6O_{18}$	$C_2H_4N_2O_6$	$C_6H_{14}N_6O_6$	$C_4H_6N_4O_{12}$	$C_5H_8N_4O_{12}$	$C_6H_2N_4O_5$	$C_6H_3N_3O_7$	$C_7H_7NO_2$	$C_7H_7NO_2$	$C_7H_7NO_2$
M [g mol^{-1}][c]	208.1700	222.2370	148.1580	91.066	452.1540	152.0620	227.0850	302.1080	316.1350	210.105	229.1040	137.1380	137.1380	137.1380
IS [J][d]	2	1.5	5	1	1	1	1	3	3	1	10	>40	>40	>40
FS [N][e]	<5	<5	5	>360	30	>360	>3601	60	60	5	>360	>360	>360	>360
ESD [J][f]	0.003	0.2	0.2	-/-	0.15	n.m.	n.m.	0.15	0.19	0.15	0.4	-/-	-/-	>1.5
Grain Size [µm][g]	<100	<100	<100	-/-	100-500	-/-	-/-	100-500	>1000	100-500	100-500	-/-	-/-	<100
N[%][h]	13.46	0	0	15.38	18.59	18.42	18.5	18.55	17.72	26.67	18.34	10.21	10.21	10.21
Ω_{CO2} [%][i]	-92.2	-151.2	-151.2	-61.49	7.08	0	3.52	5.3	-10.12	-60.92	-45.39	-180.84	-180.84	-180.84
T_{melt} [°C][j]	-/-	97-98[#]	132-133[#]	-95 [18]	109	-22 [19]	13 [20]	59	138	-/-	120	-10 [21]	16	51
T_{dec} [°C][k]	119	n.m.	n.m.	n.m.	157	n.m.	n.m.	170	179	163	237	232	243	234
ρ_{lit} [g cm^{-3}][l]	1.582	1.272	1.33	1.11	1.894	1.4817	1.59	1.759	1.827	1.727	1.822	-/-	-/-	1.353
T_{lit} [K][m]	295	180	208	293	173	298	297	291	123	295	120	-/-	-/-	100
CIF#[n]	CUXWIB	241973	[22]	[23]	1471378	[19]	[19]	1500841	632960	195236	787071	-/-	-/-	728953
ρ_{298} [g cm^{-3}][o]	1.582	1.250*	1.31*	1.11	1.784**	1.4817	1.59	1.774 **	1.750 **	1.726*	1.748 **	1.159 **	1.157 **	1.293 **
$\Delta_f H°$[kJ/mol][p]	-285	-640	-435	-174	-622	-219	-311	-433.1	-481	139	-202	-28	-44	-73
$\Delta_f U°$[kJ kg^{-1}][q]	-260	-2744	-2802	-1792	-1287	-1341	-290	-405.9	-1427	731	-810	-117	-233	-442
$-\Delta_d U°$[kJ kg^{-1}][r]	4713	3420	3194	4712	5938	6563	6320	6105	7796	4604	4604	2717	2618	2618
T_{det} [K][s]	2841	2038	2032	3130	4189	4541	4445	4225	4417	3559	3484	1878	1833	1833
p_{C-J} [kbar][t]	203	114	131	123	296	212	241	301	298	219	234	57	55	55
V_{det} [m s^{-1}][u]	7372	6322	6246	6321	8488	7576	7887	8540	7655	7331	7472	4649	4602	4602
V_0 [L kg^{-1}][v]	823	821	815	976	755	811	782	767	502	629	638	593	591	591

[a] Chemical Abstracts Service number [b] sum formula [c] molecular weight [d] impact sensitivity [e] friction sensitivity [f] electrostatic discharge sensitivity [g] grain size [h] nitrogen content [l] oxygen balance [j] melting point (onset), [k] decomposition temperature (onset), [l] literature density, [m] temperature of literature density, [n] Crystal Information File number [24], [o] density at 298 K, [p] calculated heat of formation (CBS-4M), [q] calculated energy of formation (CBS-4M), [r] energy of detonation, [s] detonation temperature, [t] detonation pressure, [u] detonation velocity, [v] volume of gaseous products *calculated density ** measured with gas pycnometer [#] measured with Buechi apparatus (5 °C min^{-1})

	2,4-DNT 15	2,6-DNT 16	TNT 17	HNS 18	RDX 19	HMX 20	CL-20 21	TETRYL 22	FOX-7 23	UN 24	UDN 25	DMDNB 26	NM 27	AN IV 28
CAS #[a]	121-14-2	606-20-2	118-96-7	51168-33-3	121-82-4	2691-41-0	135285-90-	479-45-8	14250-81-3	124-47-0	100-97-0	3964-18-9	75-52-5	6484-52-2
Formula[b]	$C_7H_6N_2O_4$	$C_7H_6N_2O_4$	$C_7H_5N_3O_6$	$C_{14}H_6N_6O_{12}$	$C_3H_6N_6O_6$	$C_4H_8N_8O_8$	$C_6H_6N_{12}O_{12}$	$C_7H_5N_5O_8$	$C_2H_4N_4O_4$	$CH_5N_3O_4$	$C_6H_{14}N_6O_6$	$C_6H_{12}N_2O_4$	CH_3NO_2	NH_4NO_3
M [g mol^{-1}][c]	182.1350	182.1350	227.1320	450.2320	222.1170	296.1560	438.1860	287.1440	148.0780	123.068	265.2140	176.1720	61.040	80.0430
IS [J][d]	>40	>40	15	5	7.5	7.4	3	3	25	>40	15	40	>40	>40
FS [N][e]	>360	>360	>360	>360	120	120	96	360	>360	>360	240	360	>360	>360
ESD [J][f]	>1.5	>1.5	0.7	1	0.15-0.20	0.22	0.10	0.6	1	>1.5	1.3	1.5	-/-	>1.5
Grain Size [µm][g]	<100	<100	100-500	<100	<100	<100	<100	<100	<100	500-1000	<100	<100	-/-	<100
N[%][h]	15.38	15.38	18.5	18.67	18.67	37.84	38.36	24,39	37.84	34.14	31.57	15.9	22.95	1.6769
Ω_{CO2} [%][i]	-114.2	-114.2	-73.97	-67.52	-21.61	-21.61	-10.95	-47,36	-21.61	-6.5	-78.43	-127.15	-39.32	19.99
T_{melt} [°C][j]	67	56	79	317	203			128		155	160	200 [25]	-28[26]	none
T_{dec} [°C][k]	n.m.	n.m.	306	320	208	276	224	190	219	159	164	227 [25]		32.2 [27]
ρ_{lit} [g cm^{-3}][l]	1.559	1.548	1.713	1.718	1.824	1.962	2.08	1.731	1.893	1.744	1.711	1.43	1.131	1.722
T_{lit} [K][m]	173	293	100	150	173	20	100	295	298	100	173	95	298	298
CIF#[n]	225823	172202	227799	246308	927276	673524	679946	[28]	679945	651076	1471377	BECJEY	[29]	2772 [#]
ρ_{298} [g cm^{-3}][o]	1.513 **	1.515 **	1.633 **	1.681*	1.785**	1.886 **	2.018 **	1.731	1.850 **	1.655 **	1.663 **	1.388*	1.131	1.722
$\Delta_f H°$[kJ/mol][p]	-72	-54	-55	67	87	116	365	42	-79	-469	-470	-343	-113	-366
$\Delta_f U°$[kJ kg^{-1}][q]	-311	-214	-166	215	491	492	919	223	-435	-3691	-1645	-1820	NIST	n.a.
$-\Delta_d U°$[kJ kg^{-1}][r]	3613	3697	4399	4612	5807	5837	6160	5619	4958	3348	3222	3116	4593	1577
T_{det} [K][s]	2707	2747	3202	3486	3800	3702	4071	4347	3318	2499	2239	2063	3126	1576
p_{C-J} [kbar][t]	158	159	183	200	340	381	445	232	335	236	210	132	130	216
V_{det} [m s^{-1}][u]	6098	6125	6817	7014	8882	9286	9778	7038	8877	7958	7726	6398	6500	7960
V_0 [L kg^{-1}][v]	615	1716	648	619	793	775	720	626	781	916	860	820	1004	1069

[a] Chemical Abstracts Service number [b] sum formula [c] molecular weight [d] impact sensitivity [e] friction sensitivity [f] electrostatic discharge sensitivity [g] grain size [h] nitrogen content [l] oxygen balance [j] melting point (onset), [k] decomposition temperature (onset), [l] literature density, [m] temperature of literature density, [n] Crystal Information File number [24], [o] density at 298 K, [p] calculated heat of formation (CBS-4M), [q] calculated energy of formation (CBS-4M), [r] energy of detonation, [s] detonation temperature, [t] detonation pressure, [u] detonation velocity, [v] volume of gaseous products. *calculated density ** measured with gas pycnometer [#] ICSD database

*Table 4 – Mass spectra of compounds **01**-**28** recorded in this work.*

HMTD 01 DEI+				TATP 02 DEI+		DADP 02 DEI+		EtONO2 4 EI+		MHN 05 DEI+		MHN 05 CI				EGDN 06 EI+		EGDN 06 CI		GTN 07 DEI+		GTN 07 CI	
m/z	Rel. Int.	m/z	Rel. Int.	m/z	Rel. Int.	m/z	Rel. Int.	m/z	Rel. Int.	m/z	Rel. Int.	m/z	Rel. Int.	m/z	Rel. Int.	m/z	Rel. Int.	m/z	Rel. Int.	m/z	Rel. Int.	m/z	Rel. Int.
15	1,27	120	6,44	15	3,53	15,03	8,56	15	5,94	15	1,47	15	0,16	145	0,06	15	1,01	27	0,51	15	16,63	29	0,87
17	2,40	121	1,67	18	0,16	16,07	0,09	17	20,82	16	0,87	19	0,30	148	0,07	17	2,24	29	1,58	16	0,53	30	0,99
18	10,86	132	2,81	26	0,13	17,04	0,23	18	34,20	17	1,03	27	0,61	149	0,08	18	3,85	30	1,76	17	0,39	39	2,43
27	1,76	133	2,57	27	1,26	18,05	0,92	27	4,99	18	0,43	28	0,05	154	0,15	28	1,17	39	5,73	18	2,58	41	0,90
28	8,04	134	2,11	28	0,20	26,07	0,46	28	6,48	26	0,53	29	0,76	157	0,06	29	6,60	41	1,95	19	0,26	43	2,29
29	1,51	135	1,34	29	2,57	27,07	1,99	29	12,18	27	1,47	30	0,17	165	0,06	30	9,48	42	0,92	25	0,40	46	10,70
30	13,50	136	3,10	31	0,81	28,05	0,70	30	3,51	28	1,15	38	0,08	173	0,05	31	1,57	43	5,57	26	2,35	56	1,82
36	2,12	137	4,96	33	0,10	29,09	0,99	32	2,92	29	13,20	39	3,15	174	0,06	41	0,57	46	24,57	27	5,06	57	100,00
38	5,60	148	1,98	39	0,26	30,06	0,07	43	8,37	30	20,26	40	0,31	181	0,16	43	1,42	56	5,02	28	6,17	58	5,28
39	2,67	149	10,66	41	1,00	31,06	0,58	46	100,00	31	4,40	41	3,23	183	0,07	44	0,61	57	100,00	29	78,31	86	0,97
41	1,55	150	2,21	42	1,36	32,03	0,58	57	3,72	32	0,21	42	1,43	190	0,09	46	100,00	58	11,95	30	82,88	88	2,62
42	4,59	153	1,04	43	100,00	37,05	0,09	71	2,97	39	0,51	43	16,95	193	0,08	47	0,52	59	1,38	31	26,17	102	1,52
43	11,78	163	1,19	44	2,24	38,06	0,15	76	38,48	41	0,48	44	0,54	219	0,09	55	0,70	71	0,93	32	1,01	104	0,56
44	2,50	164	3,83	45	1,44	39,07	0,56	85	2,07	42	1,88	46	1,00	220	0,05	57	1,14	73	5,48	37	0,64	106	0,62
46	8,13	165	3,34	47	0,16	40,07	0,10			43	3,16	48	0,60	282	0,05	60	0,54	74	0,91	38	0,80	120	1,08
50	5,97	166	4,76	55	0,37	41,08	0,54			44	1,40	51	0,09	293	0,07	69	0,58	86	1,29	39	1,59	148	1,16
61	4,75	167	2,48	57	3,32	42,05	2,19			45	0,83	53	0,26	345	0,12	71	0,67	87	2,14	40	0,24	165	3,20
52	3,68	178	2,09	58	7,55	43,05	100,00			46	100,00	55	0,67	363	0,06	76	14,45	88	9,38	41	1,21	191	1,33
53	2,16	179	2,68	59	9,50	44,05	2,18			47	0,86	56	4,87	390	0,22	83	0,51	89	0,51	42	8,19	223	3,82
59	8,44	181	32,60	60	0,34	45,06	0,67			48	0,45	57	100,00	408	0,35	97	0,51	90	30,76	43	39,66	228	0,94
61	3,33	182	2,36	73	2,41	55,08	0,08			53	0,26	58	5,52	437	0,07	102	0,66	91	0,83	44	1,68	257	6,44
62	10,41	183	2,53	74	1,71	57,07	0,32			54	0,41	59	1,19	448	0,16	256	0,86	99	1,73	45	1,10	270	2,37
63	5,53	194	13,32	75	8,59	58,07	15,05			55	2,38	60	0,07	453	0,40			100	0,36	46	100,00	273	21,09
64	8,21	195	7,44	76	0,30	59,08	14,58			56	0,56	61	0,19	454	0,05			101	1,19	47	4,56	274	1,14
65	3,73	196	2,01	59	0,11	60,08	0,51			57	0,57	67	0,06	482	0,64			102	1,27	48	3,82	284	0,54
66	3,12	197	2,37	101	0,62	73,08	0,51			58	0,52	69	0,11	483	0,07			104	0,58	53	0,21		
67	5,62	210	1,51	117	0,54	74,05	0,08			59	0,32	70	0,06	495	0,56			106	1,01	55	0,61		
68	1,21	211	2,61	222	0,13	75,07	0,16			60	0,53	71	0,09	496	0,09			108	1,52	56	0,42		
71	3,65	212	2,47			101,06	4,80			69	0,41	72	0,23	498	0,15			133	1,30	57	0,33		
73	1,15	213	3,91			102,05	0,26			71	1,03	73	0,35					134	0,70	58	6,73		
74	8,35	224	21,18			133,04	0,06			72	0,24	76	0,08					148	5,25	59	0,64		
75	21,02	241	100,00							73	0,43	79	0,05					153	1,34	60	2,85		
76	12,05	242	21,21							76	6,27	81	0,07					182	8,34	76	33,11		
77	13,65	243	2,70							83	0,35	85	0,16					195	2,04	77	1,64		
78	6,29	287	3,72							84	0,73	86	0,41					198	31,43	78	0,62		
79	2,24									85	0,62	87	0,07					199	1,21	89	0,45		
80	4,72									101	0,34	88	0,37					200	0,55	119	0,73		
87	2,31									114	0,24	89	0,07					242	0,62	151	5,22		
88	14,58									118	0,36	91	0,05							165	1,08		
89	4,11									130	0,26	97	0,05							273	2,24		
90	13,73									151	1,46	99	0,05										
91	17,25									160	0,31	101	0,09										
92	6,86									193	0,97	102	0,14										
93	2,28									226	0,22	103	0,06										
94	1,07									268	0,39	104	0,09										
102	3,46									330	0,07	106	0,18										
103	7,69									495	0,05	113	0,07										
104	6,21											115	0,06										
105	3,38											127	0,07										
106	1,40											129	0,06										
107	2,14											130	0,06										
108	1,41											133	0,06										
117	1,28											136	0,06										
118	6,55											141	0,13										
119	12,93											143	0,06										

ETN 08	DEI+	PETN 09	DEI+	PETN 09 CI		DDNP 10	DEI+	PA 11	DEI+			2-MNT 12	EI	3-MNT 13	DEI+	4-MNT 14	DEI+	2,4-DNT 15	DEI+	2,6-DNT 16	DEI+	TNT 17	DEI+
m/z	Rel. Int.	m/z	Rel. Int.	m/z	Rel. Int.	m/z	Rel. Int.	m/z	Rel. Int.	m/z	Rel. Int.	m/z	Rel. Int.	m/z	Rel. Int.	m/z	Rel. Int.	m/z	Rel. Int.	m/z	Rel. Int.	m/z	Rel. Int.
15	1,72	15	1,10	30	2,93	16	1,72	15	2,57	171	4,09	27	1,64	18	4,19	18	1,27	27	1,21	18	1,01	30	3,46
16	0,39	16	0,21	39	4,68	17	3,27	28	1,28	199	13,85	30	1,61	27	3,38	28	1,40	30	16,26	27	1,70	38	1,15
17	1,05	17	0,64	41	1,27	18	5,36	29	2,00	200	1,81	37	1,04	28	4,52	30	1,02	38	2,48	28	1,15	39	6,37
18	3,23	18	2,05	43	3,34	27	1,56	30	65,53	213	5,30	38	2,83	29	2,20	38	1,11	39	11,28	30	5,73	43	3,31
19	0,09	19	0,35	46	23,40	28	57,86	37	4,53	229	100,00	39	16,37	30	4,51	39	4,86	40	1,61	37	1,04	46	1,65
26	0,27	26	0,48	56	2,52	29	2,66	38	3,48	230	15,20	40	1,31	38	3,72	51	1,25	46	3,53	38	3,04	50	4,88
27	0,72	27	1,73	57	100,00	30	53,33	39	4,13	231	2,26	41	3,75	39	18,37	62	1,25	50	4,86	39	11,29	51	6,41
28	2,24	28	1,64	58	5,32	37	3,35	42	1,37			50	5,79	41	8,88	63	4,16	51	3,32	40	1,74	52	1,54
29	8,85	29	5,19	85	1,10	38	4,62	43	11,39			51	10,04	43	5,39	64	1,23	52	7,65	43	8,25	53	1,18
30	12,10	30	7,62	86	2,11	39	2,24	44	1,30			52	3,02	46	2,30	65	14,16	53	2,00	46	1,12	61	1,89
31	3,41	31	2,68	87	7,43	44	32,40	45	2,59			53	2,05	50	7,18	77	5,16	61	1,90	50	7,33	62	3,79
32	0,34	39	1,21	88	4,11	45	1,11	46	3,72			61	1,79	51	10,02	78	1,57	62	7,26	51	15,48	63	13,78
36	0,11	40	0,67	102	2,38	46	5,76	49	2,63			62	5,33	52	3,41	79	5,35	63	30,68	52	3,77	64	2,38
38	0,08	41	1,38	104	1,06	47	1,47	50	17,65			63	15,72	53	2,78	86	1,77	64	10,39	53	3,10	65	2,45
39	0,23	42	1,86	114	1,47	49	5,56	51	3,68			64	6,48	55	4,74	87	1,48	65	3,64	61	2,16	69	1,81
41	0,26	43	2,12	115	1,03	50	41,23	52	3,55			65	66,29	57	4,76	89	14,34	66	2,52	62	8,79	74	4,76
42	1,12	44	2,44	116	5,70	51	8,41	53	21,14			66	4,66	61	2,31	90	4,34	74	3,01	63	34,03	75	5,14
43	3,39	45	0,44	120	1,42	52	3,32	54	1,85			74	1,86	62	7,43	91	32,78	75	3,00	64	15,74	76	10,07
44	3,42	46	100,00	130	3,74	53	20,82	55	1,30			75	1,61	63	13,62	92	7,54	76	1,36	65	3,71	77	5,09
45	0,64	47	0,56	132	2,43	54	1,75	58	6,00			76	1,46	64	5,08	107	48,18	77	8,70	66	2,46	78	1,82
46	100,00	48	0,44	148	1,07	55	1,27	61	17,74			77	17,17	65	48,64	108	3,81	78	13,97	74	4,23	85	1,11
47	0,72	53	0,24	150	1,38	60	3,03	62	51,02			78	4,09	66	3,29	121	4,08	79	3,79	75	11,72	86	3,66
48	0,41	54	0,40	161	1,17	61	41,55	63	20,12			79	3,31	69	3,16	137	100,00	80	2,57	76	7,18	87	5,32
53	0,08	55	1,85	164	1,06	62	100,00	64	6,34			86	1,35	71	2,49	138	8,26	86	2,39	77	19,01	88	5,39
54	0,09	56	1,12	177	2,18	63	13,54	65	1,17			87	1,14	74	2,85			87	2,74	78	15,61	89	28,09
55	0,69	57	1,93	195	6,27	64	42,36	66	6,36			89	17,91	75	2,36			88	1,08	79	5,81	90	3,42
56	0,17	58	0,43	209	1,82	65	2,85	67	3,12			90	3,03	77	12,62			89	49,95	80	1,19	91	1,13
57	0,33	60	0,98	224	1,96	66	8,49	68	1,98			91	55,97	78	3,71			90	20,46	86	2,43	92	1,84
58	0,41	68	0,21	237	1,43	67	1,75	69	4,63			92	48,23	79	10,09			91	6,02	87	2,51	103	1,99
59	0,15	69	0,57	240	6,52	68	1,45	70	1,29			93	5,51	83	2,50			92	1,90	89	34,87	104	2,36
60	0,43	70	0,37	254	3,90	69	3,73	74	2,16			120	100,00	86	2,01			94	1,40	90	27,83	105	2,97
61	0,20	71	0,70	272	1,82	74	1,99	75	4,14			121	7,99	87	2,01			104	1,62	91	12,82	106	2,52
69	0,15	72	0,21	301	6,24	75	4,31	76	4,97			137	19,37	89	14,48			105	4,34	92	3,25	120	2,51
70	0,13	73	0,36	312	4,02	76	2,00	77	10,87			138	1,79	90	5,36			106	5,23	93	1,11	134	3,81
71	0,40	76	13,94	317	14,92	77	11,66	78	7,31					91	100,00			107	4,79	94	1,08	135	1,50
72	0,16	77	0,35	318	1,10	78	11,22	79	5,38					92	8,31			108	1,88	104	5,17	136	1,21
73	0,35	83	0,24	346	14,52	79	7,52	80	13,89					107	3,95			118	7,80	105	3,08	149	6,42
76	8,24	85	0,75	347	1,23	80	6,89	81	1,37					121	2,76			119	16,65	106	4,04	151	1,11
77	0,18	86	0,22	359	3,23	89	1,59	89	1,82					137	58,48			120	1,80	107	4,07	152	1,04
83	0,12	149	0,48	362	37,13	90	7,70	90	8,17					138	4,82			136	1,39	108	6,39	163	1,51
85	0,08	194	0,28	363	2,92	91	6,19	91	37,94									148	2,35	117	1,79	164	4,50
88	0,12			364	1,12	92	5,77	92	7,93									149	2,17	118	3,50	166	3,81
95	0,08					93	1,96	93	1,14									166	100,00	119	3,50	179	4,16
99	0,08					94	3,85	94	1,66									166	3,89	121	16,40	180	11,29
97	0,08					105	1,40	95	1,14									167	0,73	122	1,37	181	1,09
106	0,12					106	2,88	105	4,36									182	5,00	134	5,34	193	10,73
112	0,10					107	5,71	106	2,01									183	7,42	135	14,39	194	1,74
118	0,30					108	3,76	107	1,13											136	1,31	209	2,27
129	0,09					124	1,04	108	2,13											148	15,69	210	100,00
149	0,26					152	5,71	119	1,48											149	1,98	211	9,25
151	0,59					154	4,19	120	2,39											164	2,26	212	1,46
167	0,11					168	1,07	136	3,87											165	100,00	227	1,18
226	0,10					184	3,77	137	2,71											166	8,66		
						200	10,20	152	3,78											182	2,29		
						210	30,65	155	3,08														
						211	3,11	166	1,71														

HNS 18 DEI+

m/z	Rel. Int.	m/z	Rel. Int.
17	1,36	118	1,11
18	4,94	119	74,37
28	1,65	120	29,70
29	1,20	121	36,03
30	36,80	122	6,26
38	1,02	123	5,40
44	7,35	124	3,78
46	2,79	125	1,62
50	3,12	126	1,27
51	1,68	127	1,12
53	2,80	133	3,26
61	1,73	134	4,11
62	8,67	135	5,81
63	8,41	136	3,34
64	3,27	137	5,29
65	5,53	138	2,31
66	2,54	139	1,06
67	1,78	146	1,42
68	1,49	147	1,88
69	3,61	148	19,81
73	1,18	149	14,36
74	24,07	150	7,20
75	28,79	151	5,49
76	8,96	152	4,62
77	4,87	161	18,44
78	1,46	162	8,19
79	1,70	163	4,07
80	1,29	164	3,57
81	1,99	165	82,28
86	7,13	166	7,12
87	11,73	167	100,00
88	7,72	168	8,13
89	4,38	169	1,23
90	7,78	173	2,78
91	13,63	174	8,08
92	4,75	175	3,63
93	4,86	176	1,39
94	1,10	177	2,76
98	6,30	178	5,30
99	6,12	179	4,06
100	3,81	180	1,87
101	1,63	189	1,83
102	1,83	190	1,39
103	13,17	191	1,49
104	4,46	192	1,35
105	1,61	193	2,74
106	1,01	194	31,42
107	2,55	195	4,36
110	4,23	197	2,77
111	6,60	203	1,63
112	3,93	207	1,41
113	1,15	208	2,09
114	1,03	209	12,43
116	3,86	210	7,10
117	1,53	213	1,26

HNS 18 DEI+

m/z	Rel. Int.	m/z	Rel. Int.
224	12,30	225	11,63
226	2,04	235	1,76
240	23,67	241	4,31
249	1,04	281	1,81
295	2,87	341	1,25
387	6,46	388	1,37

RDX 19 DEI+

m/z	Rel. Int.	m/z	Rel. Int.
15	11,55	105	0,49
16	0,35	112	1,67
17	0,72	113	0,14
18	2,01	114	0,10
26	0,25	118	0,38
27	2,24	120	53,15
28	86,47	121	1,25
29	25,40	122	0,49
30	36,38	127	2,23
31	0,48	128	62,93
32	0,29	129	3,12
34	0,16	130	1,78
38	0,21	131	0,69
39	0,45	132	1,52
40	2,56	145	0,77
41	17,23	147	1,03
42	100,00	148	14,37
43	5,52	149	3,09
44	3,15	150	0,26
45	0,68	158	1,04
46	88,75	159	1,06
47	0,64	160	0,13
48	1,60	174	0,48
53	3,32	175	0,30
54	6,70	194	0,35
55	10,70	205	4,30
56	33,19	206	0,28
57	2,60	221	0,34
58	2,47	268	0,12
59	0,43		
60	2,19		
68	3,06		
69	0,83		
70	0,12		
71	20,77		
72	1,88		
73	3,72		
74	3,29		
75	68,44		
76	2,23		
77	0,34		
80	8,85		
81	11,16		
82	13,10		
83	3,57		
84	0,87		
85	1,32		
87	0,28		
89	0,23		
99	0,55		
100	0,35		
101	5,51		
102	12,24		
103	0,57		
104	2,87		

HMX 20 DEI+

m/z	Rel. Int.	m/z	Rel. Int.
15	6,28	158	1,45
17	0,78	174	0,93
18	2,42	175	2,09
27	1,54	176	1,96
28	27,77	194	1,00
29	8,13	205	6,89
30	18,15	206	0,53
40	0,96	221	5,63
41	7,89	222	26,62
42	100,00	223	2,78
43	3,64	342	0,86
44	2,94		
46	66,02		
47	0,58		
48	1,33		
53	0,95		
54	1,92		
55	4,92		
56	16,16		
57	1,56		
58	1,97		
60	1,11		
68	0,83		
69	0,51		
71	7,68		
72	1,11		
73	2,67		
74	6,88		
75	64,90		
76	1,90		
80	1,56		
81	4,03		
82	4,26		
83	3,61		
84	0,53		
98	5,88		
100	0,53		
101	1,71		
102	25,06		
103	0,98		
104	4,61		
105	0,88		
120	46,71		
121	1,10		
127	0,93		
128	69,41		
129	4,58		
130	3,65		
132	3,18		
145	0,71		
147	0,88		
148	83,66		
149	7,66		
150	0,95		
157	1,87		

CL-20 21 DEI+

m/z	Rel. Int.	m/z	Rel. Int.
16	1,49	259	1,01
17	2,28	270	2,61
18	2,47	273	1,12
26	2,13	300	3,68
27	5,78	316	7,46
28	15,64	347	1,05
29	5,04	392	4,60
30	34,65		
39	1,37		
40	3,05		
41	1,96		
42	1,18		
43	3,75		
44	16,68		
45	1,73		
46	100,00		
47	2,04		
52	1,70		
53	11,31		
54	26,59		
55	2,51		
66	2,60		
67	6,44		
68	1,62		
70	1,93		
73	3,05		
80	4,42		
81	14,26		
82	11,60		
83	1,53		
93	1,76		
94	11,20		
95	1,23		
100	1,05		
107	4,04		
108	23,38		
109	2,15		
120	3,23		
121	2,90		
126	1,60		
127	5,95		
135	5,75		
136	1,17		
137	1,56		
151	1,25		
154	2,04		
161	2,74		
162	3,35		
167	1,38		
178	4,49		
181	1,26		
207	1,37		
213	14,62		
214	1,18		
224	4,15		

TETRYL 22 DEI+

m/z	Rel. Int.	m/z	Rel. Int.
15	1,27	120	6,44
17	2,40	121	1,67
18	10,86	132	2,81
27	1,76	133	2,57
28	8,04	134	2,11
29	1,51	135	1,34
30	13,50	136	3,10
36	2,12	137	4,36
38	5,60	148	1,98
39	2,67	149	10,66
41	1,55	150	2,21
42	4,59	153	1,04
43	11,78	163	1,19
44	2,50	164	3,83
46	8,13	165	3,34
50	5,97	166	4,76
51	4,75	167	2,48
52	3,68	178	2,09
53	2,16	179	2,68
59	8,44	181	32,60
61	3,93	182	2,96
62	10,41	183	2,53
63	5,53	194	13,92
64	8,21	195	7,44
65	3,73	196	2,01
66	3,12	197	2,37
67	5,62	210	1,51
68	1,21	211	2,61
71	3,65	212	2,47
73	1,15	213	3,91
74	8,95	224	21,18
75	21,02	241	100,00
76	12,05	242	21,21
77	13,65	243	2,70
78	6,29	287	3,72
79	2,24		
80	4,72		
87	2,91		
88	14,58		
89	4,11		
90	13,73		
91	17,25		
92	6,86		
93	2,28		
94	1,07		
102	3,46		
103	7,69		
104	6,21		
105	3,38		
106	1,40		
107	2,14		
108	1,41		
117	1,28		
118	6,55		
119	12,93		

FOX-7 23 DEI+

m/z	Rel. Int.
17	2,39
18	11,01
27	3,08
28	14,52
29	2,98
30	22,80
41	4,48
42	19,33
43	76,16
44	55,02
46	8,00
53	3,83
55	7,19
60	5,00
69	30,86
70	4,76
72	8,44
86	19,77
118	2,89
148	100,00
149	6,96

UN24	DEI+	UDN 25	DEI+	DMDNB 26	DEI+	NM 27	DEI+	AN 28	DEI+
m/z	Rel. Int.	m/z	Rel. Int.	m/z	Rel. Int.	m/z	Rel. Int.	m/z	Rel. Int.
15	1,78	15	2,80	15	3,26	15	13,73	15	2,22
16	13,52	28	1,14	17	1,60	17	8,98	16	14,48
17	50,97	30	3,87	18	6,09	18	39,79	17	15,85
18	10,14	36	1,59	27	9,14	27	2,02	18	2,06
26	1,24	41	4,18	28	4,88	28	6,47	27	0,14
27	5,67	42	100,00	29	7,37	29	3,71	28	1,02
28	6,59	43	3,63	30	12,04	30	50,34	29	0,17
29	4,87	44	1,72	31	1,58	32	2,69	30	33,41
30	19,58	46	14,15	38	1,04	42	1,27	31	0,30
31	5,21	56	1,20	39	21,66	43	2,81	32	0,68
35	4,15	69	4,22	40	4,33	44	5,68	35	0,18
36	13,39	71	5,09	41	56,27	45	4,82	36	0,64
37	1,38	83	4,50	42	6,60	46	37,35	38	0,26
38	6,52	84	1,74	43	17,03	60	7,38	42	0,16
41	2,75	85	3,29	44	1,01	61	100,00	43	0,40
42	6,23	96	1,66	46	2,51	62	1,63	44	2,20
43	23,79	97	1,05	51	1,75			46	100,00
44	98,85	111	2,63	53	5,45			47	0,55
45	1,62	112	13,47	54	1,02			48	0,41
46	43,82	140	84,38	55	22,32			63	1,54
58	1,23	141	6,38	56	8,30			64	0,47
60	100,00			57	100,00			66	0,15
61	3,55			58	5,89			79	0,48
63	1,02			59	8,27			80	0,93
				65	1,38			81	0,43
				67	4,41			82	0,94
				68	1,83			121	0,17
				69	53,80			127	0,11
				70	3,40			128	0,12
				83	10,94			137	0,10
				84	22,81				
				85	7,11				
				100	28,31				
				101	2,04				
				112	2,23				

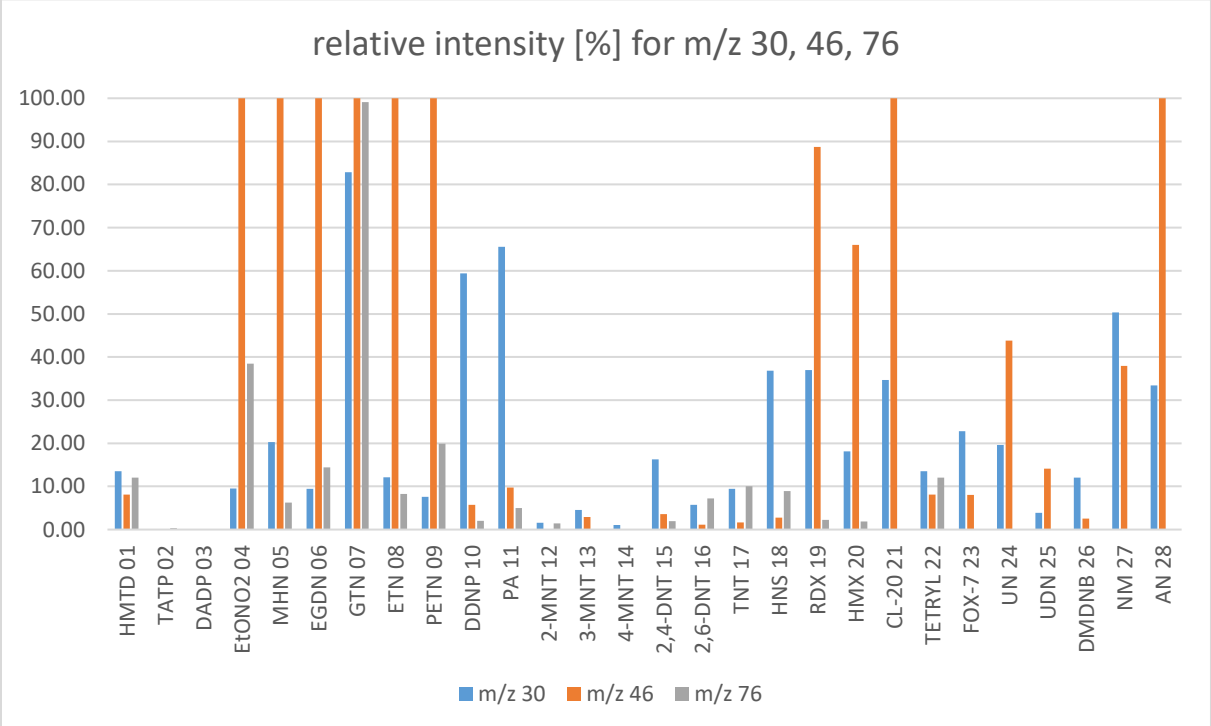

Figure 7 – Relative intensity of the m/z fragment ions m/z 30, m/z 46 and m/z 76.

In the (D)EI spectra of the nitrate esters $(M+NO)^+$ or $(M+NO_2)^+$ adducts were observed in many cases. The analysis of the spectra revealed that for almost every analyte the m/z values 30, 46 and 76 could be observed. These fragment ions correspond most probably to the nitrosonium cation NO^+ (m/z 30), the nitronium cation NO_2^+ (m/z 46) and the $N_2O_3^+$ cation (m/z 76). The latter cation may be formed by the reaction of NO_2 with NO^+ or by the reaction of NO with NO_2^+. These ions dominate the DEI/EI mass spectra of the nitrate esters and cycloaliphatic nitramines. They are also observed for different compounds like the peroxide HMTD **01** and ammonium nitrate **18**. These fragment cations and the

release of nitrogen oxides under harsh conditions like EI ionization is a promising approach for future explosive detectors. The first version of the EGIS explosive detector relied on thermal decomposition followed by chemoluminescent NO detection.[30]

In the following each compound of the ChemAir substance repertoire will be presented individually.

4.6.1 Hexamethylene Triperoxide Diamine HMTD 01

WARNING: HMTD 01 is extremely sensitive towards electrostic discharge detonating at 3 mJ at a grain size <100 µm. Protective measures against electrostatic discharge are obligatory upon handling this compound.

HMTD **01** was first synthesised by *Legler*[31] in 1885. It is a more powerful initiating explosive than mercury fulminate, but it has never found application in detonators regarding its poor thermal and chemical stability.[32]

In this work two similar syntheses of HMTD **08** were tested. The first was a reproduction of the synthesis stated by *Marotta*[33] with the washing steps suggested by *Wierzbicki et al.*[34]. Hexamethylenetetramine was dissolved in glacial acid and allowed to cool to room temperature. Hydrogen peroxide was added and the solution stood overnight at ambient conditions before a small amount of distilled water was added and the white precipitate was filtered off. It was washed with 20 mL distilled water, 20 mL ethanol and 20 mL diethyl ether before the precipitate was air suction dried for several minutes. HMTD was obtained as a crude product in 77 % yield which was impurified with acetic acid. It was tried to perform an azeotropic removal of acetic acid by codistillating the crude product five times with each three millilitres of toluene on a rotary evaporator at 40 mbar and 40 °C. It was not possible to obtain a pure product, yet its detonation could be initiated by striking it manually with a hammer on a metal plate.

Therefore a downscaled synthesis according to *Wierzbicki et al.*[34] was chosen. No decomposition was observed after storing HMTD **01** at ambient conditions in an ESD container which was sealed for three months.

HMTD **01** has an interesting conformeric behavior. In total four enantiomers of two chiral conformers exist. One chiral conformer has D_3 symmetry, the second conformer has C_2 symmetry. The X-Ray structure of solid HMTD **01** has been demonstrated to consist of equal proportions of the enantiomers disordered at the crystallographic mirror plane.[34-35]

Guo et al.[36] investigated the two solution-state conformers of HMTD **01**. It is stated that earlier spectroscopic work was only able to detect a single conformer, but published NMR data are in disagreement. On the one hand a strongly coupled AB quartet was observed performing ^{1}H-NMR in DMSO-d_6, which would be consistent with the two geminal diastereotopic protons expected from D_3 symmetry.

On the other hand *Wierzbicki et al.*[34] stated that a singulet appears in the ^{1}H-NMR spectrum of HMTD **01** in $CDCl_3$ which would be only consistent with this structure by accidental chemical shift degeneracy of the diastereotopic protons or fast exchange of the D_3 isomers.

In this work we could reconfirm the observations of *Guo et al.*[36] (cf. Figure 8) measuring the ^{1}H-NMR of HMTD **01** in DMSO-d_6 at 400.18 MHz. An AB-quartett with chemical shifts of 4.66 and 4.79 ppm and

a coupling constant of 13.5 MHz was observed. In the baseline of the ^{1}H-NMR in *Figure 8* even the small AB multiplets of the C_2 conformer superimposed with the major D_3 conformer can be observed as reported by *Guo et al.*[36]

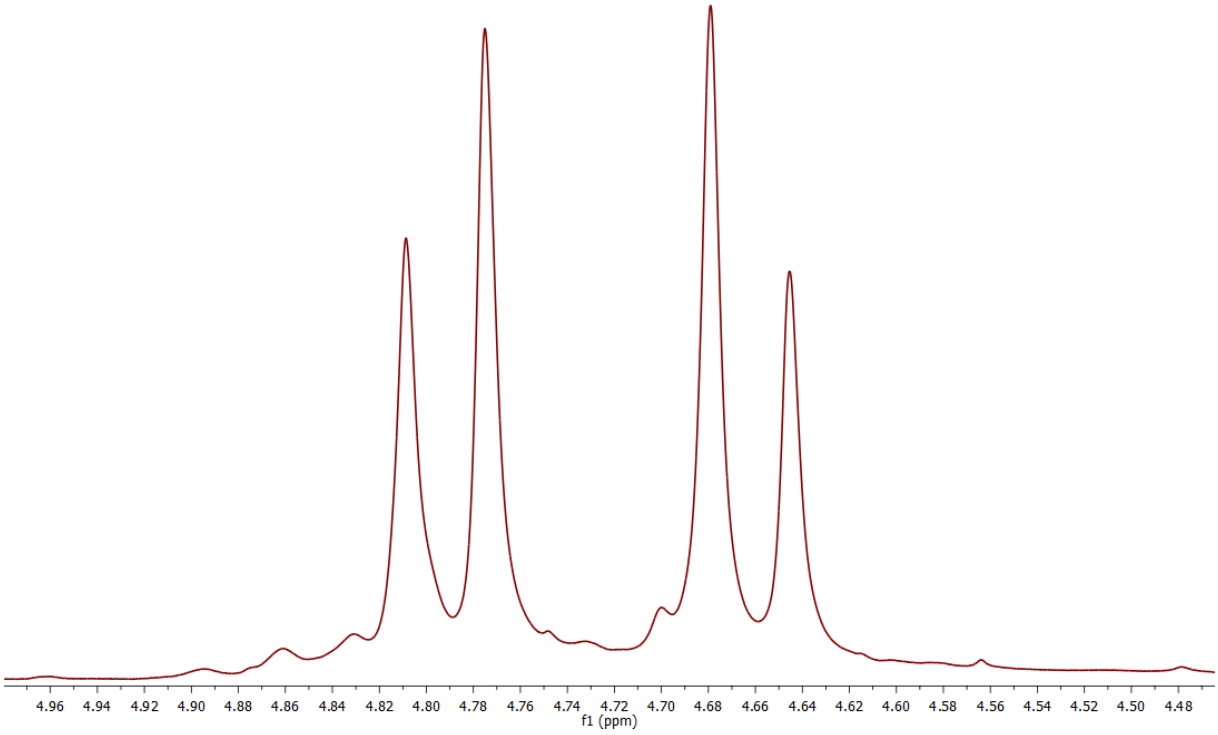

Figure 8: ^{1}H-NMR (400.18 MHz) of HMTD 01 in DMSO-d_6

The ^{13}C-NMR as it is shown in *Figure 9* contains four signals at 88.8, 89.6, 90.0 and 91.3 ppm of which the one at 89.6 ppm is the most intense signal and therefore corresponds to the D_3 conformer. The three minor signals are related to the C_2 conformer.

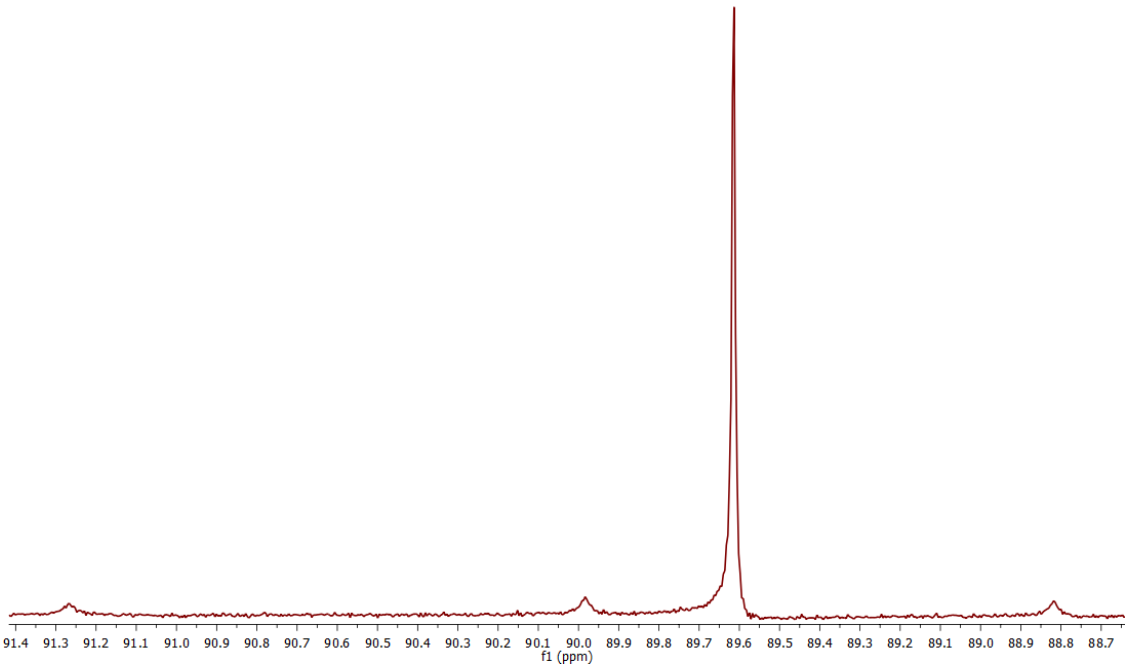

Figure 9: ^{13}C-NMR of HMTD 08 in DMSO-d_6 at 100.63 MHz.

HMTD **01** was reported to be instable in the gas-phase by *Oxley et al.* [37] who tried to measure its vapor pressure by head-space gas chromatography in the temperature range of 15-55 °C, which failed due to the thermal instability of HMTD **01**. In 2015 Aernecke et al. [38] estimated the vapor pressure of HMTD **01** using Secondary Electrospray Ionization Mass Spectroscopy using heroine and cocaine as calibrants.

At 20 °C a HMTD vapor pressure of 6.1×10^{-6}Pa (cocaine) and 4.5×10^{-6}Pa (heroine) was reported with enthalpies of sublimation of 92 ± 3 kJ mol^{-1} (cocaine) and 116 ± 4 kJ mol^{-1} (heroine).

Hydrogen peroxide (1.92 g, 56.45 mmol, 11.8 eq., 30 %, aq.) was cooled by means of an ice-salt cooling bath and hexamethylenetetramine (0.67 g, 4.78 mmol, 1.0 eq.) was dissolved within. Citric acid monohydrate (0.70 g, 3.33 mmol, 0.7 eq.) was added in small portions over a period of 10 minutes. The reaction batch was allowed to warm up gradually to room temperature. After 24 hours a white precipitate had formed, which was filtered off and washed with 20 mL distilled water, 20 mL ethanol and 20 mL diethyl ether. Subsequently it was dried under suction for five minutes and dried over orange gel in high vacuum over night. 0.56 g (56 %) of white powdery hexamethylene triperoxide diamine **01** was obtained.[34]

^{1}H-NMR[36]	(DMSO-d_6, 400 MHz): δ = 4.66, 4.79 (ABq, J = 13.5 Hz, D_3 conformer) ppm. Further signals of the C_2 minor conformer are reported in the literature given.
^{13}C-NMR[36]	(DMSO-d_6, 101 MHz): δ = 88.8 (minor conformer), 89.6 (minor conformer), 90.0 (major conformer), 91.3 (minor conformer) ppm.
EA	for $C_6H_{12}N_2O_6$ calculated: C 34.62, H 5.81, N 13.46 %; found: C 34.56, H 5.81, N 13.29 %.
IR (ATR)	$\tilde{\nu}$ = 2960 (w), 2923 (w), 2343 (w), 1684 (w), 1467 (w), 1445 (w), 1417 (w), 1386 (w), 1360 (m), 1337 (m), 1291 (w), 1257 (w), 1232 (m), 1054 (m), 1034 (m), 961 (s), 951 (s), 908 (m), 873 (s), 774 (w) cm^{-1}.
Raman	Not measured due to the sensitivity of the compound.
DTA	T_{dec}: 80/119/125/126/130 °C.

4.6.2 The Peroxides TATP 02 and DADP 03

Triacetone triperoxide **02**, also known as TATP or APEX, is the condensation product of hydrogen peroxide with acetone and was discovered accidentally by *Wolffenstein* [39] in 1895. Due to its high volatility and sensitivity toward external stimuli the medium performance explosive is not applied in neither the civil nor the military sector. With respect to the free availability of its precursors and its readiness for detonation initiation, the compound is popular in the amateur chemist and terrorist scene. Unfortunately, this was demonstrated by the recent TATP related incident in Oberursel (Germany, 2015, [40]) and the ISIS terror attack in Paris (France, 2015, [41]). A 17 year old teenager (Germany, 2006, [42]) was arrested for hoarding 2 kg of TATP **02**, which underlines the ease of TATP **02** synthesis. Oxley *et al.* investigated the factors influencing the formation of TATP **01** and its side product diacetone diperoxide (DADP, **02**) [43] as well as the destruction of TATP [44]. Lubczyk *et al.* [45] recently published a method for desensitizing TATP **02** for training and testing purposes in an ionic liquid matrix and pointed out that resublimed TATP **02** shows a higher impact (0.1 J) and friction sensitivity of (0.05 N) than the crude product from the aqueous synthesis (0.5 J, 0.2 N) that is stabilized by trace amounts of water. There exist six solid state polymorphs of TATP reported with crystal structures by Reany *et al.* [46] The resublimation of TATP **02** during storage enhances the risk of unintended detonation. Two isomers of TATP **02** have been separated by LC-NMR [47]. The synthesis of phase-pure TATP has been reported by *Peterson et al.*[48]. TATP **02** was synthesized in this work according to Milas *et al.*.[49] DADP **03** was synthesized according to Landenberger *et al*. [50]

TATP **02**: 3.14 mL 50% aqueous H_2O_2 solution (3.76 g, 0.11 mol) and 0.86 mL conc. H_2SO_4 (1.58 g, 0.016 mol) are mixed and cooled to 0 °C. 4.90 mL acetone (3.87 g, 0.07 mol) are added dropwise. After stirring the mixture at 0 °C for 3 h, it is extracted with 70 mL pentane. The pentane mixture is washed two times with 20 mL saturated ammonium sulfate solution and afterwards three times with 20 mL of water. The organic phase is dried over magnesium sulfate. After evaporation of the solvent a colorless solid is isolated. (2.07 g, 40%) [49]

^{1}H-NMR	($CDCl_3$, 400 MHz): δ = 1.45 (18 H), multiple minor conformer signals [47]
^{13}C-NMR	($CDCl_3$, 101 MHz): δ = 21.5 (CH_3), 107.7 (C_q).
EA	for $C_9H_{18}O_6$ calculated: C 48.63, H 8.18 %. found: C 48.73, H 8.26 %.
IR (ATR)	$\tilde{\nu}$ = 3005 (w), 2945 (w), 1600 (w), 1461 (w), 1376 (m), 1361 (m), 1274 (w), 1232 (m), 1200 (m), 1178 (s), 997 (w), 945 (m), 937 (m), 884 (s), 842 (m), 784 (m), 615 (m).
Raman	$\tilde{\nu}$ = 3012 (55), 3001 (54), 2948 (100), 10450 (30), 1372 (5), 1338 (6), 962 (48), 913 (50), 864 (60), 856 (48), 653 (7), 555 (61), 452 (28), 434 (30), 412 (28), 380 (8).
Melting Point	97-98 °C (determined with Buechi device, 5 °C min^{-1})

DADP **03**: 10 mL dichloromethane are cooled in an ice bath. 2.00 mL acetone (1.58 g, 0.03 mol) and 4.00 mL 30% aqueous H_2O_2 solution (4.44 g, 0.04 mol) are added. 4.00 mL concentrated perchloric acid (7.08 g, 0.07 mol) are added drop wisely and the mixture was stirred at 0 °C for 1 h. Afterwards the mixture is stored for three days at room temperature to allow complete conversion of TATP to DADP. The formed colorless precipitate is filtered off, washed with water and recrystallized from methanol. (0.23 g, 10%). [50]

^{1}H-NMR	($CDCl_3$, 400 MHz): δ = 1.35 (s, 6H), 1.79 (s, 6H)
^{13}C-NMR	($CDCl_3$, 101 MHz): δ = 20.7 (CH_3), 22.5 (CH_3), 107.7 (C_q)
EA	for $C_9H_{18}O_6$ calculated: C 48.63, H 8.18 %. found: C 48.24, H 8.13%.
IR (ATR)	$\tilde{\nu}$ = 3031 (w), 3000 (w), 2955 (w), 1603 (w), 1452 (w), 1374 (m), 1367 (m), 1284 (w), 1268 (m), 1198 (s), 1006 (w), 943 (m), 930 (m), 858 (m), 839 (w), 814 (m), 686 (m).
Raman	$\tilde{\nu}$ = 3053 (25), 3004 (100), 2980 (62), 1450 (18), 1417 (21), 1260 (17), 940 (23), 917 (19), 863 (64), 720 (65), 512 (8), 501 (58), 491 (22), 452 (10), 447 (9), 428 (17), 382 (53).
Melting Point	132-133 °C (determined with Buechi device, 5 °C min^{-1})

4.6.3 Ethyl Nitrate $EtONO_2$ 04

The first synthesis of ethyl nitrate $EtONO_2$ **04** was performed by *Feldhaus*[51] in 1863. One way was pouring a solution of potassium nitrite over a mixture of sulphuric acid and alcohol. The other way he suggested was that the mixture of sulphuric acid and alcohol was poured over solid potassium nitrite nuggets in the size of a walnut. In the framework of this thesis $EtONO_2$ 04 was synthesized according to a modified and downscaled way according to the instructions of *Gattermann*.[52] Ethyl nitrate is distilled from a mixture of nitric acid (65%, aq.), uranium nitrate and ethanol. The most important security aspect of this synthesis is that the nitric acid has to be saturated with uronium nitrate **24** before the ethanol is added. Otherwise an autocatalytic oxidation of ethanol occurs in which it is oxidized to acetaldehyde and acetic acid under exothermic conditions.

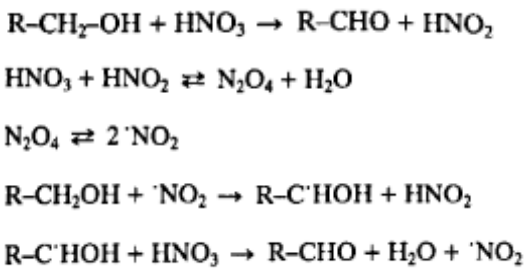

Figure 10: Suggested reaction pathway by Camera et al.[53]

This autocatalytic oxidation is induced by the formation of nitrous acid HNO_2. Nitrous acid reacts with nitric acid to nitrogen tetraoxide, which is in equilibrium with nitrogen dioxide. Nitrogen dioxide can react with the alcohol under the formation of nitrous acid. The resulting alcohol radical can react with nitric acid to an aldehyde and further nitrogen dioxide. (cf. *Figure 10*). This autocatalytic oxidation can be suppressed by the addition of urea to the mixture of sulphuric and nitric acid as it destroys nitrogen dioxide as shown in *Figure 11*. This reaction of nitrous acid with urea to gaseous nitrogen, carbon dioxide and water was investigated by *Lasalle et al.*[54].

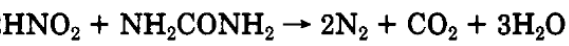

Figure 11: Reaction of nitrous acid with urea suggested by Lasalle et al.[54]

According to *Gattermann* the reaction mixture was distilled at ambient conditions at 130 °C oil bath temperature until no further raw product was obtained. After the washing steps NMR analysis showed that ethyl nitrate **10** was obtained pure (>99.9%) according to ^{1}H-NMR spectroscopy. In contrast to the literature recommendation, no dangerous second distillation was necessary. The lower explosion limit of ethyl nitrate **10** is 3.8 % by volume and it has a flash point of 10 °C.[55]

Uronium nitrate **27** (5.00 g, 40.63 mmol, 0.1 eq.) was stirred with nitric acid (21 mL, 29.40 g, 466.59 mmol, 1.3 eq., 65 %) at room temperature. After 5 minutes of stirring absolute ethanol (21 mL 16.57 g, 359.66 mmol, 1.0 eq.) was added. The solution was then distilled from the reaction mixture at an oil bath temperature of 130 °C, which was reached within one hour. The reaction is finished when the volume of the lower ethyl nitrate phase in the catching vessel remains constant. 34.50 g of the raw product, a colourless liquid, was washed with 3 x 20 mL of distilled water, sodium carbonate solution (0.50 g in 20 mL distilled water) and again with 2 x 20 mL distilled water. After drying over sodium sulphate 4.35 g (14 %) colourless liquid ethyl nitrate **10** were obtained and stored at -30 °C in a freezer under argon atmosphere.[52]

^{1}H-NMR	(400 MHz, Acetone-d_6) δ 4.58 (q, *J* = 7.1 Hz, H-1), 1.34 (t, *J* = 7.1 Hz, H-2).
^{13}C{^{1}H}-NMR	(101 MHz, Acetone-d_6) δ 70.7 (C-1), 12.4 (C-2)
^{15}N-NMR	(41 MHz, Acetone-d_6) δ -40.8 (t, *J* = 3.0 Hz, ONO_2)
IR (ATR)	$\tilde{\nu}$ = 2992 (w), 2944 (w), 2889 (w), 1618 (s), 1477 (w), 1447 (w), 1383 (w), 1367 (m), 1277 (s), 1157 (w), 1118 (w), 1091 (w), 1009 (m), 902 (m), 853 (s), 760 (m), 703 (w) cm^{-1}.
Raman	$\tilde{\nu}$ = 2981 (36), 2948 (100), 2881 (16), 2732 (8), 1629 (8), 1459 (1), 1449 (14), 1369 (8), 1281 (36), 1120 (13), 1093 (9), 1008 (1), 905 (3), 859 (27), 706 (4), 568 (23), 384 (27), 100 (56) cm^{-1}.

4.6.4 D-Mannitol Hexanitrate MHN 05

D-Mannitol Hexanitrate **05** was first synthesised by *Sobrero*[56],[57] in 1847. The so called *Nitromannit* **05** was received by pouring nitric and sulphuric acid on D-mannitol. The explosive properties were studied in 1879 by *Sokoloff* [58], who additionally improved the synthesis. In 1951 *Hayward et al.*[59] showed that pyridine causes a selective denitration of MHN **11** on the *C*-4 position. D-mannitol is a freely available polyalcohol. The synthesis was performed in this work several times according to the one of *Sokoloff*[58], which was stated by *Patterson and Todd*[60] with slight modifications. The best results were achieved when the reaction of D-mannitol and nitric acid was performed in a beaker and sulfuric acid was added as a precipitation agent in a volume slightly higher than the one of nitric acid. Pouring this viscous mixture into ice water led to a fine white precipitate of MHN **05**.

An investigation on the solubility of 50-60 mg of MHN **05** in various solvents was carried out in order to obtain measurable crystals. The best solubility was observed in acetone (45.8 g per litre), acetonitrile, dioxane, ethyl acetate, methanol, tetrahydrofuran, dichloromethane and tert-butyl-methyl ether. The solubility in benzene, trichloromethane, toluene and diethyl ether is poor and more than 5 ml of solvent were necessary to dissolve 50-60 mg of MHN **05**. The compound is insoluble in n-hexane and diisopropyl ether.

In a beaker nitric acid (15 mL, 22.69 g, 360.16 mmol, 21.9 eq., 100 %) was cooled below 0 °C by means of an acetone-ice cooling bath and D-mannitol (3.00 g, 16.47 mmol, 1.0 eq.) was added keeping the temperature below 0 °C. The obtained yellow suspension was stirred for 30 minutes while being cooled. This suspension was poured into a beaker and after adding sulfuric acid (16.5 mL, 96 %) a white viscous suspension was formed, which was poured into 300 mL ice water. A white precipitate was obtained and filtered off. It was washed with sodium carbonate solution (16.5 g in 300 mL distilled water) and with 300 mL of distilled water. 10.65 g of the wet product were recrystallized from boiling ethanol (35 mL). The fine white product was filtered off, washed with a small amount of ethanol (-30 °C cold) and dried in high vacuum (8×10^{-3} mbar) over night. 6.04 g (81 %) soft white needles of D-mannitolhexanitrate **5** were obtained and was stored at -30 °C in a freezer under argon atmosphere. [60]

^{1}H-NMR	(acetone-d_6, 400 MHz): δ = 6.33 – 6.23 (m, 1H, X-Part of $[ABMX]_2$), 6.12-6.04 (m, 1H, M-Part of $[ABMX]_2$), 5.29 (dd, *J* = 13.3, 3.3 Hz, 1H, H-1, H-6), 4.99 (dd, *J* = 13.3, 5.9 Hz, 1H, H-1, H-6).
^{13}C-NMR	(acetone-d_6, 101 MHz): δ = 77.6 (C-2, C-5), 77.1 (C-3, C-4), 69.4 (C-1, C-6).
^{15}N-NMR	(acetone-d_6, 41 MHz): δ = -47.8 (dd, *J* = 3.9, 3.0 Hz, N-1, N-6), -51.9 (d, *J* = 4.1 Hz, N-2, N-5), -53.2 – -54.6 (m, X-Part of AA'X, N-3, N-4).
EA	for $C_6H_8N_6O_{18}$ calculated: C 15.94, H 1.78, N 18.59 %; found: C 16.23, H 1.94, N 18.43 %.
IR (ATR)	$\tilde{\nu}$ = 3297 (w), 2981(m), 2916 (w), 2535 (w), 1677 (m), 1645 (s), 1637 (s), 1464 (m), 1378 (w), 1359 (w), 1340 (w), 1280 (s), 1271 (s), 1268 (s), 1224 (m), 1054 (w), 1042 (w), 1031 (m), 1001 (m), 963 (w), 930 (m), 860 (m), 826 (m), 749 (w), 733 (w), 701 (w), 681 (w) cm^{-1}.
Raman	$\tilde{\nu}$ = 3002 (16), 2976 (92), 2906 (14), 1681 (5), 1649 (31), 1467 (19), 1389 (7), 1356 (55), 1323 (13), 1302 (100), 1273 (4), 1235 (17), 1155 (12), 1092 (20), 1046 (5), 966 (5), 936 (8), 869 (99), 836 (8), 800 (4), 745 (9), 703 (31), 676 (16), 612 (18), 585 (8), 564 (7), 553 (10), 535 (27), 504 (6), 313 (22), 249 (5), 228 (96), 189 (34), 167 (5), 135 (34) cm^{-1}.
MS (CI)	m/z: 453.0 $[M+H^+]$
DSC	Melting: 107/109/111/113/119 °C Decomposition: 162/179/200/212/230 °C

Density (pycnometer)	1.784 g/cm³.

4.6.5 Ethyleneglycol Dinitrate EGDN 06

Ethylene glycol dinitrate EGDN **06** was synthesized first by *L. Henry*[61] in 1870 in a pure form. EGDN **06** was used to increase the freezing point of GTN **07** in order to improve the safety of dynamite during the winter months. It took until the 1930s for EDGN **06** to find commercial application.[62]

The synthesis of EGDN **06** was done according to the synthesis of NG **13**, but the reaction time was decreased to 1.5 hours. EGDN **06** is an oily colourless liquid which can be easily detonated, but it is not as sensitive as GTN **07**.[32]

Nitric acid (10 mL, 15.13 g, 240.10 mmol, 12.0 eq., 100 %) was stirred and cooled by means of an ice-salt cooling bath and sulfuric acid (5 mL, 96 %) was added. Afterwards ethylene glycol (1.24 g, 19.99 mmol, 1.0 eq.) was added dropwise keeping the temperature below 10 °C. Cooling and stirring was continued for 1.5 hours and the solution was then poured in 100 mL of ice water. A white oily liquid occurred at the bottom of the beaker. Most of the water above the oil was decanted and the remaining phase mixture was extracted with dichloromethane (15 mL). The organic phase was washed with 2 x 20 mL distilled water, potassium bicarbonate solution (1.33 g in 20 mL distilled water), 2 x 20 mL distilled water and once with 20 mL brine. After drying over sodium sulfate the solvent was removed with a rotary evaporator keeping the temperature of the water bath at room temperature. 0.88 g (29 %) of colourless liquid ethylene glycol dinitrate were obtained and stored at -30 °C in a freezer under argon atmosphere. [63]

^{1}H-NMR	(400 MHz, dmso-d_6) δ 4.87 (s, H-1, H-2)
^{13}C{^{1}H}-NMR	(101 MHz, dmso-d_6) δ 4.87 (s, H-1, H-2)
^{14}N-NMR	(29 MHz, dmso-d_6) δ -43 (s, ONO_2)
IR (ATR)	$\tilde{\nu}$ = 2900 (w), 1624 (s), 1455 (w), 1427 (m), 1391 (w), 1289 (m), 1265 (s), 1038 (m), 885 (m), 831 (s), 754 (m), 710 (w) cm^{-1}.
Raman	$\tilde{\nu}$ = 3014 (4), 2975 (100), 2893 (6), 2768 (2), 2731 (3), 1639 (13), 1514 (3), 1457 (9), 1429 (13), 1396 (7), 1371 (3), 1290 (85), 1238 (4), 1115 (8), 858 (51), 754 (2), 695 (7), 647 (9), 580 (6), 562 (64), 477 (9), 386 (3), 353 (1), 280 (9), 239 (4) cm^{-1}.

4.6.6 Glyceryl Trinitrate GTN 07

Glyceryl Trinitrate (GTN) **07** was first synthesized by the Italian *Ascanio Sobrero*[64] in 1846. He added glycerine to a mixture of nitric and sulphuric acid and obtained an olive-green liquid which was highly explosive. An accident with nitroglycerine caused severe injuries on Sobrero's face. Sobrero's student *Alfred Nobel*[65] found out accidentally that GTN **07** can be mixed with *Kieselgur* so that a less sensitive paste was received which he called dynamite. This mixture, which is called dynamite, could be transported without enormous hazards.[32] The hazard of transporting pure nitroglycerine is the guiding motif in the 1953 movie "The Wages of Fear". The first characterisation is mentioned in *Justus Liebigs, Annalen der Chemie* in 1848. In the following text excerpt (Figure 12) it is written that pure GTN **07** is a yellowish olive coloured oil without odour, but of spicy aromatic taste. A small amount on the tongue causes lasting migraine and S. [Sobrero] killed a dog with a small amount of it. The substance detonates upon heating".[64]

sie sich reinigen und über Schwefelsäure trocknen. Sie ist dann ein gelbes olivenfarbiges Oel ohne Geruch, von scharfem aromatischem Geschmack. Ein wenig davon auf die Zunge gebracht, erregt anhaltende Migräne und S. tödtete mit einer geringen Menge davon einen Hund. Beim Erhitzen detonirt diese Substanz.

Figure 12: Original text excerpt from Justus Liebigs Annalen der Chemie[64]

In this work the synthesis of GTN **07** was carried out according to *Urbanski and Witanowski*.[63] The nitration mixture was stirred strongly to generate a swirl at the surface. The glycerine was added and the temperature was kept below 10 °C. The intense stirring is necessary because otherwise a two-phase mixture of nitrosulfuric acid and glycerine is obtained. This two-phase state is quite dangerous as intense heating to 60°C was observed upon moving the reaction vessel. It may not be excluded that this might lead to a spontaneous detonation. Even with the highest stirring rates possible, no detonation of the reaction mixture was observed within five tries. The best yields and the highest level of safety is achieved if dichloromethane is used for the extraction of GTN **07** during its work up. In traditional syntheses GTN **07** is extracted as a pure substance. Besides the sensitivity of pure GTN **07**, it sticks to the separation equipment and separation problems occur. Furthermore, the dichloromethane solution can be efficiently dried with sodium sulfate. The dichloromethane can be evaporated at room temperature and about 20 mbar pressure using a rotary evaporator. During this, the flask with the dichloromethane/GTN **07** solution has to be in touch with room temperature water. Otherwise GTN **07** may freeze out during the evaporation of dichloromethane and might become even more sensitive.

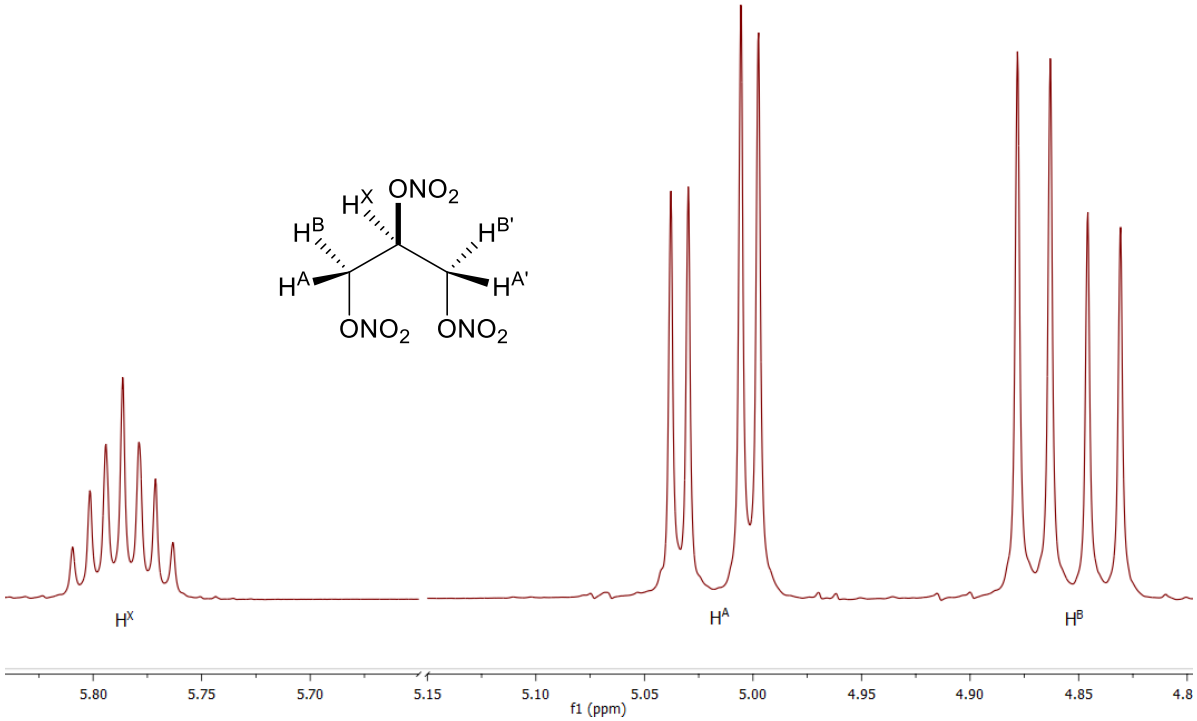

Figure 13: ^{1}H-NMR of GTN 07 in DMSO-d_6 at 400.18 MHz.

The ^{1}H-NMR spectrum of GTN **07** is shown in *Figure 13*. It consists of a triplet of triplet at 5.79 ppm (H_X) and two duplets of duplets at 5.02 ($H_{A/A'}$) and 4.85 ppm ($H_{B/B'}$). $H_{A/A'}$ and $H_{B/B'}$ were allocated according to the *Karplus*[66] relation with respect to their coupling constants to H^X. A strong coupling constant of 12.9 Hz is observed between the prochiral protons $H^{A/A'}$ and $H^{B/B'}$. Prochirality means that if one of

the two “prochiral” protons is substituted, a chiral centre would be formed. The splitting-key of the pseudo-septett signal of H^X is shown in *Figure 14.* The signals intensities are clearly different to the ones of a septet, which would be 1-6-15-20-15-6-1. Due to these facts the proton spin system of GTN **07** is AA’BB’X.

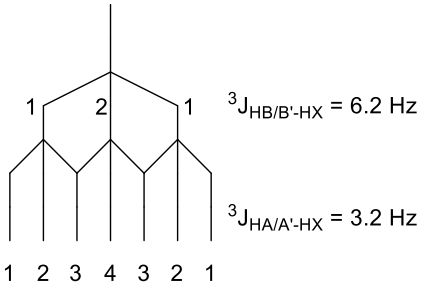

Figure 14: Splitting-key of the pseudo-septett from NG 13

Sulfuric acid (6 mL, 96 %) and nitric acid (4 mL, 6.05 g, 96.04 mmol, 6.4 eq., 100 %) were stirred so that a swirl at the surface occurred and cooled below 0 °C by means of an ice-salt cooling bath. Glycerine (1.38 g, 14.99 mmol, 1.0 eq.) was added dropwise using a syringe without cannula which was weighed before and after the addition. The temperature was kept below 10 °C. For three hours the temperature was kept below 10 °C under permanent stirring. The two phase mixture was poured into 150 mL ice water and dichloromethane (30 mL) was added. The organic phase was separated and washed with 3 x 30 mL distilled water, sodium bicarbonate solution (1.21 g in 30 mL distilled water), 2 x 30 mL distilled water and 30 mL brine. After drying over sodium sulfate the organic phase was filtered off and the solvent was evaporated with a rotary evaporator placing the flask in room temperature water. 2.56 g (75 %) colorless liquid nitroglycerine **13** were obtained and stored at -30 °C under an argon atmosphere.[64],[63]

^{1}H-NMR[67]	(400 MHz, Acetone-d_6) δ 5.89 (tt, *J* = 6.2, 3.4 Hz, H-2), 5.13 (dd, *J* = 13.0, 3.4 Hz, H-1,H-3), 4.95 (dd, *J* = 13.0, 6.2 Hz, H-1’, H-3’)
^{13}C{^{1}H}-NMR	(101 MHz, Acetone-d_6) δ = 76.78 (C-2), 70.07 (C-1,C-3).
^{15}N-NMR	(41 MHz, Acetone-d_6) δ -46.62 (dd, *J* = 3.8, 3.0 Hz, N-1, N3), -49.03 (d, *J* = 3.5 Hz, N-2).
IR (ATR)	$\tilde{\nu}$ = 3024 (w), 1986 (w), 2911 (w), 2552 (w), 1630 (s), 1455 (w), 1427 (m), 1393 (w), 1352 (w), 1292 (m), 1264 (s), 1086 (w), 1052 (w), 1006 (m), 899 (m), 822 (s), 749 (m), 701 (w) cm^{-1}.
Raman	$\tilde{\nu}$ = 2976 (66), 2914 (3), 2899 (5), 2859 (7), 1655 (11), 1459 (7), 1431 (4), 1395 (4), 1353 (5), 1293 (53), 857 (32), 682 (5), 634 (3), 590 (6), 556 (9), 456 (1), 238 (8), 98 (100) cm^{-1}.
DSC	Decomposition: 140/167/185/210/226 °C
IS	1 J (liquid).
FS [N]	> 360 N (liquid).
ESD [J]	not measurable with liquids.

4.6.7 *meso*-Erythritol Tetranitrate ETN 08

The first synthesis of *meso*-erythritol tetranitrate **08** was described by *Stenhouse*[68] in 1849. He did research on lichen and the acids they are containing. *Stenhouse* solved the so called Erythromannit in fuming nitric acid and after the cooling of the mixture sulfuric acid was added. Flat crystals like the ones of benzoic acid were obtained after crystallizing it from spirit of wine.

The freely available starting material *meso*-erythritol can be easily purchased as sweetener. *Oxley et al.*[69] and *Matyas et al*.[70] investigated the analytical and energetic material properties of *meso*-erythritol tetranitrate (ETN, **08**). *Manner et al.* [71] published a crystallographic study of **08** in 2014.

The performed synthesis is a slight modification of that stated by *Oxley et al.*[69b]. *Meso*-erythritol was not dissolved in sulfuric acid, but was directly dissolved in the nitrosulfuric acid. Furthermore the crude product was not recrystallized from methanol, but from ethanol.

It was tried to obtain different polymorphs of *meso* -erythritol tetranitrate **08** in various solvents. The best solubility was achieved with acetone (35.6 g per litre), acetonitrile, dioxane, ethyl acetate, methanol, tetrahydrofuran, dichloromethane, tert-butyl ethyl ether and diethyl ether. It was also soluble in benzene, trichloromethane, toluene, n-hexane and diisopropyl ether. The best measurable crystals were obtained by evaporation from ethanol or benzene solution.

Nitric acid (19 mL, 28.75 g, 456.20 mmol, 13.9 eq. 100 %) was added to sulfuric acid (17 mL, 96 %) while being stirred and cooled to 0 °C by means of an ice-salt cooling bath. The temperature rose to 10 °C when D-erythritol (4.00 g, 32.75 mmol, 1.0 eq.) was added. Afterwards the solution was heated to 40 °C and stirred for one hour before it was poured on 200 mL ice water. The obtained white precipitate was washed with distilled water, sodium carbonate solution (0.70 g solved in 25 mL distilled water) and again with distilled water. After drying under suction for 20 minutes 8.17 g of raw product were recrystallized from ethanol (20 mL) at 55 °C. The white crystalline product was filtered off and dried in high vacuum ($1x10^{-2}$ mbar) over night. 6.60 g (67 %) ETN **4** were obtained and stored at -30 °C in a freezer under an argon atmosphere. [69b]

^{1}H-NMR	(400 MHz, Acetone-d_6) δ 6.03 – 5.97 (m, 2H, X-Part of $[ABX]_2$), 5.27 – 5.19 (m, 2H, A-Part of $[ABX]_2$), 5.04 – 4.95 (m, 2H, B-Part of $[ABX]_2$).
^{13}C{^{1}H}-NMR	(acetone-d_6, 101 MHz): δ 68.7 (2C, *C*-1, *C*-4), 76.5 (2C, *C*-2, *C*-3) ppm.
^{15}N-NMR	(acetone-d_6, 41 MHz): δ -47.2 (dd, *J* = 3.9, 2.9 Hz, N-1, N-4), -51.1 (m, N-2, N-3, X-Part of AA'X).
EA	for $C_4H_6N_4O_{12}$ calculated: C 15.90, H 2.00, N 18.55 %; found: C 16.00, H 2.00, N 18.26 %.
IR (ATR)	$\tilde{\nu}$ = 3293 (w), 2978 (w), 2911 (w), 2555 (w), 1746 (w), 1656 (s), 1648 (s), 1631 (s), 1512 (w), 1488 (w), 1455 (m), 1375 (m), 1339 (w), 1294 (m), 1286 (m), 1277 (s), 1258 (s), 1228 (m), 1058 (m), 1032 (m), 982 (m), 918 (m), 872 (m), 827 (s), 754 (m), 740 (m), 696 (m) cm^{-1}.
Raman	$\tilde{\nu}$ = 3020 (19), 2980 (87), 2897 (9), 1673 (7), 1649 (17), 1632 (10), 1512 (2), 1488 (2), 1457 (25), 1386 (9), 1371 (5), 1358 (15), 1311 (15), 1297 (100), 1281 (5), 1270 (8), 1163 (9), 1085 (15), 1053 (5), 928 (3), 899 (6), 870 (71), 844 (5), 835 (15), 774 (8), 700 (45), 634 (17), 589 (20), 565 (58), 373 (5), 282 (16), 242 (18), 228 (82), 183 (22), 113 (7) cm^{-1}.
DSC	Melting: 56/59/62/65/71 °C Decomposition: 144/170/182/191/210 °C

4.6.8 Pentaerythritol Tetranitrate PETN 09

PETN **09** was first synthezised in 1894 through an esterification of pentaerythritol with nitric acid by the company Rheinisch-Westfälischen-Sprengstoff-AG[72]. Pentaerythritol was synthesized by Tollens and Wigand[73] in 1891 performing an alkaline condensation of acetaldehyde and formaldehyde. PETN **09** is used as one of the main components besides RDX **19** in the plastic explosive Semtex[74]. Pentaerythritol tetranitrate is still in use as a booster explosive being appreciated for its readiness for detonation and high detonation pressure.

PETN **09** can be synthesized with a mixture of nitric and sulphuric acid under permanent stirring and cooling. In the framework of this thesis PETN **09** was synthesised in analogy to a procedure by Barros.[75]

In the research group of Prof. Klapötke a synthesis using in situ generated acetyl nitrate was developed by *Stefanie Schedlbauer*. It is better in terms of product purity.

Roberts and Dinegar[76] researched the solubility of PETN **09** in acetone, ethyl acetate, benzene and ethanol. It turned out that bigger crystals are obtained when recrystallizing PETN **09** from ethanol instead of precipitating it from acetone by addition of water.

Acetic acid anhydride (10.0 ml, 107 mmol) was cooled down to 0 °C. Afterwards nitric acid (2.00 ml, 44.1 mmol, 100%) and glacial acetic acid (2.00 ml, 33.1 mmol) were added slowly. The solution was stirred at 0 °C for 30 minutes. Pentaerythritol (1.00 g, 7.35 mmol) was dissolved in the nitrating medium and stirred for 4 hours at 0 °C. The mixture was brought to ambient temperature and stirred for 12 hours. Subsequently the suspension was diluted with ice-water (250 ml) and stirred for 30 minutes. A white precipitate was obtained. It was filtered off, washed with water and $NaHCO_3$-solution (5.00 g $NaHCO_3$ in 200 ml water). After drying at ambient temperature the raw product (2.12 g) was recrystallized from ethanol (100 ml). The solution was stored in a fridge at 4 °C for 16 hours. Then the colorless needles were filtered off, washed with cold ethanol and dried in a desiccator *in vacuo* yielding 1.96 g (6.20 mmol, 84%) of white crystalline pentaerythritol tetranitrate **6**.

^{1}H-NMR	(400 MHz, dmso-d_6) δ 4.70 (s, H-1, H-3, H-4, H-5)
^{13}C-NMR	(101 MHz, dmso-d_6) δ 40.8 (C-2), 70.3 (C-1, C3, C-4, C-5)
^{14}N-NMR	(29 MHz , dmso-d_6) δ -45 (s, N-1, N-3, N-4, N-5)
EA	for $C_5H_8N_4O_{12}$ calculated: C 19.00, H 2.55, N 17.72 %; found: C 19.18, H 2.49, N 17.54 %.
IR (ATR)	$\tilde{\nu}$ = 3273 (w), 3021 (w), 2983 (w), 2905 (w) 2551 (w), 1740 (w), 1638 (s), 1506 (w), 1471 (m), 1394 (w), 1383 (w), 1304 (m), 1282 (s), 1267 (s), 1193 (w), 1035 (m), 998 (m), 937 (w), 895 (w), 840 (m), 835 (m), 752 (m), 745 (m), 701 (m) cm^{-1}.
Raman	$\tilde{\nu}$ = 3024 (46), 2985 (100), 2917 (22), 2764 (3), 1671 (7), 1660 (23), 1628 (8), 1509 (4), 1469 (31), 1403 (13), 1292 (98), 1275 (8), 1251 (23), 1193 (7), 1043 (22), 1004 (5), 938 (10), 873 (52), 838 (2), 746 (6), 704 (5), 676 (12), 624 (61), 589 (24), 539 (23), 459 (9), 322 (4), 278 (12), 259 (7), 228 (43) cm^{-1}.
MS (CI)	m/z: 317.1 [$(C_5H_8N_4O_{12} + H^+)^+$].
DSC	Melting: 132/138/140/144/150 °C Decomposition: 143/157/176/192/214 °C
Density (pycnometer)	1.750 g/cm³

4.6.9 2-Diazonium-4,6-dinitrophenolate DDNP 10

The first synthesis of 2-Diazonium-4,6-dinitrophenolate DDNP **10** as it is shown was performed by *Griess* [77],[78] in 1858 to obtain the first ever-synthesized diazonium compound. It was obtained by heating a solution of pure picramic acid to 50 °C and introducing a stream of gaseous nitrous acid. With rising temperature the color of the solution changed from red to yellow. Performing this procedure for some time led to a yellow crystalline precipitate which was recrystallized several times from alcohol. A brass- to gold-coloured precipitate was obtained which was DDNP **10**. The explosive character of the compound was reported in 1892 by *Lenze*.[79]

DDNP **10** is an important primary explosive. It has been reviewed twice by *Clark* [79] in 1933 and in a book-chapter by Matyas [80]. It is used in blasting caps and detonators, where it has replaced amongst lead azide the former used mercury fulminate.[57] According to the review of *Clark*[79] it is stable over a long period of time when exposed to diffused light, but rapidly lost its power when exposed to direct sunlight. As mentioned by *Hagel and Redecker*[81],[82], employees of the *Dynamit Nobel AG,* DDNP **10** is used in the primer composition Sintox.

The drawbacks of DDNP **10** are its flaws in terms of photosensitivity and low thermal stability and that it can be dead-pressed. [80] Most recently new isomers and derivatives of DDNP **10** were developed in our workgroup that outperform DDNP **10** [83],[84],[83] and have drawn the attention of the amateur chemist scene resulting in the illegal synthesis of 4-Diazonium-2,6-dinitrophenolate from the ubiquitious pain and fever medication Acetaminophen. [85] DDNP **10** was used as primary explosive in the bomb attack carried out by Anders Behring Breivik. (cf. section 4.1).

DDNP **10** was synthesised in the framework of this thesis according to the synthesis of the amateur chemist Megalomaniac[86] which is a detailed version similar to *Method A* in the review of *Clark*[79], who performed a related synthesis to *Abel*[87] and *Newdon*[88]. We experienced problems with the purity of the product. A recrystallization is difficult due to the intense dark red color of DDNP **10** solutions. We decided to use an excess of sodium nitrite to generate the byproduct picric acid which is better soluble in water than picramic acid and can be washed out from the final product resulting in a purity of > 99 % by ^{1}H-NMR. The remaining picramic acid is most probably included in the DDNP **10** particles since the diazotation is a heterogeneous reaction with a suspension of picramic acid in water.

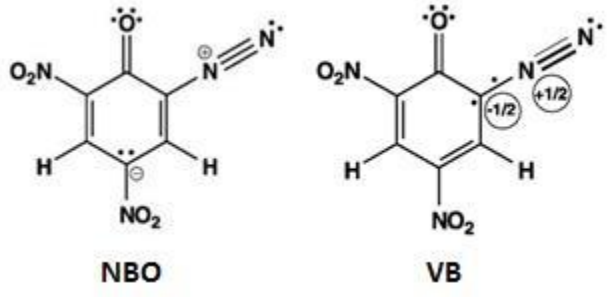

Figure 15: Optimized Lewis structures according to natural bond orbital (NBO) and increased valence bond (VB) analysis of DDNP 10 [89]

The electronic structure of DDNP **10** has been discussed by *Holl et al.*.[89] A NBO analysis (DFT density) was performed to obtain the best standard *Lewis* structure. The results of natural bond orbital and increased valence bond analysis are depicted in Figure 15. The increased valence bond structure stands in better agreement with the X-Ray structure and the formal charges are located closer to each other.

Picramic acid **41** (0.24 g, 1.21 mmol, 1.0 eq.) was suspended in hydrochloric acid (3 mL, 5 %; 5 mL 37 % hydrochloric acid was filled up to 36 mL with distilled water) while being stirred and cooled by means of an ice-salt cooling bath. Sodium nitrite (0.13 g, 1.88 mmol, 1.6 eq.) was dissolved in distilled water

(2.5 mL) and added. Light was excluded with aluminium foil and the ice-salt cooling bath removed. The mixture was stirred for one hour at room temperature. After filtration the remaining solid was washed with 25 mL distilled water and dried over orange gel *in vacuo* over night. 0.16 g (63 %) brown to orange coloured powder of 2-Diazonium-3,5-dinitrophenolate **15** were obtained. [79],[86]

^{1}H-NMR	(DMSO-d_6, 400 MHz): δ = 8.87 (9.34 (d, *J* = 3.2 Hz, 1H, H-5), 8.85 (d, *J* = 3.2 Hz, 1H, H-3) ppm.
^{13}C-NMR	(DMSO-d_6, 101 MHz): δ = 99.5 (C-2), 129.2(C-4), 130.6(C-3), 134.7 (C-5), 140.7(C-6), 164.4 (C-1) ppm.
^{15}N-NMR	(DMSO-d_6, 29 MHz): δ = -16.9 (d, J = 3.2 Hz, NO_2-6), -19.1 (t, J = 1.8 Hz, NO_2-4), -44.7 (s, diazonium terminal), -141.9 (d, J = 3.2 Hz, diazonium C-bound) ppm.
EA	for $C_6H_2N_4O_5$ calculated: C 34.30, H 1.36, N 26.67 %; found: C 34.56, H 1.10, N 26.72 %.
IR (ATR)	$\tilde{\nu}$ = 3098 (w), 2309 (w), 2195 (m), 1694 (w, b), 1631 (s), 1571 (w), 1556 (m), 1519 (m), 1414 (m), 1364 (m), 1351 (m), 1317 (s), 1277 (s), 1156 (m), 1092 (w), 1071 (m), 1044 (w), 938 (w), 921 (w), 906 (m), 826 (w), 788 (w), 774 (w), 737 (m), 723 (w), 707 (m), 673 (w) cm^{-1}.
Raman	Detonation during the measurement.
DTA	Decomposition: 150/163/169/177/196 °C

4.6.9.1 DDNP Precursor Picramic Acid

Picramic acid (2-Amino-4,6-dinitrophenolate) was used for Benedict's blood sugar determination around 1918 and is a precursor material for DDNP **10**. Due to the shortage of picric acid **11** after World War I *Egerer*[90] searched a method for the synthesis of picramic acid **41** that gives better yields than previous procedures. She criticised the methods stated by *Girard*[91] and *Lea*[92] in terms of purity and yields.

In the framework of this thesis a downscaled synthesis according to *Egerer*[90] was executed.

Picric acid **16** (10.01 g, 43.69 mmol, 1.0 eq.) was dissolved in ethanol (150 mL) and heated to 50 °C during permanent stirring. A concentrated ammonia solution (63 mL, 55.43 g, 158.19 mmol, 3.6 eq.) was added and the mixture was allowed to cool itself to 30 °C. Hydrogen sulfide gas was bubbled in the mixture for one hour. During the addition the temperature was allowed to reach 50 °C for 15 minutes and was then cooled to 0 °C by means of an ice-salt cooling bath. The excess of hydrogen sulfide gas was introduced into a potassium hydroxide solution for its disposal. The mixture was filtered off after 45 minutes of stirring at 0 °C and the precipitate was suspended in acetic acid (30 mL, 20 %) for five minutes. This suspension was filtered again and washed two times with 10 mL distilled water. 12.06 g of wet precipitate was divided up to two batches. Each batch of about 6.00 g was dissolved in 1.5 litres boiling distilled water and the resulting dark red solution was filtered while being hot. The solutions were kept in a fridge overnight and the product was filtered off and dried in a desiccator over orange gel *in vacuo* overnight. 4.48 g (51 %) of red glittering picramic acid were obtained.[90]

^{1}H-NMR	(DMSO-d_6, 400 MHz): δ = 7.56 (s, NH_2), 7.65 (d, J = 3.0 Hz, 1H, C-H), 7.93 (d, J = 3.0 Hz, 1H, C-H) ppm.
^{13}C-NMR	(DMSO-d_6, 101 MHz): δ = 108.7, 111.0, 134.4, 137.8, 140.0, 147.3 ppm.
^{15}N-NMR	(DMSO-d_6, 41 MHz): δ = -12.2 (d, J = 2.5 Hz, NO_2-6), -13.5 (pseudo-t, J = 2.1 Hz, NO_2-4), -323.1 (s, NH_2) ppm.
EA	for $C_6H_5N_3O_5$ calculated: C 36.19, H 2.53, N 21.10 %; found: C 36.24, H 2.49, N 20.84 %.
IR (ATR)	$\tilde{\nu}$ = 3595 (w), 3466 (m), 3373 (s), 3242 (m), 3119 (m), 3104 (m), 3071 (m), 2841 (m), 2634 (m), 2420 (m), 2285 (m), 1635 (m), 1614 (m), 1593 (m), 1548 (s),

	1513 (m), 1476 (m), 1440 (m), 1400 (w), 1335 (s), 1299 (s), 1230 (m), 1139 (m), 1107 (m), 1063 (m), 992 (m), 932 (w), 893 (w), 878 (w), 854 (w), 815 (w), 802 (w), 770 (w), 734 (w), 723 (w), 709 (w), 672 (w) cm^{-1}.
Raman	$\tilde{\nu}$ = 3380 (3), 3082 (2), 2576 (2), 2413 (2), 2172 (2), 2158 (2), 2137 (2), 1613 (6), 1595 (3), 1543 (3), 1517 (6), 1479 (2), 1448 (3), 1400 (30), 1344 (100), 1298 (8), 1251 (7), 1155 (5), 1112 (1), 1067 (7), 996 (3), 936 (5), 882 (1), 809 (19), 771 (1), 653 (1), 554 (1), 483 (7), 432 (1), 380 (3), 355 (6), 268 (1), 237 (3) cm^{-1}.
MS (DEI+)	m/z: 199.2 [$(C_6H_5N_3O_5)^+$].
DSC	Melting: 161/169/170/173/180 °C Decomposition: 184/201/223/239/257 °C
Density (pycnometer)	1.652 g/cm³.

4.6.10 Picric Acid PA 11

The synthesis of pure picric Acid **11** was first reported by the British chemist *Peter Woulfe*[93] in 1771. He investigated the reaction of nitric acid on indigo. The industrial production of picric acid **11** by nitrating phenol is described by *Olsen and Goldstein*[94] in 1924. The French scientist *Eugene Turpin*[57] patented a melt casting process for picric acid **11**. With this procedure it could be filled in artillery shells as high explosive filling. After the French started this, the British also used picric acid **16** as a melt-cast explosive and called it *Lyddite*[57],[93]. The British tested it in Lydd near Kent and used it later in high quantities during *World War I*. Using picric acid **16** together with metals is highly dangerous. Due to its high acidity picric acid **16** is able to form salts with metals, the so called picrates. These picrates are even more sensitive than picric acid **16** itself and led to many accidents in the past.[32] Picric acid **11** has a pK_a value of 0.40[95],[96] in water which underlines its strong acidity.

Anders Behring Breivik synthesized picric acid **11** from acetylsalicylic acid (cf. section 4.1) as a booster explosive.

It should be mentioned that picric acid **16** can be easily synthesized from *Aspirin®*. This reaction way was stated by an amateur chemist on his website.[97]

^{1}H-NMR[98]	(DMSO-d_6, 400 MHz): δ = 8.60 (s, 2H, *H*-3, *H*-5), 11.81 (s, 1H, OH) ppm.
^{13}C-NMR[98]	(DMSO-d_6, 101 MHz): δ = 125.4 (2C, *C*-3, *C*-5), 125.6 (1C, *C*-4), 141.9 (2C, *C*-2, *C*-6), 160.2 (1C, *C*-1) ppm.
^{14}N-NMR	(DMSO-d_6, 29 MHz): δ = -12 ppm.
EA	for $C_6H_3N_3O_7$ calculated: C 31.45, H 1.32, N 18.34 %; found: C 31.74, H 1.44, N 18.45 %.
IR (ATR)	$\tilde{\nu}$ = 3102 (m), 2869 (w), 2273 (w), 1859 (w), 1629 (s), 1606 (s), 1524 (s), 1462 (m), 1428 (m), 1339 (s), 1312 (s), 1261 (m), 1176 (m), 1149 (m), 1086 (m), 955 (w), 939 (w), 917 (m), 832 (w), 804 (w), 782 (w), 753 (w), 727 (m), 702 (m) cm^{-1}.
Raman	$\tilde{\nu}$ = 3109 (2), 2680 (1), 2285 (1), 1634 (9), 1612 (4), 1563 (5), 1530 (17), 1346 (100), 1280 (18), 1179 (15), 1090 (3), 943 (11), 922 (1), 832 (25), 785 (1), 741 (1), 706 (2), 544 (1), 402 (3), 350 (3), 329 (6), 209 (2) cm^{-1}.
DTA	T_{melt}: 113/120/128/133/138 °C T_{dec-1}: 180/235/256/2262/265 °C T_{dec-2}: 265/257/290/303/334 °C
Density (pycnometer)	1.748 g/cm³.

4.6.11 The Mononitrotoluenes 2-MNT 12, 3-MNT 13 and 4-MNT 14.

The mixed acid nitration of toluene yields a mixture of 55-60 % 2-Nitrotoluene (2-MNT, **12**), 3-4 % 3-Nitrotoluene (3-MNT, **13**) and 35-40% 4-Nitrotoluene (4-MNT, **14**). [99] This mixture is an intermediate of the stepwise nitration of toluene to the explosive 2,4,6-trinitrotoluene (2,4,6-TNT, **17**), which is a medium performance energetic material that was developed at the end of the 19th century. Nonetheless, TNT **17** has never lost its application in the explosive industry being appreciated for its melt cast processability. The mononitroluenes **12**-**14** are also used for the industrial synthesis of agricultural, rubber and dye chemicals and their toxicity towards mice has been demonstrated.[100] In Germany all nitrotoluenes **12**-1**4** are classified as toxic and cancerogenic [101], yet they were identified as environmental contaminants in soil and groundwater in multi-ton amounts. [99, 102] According to the Montreal Convention on the Marking of Plastic Explosives for Detection [10], 2-MNT **1** or 4-MNT **3** have to be integrated amongst two alternative compounds as detection aid agents, so-called taggants, in commercial formulations of explosives with a vapor pressure lower than 0.1 mPa.

2-MNT **12**:

^{1}H-NMR[103]	(DMSO-d_6, 400 MHz): δ = 2.50 (s, 3H, CH_3), 7.40-7.52 (m, 2H, *H*-4, *H*-6), 7.62 (td, 1H, J = 7.5, 1.3 Hz, H-5), 7.95 (dd, 1H, J = 8.2, 1.3 Hz, *H*-3)
^{13}C-NMR[103]	(DMSO-d_6, 101 MHz): δ = 19.4 (CH_3), 124.2 (*C*-3), 127.3 (*C*-4), 132.6 (C-6), 132.7 (*C*-5), 133.3 (*C*-1), 149.0 (*C*-2) ppm.
^{14}N-NMR	(DMSO-d_6, 29 MHz): δ = -5 ppm.
EA	for $C_7H_7NO_2$ calculated: C 61.31, H 5.14, N 10.21 %; found: C 61.16, H 5.14, N 10.19 %.
IR (ATR)	$\tilde{\nu}$ = 3071 (w), 2976 (w), 2933 (w), 2857 (w), 1612 (m), 1578 (w), 1517 (s), 1482 (m), 1460 (m), 1429 (w), 1323 (w), 1342 (s), 1305 (m), 1277 (w), 1202 (w), 1163 (w), 1149 (w), 1083 (w), 1050 (w), 1037 (w), 955 (w), 857 (m), 786 (m), 725 (s), 688 (w), 664 (m) cm^{-1}.
Raman	$\tilde{\nu}$ = 3158 (1), 3076 (37), 3033 (3), 2977 (4), 2936 (32), 2869 (1), 2748 (3), 2615 (2), 1613 (8), 1580 (33), 1524 (12), 1483 (3), 1430 (2), 1385 (10), 1346 (100), 1279 (2), 1203 (20), 1164 (13), 1150 (5), 1085 (6), 1052 (49), 998 (3), 859 (15), 793 (61), 732 (1), 666 (13), 566 (6), 539 (12), 476 (2), 387 (5), 352 (1), 230 (9), 151 (23), 113 (4) cm^{-1}.
DSC	Boiling: 197/232/236/239/251 °C
Density (pycnometer)	1.159 g/cm³.

3-MNT **13**:

^{1}H-NMR [104]	(DMSO-d_6, 400 MHz): δ 2.41 (s, 3H, CH_3), 7.52 (t, *J* = 7.8 Hz, 1H, H-5), 7.62 (d, *J* = 7.6 Hz, 1H, H-6), 7.94 – 8.04 (m, 2H, H-2, H-4).
^{13}C-NMR[105]	(DMSO-d_6, 101 MHz): δ = 20.5 (1C, CH_3), 120.4 (1C, *C*-4), 123.4 (1C, *C*-2), 129.5 (1C, *C*-5), 135.8 (1C, *C*-6), 139.9 (1C, *C*-1), 147.7 (1C, *C*-3) ppm.
^{14}N-NMR	(DMSO-d_6, 29 MHz): δ = -10 ppm.
EA	for $C_7H_7NO_2$ calculated: C 61.31, H 5.14, N 10.21 %; found: C 61.29, H 5.18, N 10.17 %.
IR (ATR)	$\tilde{\nu}$ = 3070 (w), 2927 (w), 2865 (w), 1585 (w), 1561 (w), 1521 (s), 1480 (m), 1381 (w), 1344 (s), 1315 (m), 1289 (w), 1215 (w), 1166 (w), 1096 (w), 1081 (w), 1043 (w), 1003 (w), 926 (w), 905 (w), 881 (w), 799 (m), 726 (m), 671 (m) cm^{-1}.
Raman	$\tilde{\nu}$ = 3072 (13), 3036 (1), 2927 (12), 2869 (1), 2744 (1), 2691 (1), 1622 (2), 1586 (19), 1529 (6), 1383 (3), 1348 (100), 1291 (2), 1217 (12), 1167 (3), 1097 (7), 1005 (27), 907 (1), 802 (25), 673 (9), 510 (4), 397 (4), 358 (4), 227 (4), 172 (8), 113 (1) cm^{-1}.
DTA	Boiling: 223/243/278/280/295 °C

Density (pycnometer)	1.157 g/cm³.

4-MNT **14**:

^{1}H-NMR[103],	(DMSO-d_6, 400 MHz): δ = 2.41 (s, 3H, CH_3), 7.39-7.46 (m, 2H, H-2, H-6), 8.05-8.11 (m, 2H, H-3, H-5) ppm.
^{13}C-NMR[103]	(DMSO-d_6, 101 MHz): δ = 21.0 (1C, CH_3), 123.2 (2C, *C*-3, *C*-5), 130.1 (2C, *C*-2, *C*-6), 145.6 (1C, *C*-1), 146.3 (1C, *C*-4) ppm.
^{14}N-NMR	(DMSO-d_6, 29 MHz): δ = -10 ppm.
EA	for $C_7H_7NO_2$ calculated: C 61.31, H 5.14, N 10.21 %; found: C 61.41, H 5.17, N 10.20 %.
IR (ATR)	$\tilde{\nu}$ = 3107 (w), 3081 (w), 2933 (w), 2841 (w), 2444 (w), 2294 (w), 1935 (w), 1804 (w), 1722 (w), 1699 (w), 1673 (w), 1596 (m), 1562 (w), 1505 (s), 1467 (m), 1421 (w), 138 (w), 1366 (w), 1339 (s), 1295 (m), 1212 (w), 1179 (m), 1043 (w), 1017 (w), 971 (w), 961 (w), 858 (m), 834 (m), 785 (w), 736 (m), 684 (w) cm^{-1}.
Raman	$\tilde{\nu}$ = 3110 (1), 3077 (11), 3060 (3), 2924 (9), 2674 (1), 2447 (1), 1598 (27), 1516 (6), 1496 (3), 1380 (5), 1340 (100), 1213 (7), 1180 (2), 1108 (23), 861 (21), 787 (5), 635 (9), 521 (1), 364 (6), 296 (3), 174 (4), 109 (3) cm^{-1}.
MS (DEI+)	m/z: 137.1 [$(C_7H_7NO_2)^+$].
DSC	Melting: 50/51/52/55/66 °C Boiling: 218/234/235/238/244 °C
IS	> 40 J (< 100 µm).
Density (pycnometer)	1.293 g/cm³.

4.6.12 The Dinitrotoluenes 2,4-DNT 15 and 2,6-DNT 16

2,4-Dinitrotoluene (2,4-DNT **15**) and 2,6-dinitrotoluene (2,6-DNT **16**) are possible intermediates of the synthesis of TNT **17**. Both compounds are produced as a mixture of technical grade DNT, containing 76% 2,4-DNT **15** and 19% 2,6-DNT **16**. DNT is used for the production of toluene diisocyanate, urethane polymers, auto airbags, dyes and explosives including TNT **17**. [106] 2,6-DNT exists in two crystal polymorphs that can be obtained by recrystallization from benzene (T_{melt}: 54.6 °C) and resolidification from the melt (T_{melt}: 66 °C). [107]

2,4-DNT **15**:

^{1}H-NMR[108]	(DMSO-d_6, 400 MHz): δ = 2.62 (s, 3H, CH_3), 7.79 (d, J = 8.5 Hz, 1H, *H*-5), 8.42 (dd, J = 8.7, 2.5 Hz, 1H, *H*-6), 8.68 (d, J =2.5 Hz, 1H, *H*-3) ppm.
^{13}C-NMR[109]	(DMSO-d_6, 101 MHz): δ = 19.6 (CH_3), 119.6 (C-3), 127.2 (*C*-5), 134.3 (*C*-6), 140.3 (*C*-1), 145.9 (*C*-4), 148.7 (*C*-2) ppm.
^{14}N-NMR	(DMSO-d_6, 29 MHz): δ = -12 ppm.
EA	for $C_7H_6N_2O_4$ calculated: C 46.16, H 3.32, N 15.38 %; found: C 46.06, H 3.50, N 15.32 %.
IR (ATR)	$\tilde{\nu}$ = 3102 (m), 3083 (m), 2988 (w), 2865 (w), 2734 (w), 1948 (w), 1818 (w), 1606 (m), 1519 (s), 1453 (m), 1439 (w), 1393 (w), 1382 (w), 1344 (s), 1268 (w), 1201 (w), 1152 (m), 1132 (w), 1068 (w), 1035 (w), 973 (w), 912 (m), 835 (m), 790 (w), 763 (w), 731 (m), 703 (w), 664 (w) cm^{-1}.
Raman	$\tilde{\nu}$ = 3105 (3), 3087 (26), 3060 (1), 3004 (3), 2980 (4), 2937 (28), 2748 (2), 2688 (2), 2618 (1), 1612 (50), 1544 (30), 1530 (9), 1457 (3), 1399 (4), 1384 (9), 1357 (10), 1347 (100), 1308 (4), 1271 (5), 1206 (13), 1154 (17), 1136 (15), 1072 (6), 1036 (2), 1008 (1), 915 (7), 837 (39), 793 (14), 766 (2), 733 (2), 706 (3), 671 (5), 639 (9), 529 (2), 478 (2), 391 (4), 356 (16), 297 (7), 160 (21), 133 (3), 113 (3) cm^{-1}.
MS (DEI+)	m/z: 182.2 [$(C_7H_6N_2O_4)^+$].

DSC	Melting: 61/67/70/72/81 °C
Density (pycnometer)	1.513 g/cm³.

2,6-DNT **16**:

^{1}H-NMR	(DMSO-d_6, 400 MHz): δ = 2.44 (s, 3H, CH_3), 7.70 (t, J = 8.2 Hz, 1H, H-4), 8.21 (d, J = 8.2 Hz, 2H, H-3, H-5) ppm.
^{13}C-NMR	(DMSO-d_6, 101 MHz): δ = 14.2 (1C, CH_3), 125.9, 127.9, 128.4, 151.0 ppm.
^{14}N-NMR	(DMSO-d_6, 29 MHz): δ = -9 ppm.
EA	for $C_7H_6N_2O_4$ calculated: C 46.16, H 3.32, N 15.38 %; found: C 46.17, H 3.40, N 15.33 %.
IR (ATR)	$\tilde{\nu}$ = 3098 (m), 3024 (w), 2984 (w), 2940 (w), 2865 (w), 1974 (w), 1917 (w), 1863 (w), 1752 (w), 1613 (w), 1577 (w), 1528 (s), 1460 (m), 1424 (m), 1390 (w), 1349 (s), 1299 (m), 1219 (w), 1206 (w), 1134 (w), 1085 (w), 1031 (w), 989 (w), 894 (m), 841 (w), 820 (m), 789 (w), 755 (w), 729 (m), 709 (m) cm^{-1}.
Raman	$\tilde{\nu}$ = 3157 (2), 3102 (7), 3081 (36), 3031 (9), 2990 (9), 2947 (46), 2882 (2), 2754 (2), 2600 (3), 1616 (8), 1582 (23), 1532 (3), 1524 (37), 1448 (5), 1426 (4), 1388 (13), 1367 (100), 1301 (4), 1207 (42), 1166 (16), 1138 (12), 1086 (28), 1029 (4), 896 (2), 843 (26), 821 (2), 797 (74), 759 (4), 731 (3), 713 (2), 689 (3), 632 (1), 579 (50), 515 (1), 467 (6), 448 (4), 387 (8), 365 (4), 330 (26), 296 (2), 242 (12), 183 (58), 131 (4), 112 (10) cm^{-1}.
MS (DEI+)	m/z: 182.2 [$(C_7H_6N_2O_4)^+$].
DSC	Melting: 54/56/58/60/66 °C
Density (pycnometer)	1.515 g/cm³.

4.6.13 2,4,6-Trinitrotoluene TNT 17

2,4,6-Trinitrotoluene TNT **17** was first synthesised by the German *Wilbrand*[110] in 1863. He used toluene as reactant which was mixed with fuming sulfuric and fuming nitric acid for some days under boiling conditions. *Karl Häussermann*[57] developed a three step nitration of toluene to TNT **17**.

In 1912 TNT **17** became the common bursting charge in high explosive shells for the field artillery in the *US Army*.[57] Furthermore, it was used during both *World Wars* with respect to its facile synthesis and the fact that it is possible to extract toluene from mineral oil. The most important advantage of TNT **17** is that owing to its thermal stability and a melting point of about 80 °C it can be melt-casted in almost any possible form.[32] *Dorey and Carper*[111] performed a modified synthesis previously carried out by *Dennis et al.*[112] which uses oleum and 2,4-DNT **15**. Instead of using Oleum (15-wt% SO_3) concentrated sulfuric acid (96 %) was used in this work. This is advantageous since the use of oleum enhances the risk of dangerous runaway reactions involving the oxidation of TNT **17** to 2,4,6-trinitrobenzoic acid.

The solubility of commercial available TNT **17** in acetone was determined to be 6 g per litre solvent at room temperature.

Sulfuric acid (9 mL, 96 %) was cooled below 0 °C by means of an ice-salt cooling bath and nitric acid (3 mL, 71.89 mmol, 3.2 eq., 100 %) was added. While being stirred this mixture was allowed to warm up to room temperature. After this 2,4-dinitrotoluene **15** (4.00 g, 22.01 mmol, 1.0 eq.) was added and the mixture was heated to 90 °C within one hour. No exothermic reaction occurred and the temperature was kept constant for two hours while nitrous fumes were observed in the flask. The acid mixture was allowed to stay overnight at room temperature and was then extracted two times with each 50 mL of dichloromethane. The combined organic phases were washed with 1 x 50 mL saturated sodium

carbonate solution, 2 x 50 mL distilled water, 1 x 50 mL brine and dried over sodium sulfate, followed by removal of the solvent using a rotary evaporator. A yellow crude product was obtained. It was recrystallized from boiling ethanol (25 mL). Light yellowish needles were obtained and dried in high vacuum (1.2×10^{-2} mbar, 16 h). 3.96 g (79 %) of yellow-pale needles of 2,4,6-trinitrotoluene **17** were obtained.[111]

^{1}H-NMR[113]	(acetone-d_6, 400 MHz): δ = 2.70 (s, 3H, CH_3), 8.98 (s, 2H, *H*-3, *H*-5) ppm.
^{13}C-NMR[113]	(acetone-d_6, 101 MHz): δ = 15.6 (1C, CH_3), 123.3 (2C, *C*-3, *C*-5), 134.6 (1C, *C*-1), 146.9 (1C, *C*-4), 152.4 (2C, *C*-2, *C*-6) ppm.
^{15}N-NMR	(acetone-d_6, 41 MHz): δ = -15.0 (NO_2-2, NO_2-6, X-part of AA'X), -21.2 (NO_2-4, X-part of A_2X).
EA	for $C_7H_5N_3O_6$ calculated: C 37.02, H 2.22, N 18.50 %; found: C 37.01, H 2.20, N 18.49 %.
IR (ATR)	$\tilde{\nu}$ = 3095 (m), 3055 (m), 3011 (w), 2956 (w), 2876 (w, b), 1615 (w), 1600 (w), 1530 (s), 1463 (m), 1435 (m), 1403 (m), 1379 (w), 1347 (s), 1207 (w), 1169 (w), 1085 (w), 1026 (w), 937 (w), 924 (w), 905 (m), 792 (w), 768 (w), 757 (w), 733 (w), 715 (m), 702 (m) cm^{-1}.
Raman	$\tilde{\nu}$ = 3103 (8), 3059 (4), 3011 (7), 2956 (29), 2702 (2), 2614 (4), 1618 (55), 1534 (38), 1466 (2), 1438 (5), 1359 (100), 1211 (31), 1172 (4), 1089 (9), 1027 (4), 940 (13), 926 (1), 908 (6), 824 (43), 793 (26), 770 (1), 761 (4), 735 (1), 719 (3), 706 (2), 640 (5), 444 (3), 368 (13), 356 (3), 328 (22), 271 (8), 239 (1) cm^{-1}.
DSC	Melting: 76/79/81/84/90 °C Decomposition: 282/306/309/312/326 °C
Density (pycnometer)	1.633 g/cm³.

4.6.14 Hexanitrostilbene 18

Hexanitrostilbene **18** melts with an onset temperature of 317 °C and is therefore used as heat-resistant explosive.[32] It is used for *Aluminium-Sheathed Linear Shaped Charges* which are used for emergency escape and stage separation in aerospace.[114] It is also used in the oil and gas industry because of its thermal stability. The first synthesis of HNS **18** was done by *Shipp*[115] who reported four different syntheses of HNS **18** in 1964.[115]

The industrial synthesis of HNS **18** is performed according to the procedure stated by *Shipp and Kaplan*.[116] TNT **17** is dissolved in a mixture of tetrahydrofuran and methanol and cooled to 0 °C. The solution is quickly added to a 0 °C cold aqueous sodium hypochlorite solution (5% of active chlorine) and after two minutes a precipitate starts to form. The reaction mixture is held at room temperature until the precipitation is complete. The resulting precipitate is filtered off, washed with methanol and dried in an oven at 100 °C. It can be recrystallized from nitrobenzene and forms yellow pale needles.

^{1}H-NMR[117]	(DMSO-d_6, 400 MHz): δ = 7.14 (s, 2H, CH=CH), 9.11 (s, 4H, *H*-Ar) ppm.
^{13}C-NMR	(DMSO-d_6, 101 MHz): δ = 123.2, 126.2, 130.5, 147.0, 149.5 ppm.
EA	for $C_{14}H_6N_6O_{12}$ calculated: C 37.35, H 1.34, N 18.67 %; found: C 37.37, H 1.36, N 18.66 %.
IR (ATR)	$\tilde{\nu}$ = 3098 (m), 3003 (w), 2876 (w), 1847 (w), 1616 (m), 1599 (m), 1536 (s), 1462 (w), 1401 (w), 1340 (s), 1304 (m), 1264 (w), 1216 (w), 1185 (w), 1179 (w), 1173 (w), 1083 (m), 956 (m), 938 (w), 919 (m), 824 (w), 807 (w), 780 (w), 760 (w), 738 (w), 722 (m), 713 (m), 687 (w) cm^{-1}.
Raman	$\tilde{\nu}$ = 3102 (9), 3064 (23), 2702 (2), 2609 (2), 1638 (56), 1614 (11), 1559 (3), 1539 (30), 1458 (1), 1366 (100), 1346 (6), 1303 (11), 1207 (20), 1182 (6), 1087 (6), 942 (9),

	927 (5), 879 (6), 826 (30), 771 (2), 756 (4), 722 (1), 696 (3), 647 (1), 533 (1), 407 (1), 376 (9), 356 (4), 329 (15), 291 (30) cm^{-1}.
DSC	Melting: 313/317/319/320/320 °C Decomposition: 320/320/339/347/378 °C

4.6.15 RDX 19

The acronym RDX **19** may be interpretated as *Royal Demolition Explosive* or *Research Department Explosive*. It is also called Cyclonite or Hexogen by the Germans. **19** was first prepared by the German chemist *Georg Friedrich Henning*[118] in 1899 who nitrated urotropine dinitrate **25**. He suggested a medical application, but the explosive properties were studied around 1920 by *Herz*[119], who nitrated hexamethylenetetramine directly. These syntheses worked with poor yields, so *Hale* based at the *Picatinny Arsenal, USA* developed a synthesis with 68 % yield in 1925.[57],[120] The most important processes for RDX **19** production during *World War II* were the *Bachmann-Process* and the *Brockman-Process*. RDX **19** impurified with 8-12 % of the better performing secondary explosive HMX **20** is produced performing the *Bachmann-Process* and pure RDX **19** is obtained with the *Brockman-Process*.[121] RDX **19** is the most important secondary explosive with military application nowadays. It is combined with other ingredients and explosives like PETN **09** in formulations of plastic explosives such as *Semtex* [74] or C-4 [57] containing 90-92 % RDX and 8-10 % polyisobutylene [57].

Synthesis in laboratory scale of pure RDX **19** can be done according to the PhD thesis of *Steemann*.[122]

Nitric acid (12 mL, 18.12 g, 287.57 mmol, 25.5 eq., 100 %) was cooled to -30 °C by means of an ethanol dry ice cooling bath. Only a few pieces of solid carbon dioxide should be within the cooling bath. Otherwise the nitric acid starts freezing. Hexamethylenetetramine (1.57 g, 11.26 mmol, 1 eq.) was added in small portions keeping the temperature below -20 °C. The solution must be cooled, otherwise a runaway reaction will occur. Temporary heating of the solution to -10 °C occurred, however, a complete runaway reaction could be avoided by cooling the solution. It was stirred below -20 °C for half an hour and then warmed up to -10°C by an ice-salt bath to obtain *Solution 1*.
In another reaction vessel nitric acid (0.8 mL, 65%) was added to sodium nitrite (0.16 g, 2.35 mmol). Three pasteur pipettes of *Solution 1* were added to this suspension. A time-delayed runaway reaction was initiated resulting in the evolution of nitrous fumes and a drastic warming of the reaction mixture. The runaway reaction was terminated by cooling the reaction mixture with an ethanol-dry-ice bath. Another pipette of *Solution 1* was added and led to the same runaway reaction, which was cancelled before reaching 70 °C followed by cooling the reaction mixture to 50 °C. The runaway reaction announces itself by the evolution of nitrous fumes. This procedure was repeated until *Solution 1* was completely consumed and the temperature should reach 65 °C performing the last addition. The runaway reaction was not cancelled that time and the solution was allowed to cool itself down.
The reaction mixture was heated again to 65 °C (73 °C oil-bath temperature) for 70 minutes followed by cooling it to 5 °C. Afterwards it was poured into an ice bath and a white precipitate was obtained, filtered off and washed with distilled water. This product was dried over orange gel in high vacuum overnight and 1.49 g (60 %) of white RDX **22** were obtained.[122]

^{1}H-NMR	(DMSO-d_6, 400 MHz): δ = 6.10 (s, 6H, CH_2) ppm.
^{13}C-NMR	(DMSO-d_6, 101 MHz): δ = 61.2 (CH_2) ppm.
^{14}N-NMR	(DMSO-d_6, 29 MHz): δ = -34 ppm.
EA	for $C_3H_6N_6O_6$ calculated: C 16.22, H 2.72, N 37.84 %; found: C 16.39, H 2.58, N 37.66 %.
IR (ATR)	$\tilde{\nu}$ = 3073 (m), 3064 (m), 3000 (w), 1588 (s), 1569 (s), 1529 (m), 1457 (m), 1431 (m), 1421 (m), 1386 (m), 1349 (m), 1308 (m), 1263 (s), 1231 (m), 1215

	(m), 1037 (m), 1016 (w), 944 (w), 908 (s), 880 (m), 851 (w), 842 (m), 779 (m), 751 (m), 736 (w), 670 (w) cm^{-1}.
Raman	$\tilde{\nu}$ = 3075 (37), 3066 (15), 3002 (52), 2948 (73), 2906 (6), 2747 (2), 1594 (18), 1572 (9), 1541 (8), 1509 (2), 1458 (6), 1435 (16), 1389 (19), 1378 (6), 1347 (10), 1310 (46), 1274 (39), 1216 (54), 1031 (11), 945 (9), 885 (100), 857 (4), 848 (28), 788 (8), 757 (3), 739 (3), 670 (6), 606 (18), 591 (9), 464 (21), 415 (7), 347 (30), 301 (2), 226 (24), 207 (5) cm^{-1}.
DSC	Melting: 200/203/204/207/208 °C Decomposition: 208/208/233/247/255 °C
Density (pycnometer)	1.785 g/cm^3.

4.6.16 HMX 20

HMX **20** stands for High Melting Explosive or Homocyclonite and is currently one of the best performing military explosives with a better energetic performance in comparison to RDX **19**. Due to its high production costs, it is limited to military use. It is used in mixtures such as Octol, a melt-cast explosive, which consists of 75 % HMX **20** and 25 % TNT **17**.[32]

HMX **20** exists in four polymorphs (α-δ) of which the β-polymorph is the one in use as an explosive with respect to its high density.[123] According to *Bachmann et al.*[124], one possibility to obtain HMX **20** is to recrystallize mixtures of RDX **19** and HMX **20** in organic solvents. HMX **20** has a poor solubility in organic solvents and so RDX **19** can be removed by this method. These mixtures can be prepared in different ways. One way is the nitration of hexamethylenetetramine at modified conditions for RDX **19** synthesis. *Castorina et al.*[125] stated a synthesis at a constant temperature of 44 °C using hexamethylenetetramine and trace amounts of paraformaldehyde treated with a mixture of acetic acid, acetic anhydride, ammonium nitrate and nitric acid. They obtained a yield of 90% containing 85 % HMX **20** and 15 % RDX **19**.[32]

Another synthesis was stated by *McKay et al.*[126], who nitrated 1,5-dinitroendomethylene-1,3,5,7-tetraazacyclooctane using a mixture of acetic anhydride, ammonium nitrate and nitric acid at a temperature of 65 - 70 °C to obtain a yield of 66 % HMX after purification.

β-HMX **20**:

^{1}H-NMR	(DMSO-d_6, 400 MHz): δ = 6.03 (s, 8H, CH_2) ppm.
^{13}C-NMR	(DMSO-d_6, 101 MHz): δ = 63.3 (4C, CH_2) ppm.
^{14}N-NMR	(DMSO-d_6, 29 MHz): δ = -37 ppm.
EA	for $C_4H_8N_8O_6$ calculated: C 16.22, H 2.72, N 37.84 %; found: C 16.47, H 2.60, N 37.54 %.
IR (ATR)	$\tilde{\nu}$ = 3035 (w), 3025 (w), 2988 (w), 1527 (s), 1460 (m), 1431 (m), 1393 (m), 1346 (w), 1324 (w), 1261 (s), 1237 (m), 1200 (s), 1140 (m), 1086 (m), 961 (m), 943 (s), 870 (w), 829 (w), 771 (w), 759 (m), 753 (m), 657 (w) cm^{-1}.
Raman	$\tilde{\nu}$ = 3037 (10), 3028 (27), 2992 (77), 2909 (3), 2865 (1), 2830 (2), 1568 (12), 1524 (9), 1454 (13), 1418 (27), 1367 (9), 1349 (25), 1310 (38), 1267 (6), 1248 (29), 1190 (11), 1168 (19), 1079 (5), 952 (49), 883 (40), 834 (66), 760 (6), 720 (3), 661 (9), 639 (12), 597 (11), 436 (15), 415 (10), 362 (32), 314 (6), 281 (12), 230 (27), 181 (10), 148 (100), 139 (14), 130 (16) cm^{-1}.
MS (DEI+)	m/z: 222.1 $[(C_4H_8N_8O_6 - NO_2 - HCN - H^+)^+]$, 148.1 $[(C_4H_8N_8O_6 - 4\ NO - 2\ CH_2)^+]$, 128.1 $[(C_4H_8N_4O)^+]$, 75.1 $[(CH_3N_2O_2)^+]$, 46.1 $[(NO_2)^+]$.
DSC	Phase Transition: 193/193/196/200/202 °C. (β→δ) [123]

	Decomposition: 266/276/278/283/299 °C.
Density (pycnometer)	1.886 g/cm³.

4.6.17 CL-20 21

CL-20 **21** was first synthesised in 1987 by *A. T. Nielsen et al.* [127],[128] at the *Naval Air Warfare Center Weapons Division* in California (USA). It is one of the most powerful non-nuclear explosive known and is industrially produced in a pilot plant scale by the *Thiokol Corporation*[32],[129] in the USA.

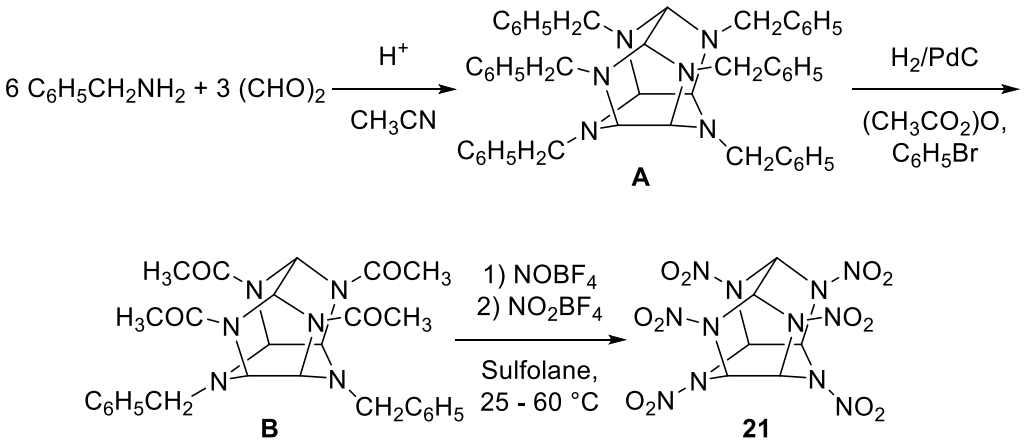

Scheme 1: Synthesis of CL-20 24 according to Nielsen at al.[130]

Five CL-20 **21** polymorphs (α-ε) are known, of which the ε-polymorph is the most thermodynamically stable and dense. The other polymorphs may be obtained by recrystallization under specific conditions. [131] A cocrystal of CL-20 **21** and HMX **20** with improved sensitivity parameters in comparison to **21** has been reported by *Bolton et al.* [132]. *Bennion et al.* [133] reported in 2016 two polymorphic hydrogen peroxide solvates of which one outperforms ε-CL-20 according to performance predictions using the Cheetah 7.0 computer code. The hydrogen peroxide solvate in the best performing polymorph is lost at 165 °C.

The most commonly used preparation of CL-20 **21** is a three step synthesis that is shown in *Scheme 1* which is not too complex, but exotic reactants are needed, such as a palladium catalyst. Two intermediates (**A** and **B**) have to be isolated during this process described by *Nielsen et al.*[130]. The caged polyazapolycyclic benzyl intermediate **A** is obtained through stoichiometric condensation of benzylamine and glyoxal in aqueous acetonitrile at 25 °C in the presence of formic acid as catalyst. Glyoxal is added dropwise to the mixture of aqueous solution of benzylamine in acetonitrile over a period of one hour so that the temperature is kept below 20 °C. The reaction mixture is allowed to stand overnight (16-18 hours) and the precipitate was filtered off and may be recrystallized from acetonitrile to obtain colourless crystals.[134] **B** is the second intermediate, which is obtained by reductive acetylation of **A**. This reaction is performed in acetic acid anhydride as solvent, using a mineral acid (HBr as best choice) as catalyst, hydrogen and a Pd/C catalyst.[127],[128] To obtain CL-20 **21** from **B** it is suspended in sulfolane containing a small amount of water as solvent. A nitrosation reaction with nitrosonium tetrafluoroborate $NOBF_4$ (3 mol eq.) is performed followed by a nitration using nitronium tetrafluoroborate NO_2BF_4 (12 mol eq.) This mixture is stirred for two hours at 25 °C and for another two hours at 55-60 °C. To increase purity of the product it may be dissolved in ethyl acetate and filtered using a silica gel column, which is washed with ethyl acetate to obtain a clear, pale yellow solution. This solution is poured into chloroform to precipitate pure crystalline CL-20 **24** in β-form.[130] Yields performing this three step synthesis are in the first step around 72 %, in the second step 60-65 % and in the last step 90 % after recrystallization.

ε-CL-20:

^{1}H-NMR[135]	(aceton-d_6, 400 MHz): δ = 8.19 – 8.25 (m, 2H), 8.32 – 8.39 (m, 4H) ppm.
^{13}C-NMR[136]	(aceton-d_6, 101 MHz): δ = 72.1 (4C, *C*-a), 75.1 (2C, *C*-b) ppm.
^{14}N-NMR	(aceton-d_6, 29 MHz): δ = -42, -45 ppm.
EA	for $C_6H_6N_{12}O_{12}$ calculated: C 16.45, H 1.38, N 38.36 %; found: C 16.69, H 1.36, N 38.03 %.
IR (ATR)	$\tilde{\nu}$ = 3044 (m), 3016 (w), 2845 (w), 1631 (w), 1603 (s), 1584 (s), 1562 (s), 1382 (w), 1326 (s), 1296 (m), 1280 (s), 1260 (s), 1252 (s), 1217 (m), 1191 (w), 1181 (m), 1135 (w), 1123 (w), 1085 (w), 1040 (m), 1018 (m), 978 (m), 959 (w), 935 (m), 912 (m), 881 (m), 854 (m), 830 (m), 818 (m), 756 (m), 749 (m), 743 (m), 736 (m), 721 (m), 704 (w), 658 (w) cm^{-1}.
Raman	$\tilde{\nu}$ = 3046 (97), 3031 (34), 3018 (13), 1625 (32), 1607 (17), 1578 (9), 1561 (2), 1503 (4), 1383 (17), 1336 (31), 1277 (12), 1263 (9), 1219 (4), 1183 (6), 1125 (15), 1088 (4), 1051 (18), 984 (19), 940 (21), 856 (22), 834 (32), 821 (84), 791 (16), 752 (8), 705 (2), 661 (6), 644 (9), 625 (5), 581 (13), 528 (19), 467 (5), 447 (13), 370 (17), 345 (54), 319 (100), 267 (34), 221 (7), 194 (33), 159 (16), 139 (87) cm^{-1}.
MS (DEI+)	m/z: 439.2 [$(C_6H_6N_{12}O_{12} + H^+)^+$].
DSC	Phase Transition: 159/160/162/165/167 °C. Decomposition: 213/224/243/252/262 °C.
Density (pycnometer)	2.18 cm^3.

4.6.18 TETRYL 22

Tetryl **22** was first prepared in 1877 by *Mertens*[137]. It can be used as a booster explosive amongst PETN **09** and RDX **19**. It is a component of high brisance composite explosives and was used in both World War I and II. In industrial scale dinitrophenylmethylamine is produced from methylamine and 2,4- or 2,6-dinitrophenylchloride. The resulting product can be nitrated to Tetryl **22**. The second synthetic approach to Tetryl **22** is the direct nitration of *N*,*N*-Dimethylaniline as described by *Urbanski et al*.[138] This approach has two disadvantages since the oxidative removal of the methyl group resulting in carbon dioxide consumes nitric acid and the strongly exothermic reaction is hard to control on industrial scale. Tetryl **22** melts at 128 °C and decomposes at 190 °C. It forms an eutecticum with TNT **17** containing 55% of **22**. This eutectic mixture is used in binary TNT-Tetryl formulations called Tetrytols. In 1979 the United States discontinued the use of Tetryl **22** in explosive devices due to its instability during storage at elevated temperatures. Existing devices were redesigned to eliminate **22** from them. [57]

In a 250 mL three neck bottle equipped with a thermometer and reflux condenser a mixture of nitric acid (37.5 mL, 65 %) and fuming nitric acid (20.0 mL, 98%) is cooled to a temperature between 5 – 7 °C. N,N-Dimethylaniline (2.10 g, 17.3 mmol) is added dropwise under evolution of fumes and a hissing sound. The reaction mixture is stirred for 15 minutes at 2 °C and then heated to an oilbath temperature between 40 and 50 °C. This led to a dark solution and evolution of nitrous gases. After the change of color the oilbath was first heated to 80 °C and then to 90 °C. After one hour at 90 °C the mixture was cooled to 10 °C using an ice bath and 3.5 mL of distilled water were added resulting in the immediate formation of crystals. After 3 hours of cooling the product was filtered off using a glass frit (Por. 3) and washed with 250 mL of water. After drying in high vacuum over orange gel 3.37 g (68 %) of Tetryl **22** were obtained as slightly yellow needle-shaped crystals.

^{1}H-NMR	(acetone-d_6, 400 MHz): δ = 3.78 (s, 3H, CH_3), 9.37 (s, 2H, H-3, H-5) ppm
^{13}C-NMR	(acetone-d_6, 101 MHz): δ = 41.0 (CH_3), 126.2, 131.8, 147.7, 149.4 ppm.
^{14}N-NMR	(acetone-d_6, 29 MHz): δ = -35, -22 ppm.
EA	for $C_2H_4N_4O_4$ calculated: C 29.28, H 1.78, N 24.39 %; found: C 29.15, H 1.75, N 24.34 %.
IR (ATR)	$\tilde{\nu}$ = 3078 (m), 3013 (w), 2950 (w), 2882 (w), 2362 (w), 2327 (w), 1858 (w), 1608 (m), 1536 (s), 1457 (m), 1427 (m), 1337 (s), 1322 (s), 1277 (s), 1198 (m), 1164 (w), 1115 (w), 1077 (m), 963 (w), 932 (w), 919 (m), 826 (w), 800 (w), 783 (w), 757 (w), 742 (w), 711 (m), 657 (w) cm^{-1}
Raman	$\tilde{\nu}$ = 3093 (6), 3074 (0), 3039 (2), 3011 (4), 2953(12), 2834 (2), 2614 (2), 1619 (30), 1551 (22), 1479 (6), 1426 (8), 1360 (100), 1341 (5), 1323 (10), 1282 (4), 1186 (7), 1119 (5), 1079 (14), 966 (7), 934 (9), 827 (30), 801 (15), 784 (7), 752 (4), 715 (4), 604 (5), 491 (2), 393 (1), 373 (9), 328 (14), 311 (2), 255 (4), 199 (26), 168 (1), 107 (9), 85 (69) cm^{-1}
MS (DEI+)	m/z: 287.2 [$(C_7H_5N_5O_8)^+$]
DTA	Melting: 126/128/133/136/141 °C Decomposition: 160/190/191/193/200 °C

4.6.19 FOX-7 23

The general information about FOX-7 is an excerpt from the authors M.Sc. Thesis:

1,1-Diamino-2,2-Dinitroethene (FOX-7, **23**) has been published as an RDX **19** replacement first in 1985 by the Swedish Defence Research Agency (FOI), although it appears to have been first isolated by Russian chemists. The first reported synthesis of FOX-7 **23** starts from 2-methylimidazole **A**, which is nitrated and oxidized by a mixture of nitric (100 %) and sulfuric acid (92 %) to afford **B** in 15 % yield under simultaneous formation of parabanic acid **C** as undesired main product with 60 % yield. **B** is unstable at room temperature and decomposes under formal loss of nitrogen oxides to 2-dinitromethyleneimidazolidine-4,5-dione **D**. **D** can be hydrolyzed with aqueous ammonia to afford FOX-7 **23** in 87 % yield. Due to the optimized overall yield of 13 %, a more direct, but related synthesis was presented within the same paper. Starting from acetamidine hydrochloride and diethyl oxalate, 2-methoxy-2-methylimidazolidine-4,5-dione **E** is formed in methanol and sodium methoxide in 64 % yield. **E** is nitrated to **D** with a mixture of sulfuric and nitric acid in 67 % yield. Taking into account the identical hydrolysis reaction to FOX-7 **23**, this route offers an overall yield of 37 %.[4, 139] (Scheme 2)

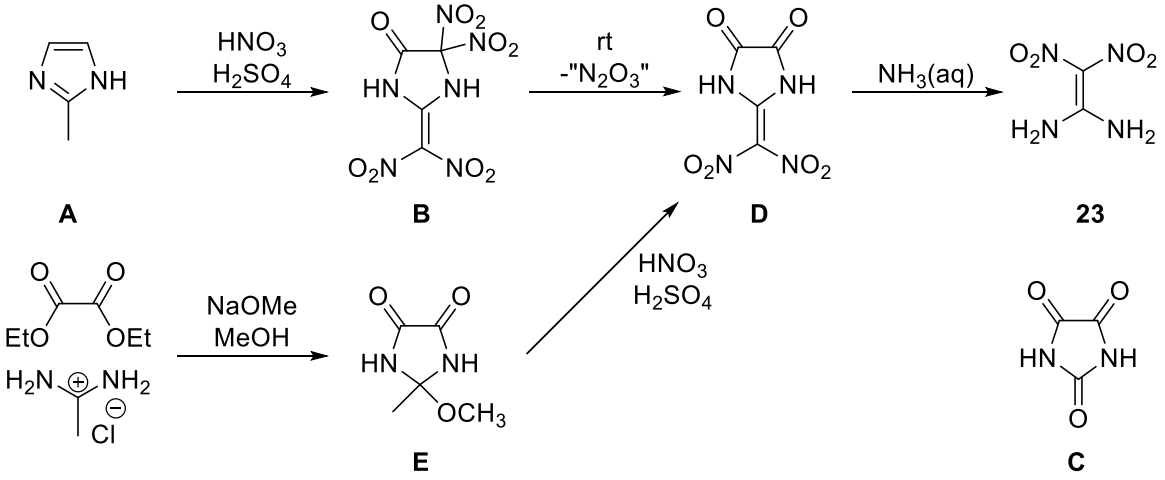

Scheme 2 - Synthesis of FOX-7 23 starting from 2-methyl-imidazole 109 or diethyloxalate and acetamidinium hydrochloride.

The overall yield of the synthesis of FOX-7 **23** has been further improved by changing the starting material. If commercially available 2-methylpyrimidine-4,6-diol **F** (which can be synthesized with the procedure provided by *Czeskis*[140]) is used for the synthesis, a FOX-7 **23** yield above 90 % can be obtained under optimized conditions. In the course of the nitration reaction **F** is quickly nitrated at its 5-position to **G**, which is slowly further nitrated to **H**. **H** can be easily hydrolyzed to FOX-7 **23** and dinitromethane by addition of the nitration mixture to water under loss of carbon dioxide. FOX-7 **23** simply precipitates from the reaction mixture, so it can be filtered off and washed affording the pure product. Dinitromethane can be extracted from the filtrate or it may be left in it to decompose. However, on large scale the formation of this byproduct may be problematic with regard to safety matters, as in practice 5.5 kg dinitromethane are generated for every 10 kg of FOX-7 **31**.[4, 141](Scheme 3)

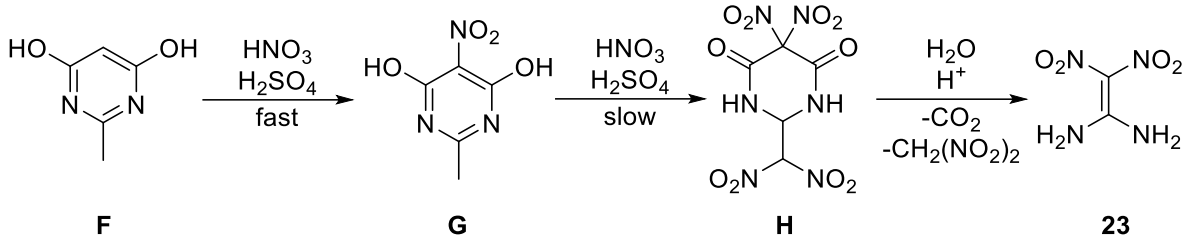

Scheme 3 - Synthesis of FOX-7 23 starting from 4,6-Dihydroxyl-2-methyl-pyrimidine F.

In comparison to RDX **19**, FOX-7 **23** has a decreased sensitivity towards external stimuli in combination with a comparable performance. FOX-7 **23** has an impact sensitivity of 25 J (RDX **19**, 7.5 J), a friction sensitivity above 360 N (RDX **19**, 120 N) and a decomposition temperature of 219 °C (RDX **19**, 203 °C). In terms of energetic performance, FOX-7 **23** has an experimental detonation velocity of 8870 km s^{-1} (RDX **49**, 8930 km s^{-1}) and a detonation pressure $p_{C\text{-}J}$ of 340 kbar (RDX **49**, 346 kbar). Furthermore, FOX-7 is reported to have a density ρ of 1.88 g cm^{-3} (RDX **49**, 1.82 g cm^{-3}) and an enthalpy of formation ΔH_f^0 of -130 kJ mol^{-1} (RDX **49**, +67 kJ mol^{-1}). This comparison is in particular of interest as FOX-7 **31** and RDX **19** both have the same empirical sum formula $CH_2N_2O_2$ and consequently the same oxygen balance Ω_{CO2}.[4, 142]

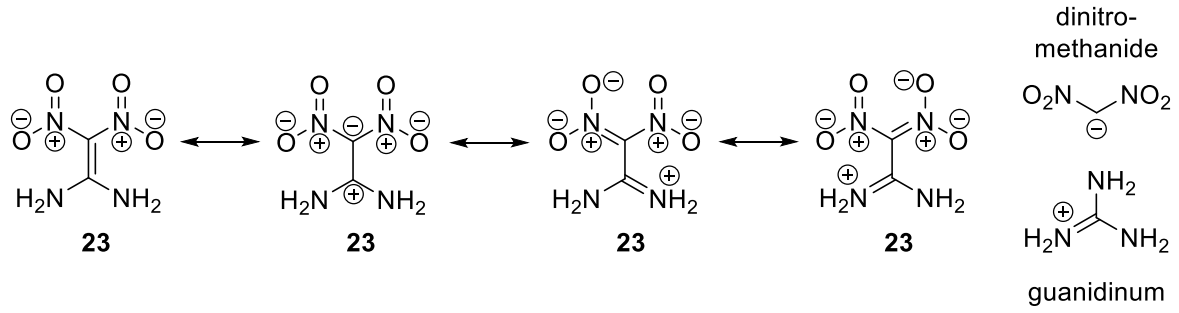

Figure 16 - Selected mesomeric structures of FOX-7 31 underlining its zwitterionic push-pull-alkene character.

Two important factors contributing to the low sensitivity of FOX-7 **23** towards external stimuli are its strong intramolecular hydrogen bonding interactions and its resonance-stabilization as a push-pull alkene. The prime example for an energetic molecule stabilized by intramolecular hydrogen bonding is the insensitive explosive 1,3,5-triamino-2,4-6-trinitrobenze (TATB), which resists heat up to 300 °C and decomposes at 350 °C.[142] In the crystal structure of FOX-7 **23**, a strong hydrogen bonding exists between amino hydrogens and nitro oxygens on both sides of the molecule. FOX-7 **23** is a push-pull-alkene with two geminal electron-pushing amino-groups in conjugation with two electron-pulling nitrogroups via a C-C double bond. The resonance-stabilization of the push-pull alkene can be further evidenced by the C-C-bond length of 1.456 Å, which is in between that of a C-C single bond (1.54 Å)

and a normal double bond (1.34 Å). Furthermore, shorter than normal C-NH_2 and C-NO_2 bonds are observed. [143] This effect can be illustrated by regarding FOX-7 **23** as the formal zwitterionic combination of a guanidinium and dinitromethanide system, which are both known for their high stability in ionic compounds. Further consequences of the zwitterionic character of FOX-7 **23** should be enhanced electrophilicity of C-1, N-H-acidity with a lower pK_a in comparison to simple amines and weak nucleophilicity of the amine N-atoms. FOX-7 **23** has an interesting temperature-dependent polymorphism involving three polymorphs, which has been extensively studied by our research group.[143-144]

FOX-7 **23** has been synthesized in this work according to *Astrat'ev et al.*[141],[145].

2-methylpyrimidine-4,6-diol (3.55 g, 0.03 mol, 1 eq.) (which can be synthesized with the procedure provided by *Czeskis*[140]) was given in small portions to sulfuric acid (98%, 10.7 mL) keeping the temperature between 15–20°C. The resulting suspension was cooled down to 5–10 °C and fuming nitric acid (100%, 15.9 mL) was added dropwise maintaining the temperature. The reaction mixture was cooled down by means of an ice-salt-bath and allowed to gradually warm up to room temperature overnight. The homogenous suspension was added to 150 mL of ice-water in one gush without stirring. The resulting clear solution changes its color from yellow to orange under evolution of carbon dioxide and is set aside in a fridge over night for complete precipitation of the product. The yellow precipitate was filtered off and washed with sodium carbonate solution (5g in 200 mL distilled water), 100 mL of distilled water and 100 mL diethyl ether. After drying 4.14 g (99 %) 1,1-diamino-2,2-dinitroethene **26** were obtained as a yellow solid.[141],[145]

^{1}H-NMR[4]	(DMSO-d_6, 270 MHz): δ = 8.77 (s, 4H, NH_2) ppm.
^{13}C-NMR[4]	(DMSO-d_6, 101 MHz): δ = 128.0 (1C, $C(NO_2)_2$), 158.0 (1C, $C(NH_2)_2$) ppm.
^{14}N-NMR	(DMSO-d_6, 29 MHz): δ = -26 (NO_2), -271 (NH_2) ppm.
EA	for $C_2H_4N_4O_4$ calculated: C 16.22, H 2.72, N 37.84 %; found: C 16.47, H 2.62, N 37.72 %.
IR (ATR)	$\tilde{\nu}$ = 3698 (w), 3399 (s), 3321 (s), 3293 (s), 3222 (m), 2468 (w), 1623 (m), 1604 (m), 1516 (m), 1498 (m), 1468 (m), 1389 (m), 1346 (m), 1214 (m), 1161 (m), 1138 (m), 1019 (m), 857 (w), 788 (w), 748 (m), 738 (w), 673 (w) cm^{-1}.
Raman	$\tilde{\nu}$ = 3423 (1), 3331 (10), 1630 (1), 1607 (12), 1525 (21), 1481 (2), 1462 (6), 1344 (100), 1208 (74), 1166 (27), 1143 (5), 1066 (9), 1026 (26), 859 (100), 792 (6), 739 (5), 681 (4), 624 (22), 587 (3), 482 (9), 458 (27), 402 (7), 320 (7) cm^{-1}.
MS (DEI+)	m/z: 148.1 [$(C_2H_4N_4O_4)^+$], 86.1 [$(C_2H_4N_4O_4 - NO_2 - NH_2)^+$], 69.1 [$(C_2H_4N_4O_4 - NO_2 - O_2 - H^+)^+$], 43.1 [$(CH_4N_2 - H^+)^+$].
DSC	Decomposition I: 215/219/228/232/236 °C Decomposition II: 237/255/257/261/272 °C
IS	25 J (< 100 µm).
Density (pycnometer)	1.850 g/cm³.

4.6.20 Uronium Nitrate 24

Uronium nitrate **24** is an explosive with freely available precursors that has been reported first by *Pelouze* in 1842 [146]. It was the main charge of the explosive device used in the *World Trade Center Bombing* in 1993 where a truck was filled with explosive material and detonated at the north tower of the *World Trade Center* in New York.[147] *Oxley et al.* [148] reported a vapor pressure for uronium nitrate 24 of 3.94×10^{-5} Pa at 25 °C in combination with an enthalpy of sublimation of 167 kJ mol^{-1} (temperature not specified) using isothermal thermogravimetic analysis. Benzoic acid was used for the conversion of pressure analog values to real vapor pressures.

Uronium nitrate **24** can be obtained by simple mixing of stoichiometric amounts of urea and nitric acid under under cooling according to *Worsham et al.*[149]

Urea (28.64 g, 476.86 mmol, 1.0 eq.) was dissolved in 200 mL distilled water and cooled below 0 °C by means of an ice-salt cooling bath while being stirred. Nitric acid (30 mL, 42.00 g, 666.56 mmol, 1.4 eq., 65 %) was added keeping the temperature below 10 °C. A white precipitate occurs after adding about two-thirds of the volume of nitric acid. The mixture was stirred for another 30 minutes while being cooled. The water was evaporated with a rotary evaporator at 60 °C and a white solid remained in the flask. This solid was recrystallized from boiling ethanol (200 mL) and filtered off after cooling in a fridge. The white crystalline product was air-dried for four days and 43.84 g (78 %) uronium nitrate **24** were obtained.[149]

^{1}H-NMR	(DMSO-d_6, 400 MHz): δ = 8.57 (s, NH_2) ppm.
^{13}C-NMR	(DMSO-d_6, 101 MHz): δ = 161.6 ppm.
^{14}N-NMR	(DMSO-d_6, 29 MHz): δ = -8 ppm.
EA	for $CH_5N_3O_4$ calculated: C 9.76, H 4.10, N 34.14 %; found: C 10.01, H 4.03, N 33.87 %.
IR (ATR)	$\tilde{\nu}$ = 3396 (s), 3351 (s), 3246 (s), 3193 (s), 2968 (m), 2880 (m), 2825 (m), 2722 (m), 2412 (m), 2269 (m), 1770 (w), 1702 (m), 1673 (m), 1568 (m), 1548 (m), 1425 (m), 1351 (m), 1303 (s), 1048 (m), 1016 (m), 891 (m), 814 (w), 747 (w), 735 (w), 718 (w), 667 (w) cm^{-1}.
Raman	$\tilde{\nu}$ = 3261 (3), 1637 (2), 1578 (2), 1422 (1), 1302 (1), 1057 (100), 1020 (39), 737 (7), 722 (3), 574 (3), 535 (10) cm^{-1}.
MS	m/z (FAB+): 61.0 [$(CH_5N_2O)^+$]; m/z (FAB-): 62.0 [$(NO_3)^-$].
DSC	Melting: 146/155/158/159/159°C Decomposition: 159/159/161/164/169 °C
Density (pycnometer)	1.655 g/cm^3.

4.6.21 Urotropine Dinitrate 25

Urotropine dinitrate **25** is a low-performing explosive, yet it is an important precursor material for the production of RDX **19**. The first application of **25** in explosive chemistry was performed by *Henning*[118] in 1899. He nitrated **25** and obtained a very powerful explosive even though he thought of a medical application for RDX **19**. The so called *Bachmann Process* was simultaneously developed by *Bachmann*[150] in the USA and *Köffler* in Germany. This process improves the one of *Henning* in terms of the yield. The obtained RDX **22** contains almost no impurities. For both processes **25** is needed as precursor material.

25 is not well storable because it is hygroscopic and decomposes in the presence of water. The main decomposition products are hexamethylenetetramine, nitric acid and formaldehyde.[151] It is stable for 24 hours when exposed to ambient conditions and shut in a vessel, however, it should be stored in a dry atmosphere.

In this work the crystal structure of **25** was determined for the first time:

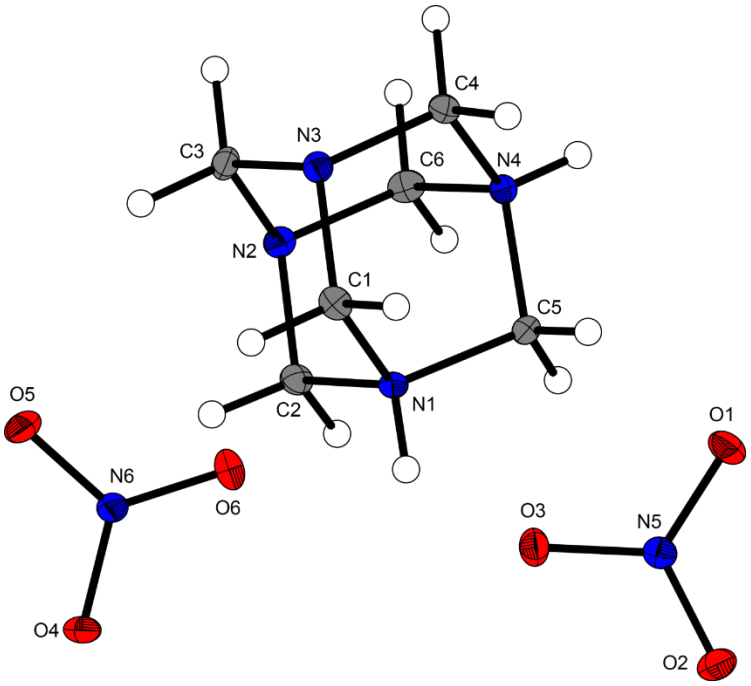

Figure 17 – Crystal structure of 25. Thermal ellipsoids of non-hydrogen atoms are generated at a 50 % probability level.

The compound crystallizes in the monoclinic spacegroup $P2_1/c$ with four molecular units in the unit cell. Further details of crystallographic refinement and other measurement parameters are compiled in Table 5.

Table 5 – Selected details of crystallographic refinement and further measurement parameters for the crystal structure of 25.

	HDN 32
measurement #	jx208
Chemical formula	$C_6H_{14}N_6O_6$
Molecular weight [g mol^{-1}]	266.23
Color, habit	colorless plate
Size [mm]	0.38x0.30x0.08
Crystal system	monoclinic
Space group	$P2_1/c$
***a* [Å]**	6.2767(3)
***b* [Å]**	18.3445(7)
***c* [Å]**	8.9984(3)
α [°]	90
β [°]	94.018(4)
γ [°]	90
***V* [Å^3]**	1033.56(7)
Z	4
ρ_{calc} [g cm^{-3}]	1.711
μ [mm^{-1}]	0.151
Irridiation [Å]	MoK_α 0.71073
F(000)	560
Θ-Bereich [°]	4.245-25.997
T [K]	173
Dataset h	-7 ≤ h ≤ 7
Dataset k	-23 ≤ k ≤ 23

Dataset l	-11 ≤ l ≤ 10
Reflecions coll.	6139
Independent refl.	2203
Observed refl.	1867
Parameters	219
R (int)	0.0211
GOOF	1.047
R_1, wR_2 ($I>\sigma I_0$)	0.0309, 0.0741
R_1, wR_2 (all data)	0.0390, 0.0789
Weighting scheme [a]	0.0366, 0.3003
Remaining density [e Å^{-3}]	-0.237, 0.224
Device type	Oxford XCalibur3
Adsorption corr.	multi-scan
CIF #	1471377

[a] $wR_2 = [\Sigma[w(F_0^2-F_c^2)^2]/\Sigma[w(F_0)^2]]^{1/2}$ where $w=[\sigma_c^2(F_0^2)+(xP)^2+yP]$ and $P=(F_0^2+2F_c^2)/3$

^{1}H-NMR[151]	(DMSO-d_6, 400 MHz): δ = 4.84 (s, 12H, CH_2), 8.83 (s, 2H, NH) ppm.
^{13}C-NMR	(DMSO-d_6, 101 MHz): δ = 71.2 (6C, CH_2) ppm.
^{14}N-NMR	(DMSO-d_6, 29 MHz): δ = -9 ppm.
EA	for $C_6H_{14}N_6O_6$ calculated: C 27.07, H 5.30, N 31.57 %; found: C 27.06, H 5.14, N 31.65 %.
IR (ATR)	$\tilde{\nu}$ = 3031 (m), 1754 (w), 1471 (w), 1426 (w), 1374 (s), 1356 (s), 1309 (s), 1264 (s), 1218 (m), 1187 (m), 1153 (m), 1080 (w), 1056 (m), 1041 (m), 1011 (m), 963 (w), 927 (w), 859 (m), 821 (w), 812 (m), 766 (w), 716 (w), 695 (w) cm^{-1}.
Raman	$\tilde{\nu}$ = 3033 (21), 3022 (7), 3006 (10), 2982 (36), 1473 (1), 1454 (5), 1425 (2), 1407 (5), 1357 (3), 1344 (7), 1316 (1), 1218 (8), 1190 (1), 1168 (1), 1060 (6), 1049 (100), 1014 (3), 967 (7), 953 (3), 931 (6), 864 (12), 818 (29), 768 (27), 718 (12), 710 (4), 696 (6), 672 (8), 644 (3), 520 (8), 505 (9), 486 (6), 442 (11), 356 (2) cm^{-1}.
MS	m/z (FAB+): 289.2 [$(C_6H_{14}N_6O_6 + Na^+)^+$]; m/z (FAB-): 62.0 [$(NO_3)^-$].
DSC	Melting: 155/160/163/164/164 Decomposition: 164/164/197/202/214
Density (pycnometer)	1.663 g/cm³.

4.6.22 2,3-Dimethyl-2,3-dinitrobutane 26

DMDNB **26** is a commercially available chemical. 2,3-Dimethyl-2,3-dinitrobutane **26** is an important detection aid agent (taggant) for commercially available explosive formulations according to the 1999 Montreal Convention on the Marking of Plastic explosives [10]. The crystal structure and thermal behavior of the compound is discussed in section 7.7.

^{1}H-NMR	(acetone-d_6, 400 MHz): δ = 1.76 (s, CH_3) ppm.
^{13}C-NMR	(acetone-d_6, 101 MHz): δ = 23.2 (CH_3), 93.0 (*C*-2, *C*-3) ppm.
^{14}N-NMR	(acetone-d_6, 29 MHz): δ = 11 ppm.
EA	for $C_6H_{12}N_2O_4$ calculated: C 40.91, H 6.87, N 15.90 %; found: C 40.81, H 6.83, N 15.63 %.
IR (ATR)	$\tilde{\nu}$ = 3031 (w), 3003 (w), 2868 (w), 1584 (w), 1546 (s), 1527 (s), 1471 (m), 1454 (m), 1433 (w), 1408 (m), 1393 (m), 1378 (m), 1340 (s), 1241 (w), 1219 (w), 1170 (m), 1132 (m), 1096 (w), 904 (w), 850 (m), 800 (w), 766 (w), 728 (w), 672 (w) cm^{-1}.

Raman	$\tilde{\nu}$ = 3033 (72), 3007 (100), 2968 (77), 2820 (4), 2788 (3), 2746 (9), 1543 (37), 1486 (12), 1460 (12), 1438 (24), 1412 (29), 1398 (5), 1379 (6), 1342 (46), 1241 (7), 1206 (11), 1133 (4), 1027 (10), 952 (5), 929 (5), 857 (63), 769 (51), 737 (12), 681 (5), 647 (8), 561 (30), 520 (53), 432 (3), 385 (40), 350 (7), 328 (5), 235 (10), 182 (7), 124 (61) cm^{-1}.
DSC	see [25]
Density (pycnometer)	1.345 g/cm^3.

4.6.23 Nitromethane 27

Nitromethane **27** is a commercially available low sensitive explosive. It is produced on industrial scale by treating propane with nitric acid at 350-450 °C. Nitromethane **29**, nitroethane, 1-nitropropane and 2-nitropropane are the four nitroalkanes that are produced by this exothermic reaction.[152]

It is used as a component in the commercial explosive *Kinepak*^{TM} which is a mixture containing ammonium nitrate **28** and nitromethane **27**.[153] Nitromethane is the main component of the Picatinny Liquid Explosive (PLX). [5] PLX is a mixture of **27** (95 %) and ethylene diamine (5 %), which is added to increase the sensitivity of the mixture by deprotonation of the C-H-acidic **27**. Selected, predicted performance parameters of PLX (Explo5 v6.03) are compiled in Table 6.

Table 6 – Selected energetic performance parameters of PLX predicted by Explo5v6.03 (ρ: 1.13 g cm^{-3}). Cf. Table 3.

$-\Delta_{ex}U^{\circ}$ [kJ kg^{-1}]	4593	$p_{C\text{-}J}$ [kbar]	130
T_{ex} [K]	3126	VoD [m s^{-1}]	6500
V_o [L kg^{-1}]	1005		

PLX filled in a whisky bottle is suspected to have been used to crash *Korean-Air-Flight-858* (*KAL-858*) in 1987 over the Andaman Sea. Two North Korean agents joined *KAL-858* at *Saddam International Airport* in Iraq and placed a time bomb in the aeroplane. They left the flight at *Abu Dhabi International Airport* and tried to escape, but were caught. One of the agents, who survived their attempt to kill themselves, said that they used *PLX* which was filled in a whisky bottle, but even newspapers regarded this statement critical. [154]

Nitromethane **29** is also used as solvent, as reference substance for $^{14/15}$N-NMR spectroscopy, fuel for dragster racing car engines and freely available as fuel for remote controlled (RC) models.

^{1}H-NMR	(DMSO-d_6, 400 MHz): δ = 4.42 (s, 3H, CH_3) ppm.
^{13}C-NMR[105]	(DMSO-d_6, 101 MHz): δ = 63.3 (1C, CH_3) ppm.
^{14}N-NMR	(DMSO-d_6, 29 MHz): δ = 0 ppm.
EA	for CH_3NO_2 calculated: C 19.68, H 4.95, N 22.95 %; found: C 19.85, H 4.80, N 23.00 %.
IR (ATR)	$\tilde{\nu}$ = 3310 (w), 2938 (w), 2472 (w), 1551 (s), 1423 (m), 1402 (s), 1375 (s), 1099 (w), 917 (w), 817 (w), 654 (m) cm^{-1}.
Raman	$\tilde{\nu}$ = 3046 (2), 2967 (55), 1557 (2), 1401 (31), 1378 (16), 1101 (2), 918 (100), 656 (20), 607 (2), 481 (7), 174 (5), 113 (2) cm^{-1}.
ΔH_f^0(l/s)(CBS-4M)	-104.6 kJ/mol.

4.6.24 Ammonium Nitrate 28

Ammonium nitrate is a chemical produced industrially on a megaton scale. Straightly used as a fertilizer it accounts for 24% of the world consumption of nitrogen fertilizers and is integrated in many more complex fertilizer compilations. Its production and physico-chemical properties have been reviewed excellently reviewed by *Zapp et al.* [27] including the temperature-dependent polymorphism involving 4 polymorphs. Although several heavy accidents occurred in the past, pure ammonium nitrate **28** will not detonate when stored properly.[155] The application of an explosive which can be stored as two non-explosive components revolutionised the mining industry. The safety in mining operations increased enormously by using a mixture of e.g. 94.5 % ammonium nitrate **28** and 5.5 % mineral oil as explosive (ANFO: ammonium nitrate fuel oil). Half of the explosives used in mining operations are ANFO formulations.[156] Ammonium nitrate **28** is also used as a component in the commercial explosive *Kinepak*^{TM} which is a mixture containing ammonium nitrate **28** and nitromethane **27**.[153] Anders Behring Breivik used ammonium nitrate **28** based fertilizers in his bomb attack. (cf. section 4.1). Ammonium nitrate is also used as an oxidizer in solid rocket propellants. For this application the polymorphism of **28** is problematic since two phase transitions occur at -16.9 °C (AN V → AN IV) and 33.2 °C (AN IV → AN III). This may result in the formation of cracks in the propellant mixture which deteriorates its burning behaviour. Phase-stable ammonium nitrate is commercially available. [157]

^{1}H-NMR	(DMSO-d_6, 400 MHz): δ = 7.22 (s, 4H, NH_4) ppm.
^{14}N-NMR	(DMSO-d_6, 29 MHz): δ = -4 (NO_3^-), -360 (NH_4) ppm.
EA	for $H_4N_2O_4$ calculated: H 5.04, N 35.00 %; found: H 4.87, N 34.74 %.
IR (ATR)	$\tilde{\nu}$ = 3238 (s), 3052 (s), 2413 (w), 2361 (w), 2329 (w), 1752 (w), 1403 (m), 1308 (m), 1041 (m), 825 (m), 711 (w) cm^{-1}.
Raman	$\tilde{\nu}$ = 3142 (2), 1655 (1), 1415 (2), 1290 (2), 1044 (100), 716 (18), 169 (8), 140 (14) cm^{-1}.
DSC	See [27] for phase transition behavior.
IS	> 40 J (< 100 µm).
FS [N]	> 360 N (< 100 µm).
ESD [J]	> 1.5 J (< 100 µm).
Density (pycnometer)	1.677 g/cm³.
ΔH_f^0(l/s)(CBS-4M)	-337.5 kJ/mol.

4.6.25 Origin and Purity of commercially available materials.

Table 7: Origin and purity of commercially available materials.

substance	purity	producer	catalogue-#	lot-#
2-nitrotoluene **12**	≥ 99 %	Sigma-Aldrich	438804-100 mL	BCBJ4334V
2,4-dinitrotoluene **15**	97 %	Sigma-Aldrich	101397	1354711 43607092
2,6-dinitrotoluene **16**	98 %	Sigma-Aldrich	D200603-100 g	1358379 45107014
3-nitrotoluene **13**	99 %	Sigma-Aldrich	N27314-100 g	12609ENV
4-nitrotoluene **14**	99 %	ABCR	AB118285	1121486
acetone	≥ 99.8% HPLC	Sigma-Aldrich	34850-2 L	SZBC351SV
ammonium nitrate **28**	99 % absolute	Grüssing	10151-1 kg	4327
CL-20 **21**	/	NEXPLO Bofors	/	/
D-mannitol	≥ 98 %	Sigma-Aldrich	M4125-100 g	BCBK8481V
meso-erythritol	/	Erylite®	/	/
ethylene glycol	98 %	VWR	24407.292	09H170514
glycerine	99 %	AppliChem	A4443.1000	0Y001741
hexamethylene tetramine	99 %	ACROS-Organics	120610010-1 kg	A0216057001
HMX **20**	/	confidential	/	/
HNS **18**	/	DYNAenergetics	/	/
sodium nitrite	99 %	AppliChem	A7014.0500	0Z004238
nitromethane **27**	98 %	ABCR	AB118236	1225507
pentaerythritol	≥ 97 % HPLC	Fluka	76640	405975/1 41601
picric acid **17**	99.8 %	Merck	Art. 623	K1371023
TNT **17**	purum	Fluka	100 g	6./122/00002
hydrogen peroxide 30 %	for synthesis	Merck	822287-1 L	K42389487
DMDNB **26**	98 %	Sigma-Aldrich	156345-10 g	MKBF0326V
urea	99 %	Grüssing	11019	0084

Literature References

1. https://en.wikipedia.org/wiki/2011_Norway_attacks#/media/File:Regjeringsbygget_22.7.2011.jpg Picture was created by Johannesen. No changes were made. Licensed under CC BY 2.0 by the Wikimedia Foundation.
2. https://fas.org/programs/tap/_docs/2083_-_A_European_Declaration_of_Independence.pdf
3. https://www.cmc-versand.de/modellbau/Motoren--und--Zubehoer/Verbrenner-Motoren/Modelltreibstoffe.html.
4. Bellamy, A., FOX-7 (1,1-Diamino-2,2-dinitroethene)

High Energy Density Materials. Klapötke, T., Ed. Springer Berlin / Heidelberg: 2007; Vol. 125, pp 1-33.
5. Meyer, R.; Köhler, J.; Homburg, A., *Explosives*. 7th ed.; WileyVCH: 2015.
6. http://home.arcor.de/chemist123/Gewinnung%20von%20Ammoniumnitrat%20aus%20KAS.pdf.
7. http://keten.pl.
8. (a) Brauer, G., *Handburch der Präparativen Anorganischen Chemie*. Ferdinand Enke Verlag: Stuttgart, 1975; Vol. 1; (b) http://youtu.be/032c5PI0yxU.
9. http://www.lambdasyn.org/synfiles/natriumnitrit.htm.
10. http://www.mcgill.ca/iasl/files/iasl/montreal1991.pdf.
11. Östmark, H.; Wallin, S.; Ang, H. G., Vapor Pressure of Explosives: A Critical Review. *Propellants, Explosives, Pyrotechnics* **2012,** *37* (1), 12-23.
12. Frisch, M. J.; Trucks, G. W.; Schlegel, H. B.; Scuseria, G. E.; Robb, M. A.; Cheeseman, J. R.; Scalmani, G.; Barone, V.; Mennucci, B.; Petersson, G. A.; Nakatsuji, H.; Caricato, M.; Li, X.; Hratchian, H. P.; Izmaylov, A. F.; Bloino, J.; Zheng, G.; Sonnenberg, J. L.; Hada, M.; Ehara, M.; Toyota, K.; Fukuda, R.; Hasegawa, J.; Ishida, M.; Nakajima, T.; Honda, Y.; Kitao, O.; Nakai, H.; Vreven, T.; Montgomery Jr., J. A.; Peralta, J. E.; Ogliaro, F.; Bearpark, M. J.; Heyd, J.; Brothers, E. N.; Kudin, K. N.; Staroverov, V. N.; Kobayashi, R.; Normand, J.; Raghavachari, K.; Rendell, A. P.; Burant, J. C.; Iyengar, S. S.; Tomasi, J.; Cossi, M.; Rega, N.; Millam, N. J.; Klene, M.; Knox, J. E.; Cross, J. B.; Bakken, V.; Adamo, C.; Jaramillo, J.; Gomperts, R.; Stratmann, R. E.; Yazyev, O.; Austin, A. J.; Cammi, R.; Pomelli, C.; Ochterski, J. W.; Martin, R. L.; Morokuma, K.; Zakrzewski, V. G.; Voth, G. A.; Salvador, P.; Dannenberg, J. J.; Dapprich, S.; Daniels, A. D.; Farkas, Ö.; Foresman, J. B.; Ortiz, J. V.; Cioslowski, J.; Fox, D. J. *Gaussian 09*, Gaussian, Inc.: Wallingford, CT, USA, 2009.
13. NATO standardization agreement (STANAG) on explosives, impact sensitivity tests, no. 4489, 1st ed., Sept. 17, 1999.
14. NATO standardization agreement (STANAG) on explosive, friction sensitivity tests, no. 4487, 1st ed., Aug. 22, 2002.
15. (a) WIWEB-Standardarbeitsanweisung 4-5.1.02, Ermittlung der Explosionsgefährlichkeit, hier der Schlagempfindlichkeit mit dem Fallhammer, Nov. 8, 2002; (b) WIWEB-Standardarbeitsanweisung 4-5.1.03, Ermittlung der Explosionsgefährlichkeit oder der Reibeempfindlichkeit mit dem Reibeapparat, Nov. 8, 2002.
16. (a) Bundesanstalt für Materialforschung und -prüfung. Available online: http://www.bam.de (accessed on 26 March 2012); (b) REICHEL & PARTNER GmbH, http://www.reichelt-partner.de; (c) Impact: Insensitive > 40 J, less sensitive ≥ 35 J, sensitive ≥ 4 J, very sensitive ≤ 3 J; Friction: Insensitive > 360 N, less sensitive = 360 N, sensitive < 360 N and > 80 N, very sensitive ≤ 80 N, extremely sensitive ≤ 10 N. According to the UN Recommendations on the Transport of Dangerous Goods.
17. Fulmer, G. R.; Miller, A. J. M.; Sherden, N. H.; Gottlieb, H. E.; Nudelman, A.; Stoltz, B. M.; Bercaw, J. E.; Goldberg, K. I., NMR Chemical Shifts of Trace Impurities: Common Laboratory Solvents, Organics, and Gases in Deuterated Solvents Relevant to the Organometallic Chemist. *Organometallics* **2010,** *29* (9), 2176-2179.
18. Gray, P.; Smith, P. L., Low-temperature calorimetry and the thermodynamic properties of ethyl nitrate. *Journal of the Chemical Society (Resumed)* **1954,** (0), 769-773.

19. Rinkenbach, W. H., The Properties of Glycol Dinitrate1. *Industrial & Engineering Chemistry* **1926,** *18* (11), 1195-1197.
20. Kemp, M. D.; Goldhagen, S.; Zihlman, F. A., Vapor Pressures and Cryoscopic Data for Some Aliphatic Dinitroxy and Trinitroxy Compounds. *The Journal of Physical Chemistry* **1957,** *61* (2), 240-242.
21. Bell; McEwen, **1922,** *14*, 536.
22. Gelalcha, F. G.; Schulze, B.; Lonnecke, P., 3,3,6,6-Tetramethyl-1,2,4,5-tetroxane: a twinned crystal structure. *Acta Crystallographica Section C* **2004,** *60* (3), o180-o182.
23. Cowley, E. G.; Partington, J. R., 293. Studies in dielectric polarisation. Parts VIII, IX, X, and XI. *Journal of the Chemical Society (Resumed)* **1933,** (0), 1252-1259.
24. Groom, C. R.; Bruno, I. J.; Lightfoot, M. P.; Ward, S. C., The Cambridge Structural Database. *Acta Crystallographica Section B* **2016,** *72* (2), 171-179.
25. Jones, D. E. G.; Lightfoot, P. D.; Fouchard, R. C.; Kwok, Q. S. M., Thermal properties of DMNB, a detection agent for explosives. *Thermochimica Acta* **2002,** *388* (1–2), 159-173.
26. Bagryanskaya, I. Y.; Gatilov, Y. V., Crystal structure of nitromethane. *Journal of Structural Chemistry* **1983,** *24* (1), 150-151.
27. Zapp, K.-H.; Wostbrock, K.-H.; Schäfer, M.; Sato, K.; Seiter, H.; Zwick, W.; Creutziger, R.; Leiter, H., Ammonium Compounds. In *Ullmann's Encyclopedia of Industrial Chemistry*, Wiley-VCH Verlag GmbH & Co. KGaA: 2000.
28. Cady, H., The crystal structure of N-methyl-N-2,4,6-tetranitroaniline (tetryl). *Acta Crystallographica* **1967,** *23* (4), 601-609.
29. Kiselev, V. D.; Kashaeva, H. A.; Shakirova, I. I.; Potapova, L. N.; Konovalov, A. I., Solvent Effect on the Enthalpy of Solution and Partial Molar Volume of the Ionic Liquid 1-Butyl-3-methylimidazolium Tetrafluoroborate. *Journal of Solution Chemistry* **2012,** *41* (8), 1375-1387.
30. Steinfeld, J. I.; Wormhoudt, J., EXPLOSIVES DETECTION: A Challenge for Physical Chemistry. *Annual Review of Physical Chemistry* **1998,** *49* (1), 203-232.
31. Legler, L., Ueber Producte der langsamen Verbrennung des Aethyläthers. *Berichte der deutschen chemischen Gesellschaft* **1885,** *18* (2), 3343-3351.
32. Agrawal, J. P.; Hodgson, R. D., *Organic Chemistry of Explosives*. 2007.
33. Marotta, D., *Gazzetta chimica italiana* **1929,** *59*, 942.
34. Wierzbicki, A.; Salter, E. A.; Cioffi, E. A.; Stevens, E. D., Density Functional Theory and X-ray Investigations of P- and M-Hexamethylene Triperoxide Diamine and Its Dialdehyde Derivative. *The Journal of Physical Chemistry A* **2001,** *105* (38), 8763-8768.
35. Schaefer, W. P.; Fourkas, J. T.; Tiemann, B. G., Structure of hexamethylene triperoxide diamine. *Journal of the American Chemical Society* **1985,** *107* (8), 2461-2463.
36. Guo, C.; Persons, J.; Harbison, G. S., Helical chirality in hexamethylene triperoxide diamine. *Magnetic Resonance in Chemistry* **2006,** *44* (9), 832-837.
37. Oxley, J. C.; Smith, J. L.; Luo, W.; Brady, J., Determining the Vapor Pressures of Diacetone Diperoxide (DADP) and Hexamethylene Triperoxide Diamine (HMTD). *Propellants, Explosives, Pyrotechnics* **2009,** *34* (6), 539-543.
38. Aernecke, M. J.; Mendum, T.; Geurtsen, G.; Ostrinskaya, A.; Kunz, R. R., Vapor Pressure of Hexamethylene Triperoxide Diamine (HMTD) Estimated Using Secondary Electrospray Ionization Mass Spectrometry. *The Journal of Physical Chemistry A* **2015,** *119* (47), 11514-11522.
39. Wolffenstein, R., Ueber die Einwirkung von Wasserstoffsuperoxyd auf Aceton und Mesityloxyd. *Berichte der deutschen chemischen Gesellschaft* **1895,** *28* (2), 2265-2269.
40. German police seize bomb, firearm in raid that foiled imminent Boston Marathon-style terror attack. http://news.nationalpost.com/news/world/german-police-seize-bomb-firearm-in-raid-that-foiled-imminent-boston-marathon-style-terror-attack
41. Paris suicide bombers used TATP, a powerful, homemade explosive: officials. http://www.nydailynews.com/news/world/paris-suicide-bombers-tatp-homemade-explosive-article-1.2435082.
42. 17-Jähriger hortete Sprengstoff. http://www.n-tv.de/panorama/17-Jaehriger-hortete-Sprengstoff-article334469.html.

43. (a) Oxley, J. C.; Smith, J. L.; Steinkamp, L.; Zhang, G., Factors Influencing Triacetone Triperoxide (TATP) and Diacetone Diperoxide (DADP) Formation: Part 2. *Propellants, Explosives, Pyrotechnics* **2013,** *38* (6), 841-851; (b) Oxley, J. C.; Smith, J. L.; Bowden, P. R.; Rettinger, R. C., Factors Influencing Triacetone Triperoxide (TATP) and Diacetone Diperoxide (DADP) Formation: Part I. *Propellants, Explosives, Pyrotechnics* **2013,** *38* (2), 244-254.
44. Oxley, J. C.; Smith, J. L.; Brady, J. E.; Steinkamp, L., Factors Influencing Destruction of Triacetone Triperoxide (TATP). *Propellants, Explosives, Pyrotechnics* **2014,** *39* (2), 289-298.
45. Lubczyk, D.; Hahma, A.; Brutschy, M.; Siering, C.; Waldvogel, S. R., A New Reference Material and Safe Sampling of Terrorists Peroxide Explosives by a Non-Volatile Matrix. *Propellants, Explosives, Pyrotechnics* **2015,** *40* (4), 590-594.
46. Reany, O.; Kapon, M.; Botoshansky, M.; Keinan, E., Rich Polymorphism in Triacetone-Triperoxide. *Crystal Growth & Design* **2009,** *9* (8), 3661-3670.
47. Haroune, N.; Crowson, A.; Campbell, B., Characterisation of triacetone triperoxide (TATP) conformers using LC-NMR. *Science & Justice* **2011,** *51* (2), 50-56.
48. Peterson, G. R.; Bassett, W. P.; Weeks, B. L.; Hope-Weeks, L. J., Phase Pure Triacetone Triperoxide: The Influence of Ionic Strength, Oxidant Source, and Acid Catalyst. *Crystal Growth & Design* **2013,** *13* (6), 2307-2311.
49. Milas, N. A.; Golubovic, A., Studies in Organic Peroxides. XXVI. Organic Peroxides Derived from Acetone and Hydrogen Peroxide. *Journal of the American Chemical Society* **1959,** *81* (24), 6461-6462.
50. Landenberger, K. B.; Bolton, O.; Matzger, A. J., Two Isostructural Explosive Cocrystals with Significantly Different Thermodynamic Stabilities. *Angewandte Chemie International Edition* **2013,** *52* (25), 6468-6471.
51. Feldhaus, S., Bereitung des Salpetrigsäure - Aethyläthers. *Justus Liebigs Annalen der Chemie* **1863,** *126* (1), 71-74.
52. Gatterman, L., *Die Praxis des organischen Chemikers*. Walter de Gruyter: Berlin / New York, 1982.
53. Camera, E.; Modena, G.; Zotti, B., On the behaviour of nitrate esters in acid solution. III. Oxidation of ethanol by nitric acid in sulphuric acid. *Propellants, Explosives, Pyrotechnics* **1983,** *8* (3), 70-73.
54. Lasalle, A.; Roizard, C.; Midoux, N.; Bourret, P.; Dyens, P. J., Removal of nitrogen oxides (NOx) from flue gases using the urea acidic process: kinetics of the chemical reaction of nitrous acid with urea. *Industrial & Engineering Chemistry Research* **1992,** *31* (3), 777-780.
55. Brandes, E.; Möller, W., *Sicherheitstechnische Kenngrößen - Band 1: Brennbare Flüssigkeiten und Gase*. Wirtschaftsverlag NW, Verlag für neue Wissenschaft GmbH, Bremerhaven: 2003.
56. Strecker, A., Ueber Nitromannit. *Justus Liebigs Annalen der Chemie* **1850,** *73* (1), 59-70.
57. *Military Explosives*. TM 9-1300-214 ed.; Headquaters, Department of the Army: Washington D.C., 1984.
58. Sokoloff, N. K., *Russian Journal of Physical Chemistry* **1879,** (11), 136.
59. Hayward, L. D., D-Mannitol-1,2,3,5,6-pentanitrate. *Journal of the American Chemical Society* **1951,** *73* (5), 1974-1975.
60. Patterson, T. S.; Todd, A. R., CCCXC.-The influence of solvents and of other factors on the rotation of optically active compounds. Part XXVIII. The rotation dispersion of mannitol and some of its derivatives. Note on rotation dispersion curves. *Journal of the Chemical Society (Resumed)* **1929,** (0), 2876-2889.
61. Henry, L., Untersuchungen über die Aetherderivate der mehratomigen Alkohole und Säuren. *Berichte der deutschen chemischen Gesellschaft* **1870,** *3* (1), 529-533.
62. NIOSH, Criteria for a recommended standard... occupational exposure to nitroglycerin and ethylene glycol dinitrate. *NIOSH-Criteria-Document* **1978**.
63. Urbanski, T.; Witanowski, M., Infra-red spectra of nitric esters. Part 1.-Influence of inductive effects of substituents. *Transactions of the Faraday Society* **1963,** *59* (0), 1039-1045.
64. Einwirkung der Mischung von Schwefelsäure und Salpetersäure auf einige organische Substanzen. *Justus Liebigs Annalen der Chemie* **1848,** *64* (3), 396-398.

65. Butler, J. A. V.; Ramchandani, C. N.; Thomson, D. W., 58. The solubility of non-electrolytes. Part I. The free energy of hydration of some aliphatic alcohols. *Journal of the Chemical Society (Resumed)* **1935,** (0), 280-285.
66. Minch, M. J., Orientational dependence of vicinal proton-proton NMR coupling constants: The Karplus relationship. *Concepts in Magnetic Resonance* **1994,** *6* (1), 41-56.
67. Lemanceau, B.; Caire-Maurisier, M., Esters nitriques de polyols. Conformation de la nitroglycérine. Résonance magnétique nucléaire et moment dipolaire. *Propellants, Explosives, Pyrotechnics* **1980,** *5* (6), 147-150.
68. Stenhouse, J., Ueber die näheren Bestandtheile einiger Flechten. *Pharmaceutisches Central Blatt* **1849,** *Band 20* (No. 40), 625-628.
69. (a) Oxley, J. C.; Smith, J. L.; Brady, J. E.; Brown, A. C., Erratum: Characterization and Analysis of Tetranitrate Esters. *Propellants, Explosives, Pyrotechnics* **2012,** *37* (6), 735-735; (b) Oxley, J. C.; Smith, J. L.; Brady, J. E.; Brown, A. C., Characterization and Analysis of Tetranitrate Esters. *Propellants, Explosives, Pyrotechnics* **2012,** *37* (1), 24-39.
70. Matyáš, R.; Lyčka, A.; Jirásko, R.; Jakový, Z.; Maixner, J.; Mišková, L.; Künzel, M., Analytical Characterization of Erythritol Tetranitrate, an Improvised Explosive. *Journal of Forensic Sciences* **2016,** *61* (3), 759-764.
71. Manner, V. W.; Tappan, B. C.; Scott, B. L.; Preston, D. N.; Brown, G. W., Crystal Structure, Packing Analysis, and Structural-Sensitivity Correlations of Erythritol Tetranitrate. *Crystal Growth & Design* **2014,** *14* (11), 6154-6160.
72. Zukas, J. A.; Walters, W. P., *Explosive Effects and Applications*. Springer-Verlag: New York, USA, 1998.
73. Tollens, B.; Wigand, P., Ueber den Penta-Erythrit, einen aus Formaldehyd und Acetaldehyd synthetisch hergestellten vierwerthigen Alkohol. *Justus Liebigs Annalen der Chemie* **1891,** *265* (3), 316-340.
74. Santos, L. M. N. B. F.; Lima, L. M. S. S.; Lima, C. F. R. A. C.; Magalhães, F. D.; Torres, M. C.; Schröder, B.; Ribeiro da Silva, M. A. V., New Knudsen effusion apparatus with simultaneous gravimetric and quartz crystal microbalance mass loss detection. *The Journal of Chemical Thermodynamics* **2011,** *43* (6), 834-843.
75. Barros, S., http://www.powerlabs.org/chemlabs/petn.htm. (accessed 02/02/14).
76. Roberts, R. N.; Dinegar, R. H., Solubility of Pentaerythritol Tetranitrate. *The Journal of Physical Chemistry* **1958,** *62* (8), 1009-1011.
77. Griefs, P., Vorläufige Notiz über die Einwirkung von salpetriger Säure auf Amidinitro- und Aminitrophenylsäure. *Justus Liebigs Annalen der Chemie* **1858,** *106* (1), 123-125.
78. Griefs, P., Ueber eine neue Klasse organischer Verbindungen, welche Wasserstoff durch Stickstoff vertreten enthalten. *Justus Liebigs Annalen der Chemie* **1860,** *113* (2), 201-217.
79. Clark, L. V., Diazodinitrophenol, a Detonating Explosive. *Industrial & Engineering Chemistry* **1933,** *25* (6), 663-669.
80. Matyáš, R.; Pachman, J., *Primary Explosives*. Springer Berlin Heidelberg: 2013.
81. Hagel, R.; Redecker, K., Sintox - A New, Non-Toxic Primer Composition by Dynamit Nobel AG. *Propellants, Explosives, Pyrotechnics* **1986,** *11* (6), 184-187.
82. Matyás, R.; Pachmann, J., *Primary Explosives*. Springer-Verlag: Berlin Heidelberg, 2012.
83. Klapötke, T. M.; Preimesser, A.; Stierstorfer, J., Synthesis and Energetic Properties of 4-Diazo-2,6-dinitrophenol and 6-Diazo-3-hydroxy-2,4-dinitrophenol. *European Journal of Organic Chemistry* **2015,** *2015* (20), 4311-4315.
84. Izsák, D.; Klapötke, T. M.; Preimesser, A.; Stierstorfer, J., Synthesis and Initiation Capabilities of Energetic Diazodinitrophenols. *Zeitschrift für anorganische und allgemeine Chemie* **2016,** *642* (1), 48-55.
85. http://www.sciencemadness.org/talk/files.php?pid=419166&aid=44191.
86. http://keisyou.gooside.com/do2.htm. (accessed 02/09/2014).
87. Abel, C. D. British Patent 10,294. 1900.
88. Newdon, H. E. British Patent 13,213. 1899.

89. Holl, G.; Klapötke, T. M.; Polborn, K.; Rienäcker, C., Structure and Bonding in 2-Diazo-4,6-Dinitrophenol (DDNP). *Propellants, Explosives, Pyrotechnics* **2003,** *28* (3), 153-156.
90. Egerer, G., A MODIFIED METHOD FOR THE PREPARATION OF PICRAMIC ACID. *Journal of Biological Chemistry* **1918,** *35* (3), 565-566.
91. Girard, A., *Ann. Pharm.* **1853,** *88*, 281.
92. Lea, M. C., On the Formation of Picramic Acid. *Am. J. Sc. and Arts* **1861,** *31*, 188.
93. Russel, C. A., *Chemistry, Society and Environment: A New History of the British Chemical Industry*. The Royal Society of Chemistry: Great Britain, 2000.
94. Olsen, F.; Goldstein, J. C., The Preparation of Picric Acid from Phenol. *Industrial & Engineering Chemistry* **1924,** *16* (1), 66-71.
95. Kortüm, G. V. W. A. K., *Dissoziationskonstanten organischer säuren in Wässeriger Lösung*. Butterworths: London, 1961.
96. Raamat, E.; Kaupmees, K.; Ovsjannikov, G.; Trummal, A.; Kütt, A.; Saame, J.; Koppel, I.; Kaljurand, I.; Lipping, L.; Rodima, T.; Pihl, V.; Koppel, I. A.; Leito, I., Acidities of strong neutral Brønsted acids in different media. *Journal of Physical Organic Chemistry* **2013,** *26* (2), 162-170.
97. http://gingerafro.tripod.com/siferonline/id10.html. (accessed 02/07/2014).
98. Lyčkaa, A.; Macháčekb , V.; Jirman, J., 15N, 13C, and 1H NMR spectra of 1-substituted-2,4,6-trinitrobenzenes. *Collect. Czech. Chem. Commun.* **1987,** *52* (12), 2946.
99. Some chemicals present in industrial and consumer products, food and drinking-water. *IARC Monogr Eval Carcinog Risks Hum* **2013,** *101*, 9-549.
100. Dunnick, J. K. *NTP technical report on toxicity studies of o-, m-, and p-nitrotoluenes (CAS Nos.: 88-72-2, 99-08-1, 99-99-0) administered in dosed feed to F344/N rats and B6C3F1 mice*; Natl. Toxicol. Program: 1992; p 133 pp.
101. Deutsche, F.; Deutsche, F., Krebserzeugende Arbeitsstoffe. In *MAK- und BAT-Werte-Liste 2015*, Wiley-VCH Verlag GmbH & Co. KGaA: 2015; pp 163-182.
102. http://www.him-stadtallendorf.de/ergebnisse/boden/bodensanierung_tab.htm.
103. http://www.oc-praktikum.de/nop/de/instructions/pdf/1001_de.pdf.
104. http://sdbs.db.aist.go.jp/sdbs/cgi-bin/direct_frame_top.cgi SDBS No.: 1151.
105. Bailey, W. F.; Cioffi, E. A., Carbon-13 NMR chemical shifts of representative nitriles and nitro compounds. *Magnetic Resonance in Chemistry* **1987,** *25* (2), 181-183.
106. https://www.epa.gov/sites/production/files/2014-09/documents/chapter_7_24_and_26_dinitrotoluene.pdf.
107. Finch, A.; Payne, J., Thermochemical study of 2,6-dinitrotoluene. *Thermochimica Acta* **1990,** *164*, 55-63.
108. Majer, V.; Svoboda, V.; Pick, J., *Heats of vaporization of fluids*. Elsevier: 1989.
109. Wan, D., Reactions of 1,1,2,2-tetranitroaminoethane and properties of its tetrasodium salt. *Proc. Int. Pyrotech. Semin.* **1991,** *17th* (Vol. 1), 231-4.
110. Wilbrand, J., Notiz über Trinitrotoluol. *Justus Liebigs Annalen der Chemie* **1863,** *128* (2), 178-179.
111. Dorey, R. C.; Carper, W. R., Synthesis and high-resolution mass-spectral analysis of isotopically labeled 2,4,6-trinitrotoluene. *Journal of Chemical & Engineering Data* **1984,** *29* (1), 93-97.
112. Dennis, W. H.; Rosenblatt, D. H.; Blucher, W. G.; Coon, C. L., Improved synthesis of TNT isomers. *Journal of Chemical & Engineering Data* **1975,** *20* (2), 202-203.
113. Wang, C.; Lyon, D. Y.; Hughes, J. B.; Bennett, G. N., Role of Hydroxylamine Intermediates in the Phytotransformation of 2,4,6-Trinitrotoluene by Myriophyllum aquaticum. *Environmental Science & Technology* **2003,** *37* (16), 3595-3600.
114. Schwarz, A. C. *APPLICATION OF HEXANITROSTILBENE (HNS) IN EXPLOSIVE COMPONENTS*; SC-RR--710673 United States10.2172/4666790Thu Aug 12 07:29:48 EDT 2010Dep. NTIS.SNL; NSA-26-035735English; 1972; p Medium: ED; Size: Pages: 45.
115. Shipp, K. G., Reactions of α-Substituted Polynitrotoluenes. I. Synthesis of 2,2',4,4',6,6'-Hexanitrostilbene. *The Journal of Organic Chemistry* **1964,** *29* (9), 2620-2623.
116. Shipp, K. G.; Kaplan, L. A., Reactions of α-Substituted Polynitrotoluenes. II. The Generation and Reactions of 2,4,6-Trinitrobenzyl Anion. *The Journal of Organic Chemistry* **1966,** *31* (3), 857-861.

117. Kayser, E. G., An Investigation of the Ship Hexanitrostilbene (HNS) Process. Center, N. S. W., Ed. Maryland, USA, 1980.
118. Henning, G. F. German patent 104280. 1899.
119. Herz, G. C. V. British patent 145793 (1921), U. S. patent 1402693. 1922.
120. Hudson, R. J. Investigating the Factors influencing RDX shock sensitivity. Cranfield University, United Kingdom, 2012.
121. Klapötke, T. M., *Chemie der Hochenergetischen Materialien*. Walter de Gruyter GmbH & Co. KG: Berlin, 2009.
122. Steemann, F. X. Beiträge zur Chemie energetischer Amin-, Nitramin- und Tetrazolverbindungen. Dissertation, LMU München, 2009.
123. http://permalink.lanl.gov/object/tr?what=info:lanl-repo/lareport/LA-02652-MS.
124. Bachmann, W. E.; Horton, W. J.; Jenner, E. L.; MacNaughton, N. W.; Scott, L. B., Cyclic and Linear Nitramines Formed by Nitrolysis of Hexamine1. *Journal of the American Chemical Society* **1951,** *73* (6), 2769-2773.
125. Castorina, T. C.; Holahan, F. S.; Graybush, R. J.; Kaufman, J. V. R.; Helf, S., Carbon-14 Tracer Studies of the Nitrolysis of Hexamethylenetetramine. *Journal of the American Chemical Society* **1960,** *82* (7), 1617-1623.
126. McKay, A. F.; Wright, G. F.; Richmond, H. H., NITROLYSIS OF HEXAMETHYLENETETRAMINE: II. NITROLYSIS OF l,5-ENDOMETHYLENE-3,7-DINITRO-1,3,5,7-TETRAZA-CYCLOÖCTANE (DPT). *Canadian Journal of Research* **1949,** *27b* (5), 462-468.
127. Nielsen, A. T. In *Synthesis of Caged Nitramine Explosives*, Joint Army, Navy, NASA, Air Force (JANNAF) Propulsion Meeting, San Diegeo, CA, San Diegeo, CA, 1987.
128. Nielsen, A. T., Caged polynitramine compound. Google Patents: 1997.
129. Braithwaite, P.; Collignon, S.; Hinshaw, J. C.; Johnstone, G.; Jones, R.; Lyon, V. A.; Poush, K.; Wardle, R. B. In *Thiokol Corporation in the US*, Proc. International Symposium on Energetic Materials Technology, American Defence Preparedness Association, 1996.
130. Nielsen, A. T.; Chafin, A. P.; Christian, S. L.; Moore, D. W.; Nadler, M. P.; Nissan, R. A.; Vanderah, D. J.; Gilardi, R. D.; George, C. F.; Flippen-Anderson, J. L., Synthesis of polyazapolycyclic caged polynitramines. *Tetrahedron* **1998,** *54* (39), 11793-11812.
131. Millar, D. I. A., *Energetic Materials at Extreme Conditions*. Springer Berlin Heidelberg: 2011.
132. Bolton, O.; Simke, L. R.; Pagoria, P. F.; Matzger, A. J., High Power Explosive with Good Sensitivity: A 2:1 Cocrystal of CL-20:HMX. *Crystal Growth & Design* **2012,** *12* (9), 4311-4314.
133. Bennion, J. C.; Chowdhury, N.; Kampf, J. W.; Matzger, A. J., Hydrogen Peroxide Solvates of 2,4,6,8,10,12-Hexanitro-2,4,6,8,10,12-hexaazaisowurtzitane. *Angewandte Chemie International Edition* **2016,** *55* (42), 13118-13121.
134. Nielsen, A. T.; Nissan, R. A.; Vanderah, D. J.; Coon, C. L.; Gilardi, R. D.; George, C. F.; Flippen-Anderson, J., Polyazapolycyclics by condensation of aldehydes with amines. 2. Formation of 2,4,6,8,10,12-hexabenzyl-2,4,6,8,10,12-hexaazatetracyclo[5.5.0.05.9.03,11]dodecanes from glyoxal and benzylamines. *The Journal of Organic Chemistry* **1990,** *55* (5), 1459-1466.
135. Bazaki, H.; Kawabe, S.; Miya, H.; Kodama, T., Synthesis and Sensitivity of Hexanitrohexaaza-isowurtzitane(HNIW). *Propellants, Explosives, Pyrotechnics* **1998,** *23* (6), 333-336.
136. Sider, A. K.; Sikdev, N.; Gandhe, B. R.; Agrawal, J. P.; Singh, H., Hexanitrohexaazaisowurtzitane or CL-20 in India: Synthesis and Characterisation. *Defence Science Journal* **2002,** *52* (2), 135-146.
137. Mertens, K., Vorläufige Notiz über neu Nitroderivate des Dimethylanilins und Bereitung des Dimethylanilins. *Chem. Ber.* **1877,** *10,* , 995.
138. Urbanski, T.; Semenczuk, A., Preparation of N,2,4,6-tetranitro-N-methylaniline by action of nitric acid on dimethylaniline. *Bull. Acad. Pol. Sci., Cl. 3* **1957,** *5* (Classe III), 649-51.
139. Latypov, N. V.; Bergman, J.; Langlet, A.; Wellmar, U.; Bemm, U., Synthesis and reactions of 1,1-diamino-2,2-dinitroethylene. *Tetrahedron* **1998,** *54* (38), 11525-11536.
140. Czeskis, B. A., Synthesis of triple [14C]-labeled moxonidine. *Journal of Labelled Compounds and Radiopharmaceuticals* **2004,** *47* (10), 699-704.

141. Astrat'ev, A. A.; Dashko, D. V.; Mershin, A. Y.; Stepanov, A. I.; Urazgil'deev†, N. A., Some Specific Features of Acid Nitration of 2-Substituted 4,6-Dihydroxypyrimidines. Nucleophilic Cleavage of the Nitration Products. *Russian Journal of Organic Chemistry* **2001,** *37* (5), 729-733.
142. Meyer, R.; Köhler, J.; Homburg, A., *Explosives*. Sixth ed.; Wiley-VCH Verlag GmbH: Weinheim, 2007.
143. Welch, J. M. Low Sensitivity Energetic Materials. University of Munich, Munich, 2008.
144. (a) Crawford, M.-J.; Evers, J.; Göbel, M.; Klapötke, T. M.; Mayer, P.; Oehlinger, G.; Welch, J. M., γ-FOX-7: Structure of a High Energy Density Material Immediately Prior to Decomposition. *Propellants, Explosives, Pyrotechnics* **2007,** *32* (6), 478-495; (b) Evers, J.; Klapötke, T. M.; Mayer, P.; Oehlinger, G.; Welch, J., α- and β-FOX-7, Polymorphs of a High Energy Density Material, Studied by X-ray Single Crystal and Powder Investigations in the Temperature Range from 200 to 423 K. *Inorganic Chemistry* **2006,** *45* (13), 4996-5007.
145. Härtel, M. A. C. Feasibility Study of Direct Polycondensation of Energetic Monomers and Related High Energy Density Material Syntheses. Master-Thesis, Ludwig-Maximilians-Universität München, München, 2012.
146. Pelouze, J., Ueber den Arsenikbrechweinstein, den Harnstoff und das Allantoin. *Justus Liebigs Annalen der Chemie* **1842,** *44* (1), 100-109.
147. Foreign Terrorists in America: Five Years After the World Trade Center. In *Senate Judiciary Committee; Subcommittee on Technology, Terrorism, and Government Information*, Childers, J. Gilmore DePippo, Henry J.: USA, 1998.
148. Oxley, J.; Smith, J. L.; Brady, J.; Naik, S., Determination of Urea Nitrate and Guanidine Nitrate Vapor Pressures by Isothermal Thermogravimetry. *Propellants, Explosives, Pyrotechnics* **2010,** *35* (3), 278-283.
149. Worsham, J. E., Jnr; Busing, W. R., The crystal structure of uronium nitrate (urea nitrate) by neutron diffraction. *Acta Crystallographica Section B* **1969,** *25* (3), 572-578.
150. Bachmann, W.; Sheehan, J. C., A new method of preparing the high explosive RDX. *Journal of the American Chemical Society* **1949,** *71* (5), 1842-1845.
151. Turhan, H.; Atalar, T.; Erdem, N.; Özden, C.; Din, B.; Gül, N.; Yildiz, E.; Türker, L., Hexamethylenetetramine Dinitrate (HDN): The Precursor for RDX Production by Bachmann Process. *Propellants, Explosives, Pyrotechnics* **2013**, n/a-n/a.
152. Markofsky, S. B., Nitro Compounds, Aliphatic. In *Ullmann's Encyclopedia of Industrial Chemistry*, Wiley-VCH Verlag GmbH & Co. KGaA: 2000.
153. Aim, K., Saturated Vapor Pressure Measurements on Isomeric Mononitrotoluenes at Temperatures between 380 and 460 K. *Journal of Chemical & Engineering Data* **1994,** *39* (3), 591-594.
154. Wilkinson, P., *Technology and Terrorism*. F. Cass: 1993.
155. Marlair, G.; Kordek, M.-A., Safety and security issues relating to low capacity storage of AN-based fertilizers. *Journal of Hazardous Materials* **2005,** *123* (1–3), 13-28.
156. Zygmunt, B.; Buczkowski, D., Agriculture Grade Ammonium Nitrate as the Basic Ingredient of Massive Explosive Charges. *Propellants, Explosives, Pyrotechnics* **2012,** *37* (6), 685-690.
157. Vargeese, A. A.; Joshi, S. S.; Krishnamurthy, V. N., Use of potassium ferrocyanide as habit modifier in the size reduction and phase modification of ammonium nitrate crystals in slurries. *Journal of Hazardous Materials* **2010,** *180* (1–3), 583-589.

5 Vacuum Outlet GC/MS for Detection and Quantification of Explosives

The following section is partially based on a previous non-peer reviewed publication by the author of this thesis, which was published in "Labo-Online" in cooperation with the Shimadzu Company. [1]

The gas-chromatographic analysis of thermolabile, heavily volatile analytes like explosives is a special challenge since it requires the transfer of the analytes into the gaseous states at operating temperatures of 30 – 280 °C. Yet the elution temperature of the analytes must remain below their temperature of decomposition, which should be avoided until the final detection. The residence time of the analyte in hotter zones should be minimized.

Considering this the principal approach in the method development for the GC-analysis of explosives is the reduction of the elution temperature of the analytes. This can be achieved by increasing the flowrate of the carrier gas, which can be realized without difficulties for atmospheric detectors like electron capture (ECD) or flame ionization (FID) detectors. In case of GC/MS applications, the maximum flowrate is limited with respect to the ultrahigh vacuum (UHV) inside the MS detector, which must be preserved. *Kirchner et al.* [2] demonstrated the advantages of analyte protectants for the GC/ECD and GC/MS-analysis of explosives. *Boeker et al.* [3] presented recently a new concept for the realization of thermogradient gas chromatography using forced convection on a resistively heated column for the analysis of explosives. In this work vacuum outlet gas-liquid-chromatography (VO-GC/MS), as established by *Leclerq et al.* [4] and *de Zeeuw et al.* [5], is used. *Brust et al.* [6] used VO-GC/MS for the impurity profiling of TNT **17**. Further applications of GC/MS for the detection of explosives have been reviewed by *Lefferts* and *Castell* [7].

In case of Vacuum Outlet GC/MS the MS detector UHV is used to lower the elution temperature of the analytes as it spreads gradually along the analytical column. This effect is directly proportional to the inner diameter of the column and causes a reduction of the elution temperature of the analytes in combination. With the reduction of the pressure the optimum carrier gas velocity is increased, which is beneficial for the separation efficiency and the lowering of the elution temperatures.

For the optimized use of these effects a Restek RTX-TNT 1 column (6m length, 0.53 mm i.d., 1.5 µm film) was used in this work. This analytical column combines the maximum of the commercially available inner diameter with a proprietary phase which was specially adjusted for the separation of explosives. The length of the column should be short enough to allow fast elution of the analytes after reaching their elution temperature with sufficient separation efficiency. If one would attach this column directly to the mass spectrometer under atmospheric conditions, the detector vacuum would collapse with respect to the resulting carrier gas flow of about 50 mL min^{-1}. Mass spectrometer tolerate maximum carrier gas flow rates from 4 – 12 mL min^{-1} depending on their vacuum system. For the preservation of the detector vacuum a restriction, a short piece of capillary with small inner diameter (1.0-1.2 cm length, 0.05 mm i.d.), must be positioned in front of the analytical column. It is advantageous to place the restriction and the necessary connector to the analytical column inside the injector of the GC/MS system. This has been described extensively in the literature. [5]

So far Restek "press-tight" connectors and uniliner were used for the connection of the analytical column with the restriction. Commercially available "press-tight" glass connectors have to be cut prior to use with a glass cutter generating active surfaces. In case of the Uniliner the pressed connection can collapse. Additionally, Uniliner are not available for every injector in a multitude of varieties and the use of "press-tight" connectors is limited by the dimensions of the part itself. Within this work the use

of a SGE Siltite µ-Union is presented as connector for analytical column and restriction inside the injector. The µ-union has a length of less than 1 cm and a diameter of 3.5 mm. Therefore it can be used in any injector with an inner diameter of at least 5 mm and the end of the restriction can be placed near the optimum splitpoint for conventional analytical columns. The high temperature inside the injector results in the expansion of the stainless steel µ-union. By this the column connection seals itself and any remaining minimal leaks are located in the inert gas atmosphere of the injector. The major advantage of placing the restriction inside the injector is that the GC-system can be operated in constant pressure mode. In conventional GC applications it is widely established to operate the system in constant flow-mode, which means to adjust the head-pressure of the injector according to the oven temperature to achieve a constant carrier gas flow-rate throughout the analysis. According to calculations that are based on the *Hagen-Poiseuille* equation [8] (cf. section 5.2), it can be demonstrated that the flow dynamics of the GC/MS setup are dominated by the restriction in the isothermal injector and that the carrier gas flow-rate depends to a negligible extent of 4% on the GC oven temperature. This allows the operation of the Vacuum Outlet GC/MS setup in constant pressure mode.

The concept of VO-GC/MS was realized in this work on a Shimadzu GCMS-QP2010 SE GC/MS device in combination with a Shimadzu AOC-20i autosampler and an Atas Optic 4 injector that was optimized for Shimadzu systems. The Labsolutions GCMSsolution v4.11 Software of the GC/MS system requires the input of the analytical column parameters (length, diameter, film thickness) to calculate the injector parameters and limits the flow-rate to 4 mL min^{-1}. Complex arrays of multiple capillaries, like the VO-GC/MS setup described in this work, cannot be entered. This problem can be solved by the use of a virtual column, which allows the configuration of the desired head pressure without exceeding the flowrate limit that is calculated for the virtual column by the software. The virtual column used in this work allowed the setting of head pressures up to 760 kPa and had the following parameters: length 100 m, 0.20 mm diameter, 0.25 µm film thickness.

The µ-union, used for the connection of restriction and analytical column, is with an outer diameter of 3.5 mm not compatible with the commercially available Atas liners. Therefore V2A stainless steel tubes were cut to 100 mm length and two split notches were added at the bottom. These notches can be found on any commercial Atas Liner for split injections. Both the µ-union and the custom stainless steel liner were inertized by coating with SilcoNert 2000 by the company SilcoTek.

5.1 Optimization for Quantification Applications

The main goal in this work is the quantification of explosives with an internal standard method. For this purpose two key requirements must be achieved, when a sample is injected repeatedly: The absolute peak areas and integral ratios of analyte and standard must be reproducible. To investigate the reproducibility of the VO-GC/MS setup established in this work a test mixture of naphthalene (NAP), 4-nitrotoluene (4-MNT 14), 2,4-Dinitrotoluene (2,4-DNT 15), 1-Nitronaphthalene (NiNAP) and Phenanthrene (PHE) was prepared. The analytes were chosen to generate a mixture of compounds with boiling points ranging from 218 °C to 340 °C to investigate the influence of analyte volatility (cf. Table 1).

Table 1 Composition of the test mixture. The analytes were dissolved in 10 mL of acetonitrile.

Analyte	Naphtalene	4-Nitrotoluene	2,4-Dinitrotoluene	1-Nitronaphtalene	Phenanthrene
Abbreviation	NAP	4-MNT **14**	2,4-DNT **15**	N-NAP	PHE
m [g]	0.0166	0.0157	0.0169	0.0169	0.0156
n [mmol]	0.1295	0.1145	0.0928	0.0976	0.0875
c [µmol/mL]	12.9511	11.4483	9.2788	9.7591	8.7525
T_{boil} [°C]	218	238	>250	304	340

For the optimization in this work the web contributions by *Matthew Klee* [9] were extremely helpful. The optimization included the following parameters: concentration of analyte (4 levels – dilution factors of stock solution: 1/8, 1/16, 1/32, 1/64), injector temperature (175 – 250 °C), glass wool inside the GC liner and MS event time (20 – 300 ms). For the facilitation of the elucidation of the optimization procedure it is stated in advance that neither the injector temperature nor the concentration of the solution had influence on the reproducibility of the VO-GC/MS measurement.

For the improvement of the reproducibility of the absolute peak areas it was crucial to insert silanized glass wool in the GC-Liner. The glass wool should be penetrated at least 2 mm by the injection needle. Capillary forces then extract the analyte solution from the canula and distribute it on the glass wool.

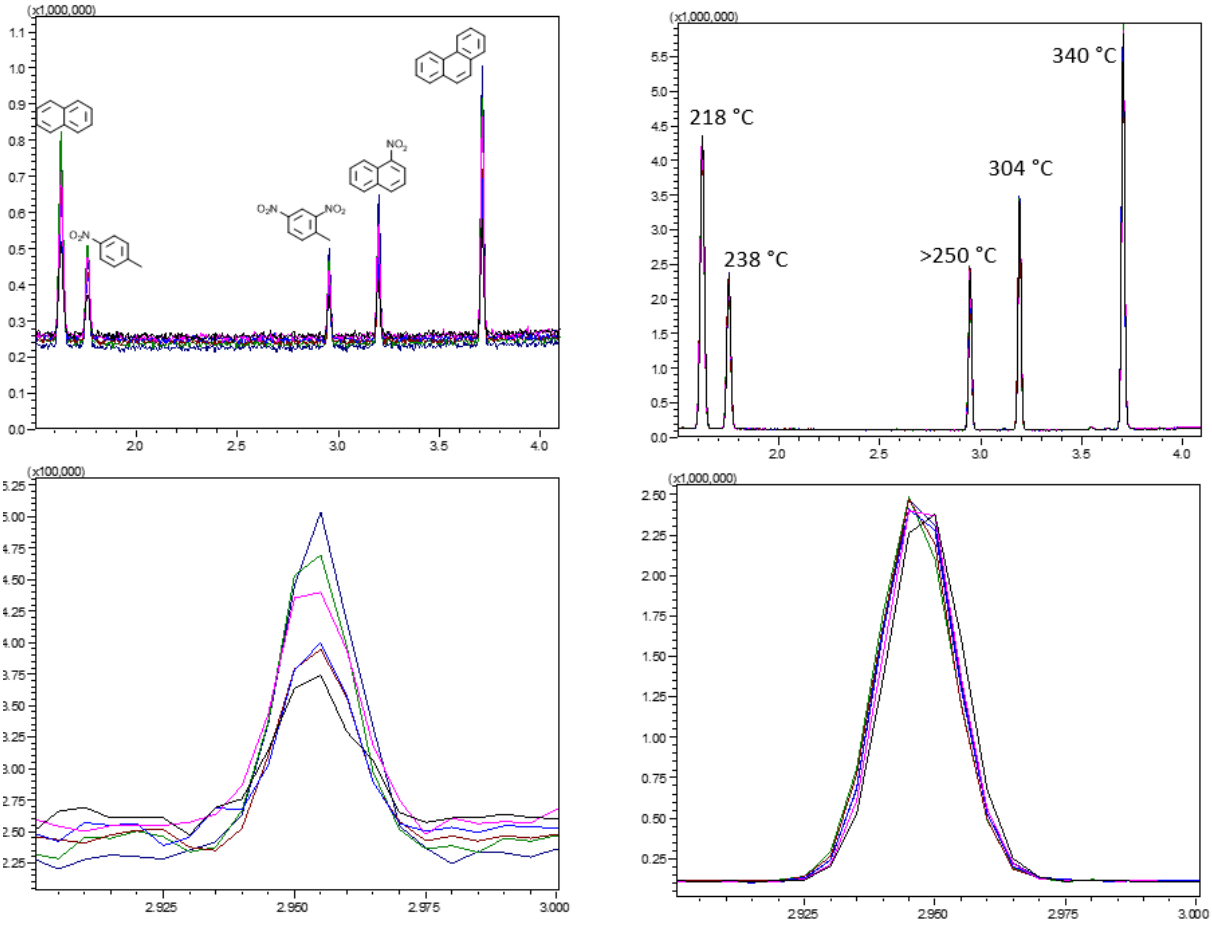

Figure 1 – Up: Superimposition of 6 chromatograms of directly repeated injections of the test mixture. Down: Zoom on single peak of identical superimposition. Left: without silanized glasswool in the liner, right: with silanized glasswool in the liner. The boiling structure formulae and the boiling points of the analytes are given in the upper chromatograms.

Table 2 – The influence of the introduction of glass wool into the liner on the absolute peak areas. Averaged results of six directly repeated injections.

Analyte	**I[counts]**	**σ [%]**	**I[counts]**	**σ [%]**	**α**
	without wool		with wool		
Naphthalene	335286	23.2	3173302	0.6	9
4-Nitrotoluene	60869	25.2	623111	1.0	10
2,4-Dinitrotoluene	38304	32.4	525603	0.6	14
1-Nitronaphthalene	55487	28.4	626790	1.4	11
Phenanthrene	235070	31.9	2516984	1.2	11

Figure 1 visualizes and Table 2 demonstrates the effect of the introduction of glass wool into the GC-liner. In Table 2 the averaged peak areas of six directly repeated injections with and without wool are stated for all five test analytes. The standard deviation is reduced by the introduction of glass wool from 23.2 – 32.4 % to 0.6 to 1.4 %. The ratio α in the range of 9 – 14 is the quotient of average peak area with glass wool to average peak area without glass wool. This means that the sensitivity of the system was increased by a factor of 9 – 14 by the introduction of glass wool into the GC-liner. Presumably, without glass wool a large fraction of the analytes are injected to the bottom of the liner and exit the system via the split flow. Yet there is another problem to solve. Taking a closer look at the peak tips of the zoom in the lower right of Figure 1 it becomes evident that the tip of the peak is not registered correctly. The chromatograms were recorded in scan mode (30 – 500 amu) with an event time of 300 ms, which means that each 300 ms a new datapoint is created. The peak mentioned has a baseline width of 3 seconds and is therefore registered with 10 datapoints. This is not sufficient for reproducible peak area ratios considering internal standard quantification. With respect to this selective ion monitoring was chosen as the mode of operation for the mass spectrometer. Instead of monitoring the 470 mass channels from 30 – 500 amu, the detector monitors 6 mass channels: 1 quantification and 5 reference ion channels for the identification of the analyte by the relative mass peak intensities.

Table 3 – Selective Ion Monitoring Program for the Mass Spectrometer

Analyte	**T_{start} [min]**	**T_{end} [min]**	**m/z 1**	**m/z 2**	**m/z 3**	**m/z 4**	**m/z 5**	**m/z 6**
NAP	0.5	1.7	128	127	129	64	51	102
4-MNT 14	1.7	2.7	91	137	65	39	107	77
2,4-DNT 15	2.7	3.1	165	89	63	90	119	39
N-NAP	3.1	3.45	127	115	173	126	77	75
PHE	3.45	4.1	178	89	76	176	179	88

The SIM program used in this work for the quantification of the analytes in the test mixture can be found in Table 3. A microscan width of 1 amu was used. This means that for mass channel 128 the mass channels from 127.0 – 129.0 amu are monitored to find the mass peak with the highest intensity.

For the investigation of the influence of the event time on the reproducibility of the peak area ratios six chromatograms of directly repeated injections were recorded for each event time ranging from 20 ms to 300 ms. Arbitrary chosen integral ratios were introduced to investigate the reproducibility of the integral ratios.

Table 4 – Example of Integral Ratio evaluation for event time 20 ms.

integral ratio	#1	#2	#3	#4	#5	#6	mean	σ
NAP/4-MNT **14**	5.05	5.05	5.06	5.05	5.06	5.05	5.05	0.005
NAP/2,4-DNT **15**	5.45	5.44	5.44	5.42	5.44	5.45	5.44	0.010
NAP/N-NAP	4.82	4.81	4.82	4.81	4.81	4.83	4.82	0.009
PHE/4-MNT **14**	4.21	4.24	4.23	4.22	4.20	4.20	4.22	0.018
PHE/2,4-DNT **15**	4.54	4.56	4.55	4.53	4.52	4.53	4.54	0.016
PHE/N-NAP	4.02	4.04	4.03	4.02	4.00	4.02	4.02	0.014
							∑σ	**0.073**
							$\overline{\sigma}$	**0.012**

Table 4 gives an example for the evaluation of the reproducibility of the integral ratios of six directly repeated injections. To judge the reproducibility at a certain event time the sum of standard deviations ∑σ and the mean standard deviation $\overline{\sigma}$ were calculated for each event time.

Table 5 – Results of the event time optimization. Sum of standard deviations ∑σ and mean standard deviation $\overline{\sigma}$ for six directly repeated injections.

event time [ms]	**20**	**50**	**100**	**150**	**200**	**250**	**300**	**80**	**100**	**120**
∑σ	0.073	0.059	0.045	0.051	0.069	0.082	0.075	0.040	0.050	0.041
$\overline{\sigma}$	0.012	0.010	0.008	0.009	0.012	0.014	0.012	0.007	0.008	0.007

Table 5 compiles the results of the event time optimization study. The reproducibility of the integral ratios is indirectly proportional to the the values of ∑σ and $\overline{\sigma}$. The first measurement series was carried out with the event times 20, 50, 100, 150, 200, 250 and 300 ms. An optimum could be found with an event time of 100 ms. To verify this result a measurement series with event times of 80, 100 and 120 ms was carried out. The reproducibility is nearly identical for event times of 80 and 120 ms. Therefore the optimum range for a SIM measurement with six simultaneous mass channels and a micro scan width of 1 amu is in the range of 80 – 120 ms and can be used for quantification applications.

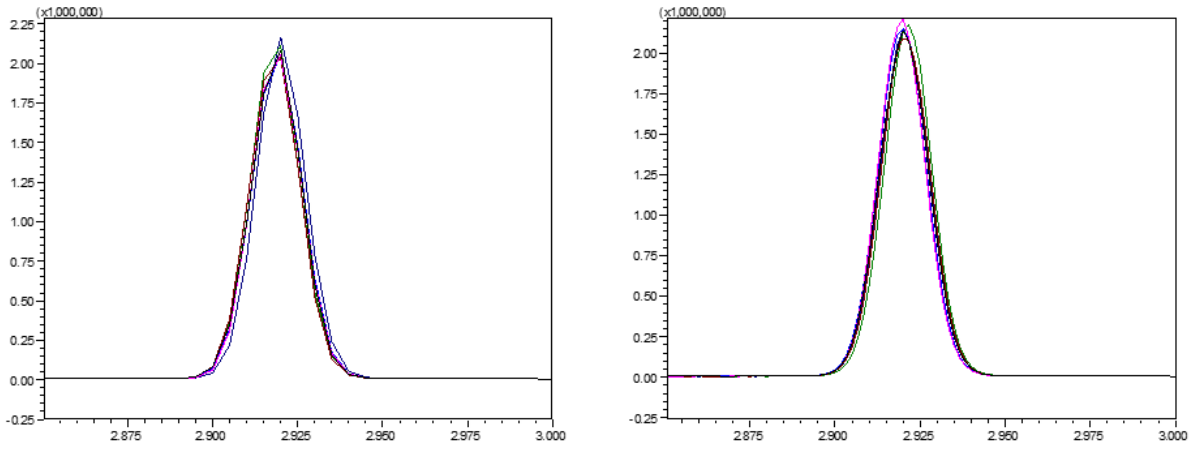

Figure 2 - Superimposition of six directly repeated injection of identical sample and peak measured with 300 ms (left) and 100 ms (right) event time. With 100 ms event time the peak is recorded more exactly with 30 instead of 10 datapoints.

The effect of the decreased event time which leads to more precise detection of peaks is visualized in Figure 2 for a peak recorded under SIM conditions with 300 ms and 100 ms event time. With 300 ms event time the tip of the peak is not properly detected, which leads to imprecise results of quantification.

Table 6 – Compilation of VO-GC/MS parameters

GC/MS	*Shimadzu QP2010SE®*
Injector	Atas Optic 4
Liner	10 mm V2A stainless steel tube, 5 mm wall thickness, equipped with silanized glass wool (2 mm injection needle penetration into wool)
Restriction	**M1**: 0.025 mm capillary, 7.76 mm length (Restek #10097) **M2**: 0.025 mm capillary, 8.11 mm length (Restek #10097) **M3**: 0.050 mm capillary, 10.10 mm length (Restek #10098)
Column connector	*SGE Siltite µ-Union®* (Restek #073562)
Analytical columns	*Restek RTX-TNT 1®* (6 m, 0.53 mm, 1.5 µm)

Oven program	**M1**: 40 °C (hold 0.10 min) → 100 °C (60 °C min^{-1}, hold 0.50 min) → 200 °C (40 °C min^{-1}, hold 0.50 min) **M2**: 40 °C (hold 0.10 min) → 100 °C (60 °C min^{-1}, hold 0.50 min) → 280 °C (40 °C min^{-1}, hold 0.50 min) **M3**: identical to M2
Injector head pressure	**M1**: 400 kPa **M2**: 400 kPa **M3**: 90 kPa
virtual column	100 m, 0.25 µm film thickness, 0.20 mm i.d.
column flow	**M1**: 2.33 mL min^{-1} **M2**: 2.33 mL min^{-1} **M3**: 3.92 – 4.08 mL min^{-1}
split ratio	**M1**: 18.7 **M2**: 24.5 **M3**: 150
split flow	**M3**: 25.38 mL min^{-1} (measured at split exit with soap film flow meter, corrected according to *Boeker et al.* [8]
purge flow	5 mL min^{-1}
injection volume	1 µL
Ion source	200 °C
MS interface	200 °C
MS	**M1**-**M3**: SCAN m/z 30 – 500, event time 0.300 s

SIM-programs for mass spectrometer:

M1 – SIM:

T_{start} [min]	T_{end} [min]	t_{event} [s]	MC1 m/z	MC2 m/z	MC3 m/z	MC4 m/z	MC5 m/z	MC6 m/z
0.5	1.7	0.020 – 0.300	128	127	129	64	51	102
1.7	2.7	0.020 – 0.300	91	137	65	39	107	77
2.7	3.1	0.020 – 0.300	165	89	63	90	119	39
3.1	3.45	0.020 – 0.300	127	115	173	126	77	75
3.45	4.1	0.020 – 0.300	178	89	76	176	179	88

M3 – SIM:

T_{start} [min]	T_{end} [min]	t_{event} [s]	MC1 m/z	MC2 m/z	MC3 m/z	MC4 m/z	MC5 m/z	MC6 m/z
0.5	1.42	0.1	46	30	43	59	120	65
1.42	1.6	0.1	120	65	57	41	91	137
1.6	2.4	0.1	91	137	65	46	30	
2.4	3	0.1	46	30	165	63	89	
3	3.5	0.1	165	89	46	30	210	
3.5	4	0.1	210	89	46	76	42	
4	6.1	0.1	46	42	194	77	30	

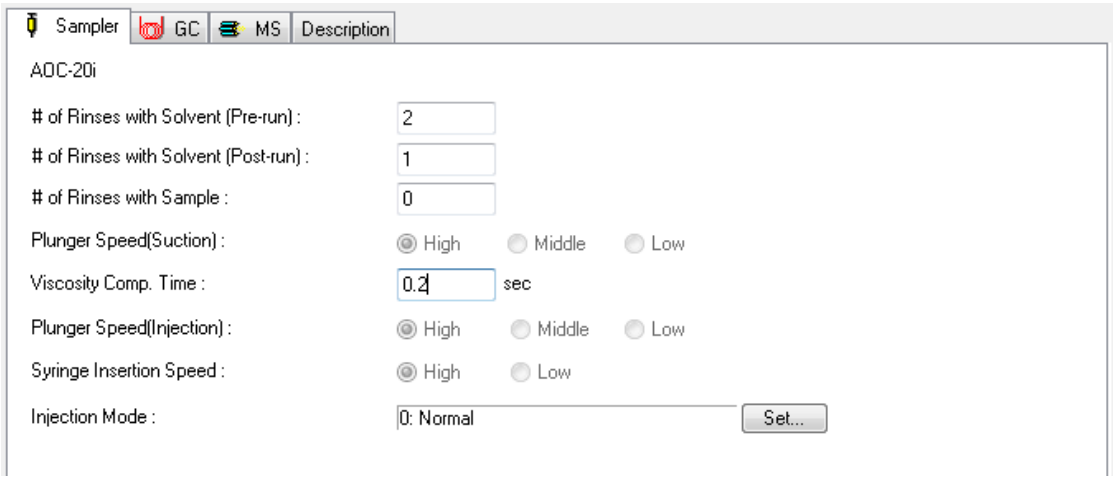

Figure 3 – Injection Parameters used for the Shimadzu QP2010SE AOC 20i Autosampler. Screenschot of LabSolutions GCMSsolution v4.11 [M3]

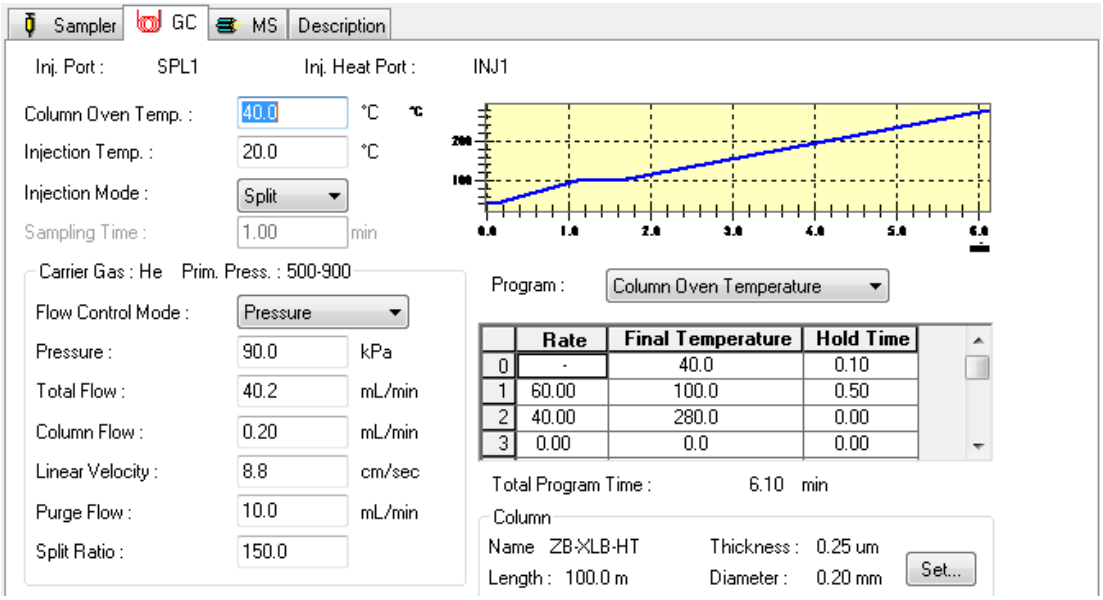

Figure 4 – Injector and GC oven parameters used for the Shimadzu QP2010SE AOC 20i Autosampler. Screenschot of LabSolutions GCMSsolution v4.11 [M3]

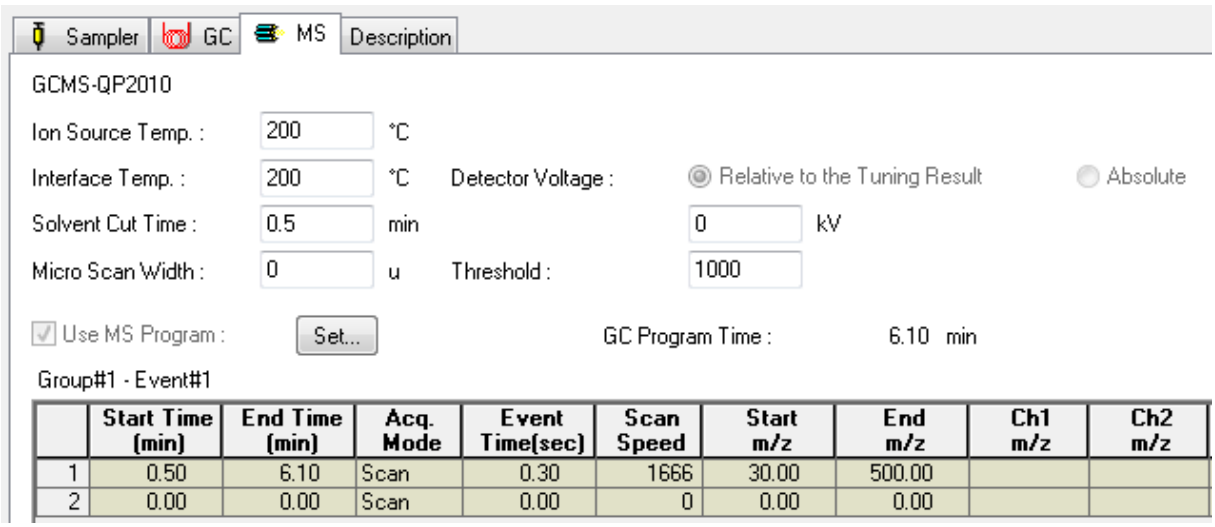

Figure 5 – Mass spectrometer parameters used for the Shimadzu QP2010SE AOC 20i Autosampler. Screenschot of LabSolutions GCMSsolution v4.11 [M3]

5.2 Calculation of the Flow in a Series of Capillaries

It was pointed out before that the VO/GC-MS setup presented in this work is operated with constant injector head pressure. The LabSolutions GCMSsolution software, that controls the injector head pressure and split flow via the advanced flow control (AFC) module of the Shimadzu QP2010SE GC/MS system cannot calculate the flow parameters for a series of capillaries. Since after each setup installation a new restriction capillary with individual length is installed, it is necessary to calculate the head pressure that is necessary to obtain the desired flow rate. In this work the flow rate 4 mL min^{-1} proved to be a good value for efficient separation and a sufficient detector vacuum (~9 Pa). The flow in a series of capillaries can be calculated according to a modified form of the Hagen-Poiseuille equation (1), which was established by *Boeker et al.* [8, 10]

$$V_{Std.} = (p_1^2 - p_2^2) \times \frac{\pi \times d^4 \times T_{Std.}}{256 \times \eta_{(T)} \times l \times p_{Std.} \times T_x} \quad (1)$$

$V_{Std.}$ = flow at standard conditions (298.15 K, 101300 Pa, [m^3/s]); p_1 = absolute input pressure [Pa]; p_2 = output pressure (0 Pa for vacuum); $p_{Std.}$ = standard pressure (101300 Pa); d = diameter of the respective capillary [m]; l = length [m]; $\eta_{(T)}$ = dynamic viscosity of Helium ($4.280 \times 10^{-8} \times T_x + 6.968 \times 10^{-6}$), [Pa·s]); T_x = temperature in the respective capillary [K]; $T_{Std.}$ = standard temperature (298.15 K)

The dynamic viscosity of Helium $\eta_{(T)}$ is calculated by:

$$\eta_{(T)} = C_1 \times T_x + C_2 \quad (2)$$

C_1: 4.280 × 10-8 Pa s K^{-1}, C_2: 6.968 × 10-6 Pa s

The values of the dynamic viscosity $\eta_{(T)}$ are temperature and carrier gas dependent and can be calculated for any temperature. (N_2: C_1: 3.500×10^{-8} Pa s K^{-1}, C_2: 7.994×10^{-6} Pa s; H_2: C_1: 1.830×10^{-8} Pa s K^{-1}, C_2: 4.416×10^{-6} Pa s) The absolute input pressure p_1 is calculated from the chosen head pressure in the injector and the standard pressure (cp. Equation (3)).

$$p_1 = p_{input} + p_{std} \quad (3)$$

p_{input} = head pressure in the injector

It is convenient to combine the constant values to a single parameter A (eq. (4)) and the dimensions of the capillary, the temperature and the viscosity to a resistance parameter K (eq. (5)).

$$A = \frac{\pi}{256} \times \frac{T_{Std.}}{p_{Std.}} = \frac{\pi}{256} \times \frac{298.15K}{101300Pa} = 3.6119 \times 10^{-5}\, {}^{K}/_{Pa} \quad (4)$$

$$K = \frac{\eta_{(T)} \times l \times T_x}{d^4} \quad (5)$$

For each part of the series of capillaries a separate K (cp. Equation (6)) has to be calculated as each part has another length l, diameter d, temperature T_x and and dynamic viscosity $\eta_{(T)}$. The individual K values of each respective capillary are summed up to K_{total}.

$$K_{total} = \sum_1^i K_i \quad (6)$$

For a series of capillaries Equation (7) can be derived from Equation (1)

$$V_{Std.} = (p_1^2 - p_2^2) \times A \times \frac{1}{\sum_1^i K_i} \quad (7)$$

With help of these equations, an example of flow calculation at 175°C for the VO-GC/MS Setup in this work will be calculated in the following:

All constant parameters used are listed in Table 7.

Table 7: Fix parameters for calculation of the flow.

p_{input}	90 kPa = 90000 Pa
p_{std}	101300 Pa
p_1	P_{input} + p_{std} =193000 Pa
p_2	0 Pa (vacuum)
T_{std}	298.15 K
C_1	4.280 x10^{-8} Pa·s/K
C_2	6.968x10^{-6} Pa·s
A	3.6119x10^{-5} K/Pa

The values of *K* for the different capillaries are calculated with Equation (5):

Table 8: Calculation of different $\eta_{(T)}$ and K for each section of the series of capillaries for an oven temperature of 40°C.

Variables / section	d [mm]	l [m]	T_x [°C]	$\eta_{(T)}$ [Pa·s]	*K* [Pa·s·K/m^3]
Injector	0.050	0.0101	175	2.615x10^{-5}	1.8937x10^{13}
Analytical Column	0.53	5.85	40	2.037x10^{-5}	4.7298x10^{11}
MS Interface	0.53	0.15	200	2.722x10^{-5}	2.4483x10^{10}

According to the respective *K* values of Table 8, the total K_{total} is calculated as a sum of all *K* (eq. (6)).

$$K_{total} = \sum_1^i K_i = 1.9435 \times 10^{13} \frac{Pa \times s \times K}{m^3} \quad (8)$$

Finally the flow at standard conditions (298.15 K, 101300 Pa) is calculated with Equation (7):

$$V_{Std} = \frac{(p_1^2 - p_2^2) \times A}{\sum_1^i K} = \frac{(191300^2 - 0^2) \times 3.6119\text{x}10^{-5}}{1.9435 \times 10^{13}} \frac{Pa^2 \times K \times m^3}{Pa \times Pa \times s \times K} = \quad (9)$$

$$= 6.80 \times 10^{-8} \frac{m^3}{s} = 4.08 mL/min$$

If the temperature of the GC oven is changed to 250 °C, the column flow will decrease to 3.92 mL min^{-1}. The corresponding calculation is shown in Figure 6.

Calculation of the flow through a series of capillaries

Input gauge pressures (above atmosphere as indicated by manometers)

Input pressure	kPa (g)	90
	bar (g)	0.9
	psi (gauge)	13.053

absolute pressure (needed for the calculation)

Input pressure abs.	Pa (abs.)	191300

Output pressure	Pa	0 (101300=atmosphere, 0=vacuum)

capillary data		Injector	Transfer	Transfer	Column	Transfer	Transfer	Detector	Sum
i.D.	mm	0.05	0.53	0.53	0.1	0.1	0.1	0.1	
T	°C	175	280	200	240	300	300	290	
eta He	Pa s	2.615E-05	3.064E-05	2.722E-05	2.893E-05	3.150E-05	3.150E-05	3.107E-05	
lenght	m	0.0101	5.85	0.15	0	0	0	0	6.010
									K_tot
Factor K		1.89E+13	1.26E+12	2.45E+10	0	0	0	0	2.02E+13
Factor A		3.61E-05							
		Input press.	intermediate pressures						Output press.
p_middle	Pa	191300	48155	6657	0	0	0	0	0
hold-up time	s	0.00	3.43	0.01	0.00	0.00	0.00	0.00	3.44
med.lin.veloc.	m/s	37.84	1.71	10.73	0.00	0.00	0.00	0.00	
	cm/s	**3784**	**171**	**1073**	**0**	**0**	**0**	**0**	

flow @25°C,1,013 bar) ml/min **3.92**

Values from HP Flow Calculator, linear equation
Speed Optimized Flow from Blumberg (1999)

	Helium	Nitrogen	Hydrogen
C1	4.280E-08	3.500E-08	1.830E-08
C2	6.968E-06	7.994E-06	4.416E-06
SOF_100	0.8	0.25	1

Helium	C1	4.280E-08
	C2	6.968E-06
	SOF_100	0.8

s 3.44 min **0.05738**

Figure 6 – The results of flow calculation for the VO-GC/MS calulation at 280 °C oven temperature. (MS Excel Screenshot)

The injector (175 °C) and the MS interface (200 °C) remain isothermal and the head pressure of the injector is kept constant at 90 kPa. Solely the column oven temperature is changed from 40 to 280 °C. This causes a change of column flow from 4.08 mL min^{-1} (cf. eq. (9)) to 3.92 mL min^{-1} (cf. Figure 6) The column flow rate change from start to end temperature is 3.9 % of the starting value and negligible. Therefore, the injector can be operated in constant pressure mode with the VO-GC/MS setup described in this work. With the calculation of the flow dynamics it is possible to calculate the scenario of an analytical column (6m, 0.53 mm i.d.) under atmospheric pressure conditions at 25 °C. The resulting helium gas flow of 50 mL min^{-1} would lead to the collapse of the MS detector vacuum. (cf. Figure 7)

Calculation of the flow through a series of capillaries

Input gauge pressures (above atmosphere as indicated by manometers)

Input pressure	kPa (g)	0
	bar (g)	0
	psi (gauge)	0.000

absolute pressure (needed for the calculation)

Input pressure abs.	Pa (abs.)	101300

Output pressure	Pa	0 (101300=atmosphere, 0=vacuum)

capillary data		Injector	Transfer	Transfer	Column	Transfer	Transfer	Detector	Sum
i.D.	mm	0.05	0.53	0.53	0.1	0.1	0.1	0.1	
T	°C	25	25	25	240	300	300	290	
eta He	Pa s	1.973E-05	1.973E-05	1.973E-05	2.893E-05	3.150E-05	3.150E-05	3.107E-05	
lenght	m	0	5.85	0.15	0	0	0	0	6.000
									K_tot
Factor K		0	4.36E+11	1.12E+10	0	0	0	0	4.47E+11
Factor A		3.61E-05							
		Input press.	intermediate pressures						Output press.
p_middle	Pa	101300	101300	16017	0	0	0	0	0
hold-up time	s	0.00	1.06	0.00	0.00	0.00	0.00	0.00	1.06
med.lin.veloc.	m/s	0.00	5.51	35.63	0.00	0.00	0.00	0.00	
	cm/s	**0**	**551**	**3563**	**0**	**0**	**0**	**0**	

flow @25°C,1,013 bar) ml/min **49.72**

Values from HP Flow Calculator, linear equation
Speed Optimized Flow from Blumberg (1999)

	Helium	Nitrogen	Hydrogen
C1	4.280E-08	3.500E-08	1.830E-08
C2	6.968E-06	7.994E-06	4.416E-06
SOF_100	0.8	0.25	1

Helium	C1	4.280E-08
	C2	6.968E-06
	SOF_100	0.8

s 1.06 min **0.01775**

Figure 7 – Calculation of the flow through a capillary (6m length, 0.53 mm inner diameter) at atmospheric pressure and 25 °C temperature. The resulting flow of 50 mL min^{-1} would result in the collapse of the MS detector vacuum. (MS Excel screenshot)

5.3 Experimental Verification of the Split-Flow

In standard applications solely the analytical column is positioned in the liner of the GC injector. In case of VO-GC/MS, the injector is filled with the µ-Union column connector (length 1 cm, diameter 3.5 mm). Since the stainless steel liner used has an inner diameter of 4.0 mm, solely 0.25 mm space remain between liner and µ-Union. Conventional analytical columns have an outer diameter of less than 1 mm. The split flow exits the liner at the bottom and has to pass the µ-Union. Since this situation is far from standard it was checked whether the space "a" between µ-union and liner does allow a sufficient splitflow.

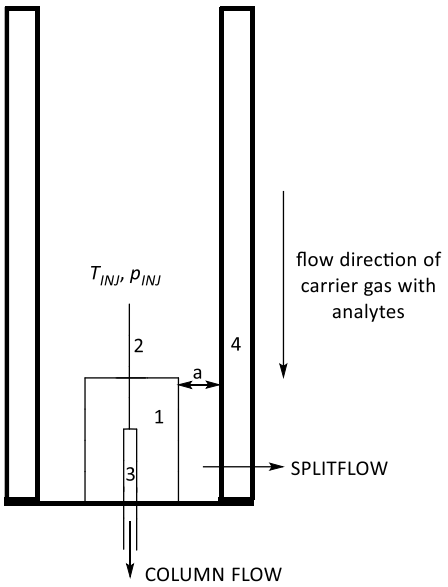

Figure 8 Schematic illustration of the cross-section of the Atas4 Injector in the VO-GC/MS configuration used in this work. (cf. Table 6) 1: SGE Siltite µ-Union (length ≈10 mm, diameter 3.5 mm), 2: restriction (10.10 mm length, 0.050 mm inner diameter), 3: Analytical column (6 m length, 0.53 mm inner diameter) 4: stainless steel liner (100 mm length, 0.5 mm wall thickness, 0.4 mm inner diameter. a: 0.25 mm. Does the space "a" between µ-union and liner allows sufficient splitflow?

To answer this question several splitflows were set keeping the remaining conditions constant. The flowrate of the splitflow was measured using a Soapfilm Flowmeter (Hewlett Packard, #0101-0113) and corrected according to the formula stated and derived by *Boeker et al.* [11]:

$$V_{Std} = V_{meas} \times \frac{T_{Std}}{T_{amb}} \times \frac{p_{amb}}{p_{std}} \times \left(1 - \frac{p_{WS}}{p_{amb}}\right) \tag{10}$$

V_{Std} = corrected flow at standard conditions (25°C, 101300 Pa, [mL min^{-1}]); V_{meas} = measured flow with soap film flowmeter [mL min^{-1}]; TStd = standard temperature (298.15 K); T_{amb} = ambient temperature [K]; p_{amb} = ambient pressure [Pa]; p_{std} = standard pressure (101300 Pa); p_{WS} = saturation pressure of water.

The flow-rate is measured with the soap film flowmeter by measuring the the time span Δt a soap film needs to pass a defined volume V_{tube} in the soap film flow meter tube:

$$V_{meas} = \frac{V_{tube}}{\Delta t} \tag{11}$$

V_{tube}: volume in soap film flowmeter [mL], Δt: time span [min]

The saturation vapor pressure of water p_{ws} is calculated by:

$$p_{ws} = 10^{\left(8.3246 - \frac{1799.73}{(T_{amb} + 238.734)}\right)} \tag{12}$$

With the tools to measure the corrected flow at standard conditions in hands, the relation between set flow and real flow was checked keeping the injector temperature and head pressure constant. The LabSolutions GCMSsolution calculated for 90 kPa head pressure a column flow of 0.20 mL min^{-1}. The splitflow is the product of column flow and split ratio. The split ratio was varied from 50 to 450 to set splitflows from 10 – 90 mL min^{-1}. (cf. Table 9)

Table 9: Deviation of the corrected flow in comparison to the employed splitflow f_{split} for a measurement series at an injector temperature of 175°C and 90 kPa head pressure and a calculated column flow of 4.08 mL min^{-1}

f_{set}[a] [mL min^{-1}]	r_{split}[b]	f_{obs}[c] [mL min^{-1}]	σ(f_{obs})[d] [mL min^{-1}]	Deviation[e] [%]	p_{split}[f]
10	50	5.24	0.02	47.65	0.438
20	100	14.61	0.05	26.97	0.218
30	150	25.37	0.02	15.07	0.139
40	200	36.16	0.01	9.61	0.101
50	250	46.93	0.04	6.15	0.080
60	300	57.24	0.04	4.60	0.067
70	350	67.50	0.13	3.57	0.057
80	400	77.95	0.10	2.56	0.050
90	450	88.00	0.35	2.22	0.044

[a] set spliflow [b] split ratio [c] observed splitflow (soap film flowmeter at split exit) [d] standard deviation of observed splitflow (3 measurements) [e] deviation of set and observed splitflow ((f_{set}-f_{obs})×100/ f_{set}) [f] split proportion (4.08 mL min^{-1} / (4.08 mL min^{-1} + f_{obs})

It could be observed that for small split ratios the deviation of measured and entered split flow is tremendous (e.g. 47.65 % for splitratio 10). With increasing split ratio the deviation of entered and calculated splitflow gets smaller (e.g. 2.23 % for Splitratio 450). With this it could be demonstrated that the µ-union is not blocking the split exit for splitflows up to 90 mL min^{-1}.

Table 10 – Results of split measurement for a mixture of explosives. Integrals from VO-GC/MS measurement for different splitflows. [M3 scan]

f_{set} [mL min^{-1}][a]	**10**[b]	σ [%][c]	**20**[b]	σ [%][c]	**30**[b]	σ [%][c]
EGDN **06**	n.m.[d]	n.m.[d]	3813982	0.61	2284176	0.62
TATP **02**	8551142	1.66	4336433	0.15	2622589	1.60
2-MNT **12**	6491403	0.51	3273470	0.97	1980013	0.46
DMDNB **26**	7525425	0.87	3723138	0.65	2258411	0.42
3-MNT **13**	7580942	0.79	3787023	0.40	2290783	0.74
4-MNT **14**	7268721	0.33	3616819	0.17	2192761	0.17
GTN **17**	6831835	1.42	3380557	0.52	2056274	0.70
2,6-DNT **16**	6359160	0.31	3154809	1.64	1946103	1.24
2,4-DNT **15**	6294029	0.21	3168982	1.31	1971343	1.19
ETN **08**	2076577	3.15	1401374	1.28	982421	1.19
TNT **17**	4994964	1.76	2640271	1.06	1692207	0.96
PETN **09**	3969225	0.68	2464785	1.37	1702811	0.49
RDX **19**	4445531	1.48	2718120	2.24	1804816	1.02
f_{set} [mL min^{-1}][a]	**40**[b]	σ [%][c]	**50**[b]	σ [%][c]	**60**[b]	σ [%][c]
EGDN **06**	1626842	1.16	1027984	0.25	1018532	1.24
TATP **02**	1869614	1.57	1182522	1.34	1171536	2.60
2-MNT **12**	1414106	1.10	1068373	1.21	901050	1.38
DMDNB **26**	1627059	0.32	1160324	0.94	1040590	0.53
3-MNT **13**	1644878	1.53	1177777	0.31	1042260	0.98
4-MNT **14**	1587645	0.85	1130952	0.47	1000842	1.07
GTN **17**	1496803	1.10	958150	1.07	959369	0.77
2,6-DNT **16**	1416536	1.29	1021631	2.15	924881	1.84
2,4-DNT **15**	1451405	0.80	1063544	1.39	944680	1.29
ETN **08**	737990	2.09	467074	1.97	464138	1.97
TNT **17**	1227180	1.42	961396	4.48	820649	0.87
PETN **09**	1276089	0.29	831385	1.37	856735	1.63
RDX **19**	1402599	4.15	922835	4.00	966061	2.58
f_{set} [mL min^{-1}]	**70**[b]	σ [%][c]	**80**[b]	σ [%][c]	**90**[b]	σ [%][c]
EGDN **06**	846697	2.08	727395	1.71	641683	1.40
TATP **02**	1006795	0.96	858360	0.93	753131	2.95
2-MNT **12**	768567	1.32	658023	1.72	578539	1.16
DMDNB **26**	876237	0.29	765975	0.68	664551	1.54
3-MNT **13**	885915	1.38	747835	0.49	658895	0.73
4-MNT **14**	850322	1.42	722042	2.81	646381	2.72
GTN **17**	813549	2.08	701505	0.53	595856	1.27
2,6-DNT **16**	793627	1.62	685661	1.86	613417	1.69
2,4-DNT **15**	801148	1.02	704120	0.96	639385	1.76
ETN **08**	376704	1.89	302815	4.98	210281	14.71
TNT **17**	695491	0.86	605734	1.39	538753	2.13
PETN **09**	703211	0.56	598880	0.21	495368	8.51
RDX **19**	808936	2.85	714698	1.65	584082	11.95

[a] set spliflow (cf. Table 9) [b] Average Integral of Analyte (3 directly repeated injections) for f_{set} stated, [c] standard deviation of integrals of 3 directly repeated injections

Table 11 – Calculation of relative average integrals $\sum_{int,rel}$ and splitproportions $p_{split,rel}$

f_{set} [mL min^{-1}][a]	10	20	30
$\sum_{int}$[b]	7.24E+07	4.15E+07	2.58E+07
$\sum_{int,rel}$[c]	**1**	**0.573**	**0.356**
p_{split}[d]	0.438	0.218	0.138
$p_{split,rel}$[e]	**1**	**0.498**	**0.315**
f_{set} [mL min^{-1}][a]	40	50	60
$\sum_{int}$[b]	1.88E+07	1.30E+07	1.21E+07
$\sum_{int,rel}$[c]	**0.259**	**0.179**	**0.167**
p_{split}[d]	0.101	0.080	0.067
$p_{split,rel}$[e]	**0.231**	**0.183**	**0.153**
f_{set} [mL min^{-1}][a]	70	80	90
$\sum_{int}$[b]	1.02E+07	8.79E+06	7.62E+06
$\sum_{int,rel}$[c]	**0.141**	**0.121**	**0.105**
p_{split}[d]	0.057	0.050	0.044
$p_{split,rel}$[e]	**0.130**	**0.114**	**0.100**

[a] set spliflow (cf. Table 9) [b] Average Integral of Analyte (3 directly repeated injections) (cf. Table 10),
[c] $\sum_{int,rel} = \sum_{int}(f_{set})/\sum_{int}$(10 mL min^{-1}), [d] split proportion (cf. Table 9)
[e] $p_{split,rel}$ = $p_{split}(f_{set})/\ p_{split}$(10 mL min^{-1})

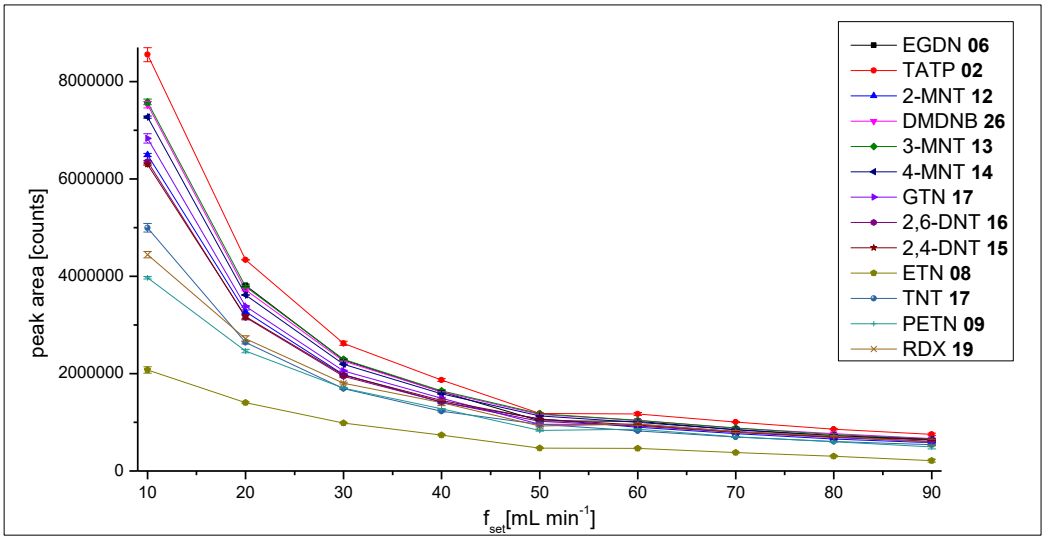

Figure 9 – Plot of $\sum_{int}$ vs. f_{set} (cf. Table 11) Error bars indicate standard deviation of three directly repeated injections. [M3 scan]

In the next step the split conditions applied (f_{set} = 10, 20, …, 90 mL min^{-1}) were tested with a mixture of explosives to investigate the influence of variation of the splitflow on the response of the detector. Table 10 is a compilation of the average integral intensities of the analytes for different values of f_{set}. From the average integral intensities of each individual analyte the sum of integrals $\sum_{int}$ of all analytes was calculated. For validation of the analyte stream splitting the value $\sum_{int,rel}$ (relative to the starting value $\sum_{int}$ (10 mL min^{-1})) was calculated. In analogy to this, the value $p_{split,rel}$ (relative to the starting value p_{split} (10 mL min^{-1}) was calculated. (cf. Table 11) It becomes evident that the values of $\sum_{int,rel}$ and $p_{split,rel}$ correlate well for each value of f_{set}. With increasing values of f_{set}, the effect of analyte dilution is decreasing from step to step. This effect is visualized in Figure 9. It can be concluded that the µ-union does not block the splitflow through the split exit at the bottom of the liner and that the stream of analyte is splitted correctly in the range of f_{set} from 10 mL min^{-1} to 90 mL min^{-1}. The value

of f_{set} correlates well with f_{obs} for higher values, but f_{obs} should always be measured manually at the split exit for the calculation of the correct value of p_{split}. (cf. Table 9).

5.4 Analysis of Explosives

For the initial testing purposes a mixture of explosives in acetone was prepared. To gain insight in the relative reponse factors of the analytes their molar concentration should be equal to introduce similar amounts of analytes:

Table 12 – Preparation of a mix of analytes with c_{sub} = 0.276 µmol mL^{-1} [M3 scan]

Analyte	m_{sub}[a] [mg]	m_{solv}[b] g	M[c] g mol^{-1}	n[d] µmol	V_{solv}[e] mL	c_{sub}[f] µmol mL^{-1}	V_{MIX}[g] mL	p_{sat}[h] Pa	T_{dec}[i] °C
HMX **22**	11.7	7.5418	296.1560	39.5	9.5345	4.1435	0.65	4.01E-13	278.3
MHN **05**	14.2	7.5260	452.1540	31.4	9.5145	3.3008	0.82	n.a.	175.8
EGDN **06**	10.7	7.6779	152.0620	70.4	9.7066	7.2493	0.37	1.02E+01	n.a.
GTN **17**	12.5	7.7132	227.0850	55.0	9.7512	5.6450	0.48	6.41E-02	n.a.
ETN **08**	15.5	7.4187	302.1080	51.3	9.3789	5.4704	0.50	6E-04*	181.9
PETN **09**	13.5	7.6749	316.1350	42.7	9.7028	4.4011	0.62	1.55E-06	199.8
DDNP **10**	11.1	7.6301	210.1050	52.8	9.6461	5.4769	0.49	n.a.	157.6
NM **27**	11.7	7.5860	61.0400	191.7	9.5904	19.9864	0.14	4.87E+03	n.a.
TNT **17**	10.7	8.4049	227.1320	47.1	10.6257	4.4335	0.61	7.33E-04	308.9
TETRYL **22**	10.2	7.7561	287.1440	35.5	9.8054	3.6227	0.75	8.68E-07	191.2
TATP **02**	17.2	7.3940	222.2370	77.4	9.3477	8.2796	0.33	6.20E+00	n.a.
PA **11**	10.3	7.7299	199.1220	51.7	9.7723	5.2932	0.51	n.a.	222.5
2-MNT **12**	15.3	7.1875	137.0477	111.6	9.0866	12.2862	0.22	1.92E+01	n.a.
3-MNT **13**	18.0	8.1599	137.0477	131.3	10.3159	12.7319	0.21	n.a.	n.a.
4-MNT **14**	9.80	7.6792	137.0477	71.5	9.7082	7.3657	0.37	6.52E+00	n.a.
2,4-DNT **15**	10.6	7.6749	182.1350	58.2	9.7028	5.9981	0.45	3.51E-02	296.0
2,6-DNT **16**	13.5	7.2924	182.1350	74.1	9.2192	8.0398	0.34	8.27E-02	n.a.
$EtONO_2$ **04**	8.10	7.8300	91.0660	88.9	9.8989	8.9855	0.30	n.a.	n.a.
CL-20 **21**	12.2	7.5631	438.1860	27.8	9.5614	2.9119	0.93	n.a.	243.4
DMDNB **26**	12.1	7.2930	176.1720	68.7	9.2200	7.4494	0.36	n.a.	n.a.
RDX **19**	14.6	7.3109	222.1170	65.7	9.2426	7.1118	0.38	4.40E-07	232.9

[a] mass of analyte, [b] mass of solvent, [c] molar mass of analyte, [d] molar amount of analyte, [e] volume of solvent (ρ(acetone): 0.791 g cm^{-3}), [f] concentration of substance, [g] volume for 2.71 µmol. Total volume of MIX: 9.84 mL. Concentration of analytes in mixture: 0.276 µmol mL^{-1} [h] vapor pressure of analyte at 298.15 K according to *Östmark et al.* [12], [i] decomposition temperature of analyte (differential scanning calorimetry, 5 °C min^{-1}), *value derived from own vapor pressure measurements.

This mixture of 21 analytes was injected in the VO-GC/MS setup with the parameters stated in Table 6 [M3]. The resulting chromatogramm is depicted in Figure 10. In total 14 of 21 Substances could be detected by the VO-GC/MS Setup. The substances that were not detectable are: HMX **22,** CL-20 **21**, MHN **05**, PA **11**, DDNP **10**. The most probable reasons for this is the combination of thermolability and low vapor pressure with these molecules. The latest eluting molecules are RDX 19 (p_{sat}: 4.40× 10^{-7} Pa, T_{dec} = 232.9 °C) and TETRYL **22** (p_{sat}: 8.68 × 10^{-7} Pa, T_{dec}: 191.2 °C). RDX **19**, HMX **22** (p_{sat}: 4.01 × 10^{-13} Pa, T_{dec}: 278.3 °C) and CL-20 **21** (p_{sat}: unknown, T_{dec}: 243.4 °C) are cycloaliphatic nitramines in high structural relations. The vapor pressure of HMX **22** is reduced by six orders of magniture in comparison to RDX 19 yet its decomposition temperature is significantly higher. The vapor pressure of CL-20 **21** (M: 438 g mol^{-1}) is unknown but it should be significantly lower than that of HMX **22** (M: 296 g mol^{-1}) due to its higher molar mass. MHN **05** is the heavier homolog of ETN **08** and contains two more methylene nitrato ($CHONO_2$) units. The repertoire of analytes tested contains several linear polynitrate

esters, which all contain two terminal CH_2ONO_2 units but different numbers of $CHONO_2$ units. EGDN 06 (p_{sat}: 10.2 Pa) contains zero, GTN **17** (p_{sat}: 6.41× 10^{-2} Pa) one, ETN **08** (p_{sat}: 6× 10^{-4} Pa) two and MHN **05** four methylene nitrato units. For each additional methylene nitrato unit the vapor pressure is reduced by about two orders of magnitude. With this in mind it can be estimated that the vapor pressure of MHN 05 (T_{dec}: 175.8 °C) is about four orders of magnitude lower than that of ETN **08** (T_{dec}: 181.9 °C) whilst the temperatures of decomposition are comparable. For PA **11** and DDNP **10** it can only be assumed that a combination thermolability and low volatility causes the non-detectability of the substances. In a separate experiment an acetonitrile solution (0.1 mg/mL) of HNS **22** (hexanitrostilbene, p_{sat}: 6.19E-16 Pa T_{dec}: 338.9 °C) was injected, but no detector response could be observed. HNS **22** is the most thermostable substance investigated and thermal degradation can be excluded as reason for its non-detectability. NM **27** and $EtONO_2$ **04** are so volatile that they can be detected in the solvent peak by mass deconvolution (m/z 46 amu). It can be concluded that VO-GC/MS is a suitable method for the detection of explosives with the upper limit of detectability in terms of T_{dec} and p_{sat} in the range of RDX **19** and TETRYL **22**. Explosives that are less thermostable than 200 °C in combination with an extrapolated vapor pressure p_{sat} at 298.15 K lower than 10^{-7} Pa will most probably not be detectable by VO-GC/MS.

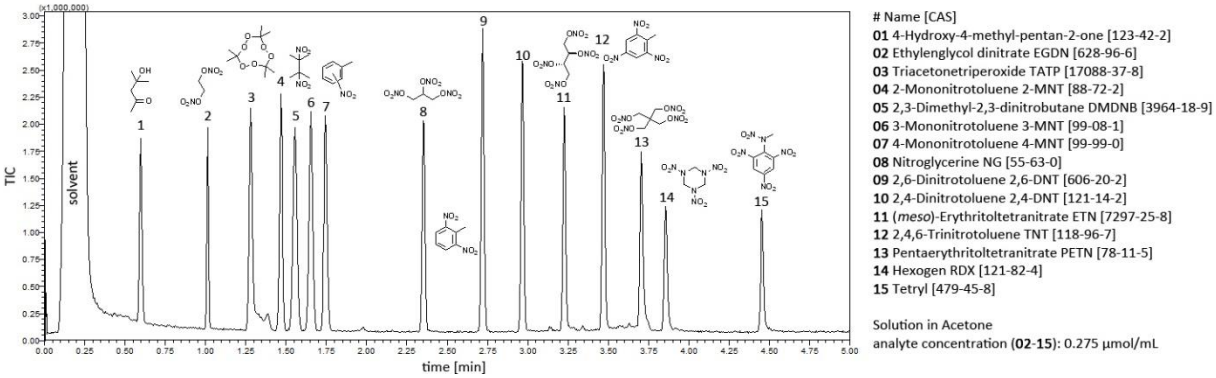

Figure 10 – Chromatogram of mixture of explosives (cf. Table 12) [M2]

In the next step the diameter of the restriction was changed from 0.025 mm to 0.050 mm. This allows the use of lower injector head pressures, accelerates the vaporization of the analytes in the injector and reduces the elution temperature. If one replaces the restriction column (10.1 mm length, 0.05 mm i.d.) in the calculation in Figure 6 with a 0.025 mm i.d. restriction of identical length, the necessary head pressure rises from 90 kPa to 641 kPa for the same column flow of 3.92 mL min^{-1}. This means that with a 0.05 mm restriction the head pressure can be reduced by a factor >7. To investigate the influences of the injector head pressure reduction a new test mixture of explosives with equimolar concentrations (0.518 – 0.543 µmol mL^{-1}) was created (cf. Table 13).

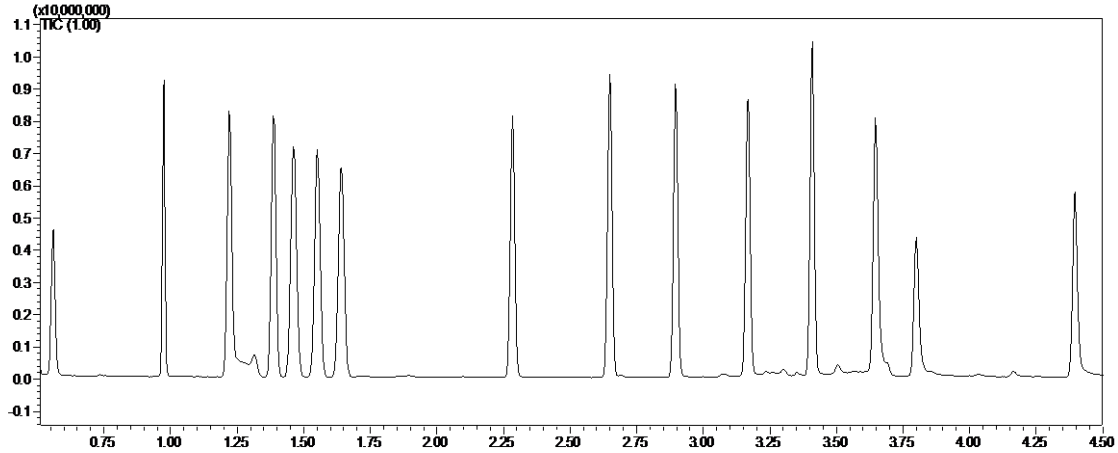

Figure 11 – Chromatogram of of MIX 1 (cf. Table 13) [M3 scan]

The mixture was analyzed by VO-GC/MS with the new restriction in SIM and SCAN mode. (cf. Table 14). The average integrals observed in SIM mode (I_{SIM}) and scan mode (I_{SCAN}) were transferred in relative response factors $R_{rel,SIM}$ and $R_{rel,scan}$, which are normalized to the exact concentration of the analyte and relative to the analyte with the best response (ETN 08): R_{rel} = $((c_{sub})^{-1} \times I)/I_{max}$. The relative response factors $R_{rel,SIM}$ and $R_{rel,SCAN}$ correlate well with each other. The trend of R_{rel} is in good correlation with the ion count in the quantification channel QC. The quantification channel QC is chosen in accordance with the most intensive peak of the mass spectrum of the analyte. δ is the relative intensity of the most intense peak in the mass spectrum of the analyte to the total intensity of its mass spectrum (total ion count, TIC). The quantification channel of the nitrate esters corresponds to the nitronium cation NO_2^+ and indicates that these molecules release a lot of nitrogen dioxide NO_2 during their fragmentation. Since erythritol tetranitrate can release 4 molecules of NO_2, it has the highest relative response factor R_{rel} observed. In terms of R_{rel}, it is followed by TATP **02**, which can release three $C_2H_3O^+$ cations with *m/z* = 44 amu and the other nitrate esters. RDX **19** has a high value for its relative quantification ion intensity δ (62.4 %), but a low value for $R_{rel,SIM}$ (0.140), which is an indicator for analyte degradation in the injector. TETRYL **22** has the lowest value for $R_{rel,SIM}$ (0.050) and δ (6.20 %). It can be concluded that $R_{rel,SIM}$ depends strongly on the fragmentation of the molecule, which is reflected by δ. Analytes, which release a lot of identical fragment ions like the nitrate esters and TATP **02**, have a high relative response factor for VO-GC/MS detection.

Table 13 - Preparation of a mix of analytes with c_{sub} = 0.518 – 0.541 µmol mL^{-1} [M3 scan]

Analyte	m_{sub} [a]	m_{solv} [b]	M [c]	n [d]	V_{solv} [e]	c_{sub} [f]	V_{MIX} [g]	c_{MIX} [h]
	[mg]	g	g mol^{-1}	µmol	mL	µmol mL^{-1}	mL	µmol/mL
HMX **22**	21.0	7.1140	296.1560	70.9	8.99	7.88	0.68	0.536
MHN **05**	24.0	7.5884	452.1540	53.1	9.59	5.53	0.96	0.531
EGDN **06**	50.5	7.2825	152.0620	332.1	9.21	36.07	0.15	0.541
GTN **17**	41.8	7.8016	227.0850	184.1	9.86	18.66	0.29	0.541
ETN **08**	24.3	7.7704	302.1080	80.4	9.82	8.19	0.65	0.532
PETN **09**	21.5	7.1871	316.1350	68.0	9.09	7.48	0.71	0.531
DDNP **10**	20.4	7.8523	210.1050	97.1	9.93	9.78	0.54	0.528
NM **27**	30.0	7.4989	61.0400	491.5	9.48	51.84	0.10	0.518
TNT **17**	29.7	7.1859	227.1320	130.8	9.08	14.39	0.37	0.533
TETRYL **22**	19.7	7.5425	287.1440	68.6	9.54	7.19	0.74	0.532
TATP **02**	19.9	7.9538	222.2370	89.5	10.06	8.91	0.60	0.534
PA **11**	20.1	7.5461	199.1220	100.9	9.54	10.58	0.50	0.529
2-MNT **12**	34.3	7.4686	137.0477	250.3	9.44	26.51	0.20	0.530
3-MNT **13**	25.0	7.7006	137.0477	182.4	9.74	18.74	0.28	0.525
4-MNT **14**	15.5	7.3701	137.0477	113.1	9.32	12.14	0.44	0.534
2,4-DNT **15**	25.6	7.3888	182.1350	140.6	9.34	15.05	0.35	0.527
2,6-DNT **16**	28.2	7.7772	182.1350	154.8	9.83	15.75	0.34	0.535
$EtONO_2$ **04**	38.3	7.9604	91.0660	420.6	10.06	41.79	0.13	0.543
CL-20 **21**	19.1	7.9301	438.1860	43.6	10.03	4.35	1.22	0.530
DMDNB **26**	27.5	7.3602	176.1720	156.1	9.30	16.78	0.32	0.537
RDX **19**	26.1	7.4412	222.1170	117.5	9.41	12.49	0.43	0.537

[a] mass of analyte, [b] mass of solvent, [c] molar mass of analyte, [d] molar amount of analyte, [e] volume of solvent (ρ(acetone): 0.791 g cm^{-3}), [f] concentration of substance, [g] volume for 2.71 µmol. Total volume of MIX: 9.84 mL. Concentration of analytes in mixture: 0.276 µmol mL^{-1} [h] concentration of analyte in mixture.

Table 14 – Results of VO-GC/MS analysis of MIX2 with SIM and SCAN mode. Order of analytes according to their relative response. [M3 SIM and scan]

Analyte	I_{SIM}[a]	σ(I_{SIM})[b]	I_{SCAN}[c]	σ(I_{SCAN})[d]	$R_{rel,SIM}$[e]	$R_{rel,scan}$[f]	C[g]	QC[h]	δ[i]
	counts	%	counts	%	SIM	scan		m/z	%
ETN **08**	6520371	1.23	6407454	0.99	1.000	1.000	0.92	46	70.5
TATP **02**	6158293	0.79	6103451	0.59	0.941	0.949	0.97	43	67.0
GTN **17**	5789515	0.37	5374869	0.28	0.873	0.825	1.04	46	74.0
PETN **09**	5488238	0.07	5195218	0.69	0.843	0.812	1.09	46	62.4
EGDN **06**	3222545	0.84	3164420	0.43	0.486	0.486	1.86	46	70.3
DMDNB **26**	1969207	0.98	2059420	1.00	0.299	0.319	3.05	57	26.5
3-MNT **13**	1756258	0.72	1882609	0.97	0.273	0.298	3.42	91	26.2
4-MNT **14**	1261903	0.66	1357363	0.75	0.193	0.211	4.75	91	19.9
2,4-DNT **15**	1304523	0.52	1335904	1.24	0.202	0.211	4.60	165	22.3
2-MNT **12**	1228116	0.79	1287346	1.45	0.189	0.202	4.89	120	21.3
TNT **17**	1094281	0.25	1126730	0.83	0.168	0.176	5.48	210	11.9
2,6-DNT **16**	1026469	0.48	1030230	1.03	0.156	0.160	5.85	165	16.8
RDX **19**	921725	0.36	813251	1.35	0.140	0.126	6.51	46	62.4
TETRYL **22**	311233	0.77	318416	2.82	0.048	0.050	19.3	194	6.206

All values were obtained for three directly repeated injections [a] average value of analyte integral (SIM) [b] standard deviation of a, [c] Average value of analyte integral (SIM) , [d] standard deviation of c, [e] relative response of analyte (SIM) [f] relative response of analyte (SCAN). R_{rel} = $((c_{sub})^{-1} \times I)/I_{max}$, I_{max}: maximum average integral observed. [g] Correction factor for equivalent peak area: $6 \times 10^6/I_{SIM}$. [h] Quantification Channel [i] Relative peak intensity of quantification ion to total ion count.

In the next step the same stock solutions were used to to generate a mixture of analytes with equivalent peak area. This is advantageous for the external standard calibration, which is required for the determination of the limits of detection and quantification according to DIN 32645:2008. TETRYL 22 was not included in the mixture with respect to its low $R_{rel,SIM}$ value. The composition of the mixture is detailed in Table 15. The results of VO-GC/MS analysis are detailed in Table 16. In SIM mode the integrals of the analytes vary from 3.45 to 3.73 Mcounts with a mean value of 3.58 Mcounts and a standard deviation of 2.59 %. In SCAN mode the integrals of the analytes vary from 3.17 to 4.04 Mcounts with a mean value of 3.61 Mcounts and a standard deviation of 7.81 %. (cf. Table 16) In general SIM mode is more precise for quantification but the sensitivity in comparison to SCAN is similar.

With a mix adjusted to similar response of the analytes (cf. Table 15, Table 16) in hands the injector temperature T_{Inj} optimum for each analyte was investigated in the range of 175 °C to 250 °C. To achieve comparable conditions of analysis the injector head pressure p_{Inj} and split ratio were adjusted to achieve a column flow f_{column} of ≈4.08 mL min^{-1} and a set splitflow f_{set} of ≈ 30 mL min^{-1}. The adjustment of the injector head pressure was carried out with the calculations discussed in section 5.2. In addition to this the splitflow f_{obs} was measured with a soapfilm flow meter (cf. section 5.3). It was possible to keep f_{col} constant in the range of 4.05 – 4.09 mL min and f_{obs} constant in the range of 25.27 – 25.99 mL min^{-1}.

Table 15 – Preparation of a mix of Analytes with equivalent peak area. [M3 scan]

	m_{sub}[a]	m_{solv}[b]	V_{MIX1}[c]	C[d]	V_{MIX2}[e]	c_{MIX2}[f]
	[mg]	g	mL	C	mL	µg mL^{-1}
ETN **08**	24.3	7.7704	0.650	0.92	0.375	92.85
TATP **02**	19.9	7.9538	0.598	0.97	0.365	72.32
GTN 17 **17**	41.8	7.8016	0.285	1.04	0.185	78.61
PETN **09**	21.5	7.1871	0.711	1.09	0.488	115.44
EGDN **06**	50.5	7.2825	0.148	1.86	0.172	94.57
DMDNB **26**	27.5	7.3602	0.317	3.05	0.607	179.29
3-MNT **13**	25.0	7.7006	0.284	3.42	0.609	156.39
4-MNT **14**	15.5	7.3701	0.439	4.75	1.308	217.65
2,4-DNT **15**	25.6	7.3888	0.354	4.60	1.021	279.80
2-MNT **12**	34.3	7.4686	0.201	4.89	0.616	223.64
TNT **17**	29.7	7.1859	0.370	5.48	1.272	415.97
2,6-DNT **16**	28.2	7.7772	0.338	5.85	1.240	355.60
RDX **19**	26.1	7.4412	0.426	6.51	1.741	482.94

[a] mass of substance [b] mass of solvent [c] volume of analyte solution in MIX1 [d] Correction factor for equivalent peak area [e] volume of analyte solution in MIX2 [f] concentration of analyte in MIX2

Table 16: Average peak areas with standard deviation and percentage standard deviation for MIX2 with adjusted concentrations of analytes with SIM and SCAN method at 175°C.

Analyte	I_{SIM}[a]	σ(I_{SIM})[b]	I_{SCAN}[c]	σ(I_{SCAN})[d]
	counts	%	counts	%
EGDN **06**	3453492	0.99	3443799	0.56
TATP **02**	3659016	1.12	3844764	0.40
2-MNT **12**	3519774	0.71	3744349	0.47
DMDNB **26**	3593660	0.83	3850053	0.76
3-MNT **13**	3708079	0.75	4044811	1.09
4-MNT **14**	3549188	0.65	3872202	1.15
GTN **17**	3739743	0.53	3500988	0.96
2,6-DNT **16**	3460140	0.53	3543313	0.49
2,4-DNT **15**	3649003	0.69	3750382	1.05
ETN **08**	3488722	0.48	3168820	1.18
TNT **17**	3633721	0.37	3718750	1.76
PETN **09**	3520674	0.43	3234234	0.72
RDX **19**	3562667	1.09	3215275	2.07

All values were obtained for three directly repeated injections [a] Average value of analyte integral (SIM) [b] standard deviation of a, [c] Average value of analyte integral (SIM) , [d] standard deviation of c

Table 17: Adjustment of pressure and split ratio SR at different injector temperatures for comparable column- and splitflow.

T_{inj}[a] °C	p_{Inj}[b] kPa	r_{split}[c]	f_{set}[d] mL min^{-1}	f_{obs}[e] mL min^{-1}	f_{col}[e] mL min^{-1}
155	83	167.0	30	25.24	4.09
175	90	150.0	30	25.37	4.08
195	97	142.9	30	25.61	4.07
213	103	136.4	30	25.99	4.05
223	107	130.4	30	25.72	4.07
232	110	125.0	30	25.27	4.06
241	114	120.0	30	25.54	4.09
250	117	115.4	30	25.41	4.08

[a] injector temperature [b] injector head pressure [c] split ratio [d] set splitflow [e] observed splitflow (soap film flowmeter at split exit (cf. section 5.3)) [e] calculated column flow (cf. section 5.2)

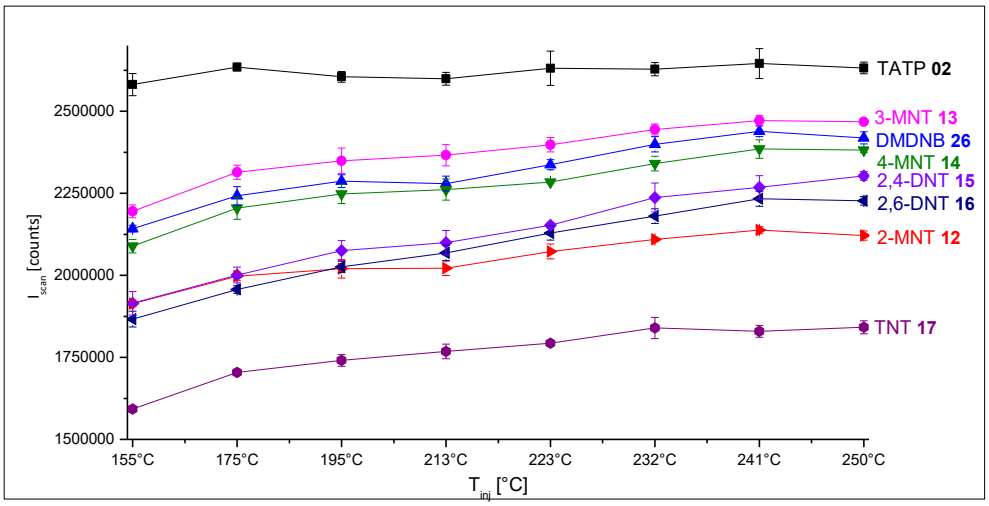

Figure 12 – Plot of injector temperature T_{inj} [°C] vs. average analyte integral I_{SCAN} [counts]. TNT 17, 2-MNT 12, 2,6-DNT 16, 4-MNT 14, DMDNB 26, 3-MNT 13 and TATP 02 profit from higher injector temperatures. Error bars indicate standard deviation σ for three directly repeated measurements. [M3 scan]

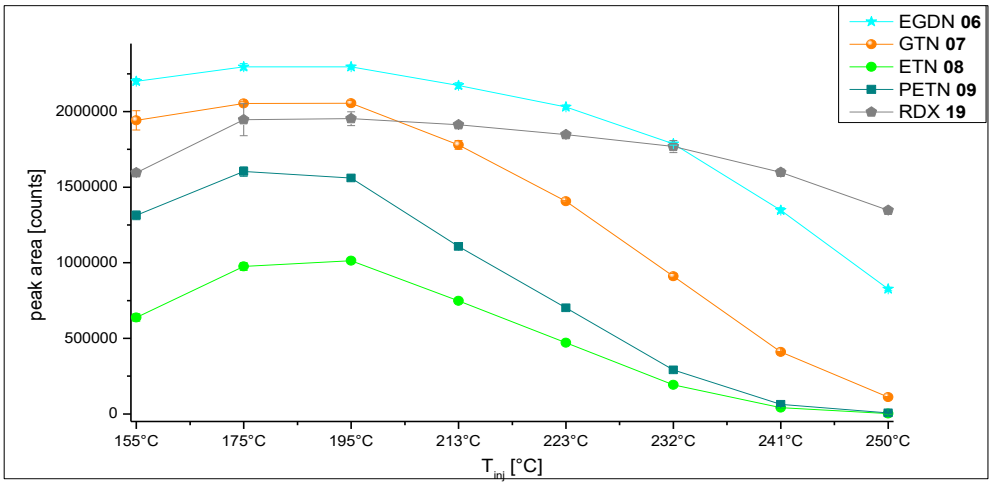

Figure 13 – Plot of injector temperature T_{inj} [°C] vs. average analyte integral I_{SCAN} [counts]. EGDN 06, GTN 17, ETN 08, PETN 09 and RDX 19 suffer from higher injector temperatures. For these analytes the optimum of T_{inj} is between 175 °C and 195 °C. Error bars indicate standard deviation σ for three directly repeated measurements. [M3 scan]

Table 18: Mean peak areas of analytes and percentage standard deviation of MIX5 at a temperature range of 155-250°C. [M3 scan]

	155°C[a]	σ [%][b]	**175°C**[a]	σ [%][b]	**195°C**[a]	σ [%][b]	**213°C**[a]	σ [%][b]
EGDN **06**	2200921	0.81	2296563	0.93	2295550	0.53	2172263	0.91
TATP **02**	2581437	1.30	2634576	0.44	2605067	0.64	2598836	0.75
2-MNT **12**	1913429	0.47	1997469	0.62	2019922	1.40	2021656	1.12
DMDNB **26**	2142185	0.47	2242209	1.26	2286706	0.85	2279415	0.99
3-MNT **13**	2195149	0.89	2314216	0.94	2349070	1.64	2366116	1.37
4-MNT **14**	2089197	0.98	2204617	1.53	2248185	1.29	2261453	1.43
GTN **17**	1942632	3.28	2053737	0.57	2055047	0.83	1779203	1.63
2,6-DNT **16**	1866393	1.29	1956952	0.60	2025862	0.86	2068501	1.15
2,4-DNT **15**	1914762	1.89	2001080	1.21	2075297	1.47	2099465	1.77
ETN **08**	638382	3.86	975531	2.62	1013508	1.61	747364	0.62
TNT **17**	1592687	0.58	1704338	0.56	1740825	1.02	1768125	1.26
PETN **09**	1313517	2.20	1603387	1.93	1561085	1.08	1108224	1.40
RDX **19**	1596046	1.44	1946346	5.47	1953192	2.32	1913227	0.77

	223°C[a]	σ [%][b]	**232°C**[a]	σ [%][b]	**241°C**[a]	σ [%][b]	**250°C**[a]	σ [%][b]
EGDN **06**	2031172	0.65	1787295	0.54	1347194	1.25	826386	1.45
TATP **02**	2630939	1.99	2628329	0.76	2645543	1.72	2631793	0.67
2-MNT **12**	2072624	1.09	2109103	0.20	2137878	0.50	2121173	0.67
DMDNB **26**	2337171	0.65	2399452	0.97	2438971	0.67	2418872	0.76
3-MNT **13**	2398076	0.90	2494378	0.67	2471417	0.65	2468047	0.24
4-MNT **14**	2284547	0.24	2340739	0.96	2384887	1.17	2381591	0.32
GTN **17**	1406324	0.30	909888	2.13	409325	1.00	111699	3.58
2,6-DNT **16**	2128973	1.03	2180499	1.02	2233271	1.04	2227137	0.60
2,4-DNT **15**	2152570	0.42	2237189	1.98	2267983	1.57	2302930	0.58
ETN **08**	471234	1.14	191959	1.03	41049	1.77	2123	115.63
TNT **17**	1793431	0.41	1839685	1.77	1829169	0.99	1841739	1.08
PETN **09**	701012	1.00	290745	1.71	62907	8.64	6743	40.23
RDX **19**	1847650	0.57	1768879	2.29	1598614	1.31	1347974	0.66

All values were obtained for three directly repeated injections [a] Average value of analyte integral (SCAN) for stated temperature [b] standard deviation of a

Table 18 compiles the results of the injector temperature optimization. The analytes can be divided into two types. All Nitrotoluene derivatives, DMDNB **26** and TATP **02** profit from higher injector temperatures. (cf. Figure 12) The average integrals I_{SCAN} of the nitrate esters and RDX **19** increase from T_{INJ} 155 °C to T_{INJ}175 °C but decrease from 195 °C. If one considers the sum of the average integrals of all analytes in Table 18, the temperature optimum for all analytes can be found in Table 19.

Table 19 – Global temperature optimum for all analytes (cf. Table 18)

T_{INJ} [°C]	155	175	195	213	223	232	241	250
$\sum_{int}$ [10^6 counts]	23.98	25.93	26.23	25.18	24.26	23.17	21.87	20.68

The highest value for $\sum_{int}$ is obtained with the injector temperatures T_{INJ} 175 °C (25.93 × 10^6 counts) and 195 °C (26.23 × 10^6 counts). Therefore the injector temperature optimum for the configuration described is 175 °C and was chosen for the determination of the limits of detection for the explosive analytes using the VO-GC/MS setup.

Table 20 – Retention times, elution temperatures, NIST match scores and selected mass spectrum data for the analytes. [M3]

Analyte	t_{ret}[a]	T_{elu}[b]	NIST[c]	30[d]	46[d]	76[d]	100%[e]
	[min]	[°C]	[%]	%	%	%	
EGDN **06**	0.975	92.50	96	12.82	100.00	0.00	46
TATP **02**	1.372	100.00	92	0.06	0.00	0.23	43
2-MNT **12**	1.386	100.00	97	2.87	0.92	1.74	120
DMDNB **26**	1.461	100.00	97	9.45	1.16	0.00	57
3-MNT **13**	1.550	100.00	96	4.21	1.09	0.84	91
4-MNT **14**	1.640	101.60	95	6.87	1.26	1.10	91
GTN **17**	2.285	127.42	81	10.25	100.00	4.85	46
2,6-DNT **16**	2.650	142.00	95	14.97	1.42	11.48	165
2,4-DNT **15**	2.895	151.81	96	24.91	1.91	2.71	165
ETN **08**	3.171	162.80	n.a.	9.60	100.00	3.47	46
TNT **17**	3.410	172.40	87	33.82	3.15	17.92	210
PETN **09**	3.645	181.81	73	7.99	100.00	9.18	46
RDX **19**	3.800	188.00	89	7.99	100.00	9.18	46
TETRYL **22**	4.395	211.80	79	87.35	4.67	66.82	194

[a] retention time, [b] elution temperature, [c] NIST08 MS database match score after background subtraction, [d] relative intensity of the corresponding m/z value, m/z value with 100 % relative intensity

Table 20 summarizes the retention time of the analytes, their elution temperature and match scores for the NIST08 mass spectra database. TETRYL **22** is the last analyte eluting after 4.395 minutes at 211.80 °C. This is less than half the elution time of TETRYL **22** in the application note of the RTX-TNT column (< 11 min) and demonstrates the potential of VO-GC/MS to reduce the total time of the analysis cycle. The NIST match scores are not lower than 73% (PETN **09**). The deviation of the recorded spectra to the NIST database can be compensated by the creation of an own library with the mass spectra recorded in this work. Most of the mass spectra of the analytes include peaks at the m/z values 30, 46 and 76, which might be corresponding to the nitrosonium cation NO^+ (m/z 30), the nitronium cation NO_2^+(m/z 46) and the $N_2O_3^+$ cation (m/z 76). The mass spectra of all analytes are compiled in Appendix 2.

5.5 VO-GC/MS Limits of Detection of Explosives

The limits of detection (LOD) and limits of quantification (LOQ) were determined for the VO-GC/MS setup according to the calibration method of DIN32645:2008-11. The Limit of Detection LOD is calculated according to:

$$LOD = \left(\frac{S_{y,x}}{b}\right) \times t_{n-2;\alpha} \sqrt{m^{-1} + n^{-1} + \frac{\bar{x}^2}{Q_x}} \quad (1)$$

$S_{y,x}$: Residual standard deviation of calibration points, b: slope of calibration function, α: level of significance for errors of first kind, $t_{n-2;\alpha}$: Student's t, m: number of measurements per datapoint, n: number of calibration points, $\bar{x}$: average value of analyte concentration, Q_x: residual sum of squares. For details see DIN32645:2008-11.

The Limit of Quantification LOQ is calculated iteratively according to:

$$LOQ = k \times \frac{S_{y,x}}{b} \times t_{n-2;\frac{\alpha}{2}} \sqrt{m^{-1} + n^{-1} + \frac{(LOQ - \bar{x})^2}{Q_x}} \quad (2)$$

k: reciprocal relative uncertainty of the results *k.* For details see DIN32645:2008-11.

For the iteration, an arbitrary (e.g. 1.00 µg mL^{-1}) starting value for LOQ is chosen and the obtained result is reinserted in equation (2) until a stable value for LOQ is obtained.

The level of significance α for errors of first kind was chosen to be 1 %. The reciprocal relative uncertainty of the results *k* was chosen to be 3. For the determination of LOD and LOQ a 1:1 (v/v) dilution series of a sample of MIX 2 (cf. Table 15) was generated resulting in samples with the concentration $c_n = 1/(2^n) \times c_{MIX2}$ (n = 0, 1,…,10). This dilution series was used for an external standard calibration. The calibration was carried out measuring from low to high concentrations to avoid analyte carryover. It was observed that the detector response stabilized after the second injection of the identical sample. This might be caused by analyte deactivation of possible active spots in the injector. With respect to this, every sample was injected four times discarding the results of the first injection. The average value of the second to fourth injection was used as input for the external standard calibration.

The peaks were integrated automatically with the exception of TATP **02** and PETN **09** using the Lab Solutions Software. TATP **02** and PETN **09** were integrated manually. All peaks were quantified using the one mass channel for quantification and one reference ion mass channel for identification of the analyte using the absolute signal intensities with a 30% default ion allowance. In case of a mismatch of the ratio of quantification and reference ion, all data corresponding to the respective concentration level was discarded from the calibration process. This boundary condition was introduced in context of an application of the VO-GC/MS device in a gas phase detection scenario. The data acquired can be found in Table 21 and is visualized for the Limit of Detection in Figure 14 and for the Limit of Quantification in Figure 15. In general it can be stated that the limit of detection LOD is directly proportional to the limit of quantification LOQ. For the data obtained in this work, LOQ can be estimated by the LOD value, since for all values in this work a conversion factor of 3.58 ± 0.07 could be determined.

$$LOQ = 3.6 \times LOD \quad (3)$$

With respect to the direct proportionality of LOD and LOQ the discussion will be limited to LOD values in the following but is also valid for LOQ values. Generally speaking the detection of early eluting analytes (from EGDN 06 to 2,4-DNT **15**, cf. Figure 10) is unproblematic since the limits of detection are

below 100 pg on column. It is problematic to distinguish TATP **02** from the acetone solvent peak tailing. Therefore this analyte has the highest LOD value in SCAN mode amongst the early eluting peaks. In most cases the LOD value measured in SIM mode is lower than in SCAN mode. This is caused by a better signal to noise ratio and a better peak identification using the intensity ratio of quantification and reference ion. In SIM mode the peak could be identified at one lower concentration level for eight analytes and at two lower concentration levels for three analytes. The identification of the analyte is less successful at lower concentration levels when three reference ions are used for analyte identification. For seven analytes the analyte can only be identified at a higher dilution step (Δn = -1) in comparison to the SCAN measurement with one reference ion. This is observed for the four latest eluting analytes (ETN **08**, TNT **17**, PETN **09**, RDX **19**) with the highest LOD values. In some cases this leads to higher limits of detection, but might ensure a more reliable analyte identification with less false positives in context of a gas phase detector application. (cf. Figure 16, Table 23) In all modes of detection the four latest eluting analytes have the highest limit of detection. Whilst the results for PETN **09**, TNT **17** and RDX **19** are similar, the limit of detection of ETN **08** is significantly higher. Both PETN **09** and ETN **08** are nitrate esters with four nitrato units per molecule. All four latest eluting analytes differ in vapor pressure (PETN **09** 1.55×10^{-6} Pa, ETN **08** 6×10^{-4} Pa, TNT **17** 7.33×10^{-4} Pa, RDX **19** 4.40×10^{-4} Pa (at 298.15 K) and decomposition temperature (PETN 09 199.8 °C, ETN 08 181.9 °C, TNT 17 308.9 °C, RDX 19 232.9 °C). All four analytes posess the lowest volatility in comparison to the earlier eluting analytes. In case of erythritol tetranitrate, partial decomposition of the analyte during analysis is suspected to deteriorate its limit of detection. (cf. Figure 14, Figure 15, Figure 16, Table 21, Table 22).

Table 21 – Results of Limit of Detection LOD and Limit of Quantification LOQ Determination [M3 SIM and scan]

EGDN 06[a]	**4**[f]	**5**	**6**	**7**	**8**	**9**			
SCAN[b]	231116	113857	54280	27109	12200	6672	**R^{2g}**	**LOD**[h]	**LOQ**[i]
σ[c]	2.42	3.47	10.29	5.41	5.00	6.55	0.99984	134	480
	5	**6**	**7**	**8**	**9**	**10**			
SIM[d]	116224	57718	28243	13654	5881	2511	**R^2**	**LOD**	**LOQ**
σ[e]	2.23	0.44	3.96	2.36	5.63	18.65	0.99999	19.9	72.8
TATP 02	**3**	**4**	**5**	**6**	**7**	**8**			
SCAN	533561	259401	143121	80189	50224	17047	**R^2**	**LOD**	**LOQ**
σ	2.96	4.36	1.81	2.53	6.07	3.96	0.99835	656	2277
	5	**6**	**7**	**8**	**9**	**10**			
SIM	123338	61553	31802	14613	8141	4387	**R^2**	**LOD**	**LOQ**
σ	5.03	1.07	1.93	4.74	0.61	13.16	0.99982	54	192
2-MNT 12	**4**	**5**	**6**	**7**	**8**	**9**			
SCAN	255472	128383	64141	31415	15542	8357	**R^2**	**LOD**	**LOQ**
σ	3.33	1.69	1.14	4.04	6.48	1.41	0.99998	118	431
	5	**6**	**7**	**8**	**9**	**10**			
SIM	117923	58237	28098	13053	5850	2544	**R^2**	**LOD**	**LOQ**
σ	2.44	1.28	2.20	3.28	4.34	8.90	0.99997	67.6	246
DMDNB 26	**4**	**5**	**6**	**7**	**8**	**9**			
SCAN	272569	140541	69913	36252	18087	9396	**R^2**	**LOD**	**LOQ**
σ	1.83	1.17	1.73	5.58	3.36	4.47	0.99979	288	1032
	5	**6**	**7**	**8**	**9**	**10**			
SIM	126949	63956	32452	15946	7860	4041	**R^2**	**LOD**	**LOQ**
σ	1.72	1.13	0.79	1.84	2.68	0.40	0.99996	66.6	242
3-MNT 13	**4**	**5**	**6**	**7**	**8**	**9**			
SCAN	274450	139789	68801	35838	18580	9809	**R^2**	**LOD**	**LOQ**
σ	1.42	2.89	2.26	2.96	7.97	13.63	0.99992	152	550
	5	**6**	**7**	**8**	**9**	**10**			
SIM	125842	61863	30585	13931	6375	2851	**R^2**	**LOD**	**LOQ**
σ	2.31	1.33	1.75	2.35	5.96	24.36	0.99995	59.8	217
4-MNT 14	**5**	**6**	**7**	**8**	**9**	**10**			
SCAN	131677	68781	36000	18903	10700	6417	**R^2**	**LOD**	**LOQ**
σ	3.46	1.95	9.00	6.23	13.19	0.12	0.99976	187	667
	4	**5**	**6**	**7**	**8**	**9**			
SIM	235806	119126	59335	29532	13708	6599	**R^2**	**LOD**	**LOQ**
σ	0.33	1.83	0.92	1.18	5.5	9.56	0.99993	201	728
GTN 17	**3**	**4**	**5**	**6**	**7**	**8**			
SCAN	423539	204153	95539	44669	20273	9493	**R^2**	**LOD**	**LOQ**
σ	0.70	2.01	2.09	0.62	6.29	5.54	0.99964	332	1179
	5	**6**	**7**	**8**	**9**	**10**			
SIM	98653	44577	19833	8383	3115	1071	**R^2**	**LOD**	**LOQ**
σ	1.49	1.19	1.08	1.34	5.06	17.83	0.99820	186	646

Table 21 – Results of Limit of Detection LOD and Limit of Quantification LOQ Determination (continued)

2,6-DNT 16	**5**	**6**	**7**	**8**	**9**	**10**			
SCAN	119158	59151	30293	17272	9443	6047	**R^2**	**LOD**	**LOQ**
σ	1.39	5.70	1.17	4.38	3.81	7.28	0.99968	358	1273
	5	**6**	**7**	**8**	**9**	**10**			
SIM	116717	58753	30310	15811	8932	5508	**R^2**	**LOD**	**LOQ**
σ	1.66	0.90	1.30	0.82	2.4	2.11	0.99997	109	397
2,4-DNT 15	**4**	**5**	**6**	**7**	**8**	**9**			
SCAN	236500	118426	58317	28470	13795	7605	**R^2**	**LOD**	**LOQ**
σ	2.36	3.25	3.70	6.17	10.6	13.14	0.99996	193	701
	5	**6**	**7**	**8**	**9**	**10**			
SIM	113758	55223	26993	12716	6334	3369	**R^2**	**LOD**	**LOQ**
σ	1.24	1.21	1.26	1.97	1.47	3.27	0.99974	252	900
ETN 08	**1**	**2**	**3**	**4**	**5**	**6**			
SCAN	2908795	1306808	531020	194638	61021	18813	**R^2**	**LOD**	**LOQ**
σ	1.75	1.6	1.8	0.75	2.20	6.79	0.99733	8589	29728
	2	**3**	**4**	**5**	**6**	**7**			
SIM	1354414	537503	188144	59068	14554	2442	**R^2**	**LOD**	**LOQ**
σ	2.06	2.06	2.98	7.44	5.56	6.54	0.98919	8669	32488
TNT 17	**3**	**4**	**5**	**6**	**7**	**8**			
SCAN	466317	218110	104594	46392	20787	8762	**R^2**	**LOD**	**LOQ**
σ	1.1	1.4	1.43	2.6	6.3	3.75	0.99927	2518	8850
	5	**6**	**7**	**8**	**9**	**10**			
SIM	99674	45010	19826	8542	3989	1842	**R^2**	**LOD**	**LOQ**
σ	1.00	0.92	1.62	1.61	1.81	8.43	0.99741	1184	4099
PETN 09	**2**	**3**	**4**	**5**	**6**	**7**			
SCAN	1670161	795020	352890	153512	64265	25802	**R^2**	**LOD**	**LOQ**
σ	1.89	1.03	0.15	2.98	3.47	6.24	0.99927	2782	9779
	4	**5**	**6**	**7**	**8**	**9**			
SIM	158763	63874	23905	7919	2020	449	**R^2**	**LOD**	**LOQ**
σ	1.73	1.95	2.42	3.78	2.52	11.79	0.99100	1228	4471
RDX 19	**4**	**5**	**6**	**7**	**8**	**9**			
SCAN	179616	83584	40349	19023	8828	4519	**R^2**	**LOD**	**LOQ**
σ	2.57	6.09	7.46	3.06	5.6	3.56	0.9989	1786	6237
	5	**6**	**7**	**8**	**9**	**10**			
SIM	91589	43443	20469	9134	4469	2503	**R^2**	**LOD**	**LOQ**
σ	0.99	1.49	3.64	2	8.79	17.39	0.99913	796	2792

[a] Analyte according to Figure 18. [b] Integral of analyte peak in SCAN Mode for respective concentration [counts] [c] standard deviation of b [%] [d] Integral of analyte peak in SIM Mode for respective concentration [counts] [e] standard deviation of d [%] [f] analyte concentration c_n (cf. Table 15) $c_n = 1/(2^n) \times c_{MIX2}$ (n = 0, 1,…,10) [g] Coefficient of determination for external standard calibration [h] Limit of Detection [ng mL^{-1}] [i] Limit of Quantification [ng mL^{-1}]. g-i given for both SIM and SCAN mode in the respective line.

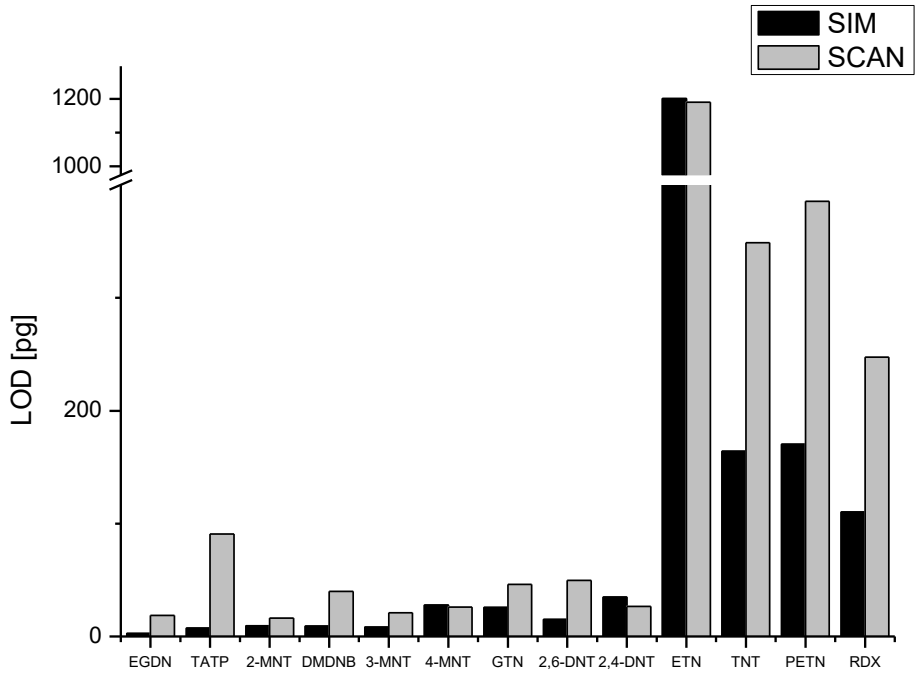

Figure 14 – Visualization of results for Limit of Detection determination for SIM and SCAN mode (cf. Table 21) [M3]

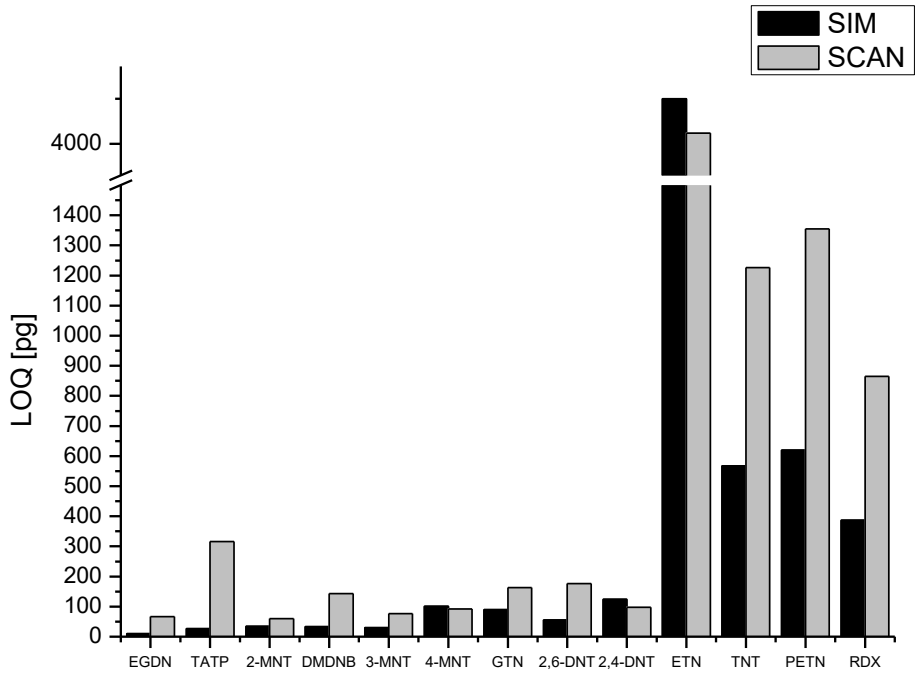

Figure 15 - Visualization of results for Limit of Quantification determination for SIM and SCAN mode (cf. Table 21) [M3]

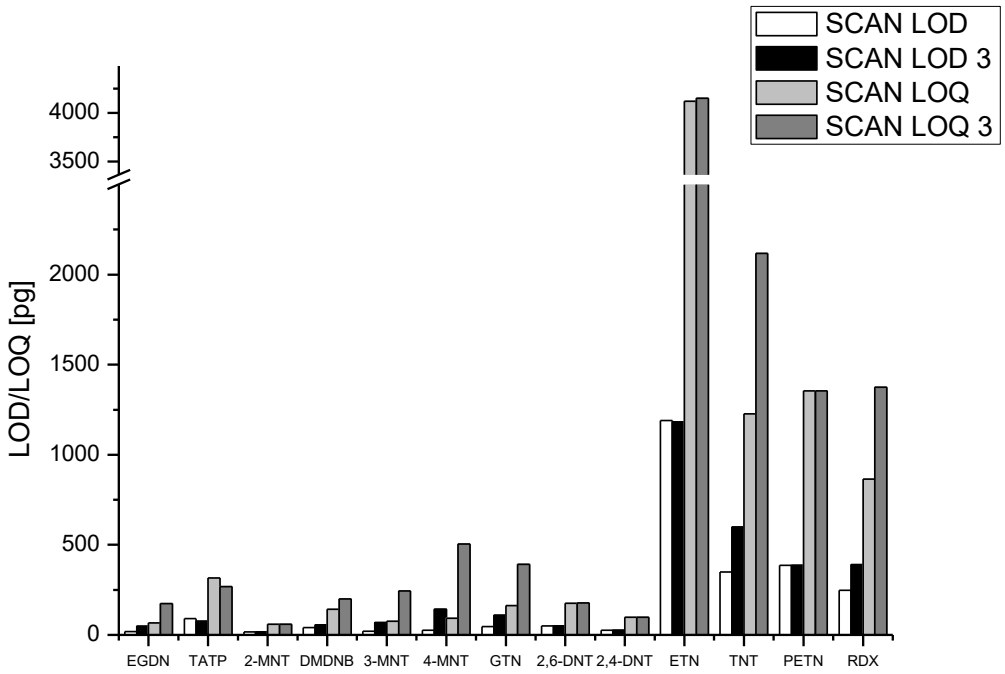

Figure 16 Visualization of results for Limit of Quantification determination for SIM and SCAN mode with one and three reference ions (indicated by 3) for analyte identification. [M3]

Table 22 – Results for Limit of Detection and Limit of Quantification in SIM and SCAN mode [M3]

	LOD SIM [pg][a]	**LOD SCAN [pg][a]**	**LOD SCAN 5 [pg][a]**	**LOQ SIM [pg][a]**	**LOQ SCAN [pg][a]**	**LOQ SCAN 5 [pg][a]**	Δn^{b}
EGDN **06**	2.76	18.5	48.2	10.1	66.4	175	-1
TATP **02**	7.43	90.8	75.4	26.6	316	269	0
2-MNT **12**	9.36	16.4	16.4	34.1	59.7	59.7	1
DMDNB **26**	9.23	39.9	55.2	33.5	143	199	0
3-MNT **13**	8.29	21.1	68.0	30.1	76.2	244	0
4-MNT **14**	27.9	25.9	142	100.9	92.5	504	-1
GTN **17**	25.8	46.0	109	89.5	163	392	-1
2,6-DNT **16**	15.1	49.6	49.9	55.0	176	177	0
2,4-DNT **15**	34.9	26.7	26.7	125	97.1	97	0
ETN **08**	1201	1190	1182	4502	4119	4151	-1
TNT **17**	164	349	599	568	1226	2117	-1
PETN **09**	170	385	385	620	1355	1355	-1
RDX **19**	110	247	391	387	864	1374	-1

[a] values given in pg on column (cf. eq. (4))Δn: n (1 reference ion channel) – n (5 reference ion channels). n: lowest concentration level with positive analyte identification. analyte concentration c_n $c_n = 1/(2^n) \times c_{MIX2}$ (n = 0, 1,…,10) (cf. Table 15)

Table 23 – Calculation of necessary enrichment volume for successful detection of the explosive. [M3]

Mode Analyte	LOD[a] SIM [pg]	LOD[b] SCAN [pg]	p_{sat}[c] [Pa]	c_{sat}[d] [ng L^{-1}]	c_{dif}[e] [ng L^{-1}]	V_{sat}[f] SIM [L]	V_{sat}[g] SCAN [L]	V_{dif}[h] SIM [L]	V_{dif}[i] SCAN [L]
EGDN **06**	2.76	18.5	1.02E+01	6.26E+05	4.36E+00	4.41E-09	2.96E-08	6.34E-04	4.25E-03
TATP **02**	7.43	90.8	6.20E+00	5.56E+05	2.84E+00	1.34E-08	1.63E-07	2.61E-03	3.20E-02
2-MNT **12**	9.36	16.4	1.92E+01	1.06E+06	6.97E+00	8.82E-09	1.55E-08	1.34E-03	2.35E-03
DMDNB **26**	9.23	39.9	2.20E-01	1.56E+04	8.84E-02	5.90E-07	2.55E-06	1.04E-01	4.52E-01
3-MNT **13**	8.29	21.1	1.17E+01	6.47E+05	4.20E+00	1.28E-08	3.26E-08	1.98E-03	5.03E-03
4-MNT **14**	27.9	25.9	6.52E+00	3.60E+05	2.49E+00	7.74E-08	7.19E-08	1.12E-02	1.04E-02
GTN **17**	25.8	46.0	6.41E-02	5.87E+03	3.13E-02	4.39E-06	7.83E-06	8.25E-01	1.47E+00
2,6-DNT **16**	15.1	49.6	8.27E-02	6.08E+03	3.88E-02	2.49E-06	8.16E-06	3.89E-01	1.28E+00
2,4-DNT **15**	34.9	26.7	3.51E-02	2.58E+03	1.62E-02	1.35E-05	1.04E-05	2.15E+00	1.64E+00
ETN **08**	1201	1190	6.00E-04	7.31E+01	3.87E-04	1.64E-02	1.63E-02	3.10E+03	3.08E+03
TNT **17**	164	349	7.33E-04	6.72E+01	3.91E-04	2.44E-03	5.20E-03	4.20E+02	8.93E+02
PETN **09**	170	385	1.55E-06	1.98E-01	9.78E-07	8.60E-01	1.95E+00	1.74E+05	3.94E+05
RDX **19**	110	247	4.40E-07	3.94E-02	2.21E-07	2.79E+00	6.27E+00	4.98E+05	1.12E+06

[a] Limit of detection according to DIN 32645:2008 (α = β = 0.01, k = 3) in SIM mode. [b] Limit of detection in SCAN mode. [c] Vapor pressure at 298.15 K [12] (**13**, **08**: results from transpiration experiment in this work), [d] Saturation concentration at 298.15 K, [e] Diffusion controlled concentration at 298.15 K according to section 5.7 with 200 cm² of exposed explosive surface, [f] Minimum volume of air that needs to be enriched with 100 % efficiency under saturation conditions for successful detection of analyte in SIM mode [g] see f but SCAN mode [h] see f but diffusion-controlled conditions [i] see h but SCAN mode.

Both LOD and LOQ are measured in ng mL^{-1} depending on their sample concentration. The LOD in terms of mass of analyte that was transferred into the analytical column (LOD [pg]) can be estimated by:

$$LOD\ [pg] = LOD[ng\ mL^{-1}] \times V_{inj} \times p_{split} \quad (4)$$

$LOD\ [pg]$: limit of detection [pg], $LOD[ng\ mL^{-1}]$: limit of detection [ng mL^{-1}], V_{inj} injection volume [µL], p_{split}: split proportion (cf. Table 9)

For V_{inj} = 1 µL (cf. Table 6) and p_{split} = 0.139 a conversion factor of 0.139 can be calculated. The unit pg stands for values that were converted with this factor as preparation for the discussion in the following.

Table 23 summarizes the results of the study to give a facit for the availability of the analytes for their gas phase detection. The limits of detection of the analytes in SIM and SCAN mode at 175 °C (cf. Table 22) were used for the calculation of the volume of air that is necessary for the successful gas phase

detection. The first step is the air stream enrichment of the analytes on a sorbent of choice followed by thermal desorption and introduction into the analytical column in a splitless injection. For a better understanding of this concept it is helpful to get familiar with the technology employed in project SEDET [13], which has realized this technique for a different type of detector. The estimation is under the assumption that analyte enrichment, desorption and injection are performed with 100 % efficiency. This is the best option until a prototype for measurements under real conditions is available. The estimated values calculated in this work are useful for the conception of the air sampling unit of this prototype. For the calculation of the concentration of the analyte under saturation conditions the Ideal Gas Equation is used:

$$c_{sat} = \frac{p_{sat} \times M}{R \times T} \tag{13}$$

c_{sat}: saturation concentration [mg L^{-1}], R: ideal gas constant (8.3145 J mol^{-1} K^{-1}), T: temperature [K]

The volume V_{sat} that is necessary for the analyte enrichment and successful detection under saturation conditions is calculated by:

$$V_{sat} = \frac{LOD}{c_{sat}} \tag{14}$$

V_{sat}: Minimum volume of air that needs to be enriched with 100 % efficiency under saturation conditions for successful detection of analyte [L], LOD: limit of detection of analyte [pg], c_{sat}: saturation concentration of analyte [pg L^{-1}]

Vapor pressures are measured under ideal saturation conditions. In a real case scenario the saturation equilibrium of the analyte will not be reached and diffusion processes will dictate the air concentration of the analyte. *Dravnicks et al.* [14] have stated a mathematical model for the estimation of the non-equilibrium air concentration c_{dif} of an explosive, which was applied to the analytes in this work using the equations and values provided by *Bird et al.* [15]. The calculation is detailed in section 5.7. The corresponding V_{dif} value is calculated in analogy to V_{sat} using c_{dif}.

The results of the calculation of V_{sat} and V_{dif} are summarized in Table 23. For the analytes investigated in this work, V_{sat} ranges from 4.41 × 10^{-9} L (EGDN **06,** SIM) to 6.27 L (RDX **19**, SCAN). These values are several magnitudes lower in comparison to the results based on the analyte concentration under diffusion conditions. V_{dif} ranges from 6.34 × 10^{-4} L (EGDN **06**, SIM) to 1120 m³ (RDX **19**, SCAN)

5.6 Facit

In terms of the availability of the analytes for gas phase detection with the VO-GC/MS setup presented in this work ETN **08** and RDX **19** are the most interesting analytes. ETN **08** has the highest LOD values (SIM: 1201 pg, SCAN: 1190 pg). RDX **19** has the lowest vapor pressure at 298.15 K (4.40×10^{-7} Pa) in combination with medium LOD values (SIM: 110 pg, SCAN: 247 pg). Despite the lower limits of detection the volume of air that needs to be sampled for the successful detection of the explosive is higher for RDX **19**, since the concentration c_{sat} and c_{dif} are both directly proportional to the vapor pressure of the analyte. Therefore RDX **19** is the benchmark analyte for the dectability of the explosives in this study. Since saturation conditions do not occur in a real detection scenario the volume for diffusion conditions V_{dif} is more relevant. In SIM mode 498 m³ of air need to be sampled for the successful detection of RDX **19**. In SCAN mode 1120 m³ litres of air must be sampled. Typical vacuum cleaners work with suction flow rates of 4 m³ min^{-1}. That means for the air enrichment of RDX **19** 124 (SIM) and 280 (SCAN) minutes are necessary. For PETN **09** these times reduce to 43 (SIM) and 98 (SCAN) minutes. For all other analytes the sampling time necessary for the enrichment of an amount of sample above the limit of detection is below one minute. (cf. Table 24) The values stated for V_{dif} in this work are estimates and neglect further transport barriers like foil wrapped around the explosive, which

additionally lower the air concentration of the analyte. The next right step would be the development of a sampling prototype and real-environment measurements to evaluate the validity of the estimates given in this work.

For the nitrate esters **04** – **08** an optimized GC/MS method was developed and improved limits of detection could be achieved. (cf. section 7.3)

Table 24 – Necessary time for the gas-phase enrichment of the analytes for their successful detection with the VO-GC/MS setup presented in this work in SIM and SCAN mode based on a sampling flowrate of 4 m³ per minute. [M3]

Analyte	SIM [min]	SCAN [min]
EGDN **06**	1.58E-07	1.06E-06
TATP **02**	6.54E-07	7.99E-06
2-MNT **12**	3.36E-07	5.88E-07
DMDNB **26**	2.61E-05	1.13E-04
3-MNT **13**	4.94E-07	1.26E-06
4-MNT **14**	2.81E-06	2.60E-06
GTN **17**	2.06E-04	3.68E-04
2,6-DNT **16**	9.72E-05	3.19E-04
2,4-DNT **15**	5.38E-04	4.11E-04
ETN **08**	7.76E-01	7.69E-01
TNT **17**	1.05E-01	2.23E-01
PETN **09**	4.34E+01	9.84E+01
RDX **19**	1.24E+02	2.79E+02

It was demonstrated that VO-GC/MS is a robust method for the detection of explosives and is suitable for the quantification of compounds with limitations. The detectability and quantifiability of the analytes from the ChemAir substance repertoire is summarized in Figure 18. All substances besides MHN **05**, DDNP **10**, HNS **18**, HMX **20**, CL-20 **21** and FOX-7 **23** could be detected. For the ionic substances UN **24**, UDN **25** and AN **28** thermal decomposition products of the salts (nitrogen oxides, neutral compounds) could be detected. The peroxides TATP **02**, DADP **03**, the nitrate esters EGDN **06**, GTN **07**, ETN **08**, the nitrotoluenes **12** – **17** and DMDNB **26** could be quantified with the necessary precision (reproducibility:<1.00 % standard deviation) for the transpiration method experiment. In the other cases the analytes can be detected but not quantified due to their thermolability. The GC/MS method can even be accelerated to a total time of analysis of 3.10 minutes when a linear heating rate of 60 °C min^{-1} from 40 to 280 °C is used. This effect is visualized in Figure 10.

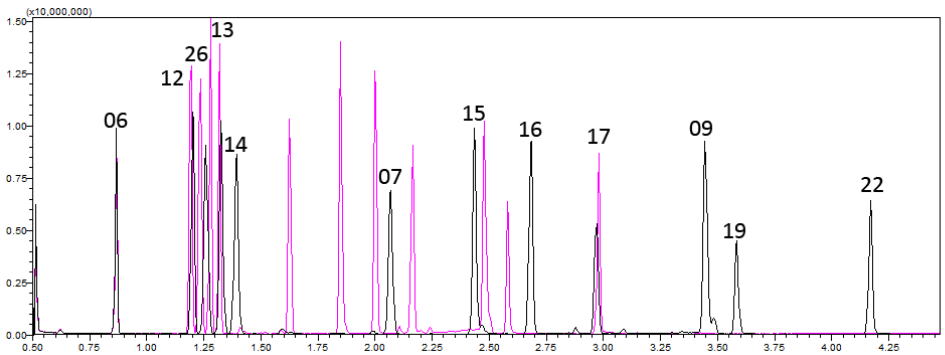

Figure 17 – Comparison of chromatogram of a mixture of explosives measured with [M3] (black) and with a linear heating rate of 60 °C min^{-1} from 40 °C to 280 °C. The retention time of Tetryl 22 is reduced from 4.18 min to 2.98 minutes.

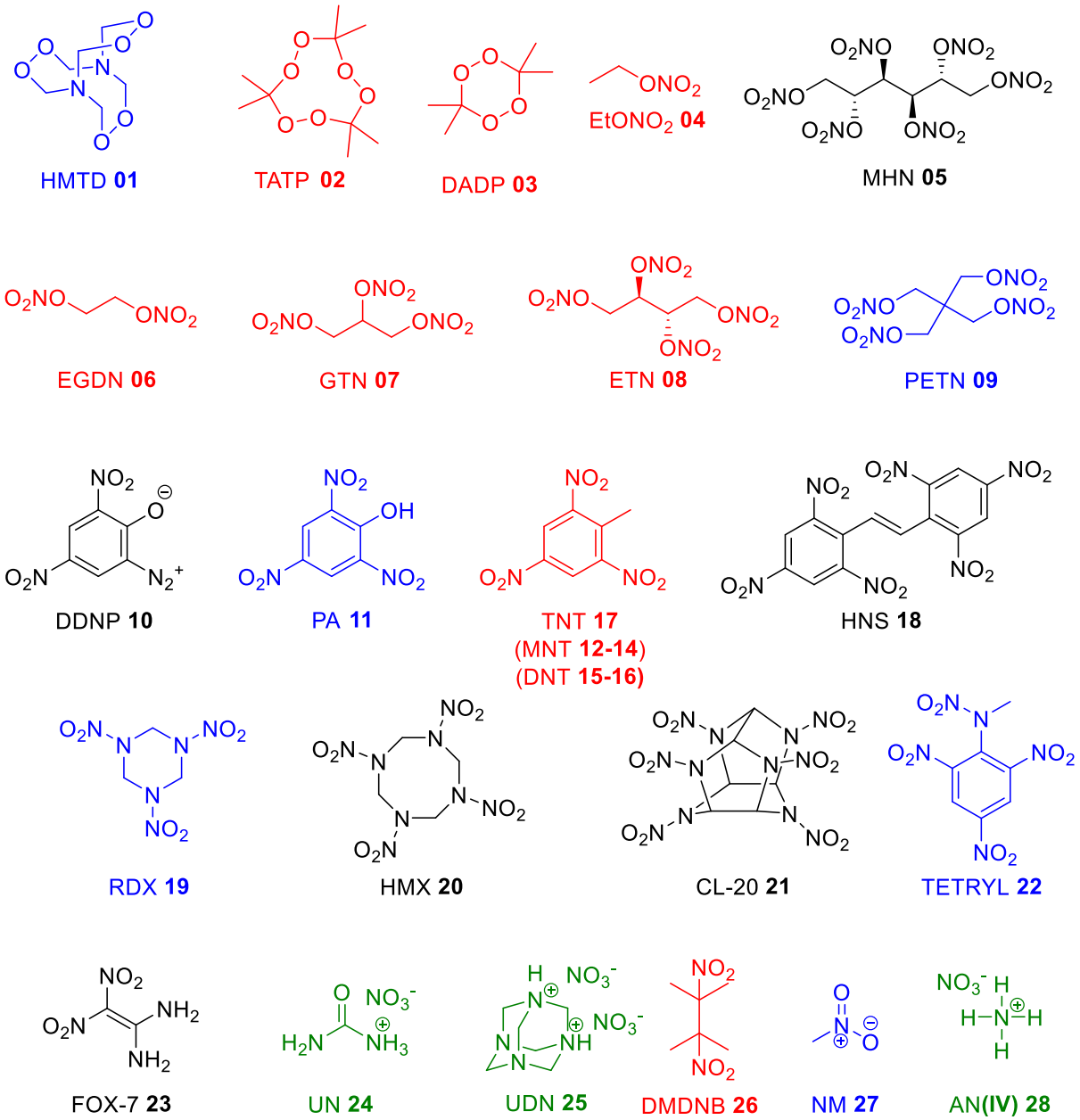

Figure 18 – The structures of the explosives that were included in the ChemAir substance repertoire. For VO-GC/MS (cf. section 5): black: substance not detectable, blue: substance detectable but not quantifiable, red: substance detectable and quantifiable, green: decomposition products of salts can be detected)

However, it has to be taken into account that PETN **09** decomposes under these conditions on the analytical column under release of nitrogen monoxide. This will have a negative influence on its limit of detection, which was not determined with this method.

In this work it was demonstrated that HPLC with a diode array UV-detector is a suitable tool for the quantification of explosives that are not detectable by VO-GC/MS. This was proven by test measurements with MHN **05**, DDNP **10**, HMX 20, CL-20 **21**, FOX-7 **23** and other analytes (cf. section 7.9). The LOD-comparison with the results for the LTM-FF-TG-GC/TOF-MS setup by Boeker and Leppert could not be established in this work but will be performed in a peer-reviewed publication during the year 2017.

Literature References

1. http://www.labo.de/chromatographie/milde-analytikmethode-fuer-explosivstoffe----------vakuum-gc-ms-mit--saeulenrestriktion-im-injektor.htm.
2. Kirchner, M.; Matisova, E.; Hrouzkova, S.; Huskova, R., Fast GC and CG-MS analysis of explosives. *Pet. Coal* **2007,** *49* (2), 72-79.
3. Boeker, P.; Leppert, J., Flow Field Thermal Gradient Gas Chromatography. *Analytical Chemistry* **2015,** *87* (17), 9033-9041.
4. (a) Cramers, C. A.; Scherpenzeel, G. J.; Leclerq, P. A., Increased speed of analysis in directly coupled gas chromatography-mass spectrometry systems : Capillary columns at sub-atmospheric outlet pressures. *Journal of Chromatography A* **1981,** *203* (0), 207-216; (b) Leclercq, P. A.; Scherpenzeel, G. J.; Vermeer, E. A. A.; Cramers, C. A., Increased speed of analysis in directly coupled gas chromatography-mass spectrometry systems : II. Advatages of vacuum outlet operation of thick-film capillary columns. *Journal of Chromatography A* **1982,** *241* (1), 61-71.
5. de Zeeuw, J.; Reese, S.; Cochran, J.; Grossman, S.; Kane, T.; English, C., Simplifying the setup for vacuum-outlet GC: Using a restriction inside the injection port. *Journal of Separation Science* **2009,** *32* (11), 1849-1857.
6. Brust, H.; Willemse, S.; Zeng, T.; van Asten, A.; Koeberg, M.; van der Heijden, A.; Bolck, A.; Schoenmakers, P., Impurity profiling of trinitrotoluene using vacuum-outlet gas chromatography–mass spectrometry. *Journal of Chromatography A* **2014,** *1374*, 224-230.
7. Lefferts, M. J.; Castell, M. R., Vapour sensing of explosive materials. *Analytical Methods* **2015,** *7* (21), 9005-9017.
8. Boeker, P.; Leppert, J.; Mysliwietz, B.; Lammers, P. S., Comprehensive Theory of the Deans' Switch As a Variable Flow Splitter: Fluid Mechanics, Mass Balance, and System Behavior. *Analytical Chemistry* **2013,** *85* (19), 9021-9030.
9. http://www.sepscience.com/Techniques/GC especially #5, #33, #36.
10. Boeker, P.; Haas, T.; Schulze Lammers, P., Theory and practice of a variable dome splitter for gas chromatography-olfactometry. *Journal of Chromatography A* **2013,** *1286*, 200-207.
11. P. Boeker; J. Leppert; B. Mysliwietz; Lammers, P. S., Supporting Information: Comprehensive Theory of the Deans' Switch As a Variable Flow Splitter: Fluid Mechanics, Mass Balance, and System Behavior. *Anal. Chem.* **2013,** *85*, 9021-9030.
12. Östmark, H.; Wallin, S.; Ang, H. G., Vapor Pressure of Explosives: A Critical Review. *Propellants, Explosives, Pyrotechnics* **2012,** *37* (1), 12-23.
13. http://www.sedet.com/Technology.html.
14. Dravnicks, A.; Brabets, R.; Stanley, T. A. *Evaluating Sensitivity Requirements of Explosive Vapor Detector Systems*; IIT Research Institute Technology Center: Chicago Illinois, 1972.
15. Bird, R. B.; Stewart, W. E.; Lightfoot, E. N., *Transport Phenomena*. John Wiley & Sons, Inc. : New Jork, 2002.
16. Rinkenbach, W. H., The Properties of Glycol Dinitrate1. *Industrial & Engineering Chemistry* **1926,** *18* (11), 1195-1197.
17. Lagemann, R. T.; McMillan, D. R.; Woolf, W. E., Temperature Variation of Ultrasonic Velocity in Liquids. *The Journal of Chemical Physics* **1949,** *17* (4), 369-373.
18. Sutton, T. C.; Harden, H. L., Surface Tension and Molecular Volume of Nitroglycerine. *The Journal of Physical Chemistry* **1933,** *38* (6), 779-781.
19. Groom, C. R.; Bruno, I. J.; Lightfoot, M. P.; Ward, S. C., The Cambridge Structural Database. *Acta Crystallographica Section B* **2016,** *72* (2), 171-179.
20. Jones, D. E. G.; Lightfoot, P. D.; Fouchard, R. C.; Kwok, Q. S. M., Thermal properties of DMNB, a detection agent for explosives. *Thermochimica Acta* **2002,** *388* (1–2), 159-173.
21. Meyer, R.; Köhler, J.; Homburg, A., *Explosives*. 7th ed.; WileyVCH: 2015.

5.7 APPENDIX 1 – Estimation of Air Concentration of Explosives

Vapor pressures are measured under ideal saturation conditions. In a real case scenario the saturation equilibrium of the analyte will not be reached and diffusion processes will dictate the air concentration of the analyte. *Dravnicks et al.* [14] have stated a mathematical model for the estimation of the non-equilibrium air concentration of an explosive, which shall be applied to compounds **I** – **VIII** in the following using the equations and values provided by *Bird et al.* [15].

Fick's Law of Diffusion provides a suitable approximation for the rate of molecular vapor emission per cm² J:

$$J = A \times D_{AB} \times \frac{n_c - n_a}{d} \tag{5}$$

J:emission flux [molecules s^{-1}], A: area of analyte exposed to air [cm²], D_{AB}: diffusivity of analyte vapor in air [cm^2 s^{-1}], n_c: concentration of analyte under saturation conditions [molecules cm^{-3}], n_a: concentration of the analyte in air [molecules cm^{-3}], d: thickness of non-turbulent layer air [cm]

The concentration of the analyte in the air is considered to be negligibly small ($\rightarrow n_a$ = 0) and the thickness of the non-turbulent layer of air surrounding the analyte is considered to be 0.2 cm [14].

The diffusivity D_{AB} can be calculated by the following formula:

$$D_{AB} = 0.0018583 \sqrt{T^3 (\frac{1}{M_A} + \frac{1}{M_B})} \frac{1}{p \sigma_{AB}^2 \Omega_{D,AB}} \tag{6}$$

T: Temperature [K] (298.15 K), M_A: Molecular Mass of Analyte [g mol^{-1}], M_B: Molecular Mass of Air [g mol^{-1}] (28.97 g mol^{-1}), p: total pressure [atm] (1 atm), σ_{AB}: combined collision diameter [Å], $\Omega_{D,AB}$: collision integral for diffusion

$$\sigma_{AB} = 1/2(\sigma_A + \sigma_B) \tag{7}$$

σ_A: collision diameter of analyte [Å], σ_B: collision diameter of air [Å] (3.617 Å) [15]

$$\varepsilon_{AB} = \sqrt{\varepsilon_A \varepsilon_B} \tag{8}$$

ε_A: characteristic energy of analyte, ε_B: characteristic energy of air

Whilst the collision diameter σ_B (3.617 Å) [15] and the characteristic energy ε_B (ε_B/κ = 97.0 K) [15] of air is known, the collision diameter of the analyte σ_A and its characteristic energy ε_A have to be estimated. These values may be estimated from the the liquid at the boiling point (b):

$$\varepsilon/\kappa = 1.15 T_b; \quad \sigma = 1.166 \sqrt[3]{V_b} \tag{9}$$
$$\varepsilon/\kappa = 1.92 T_m; \quad \sigma = 1.222 \sqrt[3]{V_m}$$

T_b: boiling point [K], V_b: molar volume of the liquid at the boiling point [cm^3 mol^{-1}] κ: Boltzmann's constant (1.38066 × 10^{-23} J K^{-1})

With ε_{AB} the collision integral for diffusion $\Omega_{D,AB}$ can be calculated according to:

$$\Omega_{D,AB} = \frac{1.16145}{T^{*0.15610}} + \frac{0.19300}{\exp(0.47635 T^*)} + \frac{1.03587}{\exp(1.52996 T^*)} + \frac{1.76474}{\exp(3.89411 T^*)} \tag{10}$$

$$T^* = \kappa T/\varepsilon_{AB} \tag{11}$$

In case of liquid explosives the diffusion coefficient can be calculated from the boiling point, which is estimated by extrapolation of the p-T-data obtained from own, unpublished vapor pressure measurements to the atmospherical pressure (101325 Pa). The needed molar volume V_b at the boiling point can be approximated. The thermal expansion coefficient α was calculated by linear regression of the temperature density data for the liquids EGDN **06** [16], 2-MNT **12** [17] and 3-MNT **13** [17] according to:

$$\rho_b = \alpha T_b + \rho_{0°C} \quad (12)$$

ρ_b: density at boiling point [g cm^{-3}], α: thermal expansion coefficient [g cm^{-3} °C^{-1}] $\rho_{0°C}$: density at 0 °C

For GTN 17 no reliable density data could be found. Instead its density at 20.5 °C $\rho_{20.5\,°C}$ [18] and the thermal expansion coefficient of EGDN 06 was used according to:

$$\rho_b = \rho_T + \alpha(T_b - T) \quad (13)$$

ρ_b: density at boiling point [g cm^{-3}], ρ_T density at temperature T [g cm^{-3}]

The molar volume at the boiling point can be calculated by:

$$V_b = M/\rho_b \quad (14)$$

For the solid explosives X-Ray diffraction densities from the CCDC database [19] were adjusted to the melting point of the explosive using the following equation (cf. Table 25):

$$\rho_m = \rho_{XRD}/(1 + 0.00015(T_m - T_{XRD})) \quad (15)$$

ρ_m: density at melting point [g cm^{-3}], ρ_{XRD}: density from X-Ray diffraction [g cm^{-3}], T_{XRD}: temperature of XRD-experiment [K]

Table 25 Melting points of room temperature solid explosives.

Ana-lyte	TATP 02	DMDNB 26	4-MNT 14	2,6-DNT 16	2,4-DNT 15	ETN 08	TNT 17	PETN 09	RDX 19
T_m[b] [°C]	97	200 [20]	52 [12]	57 [12]	71 [12]	56	81 [21]	133 [21]	204 [21]

[a] melting point, determined with differential scanning calorimetry [5 °C min^{-1}] if no literature citation is given

With equations 1 to 11 the diffusion coefficient of a liquid analyte in air can be approximated when solely its melting point and a density are known and equation (1) can be used to calculate the mass flux of material from the analyte to the air:

$$J = A \times D_{AB} \times \frac{n_c - n_a}{d}$$

With A = 1 cm², n_a= 0 and d = 0.2 cm it can be written:

$$J = \frac{D_{AB}}{0.2\ \text{cm}} \times n_c \quad (16)$$

If the concentration n_c is converted to partial pressure (n_c = 3.3×10^{16}p, p: vapor pressure [Torr]) and the emission flux is converted into a mass flux (unit conversion factor: M/N_A) the mass flux can be calculated:

$$Q = \frac{D_{AB}}{0.2} \times 3.3\times10^{16} p \times (M/N_A) \quad (17)$$

Q: emission flux of analyte [g s^{-1} cm^{-2}], N_A: Avogadro Constant (6.022 × 10^{23} mol^{-1})

An example of this calculation can be found for EGDN **06** and TATP **02** in Table 26:

*Table 26 – Example of Calculation for the emission flux of Amitone **I** at STP conditions (298.2 K, 1 atm)*

Calculation for the emission flux of explosive Q for TATP 02 and DADP at STP conditions (298.2 K, 1 atm)

	EGDN 06		**TATP 02**	**Unit**
T_b	475.36	T_m	370.2[a]	K
$\rho_{0°C}$	1.52	ρ_{XRD}	1.27[b]	g cm^{-3}
		T_{XRD}	180[b]	K
ρ_b	1.22	ρ_m	1.24	g cm^{-3}
M	152.062	M	222.237	g mol^{-1}
V_m	123.879	V_m	179.981	cm^3 mol^{-1}
σ_A	5.813	σ_A	6.899	Å
ε_B/κ	546.664	ε_B	710.688	K
σ_{AB}	4.715	σ_{AB}	5.258	Å
ε_{AB}/κ	230.275	ε_{AB}	262.558	K
$\kappa T/\varepsilon_{AB}$	1.295	$\kappa T/\varepsilon_{AB}$	1.136	[]
$\Omega_{D,AB}$	1.277	$\Omega_{D,AB}$	1.355	[]
D_{AB}	0.068	D_{AB}	0.050	cm^2 s^{-1}
p_{sat}	10.2	p_{sat}	6.7[a]	Pa
p_{sat}	0.077	p_{sat}	0.050[a]	mmHg
Q	0.218	Q	0.154	µg/cm² s

With the emission flux Q in hands the concentration of the analyte in air can be calculated:

$$c_{dif} = S \times Q \times r \quad (18)$$

c_{dif}: concentration of analyte in air, S: surface of analyte exposed to air, r: attenuation factor (10^{-4})

The attenuation factor r has been established in the study by *Dravnicks et al.* [14] For a surface of 200 cm² the values for c_{dif} stated in Table 23 were obtained. These values must be regarded as the maximum concentrations of analyte that can be present for detection in air in an open-exposure scenario.

5.8 APPENDIX 2: EI-Mass Spectra measured by VO-GC/MS

EGDN

# of Peaks	21
Raw Spectr	0.370 (scan : 35)
Backgroun	0.855 -> 0.915 (scan : 72 -> 84)
Base Peak	m/z 46.00 (Inten : 4,740,402)
Event#	1

m/z	Absolute In	Relative Intensity
30	607662	12.82
31.05	93539	1.97
32	6711	0.14
41.05	4344	0.09
42	19749	0.42
43	36465	0.77
44.05	1236	0.03
45.05	37443	0.79
46	4740402	100
47	24255	0.51
48	22546	0.48
54.9	881	0.02
55.95	1065	0.02
57.05	871	0.02

TATP

# of Peaks	32
Raw Spectr	1.220 (scan : 145)
Backgroun	1.060 -> 1.145 (scan : 113 -> 130)
Base Peak	m/z 43.00 (Inten : 5,865,627)
Event#	1

m/z	Absolute In	Relative Intensity
30.05	3800	0.06
31.05	71556	1.22
32	10486	0.18
33	7666	0.13
36.95	2304	0.04
37.95	2694	0.05
39.05	14420	0.25
40.05	5095	0.09
41.05	61956	1.06
42.05	117162	2
43	5865627	100
44	162940	2.78
45.05	82933	1.41
47.05	12605	0.21
53	1353	0.02
55	25592	0.44
56.15	3085	0.05
57.05	185808	3.17
58.05	342585	5.84
59.05	610694	10.41
60.05	25335	0.43
61.1	1910	0.03
71	1792	0.03
73.05	82628	1.41
74	70969	1.21
75.05	424844	7.24
76.05	13442	0.23
77.05	2100	0.04
89.05	4701	0.08
91.05	1619	0.03
101	12505	0.21
117.1	8713	0.15

2-MNT

# of Peaks	63
Raw Spectr	1.385 (scan : 178)
Backgroun	0.815 -> 0.925 (scan : 64 -> 86)
Base Peak	m/z 120.05 (Inten : 1,538,090)
Event#	1

m/z	Absolute In	Relative Intensity
30.05	45817	2.87
31.05	3558	0.22
35.95	1300	0.08
37	23975	1.5
38	70575	4.42
39	487041	30.48
40	33026	2.07
41.05	103017	6.45
42	4152	0.26
43.05	7091	0.44
45.05	1058	0.07
46	14779	0.92
46.9	864	0.05
47.85	1459	0.09
49	10713	0.67
50.05	127896	8
51.05	229634	14.37
52.05	71447	4.47
53.05	42362	2.65
54.05	4595	0.29
55.05	3758	0.24
60	3023	0.19
61	31766	1.99
62.05	97741	6.12
63	331212	20.73
64.05	135450	8.48
65.05	1472026	92.11
66.05	101952	6.38
67.05	8126	0.51
67.95	3170	0.2
73.05	5338	0.33
74.05	29769	1.86
75	26903	1.68
76.05	27868	1.74
77	321833	20.14
78.05	69275	4.33
79.05	45252	2.83
80	11852	0.74
81	5418	0.34
83.9	2716	0.17
85	7580	0.47
86	17682	1.11
87	16714	1.05
88.05	7456	0.47
89.05	360087	22.53
90.05	130958	8.19
91.05	746520	46.71
92.05	770933	48.24
93.1	114658	7.17
94	6601	0.41
102.95	1192	0.07
103.9	4225	0.26
105	5086	0.32
106.05	1519	0.1
107	7334	0.46
108.05	1442	0.09
119.15	10316	0.65
120.05	1538090	100
121.05	136036	8.51
122	9393	0.59
136.05	1395	0.09
137.05	105775	6.62
138.05	9012	0.56

DMDNB

# of Peaks	51
Raw Spectr	1.460 (scan : 193)
Backgroun	0.830 -> 0.925 (scan : 67 -> 86)
Base Peak	m/z 57.10 (Inten : 2,014,008)
Event#	1

m/z	Absolute In	Relative Intensity
30	190411	9.45
31.05	37764	1.88
32	1438	0.07
36.9	4039	0.2
38	12497	0.62
39	302257	15.01
40.05	67611	3.36
41.05	983288	48.82
42.05	111900	5.56
43	251197	12.47
44.05	3838	0.19
44.95	1777	0.09
45.9	23457	1.16
47.1	546	0.03
47.9	1569	0.08
48.8	1095	0.05
50	6110	0.3
51	18646	0.93
52.1	9743	0.48
53.1	70655	3.51
54.05	13484	0.67
55.05	423591	21.03
56.1	173415	8.61
57.1	2014008	100
58.1	156750	7.78
59.05	124345	6.17
60	5950	0.3
63	5881	0.29
64.05	1008	0.05
65	21551	1.07
66	6546	0.33
67.05	81075	4.03
68.15	15601	0.77
69.05	938966	46.62
70.1	53838	2.67
71.05	2337	0.12
72.05	12194	0.61
73.1	1398	0.07
77.1	3545	0.18
79	4609	0.23
80.15	1147	0.06
81.1	4382	0.22
82.15	2776	0.14
83.1	129998	6.45
84.05	319790	15.88
85.05	190730	9.47
86.1	10214	0.51
89	9826	0.49
99.15	2458	0.12
100.05	274114	13.61
101.05	17213	0.85

3-MNT

# of Peaks	60
Raw Spectr	1.550 (scan : 211)
Backgroun	1.705 -> 1.765 (scan : 242 -> 254)
Base Peak	m/z 91.05 (Inten : 1,909,610)
Event#	1

m/z	Absolute In	Relative Intensity
30	80443	4.21
31.05	1920	0.1
37	19063	1
38.05	58658	3.07
39.05	422443	22.12
40	30025	1.57
41.05	93876	4.92
43	13354	0.7
43.95	2724	0.14
45	1060	0.06
45.9	20737	1.09
49.05	6149	0.32
50.05	101544	5.32
51	155170	8.13
52.05	43229	2.26
53.1	27978	1.47
54	2250	0.12
55.1	1483	0.08
58.05	686	0.04
60	1574	0.08
61.05	27765	1.45
62	85386	4.47
63	280697	14.7
64.05	73387	3.84
65.05	1122551	58.78
66	57767	3.03
67.1	2015	0.11
68.9	1072	0.06
73.05	5218	0.27
74.05	24198	1.27
75.05	22612	1.18
76.05	16135	0.84
77.05	152785	8
78	30960	1.62
79.05	145306	7.61
80.1	13586	0.71
81	1105	0.06
83.95	2384	0.12
85.05	6109	0.32
86.05	16830	0.88
87.05	14360	0.75
88.05	4162	0.22
89.05	232275	12.16
90.15	91221	4.78
91.05	1909610	100
92.05	150596	7.89
93.15	4742	0.25
103	1359	0.07
104	4560	0.24
104.95	2156	0.11
106.15	1792	0.09
107.05	180831	9.47
108.05	15148	0.79
120.05	8596	0.45
121	8921	0.47
135.05	1632	0.09
136.05	14130	0.74
137.05	1160429	60.77
138.05	95448	5
139	5641	0.3

4-MNT

# of Peaks	59
Raw Spectr	1.640 (scan : 229)
Backgroun	1.725 -> 1.830 (scan : 246 -> 267)
Base Peak	m/z 91.05 (Inten : 1,314,057)
Event#	1

m/z	Absolute In	Relative Intensity
30	90252	6.87
31.15	1399	0.11
37.05	19992	1.52
38.05	51239	3.9
39	407014	30.97
40	27388	2.08
41.05	83687	6.37
43	10717	0.82
44	2079	0.16
45.05	1191	0.09
46	16530	1.26
49	7271	0.55
50	119356	9.13
51.05	161207	12.27
52.05	46134	3.51
53.05	30886	2.35
54.1	1823	0.14
55.05	2840	0.22
59.95	1869	0.14
61	28030	2.13
62	85438	6.5
63	262494	19.98
64.05	63247	4.81
65.05	1038576	83.6
66.05	59970	4.56
67	1449	0.11
73	4116	0.31
74	23313	1.77
75	19601	1.49
76	14508	1.1
77.05	239092	18.19
78	47975	3.65
79.05	190043	14.46
80	13524	1.03
84.05	2247	0.17
84.95	7666	0.58
86	16154	1.23
87.05	12928	0.98
88.05	4643	0.35
89	214526	16.33
90.1	61924	4.71
91.05	1314057	100
92.05	101901	7.75
93.1	2460	0.19
103	1159	0.09
104.1	1913	0.15
105	2204	0.17
106.05	5880	0.45
107.05	331964	25.26
108.05	27546	2.1
109.1	1847	0.14
120.05	2485	0.19
121.05	18073	1.38
122.05	1715	0.13
134.95	1598	0.12
136.05	4363	0.33
137.05	1048315	79.78
138.05	87908	6.69
139.05	7725	0.59

GTN

# of Peaks	29
Raw Spectr	2.285 (scan : 358)
Backgroun	1.930 -> 2.065 (scan : 287 -> 314)
Base Peak	m/z 46.00 (Inten : 6,673,543)
Event#	1

m/z	Absolute In	Relative Intensity
30	683897	10.25
31.05	199994	3
32	9384	0.14
38.95	2218	0.03
39.9	1042	0.02
41	4538	0.07
42	24874	0.37
43	47482	0.71
44	5513	0.08
45.05	43689	0.65
46	6673543	100
46.95	38171	0.57
48	26146	0.39
55.15	3090	0.05
55.95	2629	0.04
57.05	1176	0.02
58	1850	0.03
58.95	1235	0.02
60.05	8713	0.13
61.25	1266	0.02
75.05	2860	0.04
76	323670	4.85
77	5033	0.08
78.1	2378	0.04
89.1	1583	0.02
91.15	1838	0.03
119.1	2110	0.03
150.95	8354	0.13
164.95	1342	0.02

5.8 APPENDIX 2: EI-Mass Spectra measured by VO-GC/MS

2,6-DNT

# of Peaks	94
Raw Spectr	2.650 (scan : 431)
Backgroun	2.700 -> 2.745 (scan : 441 -> 450)
Base Peak	m/z 165.05 (Inten : 1,263,422)
Event#	1

m/z	Absolute In	Relative Intensity
30	189079	14.97
31	12660	1
31.95	37	0.01
36.05	1539	0.13
37.05	24359	1.96
38.05	75039	5.94
39	328569	26.01
40	54145	4.29
41	14915	1.18
42.05	16221	1.28
43	231377	18.31
44.05	9373	0.79
45.05	2515	0.2
45.95	17960	1.42
46.9	2009	0.16
47.95	1748	0.14
49	10574	0.84
50	160588	12.71
51	377460	29.88
52.05	257485	20.38
53.05	85618	6.78
54	17978	1.42
55	15130	1.2
55.95	4161	0.33
59.05	1553	0.12
60.05	8871	0.7
61.05	36345	2.88
62	172182	13.63
63.05	743695	58.86
64.05	335149	26.53
65.05	88970	7.04
66.05	55884	4.42
66.95	13908	1.1
67.95	8386	0.66
69.1	2588	0.2
70.8	457	0.04
73.05	7437	0.59
74	71050	5.62
75	213618	16.91
76	145009	11.48
77	396065	31.35
78	328419	25.99
79	101396	8.03
80.05	24353	1.96
81.05	4405	0.35
82	2726	0.22
83.1	1991	0.16
84.05	1930	0.15
85.05	10971	0.87
86.05	34931	2.76
87.05	30148	2.39
88.05	13212	1.05
89.05	737382	58.36
90.05	433878	33.09
91.05	278331	22.03
92	64446	5.1
93	17172	1.36
94.05	13932	1.1
94.9	2070	0.16
96	1026	0.08
98.9	1993	0.16
100.15	1017	0.08
102.05	3367	0.27
103.05	3844	0.3
104.05	118702	9.4
105.05	50465	3.99
106	57934	4.59
107.05	83470	6.61
108	114742	9.08
109	9948	0.79
117	28649	2.27
118	58129	4.6
119.05	116395	9.21
120.05	14970	1.18
121	260649	20.63
122.05	16993	1.34
123	2279	0.18
133.05	1282	0.1
134	92257	7.3
135.05	194844	15.42
136	19514	1.54
136.95	10857	0.86
138.05	1328	0.11
148.05	308122	24.39
149	28705	2.27
149.85	2667	0.21
163.05	1010	0.08
164.05	30359	2.4
165.05	1263422	100
166.05	113169	8.96
167.05	12274	0.97
168	1031	0.08
181.1	2377	0.19
182.1	5542	0.44

2,4-DNT

# of Peaks	90
Raw Spectr	2.895 (scan : 480)
Backgroun	2.350 -> 2.590 (scan : 371 -> 413)
Base Peak	m/z 165.05 (Inten : 1,748,706)
Event#	1

m/z	Absolute In	Relative Intensity
30	435516	24.91
31	7801	0.45
32.05	2345	0.13
37.05	21024	1.2
38	66444	3.8
39	349722	20
40.05	52393	3.03
41.05	16909	0.97
42.05	5020	0.29
43	17342	0.99
44	2917	0.17
44.95	2342	0.13
46	33403	1.91
47	1314	0.08
48.05	1473	0.08
49	11202	0.64
50	119156	6.81
51.05	274150	15.68
52.05	208553	11.93
53.05	62265	3.56
54	10914	0.62
55	14902	0.85
56.05	2123	0.12
57.05	716	0.04
59.95	3280	0.19
61.05	40362	2.31
62	147385	8.43
63	758178	43.36
64	267814	15.31
65.05	80643	4.61
66.05	58658	3.35
66.95	10107	0.58
68	10271	0.59
69	13138	0.75
71.1	5662	0.32
73.05	5718	0.33
74.05	51078	2.92
75.05	61739	3.53
76.05	47420	2.71
77.05	206686	11.82
78	282454	16.15
79.05	90904	5.2
80.05	45878	2.62
81	8764	0.5
82.1	2236	0.13
84.05	2047	0.12
85.05	10339	0.59
86.05	35087	2.01
87	38786	2.22
88.05	17109	0.98
89.05	1243719	71.47
90.05	480054	27.45
91.05	140031	8.01
92.05	40433	2.31
93.05	11976	0.68
94.05	14634	0.84
95	7065	0.4
96	1633	0.09
99.05	1059	0.06
100.1	1295	0.07
102	1905	0.11
103.05	4837	0.28
104.05	4346	0.25
105.05	70906	4.05
106.05	77876	4.45
107	81332	4.65
108.05	34447	1.97
109	4145	0.24
117.05	2313	0.13
118	168638	9.65
119.05	473078	27.05
120.05	40354	2.31
121.05	8870	0.51
121.9	1820	0.1
122.9	1034	0.06
133.95	2830	0.16
135	15434	0.88
136.05	16109	0.92
136.95	5465	0.31
138	3586	0.21
148	47438	2.72
149.05	25827	1.48
149.95	2101	0.12
164.05	7222	0.41
165.05	1748706	100
166	160540	9.18
167	14130	0.81
182	91066	5.21
183	10585	0.61
183.95	2188	0.13

ETN

# of Peaks	35
Raw Spectr	3.165 (scan : 534)
Backgroun	2.395 -> 2.600 (scan : 380 -> 421)
Base Peak	m/z 46.00 (Inten : 7,066,386)
Event#	1

m/z	Absolute In	Relative Intensity
30	678649	9.6
31.05	223150	3.16
32.05	18100	0.26
38.9	2238	0.03
39.95	1733	0.02
41	5100	0.07
41.95	28541	0.4
43	65704	0.93
44	13301	0.19
45.05	50771	0.72
46	7066386	100
47	37839	0.54
48	27081	0.38
53.05	1168	0.02
54.05	1426	0.02
55.05	16070	0.23
56.15	2899	0.04
57.05	4209	0.06
58	4707	0.07
58.9	5078	0.07
60.05	15657	0.22
61.05	4138	0.06
63.05	1202	0.02
63	2985	0.04
71	8226	0.12
73.1	3144	0.04
75.05	1049	0.01
76	245417	3.47
77.05	4265	0.06
77.95	1840	0.03
89.05	1308	0.02
106	1842	0.03
117.95	2990	0.04
151	8735	0.12
165.05	1080	0.02

TNT

# of Peaks	115
Raw Spectr	3.400 (scan : 581)
Backgroun	3.445 -> 3.480 (scan : 590 -> 597)
Base Peak	m/z 209.95 (Inten : 872,130)
Event#	1

m/z	Absolute In	Relative Intensity
30	294966	33.82
31	4653	0.53
32.05	1736	0.2
37.05	11897	1.36
38	23001	2.64
39	151850	17.41
40	7511	0.86
41.1	2547	0.29
42.05	455	0.05
43.05	66301	7.67
44.1	2880	0.33
45.05	365	0.04
46	27432	3.15
47	1995	0.23
48.05	2634	0.3
49.05	3271	0.38
50	91012	10.44
51	125344	14.37
52.1	29474	3.38
53	26935	3.09
54.1	5367	0.62
55.05	7977	0.91
56	2049	0.23
56.95	115	0.01
59.15	715	0.08
59.9	8257	0.95
61.05	28448	3.26
62	166644	19.11
63.05	352858	40.46
64	59689	6.84
65.05	51625	5.92
66	21268	2.44
67.05	18784	2.15
68.05	11517	1.32
68.95	38165	4.49
70.1	2346	0.27
70.9	2539	0.29
71.85	2035	0.23
73	7426	0.85
74	74371	8.6
75.05	82641	9.48
76	156287	17.92
77.05	84829	9.73
78	30701	3.52
79.05	14099	1.62
80	12822	1.47
81	3763	0.43
83	1513	0.17
83.95	3296	0.38
85	14585	1.67
86	46839	5.37
87.05	66328	7.61
88.05	93814	10.76
89.05	427482	49.02
90.05	64855	7.44
91.05	20834	2.39
92.05	32721	3.75
93	14380	1.65
94.05	15122	1.73
95	4382	0.5
96	5305	0.68
99.05	2604	0.3
100.05	1416	0.16
101.1	1230	0.14
102.05	1627	0.19
103	32346	3.71
104	29403	3.37
105.05	33076	3.79
106.05	34580	3.97
106.95	13618	1.56
108.05	2261	0.26
111.9	1494	0.17
116	7130	0.82
117.05	15576	1.79
118	12386	1.42
119	6706	0.77
120	36194	4.15
121.1	7585	0.87
122	3356	0.38
123.05	1783	0.2
132.05	1862	0.21
133	11670	1.34
134	118253	13.56
135.05	20082	2.3
135.95	16111	1.85
137	2625	0.3
147.05	1119	0.13
148.05	2154	0.25
149	97218	11.15
150.05	9482	1.09
151	13036	1.49
151.95	10191	1.17
153.1	1241	0.14
161.9	1481	0.17
163	18914	2.17
164	75410	8.65
165	7750	0.89
166	29519	3.38
166.95	4919	0.56
168	1270	0.15
179	37591	4.31
180	98668	11.31
181	10282	1.18
181.95	3237	0.37
193	119403	13.69
193.95	15500	1.78
194.9	2393	0.27
197	1282	0.15
209.05	23885	2.74
209.95	872130	100
211	80878	9.27
212	12079	1.38
212.7	1700	0.19
226	2217	0.25
227	2202	0.25

5.8 APPENDIX 2: EI-Mass Spectra measured by VO-GC/MS

PETN

# of Peaks	50
Raw Spectr	3.645 (scan : 630)
Backgroun	3.530 -> 3.570 (scan : 607 -> 615)
Base Peak	m/z 46.00 (Inten : 5,938,976)
Event#	1

m/z	Absolute In	Relative Intensity
30	474633	7.99
31.05	182284	3.07
32.05	1076	0.02
38	3345	0.06
39.05	38329	0.65
40.05	18272	0.31
41.05	61470	1.04
42	72223	1.22
43	70671	1.19
44	37584	0.63
45.05	52313	0.88
46	5938976	100
46.95	30625	0.52
47.95	24741	0.42
50	1081	0.02
50.9	504	0.01
53.1	6527	0.11
54	13210	0.22
55	56333	0.95
56	38697	0.65
57.05	66947	1.13
58	11887	0.2
59.05	3714	0.06
59.95	28232	0.48
60.8	2228	0.04
61.95	1648	0.03
63.85	1377	0.02
68.05	3125	0.05
69.05	14455	0.24
70.05	5332	0.09
71.05	23262	0.39
72	6620	0.11
73	9272	0.16
74.05	3025	0.05
75.05	4358	0.07
76	544396	9.18
76.95	10228	0.17
78	4941	0.08
83.1	3705	0.06
83.95	2028	0.03
85.05	14701	0.25
86.05	3321	0.06
87.2	1510	0.03
89.05	62	0
101.05	2072	0.03
102	7516	0.13
116	1337	0.02
118.05	392	0.01
134	266	0
209.1	3489	0.06

RDX

# of Peaks	50
Raw Spectr	3.645 (scan : 630)
Backgroun	3.530 -> 3.570 (scan : 607 -> 615)
Base Peak	m/z 46.00 (Inten : 5,938,976)
Event#	1

m/z	Absolute In	Relative Intensity
30	474633	7.99
31.05	182284	3.07
32.05	1076	0.02
38	3345	0.06
39.05	38329	0.65
40.05	18272	0.31
41.05	61470	1.04
42	72223	1.22
43	70671	1.19
44	37584	0.63
45.05	52313	0.88
46	5938976	100
46.95	30625	0.52
47.95	24741	0.42
50	1081	0.02
50.9	504	0.01
53.1	6527	0.11
54	13210	0.22
55	56333	0.95
56	38697	0.65
57.05	66947	1.13
58	11887	0.2
59.05	3714	0.06
59.95	28232	0.48
60.8	2228	0.04
61.95	1648	0.03
63.85	1377	0.02
68.05	3125	0.05
69.05	14455	0.24
70.05	5332	0.09
71.05	23262	0.39
72	6620	0.11
73	9272	0.16
74.05	3025	0.05
75.05	4358	0.07
76	544396	9.18
76.95	10228	0.17
78	4941	0.08
83.1	3705	0.06
83.95	2028	0.03
85.05	14701	0.25
86.05	3321	0.06
87.2	1510	0.03
89.05	62	0
101.05	2072	0.03
102	7516	0.13
116	1337	0.02
118.05	392	0.01
134	266	0
209.1	3489	0.06

TETRYL

# of Peaks	133
Raw Spectr	4.395 (scan : 780)
Backgroun	4.270 -> 4.330 (scan : 755 -> 767)
Base Peak	m/z 193.95 (Inten : 362,145)
Event#	1

m/z	Absolute In	Relative Intensity
30	316347	87.35
31.05	17073	4.71
32	2490	0.69
36.95	14053	3.88
38.05	25063	6.92
39.05	62732	17.32
39.95	21854	6.03
41.05	19843	5.48
42	34189	9.44
43.05	4478	1.24
44	40084	11.07
44.95	3497	0.97
45.95	16911	4.67
48	2172	0.6
49.05	3270	0.9
50.05	90759	25.06
51	225173	62.18
52	102346	28.26
53	61199	16.9
54.05	17949	4.96
55	10589	2.92
56.05	10050	2.78
57.1	448	0.12
58.1	21193	5.85
59.95	3655	1.01
61	52354	14.46
62	155772	43.01
63.05	87804	24.25
64	121136	33.45
65.05	133623	36.9
66.05	113122	31.24
67	20566	5.68
68.1	18081	4.99
69.05	11850	3.27
70.05	4003	1.11
71.05	179	0.05
72.05	4877	1.35
73.05	8913	2.46
74.05	89520	24.72
75	244725	67.58
76	241983	66.82
77	338032	93.36
78	190804	52.69
79.05	48225	13.32
80	57818	15.97
81	14278	3.94
82.05	8240	2.28
83.05	5360	1.48
84	2343	0.65
86	3366	0.93
87.05	19099	5.27
88	85566	23.63
89	65548	18.1
90.05	77075	21.28
91.05	110951	30.64
92.05	159734	44.12
93.05	46023	12.71
94	10110	2.79
95.1	6639	1.83
96	3434	0.95
98.05	1282	0.35
99	1654	0.46
100	4326	1.19
101	7263	2.01
102.05	76135	21.02
103	102716	28.36
104.1	101063	27.91
105	48945	13.52
106	19582	5.41
107	15926	4.4
107.95	12383	3.42
109	5106	1.41
111	1100	0.3
115.05	3170	0.88
116	6721	1.86
117.05	31897	8.81
118	120287	33.22
119.1	57927	16
120.05	65925	18.2
121.05	20241	5.59
122	4970	1.37
122.95	3923	1.08
123.9	1538	0.42
131	7902	2.18
132.05	55962	15.45
133.05	37656	10.4
134.1	18119	5
135.05	3993	1.1
136	32314	8.92
137.05	29411	8.12
138.1	4166	1.15
139	7094	1.96
147.05	4061	1.12
148	30102	8.31
149	71353	19.87
150.05	23311	6.44
151.1	6246	1.72
152.1	1062	0.29
162	1903	0.53
163.05	19073	5.27
164	41068	11.34
165	11370	3.14
166	24434	6.75
167.05	34945	9.65
168.1	3018	0.83
169.1	1108	0.31
178	26415	7.29
179	32191	8.89
180	6503	1.8
180.9	1420	0.39
182.1	3015	0.83
183.05	5520	1.52
184.1	1282	0.35
193.05	2673	0.74
193.95	362145	100
195	43274	11.95
195.95	6554	1.81
197	35554	9.82
197.95	3395	0.94
208	4182	1.15
208.9	2628	0.73
209.9	1623	0.45
212	28060	7.75
212.95	12958	3.58
213.95	2897	0.8
224	13551	3.74
225	54706	15.11
225.9	7567	2.09
226.95	1761	0.49
241.05	1950	0.54
242	207404	57.27
243	16225	4.48
244	3531	0.99

6 The Determination of Vapor Pressures with the Transpiration Method Experiment

A multitude of experiments exist for the measurement of vapor pressures. These include static method measurements, ebulliometry, *Knudsen*-effusion methods, the transpiration method and chromatographic methods. The techniques for the measurement of vapor pressures have been reviewed excellently by *Verevkin* [1]. The basic principle of the transpiration method experiment is the saturation of a well-defined carrier gas stream in a thermostatted environment. The analyte is recondensed from the carrier gas in a cooling trap or on an adsorbent and quantified using standard analytical techniques including gas chromatography. Based on temperature, the volume of the carrier gas used, the transported mass of the analyte and other parameters the vapor pressure of the analyte can be calculated. In the following the experimental setup used, the mathematical evaluation of the transpiration experiment results, the uncertainty of the transpiration method experiment and practical advices will be elucidated.

6.1 The Experimental Setup

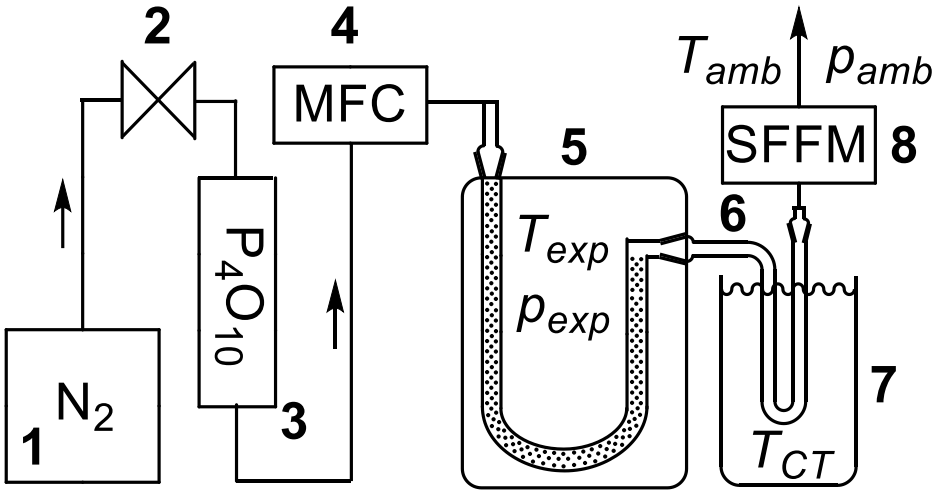

*Figure 1 – Schematic Illustration of the Transpiration Experiment Setup. **1**: nitrogen reservoir, **2**: pressure reduction valve, **3**: P_4O_{10} drying tower, **4**: mass flow controller, **5**: saturator, **6**: condenser pipe, **7**: cooling trap, **8**: soapfilm flowmeter*

The carrier gas is passed from a liquid Nitrogen reservoir **1** through a pressure reduction valve **2** to reduce the pressure from 10 bar to 1.5 bar. The reduction of the pressure is necessary to pass the gas through a drying column **3**, which is filled with phosphorous pentoxide on silica to remove any remaining contents of water. The flow-rate of the dried gas is regulated by a mass flow controller **4** before the gas enters the saturator **5**. The saturator **5** is a cylindrical glass-vessel whose temperature is controlled by a circulation thermostat, which circulates monoethylene glycol (50%, aq.) through it. The gas-stream is conducted through a U-shaped glass-pipe, which is positioned within the saturator. The glass-pipe is filled with 1 mm glass beads onto which the substance is coated. By passing the carrier-gas through the saturator it reaches the analyte saturation equilibrium before the end of the saturator. After its saturation with analyte the carrier gas is directed into a U-shaped condensation pipe **6**, which is cooled by isopropanol in a Dewar vessel cooling trap **7**. The isopropanol temperature T_{CT} (-30 ○C) is controlled by an immersion cooler. The carrier gas flow-rate is measured with a soap film flow-meter. The ambient temperature T_{amb} and pressure p_{amb} are measured with a thermo-/barometer (Greisinger GFTB200). Selected components of the experimental setup are depicted in Figure 2.

Carrier Gas Supply 1

Nitrogen (Air Liquide, Stickstoff HG Flüssig, 99.999 vol.-% purity, < 3 ppm O_2/H_2O v/v) is taken from an institute-internal distribution system, which operates with a pressure of 10 bar. The pressure is reduced to 1.5 bar with a pressure reduction valve.

Gas Drying Tower 3

The gas drying tower is a glass-pipe (80 cm length, 45 mm diameter), which is filled with phosphorus pentoxide coated on a silica support (Sicapent®, SigmaAldrich, cat. #79610). The dessicant contains an internal moisture indicator, which changes its color from white to blue upon contact with moisture. The ground glass joints are equipped with PTFE sealings and secured with safety clips.

Mass Flow Controller 4

MC-100 CCM mass flow controllers (MFC) by Natec Sensors GmbH (Garching, Germany) were used. The massflow controllers were controlled using the BB9-USB-Multi-Drop Box in combination with the Flow Vision Software (Alicat Scientic, v1.1.44.0). The high-precision calibration of the MFC was carried out by IAS GmbH (Oberursel, Germany). The MFC were operated in Mass Flow close loop mode.

Saturator 5

The saturator is a cylindrical glass vessel with a height of 25 cm and a diameter of 10 cm. Inside the glass-vessel a U-shaped glass pipe with an inner diameter of 8 mm and a total length of 50 cm is installed. The top of the saturator cylinder is penetrated by the U-shaped pipe which is terminated with a NS10 short socket. The other end of the saturator pipe terminates with a perpendicular bending to a NS 10 long socket. The end of this socket penetrates the sidewall of the saturator. It is of utmost importance that the terminal NS 10 long socket is within the saturator since collection of the analyte must start at T_{exp}. Two hose connectors are installed at the top and at the bottom of the sidewall of the saturator in a horizontally shifted fashion, which generates a swirl movement of the tempering fluid inside the saturator over the saturator pipe.

The carrier gas stream is connected with a hose connector attached to a NS 10 ground cone, which can be attached to the saturator pipe entry.

The saturator temperature is controlled with a Huber Ministat 230 circulation thermostat. It is connected to the saturator via Viton PTFE hoses, which remain operational up to 200 °C. A monoethylene glycol water mixture (50 vol.-%, aq.) can be used as cooling liquid in the temperature range from 1 °C to 100 °C. For higher temperatures pure di- or triethylene glycol can be used. Temperatures under 1 °C should be avoided due to ice crust formation on the saturator.

The thermostat is equipped with a class A PT100 sensor for the measurement of T_{exp} inside the saturator. The circulation thermostat is operated in the internal temperature control mode. The use of the external temperature control mode (tempering the saturator) increases the time until a new setpoint temperature has stabilized drastically.

The circulation thermostat bath is equipped with a gas pre-heating spiral (copper pipe, 5 mm inner diameter, 1m length) through which the gas stream is conducted before entering the saturator. For measurements below 25 °C the preheating pipe is excluded from the measurement setup.

Condenser Pipe 6

The condenser pipe is a glass pipe with 5 mm inner diameter, which is terminated at one end with a NS 10 long ground cone that can be attached to the saturator. At the end of the cone a straight piece of pipe with 12 cm length is attached before the perpendicular bent to the U-shaped part. The U-

shaped part is 11 cm long and has an inner pipe distance of 2 cm. At the end of the pipe a NS 10 short socket is installed.

The condenser pipe can be closed with a ground stopper at the ground cone. At the socket it can be closed with a polyethylene cap (laborshop24.de, Lamellenstopfen 8 x dm 9mm transparent, #10-2289).

Dewar Vessel Cooling Trap 7

The cooling trap is a Dewar vessel filled with isopropanol. The liquid is cooled to -30.0 °C with a Huber TC45E immersion cooler equipped with a PT-100 temperature sensor. The cooling liquid should be miscible with water and exchanged when ice-crystals form. Attempts to replace the isopropanol cooling liquid with isohexane resulted immediately in the rapid formation of ice crystals.

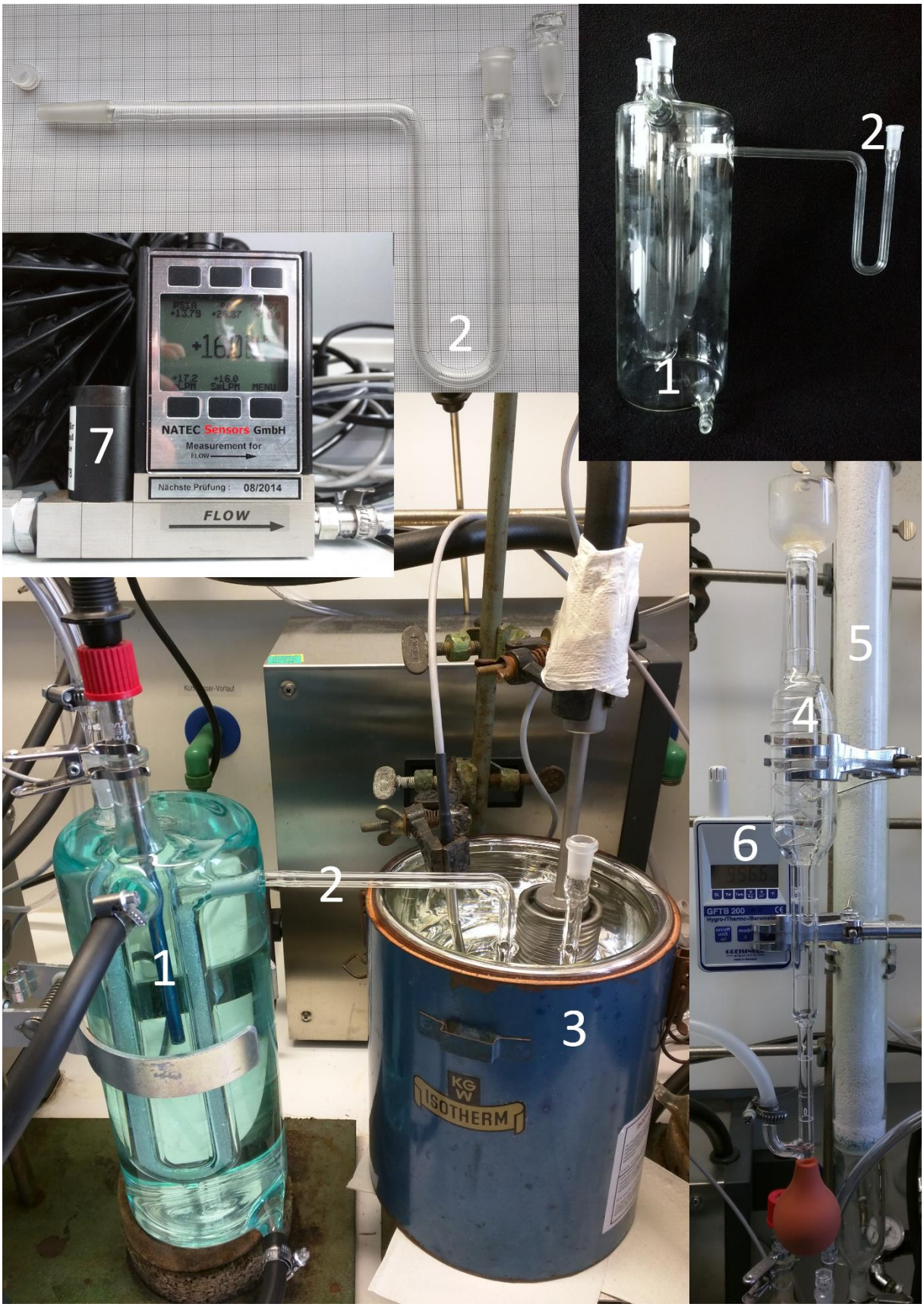

Figure 2 – Selected Components of the Transpiration Experiment Setup: 1: Saturator, 2: Condenser Pipe, 3: Cooling Bath with Immersion Cooler, 4: Soap Film Flow Meter, 5: P_4O_{10} Drying Tower, 6: Thermohygrobarometer, 7: Mass Flow Controller (MFC)

6.2 Mathematical Evaluation of the Transpiration Method Experiment Results

The pressure of an ideal gas is described by the Ideal Gas Law:

$$p = \frac{nRT}{V} \tag{1}$$

Ideal gas behavior of the analyte can be assumed since analyte-analyte interactions can be excluded due to its low concentration in the carrier gas.

The experimental transpiration experiment vapor pressure p_{sat} at an experimental temperature T_{exp} is calculated using the following equation (cf. Figure 1):

$$p_{sat}(T_{exp}) = \frac{m_a R T_{amb}}{M V_{amb}} \tag{2}$$

Derivation:

The ideal gas law can be written as follows:

$$p = \frac{nRT}{V} = \frac{mRT}{MV} \tag{3}$$

Dalton's Law of partial pressures states that the total pressure p_{total} at a constant experimental temperature T_{exp} is the sum of the partial pressures of the gas mixture components. For the transpiration experiment it can be stated that the total pressure p_{total} is the sum of the vapor pressure p_{sat} of the analyte and p_{N2} of the nitrogen carrier gas.

$$p_{total}(T_{exp}) = p_{sat}(T_{exp}) + p_{N2}(T_{exp}) = (n_{sat} + n_{N2}) \times \left(\frac{RT_{exp}}{V_{exp}}\right) \tag{4}$$

Furthermore it can be approximated that the total volume V_{exp} under experimental conditions is the volume of the carrier gas since the volume of the gaseous analyte is negligibly small. This allows the measurement of the carrier gas volume V_{amb} under ambient conditions after freezing out the analyte in the cooling trap as a good approximation for V_{exp}, which will be demonstrated in the following.

The molar amount of carrier gas and analyte transported for one experimental datapoint remains constant under ambient and experimental conditions:

$$n_{amb} = n_{exp} = \frac{m_a}{\mathrm{M}} = \frac{p_{amb} V_{amb}}{\mathrm{R} T_{amb}} = \frac{p_{exp} V_{exp}}{\mathrm{R} T_{exp}} \tag{5}$$

The gas volume V_{exp} should ideally be measured under experimental conditions. Since this is hardly possible the Volume V_{amb} is measured under ambient conditions. The measurement system is open and only a low pressure drop occurs while passing the gas through the saturator, condenser and flow-meter. With this it can be assumed that the total experimental pressure p_{exp} is equal to the total ambient pressure p_{amb}:

$$p_{exp} = p_{amb} \tag{6}$$

Using equation 6 in equation 5 leads to:

$$\frac{V_{amb}}{T_{amb}} = \frac{V_{exp}}{T_{exp}} \tag{7}$$

Inserting equation 7 into equation 4 results in:

$$p_{sat}(T_{exp}) = \frac{m_a \mathrm{R} T_{amb}}{\mathrm{M} V_{amb}} \tag{8}$$

Equation 8 is directly linked to the Ideal Gas Law, which is the fundamental equation of the Transpiration Method. Furthermore it demonstrates that the ambient conditions can be linked to the experimental ones.

Determination of the Mass m_a

The mass m_a is determined in this work by an internal standard GC/MS quantification method. The GC/MS analysis of the sample results in the output of two integral areas: the analyte integral I_a and the standard integral I_s. The masses of analyte m_a and standard m_s are related to their integrals in a linear relationship:

$$\frac{I_a}{I_s} = X\frac{m_a}{m_s} + Y \tag{9}$$

The GC/MS device is calibrated by determination of the device-dependent slope X and offset Y by measuring different integral ratios I_a/I_s. Typically for I_a/I_s = 1.0, 1.5, 2.0, 2.5 and 3.0. The mass of analyte can be calculated by using the calibration function:

$$m_a = \frac{m_s}{X}\left(\frac{I_a}{I_s} - Y\right) \tag{10}$$

Determination of the Volume V_{amb}

The Volume V_{amb} is determined by measuring the flow-rate of the gas using a soap film flow meter. The soap film flowmeter (Hewlett Packard No.: 0101-0113) is a modified volumetric pipette. The gas flow is passed through it and a soap film is pushed through the soap film flow meter. By measuring the time needed for passing the soap film through a fixed volume the gas flow-rate R_{flow} can be calculated:

$$R_{flow} = \frac{V_{pipette}}{t_{meas}} \tag{11}$$

As stated before the flow-rate measurement is carried out under ambient conditions at the ambient temperature T_{amb} so the volume at ambient conditions V_{amb} can be calculated using the flow-rate R_{flow}:

$$V_{amb} = R_{flow}\, t_{exp} \tag{12}$$

It should be stated that with this method only the volume of the carrier gas is measured as the analyte gets almost completely trapped in the condenser pipe at T_{CT}. The volume of the analyte can be neglected since it is small in comparison to that of the carrier gas as stated before.

p_{rest}-Correction

Especially for highly volatile analytes it has to be taken into account that the analyte will have a remaining vapor pressure inside the condenser pipe in the cooling trap at the cooling trap temperature T_{CT}. For the correction of this phenomenon the vapor pressure p_{rest} of the substance at T_{CT} has to be calculated and added to the vapor pressure:

$$p_{corr} = p_{sat} + p_{rest} \tag{13}$$

p_{rest} is calculated by fitting the p_{sat}- T_{exp} data to a fitting function with the fitting coefficients U and V:

$$lnp_{sat} = U + V/T_{exp} \tag{14}$$

This fitting function is extrapolated to the cooling trap temperature T_{CT} and p_{rest} can be calculated:

$$p_{rest} = p_{sat}(T_{CT}) = e^{(U+\frac{V}{T_{CT}})} \tag{15}$$

p_{corr} is obtained and can be reinserted in equation 13. The corrected vapor pressure is iteratively used to evaluate the value of p_{rest}. After five iteration cycles the final p_{rest} was not effected by further iterative evaluations. This means p_{rest} is evaluated by five iterative steps trough equation 13 – 15.

All further calculations are carried out with p_{rest}-corrected values. Since this correction is only necessary for transpiration experiments "p_{corr}" will be referred to as "p_{sat}" in the previous and following chapters by convention.

The Clausius Clapeyron Equation

The elucidations in this chapter were adapted from the comprehensive work of *Salzman*. [2]

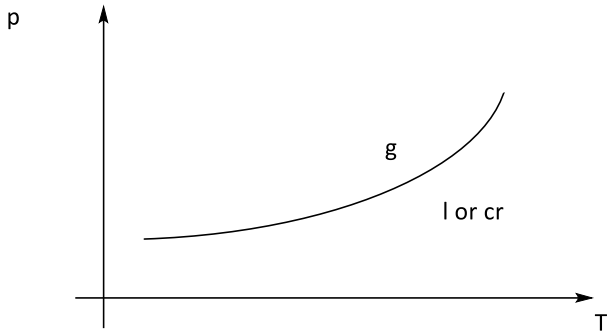

Figure 3 - Plot of Vapor Pressure against Temperature.

In the depicted phase diagram the vapor pressure p of a substance is plotted against its temperature T. This line of the vapor pressure is also called a phase boundary. Under these p-T-conditions the liquid (l) or crystalline (cr) phase is in equilibrium with the gaseous phase:

$$l/cr \rightleftharpoons g$$

For a liquid this process is called vaporization. For a solid this process is called sublimation. **By convention: If the following equations can be applied for either one of both processes this will be indicated by the label "l/cr".** Under equilibrium conditions it can be stated for vaporization and sublimation that:

$$\Delta^{g}_{l/cr}G = 0 \tag{16}$$

From the Gibbs-Helmholtz equation it can be derived that the change in Gibbs free energy is related to the change in Enthalpy and Entropy:

$$0 = \Delta^{g}_{l/cr}G = \Delta^{g}_{l/cr}H - T\Delta^{g}_{l/cr}S \tag{17}$$

$$\Delta^{g}_{l/cr}S = \frac{\Delta^{g}_{l/cr}H}{T} \tag{18}$$

The variables in equation 17 are defined by:

$$\Delta^{g}_{l/cr}G = G_g - G_{l/cr} \tag{19}$$

$$\Delta^{g}_{l/cr}S = S_g - S_{l/cr} \tag{20}$$

$$\Delta^{g}_{l/cr}H = H_g - H_{l/cr} \tag{21}$$

The change in volume which occurs during the phase transition is defined by:

$$\Delta^{g}_{l/cr}V = V_g - V_{l/cr} \tag{22}$$

The slope of the phase-boundary line $\left(\frac{\partial p_{sat}}{\partial T}\right)_{\Delta^{g}_{l/cr}G=0}$ can be derived using Euler's chain rule. $\Delta^{g}_{l/cr}G$ is assumed to be constantly zero.

$$\left(\frac{\partial p_{sat}}{\partial T}\right)_{\Delta^{g}_{l/cr}G} = -\frac{\left(\frac{\partial \Delta^{g}_{l/cr}G}{\partial T}\right)_{p_{sat}}}{\left(\frac{\partial \Delta^{g}_{l/cr}G}{\partial p}\right)_{T}} \tag{23}$$

With dG = -SdT + Vdp or d$\Delta^{g}_{l/cr}G$ = -$\Delta^{g}_{l/cr}S$ dT + $\Delta^{g}_{l/cr}V$ dp it can be stated that:

$$\left(\frac{\partial \Delta^{g}_{l/cr}G}{\partial T}\right)_{p_{sat}} = -\Delta^{g}_{l/cr}S \tag{24}$$

$$\left(\frac{\partial \Delta^{g}_{l/cr}G}{\partial p}\right)_{T} = \Delta^{g}_{l/cr}V \tag{25}$$

Using this the **Clapeyron Equation** can be established:

$$\left(\frac{\partial p_{sat}}{\partial T}\right)_{\Delta^{g}_{l/cr}G} = -\frac{\left(\frac{\partial \Delta^{g}_{l/cr}G}{\partial T}\right)_{p_{sat}}}{\left(\frac{\partial \Delta^{g}_{l/cr}G}{\partial p}\right)_{T}} = \frac{\Delta^{g}_{l/cr}S}{\Delta^{g}_{l/cr}V} \tag{26}$$

Using equation 18 the following relation can be derived:

$$\left(\frac{\partial p_{sat}}{\partial T}\right)_{\Delta^{g}_{l/cr}G} = \frac{\Delta^{g}_{l/cr}H}{T\Delta^{g}_{l/cr}V} \tag{27}$$

This equation is useful since the Enthalpy $\Delta^{g}_{l/cr}H$ varies more slowly with the temperature than the Entropy $\Delta^{g}_{l/cr}S$. Equation 27 can be integrated as follows:

$$dp_{sat} = \frac{\Delta^{g}_{l/cr}H}{T\Delta^{g}_{l/cr}V}\,dT \tag{28}$$

$$p_{sat_2} - p_{sat_1} = \frac{\Delta^{g}_{l/cr}H}{\Delta^{g}_{l/cr}V}\,ln\frac{T_2}{T_1} \tag{29}$$

For vaporization and sublimation it can be approximated that the change of volume $\Delta^{g}_{l/cr}V$ is the newly generated volume of the gas phase:

$$\Delta^{g}_{l/cr}V = V_g - V_{l/cr} \approx V_g \tag{30}$$

Using this and assuming ideal gas behavior ($V_g = nRT/p_{sat}$) for weakly associated or non-associated vapors the **Clausius-Clapeyron** equation can be established.

$$\left(\frac{\partial p_{sat}}{\partial T}\right)_{\Delta^{g}_{l/cr}G} = \frac{\Delta^{g}_{l/cr}H^{\circ}}{T\frac{n\mathrm{R}T}{p_{sat}}} = \frac{\Delta^{g}_{l/cr}H^{\circ}_{m}}{\mathrm{R}}\frac{p_{sat}}{T^2} \tag{31}$$

Equation 31 can be integrated as follows:

$$\frac{dp_{sat}}{dT} = \frac{\Delta^{g}_{l/cr}H^{\circ}_{m}}{R}\frac{p_{sat}}{T^2} \tag{32}$$

$$\ln\left(\frac{p_{sat\,2}}{p_{sat\,1}}\right) = \frac{\Delta^{\mathrm{g}}_{\mathrm{l/cr}}H^{\circ}_{m}}{R}\left(\frac{1}{T_2} - \frac{1}{T_1}\right) \tag{33}$$

$$\ln(p_{sat\,2}) = \frac{\Delta^{\mathrm{g}}_{\mathrm{l/cr}}H^{\circ}_{m}}{R}\left(\frac{1}{T_2} - \frac{1}{T_1}\right) + \ln(p_{sat\,1}) \tag{34}$$

Equation 34 shows that with a known point (p_{sat_1}, T_1) and a known enthalpy of vaporization $\Delta^{\mathrm{g}}_{\mathrm{l/cr}}H^{\circ}_{m}$ a pressure p_{sat_2} at T_2 can be calculated. This is valid for a limited range of temperature since $\Delta^{\mathrm{g}}_{\mathrm{l/cr}}H^{\circ}_{m}$ changes with the temperature.

The variables of equation 31 can also be separated in a different fashion:

$$\frac{dp_{sat}}{dT} = \frac{\Delta^{\mathrm{g}}_{\mathrm{l/cr}}H^{\circ}_{m}}{R}\frac{p_{sat}}{T^2} \tag{35}$$

$$\frac{dp_{sat}}{p_{sat}} = \frac{\Delta^{\mathrm{g}}_{\mathrm{l/cr}}H^{\circ}_{m}}{R}\frac{dT}{T^2} \tag{36}$$

$$d\ln(p_{sat}) = -\frac{\Delta^{\mathrm{g}}_{\mathrm{l/cr}}H^{\circ}_{m}}{R}d\left(\frac{1}{T}\right) \tag{37}$$

$$-\frac{Rd(ln(p_{sat}))}{d(1/T)} = \Delta^{\mathrm{g}}_{\mathrm{l/cr}}H^{\circ}_{m} \tag{38}$$

Equation 38 demonstrates the linear relationship of $ln(p_{sat})$ and $1/T$, which can be used for the elucidation of $\Delta^{\mathrm{g}}_{\mathrm{l/cr}}H^{\circ}_{m}$ from experimental p_{sat}- T-data.

Enthalpy of Vaporization $\Delta^{\mathrm{g}}_{\mathrm{l}}H^{\circ}_{m}$ & Enthalpy of Sublimation $\Delta^{\mathrm{g}}_{\mathrm{cr}}H^{\circ}_{m}$

Equation 38 shows that a linear relation between $ln(p)$ and reciprocal temperature $1/T$ exists. A plot of $ln(p)$ as ordinate and $1/T$ as abscissa shows a linear relationship. The slope $Z = d(ln(p_{sat}))/d(1/T)$ can be determined by linear regression analysis and allows a direct calculation of $\Delta^{\mathrm{g}}_{\mathrm{l/cr}}H^{\circ}_{m}$.

$$-RZ = \Delta^{\mathrm{g}}_{\mathrm{l/cr}}H^{\circ}_{m} \tag{39}$$

For the uncertainty of $\Delta^{\mathrm{g}}_{\mathrm{l/cr}}H^{\circ}_{m}$. at the average temperature of the measurement T_{avg} the standard deviation of the slope from the linear regression analysis is used.

Reference Temperature Extrapolation of $\Delta^{\mathrm{g}}_{\mathrm{l/cr}}H^{\circ}_{m}$ and $\Delta^{\mathrm{l}}_{\mathrm{cr}}H^{\circ}_{m}$ by *Chickos et al.*

The enthalpy of vaporization or sublimation $\Delta^{\mathrm{g}}_{\mathrm{l/cr}}H^{\circ}_{m}$ stated above is valid for the average temperature T_{avg} of the measurement. It must be extrapolated to a standard reference temperature $T_{ref} = 298.15\ \mathrm{K}$ for comparison with other sets of data. According to *Chickos et al.* [3] this can be done in the following fashion:

$$\Delta^{\mathrm{g}}_{\mathrm{l}}H^{\circ}_{m}\ (298.15\ \mathrm{K}) = \Delta^{\mathrm{g}}_{\mathrm{l}}H^{\circ}_{m}\left(T_{avg}\right) - (C^{\circ}_{p,m}(l) - C^{\circ}_{p,m}(g))(T_{ref}\text{-}T_{avg}) \tag{40}$$

$$\Delta^{\mathrm{g}}_{\mathrm{cr}}H^{\circ}_{m}\ (298.15\ \mathrm{K}) = \Delta^{\mathrm{g}}_{\mathrm{cr}}H^{\circ}_{m}\left(T_{avg}\right) - (C^{\circ}_{p,m}(cr) - C^{\circ}_{p,m}(g))(T_{ref}\text{-}T_{avg}) \tag{41}$$

With : $\Delta T = T_{avg} - T_{ref}$, $\Delta^{g}_{l}C^{\circ}_{p,m} = C^{\circ}_{p,m}(l) - C^{\circ}_{p,m}(g)$ and $\Delta^{g}_{cr}C^{\circ}_{p,m} = C^{\circ}_{p,m}(cr) - C^{\circ}_{p,m}(g)$ it can be written:

$$\Delta^{\mathrm{g}}_{\mathrm{l}}H^{\circ}_{m}\ \left(T_{ref}\right) = \Delta^{\mathrm{g}}_{\mathrm{l}}H^{\circ}_{m}\ \left(T_{avg}\right) - \Delta^{g}_{l}C^{\circ}_{p,m}\Delta T \tag{42}$$

$$\Delta^{\mathrm{g}}_{\mathrm{cr}}H^{\circ}_{m}\ (T_{ref}) = \Delta^{\mathrm{g}}_{\mathrm{cr}}H^{\circ}_{m}\ \left(T_{avg}\right) - \Delta^{g}_{cr}C^{\circ}_{p,m}\Delta T \tag{43}$$

Chickos et al. provide an empiric method [4] for the estimation of $\Delta_l^g C_{p,m}^\circ$ (R^2 = 0.886, 289 compounds) and $\Delta_{cr}^g C_{p,m}^\circ$ (R^2 = 0.668, 114 compounds), which is based on linear regression analysis of experimental and calculated heat capacity differences:

$$\Delta_{\mathrm{l}}^{\mathrm{g}} H_m^\circ\left(T_{ref}\right) = \Delta_{\mathrm{l}}^{\mathrm{g}} H_m^\circ\left(T_{avg}\right) - (10.58 + 0.26 C_{p,m}^\circ(l))\,\Delta T \quad (44)$$

$$\Delta_{\mathrm{cr}}^{\mathrm{g}} H_m^\circ\left(T_{ref}\right) = \Delta_{\mathrm{cr}}^{\mathrm{g}} H_m^\circ\left(T_{avg}\right) - (0.75 + 0.15 C_{p,m}^\circ(cr))\,\Delta T \quad (45)$$

For a large variety organic molecules $C_{p,m}^\circ(l)$ and $C_{p,m}^\circ(cr)$ can be estimated using the increments provided within the literature. Experimental values may be used as well.

Chickos et al. also provide a method to adjust enthalpies of fusion $\Delta_{\mathrm{cr}}^{\mathrm{l}} H_m^\circ$ to a reference temperature [5]:

$$\Delta_{\mathrm{cr}}^{\mathrm{l}} H_m^\circ\left(T_{ref}\right) = \Delta_{\mathrm{cr}}^{\mathrm{l}} H_m^\circ\left(T_{fus}\right) - (\Delta_{cr}^g C_{p,m}^\circ - \Delta_l^g C_{p,m}^\circ) \times \left(T_{fus} - T_{ref}\right) \quad (46)$$

The error of the adjusted enthalpy of fusion is calculated by:

$$u\left(\Delta_{\mathrm{cr}}^{\mathrm{l}} H_m^\circ\left(T_{ref}\right)\right) = \left(\Delta_{\mathrm{cr}}^{\mathrm{l}} H_m^\circ\left(T_{fus}\right) - \Delta_{\mathrm{cr}}^{\mathrm{l}} H_m^\circ\left(T_{ref}\right)\right) \times 0.3 \quad (47)$$

Fit-Function

The Clarke-Glew Equation [6] can be stated as follows:

$$\ln {}^{p_{\mathrm{sat}}}/_{p^{\mathrm{o}}} = \frac{\Delta_{\mathrm{l/c}}^{\mathrm{g}} S_{\mathrm{m}}^{\mathrm{o}}(T_0)}{R} - \frac{\Delta_{\mathrm{l/cr}}^{\mathrm{g}} H_{\mathrm{m}}^{\mathrm{o}}(T_0) - \Delta_{\mathrm{l/cr}}^{\mathrm{g}} C_{p,m}^\circ(l/cr) T_0}{RT} + \frac{\Delta_{\mathrm{l/cr}}^{\mathrm{g}} C_{p,m}^\circ(l/cr)}{R} ln \frac{T}{T_0} \quad (48)$$

For a more compact form the coefficients A and B can be introduced:

$$A = \frac{\Delta_{\mathrm{l/cr}}^{\mathrm{g}} S_{\mathrm{m}}^{\mathrm{o}}(T_0)}{R} \quad (49)$$

$$B = \frac{\Delta_{\mathrm{l/cr}}^{\mathrm{g}} H_{\mathrm{m}}^{\mathrm{o}}(T_0) - \Delta_{\mathrm{l/cr}}^{\mathrm{g}} C_{p,m}^\circ(T_0)}{R} \quad (50)$$

These coefficients can be inserted in the Clarke-Glew-Equation:

$$\ln {}^{p_{\mathrm{sat}}}/_{p^{\mathrm{o}}} = A - \frac{B}{T} + \frac{\Delta_{\mathrm{l/cr}}^{\mathrm{g}} C_{p,m}^\circ}{R} ln \frac{T}{T_0} \quad (51)$$

The Clarke-Glew equation can be modified to obtain the so-called Fit-Function:

$$\ln {}^{p_{\mathrm{sat}}}/_{p^{\mathrm{o}}} - \frac{\Delta_{\mathrm{l/cr}}^{\mathrm{g}} C_{p,m}^\circ}{R} ln \frac{T}{T_0} = A - \frac{B}{T} \quad (52)$$

For the least square Method fitting of equation 52 every experimental p-T datapoint with its temperature T is included. T_0 is a reference temperature that can be freely chosen.

Equation 52 is obviously a linear relationship of $\ln {}^{p_{\mathrm{sat}}}/_{p^{\mathrm{o}}} - \frac{\Delta_{\mathrm{l/cr}}^{\mathrm{g}} C_{p,m}^\circ}{R} ln \frac{T}{T_0}$ against the reciprocal temperature $1/T$. Hence the obtained data can be analysed via a linear regression method to obtain the coefficients A and B. According to NIST[7] the extended uncertainty of A and B can be calculated using the standard deviations from the linear regression analysis:

$$\Delta A = 2\sigma_A \quad (53)$$

$$\Delta B = 2\sigma_B \quad (54)$$

The Fit-Function can be used to calculate various other variables and their errors:

Molar Gibbs Helmholtz Enthalpy of vaporization/sublimation:

$$\Delta^{\mathrm{g}}_{\mathrm{l/cr}}G^{\mathrm{o}}_{\mathrm{m}}(T_0) = -RT\ln\frac{p_{\mathrm{sat}}}{p^{\mathrm{o}}} \tag{55}$$

$$\Delta\Delta^{\mathrm{g}}_{\mathrm{l/cr}}G^{\mathrm{o}}_{\mathrm{m}}(T_0) = -RT\ln\frac{p_{\mathrm{sat}} + |\Delta p_{\mathrm{sat}}|}{p^{\mathrm{o}}} \tag{56}$$

Molar Entropy of of vaporization/sublimation:

$$\Delta^{\mathrm{g}}_{\mathrm{l/cr}}S^{\mathrm{o}}_{\mathrm{m}}(T_0) = \mathrm{R}A \tag{57}$$

$$\Delta\Delta^{\mathrm{g}}_{\mathrm{l/cr}}S^{\mathrm{o}}_{\mathrm{m}}(T_0) = \mathrm{R}\Delta A = \mathrm{R}2\sigma_A \tag{58}$$

Molar Enthalpy of vaporization/sublimation:

$$\Delta^{\mathrm{g}}_{\mathrm{l/cr}}H^{\mathrm{o}}_{\mathrm{m}}(T_0) = \mathrm{R}B + \Delta^{\mathrm{g}}_{\mathrm{l/cr}}C^{\circ}_{p,m}T_0 \tag{59}$$

$$\Delta\Delta^{\mathrm{g}}_{\mathrm{l/cr}}H^{\mathrm{o}}_{\mathrm{m}}(T_0) = \sqrt{R(2\sigma_B)^2 + 2(\Delta\Delta^{\mathrm{g}}_{\mathrm{l/cr}}C^{\circ}_{p,m}T_0)^2} \tag{60}$$

The Heat Capacity Error $\Delta\Delta^{\mathrm{g}}_{\mathrm{l/cr}}C^{\circ}_{p,m}$ is normally set to zero and only used in rare cases when experimental heat capacities are used. If empirical increments from *Chickos et al.* [4] are used for extrapolation to standard conditions this term is neglected.

Vapor Pressure:

The vapor pressure at a temperature T can be calculated from a complete p-T-dataset by the following formula:

$$p_{\mathrm{sat}}(T) = e^{p^{\mathrm{o}}(A-\frac{B}{T}+\frac{\Delta^{\mathrm{g}}_{\mathrm{l/cr}}C^{\circ}_{p,m}}{R}ln\frac{T}{T_0})} \tag{61}$$

6.3 Critical Discussion of Pressure-Correction for V_{amb}

In the literature [8] it is stated that the gas volume determined with the Soap Film Flow Meter must be corrected to standard conditions according to the formula:

$$V_{corr} = V_{meas} \frac{p_{amb}}{p_{std}} \frac{T_{std}}{T_{amb}} \tag{62}$$

For the Transpiration experiment this correction is not necessary since the volume needs to be measured under ambient – not standardized – conditions, which are linked directly to the experimental conditions in the saturator (cf. section 6.2).

$$p_{sat}(T_{exp}) = \frac{m_a \mathrm{R} T_{amb}}{\mathrm{M} V_{amb}} \tag{63}$$

Further pressure dependence of the measurement method can be excluded by the following consideration:

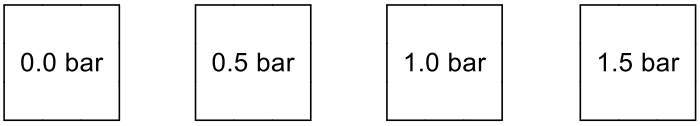

Four discrete identic volumes representing the saturator in different pressure states are in contact with the liquid/crystalline analyte at one temperature. The total carrier gas transport of the transpiration experiment can be regarded as a discrete series of volumes. The boxes are filled with an inert carrier gas at different pressures. For this isothermic thought experiment at constant volume the Helmholtz Energy should be used as State function. After reaching the saturation equilibrium the Helmholtz Energy of the liquid/crystalline and gaseous phase will be identical.

$$\Delta^{\mathrm{g}}_{\mathrm{l/cr}} F = F_g - F_{l/cr} = \Delta^{\mathrm{g}}_{\mathrm{l/cr}} F^{\circ} + RT \ln\left(\frac{n}{V}\right) = \Delta^{\mathrm{g}}_{\mathrm{l/cr}} F^{\circ} + RTln(c) = 0 \tag{64}$$

This relation shows that the concentration of analyte molecules in the gaseous phase at equilibrium conditions will be identical without dependence on the pressure, but on the temperature.

A pressure dependence can be found only for Gibbs Energy:

$$\left(\frac{d\Delta^{\mathrm{g}}_{\mathrm{l/cr}} G_m}{dp}\right)_T = V \tag{65}$$

$$\Delta^{\mathrm{g}}_{\mathrm{l/cr}} G_m = V \Delta p \tag{66}$$

$$\Delta^{\mathrm{g}}_{\mathrm{l/cr}} G_m = -RT \ln\left(\frac{p_{\mathrm{sat}}}{p^{\mathrm{o}}}\right) \tag{67}$$

For the condensed phase the molar volume V_{m} is at the level of 10^{-4} $\mathrm{m^3 \cdot mol^{-1}}$. If a pressure change Δp of 100000 Pa (from 0 to 1 bar) is assumed:

$$\Delta G = 10^{-4}\ \mathrm{m^3\ mol^{-1}} * 100000\ \mathrm{N\ m^{-2}} = 10\ \mathrm{Nm\ mol^{-1}} = 10\ \mathrm{J\ mol^{-1}}$$

How high will be effect of purge gas pressure change on vapor pressure/ vapor concentration?

$$\Delta\Delta^{\mathrm{g}}_{\mathrm{l/cr}} G_m = -RT \ln\left(\frac{p_{\mathrm{sat2}}}{p_{\mathrm{sat1}}}\right) = 10 \frac{J}{mol}$$

$$\ln\left(\frac{p_{\mathrm{sat2}}}{p_{\mathrm{sat1}}}\right) = -\frac{10}{8.314462 \cdot 300} = -0.004$$

$$\frac{p_{\mathrm{sat2}}}{p_{\mathrm{sat1}}} = \exp(-0.004) = 0.996$$

That corresponds to a pressure difference of 0.4% in vapor pressure of gas concentration for a pressure change of 1 bar from absolute vacuum to atmospheric pressure. This effect is significantly lower than the uncertainty of determination of the transpiration experiment. If the deviation of the ambient pressure from the standard state is at the level of 10-20% the effect will be at the level of 0.1% and lower and can be neglected.

6.4 Uncertainty Estimations for the Transpiration Method Experiment

6.4.1 Uncertainty of the Vapor Pressure p_{sat}

The uncertainty of the transpiration experiment for the setup used in this work has been estimated by *Verevkin et al.* [9-10] In this chapter their elucidations are adapted to the exact equipment and modifications used in this work.

For the determination of the mass m_a of the analyte which was trapped inside the condenser pipe GC/MS was used in combination with an external standard calibration method. For this purpose two reference solutions of analyte and standard were prepared separately by weighing 0.08 g of analyte and standard into a 100 mL calibrated pycnometer. The samples were weighed with a Mettler Toledo XA204 DR scale equipped with an anti-electrostatic kit and a resolution of ±0.0001 g. The pycnometers were filled with solvent to 100.0 mL with an accuracy of ±0.1 mL. The calibration samples were prepared with gas-tight Hamilton syringues (1700 series, 22s gauge, 2 inch, point style 2, 100 or 250 µL volume). The calibration samples were analyzed via GC/MS with a reproducibility of the integral ratios below 1 %. For the quantification of the analyte mass m_a a defined amount of standard was added to the condenser pipe using the syringues identical to those of the GC calibration. A volume of at least 30 µL standard solution (prepared in the same fashion as the calibration solutions) was injected from the 100 µL calibration syringue. The maximum volume of standard solution added were 500 µL from a 500 µL syringue. The manual syringue volume addition reproducibility and precision relies on the operator and is estimated to be 10% of the grading of the syringue (1% grading steps of the total volume).

The volume flow rate R_{flow} of the carrier gas was kept constant using Natec Sensors MC-100 CCM Massflow controllers with an accuracy of 1%. The flow-rate R_{flow} was measured with a soap film flow-meter (HP Nr.: 0101-0113) with an estimated accuracy of 1%. The flow-rate R_{flow} was measured with the temperature T_{amb} once for measurements below one hour. For longer measurements the determination was carried out at the beginning and at the end of the experiment and the values of R_{flow} and T_{amb} averaged. V_{amb} was calculated from flow-rate and time measurements. The experimental standard deviation of the total carrier gas volume under constant conditions is <1%. The ambient temperature T_{amb} was measured with a Greisinger GFTB200 equipped with a PT-1000 temperarature sensor with a resolution of 0.1 K. For the uncertainty estimation an ambient temperature of 298 K was chosen.

The saturator temperature T_{exp} is kept constant within ±0.1 K using a Huber Ministat 230 circulation thermostat equipped with a PT-100 temperature sensor (class A, four wire connection, ΔT_{exp} = ±0.2 K according to DIN EN 60751) with a resolution of 0.01 K. For the temperature uncertainty estimation a measurement temperature of 298 K was chosen.

With these Parameters in hands the following uncertainties can be calculated:

Uncertainty of reference and standard sample mass:

u(P)/P = ((0.0001 g/0.0800 g)^2 + (0.0001 g/0.0800g)^2)$^{1/2}$ = **0.177 %**

Uncertainty of the calibrated pycnometer volume:

u(P)/P = ((0.01 mL/100 mL)^2 + (0.01 mL/100 mL)^2)$^{1/2}$ = **0.014 %**

Uncertainty of standard addition volume:

u(P)/P = ((0.1 µL/30 µL)^2 + (0.01 mL/100 mL)^2)$^{1/2}$ = **0.33 %** for 30 µL in a 100 µL syringe. This conservative value is used for the further calculations.

(u(P)/P = ((0.25 µL/250 µL)^2 + (0.01 mL/100 mL)^2)$^{1/2}$ = **0.10** % for 250 µL in a 250 µL syringe

(u(P)/P = ((0.50 µL/500 µL)^2 + (0.01 mL/100 mL)^2)$^{1/2}$ = **0.10** % for 500 µL in a 500 µL syringe

The uncertainty of the GC/MS external standard quantification (calibration + determination):

u(P)/P = (0.01^2 + 0.01^2)$^{1/2}$ = **1.41 %**

Uncertainty of Stability of Carrier Gas Flow: u(P)/P = **1.00 %** (Mass Flow Controller specification)

Uncertainty of Soap Film Flowmeter Measurements: u(P)/P = **1.00 %**

Uncertainty of the temperature measurements: u(P)/P = ((0.2/298 K)^2 + (0.2/298 K)^2)$^{1/2}$ = **0.09 %**

Combined Uncertainties: u(P)/P = (u_1^2+u_2^2+…)$^{0.5}$ = **2.04 %**

For each individual data point a pressure uncertainty is calculated by the following formulae [9]:

$$u(p_{sat}/\text{Pa}) = 0.025 + 0.025(p_{sat}/\text{Pa}) \text{ for p >5 to 3000 Pa} \quad (68)$$

$$u(p_{sat}/\text{Pa}) = 0.005 + 0.025(p_{sat}/\text{Pa}) \text{ for p <5 Pa} \quad (69)$$

6.4.2 Uncertainty of Phase Transition Enthalpy $\Delta^{g}_{l/cr}H^{\circ}_{m}$ at T_{avg}

The uncertainty of the phase transition enthalpy $\Delta^{g}_{l/cr}H_m$ depends on the uncertainty of the vapor pressures, which has been assessed to a level of 2% in chapter 6.4.1. For the following elucidations the reference measurement of Anthracene (cf. chapter 7.1.2) was chosen. The vapor pressure measurement of Anthracene was carried out in the temperature regime of 323.2 to 372.8 K with an average measurement temperature of 348.0 K. The measurement temperature range is in this case 49.6 K. The Clausius-Clapeyron Equation 31 allows the estimation of the uncertainty of the phase transition enthalpy:

$$\Delta^{g}_{l/cr}H^{\circ}_{m} = (d\ ln\ p_{sat}/dT)RT^2 \quad (70)$$

$$\Delta\Delta^{g}_{l/cr}H^{\circ}_{m} = \Delta(d\ lnp_{sat}/\Delta T)RT^2 \quad (71)$$

$\Delta\Delta^{g}_{cr}H_m$=(0.02/49.6 K) × 8.314462 J mol^{-1} × (348.0 K)^2 = 406 J mol^{-1}

For the enthalpy of sublimation of Anthracene of 99.90 kJ/mol it can be approximated that the procentual error is:

$$u_1(\Delta^{g}_{cr}H^{\circ}_{m}) = 0.406 \text{ kJ mol}^{-1} / 99.90 \text{ kJ mol}^{-1} = 0.41\ \%$$

Additionally the uncertainty of the temperature measurement of the experimental temperature $\boldsymbol{T_{exp}}$ has to be taken into account.

The used class A PT100 temperature sensors are in accordance with DIN EN 60751 with a temperature uncertainty ΔT = ±0.2 K.

$$\Delta\Delta^{g}_{l/cr}H^{\circ}_{m} = (d\ lnp_{sat}/\Delta T)RT(2\Delta T) \quad (72)$$

$$\Delta\Delta^{\mathrm{g}}_{\mathrm{l/cr}}H^{\circ}_{m}/\Delta^{\mathrm{g}}_{\mathrm{l/cr}}H^{\circ}_{m} = 2\Delta T/T \quad (73)$$

$\underline{u_2(\Delta^{\mathrm{g}}_{\mathrm{cr}}H^{\circ}_{m})}$= (2 × 0.2K) / 348.0 K = 0.11 %

The linear regression analysis the experimental p_{sat}-T_{exp}-data by equation 52 is used for the calculation of the molar enthalpy of sublimation.

The obtained uncertainty $\Delta\Delta^{\mathrm{g}}_{\mathrm{cr}}H^{\circ}_{m}(T_{\mathrm{avg}})$ of Anthracene is 0.4 kJ/mol. The sublimation enthalpy $\Delta^{\mathrm{g}}_{\mathrm{l/cr}}H_{\mathrm{m}}$ is 99.9 kJ/mol. So it can be demonstrated for Anthracene that:

$\underline{u_3(\Delta^{\mathrm{g}}_{\mathrm{cr}}H^{\circ}_{m})}$= 0.4 kJ mol^{-1} / 99.9 kJ mol^{-1} = 0.40 %

The uncertainties of the enthalpy of vaporization can be summed up:

$u(\Delta^{\mathrm{g}}_{\mathrm{cr}}H^{\circ}_{m}) = (u_1^2+u_2^2+u_3^2)^{0.5} = (u_1^2+u_2^2+u_3^2)^{0.5} = ((0.41\%)^2+(0.11\%)^2+(0.40\%)^2)^{0.5}$ = **$\underline{0.58\ \%}$**

6.4.3 Uncertainty of Phase Transition Enthalpy $\Delta^{\mathbf{g}}_{l/cr}H^{\circ}_{m}$ at T_{ref} = 298.15 K

Phase transition enthalpies $\Delta^{\mathrm{g}}_{\mathrm{l/cr}}H^{\circ}_{m}$ are measured at the average temperature of the experiment T_{avg}. For comparison of different experiments measured in different temperature intervals the vaporization enthalpy must be adjusted to a reference temperature, which is set to the standard temperature 298.15 K by convention. For the details of the adjustment method refer to chapter 6.2. The uncertainty of the phase change enthalpy at the average temperature of the experiment $\Delta\Delta^{\mathrm{g}}_{\mathrm{l/cr}}H_{m}(T_{avg})$ is not valid at T_{ref} since the extrapolation process is an additional source of uncertainty, that needs to be integrated in the error estimation to extrapolate $u(\Delta^{\mathrm{g}}_{\mathrm{l/cr}}H^{\circ}_{m})$ from T_{avg} to T_{ref}.

The temperature adjustment (cf. section 6.2) relies on the heat capacity $C^{o}_{p,m}$(l) or $C^{o}_{p,m}$(cr) and the length of the extrapolation path: $\Delta T = T_{avg} - T_{ref}$:

$$\Delta^{\mathrm{g}}_{l}H^{\circ}_{m}\left(T_{ref}\right) = \Delta^{\mathrm{g}}_{l}H^{\circ}_{m}\left(T_{avg}\right) - \Delta^{g}_{l}C^{o}_{p,m}\Delta T$$

$$\Delta^{\mathrm{g}}_{\mathrm{cr}}H^{\circ}_{m}\left(T_{ref}\right) = \Delta^{\mathrm{g}}_{\mathrm{cr}}H^{\circ}_{m}\left(T_{avg}\right) - \Delta^{g}_{cr}C^{o}_{p,m}\Delta T$$

The extrapolation uncertainty u_4 is the product of the uncertainty of heat capacity $C^{o}_{p,m}$ and ΔT. The error of the experimental heat capacity of organic solids is in the range of ±30 J mol^{-1} K^{-1}. The error for organic liquids is in the range of ±16 J mol^{-1} K^{-1}. [11]

$$u\left(C^{o}_{p,m}(\mathrm{cr})\right) = \frac{30\ \mathrm{J}\ mol^{-1}K^{-1}}{C^{o}_{p,m}(\mathrm{cr})} \quad (74)$$

$$u(C^{o}_{p,m}(\mathrm{l})) = \frac{16\ \mathrm{J}\ mol^{-1}K^{-1}}{C^{o}_{p,m}(\mathrm{l})} \quad (75)$$

$$u_4(\Delta^{\mathrm{g}}_{\mathrm{cr}}H^{\circ}_{m}) = \Delta(\Delta^{g}_{l/cr}C^{o}_{p,m}\Delta T) \quad (76)$$

For Anthracene with $C^{o}_{p,m}$(cr) = 211.7 J mol^{-1} K^{-1}, $\Delta^{g}_{cr}C^{o}_{p,m}$ = 32.5 J mol^{-1} K^{-1} and ΔT = 49.9 K it can be calculated:

$\Delta^{g}_{cr}C^{o}_{p,m}\Delta T$ = 32.5 J mol^{-1} K^{-1} × 49.9 K = 1621.8 J mol^{-1} = 1.622 kJ mol^{-1}

$u\left(C^{o}_{p,m}(\mathrm{cr})\right)$ = 30 J mol^{-1} K^{-1} / 211.7 J mol^{-1} K^{-1} = 14.17 %

$u_4(\Delta^{\mathrm{g}}_{\mathrm{cr}}H^{\circ}_{m}) = u\left(C^{o}_{p,m}(\mathrm{cr})\right) \times \Delta^{g}_{cr}C^{o}_{p,m}\Delta T$= 0.230 kJ mol^{-1}

u_4(P)/P= 0.230 kJ mol^{-1} / 99.9 kJ/mol = 0.23 %

$$u(\Delta^{g}_{l/cr}H_m) = (u_1^2+u_2^2+ u_3^2+u_4^2)^{0.5} = ((0.41\%)^2+(0.11\%)^2+ (0.40\%)^2+(0.23\ \%)^2)^{0.5} = \underline{\mathbf{0.63\ \%}}$$

In this case the the adjustment to T_{ref} adds 0.05 % of uncertainty in comparison to the 0.58 % uncertainty at the average temperature of the measurement.

6.5 Practical Advices for the Transpiration Method Experiment

6.5.1 Calibration of the Gas Chromatograph

For the quantification of the analyte the GC/MS device needs to be calibrated. An internal standard calibration method is chosen since its precision relies on the amount of added standard. Once the standard and analyte are combined the resulting solution can be diluted with lower precision.

The initial step is the preparation of analyte and standard solutions. First a solvent needs to be chosen. The solvent must be inert towards the analyte considering the harsh temperature conditions inside the GC injector. For the GC-Analysis itself the boiling point of the solvent should be low to ensure sufficient separation of solvent and analytes. The second criterion for solvent choice is the capability to dissolve analyte and standard completely in the concentration range needed throughout the experiment. For the repertoire of standards the linear alkane molecules dodecane C-12, tetradecane C-14 and hexadecane C-16 were chosen. The solvents acetone and tert-butyl methyl ether (TBME) proved to be excellent solvents for the chosen standards and the analytes investigated.

The statement that in general only deuterated derivatives of the analytes are suitable standards for internal standard quantifications is an erroneous misbelief. This statement is valid for analyses with complex sample preparation and enrichment procedures. In this case the behaviour of analyte and standard should be similar or identical. In case of the transpiration experiment the sample preparation is carried out by addition of the dissolved standard to the matrix-free sample and further dilution with solvent. The only criterion, which must be fulfilled is the complete dissolvation of analyte and standard. Alkane standards have further advantages, since they are available in high purity for a low price, chemically inert and their GC retention time can be chosen by varying their chain length to avoid co-elution with analytes. The different behaviour of analyte and standard during the GC-analysis is compensated by the device calibration.

With solvent and standard chosen reference solutions of both must be prepared. Weighing is carried out with a Mettler Toledo XA204 DR scale (0.0001 g resolution) in combination with an anti-electrostatic kit. For liquid samples a 100 mL volumetric flask with an accuracy of ±0.1 mL is placed directly onto the scale, the scale tared and the substance directly transferred into the flask. For volatile liquids the flask was closed for weighing the substance. For solid substances it proved to be more accurate to place folded weighing paper into the scale and to transfer the weighed substance with the weighing paper and long tweezers into the volumetric flask. In any case the weight displayed by the scale must be constant (± 0.1 mg) for 1 minute. In case of weight drifting the error source must be found and the weighing process repeated.

After weighing the substance the volumetric flasks are filled with solvent until the lower meniscus is superimposing with the calibration mark. Analyte solutions are preferably stored in a fridge, but should be warmed to room temperature for calibration use regarding the temperature-dependency of the density of the solvent.

For the calibration sample preparation gas-tight Hamilton syringues (22s gauge, 2 inch, point style 2, 100 or 250 µL volume) are used. Initially three samples with random volume combinations are used to gather information on the response factors of analyte and standard. The samples are diluted with about 1 mL of solvent. Each sample is analyzed three times and the average analyte / standard signal integral ratios I_a/I_s are used for linear regression analysis.

Sample	A	B	C
$V_{analyte}$ [µL]	50	70	50
$V_{standard}$ [µL]	200	100	100
I_a/I_s	0.27	0.74	0.53

With this information a preliminary calibration curve is established, which is used for the calculation of analyte/standard volumes that are in linearity with the preliminary calibration curve for the calibration points (I_a/I_s) 1.0, 1.5, 2, 2.5 and 3.0.

Sample	A	B	C	1	2	3	4	5
$V_{analyte}$ [µL]	50	70	50	90	100	100	100	100
$V_{standard}$ [µL]	200	100	100	94	69	52	41	34
I_a/I_s	0.27	0.74	0.53	1.00	1.49	1.99	2.50	3.06

The calibration points are chosen in the integral ratio range of 1.0 to 3.0. Integral ratios lower than 1 should be avoided regarding the device-dependent offset (0.00493) of the calibration curve. Integrals above 3.0 should be avoided due to the peak-tailing of large peaks.

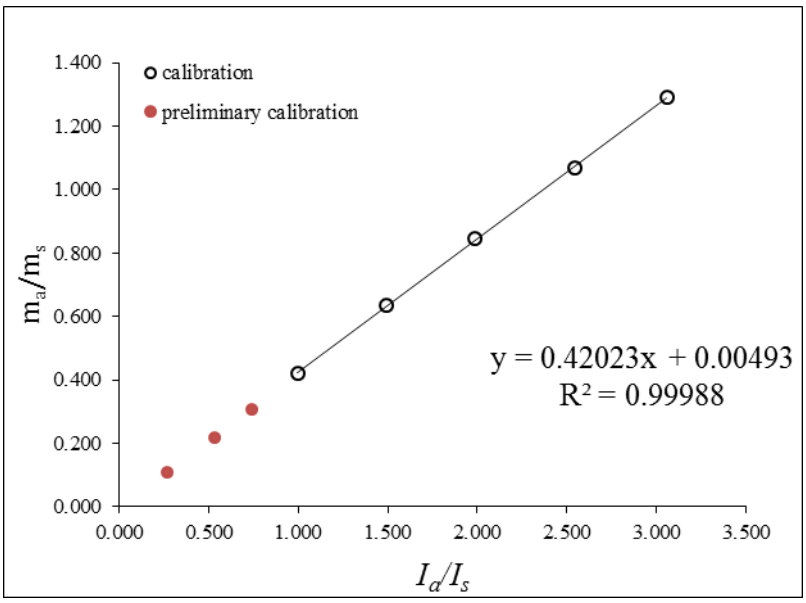

The calibration curve obtained shows a linear relationship between the mass- and integral-ratio of analyte and standard. Each calibration sample is measured three times and the mean values are used for the calibration curve. The standard deviation of the integral ratio I_a/I_s should be below 1 % of the mean value of I_a/I_s.

The second criterion for a successful quantification is to find a working range without concentration dependency effects. For this a high-concentrated sample with the integral ratio $I_a/I_s \approx 2.00$ is diluted repeatedly:

dilution step	0	1	2	3	4	5
I_a [counts]	4027016	2015182	1005780	503545	253283	125619
$\sigma(I_a)$ [counts]	8416	974	2733	3610	2487	292
I_s [counts]	2028268	1001656	499107	251083	126487	63833
$\sigma(I_s)$ [counts]	2819	2820	633	1856	1896	702
I_a/I_s	**1.99**	**2.01**	**2.02**	**2.01**	**2.00**	**1.97**
$\sigma(I_a/I_s)$	0.00	0.00	0.01	0.02	0.01	0.03

The integral ratio I_a/I_s may vary within a ±1% tolerance interval (1.98 to 2.02). In the case presented the analyte integral I_a may vary from ≈4000000 to ≈250000 counts. Below 250000 counts concentration dependent effects arise and the precision of the analysis decreases since $\sigma(I_a/I_s)$ increases.

The duration of a transpiration experiment varies usually from 1 to 14 days depending on the volatility of the analyte. The calibration should be validated at least daily (preferably after each quantification) by the injection and analysis of a reference calibration sample. The integral ratio I_a/I_s of the reference sample may vary within a ± 1% tolerance interval. The best solution is to store all transpiration samples in a fridge and to run the quantification of all samples after a new calibration of the device to avoid time-dependent calibration drifts.

6.5.2 Filling of the Saturator

The U-shaped pipe in the saturator is filled with 40 g of glass beads (1-1.25 mm diameter, Edmund Bühler GmbH #0001067) onto which the substance has to be coated to generate a sufficient analyte surface in contact with the carrier gas stream. The amount of analyte substance used for the coating should range from 500 mg to 1000 mg. The volume of 40 g glass beads is about 25 mL. Taking into account the packing density (≈74%) and the average volume of a glass bead (0.75 mm^3) it can be estimated that 25000 glass beads are filled into the device, which generates a surface of ≈1000 cm^2.

For the optimal use of the bead surface they need to be coated homogeneously. Especially in case of sensitive explosive samples each method presented in the following should be tested with a small batch prior to the full scale coating. The beaker involved should be manipulated with a support clamp.

For liquids and sticky solids the coating can be carried out easily by mixing the beads with the substance and filling the mixture into the saturator device.

For solids that can be molten without decomposition it is preferable to heat the substance and beads in a glass beaker over a heat gun which is set to a temperature above the melting point of the substance. Under continuous stirring the beads are coated with the melt. The melt-coated beads can be transferred into the preheated (5 °C above melting point) saturator. Alternatively the heated mixture can be cooled down under stirring if the substance solidifies homogeneously on the beads. If thermal decomposition needs to be excluded the residues of the mixture in the beaker can be used for qualitative analysis (e.g. ^{1}H-NMR).

For thermolabile solids the coating of the beads can be carried out by mixing beads and substance with a small amount of a volatile solvent (diethyl ether, dichloromethane, acetone,…). The volume of the solvent should be minimized avoiding the appearance of a liquid level in the mixture. The solvent-analyte-bead suspension can be filled directly in the saturator. This procedure can be used for impact/friction sensitive compounds which are preferably operated in a wet state. Alternatively the suspension can be dried with a rotary evaporator, which can also result in a homogeneous coating of the beads that can be filled into the saturator. In any case the sample needs to be conditioned with the carrier gas stream inside the saturator to eliminate any traces of solvent.

If every procedure detailed above fails the beads and analyte may be added in a layered fashion directly into the device.

6.5.3 Measuring a Datapoint with the Transpiration Method Experiment

The Transpiration Experiment is an indirect measurement of the vapor pressure of medium to low volatility analytes. A carrier gas stream is saturated with the analyte of interest at a constant temperature T_{exp} and flow-rate R_{flow} for a defined interval of time t_{exp}. The analyte is collected in a condenser trap and its mass m is quantified by a suitable analytical method. Within the framework of this thesis GC/MS in combination with an internal standard calibration was used. The vapor pressure p_{sat} of the analyte can be calculated approximatily by using the ideal gas law:

$$p_{sat}(T_{exp}) = \frac{m_a \mathrm{R} T_{amb}}{M t_{exp} R_{flow}}$$

For the derivation and further information on the exact mathematical processing of the data refer to chapter 6.2.The range of the experimental temperature T_{exp} should be at least 40 °C generating at least 9 equally distributed points of data. With the quantification device calibrated and the saturator filled the experiment can start. Several parameters can be used to optimize the total duration and accuracy of the experiment:

- **Mass m_a:** the mass of analyte transported should range ideally between 1 and 3 mg. For high volatility compounds a maximum of 8 mg is tolerable. For low volatility compounds the mass of analyte can be reduced to 0.3 mg and less. The mass of analyte is directly proportional to the amount of internal standard added since an integral ratio I_a/I_s of 2.00 should be targeted. Differently concentrated standard solutions may be used within one experiment to optimize the experiment for low and high volatility (temperature) regimes.
- **Temperature T_{exp}:** The experimental temperature range is often dictated by the thermal properties of the analyte. Those may include melting or decomposition points and other phase transitions, which should be investigated prior to the experiment via DSC/DTA measurements or literature research. Each phase transition point should be avoided within a ± 5 °C interval. Measurements near standard conditions should be preferred over high temperature measurements. Decomposition points of thermolabile compounds should be avoided as slow long-term decomposition might already occur at lower temperatures. The lower temperature limit is 1 ○C due to ice crust formation on the saturator at lower temperatures.
- **Rate of Flow R_{flow}:** The flow-rate may be varied in the interval of 1 to 5 L/h. Flow-rates lower than 1 L/h should be avoided since the results will be falsified due to thermal diffusion of the analyte into the condenser trap. High flow-rates should be avoided since reaching the saturation equilibrium of the carrier gas stream with analyte is harder at high flow-rates. This problem arises especially at low temperatures.
- **Time t:** The experimental time for one datapoint should be at least 15 minutes. The upper limit is dictated by the fluctuations of the flowrate and ambient parameters. Datapoints with experimental times above 24 hours should be avoided.

Lowering the mass m_a or the experimental time t_{exp} and increasing the Temperature T_{exp} or the flowrate R_{flow} will accelerate the experiment but might decrease its accuracy or even falsify the results. It is the task of the experimentator to find a reasonable compromise for each analyte.

For the initial data points all parameters stated above have to be guessed and optimized until two datapoints with a reasonable integral ratio I_a/I_s have been obtained. For the third and all other datapoints the linear relationship of $\ln p_{sat}$ and $1/T_{exp}$ in the Clausius-Clapeyron plot (cf. section 6.2) may be used to predict experimental conditions that will be in further linearity with the existing datapoints. In case of existing literature data this process may be accelerated drastically by the prediction of data points that are in (linear) agreement with the literature data.

In any case the analyte needs to be conditioned prior to the measurement, which includes the removal of moisture, solvent traces and impurities by passing carrier gas through the saturator at a suitable temperature. The presence of impurities can be easily checked with qualitative GC/MS chromatography in the scan-mode. A further check is the repeated measurement under identical experimental conditions. Conditioning must be continued until constant results within the accuracy of the experiment are obtained.

In case of a low level of trace impurities the initial preliminary datapoints might be enough for the conditioning of the substance. In other cases conditioning must be carried out over a longer period of time at elevated temperatures. It is always preferable to have some preliminary datapoints that enable the estimation of the mass loss during the conditioning phase.

With the sample conditioned the true experiment can be started. For each datapoint the following procedure should be performed:

1) The temperature is set to the desired value of T_{exp}. The saturator is closed with ground stoppers.
2) After stabilization of the temperature the saturator is opened and the carrier gas source is attached followed by an equilibrium stabilization interval of at least 30 s.
3) The condenser pipe is attached to the saturator and simultaneously the time measurement is started.
4) The soap film flowmeter is attached to the condenser pipe and the flow rate R_{flow} measurement is carried out two times. During the flow rate measurement the experimental temperature T_{exp}, the ambient temperature T_{amb} and the ambient pressure p_{amb} are measured. For measurements above one hour the measurement of R_{flow}, T_{exp}, p_{amb} and T_{amb} is repeated prior to the end of the vapor pressure measurement. The results are averaged for the further mathematical processing. The condenser piper stays attached to the saturator for t_{exp}.
5) The condenser pipe is detached from the saturator and simultaneously the time measurement is stopped.
6) The condenser pipe is immediately closed with a ground stopper and a plastic cap. The circulator thermostat is set to the next experimental temperature T_{exp} and the saturator is closed with ground stoppers.
7) The plastic cap is removed and a defined volume of standard is added with a calibration syringue. An additional volume of solvent is added and the condenser pipe rinsed thoroughly until the analyte has completely dissolved its concentration is distributed homogeneously.
8) The obtained solution may be further diluted or transferred directly to the quantification system.
9) Quantification analysis is performed 3 times for each sample and the result is averaged. The sample is stored in a fridge.

As stated above (cf. section 6.5.1) the analyte concentration must be within the working concentration range established within the calibration of the quantification instrument. If the sample is too concentrated it can be diluted easily. For the calibration example stated above (cf. section 6.5.1) the working range is 4.000.000 to 250.000 counts referring to the analyte integral I_a. In this case a reasonable target concentration results in an analyte integral I_a of 2.000.000 counts in the mid working range.

The calibration sample 3 (cf. section 6.5.1) (I_a/I_s = 1.99) contained 100 µL of analyte solution (c = 0.477 mg/mL) and 52 µL of standard solution (c = 1.087 mg/mL). The calibration sample was further diluted with 1 mL of solvent. The mass of analyte in the sample is 0.0477 mg (0.100 mL*0.477 mg/mL) which

has been dissolved in a total volume of 1.152 mL ((1.000 + 0.100 +0.052)mL) of solvent. This results in a concentration of 41.4 µg/mL (47.7 µg/ 1.152 mL).

Calibration sample 3 had an integral of ≈4.000.000 counts. For the ideal mid working-range concentration it should be diluted to 50% which results in an ideal sample concentration of 20.7 µg/mL.

For the transpiration experiment 1 mg of analyte was transported for each data point. It can be easily calculated how much standard is needed for an integral ratio I_a/I_s of 2.00. The calibration sample contained 0.0477 mg of analyte and 0.0565 mg of standard. This results in a mass ratio m_a/m_s of 0.844. This means that for 1.000 mg of analyte 1.184 mg of standard are necessary.

As a consequence a measurement standard with the concentration 11.84 mg/mL is generated and 100 µL of it are added to the condenser pipe containing 1 mg of analyte. The sample is further diluted with 3.9 mL of solvent resulting in an analyte concentration of 250 µg/mL. This solution needs to be further diluted by a factor of 12 to reach a concentration of 20.8 µg/mL which is reasonably near the ideal concentration. This is carried out by diluting 0.1 mL of condenser pipe solution with 1.1 mL of solvent.

This example can be used as an orientation for any transpiration experiment. Of course the mass of analyte can be reduced according to the sensitivity of the quantification instrument in agreement with the boundary conditions (T_{exp}, R_{flow}, t) of the transpiration experiment. The sensitivity of a GC/MS device can be adjusted by manipulating the injection volume and the split ratio of the injector. However these GC-parameters should be kept constant for the complete calibration and quantification of all transpiration samples.

6.6 Validation of the Experimental Results

For a statistical correct evaluation of the experiment it would be necessary to measure each datapoint at least three, better five or more times to generate data points with reliable error bars. As the transpiration experiment is time-consuming for low-volatility analytes this would result in enormous measurement times. With respect to this the standard deviations of the measurement values are calculated from linear regression analysis of the p_{sat}-T_{exp}-data obtained.

For the additional direct validation of the accuracy of the experiment the lowest, mid and highest experimental point should be measured three times under the same experimental conditions, which allows an insight in the experimental accuracy.

Furthermore it must be proven that the saturation criterion has been fulfilled for the lowest temperature regarding the flowrate R_{flow} of the experiment. The carrier gas stream must have reached its saturation equilibrium with the analyte at the end of the saturator to obtain correct experimental values. This can be demonstrated by the independence of the experimental result from the flow-rate R_{flow}. If the measurement at the lowest temperature is carried out at a lower or higher flow-rate (typically ±0.5 L/h) and the measured vapor pressure is identical within the accuracy of the experiment the saturation criterion is fulfilled for the original flow-rate R_{flow}.

Furthermore it must be checked that the analyte did not decompose during the measurement. For this reason a qualitative chromatogram (scan mode for GC/MS) of each transpiration sample should be run. If additional decomposition product peaks appear during the experiment it should be aborted. In case of doubt a sample of analyte-coated glass-beads may be collected from the saturator at the end of the experiment and used for a NMR-spectroscopy analysis of the analyte.

Further methods for the validation of the results obtained with the transpiration method experiment can be found in chapters 7.4 and 7.7.

6.7 Variables and Constants in order of Appearance

Variable	Explanation	Unit
p	Pressure	N m^{-2}
V	Volume	m³
T	Temperature	K
n	molar amount	Mol
p_{sat}	vapor pressure	N m^{-2}
T_{exp}	experimental temperature	K
V_{amb}	volume under ambient conditions	m³
n_{sat}	molar amount of analyte	mol
n_{N2}	molar amount of analyte	mol
M	Molar weight of substance	g mol^{-1}
p_{total}	total pressure	N m^{-2}
m_a	transported mass	kg
T_{amb}	ambient temperature	K
$n_{amb/exp}$	molar amount under ambient / experimental conditions	Mol
$p_{amb/exp}$	total pressure under ambient / experimental conditions	N m^{-2}
$V_{amb/exp}$	total volume of carrier gas under ambient / experimental conditions	m³
$I_{a/s}$	integral of analyte/standard GC-signal	counts
$m_{a/s}$	mass of analyte/standard	G
X/Y	quantification-device dependent calibration coefficients	
R_{flow}	flow-rate	m³/s
$V_{pipette}$	volume of pipette	m³
t_{meas}	measured time	S
t_{exp}	flow-time of the experiment for one data-point	S
T_{CT}	cooling trap temperature	K
p_{corr}	prest corrected vapor pressure	N m^{-2}
p_{rest}	vapor pressure at Tct	N m^{-2}
U/V	Fitting coefficients for p_{rest} extrapolation	
$\Delta^{\mathrm{g}}_{\mathrm{l/cr}}G$	Change of Gibbs free energy for vaporization or sublimation	J = Nm
$\Delta^{\mathrm{g}}_{\mathrm{l/cr}}H$	Change Enthalpy for vaporization or sublimation	J = Nm
$\Delta^{\mathrm{g}}_{\mathrm{l/cr}}S$	Change of Entropy for vaporization	J/K = Nm/K
G_g	Gibbs free energy in gaseous state	J = Nm
$G_{l/cr}$	Gibbs free energy in liquid or crystalline state	J = Nm
H_g	Enthalpy in gaseous state	J = Nm
$H_{l/cr}$	Enthalpy in liquid or crystalline state	J = Nm
S_g	Entropy in gaseous state	J = Nm
$S_{l/cr}$	Entropy in liquid or crystalline state	J = Nm
V_g	Volume in gaseous state	L = dm³ = 0.001 m³
$V_{l/cr}$	Volume in liquid or crystalline state	L = dm³ = 0.001 m³
$\Delta^{\mathrm{g}}_{\mathrm{l/cr}}H_m$	molar change Enthalpy for vaporization or sublimation	J mol^{-1} = Nm mol^{-1}
$\Delta^{\mathrm{g}}_{\mathrm{l/cr}}G^{\circ}_m$	Change of Gibbs free energy for vaporization or sublimation	J mol^{-1}
$\Delta^{\mathrm{g}}_{\mathrm{l/cr}}H^{\circ}_m$	Change Enthalpy for vaporization or sublimation	J mol^{-1}
$\Delta^{\mathrm{g}}_{\mathrm{l/cr}}S^{\circ}_m$	Change of Entropy for vaporization or sublimation	J K mol^{-1}
$\Delta^{\mathrm{g}}_{\mathrm{l/cr}}V^{\circ}_m$	Change of Volume for vaporization or sublimation	m³
Z	slope of ln p vs. 1/T plot	K

T_{avg}	average temperature of measurement	K
T_{ref}	reference temperature	K
$C^{\circ}_{p,m}(l)$	molar heat capacity at constant pressure in liquid state	J/K = Nm/K
$C^{\circ}_{p,m}(cr)$	molar heat capacity at constant pressure in solid state	J/K = Nm/K
$C^{\circ}_{p,m}(g)$	molar heat capacity at constant pressure in gaseous state	J/K = Nm/K
p^{o}	reference pressure of Fit-Funktion	N m^{-2}
T_0	reference temperature of Fit function	K
A	Fitting coefficient of Fit-Function	mol
B	Fitting coefficient of Fit-Function	K mol
σ_A	standard deviation of A from linear regression analysis	mol
σ_B	standard deviation of A from linear regression analysis	K mol
$\Delta^{g}_{l/cr}F^{0}$	Change of Helmholtz Energy for vaporization or sublimation	J

Constant	explanation	Value	Unit
R	universal gas constan	8.3144598(48)	Nm / K mol
M	molar mass	analyte-dependent	g / mol
X	device-dependent slope calibration constant		
Y	device-dependent offset calibration constant		

6.8 Literature References

1. Verevkin, S. P., *Phase Changes in Pure Component Systems: Liquids and Gases*. 1st ed.; Elsevier B.V.: Amsterdam, Netherlands, 2005.
2. http://www.chem.arizona.edu/~salzmanr/480a/480ants/clapeyro/clapeyro.html
3. Chickos, J. S.; Hosseini, S.; Hesse, D. G.; Liebman, J. F., Heat capacity corrections to a standard state: a comparison of new and some literature methods for organic liquids and solids. *Structural Chemistry* **1993,** *4* (4), 271-278.
4. Acree, W.; Chickos, J. S., Phase Transition Enthalpy Measurementsof Organic and Organometallic Compounds. Sublimation, Vaporizationand Fusion Enthalpies From 1880 to 2010. *Journal of Physical and Chemical Reference Data* **2010,** *39* (4), 043101.
5. Chickos, J. S.; Acree, W. E., Enthalpies of Vaporization of Organic and Organometallic Compounds, 1880–2002. *Journal of Physical and Chemical Reference Data* **2003,** *32* (2), 519-878.
6. Clarke, E. C. W.; Glew, D. N., Evaluation of thermodynamic functions from equilibrium constants. *Transactions of the Faraday Society* **1966,** *62* (0), 539-547.
7. NIST Technical Note 1297 http://www.nist.gov/pml/pubs/tn1297/.
8. Boeker, P.; Leppert, J.; Mysliwietz, B.; Lammers, P. S., Comprehensive Theory of the Deans' Switch As a Variable Flow Splitter: Fluid Mechanics, Mass Balance, and System Behavior. *Analytical Chemistry* **2013,** *85* (19), 9021-9030.
9. Emel'yanenko, V. N.; Verevkin, S. P., Benchmark thermodynamic properties of 1,3-propanediol: Comprehensive experimental and theoretical study. *The Journal of Chemical Thermodynamics* **2015,** *85*, 111-119.
10. Verevkin, S. P.; Sazonova, A. Y.; Emel'yanenko, V. N.; Zaitsau, D. H.; Varfolomeev, M. A.; Solomonov, B. N.; Zherikova, K. V., Thermochemistry of Halogen-Substituted Methylbenzenes. *Journal of Chemical & Engineering Data* **2015,** *60* (1), 89-103.
11. Gobble, C.; Chickos, J.; Verevkin, S. P., Vapor Pressures and Vaporization Enthalpies of a Series of Dialkyl Phthalates by Correlation Gas Chromatography. *Journal of Chemical & Engineering Data* **2014,** *59* (4), 1353-1365.

7 Measurement of Vapor Pressures with the Transpiration Method

The vapor pressure of a compound is the characteristic parameter which describes the pressure at which a compound is in equilibrium with its gaseous phase. (cf. section 6.2) For this reason the vapor pressure can be determined with a pressure gauge connected to a closed vessel, which has been evacuated prior to the measurement of the degassed analyte. This method of measurement is called a static method. Depending on the vapor pressure and enthalpy of vaporization or sublimation of a compound a multitude of experiments can be performed including static method measurements, ebulliometry, *Knudsen*-effusion methods, transpiration method and chromatographic methods. The techniques for the measurement of vapor pressures have been reviewed excellently by *Verevkin* [1].

As the static method measurement already indicates, the vapor pressure is directly linked to the saturation concentration of an analyte. For low vapor pressures the concentration of the analyte can be derived directly from the Ideal Gas law:

$$c_{sat} = \frac{p_{sat} \times M}{R \times T} \quad (1)$$

p_{sat}: vapor pressure [Pa], c_{sat}: saturation concentration [mg L^{-1}], R: ideal gas constant (8.3145 J mol^{-1} K^{-1}), T: temperature [K], M: molar mass of analyte [g mol^{-1}]

The air-concentration of an analyte is important for its gas-phase detection. For this reason the vapor pressure is used in diffusion-based models to estimate the concentration of analytes under real (non-saturation) conditions. [2] The vapor pressure is an important parameter for modelling the evaporation of droplets. [3]

If a vapor pressure measurement is performed over a sufficient temperature range, the enthalpy of sublimation (for solid analytes) or vaporization (for liquid analytes) can be derived from the measurement. (cf. section 6.2) With the vapor pressure and the enthalpy of sublimation or vaporization the ambient reference temperature 298.15 K, the vapor pressure at close temperatures can be calculated with respect to the linear relation in the *Clausius-Clapeyron* equation. (cf. section 6.2, equation 31). For each compound that was measured in this work both parameters are stated together with the coefficients for the fitting equation (cf. section 6.2, equation 48).

In scientific literature physico-chemists mostly avoid the discussion of absolute vapor pressures and limit their discussion to enthalpies of vaporization or sublimation. The reason for this is simple: In contrast to the vapor pressure the temperature-dependency of the enthalpies of volatilization is relatively low. Additionally the vapor pressure is more sensitive to systematic experimental errors.

The enthalpy of volatilization is a useful parameter for the transfer of the results of quantum-chemical gas-phase calculation to the condensed state:

$$\Delta_f H_m^\circ \text{ (298.15, g) - } \Delta_l^g H_m^\circ \text{ (298.15 K) = } \Delta_f H_m^\circ \text{ (298.15, liq)} \quad (2)$$

$$\Delta_f H_m^\circ \text{ (298.15, g) - } \Delta_{cr}^g H_m^\circ \text{ (298.15 K) = } \Delta_f H_m^\circ \text{ (298.15, cr)} \quad (3)$$

$\Delta_f H_m^\circ$ (298.15, g): molar enthalpy of formation in gaseous state at 298.15 K, $\Delta_l^g H_m^\circ$ (298.15 K): molar enthalpy of vaporization at 298.15 K, $\Delta_{cr}^g H_m^\circ$ (298.15 K): molar enthalpy of sublimation at 298.15 K.

Since the vapor pressure of explosives is an important parameter for the gas-phase detection of explosives, it has been recently reviewed twice by *Östmark et al.*[4] in 2012 and by *Ewing et al.* [5] in 2013. *Ewing et al.* [5] have summarized the vapor pressures of explosives at 298.15 K in comparison with the results by *Östmark et al.* [4]. (cf. Figure 1)

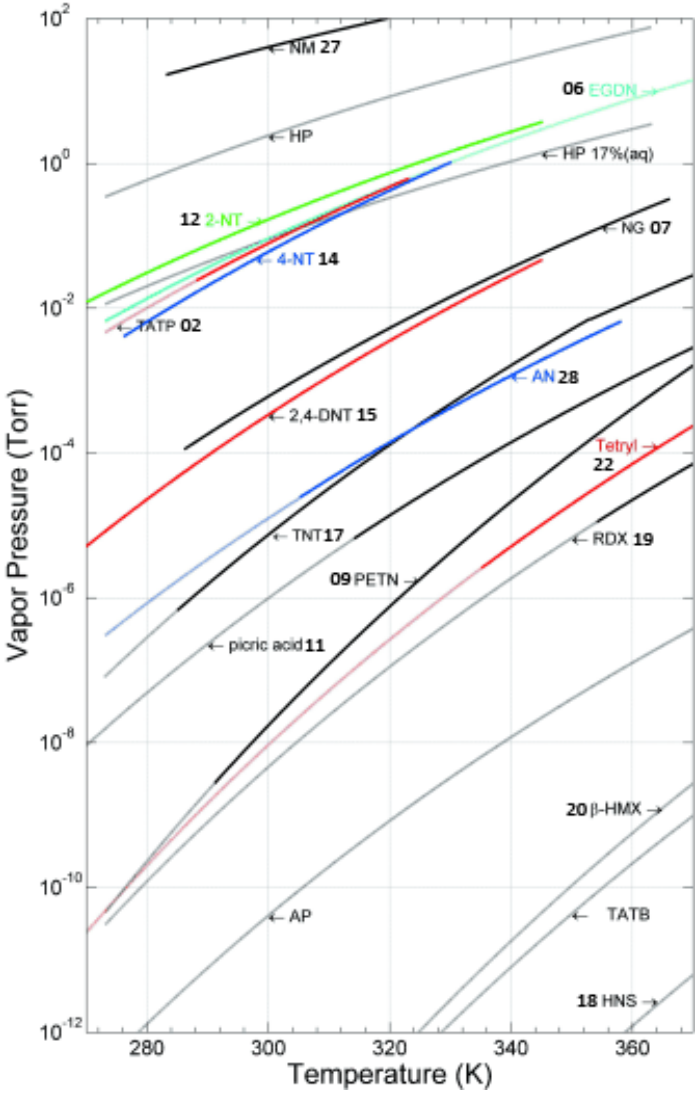

Table 3. Vapor pressures at 25°C

Explosive	Vapor pressure (atm)	Standard deviation (atm)	Number of sources[a]	Vapor pressure (ppb_v)	Vapor pressure from Ostmark (atm)	Ratio Ostmark/ this review
NM	4.68E-02	1.06E-03	3	46,800,000	4.80E-02	1.03
HP	2.88E-03	n/a	1	2880,000	2.80E-03	0.97
DADP	2.44E-4	0.93E-4	2	244,000	1.75E-04	0.72
TATP	6.31E-5	2.18E-5	3	63,100	6.12E-05	0.97
EGDN*	1.02E-4	0.09E-4	3	102,000	1.00E-04	0.98
p-MNT	6.47E-05	n/a	1	647	6.43E-05	0.99
2,4-DNT	4.11E-7	1.46E-7	5	411	3.46E-07	0.84
2,6-DNT	8.93E-7	2.08E-7	2	893	8.16E-07	0.91
NG	6.45E-7	2.37E-7	4	645	6.33E-07	0.98
TNM	4.06E-9	n/a	1	4.06		
TNT	9.15E-9	4.46E-9	6	9.15	7.24E-09	0.79
TNB	2.00E-8	n/a	1	20.0		
AN	1.47E-08	6.26E-09	5	14.7	1.29E-08	0.88
TNC	1.71E-09	n/a	1	1.71		
picric acid	9.71E-10	n/a	1	0.971	9.84E-10	1.01
TNX	1.61E-10	n/a	1	0.161		
styphnic acid	6.03E-11	n/a	1	0.0603		
UN	3.88E-10	n/a	1	0.388		
PETN	1.07E-11	0.54E-11	4	0.0107	1.53E-11	1.43
tetryl	7.41E-12	n/a	1	0.00741	8.57E-12	1.16
TNA	1.51E-11	0.98E-11	2	0.0151		
RDX	4.85E-12	1.55E-12	3	0.00485	4.34E-12	0.89
AP	4.01E-14	n/a	1	0.0000401	3.91E-14	0.98
DATB	3.76E-14	2.38E-14	2	0.0000376		
nitroguanidine	1.86E-14	n/a	1	0.0000186	2.14E-15	0.12
HMX	2.37E-17	2.79E-17	2	0.0000000237	3.96E-18	0.17
TATB	2.38E-18	n/a	1		2.45E-18	1.03
HNS	6.09E-21	n/a	1		6.11E-21	1.00
GN	2.62E-23	n/a	1			

[a]Number of sources acceptable for calculating average vapor pressure at 25 °C.

Figure 1 – left: p-T-plot of the vapor pressure of numerous explosives by Östmark et al. [4]. Reprinted with permission from [4] *Copyright 2012 John Wiley and sons. right: The vapor pressure of numerous explosives at 298.15 K. For the meaning of the acronyms see reference [5]. Reprinted with permission from [5] Copyright 2012 Elsevier Ltd.*

In general the results derived from literature data by both groups are in good agreement as demonstrated by the ratio of the vapor pressure calculated by *Östmark* and *Ewing*, which ranges from 0.72 to 1.43 besides two exceptions for the extremely low-volatile nitroguanidine and HMX **20**. As indicated by *Ewing et al.* [5] the saturation equilibrium concentration of explosives is in the ppb_v- and ppt_v-regime of equilibrium concentration. For some explosives the concentration is drastically lower (e.g. HMX **20**). State-of the art gas-phase explosive detection equipment is capable to detect the vapor of RDX **19** without preconcentration.[6]

The data collected by both reviews [4-5] is based on 31 publications, which partially date back to 1916. It would be desirable to establish a vapor pressure data base for explosives measured with state of the art equipment, which was validated with well-investigated reference compounds.

In comparison to stable analytes like hydrocarbons the vapor pressures of explosives reported in the literature are less consistent with each other. To cite Dr. Joda C. Wormhoudt, who is concerned with a program of literature reviews and laboratory measurements in support of an explosives vapor pressure database [7]:

"I did learn one thing, that the small world of explosives vapor pressure measurements is different than the great world of vapor pressure measurements on stable compounds. The common situation for explosives is that if you had 10 groups whose measurements on reference compounds agree to within a few per cent, 9 out of the 10 would have disagreements far in excess of their error estimates, factors of 2 or 3 or the like, with no idea as to the cause, and the tenth would be off by an order of magnitude or more, perhaps due to some blunder but perhaps unknown as well.'' [8]

For the reasons stated above we decided to establish the transpiration method (cf. section 6) as established by *Verevkin et al.* [9] in our workgroup. After the initial establishment of the experimental setup it was tested with reference substances that included volatile (iso-amyl acetate), medium-volatile (n-hexanol, n-octanol, naphthalene) and low-volatile (anthracene) analytes with reliable literature data.

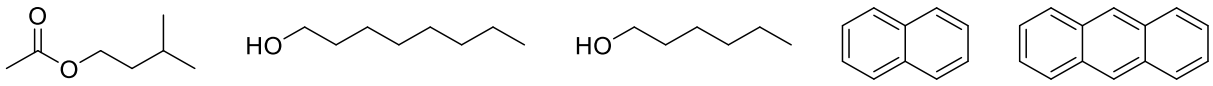

Figure 2 – Reference Compounds studied in this work: iso-amyl acetate, n-octanol, n-hexanol, naphthalene, anthracene

Since all reference analytes could be measured successfully, the transpiration method was applied to peroxides (TATP **02**, DADP **03**), nitrate esters (EGDN **06**, GTN **07**, ETN **08**), nitrotoluenes (2-MNT **12**, 3-MNT **13**, 4-MNT **14**, 2,4-DNT **15**, 2,6-DNT **16**, TNT **17**), nitroalkanes (DMBNB **26**, 2-nitrobutane, 2-methyl-2-nitrobutane), nitronaphthalenes (1-nitronaphthalene, 2-methyl-1-nitronaphthalene) and seven structurally related organo(thio)phosphates (**I**-**VIII**) including the pesticide amitone. (cf. Figure

3). In the following all experiments that were performed with the transpiration method will be presented. Published results will be given as original publications.

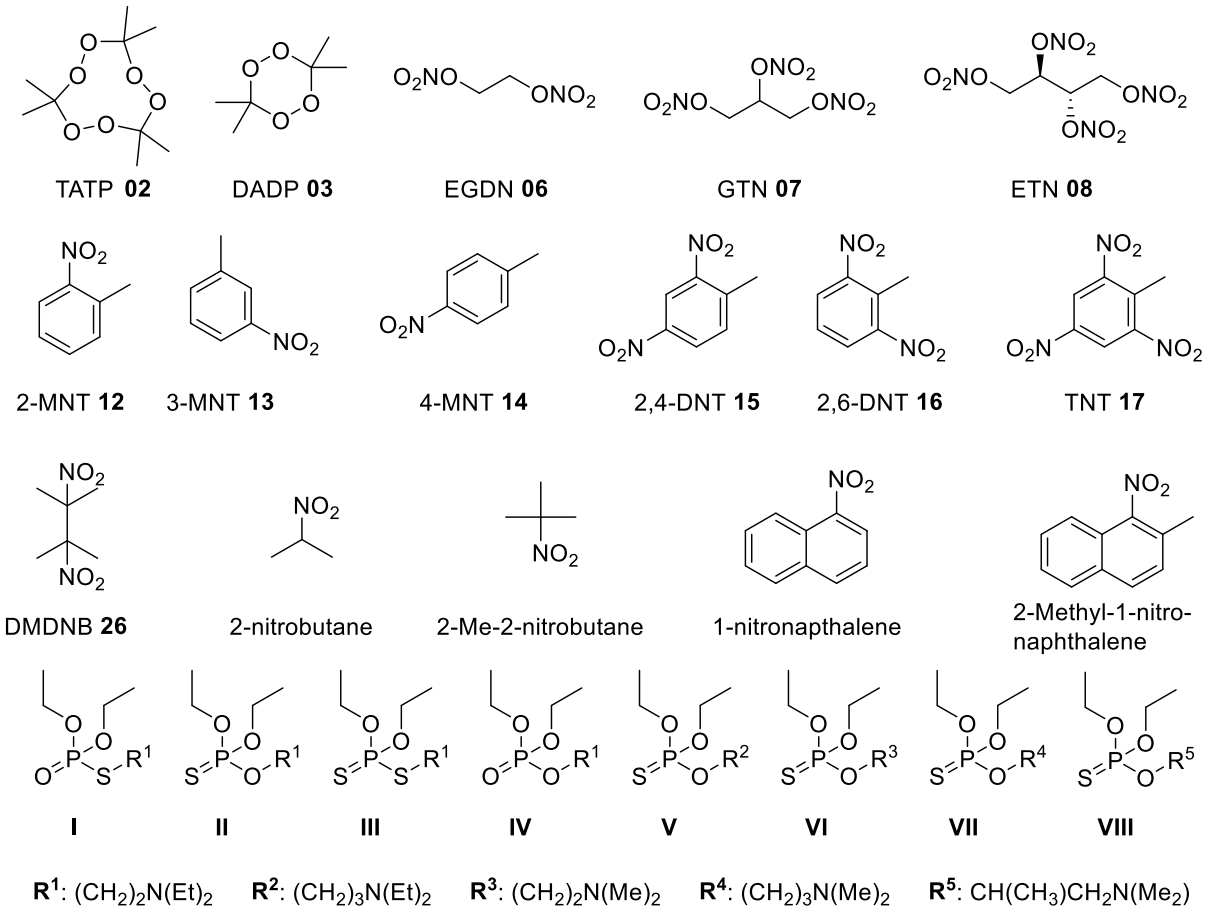

Figure 3 – Molecular Structures of all analytes characterized with the transpiration method in this work.

The transpiration method experiment and the mathematical processing are detailed in section 6.2. Published results will be given as original publications. A summary of the most important aspects is given for all unpublished results including the reference compound measurements in the following:

All p-T sets of data discussed were analyzed with the the Fit-Function using the heat capacity differences stated in the corresponding section.

$$\ln {}^{p_{\mathrm{sat}}}\!/_{p^{\mathrm{o}}} - \frac{\Delta_{\mathrm{l}}^{\mathrm{g}} C_{p,m}^{\circ}}{R} ln\frac{T}{T_0} = A - \frac{B}{T} \quad (4)$$

$$\ln {}^{p_{\mathrm{sat}}}\!/_{p^{\mathrm{o}}} - \frac{\Delta_{\mathrm{cr}}^{\mathrm{g}} C_{p,m}^{\circ}}{R} ln\frac{T}{T_0} = A - \frac{B}{T} \quad (5)$$

p^{o}: reference pressure being 1[Pa], $\Delta_{\mathrm{l}}^{\mathrm{g}} C_{p,m}^{\circ}$: molar heat capacity difference from liquid to gaseous state [J K^{-1} mol^{-1}], $\Delta_{\mathrm{cr}}^{\mathrm{g}} C_{p,m}^{\circ}$:molar heat capacity difference from solid to gaseous state [J K^{-1} mol^{-1}], T: temperature [K], T_0: reference temperature [K], A, B: fitting coefficients (A: [ ], B: [K]).

In this way the fitting coefficients A and B can be obtained for each individual set of data, which allows the calculation of enthalpies of vaporization and sublimation at the average temperature of the measurement:

$$\Delta_{\mathrm{l}}^{\mathrm{g}} H_{\mathrm{m}}^{\mathrm{o}}(T) = \mathrm{R}B + \Delta_{\mathrm{l}}^{\mathrm{g}} C_{p,m}^{\circ} T \quad (6)$$

$$\Delta_{cr}^{g} H_m^o(T) = RB + \Delta_{cr}^{g} C_{p,m}^{\circ} T \quad (7)$$

$\Delta_l^g H_m^o(T)$: molar enthalpy of vaporization [J mol^{-1}] $\Delta_{cr}^g H_m^o(T)$ molar enthalpy of sublimation [J mol^{-1}]

The obtained enthalpies of vaporization (eq. (6)) or sublimation (eq. (7)) are adjusted for comparison to *T* = 298.15 K according to the method provided by *Chickos et al.* [10] using the heat capacity differences and heat capacities stated in each section. Furthermore, p_{sat} at *T* = 298.15 K can be evaluated from each individual complete *p*-*T*-dataset using equation (1) or (2). The commercial source and purity of each reference compound is detailed in each section.

All *p*-*T*-datasets discussed will be visualized for comparison using *Clausius*-*Clapeyron* plots. The enthalpies of sublimation and vaporization at 298.15 K will be compared with literature values that were derived from the literature *p*-*T*-data by identical data treatment using equations (4) to (7) and the error estimation stated elsewhere [9b] for the sake of comparability. If sufficient data is available for comparison an uncertainty-weighted average value of own and literature data is calculated, which is used as a benchmark for the precision of the own transpiration method experiments with reference compounds. Furthermore an average value for the vapor pressure at 298.15 K derived by equation (1) or (2) from the *p*-*T*-dataset will be stated for each compound.

Literature References

1. Verevkin, S. P., *Phase Changes in Pure Component Systems: Liquids and Gases*. 1st ed.; Elsevier B.V.: Amsterdam, Netherlands, 2005.
2. (a) Dravnicks, A. *Bomb Detection System Study*; IIT Research Institute: Chicago, Illinois, 1965; (b) Dravnicks, A.; Brabets, R.; Stanley, T. A. *Evaluating Sensitivity Requirements of Explosive Vapor Detector Systems*; IIT Research Institute Technology Center: Chicago Illinois, 1972.
3. (a) Birdi, K. S.; Vu, D. T.; Winter, A., A study of the evaporation rates of small water drops placed on a solid surface. *The Journal of Physical Chemistry* **1989,** *93* (9), 3702-3703; (b) Charlesworth, D. H.; Marshall, W. R., Evaporation from drops containing dissolved solids. *AIChE Journal* **1960,** *6* (1), 9-23; (c) Melnikov, N. N., *Residue reviews : residues of pesticides and other foreign chemicals in foods and feeds. 40.1971. With cumulative table of subjects covered, detailed subject-matter index, and author index of volumes 31 - 40*. Springer: Berlin, 1971.
4. Östmark, H.; Wallin, S.; Ang, H. G., Vapor Pressure of Explosives: A Critical Review. *Propellants, Explosives, Pyrotechnics* **2012,** *37* (1), 12-23.
5. Ewing, R. G.; Waltman, M. J.; Atkinson, D. A.; Grate, J. W.; Hotchkiss, P. J., The vapor pressures of explosives. *TrAC Trends in Analytical Chemistry* **2013,** *42*, 35-48.
6. Ewing, R. G.; Clowers, B. H.; Atkinson, D. A., Direct Real-Time Detection of Vapors from Explosive Compounds. *Analytical Chemistry* **2013,** *85* (22), 10977-10983.
7. http://www.aerodyne.com/employees/joda-c-wormhoudt.
8. Personal correspondence with Dr. Joda C. Wormhoudt from Aerodyne Research Inc.
9. (a) Emel'yanenko, V. N.; Verevkin, S. P., Benchmark thermodynamic properties of 1,3-propanediol: Comprehensive experimental and theoretical study. *The Journal of Chemical Thermodynamics* **2015,** *85*, 111-119; (b) Verevkin, S. P.; Sazonova, A. Y.; Emel'yanenko, V. N.; Zaitsau, D. H.; Varfolomeev, M. A.; Solomonov, B. N.; Zherikova, K. V., Thermochemistry of Halogen-Substituted Methylbenzenes. *Journal of Chemical & Engineering Data* **2015,** *60* (1), 89-103; (c) Verevkin, S. P., 2 Phase changes in purecomponent systems: Liquids and gases. In *Experimental Thermodynamics*, Weir, R. D.; Loos, T. W. D., Eds. Elsevier: 2005; Vol. Volume 7, pp 5-30.
10. Acree, W.; Chickos, J. S., Phase Transition Enthalpy Measurementsof Organic and Organometallic Compounds. Sublimation, Vaporizationand Fusion Enthalpies From 1880 to 2010. *Journal of Physical and Chemical Reference Data* **2010,** *39* (4), 043101.

7.1 Measurement of Reference Compounds

For the initial validation of the experimental setup the following reference compounds were chosen: naphthalene, anthracene, *iso*-amyl acetate, n-hexanol and n-octanol. (see Figure 1)

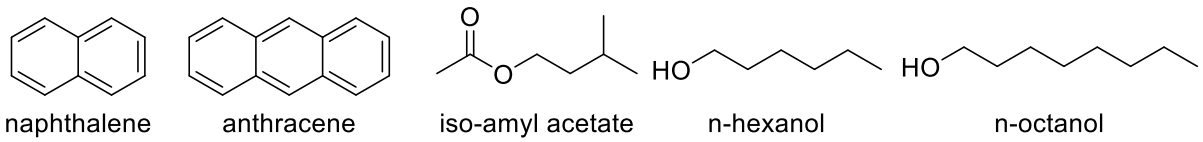

Figure 1 - Chemical structures of the reference compounds investigated in this work: naphthalene, anthracene, iso-amyl acetate, n-hexanol and n –octanol.

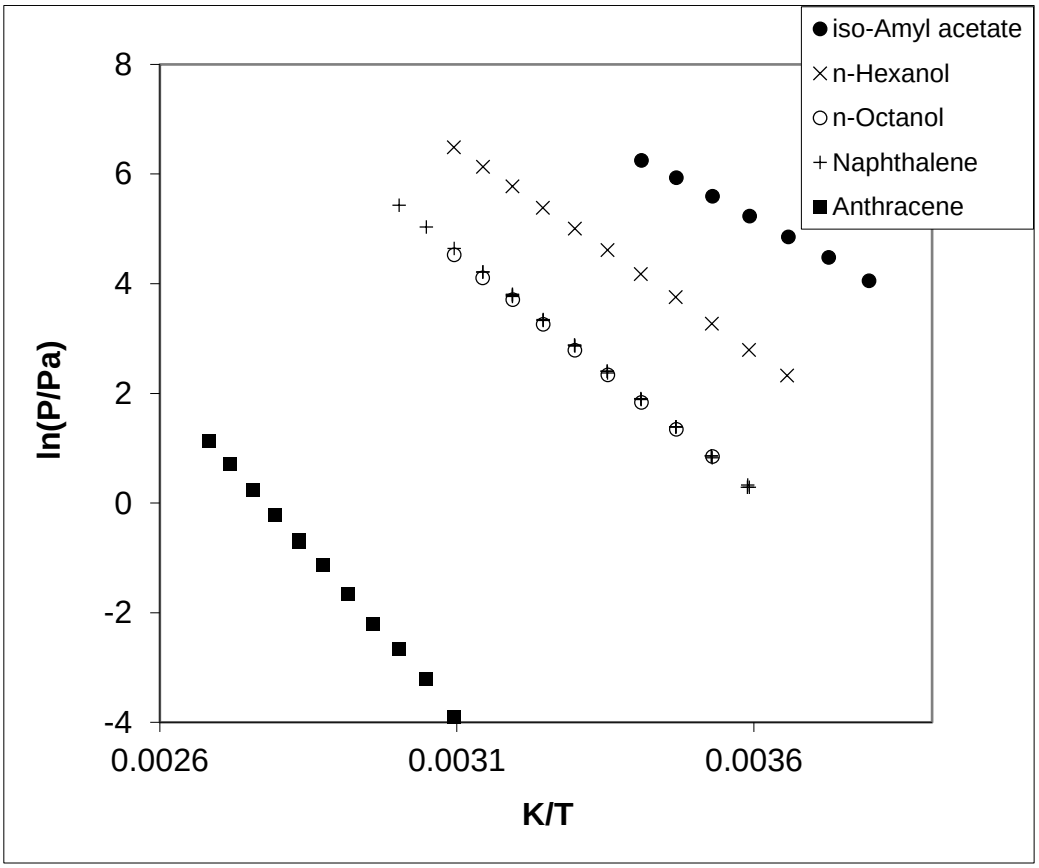

Figure 2 - Experimental vapor pressures of iso-amyl acetate, n-hexonal, n-octanol, naphthalene and anthracene obtained in this work.

A *Clausius-Clapeyron* plot of all reference compound p-T datasets measured in this work is compiled in Figure 2. The reference compounds cover measurement scenarios for compounds with high volatility (*iso*-amyl acetate), medium volatility (*n*-hexanol, *n*-octanol, naphthalene) and low volatility (anthracene). In the following the measurement of each reference compound will be discussed in detail including the p-T-data measured in this work in comparison with literature p-T-datasets. All p-T sets of data discussed were analyzed with the the Fit-Function using the heat capacity differences stated in Table 11.

7.1.1 Naphthalene

Table 1 - Naphthalene: absolute vapor pressures p_{sat} and thermodynamic properties of sublimation obtained by the transpiration method in this work.

Naphthalene: $\Delta_{cr}^{g} H_m^{\circ}$ (298.15 K) = 72.76 ± 0.32 kJ mol^{-1}

$$\ln p_{sat}/p^{\circ} = \frac{289.5}{R} - \frac{80397.1}{RT} + \frac{25.6}{R} ln \frac{T}{298.15\text{K}}$$

T_{exp}[a]	m[b]	V_{N2}[c]	T_{amb}[d]	Gasflow	p_{sat}[e]	$u(p_{sat})$[f]	$\Delta_{cr}^{g} H_m^{\circ}$	$\Delta_{cr}^{g} S_m^{\circ}$
[K]	[mg]	[dm³]	[K]	[dm³ h^{-1}]	[Pa]	[Pa]	[kJ mol^{-1}]	[J mol^{-1} K^{-1}]
278.6	0.28	3.95	297.8	1.98	1.39	0.04	73.27	170.0
278.4	1.02	14.8	296.0	4.94	1.33	0.04	73.27	169.9
278.6	0.25	3.58	297.7	1.96	1.34	0.04	73.27	169.6
283.4	0.26	2.13	297.4	1.94	2.36	0.06	73.14	169.5
283.4	0.26	2.16	297.7	1.96	2.36	0.06	73.14	169.5
283.3	1.02	8.65	295.9	1.97	2.28	0.06	73.14	169.3
288.3	1.15	5.54	297.0	1.98	4.01	0.11	73.02	169.1
288.3	0.52	2.51	297.6	1.93	4.01	0.11	73.02	169.1
288.3	0.52	2.54	298.2	1.95	3.98	0.10	73.02	169.0
293.3	0.22	0.652	299.0	1.96	6.70	0.19	72.89	168.6
293.3	0.44	1.28	297.6	1.92	6.64	0.19	72.89	168.6
293.2	1.21	3.57	297.5	1.98	6.58	0.19	72.89	168.5
298.2	0.32	0.56	299.9	1.96	11.1	0.3	72.76	168.3
298.2	0.54	0.96	297.7	1.91	11.0	0.3	72.76	168.2
298.2	0.98	1.75	295.9	1.99	10.7	0.3	72.76	168.0
303.2	0.53	0.57	297.8	1.91	17.8	0.5	72.64	167.8
303.2	0.50	0.55	300.3	1.95	17.8	0.5	72.64	167.8
303.2	1.97	2.18	296.4	1.98	17.4	0.5	72.64	167.7
308.1	1.53	1.04	298.0	1.90	28.4	0.7	72.51	167.4
308.2	0.75	0.520	300.2	1.95	28.0	0.7	72.51	167.3
308.2	0.91	0.628	297.0	1.98	27.9	0.7	72.51	167.2
313.1	1.06	0.453	297.3	1.01	44.9	1.2	72.38	167.1
313.1	1.48	0.643	298.4	1.93	44.5	1.1	72.38	167.0
313.1	1.44	0.632	297.8	1.90	44.1	1.1	72.38	166.9
313.1	1.44	0.649	300.1	1.95	43.2	1.1	72.38	166.7
318.1	1.68	0.482	298.6	1.93	67.7	1.7	72.25	166.5
318.1	1.17	0.334	296.5	1.00	67.4	1.7	72.25	166.4
323.0	2.54	0.474	297.5	1.90	104	3	72.13	166.1
328.0	3.75	0.471	297.6	1.88	154	4	72.00	165.6
333.0	5.65	0.480	297.9	1.92	228	6	71.87	165.2

[a] Saturation temperature ($u(T)$ = 0.1 K). [b] Mass of transferred sample condensed at T = 243 K [c] Volume of nitrogen ($u(V)$ = 0.005 dm³) used to transfer m ($u(m)$ = 0.0001 g) of the sample. [d] T_a is the temperature of the soap bubble meter used for measurement of the gas flow. [e] Vapor pressure at temperature T, calculated from the m and the residual vapor pressure at the condensation temperature calculated by an iteration procedure; p° = 1 Pa. [f] Standard uncertainty in p was calculated with $u(p/\text{Pa})$ = 0.005+0.025(p/Pa) for p < 5 Pa and $u(p/\text{Pa})$ = 0.025+0.025(p/Pa) for p > 5 to 3000 Pa.

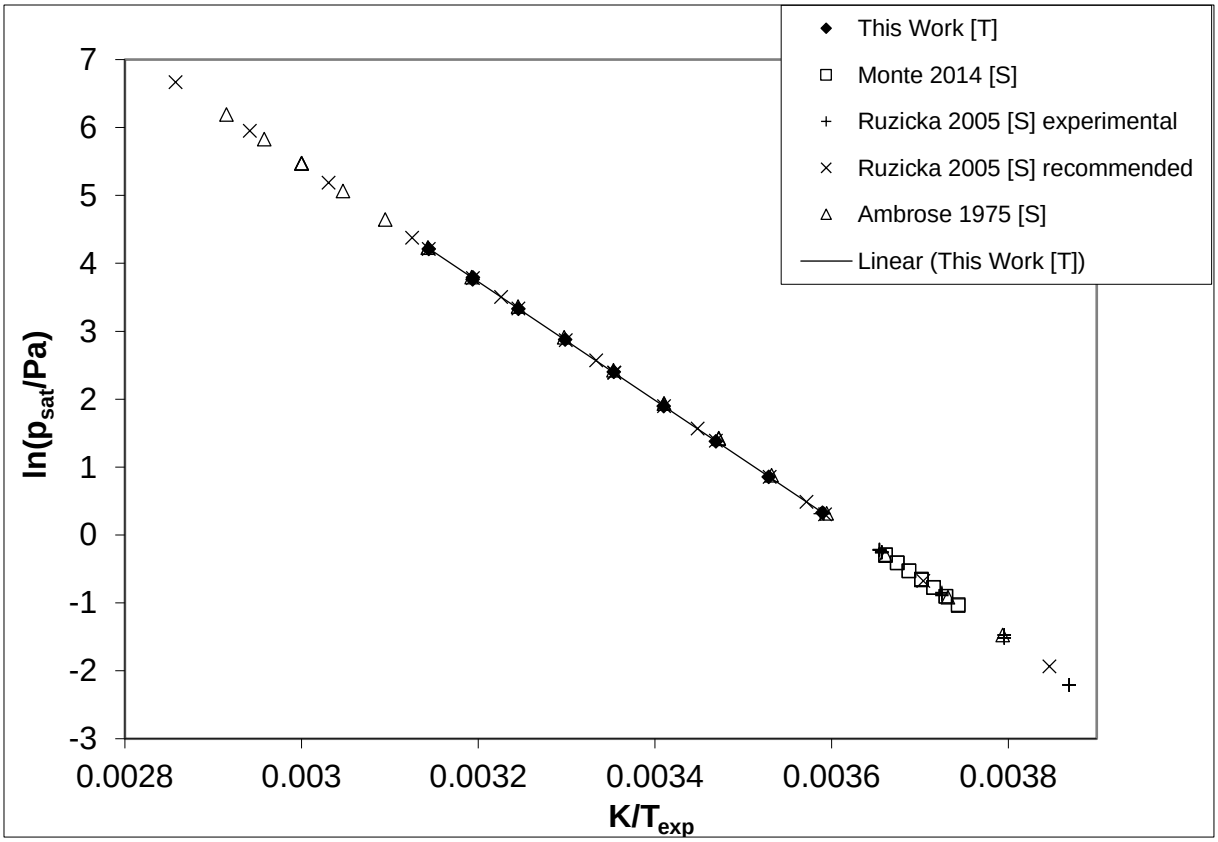

Figure 3 – Experimental vapor pressure of naphthalene in comparison with literature values.

Table 2 – Compilation of data on enthalpies of sublimation $\Delta_{cr}^{g}H_{m}^{\circ}$ of naphthalene

Experiment[a]	Method[b]	T-Range	T_{avg}	$\Delta_{cr}^{g}H_{m}^{\circ}(T_{avg})$	$\Delta_{cr}^{g}H_{m}^{\circ}$(298.15K)[c]	p_{sat}[d]
		K	K	kJ mol^{-1}	kJ mol^{-1}	
This work	T	278.4-333.0	300.3	72.7±0.1	72.8±0.2	10.8
Monte 2006 [1]	S	267.2-273.2	270.2	74.6±0.4	73.8±2.1	11.6
Ruzicka 2005 [2]	S	258.5-278.8	268.1	75.7±0.3	74.9±0.7	12.0
Ambrose 1975 [3]	S	263.6-343.1	303.6	72.2±0.1	72.3±0.3	11.2
					72.8±0.2[e]	11.4[f]

[a] First author and year of publication, [b] Methods: T: Transpiration Method, S: Static Method [c] Enthalpies of Sublimation were adjusted according to *Chickos et al.* [4] with $\Delta_{cr}^{g}C_{p,m}^{\circ}$= -25.6 J mol^{-1} K^{-1} and $C_{p,m}^{\circ}$(cr)= 165.7 J mol^{-1} K^{-1} (see Table 11). [d] Weighted average value, calculated using uncertainty as the weighing factor. [e] Vapor pressure at 298.15 K [f] Average value.

Naphthalene is the common reference compound for validation of vapor pressure measurements since reliable experimental data exists. (cf. Table 2) The sublimation behavior of naphthalene was measured with the transpiration method in this work. The results obtained are compared with three static method datasets by *Monte et al*. [1], *Ruzicka et al*. [2] and *Ambrose et al.* [3]. *Ruzicka et al*. [2] provide for the temperature range 150 – 350 K a set of recommended vapor pressures of naphtalene that was developed by a multi-property simultaneous correlation of vapor pressures and related thermal data. The excellent agreement of the *p*-*T*-data obtained by the transpiration experiment with the literature values can be visualized by graphical comparison in a *Clausius-Clapeyron* plot (cf. Figure 3). It reveals the high agreement of all sets of data.

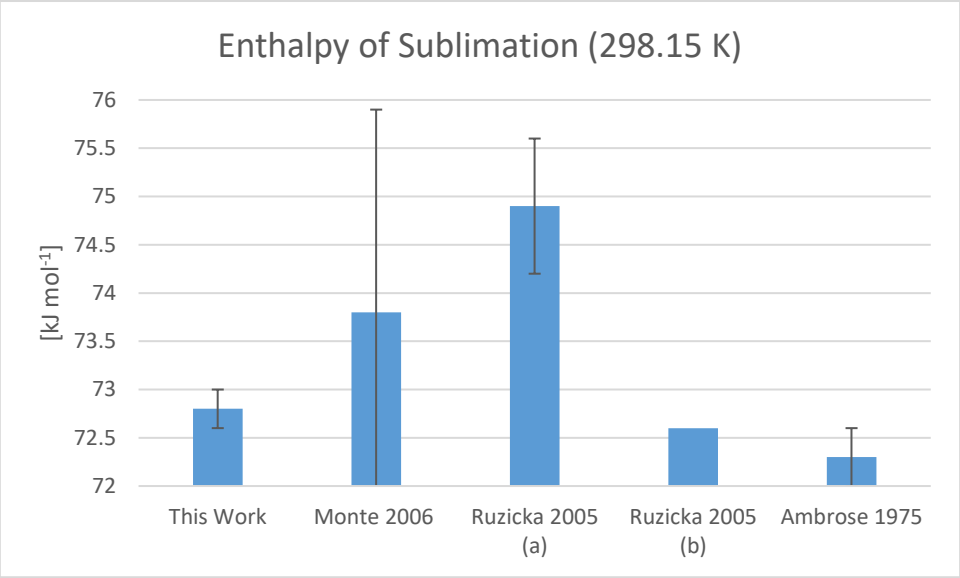

Figure 4 - Comparison of enthalpies of sublimation at 298.15 K for naphthalene. (cf. Table 2) a) experimental values, b) recommended, compiled literature data.

The enthalpies of sublimation at 298.15 K obtained by this work in comparison with literature values are compiled in Table 2 and visualized in Figure 4. The value measured in this work (72.8 ± 0.2 kJ mol^{-1}) is in agreement the static method measurements by *Ambrose et al.* [3] and *Monte et al.* [1] and the compiled data recommended by *Ruzicka et al.* [2]. Based on the data available, a weighted average sublimation enthalpy of 72.8 ± 0.2 kJ mol^{-1} was calculated using the uncertainty as the weighing factor. The vapor pressures of naphthalene at 298.15 K that were calculated from each individual complete dataset are compiled in Table 2. The mean value of 11.4 Pa can be considered as a recommendation for the ambient condition vapor pressure of naphthalene. *Ruzicka et al*. [2] provide a dataset of recommended vapor pressures of naphtalene that was developed by a multi-property simultaneous correlation of vapor pressures and related thermal data. For the temperature T = 298.15 K an enthalpy of sublimation of 72.44 kJ mol^{-1} and a vapor pressure of 10.92 Pa are recommended. The values recommended by *Ruzicka et al*. [2] are in fair agreement with the enthalpy of sublimation and absolute vapor pressures evaluated in this work (72.8 ± 0.2 kJ mol^{-1}; 11.4 Pa) considering the fact that *Ruzicka et al*. used the highly sophisticated SimCor Method for the temperature correlation of vapor pressures and related thermal data. This method outperforms the two parameter *p*-*T*-data fitting approach (equation (1)) in this work, yet the results are in sufficient agreement.

7.1.2 Anthracene

Table 3 - Anthracene: absolute vapor pressures p_{sat} and thermodynamic properties of sublimation obtained by the transpiration method in this work

Anthracene: $\Delta_{cr}^{g}H_m^{\circ}$(298.15 K) = 101.50 ± 0.59 kJ mol^{-1}

$$\ln p_{sat}/p^{\circ} = \frac{314.9}{R} - \frac{111194.6}{RT} + \frac{32.5}{R} ln \frac{T}{298.15K}$$

T_{exp}[a] [K]	m[b] [mg]	V_{N2}[c] [dm³]	T_{amb}[d] [K]	Gasflow [dm³ h^{-1}]	p_{sat}[e] [Pa]	$u(p_{sat})$[f] [Pa]	$\Delta_{cr}^{g}H_m^{\circ}$ [kJ mol^{-1}]	$\Delta_{cr}^{g}S_m^{\circ}$ [J mol^{-1} K^{-1}]
323.2	0.34	223	297	5.03	0.02	0.01	100.69	183.9
328.0	0.30	111	297.1	5.05	0.04	0.01	100.53	183.4
333.0	0.32	65.5	297.1	5.04	0.07	0.01	100.37	183.4
333.0	0.34	73.0	297.3	5.05	0.07	0.01	100.37	182.9
338.0	0.28	35.4	296.7	5.03	0.11	0.01	100.21	182.4
338.0	0.30	36.8	296.6	2.55	0.11	0.01	100.21	182.6
343.0	0.29	21.1	296.8	5.04	0.19	0.01	100.05	182.2
347.9	0.30	13.3	296.6	5.03	0.32	0.01	99.89	181.7
352.9	0.28	7.96	295.9	5.03	0.49	0.02	99.72	180.9
352.9	0.27	7.54	297.1	5.03	0.49	0.02	99.72	180.9
352.9	0.29	7.92	298.0	2.56	0.51	0.02	99.72	181.1
357.9	0.29	5.02	296.5	5.02	0.80	0.02	99.56	180.6
362.9	0.28	3.12	296.3	5.05	1.28	0.04	99.40	180.2
367.8	0.24	1.67	296.3	5.02	2.03	0.06	99.24	179.9
372.8	0.28	1.25	296.3	5.01	3.12	0.08	99.08	179.5

[a] Saturation temperature ($u(T)$ = 0.1 K). [b] Mass of transferred sample condensed at T = 243 K [c] Volume of nitrogen ($u(V)$ = 0.005 dm^3) used to transfer m ($u(m)$ = 0.0001 g) of the sample. [d] T_a is the temperature of the soap bubble meter used for measurement of the gas flow. [e] Vapor pressure at temperature T, calculated from the m and the residual vapor pressure at the condensation temperature calculated by an iteration procedure; p° = 1 Pa. [f] Standard uncertainty in p was calculated with $u(p/\text{Pa})$ = 0.005+0.025(p/Pa) for p < 5 Pa and $u(p/\text{Pa})$ = 0.025+0.025(p/Pa) for p > 5 to 3000 Pa.

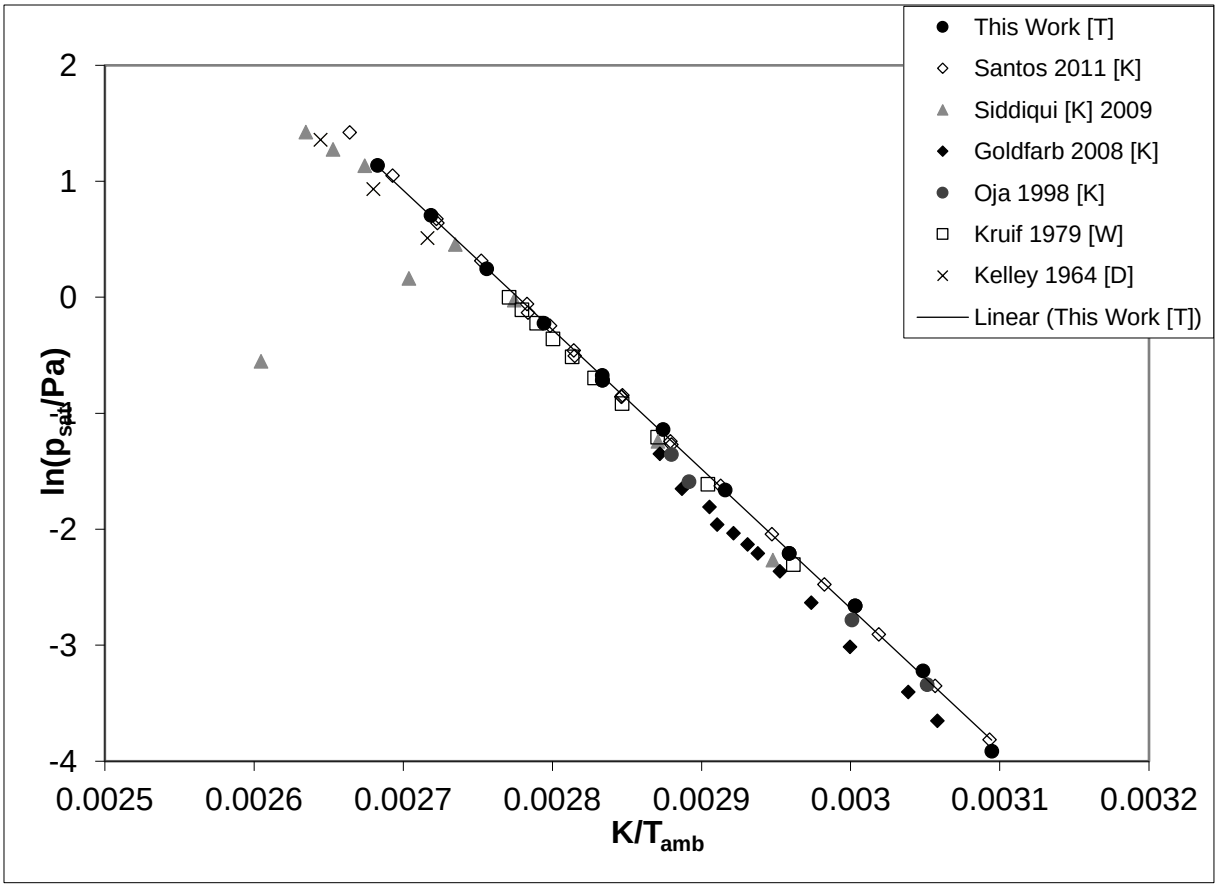

Figure 5 – Experimental vapor pressure of anthracene in comparison with literature values.

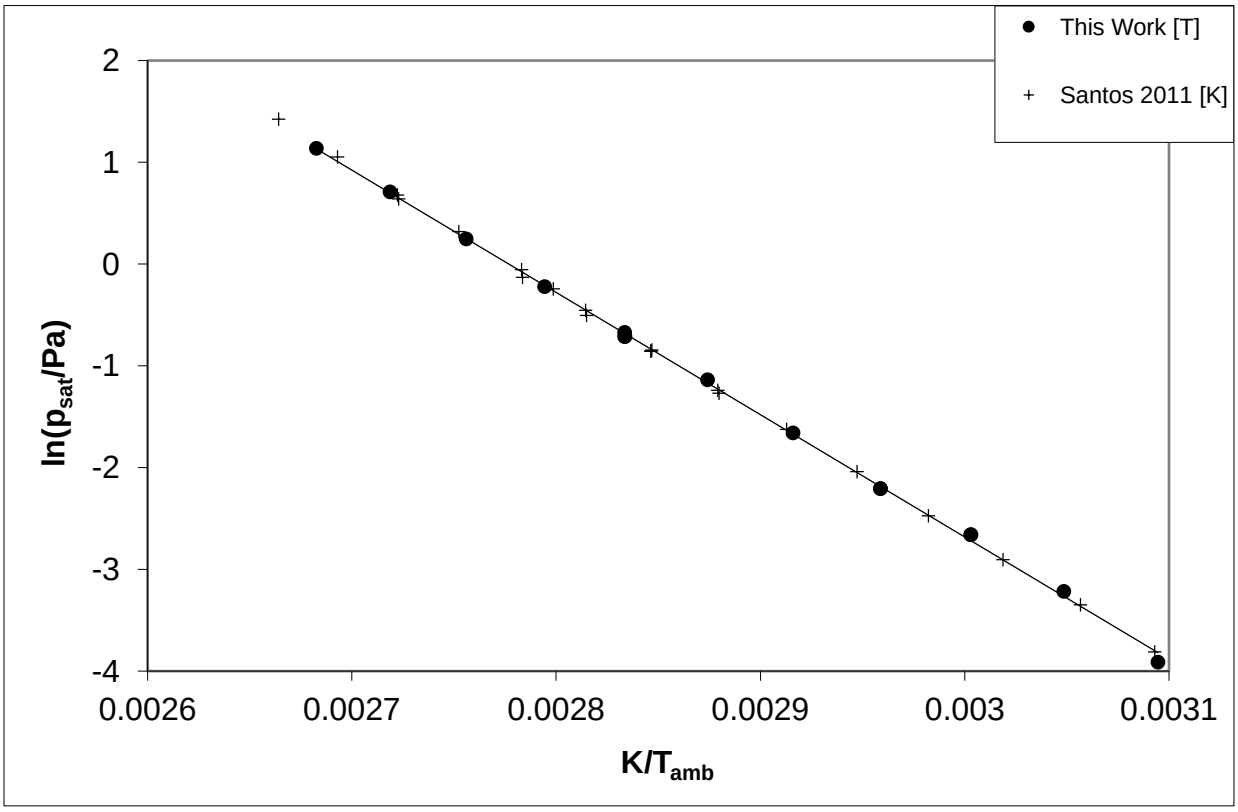

Figure 6 – Experimental vapor pressure of anthracene. Internal comparison of own experimental results with the literature data from Santos et al. [5].

Table 4 – Compilation of data on enthalpies of sublimation $\Delta_{cr}^{g}H_{m}^{\circ}$ of anthracene

Experiment[a]	Method[b]	T-Range	T_{avg}	$\Delta_{cr}^{g}H_{m}^{\circ}(T_{avg})$	$\Delta_{cr}^{g}H_{m}^{\circ}$(298.15K)[c]	p_{sat}[d]
		K	K	kJ mol^{-1}	kJ mol^{-1}	mPa
This Work	T	323.2-372.8	346.4	99.9±0.4	101.5±0.6	0.93
Santos 2011 [5]	K	323.3-375.4	350.8	100.5±0.5	102.2±0.7	0.89
Siddiqi 2009 [6]	K	339.3-398.6	379.1	96.2±1.4	98.5±1.5[e]	0.99[e]
Goldfarb 2008 [7]	K	322.2-348.2	337.8	98.4±1.6	99.6±1.7	0.77
Bender 2008 [8]	T	353.6-398.6	374.8	94.7±0.6	97.2±0.9	1.29
Chen 2006 [9]	K	320.2-354.1	337.9	93.4±2.5	94.6±2.6	1.44
R. da Silva 2006 [10]	K	340.4-360.4	349.8	107.0±0.6	108.6±1.2	0.56
Oja 1998 [11]	K	300.9-347.3	326.2	100.1±1.6	100.9±1.6	0.85
Hansen 1986 [12]	T	313.2-363.2	337.4	102.6±1.3	103.9±1.4	0.78
Macknick 1979 [13]	T	358.4-393.1	375.9	94.7±0.1	97.3±0.8	1.29
Kruif 1979 [14]	W	337.7-360.9	352.6	100.4±0.0	102.1±0.9	0.83
Kelley 1964 [15]	D	368.2-378.2	373.1	98.2±0.8	100.6±2.5	0.80
					100.9±0.3[f]	0.95[g]

[a] Author and year of publication [b] Methods: T: Transpiration Method, K: Knudsen Effusion, W: Torsion- and Weighing-Effusion, D: dynamic method, [c] Enthalpies of Sublimation were adjusted according to *Chickos et al.* [4] with $\Delta_{cr}^{g}C_{p,m}^{\circ}$ = 32.5 J mol^{-1} K^{-1} and $C_{p,m}^{\circ}$(cr) = 211.7 J mol^{-1} K^{-1} (see Table 11) [d] Vapor pressure at 298.15 K. [e] For data analysis the apparently erroneous data points (p_{sat}/T_{exp}): 1.18 Pa / 369.85 K and 0.577 Pa / 383.95 K were disregarded. [f] Weighted average value, calculated using uncertainty as the weighing factor. [g] Average value.

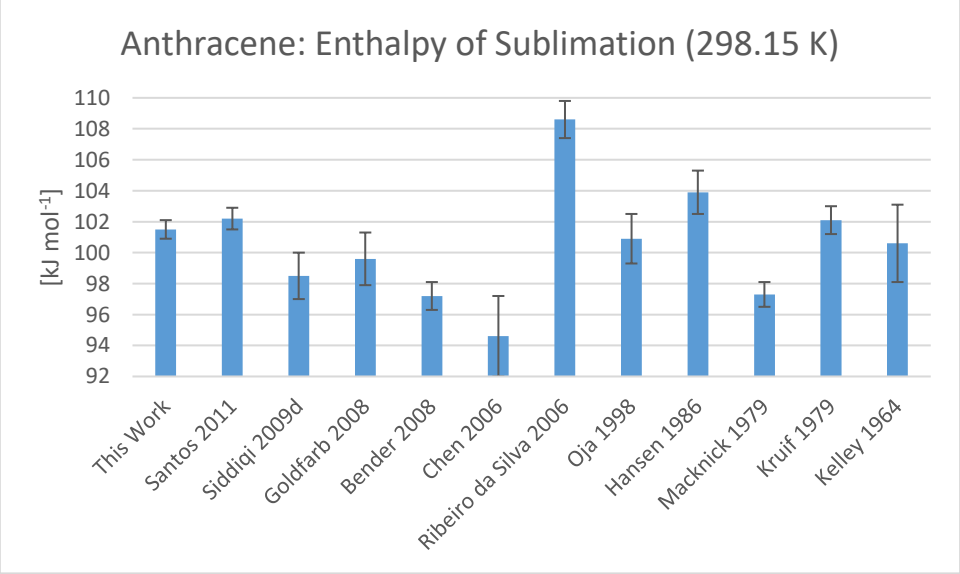

Figure 7 - Comparison of Enthalpies of Sublimation at 298.15 K for Anthracene. (cf. Table 4)

Anthracene is the reference compound with the lowest volatility analyzed within this work. The literature data compiled in Table 4 includes six Knudsen-effusion measurements, four transpiration method experiments, one torsion- and weighing-effusion experiment and one dynamic method measurement. (cf. Table 4) The enthalpies of sublimation $\Delta_{cr}^{g}H_{m}^{\circ}$(298.15 K) available in the literature spread from 94.6 ± 2.6 kJ mol^{-1} reported by *Chen et al.* [9] to 108.6 ± 1.2 kJ mol^{-1} reported by *Ribeiro da Silva et al.* [10]. A graphic visualization of all sublimation enthalpies $\Delta_{cr}^{g}H_{m}^{\circ}$(298.15 K) compiled in Table 4 for anthracene can be found in Figure 7. The value obtained in this work (101.5 ± 0.6 kJ mol^{-1}) is in very good agreement with the uncertainty-weighted average value 100.9±0.3 kJ mol^{-1} derived from all available $\Delta_{cr}^{g}H_{m}^{\circ}$(298.15 K)-values. (cf. Table 4) A Clausius-Clapeyron plot of selected datasets

can be found in Figure 5. The data from this work was plotted together with the set of data from *Santos et al.* [5] in Figure 6. The absolute vapor pressures measured in this work are in a good agreement with this most recent measurement. Few points from the dataset reported by *Siddiqi et al.* [6] (p_{sat}/T_{exp}): 1.18 Pa/369.85 K and 0.577 Pa / 383.95 K. (cf. Figure 5) seem to be erroneous. They were excluded from data treatment (see Table 4).

The vapor pressures of anthracene at 298.15 K that were calculated from each individual complete dataset are compiled in Table 4. The mean value of 0.95 mPa can be considered as a recommendation for the ambient condition vapor pressure of anthracene.

7.1.3 *iso*-amyl acetate

Table 5 - iso-Amyl acetate: absolute vapor pressures p_{sat} and thermodynamic properties of vaporization obtained by the transpiration method in this work

iso-amyl acetate : $\Delta_l^g H_m^\circ$ (298.15 K) = 46.28 ± 0.40 kJ mol^{-1}

$$\ln p_{sat}/p^\circ = \frac{285.8}{R} - \frac{68908.5}{RT} + \frac{75.9}{R} ln \frac{T}{298.15K}$$

T_{exp}[a] [K]	m[b] [mg]	V_{N2}[c] [dm³]	T_{amb}[d] [K]	Gasflow [dm³ h^{-1}]	p_{sat}[e] [Pa]	$u(p_{sat})$[f] [Pa]	$\Delta_l^g H_m^\circ$ [kJ mol^{-1}]	$\Delta_l^g S_m^\circ$ [J mol^{-1} K^{-1}]
263.6	2.69	1.07	296.0	2.00	56.9	1.5	48.90	123.4
268.4	3.03	0.730	295.9	1.99	87.6	2.2	48.54	122.3
273.4	2.95	0.471	296.0	1.01	127	3	48.16	120.8
278.3	3.31	0.353	296.0	1.01	187	5	47.78	119.4
283.3	4.64	0.337	295.6	1.01	269	7	47.41	118.2
288.2	6.57	0.337	295.7	1.01	378	9	47.03	116.8
293.2	6.78	0.252	295.8	1.01	517	13	46.66	115.4

[a] Saturation temperature ($u(T)$ = 0.1 K). [b] Mass of transferred sample condensed at T = 243 K [c] Volume of nitrogen ($u(V)$ = 0.005 dm³) used to transfer m ($u(m)$ = 0.0001 g) of the sample. [d] T_a is the temperature of the soap bubble meter used for measurement of the gas flow. [e] Vapor pressure at temperature T, calculated from the m and the residual vapor pressure at the condensation temperature calculated by an iteration procedure; p° = 1 Pa. [f] Standard uncertainty in p was calculated with $u(p/\text{Pa})$ = 0.005+0.025(p/Pa) for p < 5 Pa and $u(p/\text{Pa})$ = 0.025+0.025(p/Pa) for p > 5 to 3000 Pa.

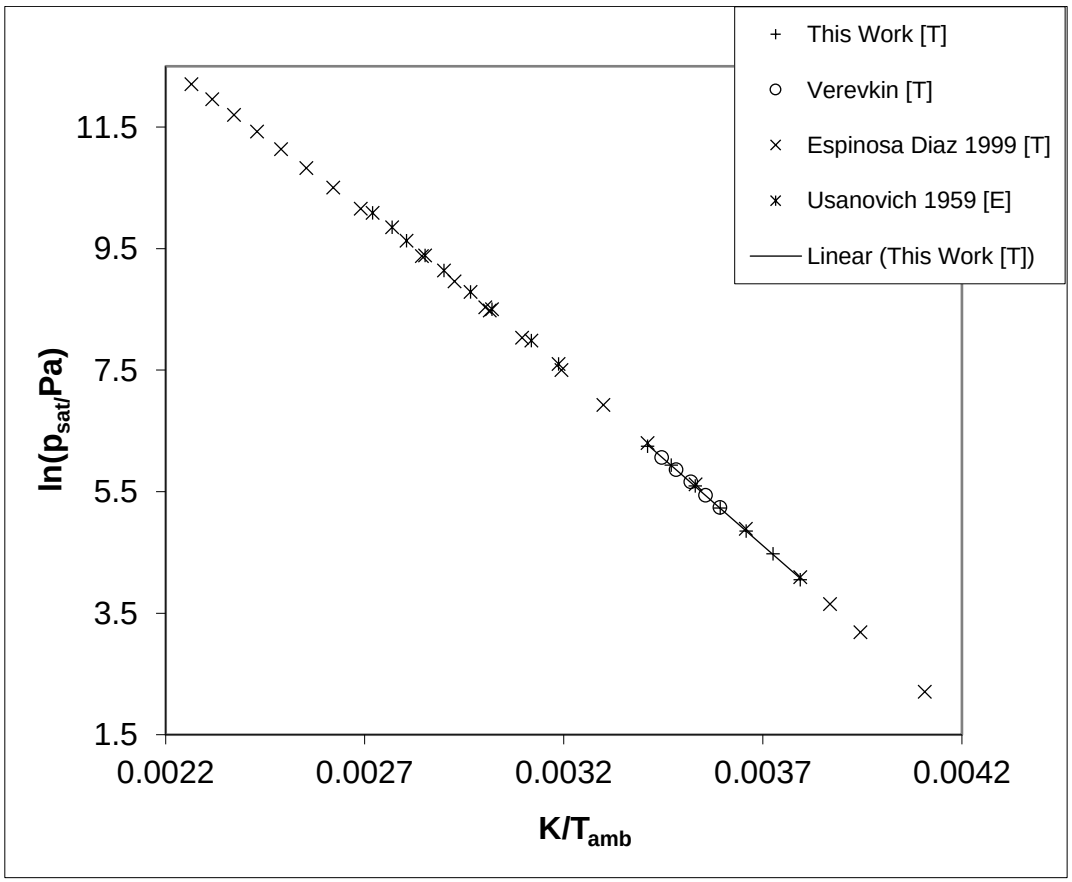

Figure 8 – Experimental vapor pressure of iso-amyl acetate in comparison with literature values.

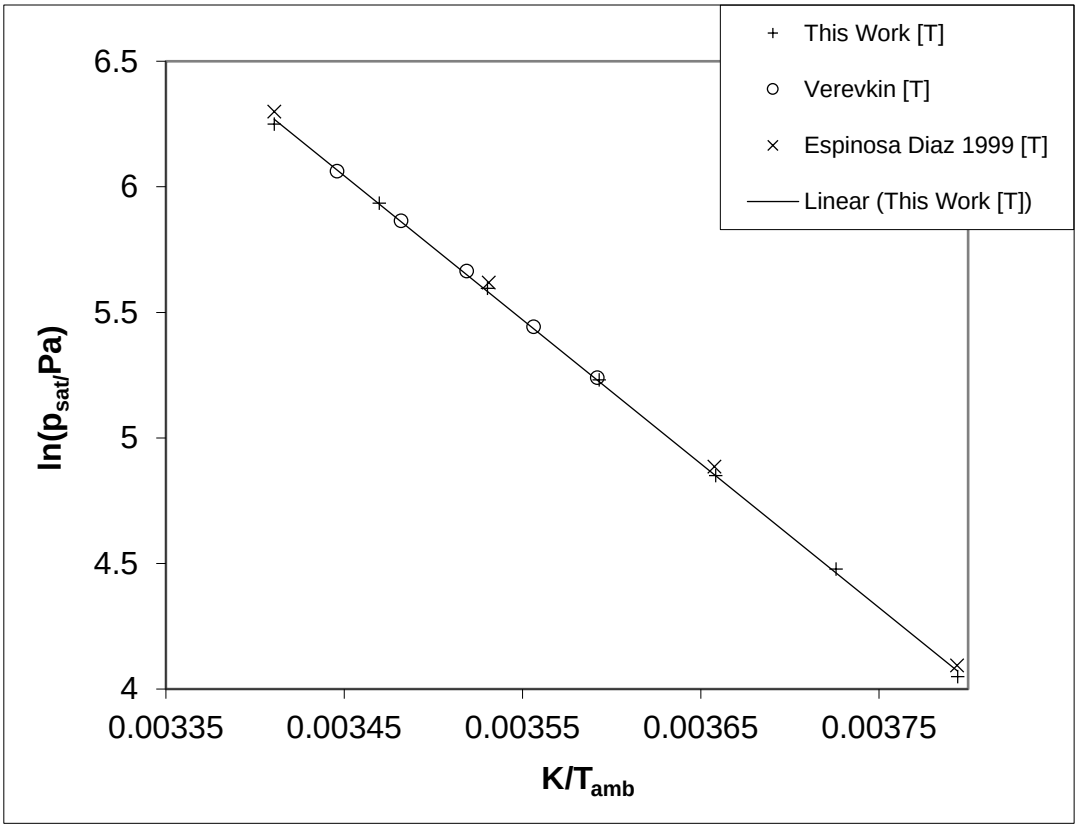

Figure 9 – Experimental vapor pressure of iso-amyl acetate. Zoom on datapoints measured within this work.

Table 6 – Compilation of Data on Enthalpies of Vaporisation $\Delta_c^g H_m$ of iso-amyl acetate

Experiment[a]	Method[b]	T-Range	T_{avg}	$\Delta_l^g H_m^\circ(T_{avg})$	$\Delta_l^g H_m^\circ$(298.15K)[c]	p_{sat}[d]
		K	K	kJ mol^{-1}	kJ mol^{-1}	Pa
This Work	T	263.6-293.2	278.0	48.0±0.3	46.3±0.4	720
Verevkin 1999 [16]	T	278.4-290.2	284.2	46.9±0.4	45.8±0.7	718
Espinosa D. 1999 [17]	S	225-442	315.2	45.7±0.6	46.8±0.2	763
Usanovich 1959 [18]	E	313.8-367.7	341.74	44.2±0.3	47.3±0.4	779
					46.7±0.2[e]	745[f]

[a] Author and year of publication, [b] Methods: T: Transpiration Method, S: Static Method, E: Ebulliometry [c] Enthalpies of vaporization were adjusted according to *Chickos et al.* [4] with $\Delta_l^g C_{p,m}^\circ$= 75.9 J mol^{-1} K^{-1} and $C_{p,m}^\circ$(liq) = 251.4 J mol^{-1} K^{-1} (see Table 11) [d] Vapor pressure at 298.15 K. [e] Weighted average value, calculated using uncertainty as the weighing factor. [f] Average value.

Iso-amyl acetate is the most volatile reference compound whose vaporization characteristics were analyzed. Literature data for comparison was reported by *Verevkin et al*. [16] with a transpiration method dataset, *Espinosa Díaz et al.* [17] with a static method dataset and *Usanovich et al.* [18] with a high temperature ebulliometry dataset. The high precision static method measurement by *Espinosa Díaz et al.* [17] is ideal for benchmarking of the data obtained with the transpiration method since it was generated by a highly reliable direct measurement of the vapor pressure.

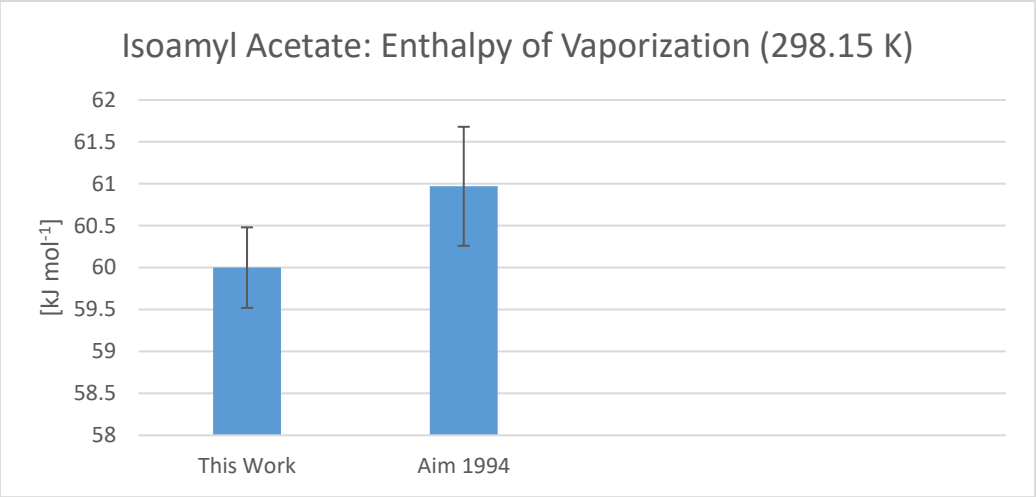

Figure 10 - Comparison of enthalpies of sublimation at 298.15 K for iso-amyl acetate. (cf. Table 6)

The enthalpies of vaporization of *iso*-amyl acetate at 298.15 K are compiled in Table 6 and visualized in Figure 10. The value measured in this work (46.3 ± 0.4 kJ mol^{-1}) is in agreement with the measurements by *Verevkin et al*. [16], *Espinosa Díaz et al.* [17] and *Usanovich et al.* [18]. A weighted average value of 46.7 ± 0.2 kJ mol^{-1} was calculated from all available data using the uncertainty of the values as the weighing factor.

The vapor pressures of *iso*-amyl acetate at 298.15 K that were calculated from each individual complete dataset are compiled in Table 6. The mean value of 745 Pa can be considered as a recommendation for the ambient condition vapor pressure of *iso*-amyl acetate.

7.1.4 n-Hexanol

Table 7 – n-Hexanol: absolute vapor pressures p_{sat} and thermodynamic properties of vaporization obtained by the transpiration method in this work

n-Hexanol: $\Delta_l^g H_m^\circ$ (298.15 K) = 61.70 ± 0.23 kJ mol^{-1}

$$\ln p_{sat}/p^\circ = \frac{329.4}{R} - \frac{86832.2}{RT} + \frac{84.3}{R} ln \frac{T}{298.15K}$$

T_{exp} [a] [K]	m [b] [mg]	V_{N2} [c] [dm³]	T_{amb} [d] [K]	Gasflow [dm³ h^{-1}]	p_{sat} [e] [Pa]	$u(p_{sat})$ [f] [Pa]	$\Delta_l^g H_m^\circ$ [kJ mol^{-1}]	$\Delta_l^g S_m^\circ$ [J mol^{-1} K^{-1}]
273.5	1.07	2.61	297.3	2.00	10.2	0.3	63.78	156.8
278.4	1.12	1.69	295.9	2.01	16.3	0.4	63.36	155.1
283.3	0.99	0.929	298.0	1.99	26.3	0.7	62.95	153.6
288.3	3.08	1.75	295.9	1.98	42.7	1.1	62.53	152.4
293.3	3.11	1.16	295.9	1.98	65.2	1.7	62.11	150.8
298.2	3.01	0.729	298.5	1.99	101	3	61.7	149.5
303.2	3.06	0.497	298.1	1.99	149	4	61.28	148.0
308.2	5.70	0.633	297.6	2.00	218	5	60.85	146.5
313.1	6.02	0.454	298.0	1.01	322	8	60.44	145.3
318.1	5.74	0.302	298.0	1.01	461	12	60.02	144.0
323.1	5.45	0.202	298.1	1.01	656	16	59.60	142.7

[a] Saturation temperature ($u(T)$ = 0.1 K). [b] Mass of transferred sample condensed at T = 243 K [c] Volume of nitrogen ($u(V)$ = 0.005 dm^3) used to transfer m ($u(m)$ = 0.0001 g) of the sample. [d] T_a is the temperature of the soap bubble meter used for measurement of the gas flow. [e] Vapor pressure at temperature T, calculated from the m and the residual vapor pressure at the condensation temperature calculated by an iteration procedure; p° = 1 Pa. [f] Standard uncertainty in p was calculated with $u(p/\text{Pa})$ = 0.005+0.025(p/Pa) for p < 5 Pa and $u(p/\text{Pa})$ = 0.025+0.025(p/Pa) for p > 5 to 3000 Pa.

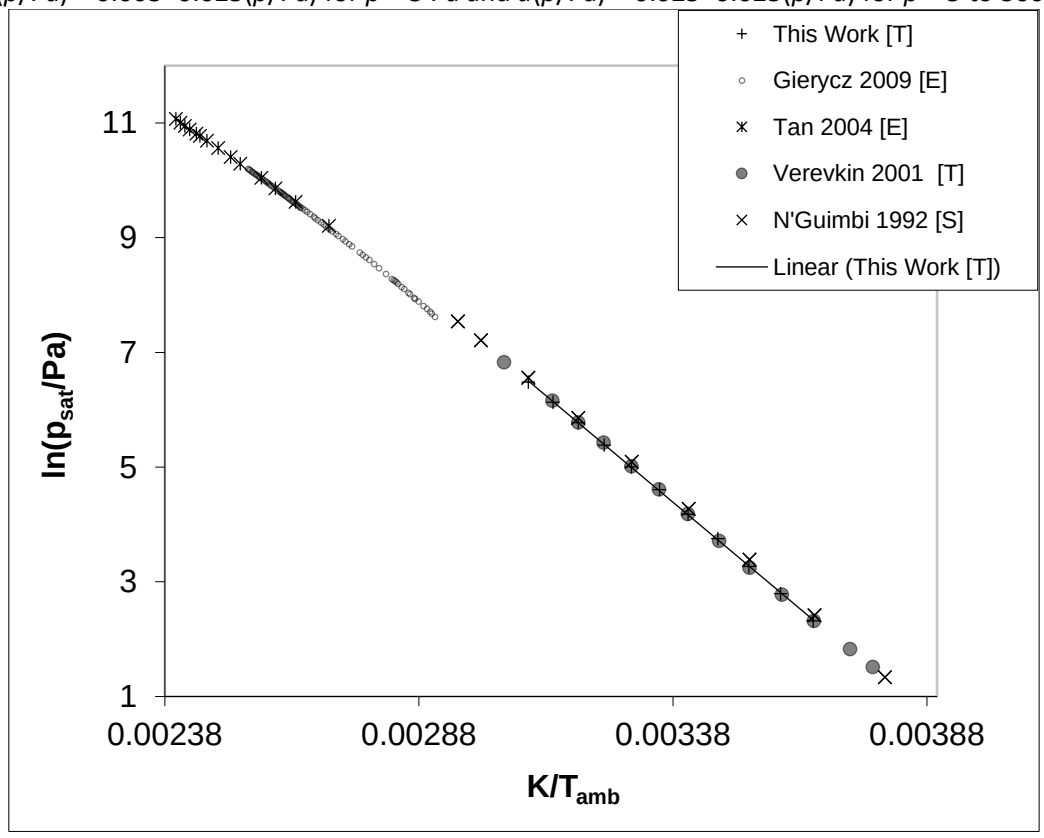

Figure 11 – Experimental vapor pressure of n-hexanol in comparison with literature values.

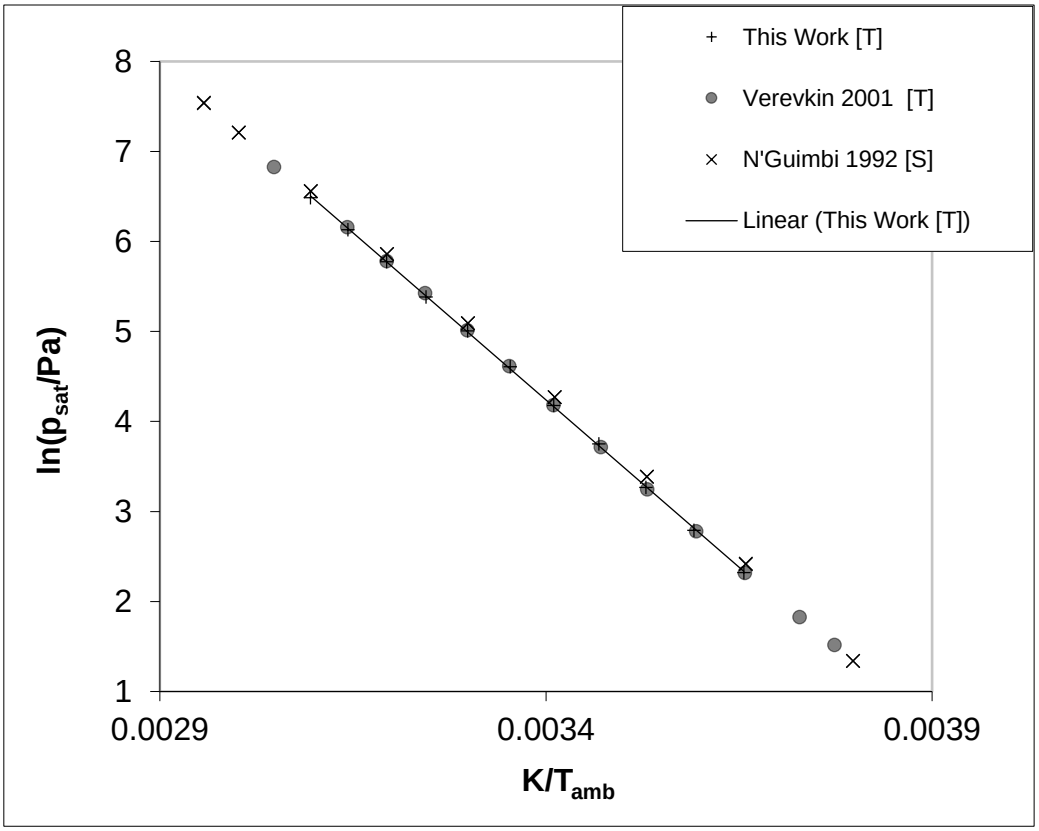

Figure 12 – Experimental vapor pressure of n-hexanol. Zoom on datapoints measured within this work.

Table 8 – Compilation of Data on Enthalpies of Vaporization $\Delta_l^g H_m^\circ$ of n-Hexanol.

Experiment[a]	Method[b]	T-Range	T_{avg}	$\Delta_l^g H_m^\circ(T_{avg})$	$\Delta_l^g H_m^\circ$(298.15K)[c]	p_{sat}[d]
		K	K	kJ mol^{-1}	kJ mol^{-1}	Pa
This Work	T	273.5-323.1	297.4	61.8±0.15	61.7±0.2	99
Gierycz 2009 [19]	E	343.46-393.15	371.84	57.5±0.14	63.4±0.5	81
Tan 2004 [20]	E	369.95-416.39	399.47	51.0±0.14	59.1±0.6	121
Verevkin 2001 [21]	T	265.0-328.1	292.5	61.5±0.31	61.1±0.4	100
N'Guimbi 1992 [22]	S	253.4-338.2	297.6	61.4±0.06	61.1±0.1	109
Mansson 1977 [23]	C				61.85±0.20	
Wadsö 1966 [24, 25]	C				61.63±0.17	
Green 1960 [26]	C				62.8±1.3	
					61.4±0.1[e]	102[f]

[a] First author and year of publication, [b] Methods: T: Transpiration, E: Ebulliometry, S: Static Method C: Calorimetry [c] Enthalpies of vaporization were adjusted according to *Chickos et al.* [4] with $\Delta_l^g C_{p,m}^\circ$= -84.3 J mol^{-1} K^{-1} and $C_{p,m}^\circ$(liq)= 240.1 J mol^{-1} K^{-1} (see Table 11) [d] Vapor pressure at 298.15 K. [e] Weighted average value, calculated using uncertainty as the weighing factor. [f] Average value

n-Hexanol is a medium volatility reference compound. The literature data compiled in Table 8 includes direct calorimetric vaporization enthalpy measurements by *Mansson et al.* [23], *Wadsö et al.* [24] and *Green et al.* [26], a static method measurement by *N'Guimbi* [22], two recent high temperature ebuliometric measurements by *Tan et al.* [20] and *Gierycz et al.* [19] and a transpiration experiment *by Verevkin et al.* [21]. In this work the vapor pressure of the medium volatility compound n-hexanol was

measured in the temperature range from 273.5 K to 323.1 K. The enthalpies of vaporization of n-hexanol at 298.15 K are compiled in Table 8 and visualized in Figure 13. The value measured in this work (61.7 ± 0.2 kJ mol^{-1}) is in a good agreement with all literature data values besides the high temperature ebuliometry measurements by *Tan et al.* [20] and *Gierycz et al.* [20] and the static method data measured by *N'Guimbi et al.* [22]. The best agreement can be found by comparing the data obtained in this work with the direct calorimetric measurements.

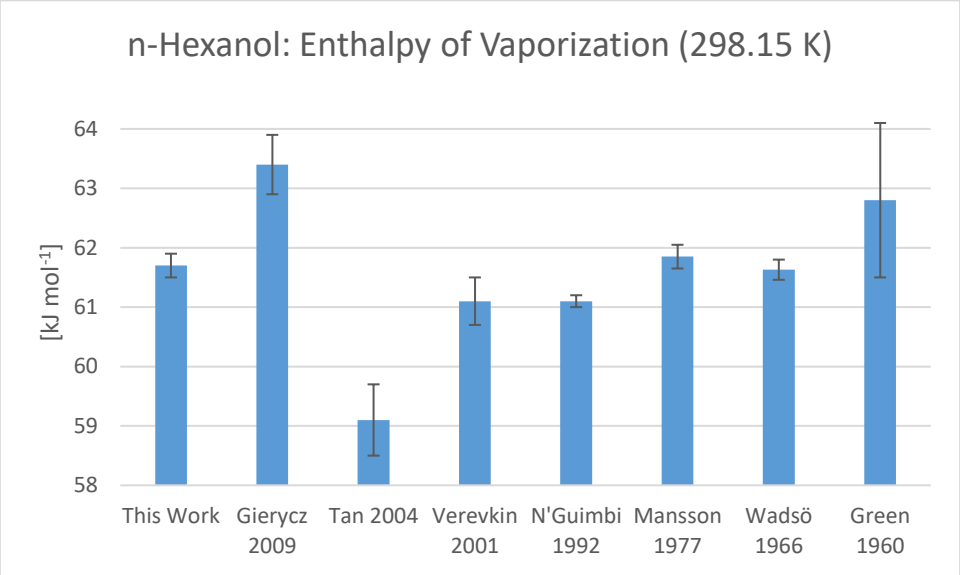

Figure 13 - Comparison of Enthalpies of Vaporization at 298.15 K for n-hexanol. (cf. Table 8)

Based on the data available a weighted average value of 61.4 ± 0.1 kJ mol^{-1} was calculated using the uncertainty of the values as the weighing factor.

The *p*-*T*-data of this work was plotted together with that of the literature in Figure 11 and Figure 12. The vapor pressures of n-hexanol at 298.15 K that were calculated from each individual complete dataset are compiled in Table 8. The mean value of 102 Pa can be considered as a recommendation for the ambient condition vapor pressure of n-hexanol.

7.1.5 n-Octanol

Table 9 – n-Octanol: absolute vapor pressures p_{sat} and thermodynamic properties of vaporization obtained by the transpiration method in this work

n-Octanol: $\Delta_l^g H_m^\circ$ (298.15 K) = 71.02 ± 0.43 kJ mol^{-1}

$$\ln p_{sat}/p^\circ = \frac{361.4}{R} - \frac{101940.0}{RT} + \frac{103.7}{R} ln \frac{T}{298.15K}$$

T_{exp} [a] [K]	m [b] [mg]	V_{N2} [c] [dm³]	T_{amb} [d] [K]	Gasflow [dm³ h^{-1}]	p_{sat} [e] [Pa]	$u(p_{sat})$ [f] [Pa]	$\Delta_l^g H_m^\circ$ [kJ mol^{-1}]	$\Delta_l^g S_m^\circ$ [J mol^{-1} K^{-1}]
283.3	1.10	8.99	295.7	1.99	2.33	0.06	72.57	167.5
288.2	1.17	5.79	296.1	2.00	3.84	0.10	72.05	165.4
293.2	0.99	3.00	296.1	2.00	6.24	0.18	71.54	163.5
298.2	1.15	2.10	295.8	2.00	10.4	0.3	71.02	161.9
303.2	1.00	1.17	296.1	2.00	16.2	0.4	70.5	160.0
308.2	1.03	0.745	295.9	1.02	26.0	0.7	69.98	158.5
313.1	1.02	0.475	297.4	1.02	40.7	1.0	69.47	157.0
318.1	2.03	0.635	297.5	1.00	60.6	1.5	68.95	155.2
323.1	2.06	0.422	296.4	1.01	92.5	2.3	68.44	153.8

[a] Saturation temperature ($u(T)$ = 0.1 K). [b] Mass of transferred sample condensed at T = 243 K [c] Volume of nitrogen ($u(V)$ = 0.005 dm³) used to transfer m ($u(m)$ = 0.0001 g) of the sample. [d] T_a is the temperature of the soap bubble meter used for measurement of the gas flow. [e] Vapor pressure at temperature T, calculated from the m and the residual vapor pressure at the condensation temperature calculated by an iteration procedure; p° = 1 Pa. [f] Standard uncertainty in p was calculated with $u(p/\text{Pa})$ = 0.005+0.025(p/Pa) for p < 5 Pa and $u(p/\text{Pa})$ = 0.025+0.025(p/Pa) for p > 5 to 3000 Pa.

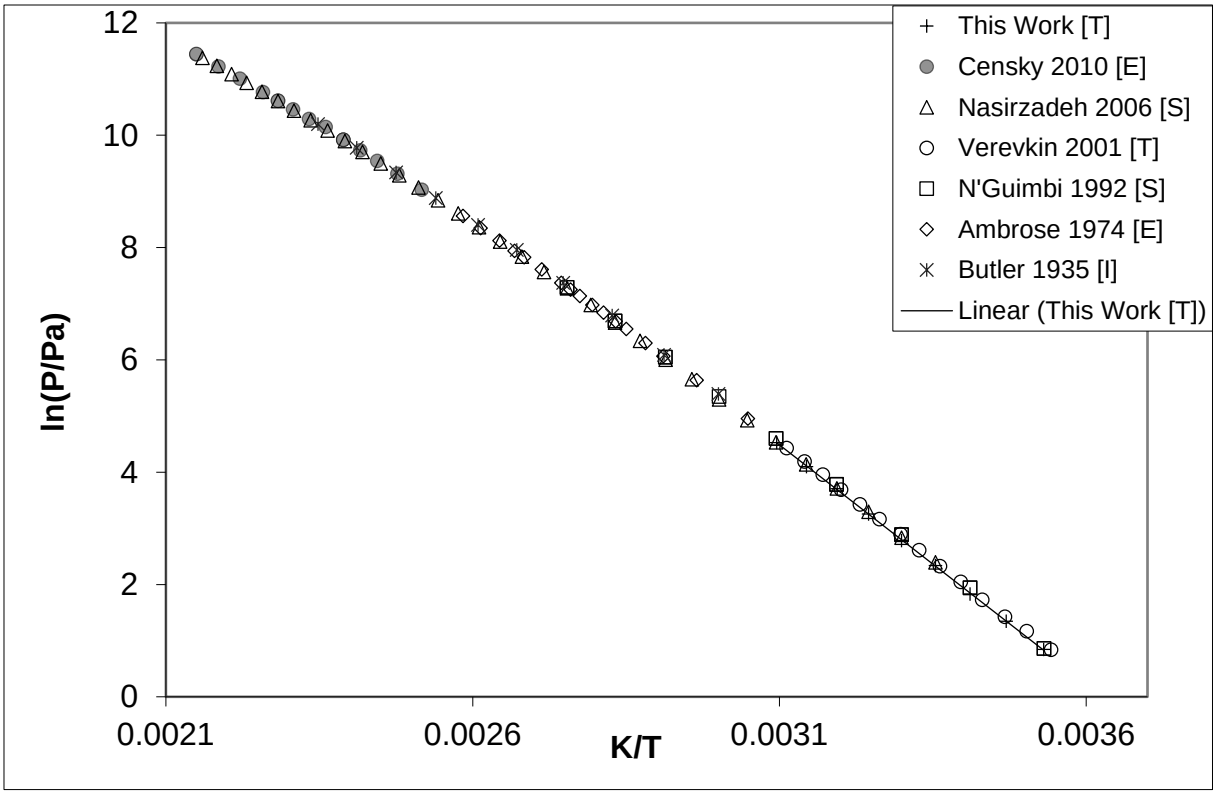

Figure 14 – Experimental vapor pressure of n-octanol in comparison with literature values.

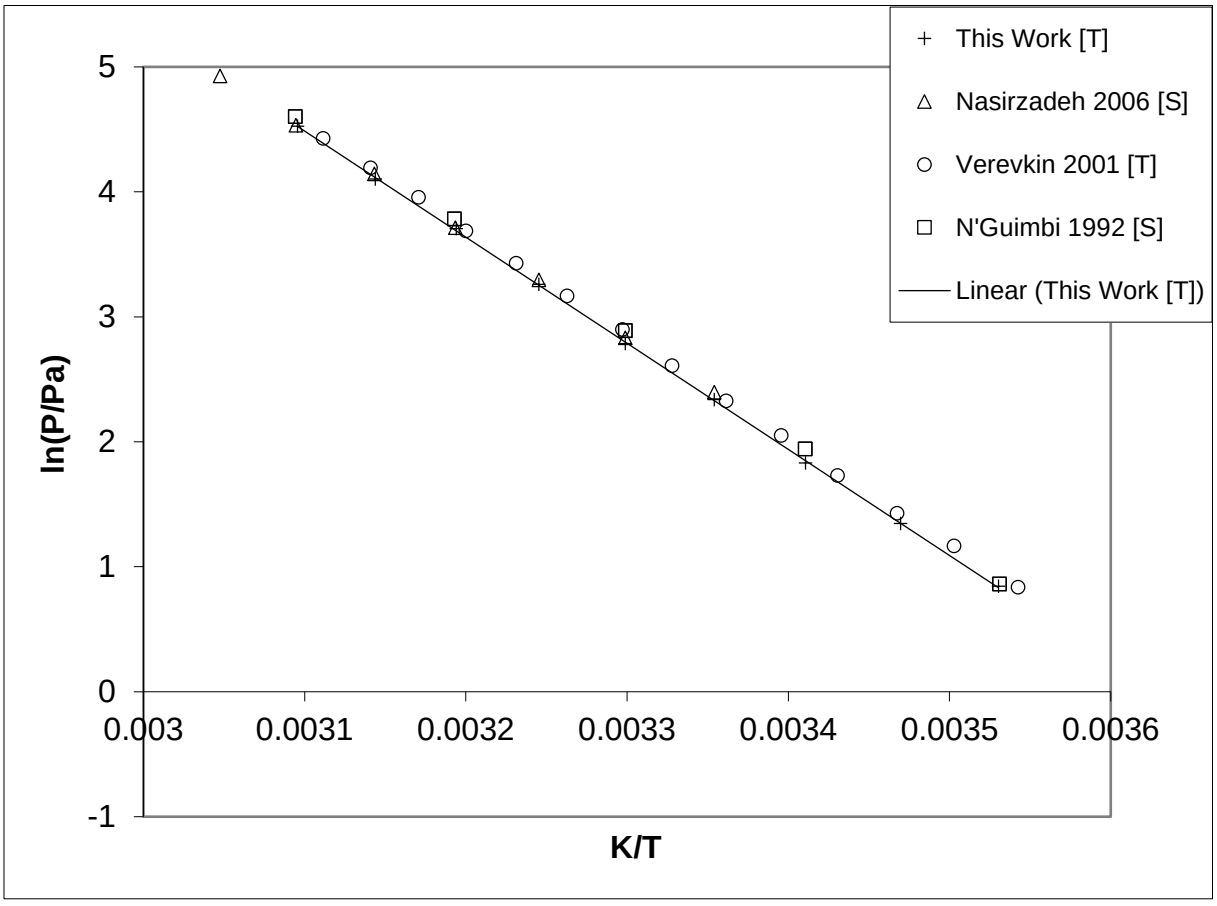

Figure 15 – Experimental vapor pressure of n-octanol. Zoom on datapoints measured within this work.

Table 10 – Compilation of data on enthalpies of vaporization $\Delta_l^g H_m^\circ$ of n-octanol

Experiment[a]	Method[b]	T-Range	T_{avg}	$\Delta_l^g H_m^\circ(T_{avg})$	$\Delta_l^g H_m^\circ$(298.15K)[c]	p_{sat}[d]
		K	K	kJ mol^{-1}	kJ mol^{-1}	
This Work	T	283.3-323.1	302.61	70.6±0.4	71.0±0.4	10.4
Censky 2010 [27]	E	397.31-465.29	429.85	54.2±0.2	(68.0±0.7)	(14.4)
Nasirzadeh 2006 [28]	S	298.2-463.2	374.24	62.6±0.1	70.1±0.5	11.1
Verevkin 2001 [21]	T	282.3-321.4	301.46	69.8±0.3	70.1±0.4	11.1
N'Guimbi 1992 [22]	S	273.3-363.2	314.72	69.5±0.2	71.2±0.2	11.1
Ambrose 1974 [29]	E	328.03-386.96	359.56	64.4±0.1	70.5±0.4	11.4
Butler 1935 [30]	I	333.3-425.9	376.79	61.1±0.3	(69.2±0.3)	(12.8)
Mansson 1977 [23]	C				71.98±0.42	
Green 1960 [26]	C				72.8±1.7	
					71.0±0.1[e]	11.0[f]

[a] First author and year of publication, [b] Methods: T: Transpiration, E: Ebulliometry, S: Static Method, I: Isoteniscope, C: Compiled Data [c] Enthalpies of vaporization were adjusted according to *Chickos et al.* [4] with $\Delta_l^g C_{p,m}^\circ$= -103.7 J mol^{-1} K^{-1} and $C_{p,m}^\circ$(liq) = 305.2 J mol^{-1} K^{-1} (see Table 11) [d] Vapor pressure at 298.15 K. [e] Weighted average value, calculated using uncertainty as the weighing factor. [f] Average value. Values in brackets were not used for calculation of average value.

The vapor pressure of the medium volatility compound n-octanol was measured in this work in the temperature range from 283.3 K to 323.1 K. An enthalpy of vaporization $\Delta_l^g H_m^\circ$(298.15 K) of 71.0 ± 0.4 kJ mol^{-1} was derived from the transpiration experiment in this work. (cf. Table 9) Literature data is compiled for comparison in

Table 10 and illustrated in Figure16.

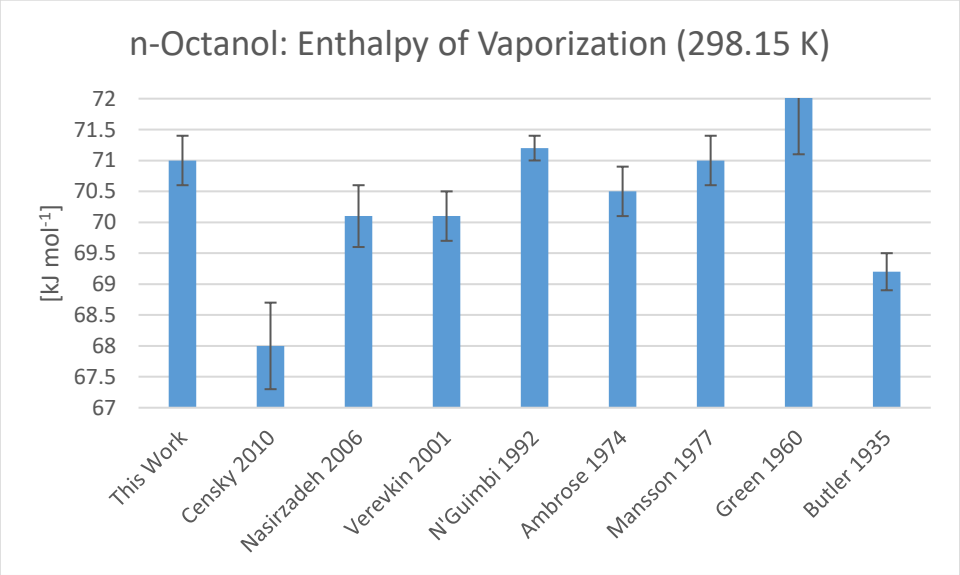

Figure16 Comparison of enthalpies of vaporization at 298.15 K for n-octanol. (cf. Table 10).

The vaporization enthalpy measured in this work is in very good agreement with those derived from the static method measurement by *N'Guimbi et al.* [22], the Ebuliometry measurement by Ambrose and the calorimetric measurements. Based on the data available, a weighted average value of 71.0 ± 0.1 kJ mol^{-1} was calculated using the uncertainty of the literature values as the weighing factor. Our value (71.0 ± 0.4 kJ mol^{-1}) is in agreement with the averaged result. Vaporization enthalpies derived from *Censky et al.* [27] and *Butler et al*. [30] are in poor agreement with other results and they were

excluded from the average value calculation. The *p*-*T*-data for n-octanol (cf. Figure 14, Figure 15) available in the literature are in very good agreement.

Regarding the p-T-data all measurements agree excellently based on graphical comparison. The vapor pressures of n-octanol at 298.15 K (see Table 10) that were calculated from each individual complete dataset are compiled in Table 6. The arithmetic mean value of 11.0 Pa can be considered as a recommendation for the ambient condition vapor pressure of *n*-octanol.

7.1.6 Purity of used Chemicals

Table 11 - Origin and Purity of the Compounds Investigated

compound	CAS#	Distributor	Product #	Lot #	purity	GC-FID-purity
iso-Amyl acetate	123-92-2	Fisher Chemicals	A/6880/08	1378565	>0.98	0.999
Naphthalene	91-20-2	Bayer	LLB LEV-C703	5H531	„pure“	0.999
Anthracene	120-12-7	Acros Organics	104861000	A0345887	0.99	0.999
n-Hexanol	111-27-3	Sigma-Aldrich	471402	SHBF4653V	≥0.99	0.999
n-Octanol	111-87-5	Sigma-Aldrich	297887	STBD7196V	≥0.99	0.999

Table 11 lists Name, CAS#, distributer, Product #, Lot #, manufacturer purity statement and GC-FID-purity. All purities were checked with a GC-FID setup and the mass of analyte sample used for GC/MS quantification corrected by the purity obtained.

7.1.7 Compilation of Heat Capacities and Heat Capacity Differences

Table 12 - Calculation of Molar Heat Capacity Differences at T = 298.15 K

compound	$C^o_{p,m}$(l)	$C^o_{p,m}$(cr)	$C^o_{p,m}$(l)	$C^o_{p,m}$(cr)	$\Delta^g_l C^o_{p,m}$	$\Delta^g_{cr} C^o_{p,m}$
	exp.	exp.	calc.	calc.		
	[J mol^{-1} K^{-1}]	[J mol^{-1} K^{-1}]	[J mol^{-1} K^{-1}]	[J mol^{-1} K^{-1}]	[J mol^{-1} K^{-1}]	[J mol^{-1} K^{-1}]
iso-Amyl acetate	251.4[31]		(254.1)		-75.9[a]	
Naphthalene		165.7[32, 33]		(158.2)		-25.6[a]
Anthracene		211.7[33]		(211.4)		-32.5[a]
n-Hexanol	240.1[21]		(247.5)		-84.3[b]	
n-Octanol	305.2[21]		(311.3)		-103.7[b]	

Bracketed values not used for calculation of heat capacity differences. a) calculated by $\Delta^g_l C^o_{p,m} = 10.58 + C^o_{p,m}(\mathrm{l}) \times 0.26$ [4] b) calculated with experimental values for $C^o_{p,m}$(g) [34] c) calculated by $\Delta^g_{cr} C^o_{p,m} = 0.75 + C^o_{p,m}(\mathrm{cr}) \times 0.15$ [4]

Literature References

[1] M.J.S. Monte, L.M.N.B.F. Santos, M. Fulem, J.M.S. Fonseca, C.A.D. Sousa, New Static Apparatus and Vapor Pressure of Reference Materials: Naphthalene, Benzoic Acid, Benzophenone, and Ferrocene, Journal of Chemical & Engineering Data, 51 (2006) 757-766.
[2] K. Růžička, M. Fulem, V. Růžička, Recommended Vapor Pressure of Solid Naphthalene, Journal of Chemical & Engineering Data, 50 (2005) 1956-1970.
[3] D. Ambrose, I.J. Lawrenson, C.H.S. Sprake, The vapour pressure of naphthalene, The Journal of Chemical Thermodynamics, 7 (1975) 1173-1176.
[4] W. Acree, J.S. Chickos, Phase Transition Enthalpy Measurementsof Organic and Organometallic Compounds. Sublimation, Vaporizationand Fusion Enthalpies From 1880 to 2010, Journal of Physical and Chemical Reference Data, 39 (2010) 043101.
[5] L.M.N.B.F. Santos, L.M.S.S. Lima, C.F.R.A.C. Lima, F.D. Magalhães, M.C. Torres, B. Schröder, M.A.V. Ribeiro da Silva, New Knudsen effusion apparatus with simultaneous gravimetric and quartz crystal microbalance mass loss detection, The Journal of Chemical Thermodynamics, 43 (2011) 834-843.
[6] M.A. Siddiqi, R.A. Siddiqui, B. Atakan, Thermal Stability, Sublimation Pressures, and Diffusion Coefficients of Anthracene, Pyrene, and Some Metal β-Diketonates, Journal of Chemical & Engineering Data, 54 (2009) 2795-2802.
[7] J.L. Goldfarb, E.M. Suuberg, Vapor Pressures and Enthalpies of Sublimation of Ten Polycyclic Aromatic Hydrocarbons Determined via the Knudsen Effusion Method, Journal of Chemical & Engineering Data, 53 (2008) 670-676.
[8] R. Bender, V. Bieling, G. Maurer, The vapour pressures of solids: anthracene, hydroquinone, and resorcinol, The Journal of Chemical Thermodynamics, 15 (1983) 585-594.
[9] X. Chen, V. Oja, W.G. Chan, M.R. Hajaligol, Vapor Pressure Characterization of Several Phenolics and Polyhydric Compounds by Knudsen Effusion Method, Journal of Chemical & Engineering Data, 51 (2006) 386-391.
[10] M.A.V. Ribeiro da Silva, M.J.S. Monte, L.M.N.B.F. Santos, The design, construction, and testing of a new Knudsen effusion apparatus, The Journal of Chemical Thermodynamics, 38 (2006) 778-787.
[11] V. Oja, E.M. Suuberg, Vapor Pressures and Enthalpies of Sublimation of Polycyclic Aromatic Hydrocarbons and Their Derivatives, Journal of Chemical & Engineering Data, 43 (1998) 486-492.
[12] P.C. Hansen, C.A. Eckert, An improved transpiration method for the measurement of very low vapor pressures, Journal of Chemical & Engineering Data, 31 (1986) 1-3.
[13] A.B. Macknick, J.M. Prausnitz, Vapor pressures of high-molecular-weight hydrocarbons, Journal of Chemical & Engineering Data, 24 (1979) 175-178.
[14] C.G. De Kruif, Enthalpies of sublimation and vapour pressures of 11 polycyclic hydrocarbons, The Journal of Chemical Thermodynamics, 12 (1980) 243-248.
[15] J.D. Kelley, F.O. Rice, The Vapor Pressures of Some Polynuclear Aromatic Hydrocarbons1, The Journal of Physical Chemistry, 68 (1964) 3794-3796.
[16] S.P. Verevkin, A. Heintz, Determination of Vaporization Enthalpies of the Branched Esters from Correlation Gas Chromatography and Transpiration Methods, Journal of Chemical & Engineering Data, 44 (1999) 1240-1244.
[17] M.A. Espinosa Díaz, T. Guetachew, P. Landy, J. Jose, A. Voilley, Experimental and estimated saturated vapour pressures of aroma compounds, Fluid Phase Equilibria, 157 (1999) 257-270.
[18] M. Usanovich, Dembitskii A., Vapor Pressure of Systems Formed by Stannic Chloride with Esters., Zhurnal Obshchei Khimii, 29 (1959) 1744-1753.
[19] P. Gierycz, A. Kosowski, R. Swietlik, Vapor−Liquid Equilibria in Binary Systems Formed by Cyclohexane with Alcohols, Journal of Chemical & Engineering Data, 54 (2009) 2996-3001.
[20] T. Tan, H. Li, C. Wang, H. Jiang, S. Han, Isothermal and isobaric vapor–liquid equilibria for the binary system trimethylbenzoquinone + n-hexanol, Fluid Phase Equilibria, 224 (2004) 279-283.
[21] D. Kulikov, S.P. Verevkin, A. Heintz, Enthalpies of vaporization of a series of aliphatic alcohols: Experimental results and values predicted by the ERAS-model, Fluid Phase Equilibria, 192 (2001) 187-207.

[22] J. N'Guimbi, H. Kasehgari, I. Mokbel, J. Jose, Tensions de vapeur d'alcools primaires dans le domaine 0,3 Pa à 1,5 kPa, Thermochimica Acta, 196 (1992) 367-377.
[23] M. Månsson, P. Sellers, G. Stridh, S. Sunner, Enthalpies of vaporization of some 1-substituted n-alkanes, The Journal of Chemical Thermodynamics, 9 (1977) 91-97.
[24] I. Wadsö, A Heat of Vaporization Calorimeter for Work at 25 °C and for Small Amounts of Substances, Acta Chem. Scand., 20 (1966) 536-543.
[25] I. Wadsö, Heats of Vaporization for a Number of Organic Compounds at 25 degrees C., Acta Chem. Scand., 20 (1966) 554-552.
[26] J.H.S. Green, Revision of the values of the heats of formation of normal alcohols, Chem. Ind. (London, U. K.), (1960) 1215-1216.
[27] M. Čenský, V. Roháč, K. Růžička, M. Fulem, K. Aim, Vapor pressure of selected aliphatic alcohols by ebulliometry. Part 1, Fluid Phase Equilibria, 298 (2010) 192-198.
[28] K. Nasirzadeh, R. Neueder, W. Kunz, Vapor Pressure Determination of the Aliphatic C5 to C8 1-Alcohols, Journal of Chemical & Engineering Data, 51 (2006) 7-10.
[29] D. Ambrose, J.H. Ellender, C.H.S. Sprake, Thermodynamic properties of organic oxygen compounds XXXV. Vapour pressures of aliphatic alcohols, The Journal of Chemical Thermodynamics, 6 (1974) 909-914.
[30] J.A.V. Butler, C.N. Ramchandani, D.W. Thomson, 58. The solubility of non-electrolytes. Part I. The free energy of hydration of some aliphatic alcohols, Journal of the Chemical Society (Resumed), (1935) 280-285.
[31] L. Becker, J. Gmehling, Measurement of Heat Capacities for 12 Organic Substances by Tian−Calvet Calorimetry, Journal of Chemical & Engineering Data, 46 (2001) 1638-1642.
[32] J.P. McCullough, H.L. Finke, J.F. Messerly, S.S. Todd, T.C. Kincheloe, G. Waddington, The Low-Temperature Thermodynamic Properties of Naphthalene, l-Methylnaphthalene, 2-Methylnaphthalene, 1,2,3,4-Tetrahydronaphthalene,trans-Decahydronaphthalene and cis-Decahydronaphthalene, The Journal of Physical Chemistry, 61 (1957) 1105-1116.
[33] M. Radomska, R. Radomski, Calorimetric studies of binary systems of 1,3,5-trinitrobenzene with naphthalene, anthracene and carbazole. I. Phase transitions and heat capacities of the pure components and charge-transfer complexes, Thermochimica Acta, 40 (1980) 405-414.
[34] E.S. Domalski, E.D. Hearing, Estimation of the Thermodynamic Properties of C-H-N-O-S-Halogen Compounds at 298.15 K, Journal of Physical and Chemical Reference Data, 22 (1993) 805-1159.

7.2 Measurement of the Peroxides TATP 02 and DADP 03

This chapter deals with the measurement of the vapor pressure of the peroxides TATP **02** and DADP **03**:

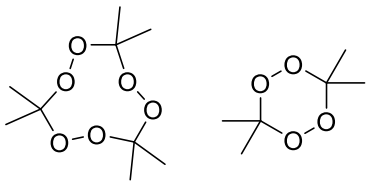

TATP **02** DADP **03**

DOI: 10.1002/prep.201700034

The original publication of the data follows.

1. Härtel, M. A. C.; Klapötke, T. M.; Stiasny, B.; Stierstorfer, J., Gas-phase Concentration of Triacetone Triperoxide (TATP) and Diacetone Diperoxide (DADP). *Propellants, Explosives, Pyrotechnics* **2017,** *42* (6), 623-634.

Full Paper

Propellants, Explosives, Pyrotechnics

DOI: 10.1002/prep.201700034

Gas-phase Concentration of Triacetone Triperoxide (TATP) and Diacetone Diperoxide (DADP)

Martin A. C. Härtel,[a] Thomas M. Klapötke,*[a] Benedikt Stiasny,[a] and Jörg Stierstorfer[a]

Abstract: The present investigation is about the determination of the gas phase concentration parameters of the notorious explosives triacetone triperoxide (TATP, **1**) and diacetone diperoxide (DADP, **2**), which have been frequently used in improvised explosive devices. According to calculations with EXPLO5 the energetic performance of both explosives is similar. The enthalpy of sublimation $\Delta^{g}_{cr}H^{\circ}_{m}$ (298.15 K) (**1:** 76.7 ± 0.7 kJ mol^{-1}; **2:** 75.0 ± 0.5 kJ mol^{-1}) and vapor pressures p_{sat}(298.15 K) (**1:** 6.7 Pa, **2:** 26.6 Pa) of both compounds have been studied using the transpiration method in the ambient temperature range of 274–314 K. The results obtained in this work were compared critically with the existing literature values. Data for DADP (**2**) mostly shows agreement with literature ones. However data of TATP (**1**) obtained in this work revealed insufficient agreement of all sets of data available in literature, which might be explained by the rich polymorphism of TATP **1.** The saturation and diffusion equilibrium concentration of both analytes was calculated at 298.15 K. In comparison to the saturation equilibrium concentration measured in this work (**1:** 600 μg L^{-1}, **2:** 1589 μg L^{-1}) the corresponding estimated diffusion condition air concentrations (**1:** 3.1 ng L^{-1}, **2:** 10 ng L^{-1}, for a surface of 200 cm^2) are lower by five orders of magnitude.

Keywords: Peroxides · Vapor Pressure · Energetic Materials · Air Concentration · Explosive Detection

1 Introduction

Triacetone triperoxide (**1**), also known as TATP, is the condensation product of hydrogen peroxide with acetone and was discovered accidentally by *Wolffenstein* [1] in 1895.

Due to its high volatility and sensitivity toward external stimuli the medium performance explosive is not applied in neither the civil nor the military sector.

With respect to the free availability of its precursors and its readiness for detonation initiation the compound is popular in the amateur chemist and terrorist scene. Unfortunately this was demonstrated by the recent TATP related incident in Oberursel (Germany, 2015, [2]) and the ISIS terror attack in Paris (France, 2015, [3]). A 17 year old teenager (Germany, 2006, [4]) was arrested for hoarding 2 kg of TATP **1**, which underlines the ease of TATP **1** synthesis. Oxley *et al.* investigated the factors influencing the formation of TATP **1** and its side product diacetone diperoxide (DADP, **2**) [5] as well as the destruction of TATP [6]. Lubczyk *et al.* [7] recently published a method for desensitizing TATP for training and testing purposes in an ionic liquid matrix and pointed out that resublimed TATP **1** shows a higher impact (0.1 J) and friction sensitivity of (0.05 N) than the crude product from the aqueous synthesis (0.5 J, 0.2 N) that is stabilized by trace amounts of water. The resublimation of TATP during storage enhances the risk of unintended detonation. With respect to this and the challenging gas phase detection of explosives [8] one of the most interesting parameters of TATP and DADP is their vapor pressure. The sublimation behavior of both peroxides **1** and **2** was measured in this work with the transpiration method and compared critically with the existing literature data. Recommendations for the ambient condition (298.15 K) vapor pressure, saturation and diffusion equilibrium air concentration and enthalpy of sublimation are given (Figure 1).

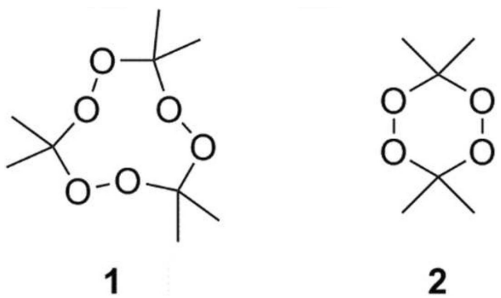

Figure 1. Chemical structures of TATP **1** and DADP **2.**

2 Experimental

All reagents and solvents were used as received (Sigma-Aldrich, Fluka, Acros Organics, ACBR). NMR spectra were

[a] *M. A. C. Härtel, T. M. Klapötke, B. Stiasny, J. Stierstorfer*
Department of Chemistry
University of Munich
Butenandtstr. 9, 81377 Munich, Germany
**e-mail: tmk@cup.uni-muenchen.de*

measured with a *JEOL* ECX-400 and a *Bruker* AVANCE 400 MHz NMR instrument. The chemical shift of the solvent peaks were adjusted according to literature values [38]. Infrared spectra were measured with a *Perkin-Elmer* FT-IR Spektrum BXII instrument equipped with a Smith Dura SampIIR II ATR unit. Transmittance values are described as "strong" (s), "medium" (m), and "weak" (w). Raman spectra were recorded on a *Bruker RAM II* device (1064 nm, 300 mW). Relative peak intensities are given in brackets. Elemental analyses (EA) were performed with a *Netzsch* STA 429 simultaneous thermal analyzer. Sensitivity data were determined using a BAM drophammer and a BAM friction tester. The electrostatic sensitivity tests were carried out using an Electric Spark Tester ESD 2010 EN (*OZM Research*). The particle sizes stated are valid for all sensitivity measurements. Melting points were measured with a *Buechi B-540* melting point apparatus using a heating rate of 5 °C min^{-1}. For the powder diffraction experiment on TATP the analytes were filled into a 0.5 mm Lindemann capillary. The material was then investigated on a Huber G644 Guinier diffractometer with the angle calibrated using electronic grade germanium (a = 5.6575 Å). Measurements with Mo$K_{\alpha 1}$ radition were made over the 2θ range 2–12° with an increment of 0.02° and a counting time of 20 seconds per increment at 25 °C.

CAUTION! TATP ***1*** *and DADP* ***2*** *are energetic materials with sensitivity to various stimuli. While we encountered no issues in the handling of these materials, proper protective measures (face shield, ear protection, body armor, Kevlar gloves, and earthed equipment) should be used during the handling of both compounds at all times including vapor pressure measurements.*

TATP **1:** 3.14 mL 50 % aqueous H_2O_2 solution (3.76 g, 0.11 mol) and 0.86 mL conc. H_2SO_4 (1.58 g, 0.016 mol) are mixed and cooled to 0 °C. 4.90 mL acetone (3.87 g, 0.07 mol) are added dropwise. After stirring the mixture at 0 °C for 3 h, it is extracted with 70 mL pentane. The pentane mixture is washed two times with 20 mL saturated ammonium sulfate solution and afterwards three times with 20 mL of water. The organic phase is dried over magnesium sulfate. After evaporation of the solvent a colorless solid is isolated. (2.07 g, 40 %) [9]

^{1}H NMR ($CDCl_3$, 400 MHz, 300 K): δ = 1.45 (18 H). **^{13}C NMR** ($CDCl_3$, 100 MHz, 300 K): δ = 21.5 (CH_3), 107.7 (*C*). **IR** (ATR): $\tilde{\nu}$ (cm^{-1}) = 3005 (w), 2945 (w), 1600 (w), 1461 (w), 1376 (m), 1361 (m), 1274 (w), 1232 (m), 1200 (m), 1178 (s), 997 (w), 945 (m), 937 (m), 884 (s), 842 (m), 784 (m), 615 (m). **Raman** (1064 nm) $\tilde{\nu}$ (cm^{-1}) = 3012 (55), 3001 (54), 2948 (100), 10450 (30), 1372 (5), 1338 (6), 962 (48), 913 (50), 864 (60), 856 (48), 653 (7), 555 (61), 452 (28), 434 (30), 412 (28), 380 (8). **EA** found (calcd.): C 48.73 (48.63), H: 8.26 (8.18). **IS:** 1.5 J, **FS:** < 5 N, **ESD:** 0.2 J (< 100 μm), **T_{melt}:** 97–98 °C.

DADP **2:** 10 mL dichloromethane are cooled in an ice bath. 2.00 mL acetone (1.58 g, 0.03 mol) and 4.00 mL 30 % aqueous H_2O_2 solution (4.44 g, 0.04 mol) are added. 4.00 mL concentrated perchloric acid (7.08 g, 0.07 mol) are added drop wisely and the mixture was stirred at 0 °C for 1 h. Afterwards the mixture is stored for three days at room temperature to allow complete conversion of TATP to DADP. The formed colorless precipitate is filtered off, washed with water and recrystallized from methanol. (0.23 g, 10 %) [10].

^{1}H NMR ($CDCl_3$, 400 MHz, 300 K): δ = 1.35 (s, 6H), 1.79 (s, 6H). **^{13}C NMR** ($CDCl_3$, 100 MHz, 300 K): δ = 20.7 (CH_3), 22.5 (CH_3), 107.7 (*C*). **IR** (ATR): $\tilde{\nu}$ (cm^{-1}) = 3031 (w), 3000 (w), 2955 (w), 1603 (w), 1452 (w), 1374 (m), 1367 (m), 1284 (w), 1268 (m), 1198 (s), 1006 (w), 943 (m), 930 (m), 858 (m), 839 (w), 814 (m), 686 (m). **Raman** (1064 nm) $\tilde{\nu}$ (cm^{-1}) = 3053 (25), 3004 (100), 2980 (62), 1450 (18), 1417 (21), 1260 (17), 940 (23), 917 (19), 863 (64), 720 (65), 512 (8), 501 (58), 491 (22), 452 (10), 447 (9), 428 (17), 382 (53). **EA** found (calcd.): C 48.24 (48.63), H: 8.13 (8.18), **IS:** 5 J, **FS:** 5 N, **ESD:** 0.2 J (< 100 μm). **T_{melt}:** 132–133 °C.

3 Results and Discussion

3.1 Polymorphism of TATP

TATP was synthesized according to Milas *et al.* [9]. DADP was synthesized according to Landenberger *et al.* [10]. The complete chemical characterization of both compounds can be found in the experimental section. With respect to the six possible solid state polymorphs of TATP reported with crystal structures by Reany *et al.* [11] the TATP synthesized in this work was analyzed with powder X-Ray diffraction to determine its polymorphic composition (see Figure 2). It could be found that the investigated TATP consisted mainly of the main polymorph reported for TATP crude products

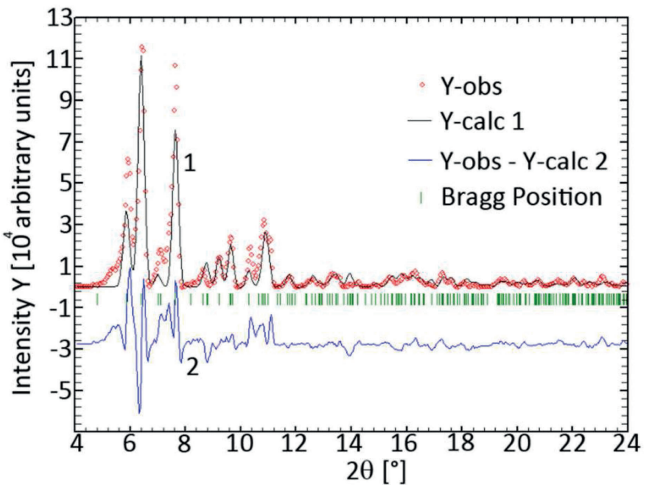

Figure 2. Powder diffractogram of the **TATP** synthesized in this work after Rietveld Refinement in comparison with the calculated diffractogram of the major polymorph (Cif-File #241973, [11–12]) found in TATP crude products. Y-obs: observed reflexes, Y-calc: calculated reflexes, Y-obs – Y-calc: difference of observed and calculated reflexes.

Table 1. Selected energetic parameters and relevant properties of crystalline TATP and DADP synthesized in this work in comparison with crystalline TNT.

	TATP **1**	DADP **2**	TNT
Formula	$C_9H_{18}O_6$	$C_6H_{12}O_4$	$C_7H_5N_3O_6$
MW/g mol^{-1}	222.24	148.16	227.13
IS[a]/J	1.5	5	15
FS[b]/N	<5	5	>360
ESD[c]/mJ	0.2	0.2	0.7
Grain Size/μm	<100	<100	100-500
Ω_{CO}; Ω_{CO2}/ %[d]	−86.4; −151.2	−86.4; −151.2	−24.7; −74.0
T_m [e]./°C	97–98	132–133	80–81
ρ[f]/g cm^{-3}	1.27 [180 K] [15]	1.33 [208 K] [16]	1.71 [100 K]
ρ_{298K}[g]/g cm^{-3}	1.25 [298 K]*	1.31 [298 K]*	1.66 [298 K]*
$\Delta_f H^{\circ}$[h]/kJ mol^{-1}	−640	−435	−54
$\Delta_f U^{\circ}$[i]/kJ kg^{-1}	−2744	−2802	−163
EXPLO5 v6.03 values (calculated for ρ_{298K}[g] of crystalline material)			
$-\Delta_{ex}U$[k]/kJ kg^{-1}	3420	73194	4425
p_{CJ}[l]/[10^8 Pa]	114	131	191
V_{det}[m]/m s^{-1}	6322	6246	6906
V_0[n]/L kg^{-1}	821	815	642

[a] impact sensitivity, BAM drophammer (method 1 of 6); [b] friction sensitivity, BAM friction tester (method 1 of 6); [c] sensitivity toward electrostatic discharge; [d] oxygen balance; [e] melting point range (5 °C min^{-1}, glass capillary); [f] density from X-Ray diffraction; [g] density at 298 K (calculated using the equation ($\rho_{298K}=\rho_T/(1+\alpha_V(298\text{-}T_0)$; $\alpha_V=1.5\ 10^{-4}\,K^{-1}$; [h] calculated heat of formation (CBS-4M); [i] calculated energy of formation (CBS-4M); [j] heat of detonation; [k] detonation pressure; [l] detonation velocity; [m] volume of gases after detonation.

(Cif-File #241973, [11–12]). The discrepancies between the observed and calculated diffractograms can be explained by the presence of further unknown polymorphs.

3.2 Sensitivities and Energetic Properties

Table 1 gives an overview about the energetic properties and other selected parameters of TATP and DADP synthesized in this work and the melt-cast explosive 2,4,6-trinitrotoluene (TNT) for comparison. TATP is very sensitive, while DADP is less sensitive toward impact. Both peroxides are extremely sensitive toward friction. [13] The sensitivity values for TATP are slightly higher than the values stated by Lubczyk *et al.* [7], yet the friction sensitivity measured in this work is at the lower limit of the measurement range of the testing device used (5 N). Both compounds have 200 mJ sensitivity toward electrostatic discharge. With a room temperature density of 1.25 g cm^{-3} (see Table 1) the nine-membered ring system TATP is less dense than the six-membered DADP (1.31 g cm^{-3}). The denser crystal packing in DADP results in the higher melting point range (heating rate 5 °C min^{-1}) of 132–133 °C in comparison to 97–98 °C for TATP. The exothermic enthalpies of formation of both compounds (**1:** −640 kJ mol^{-1}; **2:** −435 kJ mol^{-1}) were calculated on a CBS-4 M level using the *Gaussian 09* [14] software. Based on these values and the theoretical maximum density at 298 K the energetic characteristics were calculated using EXPLO5 v6.03 (BKW EOS, BKWN constants, initial temperature 3600 K). Both peroxides have a similar theoretical detonation pressure p_{CJ} (**1:** 114×10^8 Pa), **2:** 131×10^8 Pa) and detonation velocity V_{det} (**1:** 6322 m s^{-1}, **2:** 6246 m s^{-1}). When compared to crystalline TNT (p_{CJ}: 191×10^8 Pa, V_{det}: 6906 m s^{-1}), the energetic performance of both peroxides is lower.

3.3 VO-GC/MS of TATP and DADP

TATP and DADP were analyzed using vacuum outlet gas chromatography as established by *de* Zeeuw *et al.* [17] using a Shimadzu GC/MS QP2010 SE device equipped with an Atas Optic 4 injector and a Shimadzu AOC-20i autosampler. The necessary restriction (10.1 mm length, 0.05 mm inner diameter, Restek® cat. #10098) was connected to a Restek® RTX TNT 1 column (cat. #12998) with a SGE Siltite® μ-Union (cat. #073562) inside the injector. Due to the incompatibility of the inner diameter of the commercially available Atas liners a custom V2A stainless steel liner (10 mm length, 5 mm outer diameter, 0.5 mm wall thickness, split notches at bottom end) was used. Both the liner and the μ-union were inertized with a Silconert® 2000 coating. The injector was operated at 175 °C in the constant pressure mode with a head pressure of 90 kPa Helium 5.0 carrier gas and a split ratio of 150 in combination with a virtual column (100 m length, 0.25 μm film thickness, 0.20 mm diameter) for the LabSolutions GCMS Solution Software. The injection volume was 1 μL. The GC oven program start temperature was 30 °C with a hold time of 6 seconds followed by a temperature ramp to 204 °C with 60 °C min^{-1}. The temperature of the MS-Interface and the ion source was 200 °C. The mass spectrometer was operated in the single ion monitoring mode

with an event time of 0.10 s and a micro scan width of 0.1 amu. From 0.50 to 2.00 min the mass channels 43, 59, 58 and 75 were monitored for the detection of the peroxides **1** and **2.** From 2.00 to 3.00 min the mass channels 57, 43, 71 and 85 were monitored for the detection of *n*-docecane C-12 as analytical standard in quantification applications.

Figure 3 shows a chromatogram of TATP and DADP in *tert*-butyl methyl ether using the method stated before. DADP elutes after 0.72 min at 67 °C as a single peak whilst one TATP conformer A elutes after 1.37 min at 106 °C and a second TATP conformer B elutes after 1.44 min at 110 °C. The augmented baseline between both conformers indicates the conversion of conformer A to the more stable conformer B during the GC/MS analysis. The solid state polymorphism of TATP has been reported before [11] and two isomers of TATP have been separated by LC-NMR [18]. The activation barrier of an exothermic TATP polymorph interconversion has been calculated to be 110 kJ mol^{-1} [19]. With respect to this the GC/MS behavior of TATP observed in this work can be justified. Both TATP ($R^2 = 0.99995$) and DADP ($R^2 = 0.9998$) could be excellently quantified in concentrations of 20 to 60 μg/mL with an internal standard (C-12) method using the GC/MS configuration detailed above.

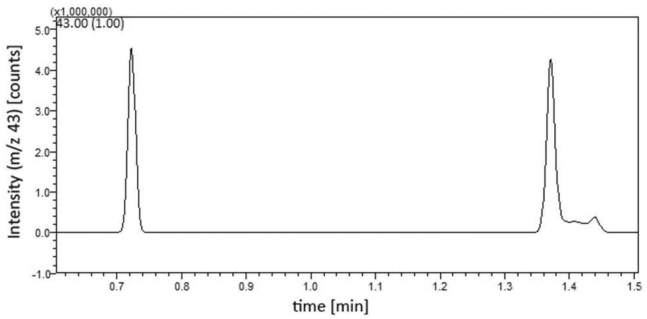

Figure 3. SIM mode (m/z 43) GC/MS chromatogram of TATP (right) and DADP (left).

3.4 Vapor Pressure Measurement

Since the vapor pressure of a compound is the key parameter for its gas phase detectability the vapor pressure of TATP and DADP was measured in this work using the transpiration method. The transpiration method setup adapted in this work has been established by Verevkin *et al.* [20]. For the experiments in this work nitrogen (99.999 % purity) was used as carrier gas. The flow-rate ranging from 1–3 L h^{-1} was adjusted and kept constant using a mass flow controller (Natec Sensors MC-100 CCM). The gas flow is conducted through the saturator, which is a glass vessel surrounding a U-shaped tube (8 mm inner diameter, 50 cm length) and containing a thermofluid, which is pumped through the saturator vessel with a circulation thermostat (Huber Ministat 230 with external class A PT-100 temperature sensor inside the saturator vessel). The peroxide (0.8 g) is coated on glass beads (1 mm diameter, 40 g) and filled into the saturator tube. For the coating of the glass beads with the sensitive peroxide explosives they were dispersed in a minimum amount of *n*-pentane and the resulting slurry filled into the saturator tube followed by removal of the *n*-pentane by application of the carrier gas stream at room temperature. After leaving the saturator and reaching the saturation equilibrium with the analyte the carrier gas stream is conducted through a condenser tube, which is positioned in a dewar vessel containing *iso*-propanol that is cooled to −30 °C by an immersion cooler (Huber TC45E). The exact carrier gas flow-rate is measured with a soap film flow meter (Hewlett Packard No.: 0101–0113) and the ambient temperature is recorded for the volume measurement (Greisinger GFTB 200) for each datapoint. The time frame from insertion of the condenser tube into the saturator to its removal was measured for the calculation of the total volume of carrier gas. After its removal from the saturator the condenser tube was closed at both ends and *tert*-butyl methyl ether solvent was filled into it containing a known amount of *n*-dodecane as internal standard for the subsequent GC/MS quantification. With the temperature of the saturator T_{exp}, the mass of the analyte trapped in the condenser tube m_a, the ambient temperature T_{amb} and the volume of carrier gas measured at ambient conditions V_{amb} the vapor pressure p_{sat} of the analyte can be calculated. The calculation of the vapor pressure relies on the Ideal Gas Law, the Dalton's Law of partial pressures and the assumption that the volume of the gaseous analyte is negligibly small in comparison to that of the carrier gas:

$$p_{sat}\left(T_{exp}\right) = \frac{m_a R T_{amb}}{M V_{amb}} \quad (1)$$

p_{sat}: vapor pressure of the analyte [Pa], T_{exp}: temperature of the saturator [K], m_a: mass of analyte [kg], T_{amb}: ambient temperature [K], V_{amb}: volume of carrier gas at ambient conditions [m^3], M: molecular weight of the analyte [kg mol^{-1}], R: universal gas constant: 8.3145 J mol^{-1} K^{-1}

The obtained values of the experimental vapor pressure p_{sat} at the saturator temperature T_{exp} are processed mathematically with a fitting function that is based on the *Clarke-Glew* equation [21]:

$$ln\, {}^{p_{sat}}/_{p^\circ} - \frac{\Delta_{cr}^{g} C_{p,m}^{\circ}}{R} ln\frac{T}{T_0} = A - \frac{B}{T} \quad (2)$$

p°: reference pressure (1 Pa), $\Delta_{cr}^{g} C_{p,m}^{\circ}$: heat capacity difference from crystalline to gaseous state [J mol^{-1} K^{-1}], T: temperature [K], T_0: reference temperature [K], A/B: fitting coefficients (A: [ ], B: [K]).

The enthalpy of sublimation at the temperature T is calculated by:

$$\Delta^{g}_{cr}H^{o}_{m}(T) = RB + \Delta^{g}_{cr}C^{o}_{p,m}T \quad (3)$$

$\Delta^{g}_{cr}H^{o}_{m}(T)$: molar enthalpy of sublimation at temperature T [J mol^{-1}]

The experimental heat capacities $C^{o}_{p,m}$ (cf. Table 5) of both peroxides at room temperature were reported by Pilar *et al.* [22] and are in good agreement with the values calculated by the empiric elemental composition approached by Hurst *et al.* [23] ($C^{o}_{p,m}$ (cr, 298.15 (calculated/experimental) [J mol^{-1} K^{-1}], **1:** 314.6/271.8, **2:** 209.7/223.4). In this work the experimental values were used and the corresponding heat capacity differences $\Delta^{g}_{cr}C^{\circ}_{p,m}$ calculated according to Chickos *et al.* [24]. The method for the calculation of the sublimation enthalpy and its uncertainty is described elsewhere [20b]. The available literature vapor pressure data for TATP and DADP was also collected. In some works the sublimation enthalpy was not derived from the vapor pressures or it was carried out in a different manner. In this work the literature vapor pressures were treated with equations (2) and (3) and the corresponding uncertainties were estimated according to [20b]. The obtained enthalpies of sublimation and vapor pressures at 298.15 K are compiled in comparison with our results in Table 4.

For TATP a value for $\Delta^{g}_{cr}H^{o}_{m}(298.15\ K)$ of 76.7 ± 0.7 kJ mol^{-1} and a vapor pressure p_{sat}(298.15 K) of 6.7 Pa and for DADP a value for $\Delta^{g}_{cr}H^{o}_{m}(298.15\ K)$ of 75.0 ± 0.5 kJ mol^{-1} and a vapor pressure p_{sat}(298.15 K) of 26.6 Pa was derived from the data obtained with the transpiration method in this work. (cf. Table 2)

The sublimation behavior of TATP was studied in this work in the temperature range from 274.3–314.1 K. The absolute vapor pressures p_{sat} and thermodynamic properties of sublimation obtained by the transpiration method in this work for TATP are compiled in Table 2. A comparison our of own data with literature experiments regarding the enthalpies of sublimation is compiled in Table 4, Figure 4 shows a Clausius-Clapeyron plot of the own and literature p-T data for the sublimation of TATP. Available p-T literature data for comparison are four headspace gas chromatography measurements by Mbah *et al.* [25] and Oxley *et al.* [26], three thermogravimetric measurements by Mbah *et al.* [27], Oxley *et al.* [28] and Rivera *et al.* [29], one static method measurement by Egorshev *et al.* [30], a Knudsen-effusion measurement by Damour *et al.* [31] and a Quantum Cascade Laser Photoacoustic Spectroscopy measurement by Dunayevskiy *et al.* [32]. The thermogravimetric analysis (TGA) measurements may result in correct enthalpies of sublimation, yet they need to be calibrated with a reference material for the derivation of correct pressure values from the data measured. It has not been proven that this reference material calibration is suitable for a precise measurement of absolute vapor pressures. Therefore TGA measurements will be disregarded in the discussion of absolute vapor pressures. The data published by Dunayevskiy *et al.* [32] have been scaled to a measurement by Oxley *et al.* [26b]. Dunayevskiy *et al.* [32] published solely a p-T-equation of their data combined with that of Oxley *et al.* [26b] and no discrete pressure analog-temperature values which would allow fitting to other sets of data. Additionally it was mentioned by Damour *et al.* [31] that the dataset provided by Dunayevskiy *at al.* [32] seems to be systematically erroneous in the low temperature regime and needs to be cut. Therefore the data published by Dunayevskiy *et al.* [32] is excluded from the calculation of average values. Mbah *et al.* [25] measured TATP crude products that were synthesized under acid catalysis with hydrochloric and sulfuric acid. The crude product synthesized with sulfuric acid contained a large fraction of DADP impurity and therefore its measurement is disregarded in the calculation of average values and the discussion of measurement results.

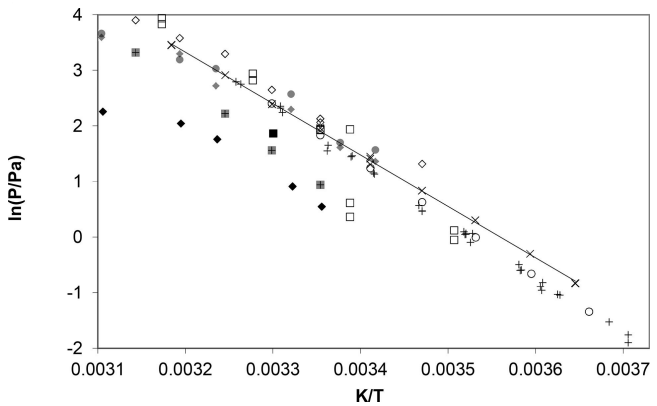

Figure 4. Experimental vapor pressure of TATP in comparison with literature values. × this work, grey circle [25] (HCl), grey diamond [25] (H_2SO_4), black diamond [27], black square [34], + [30], black triangle [28], white diamond [26a], white circle [32], grey + [29], white quare [26b]. Linear regression line for this work.

Regarding the enthalpies of sublimation $\Delta^{g}_{cr}H^{\circ}_{m}$ that were adjusted to 298.15 K (cf. Table 4) it becomes obvious that the values spread from 68.0 ± 6.3 kJ mol^{-1} derived from the data reported by Mbah *et al.* [27] to 103.8 ± 6.4 kJ mol^{-1} derived from the data reported by Oxley *et al.* [26b]. The scattering of the measurement values may be explained by the polymorphism of TATP reported by Reany *et al.* [11]. It was demonstrated that crude products of TATP contain one major and two minor mass fraction polymorphs of TATP and three additional polymorphs can be synthesized by recrystallization in organic solvents (hexane, tetrachloromethane, ethanol). Four of these polymorphs were analyzed by differential scanning calorimetry with reported sublimation enthalpies ranging from 14.6 kJ mol^{-1} at 93.6 °C onset temperature to 77.2 kJ mol^{-1} at 91.6 °C onset temperature. A sublimation enthalpy of 14.6 kJ mol^{-1} is not in accordance with the values measured by other methods for the TATP molecule (cf. Table 4). Despite that it cannot be neglected that polymorphism influences the sublimation behavior of TATP. It cannot be excluded that all measurements discussed in this work were measurements of polymorph mixtures or different pure polymorphs of **1.** The relevant in-

Table 2. TATP: absolute vapor pressures p_{sat} and thermodynamic properties of sublimation obtained by the transpiration method in this work

TATP: $\Delta_{cr}^{g}H_m^{\circ}$ (298.15 K) = 76.7 ± 0.7 kJ mol^{-1}

$\ln {}^{p_{sat}}/_{p^{\circ}} = \frac{314.7}{R} - \frac{89091.1}{RT} + \frac{41.5}{R} ln \frac{T}{298.15\ K}$

T_{exp} [a] [K]	m_a [b] [mg]	V_{N2} [c] [dm^3]	T_{amb} [d] [K]	Gasflow [dm^3 h^{-1}]	p_{sat} [e] [Pa]	u(p_{sat}) [f] [Pa]	$\Delta_{cr}^{g}H_m^{\circ}$ [kJ mol^{-1}]	$\Delta_{cr}^{g}S_m^{\circ}$ [J mol^{-1} K^{-1}]
274.3	0.11	2.80	296.6	2.58	0.43	0.02	77.71	180.6
274.4	0.09	2.43	296.5	1.62	0.44	0.02	77.71	180.6
278.3	0.11	1.65	296.5	1.62	0.74	0.02	77.54	180.4
283.2	0.11	0.926	296.4	2.14	1.4	0.0	77.34	179.9
288.2	0.24	1.16	296.9	2.17	2.3	0.1	77.13	178.9
293.2	0.23	0.610	296.5	2.15	4.2	0.1	76.92	178.7
293.2	0.23	0.611	297.1	2.16	4.1	0.1	76.92	178.4
298.2	0.57	0.898	297.0	2.15	7.1	0.2	76.72	177.9
293.2	0.20	0.613	296.5	2.16	3.7	0.1	76.92	177.5
303.1	0.53	0.538	296.8	2.15	10.9	0.3	76.51	176.5
308.1	1.25	0.751	296.3	2.15	18.4	0.5	76.30	176.1
314.1	1.55	0.540	296.7	2.16	31.8	0.8	76.06	175.2
314.1	1.54	0.538	296.3	2.15	31.7	0.8	76.06	175.2
314.1	1.53	0.539	296.7	2.16	31.5	0.8	76.06	175.1

DADP: $\Delta_{cr}^{g}H_m^{\circ}$ (298.15 K) = 75.0 ± 0.5 kJ mol^{-1}

$\ln {}^{p_{sat}}/_{p^{\circ}} = \frac{313.2}{R} - \frac{85244.0}{RT} + \frac{34.3}{R} ln \frac{T}{298.15\ K}$

T_{exp} [a] [K]	m_a [b] [mg]	V_{N2} [c] [dm^3]	T_{amb} [d] [K]	Gasflow [dm^3 h^{-1}]	p_{sat} [e] [Pa]	u(p_{sat}) [f] [Pa]	$\Delta_{cr}^{g}H_m^{\circ}$ [kJ mol^{-1}]	$\Delta_{cr}^{g}S_m^{\circ}$ [J mol^{-1} K^{-1}]
274.7	0.16	1.38	296.6	2.02	1.98	0.05	75.82	186.0
274.7	0.15	1.27	296.6	1.52	1.95	0.05	75.82	185.8
278.5	0.16	0.862	296.6	1.52	3.13	0.08	75.69	185.6
288.3	0.38	0.635	296.4	2.01	9.95	0.27	75.36	184.8
283.4	0.34	1.07	296.5	2.01	5.36	0.16	75.52	184.8
293.3	0.74	0.740	296.8	2.02	16.6	0.44	75.18	184.0
293.3	0.72	0.740	296.3	2.02	16.3	0.43	75.19	183.9
293.3	0.69	0.741	296.6	2.02	15.6	0.42	75.19	183.5
298.2	1.33	0.805	296.9	2.01	27.6	0.71	75.02	183.4
293.3	0.68	0.739	297.1	2.02	15.4	0.41	75.19	183.4
303.2	1.29	0.501	297.2	2.00	43.0	1.10	74.85	182.4
308.1	3.78	0.871	297.5	2.01	72.4	1.84	74.68	182.2
314.1	3.70	0.499	296.5	1.99	123	3.11	74.47	181.4
314.1	3.45	0.467	297.0	2.00	123	3.11	74.47	181.4
314.1	3.59	0.500	296.7	2.00	120	3.02	74.47	181.2

[a] Saturation temperature ($u(T)$ = 0.1 K). [b] Mass of transferred sample condensed at T = 243 K [c] Volume of nitrogen ($u(V)$ = 0.005 dm^3) used to transfer m ($u(m)$ = 0.0001 g) of the sample. [d] T_a is the temperature of the soap bubble meter used for measurement of the gas flow. [e] Vapor pressure at temperature T, calculated from the m and the residual vapor pressure at the condensation temperature calculated by an iteration procedure; p° = 1 Pa. [f] Standard uncertainty in p was calculated with $u(p/\text{Pa}) = 0.005 + 0.025(p/\text{Pa})$ for $p < 5$ Pa and $u(p/\text{Pa}) = 0.025 + 0.025(p/\text{Pa})$ for $p > 5$ to 3000 Pa.

formation about the synthesis of the TATP used in this work and in literature publications is summarized in Table 3.

In many cases no sufficient data about the details of sample synthesis have been provided, whilst samples that have been recrystallized from methanol were reported with different sublimation characteristics regarding the enthalpy of sublimation at 298.15 K. In this work the crude product was extracted from the reaction mixture with pentane. The data published by Mbah *et al.* [25] for the crude product of synthesis under hydrochloric acid catalysis is in fair agreement with the data obtained in this work. (cf. Table 4, Figure 4) For TATP an average uncertainty-weighted value for $\Delta_{l}^{g}H_m^{\circ}$ (298.15 K) of 80.8 ± 0.5 kJ mol^{-1} is calculated considering all available sets of data. This value is not in agreement with the one obtained in this work (76.7 ± 0.7 kJ mol^{-1}), which is supposedly caused by the polymorphism of TATP and different methods of synthesis in all measurements. The vapor pressures of TATP at 298.15 K that were calculated from each individual complete dataset are compiled in Table 4. The mean value of 6.9 Pa is in agreement with the value measured in this work (6.7 Pa).

Table 3. Details of TATP synthesis in this work and in literature references.

Experiment[a]	Acid[b]	Solvent	Purity	Melting Point Range °C	$\Delta^g_{cr}H^\circ_m$(298.15 K)[d] kJ mol^{-1}
This Work	H_2SO_4	Pentane	99.9 %[e]	97–98	76.7 ± 0.7
Mbah 2015 HCl [25]	HCl	–	–	–	71.6 ± 6.9
Mbah 2015 H_2SO4 [25]	H_2SO_4	–	impure	–	66.6 ± 3.8
Mbah 2014 [27]	–	–	–	86	68.0 ± 6.3
Egorshev 2013 [30]	HCl	–	–	95–97	98.7 ± 7.7
Rivera 2011 [34]	–	–	–	–	(73.0)
Damour 2010 [31]	CAR[c]	Methanol	–	94.2–95.2	85.7 ± 0.9
Oxley 2010 [28]	H_2SO_4	Methanol	"good"	–	92.8 ± 2.7
Oxley 2009 [26a]	–	–	–	–	72.0 ± 3.3
Dunayevskiy 2007 [32]	–	–	–	–	(85.4)
Rivera 2006 [29]	–	–	–	95.9	86.8 ± 2.2
Oxley 2005 [26b]	H_2SO_4	Methanol	"good"	–	103.8 ± 6.4

[a] First author and year of publication, [b] Acid catalyst used in synthesis, [c] CAR: Cationic Acid Resin [d] Molar Enthalpy of Sublimation at 298.15 K [e] (VO-GC/MS)

The sublimation behavior of DADP was studied in this work in the temperature range from 274.7–314.1 K. The absolute vapor pressures p_{sat} and thermodynamic properties of sublimation obtained by the transpiration method in this work for DADP are compiled in Table 2. A comparison of own data with literature experiments regarding the enthalpies of sublimation is compiled in Table 4. Figure 5 shows a *Clausius-Clapeyron* plot of the own and literature p-T data for the sublimation of DADP.

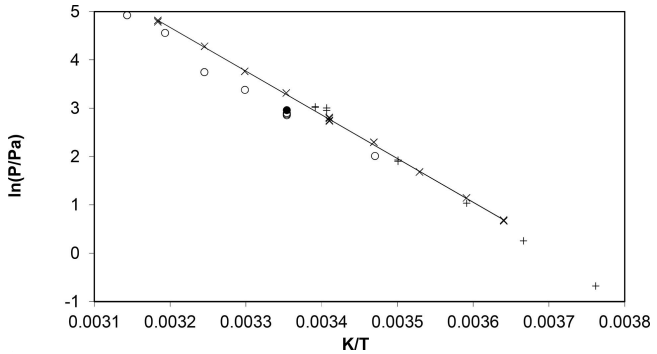

Figure 5. Experimental vapor pressure of DADP in comparison with literature values ×: this work, + [31], ● [33], ○ [26a] Linear regression line for this work.

Available p-T literature measurement data for comparison are provided by Egorshev *et al.* [30] (static method), Brady *et al.* [33] (thermogravimetry), Damour *et al.* [31] (Knudsen effusion), and Oxley *et al.* [26a] (headspace). The thermogravimetric analysis measurement by Brady *et al.* [33] is excluded from data comparison and average value calculation since solely a p-T-equation and a vapor pressure extrapolation to 298.15 K was published. For DADP an average uncertainty-weighted value for $\Delta^g_{cr}H^\circ_m$(298.15 K) of 76.4 ± 0.4 kJ mol^{-1} is recommended considering all available sets of data. This value is in fair agreement with the one obtained in this work (75.0 ± 0.5 kJ mol^{-1}). The vapor pressures of DADP at 298.15 K that were calculated from each individual complete dataset are compiled in Table 4. The mean value of 25.5 Pa is in fair agreement with the value measured in this work (26.6 Pa).

3.5 Estimation of the Air Concentration of Peroxides 1 and 2

Vapor pressures are measured under ideal saturation conditions. In a real case scenario the saturation equilibrium of the explosive will not be reached and diffusion processes will dictate the air concentration of the explosive. Dravnicks *et al.* [35] have stated a mathematical model for the estimation of the non-equilibrium air concentration of an explosive, which shall be applied to TATP and DADP in the following using the equations and values provided by Bird *et al.* [36].

Fick's Law of Diffusion provides a suitable approximation for the rate of molecular vapor emission per cm^2 J:

$$J = A \times D_{AB} \times \frac{n_c - n_a}{d} \quad (4)$$

J : emission flux [molecules s^{-1}], A: area of explosive exposed to air [cm^2], D_{AB}: diffusivity of explosive vapor in air [cm^2 s^{-1}], n_c: concentration of explosive under saturation conditions [molecules cm^{-3}], n_a: concentration of the explosive in air [molecules cm^{-3}], d: thickness of non-turbulent layer air [cm]

The concentration of the explosive in the air is considered to be negligibly small ($\rightarrow n_a = 0$) and the thickness of the non-turbulent layer of air surrounding the explosive is considered to be 0.2 cm [35].

Table 4. Compilation of data on the enthalpy of sublimation and vapor pressures obtained in this work and from literature values for TATP and DADP.

Experiment[a]	Method[b]	T-Range	T_{avg}	$\Delta^{g}_{cr}H^{\circ}_{m}(T_{avg})$	$\Delta^{g}_{cr}H^{\circ}_{m}$(298.15 K)[c]	p_{sat}[d]
		K	K	kJ mol^{-1}	kJ mol^{-1}	Pa
TATP						
This Work	T	274.3–314.1	294.3	76.9 ± 0.6	76.7 ± 0.7	6.7
Mbah 2015 HCl [25]	H	292.7–327.2	310.3	71.1 ± 6.9	71.6 ± 6.9	7.6
Mbah 2015 H_2SO_4 [25]	H	292.7–327.2	310.3	66.1 ± 3.7	(66.6 ± 3.8)	(6.5)
Mbah 2014 [27]	G	298.0–327.0	313.2	67.4 ± 6.2	68.0 ± 6.3	(1.9)
Egorshev 2013 [30]	S	348.2–367.2	357.9	96.2 ± 7.6	98.7 ± 7.7	(1.6)
Rivera 2011 [34]	G,O	303.0–338.0	320.5	72.1	(73.0)	-
Damour 2010 [31]	K	269.9–307.0	287.0	86.6 ± 0.8	85.7 ± 0.9	5.9
Oxley 2010 [28]	G	313.9–332.5	321.9	91.7 ± 2.5	92.8 ± 2.7	(24.4)
Oxley 2009 [26a]	H	288.2–323.2	305.0	71.7 ± 3.2	72.0 ± 3.3	8.7
Dunayevskiy 2007 [32]	Q,O	243.2–331.2	285.5	86.0	(85.4)	(6.3)
Rivera 2006 [29]	G	298.2–348.2	319.4	85.8 ± 2.2	86.8 ± 2.2	(2.8)
Oxley 2005 [26b]	H	285.2–331.2	305.3	103.4 ± 6.4	103.8 ± 6.4	5.8
DADP						
This Work	T	274.7–314.1	294.4	75.2 ± 0.4	75.0 ± 0.5	26.6
Egorshev 2013 [30]	S	340.7–393.0	358.5	74.3 ± 1.5	76.6 ± 1.5	25.6
Brady 2012 [33]	G,O	333.2–369.2	351.2	73	(74.8)	(19.3)
Damour 2010 [31]	K	265.9–294.9	284.7	84.6 ± 1.1	84.0 ± 1.2	31.2
Oxley 2009 [26a]	H	288.2–323.2	305.0	79.4 ± 3.4	79.6 ± 3.4	18.6
					76.4 ± 0.4[e]	25.5[f]

[a] First author and year of publication, [b] Methods: T: Transpiration, H: Headspace, S: Static Method, G: Thermogravimetric Analysis, K: Knudsen-Effusion, Q: Quantum-Cascade Laser Photoacoustic Spectroscopy, O: Equation Only [c] Enthalpies of vaporization were adjusted according to Chickos *et al.* [24] with the values for $^{g}_{cr}C^{\circ}_{p,m}$ and $C^{\circ}_{p,m}$(cr) stated in Table 5 [d] Vapor pressure at 298.15 K, calculated according to equation (2). [e] Weighted average value, calculated using the uncertainty as the weighing factor. [f] Average value. Values in brackets were excluded from average value calculation.

Table 5. Calculation of Molar Heat Capacity Differences at T = 298.15 K

compound	$C^o_{p,m}$(l) calc. [J mol^{-1} K^{-1}]	$C^o_{p,m}$(cr) calc. [J mol^{-1} K^{-1}]	$C^o_{p,m}$(l) lit. [J mol^{-1} K^{-1}]	$C^o_{p,m}$(cr) lit. [J mol^{-1} K^{-1}]	$\Delta^g_l C^o_{p,m}$ [J mol^{-1} K^{-1}]	$\Delta^g_{cr} C^o_{p,m}$ [J mol^{-1} K^{-1}]
TATP	379.3[a]	(314.6)[a]	n.a.	271.8 [22]	−109.2	−41.5
DADP	252.9[a]	(209.7)[a]	n.a.	223.4 [22]	−76.3	−34.3

Bracketed values not used for calculation of heat capacity differences. n.a.: not available a) calculated according to the increment method and data by Hurst et al. [23] b) calculated by ${}^g_l C^o_{p,m} = 10.58 + C^o_{p,m}(\mathrm{l}) \times 0.26$ according to [24] c) calculated by ${}^g_{cr} C^o_{p,m} = 0.75 + C^o_{p,m}(\mathrm{cr}) \times 0.15$ according to [24]

The diffusivity D_{AB} can be calculated by the following formula:

$$D_{AB} = 0.0018583\sqrt{T^3\left(\frac{1}{M_A}+\frac{1}{M_B}\right)}\frac{1}{p\sigma^2_{AB}\Omega_{D,AB}} \quad (5)$$

T: Temperature [K] (298.15 K), M_A: Molecular Mass of Explosive [g mol^{-1}], M_B: Molecular Mass of Air [g mol^{-1}] (28.97 g mol^{-1}), p: total pressure [atm] (1 atm), σ_{AB}: combined collision diameter [Å], $\Omega_{D,AB}$: collision integral for diffusion [ ]

$$\sigma_{AB} = 1/2(\sigma_A + \sigma_B) \quad (6)$$

σ_A: collision diameter of explosive [Å], σ_B: collision diameter of air [Å] (3.617 Å) [36]

$$\varepsilon_{AB} = \sqrt{\varepsilon_A \varepsilon_B} \quad (7)$$

ε_A: characteristic energy of explosive [J], ε_B: characteristic energy of air [J]

Whilst the collision diameter of σ_B (3.617 Å) [36] and the characteristic energy ε_B ($\varepsilon_B/\kappa = 97.0$ K) [36] of air is known, the collision diameter of the explosive σ_A and its characteristic energy ε_A have to be estimated. These values may be estimated from the solid at the melting point (m):

$$\varepsilon/\kappa = 1.92T_m;\ \sigma = 1.222^a\sqrt{V_m} \quad (8)$$

T_m: melting point [K], V_m: volume of the solid at the melting point [cm^3 mol^{-}], κ: Boltzmann's constant (1.38066×10^{-23} J K^{-1})

With ε_{AB} the collision integral for diffusion $\Omega_{D,AB}$ can be calculated according to:

$$\Omega_{D,AB} = \frac{1.16145}{T^{*0.15610}} + \frac{0.19300}{\exp(476335T^*)} + \frac{1.03587}{\exp(1.52996T^*)} + \frac{1.76474}{\exp(3.89411T^*)} \quad (9)$$

In case of TATP and DADP the diffusion coefficient can be calculated from their melting point (eq. (8)). The needed molar volume V_m can be approximated from the crystal structure density at the temperature T_{XRD}: The density can be adjusted to the melting point by the following equation [37]:

$$T^* = \kappa T/\varepsilon_{AB} \quad (10)$$

ρ_m: density at melting point [g cm^{-3}], ρ_{XRD}: density from X-Ray diffraction [g cm^{-3}], T_{XRD}: temperature of XRD-experiment [K]

$$\rho_m = \rho_{XRD}/(1 + 0.00015(T_m - T_{XRD}) \quad (11)$$

The molar volume at the melting point can be calculated by:

$$V_m = M/\rho_m \quad (12)$$

With equations (4) to (12) the diffusion coefficient of a solid explosive in air can be approximated when solely its melting point and a density are known and equation (4) can be used to calculate the mass flux of material from the explosive to the air with $A = 1$ cm^2, $n_a = 0$ and d = 0.2 cm.

If the concentration n_c is converted to partial pressure ($n_c = 3.3 \times 10^{16} p$, p: vapor pressure [Pa]) and the emission flux is converted into a mass flux (unit conversion factor: M/N_A) the mass flux can be calculated:

$$Q = \frac{D_{AB}}{0.2\ \mathrm{cm}} \times 3.3 \times 10^{16} \times \left(\frac{760}{101325}\right) p \times (M/N_A) \quad (14)$$

Q: emission flux of explosive [g s^{-1} cm^{-2}], N_A: Avogadro Constant (6.022×10^{23} mol^{-1})

An example of this calculation can be found for TATP **1** and DADP **2** in Table 6:

With the emission flux Q in hands the concentration of the explosive in air at the diffusion equilibrium state can be calculated:

$$c_{dif} = S \times Q \times r \quad (15)$$

c: concentration of explosive in air at diffusion equilibrium, S: surface of explosive exposed to air, r : attenuation factor (10^{-4})

The attenuation factor r has been established in the study by Dravnicks *et al.* [35]. For a surface of 200 cm^2 the

Table 6. Example of calculation for the emission flux of explosive *Q* for TATP and DADP at STP conditions (298.2 K, 1 atm)

	TATP	DADP	Unit
T_m	370.2[a]	405.2[a]	K
ρ_{XRD}	1.27[b]	1.33[b]	g cm^{-3}
T_{XRD}	180[b]	208[b]	K
ρ_m	1.24	1.292	g cm^{-3}
M	222.237	148.158	g mol^{-1}
V_m	179.981	114.691	cm^3 mol^{-1}
σ_A	6.899	5.937	Å
ε_B/κ	710.688	777.888	K
σ_{AB}	5.258	4.777	Å
ε_{AB}/κ	262.558	274.691	K
$\kappa T/\varepsilon_{AB}$	1.136	1.085	
$\Omega_{D,AB}$	1.355	1.385	
D_{AB}	0.050	0.062	cm^2 s^{-1}
p_{sat}	6.7[a]	26.6[a]	Pa
Q	0.154	0.498	µg cm^{-2} s

[a] value obtained in this work, [b] values obtained from the literature for TATP [15] and DADP[16].

following values for c_{dif} can be obtained: TATP: 3.1 ng L^{-1}, DADP: 10 ng L^{-1}. These values must be regarded as the maximum concentrations of explosive that can be present for detection since further diffusion barriers like foil wrapped around the explosive are highly probable. c_{dif} is directly proportional to the exposed surface of the explosive (Equation 15) and was calculated in this work for an exemplary surface of 200 cm^2.

Using the Ideal gas equation the saturation concentration of an explosive can be calculated:

$$c_{sat} = \frac{p_{sat} \times M}{R \times T} \quad (16)$$

c_{sat}: saturation concentration [mg L^{-1}], R: ideal gas constant (8.314 J mol^{-1} K^{-1}), T: temperature [K]

For TATP a value of 600 µg L^{-1} and for DADP a value of 1589 µg L^{-1} can be calculated using the vapor pressures stated in Table. This indicates that the diffusion phenomenon discussed lowers the gas phase concentration of the explosive by about five orders of magnitude (10^5).

4 Conclusions

Based on theoretical predictions using the EXPLO5 v6.03 code, TATP and its side product DADP are considered to be medium performance explosives that are easily accessible from openly available chemicals. Whilst for DADP the p-T-values obtained in this work are in agreement with literature values the p-T-values obtained for TATP are not in agreement with literature values. This might be due to the rich polymorphism of TATP. It would be recommendable to carry out future vapor pressure measurements of TATP with the synthetic procedure detailed in this work for the reason of comparability. The saturation equilibrium concentrations of TATP (600 µg L^{-1}) and DADP (1589 µg L^{-1}) are about five magnitudes higher than at the diffusion equilibrium state (**1:** 3.1 ng L^{-1}, **2:** 10 ng L^{-1}) for a surface of 200 cm^2. The latter concentrations correspond to a ppt-concentration level and are valuable for the conception of gas phase detection devices.

Acknowledgements

Financial support of this work by the Ludwig-Maximilian University of Munich (LMU), the Office of Naval Research (ONR) under grant no. ONR.N00014-16-1-2062, and the Bundeswehr – Wehrtechnische Dienststelle für Waffen und Munition (WTD 91) under grant no. E/E91S/FC015/CF049 and the German Ministry of Education and Research (BMBF) under grant no. 13N12583 is gratefully acknowledged. We would like to thank Prof. Sergey Verevkin (University of Rostock) for help with establishing the transpiration method at our laboratory. Dr. Peter Boeker and Dr. Jan Leppert (University of Bonn) are thanked for fruitful discussions and advice in gas-chromatographic aspects. Prof. Jürgen Evers is thanked for the measurement and evaluation of the powder X-Ray diffractograms. The authors acknowledge collaborations with Dr. Mila Krupka (OZM Research, Czech Republic) in the development of new testing and evaluation methods for energetic materials and with Dr. Muhamed Suceska (Brodarski Institute, Croatia) in the development of new computational codes to predict the detonation and propulsion parameters of novel explosives. We are indebted to and thank Drs. Betsy M. Rice, Jesse Sabatini and Brad Forch (ARL, Aberdeen, Proving Ground, MD) for many inspired discussions.

References

[1] R. Wolffenstein, Über die Einwirkung von Wasserstoffsuperoxyd auf Aceton und Mesityloxyd, *Ber. Dtsch. Chem. Ges.* **1895**, *28*, 2265–2269.
[2] http://news.nationalpost.com/news/world/german-police-seize-bomb-firearm-in-raid-that-foiled-imminent-boston-marathon-style-terror-attack
[3] http://www.nydailynews.com/news/world/paris-suicide-bombers-tatp-homemade-explosive-article-1.2435082
[4] http://www.n-tv.de/panorama/17-Jaehriger-hortete-Sprengstoff-article334469.html
[5] a) J. C. Oxley, J. L. Smith, L. Steinkamp, G. Zhang, Factors Influencing Triacetone Triperoxide (TATP) and Diacetone Diperoxide (DADP) Formation: Part 2, *Propellants, Explos., Pyrotech.* **2013**, *38*, 841–851; b) J. C. Oxley, J. L. Smith, P. R. Bowden, R. C. Rettinger, Factors Influencing Triacetone Triperoxide (TATP) and Diacetone Diperoxide (DADP) Formation: Part I, *Propellants, Explos., Pyrotech.* **2013**, *38*, 244–254.
[6] J. C. Oxley, J. L. Smith, J. E. Brady, L. Steinkamp, Factors Influencing Destruction of Triacetone Triperoxide (TATP), *Propellants, Explos., Pyrotech.* **2014**, *39*, 289–298.
[7] D. Lubczyk, A. Hahma, M. Brutschy, C. Siering, S. R. Waldvogel, A New Reference Material and Safe Sampling of Terrorists Per-

oxide Explosives by a Non-Volatile Matrix, *Propellants, Explos., Pyrotech.* **2015**, *40*, 590–594.

[8] a) R.-M. Räsänen, M. Nousiainen, K. Peräkorpi, M. Sillanpää, L. Polari, O. Anttalainen, M. Utriainen, Determination of gas phase triacetone triperoxide with aspiration ion mobility spectrometry and gas chromatography–mass spectrometry, *Anal. Chim. Acta* **2008**, *623*, 59–65; b) J. L. Anderson, A. A. Cantu, A. W. Chow, P. S. Fussell, R. G. Nuzzo, J. E. Parmeter, G. S. Sayler, J. n. M. Shreeve, R. E. Slusher, M. Story, W. Trogler, V. Venkatasubramaniam, L. A. Waller, J. Young, C. F. Zukoski, Existing and Potential Standoff Explosives Detection Techniques, National Academies Press, Washington, DC, **2004**; c) C. L. Rhykerd, D. W. Hannum, D. W. Murray, J. E. Parmeter, Guide for the Selection of Commercial Explosives Detection Systems for Law Enforcement Applications, National Institute of Justice Office of Science and Technology, Washington, DC, **1999**; d) J. Cabalo, R. Sausa, Trace detection of explosives with low vapor emissions by laser surface photofragmentation–fragment detection spectroscopy with an improved ionization probe, *Appl. Opt.* **2005**, *44*, 1084–1091; e) J. I. Steinfeld, J. Wormhoudt, Explosives Detection: A Challenge for Physical Chemistry, *Ann. Rev. Phys. Chem.* **1998**, *49*, 203–232; f) G. Bunte, J. Hürttlen, H. Pontius, K. Hartlieb, H. Krause, Gas phase detection of explosives such as 2,4,6-trinitrotoluene by molecularly imprinted polymers, *Anal. Chim. Acta* **2007**, *591*, 49–56; g) http://www.sedet.com/Technology.html

[9] N. A. Milas, A. Golubovic, Studies in Organic Peroxides. XXVI. Organic Peroxides Derived from Acetone and Hydrogen Peroxide, *J. Am. Chem. Soc.* **1959**, *81*, 6461–6462.

[10] K. B. Landenberger, O. Bolton, A. J. Matzger, Two Isostructural Explosive Cocrystals with Significantly Different Thermodynamic Stabilities, *Angew. Chem., Int. Ed.* **2013**, *52*, 6468–6471.

[11] O. Reany, M. Kapon, M. Botoshansky, E. Keinan, Rich Polymorphism in Triacetone-Triperoxide, *Cryst. Growth Des.* **2009**, *9*, 3661–3670.

[12] C. R. Groom, I. J. Bruno, M. P. Lightfoot, S. C. Ward, The Cambridge Structural Database, *Acta Crystallogr.*, **2016**, *B72*, 171–179.

[13] Impact: Insensitive $>$ 40 J, less sensitive $\geq$ 35 J, sensitive $\geq$ 4 J, very sensitive $\leq$ 3 J; Friction: Insensitive $>$ 360 N, less sensitive $=$ 360 N, sensitive $<$ 360 N and $>$ 80 N, very sensitive $\leq$ 80 N, extremely sensitive $\leq$ 10 N. According to the UN Recommendations on the Transport of Dangerous Goods.

[14] M. J. Frisch, G. W. Trucks, H. B. Schlegel, G. E. Scuseria, M. A. Robb, J. R. Cheeseman, G. Scalmani, V. Barone, B. Mennucci, G. A. Petersson, H. Nakatsuji, M. Caricato, X. Li, H. P. Hratchian, A. F. Izmaylov, J. Bloino, G. Zheng, J. L. Sonnenberg, M. Hada, M. Ehara, K. Toyota, R. Fukuda, J. Hasegawa, M. Ishida, T. Nakajima, Y. Honda, O. Kitao, H. Nakai, T. Vreven, J. A. Montgomery Jr., J. E. Peralta, F. Ogliaro, M. J. Bearpark, J. Heyd, E. N. Brothers, K. N. Kudin, V. N. Staroverov, R. Kobayashi, J. Normand, K. Raghavachari, A. P. Rendell, J. C. Burant, S. S. Iyengar, J. Tomasi, M. Cossi, N. Rega, N. J. Millam, M. Klene, J. E. Knox, J. B. Cross, V. Bakken, C. Adamo, J. Jaramillo, R. Gomperts, R. E. Stratmann, O. Yazyev, A. J. Austin, R. Cammi, C. Pomelli, J. W. Ochterski, R. L. Martin, K. Morokuma, V. G. Zakrzewski, G. A. Voth, P. Salvador, J. J. Dannenberg, S. Dapprich, A. D. Daniels, Ö. Farkas, J. B. Foresman, J. V. Ortiz, J. Cioslowski, D. J. Fox, Gaussian 09, Revision A02, Gaussian, Inc., Wallingford, CT, USA, **2009**.

[15] F. Dubnikova, R. Kosloff, J. Almog, Y. Zeiri, R. Boese, H. Itzhaky, A. Alt, E. Keinan, Decomposition of triacetone triperoxide Is an entropic explosion, *J. Am. Chem. Soc.* **2005**, *127*, 1146–1159.

[16] F. G. Gelalcha, B. Schulze, P. Lonnecke, 3,3,6,6-Tetramethyl-1,2,4,5-tetroxane: a twinned crystal structure, *Acta Crystallogr.* **2004**, *C60*, o180-o182.

[17] J. de Zeeuw, S. Reese, J. Cochran, S. Grossman, T. Kane, C. English, Simplifying the setup for vacuum-outlet GC: Using a restriction inside the injection port, *J. Sep. Sci.* **2009**, *32*, 1849–1857.

[18] N. Haroune, A. Crowson, B. Campbell, Characterisation of triacetone triperoxide (TATP) conformers using LC-NMR, *Sci. Justice* **2011**, *51*, 50–56.

[19] C. Denekamp, L. Gottlieb, T. Tamiri, A. Tsoglin, R. Shilav, M. Kapon, Two Separable Conformers of TATP and Analogues Exist at Room Temperature, *Org. Lett.* **2005**, *7*, 2461–2464.

[20] a) V. N. Emel'yanenko, S. P. Verevkin, Benchmark thermodynamic properties of 1,3-propanediol: Comprehensive experimental and theoretical study, *J. Chem. Thermodyn.* **2015**, *85*, 111–119; b) S. P. Verevkin, A. Y. Sazonova, V. N. Emel'yanenko, D. H. Zaitsau, M. A. Varfolomeev, B. N. Solomonov, K. V. Zherikova, Thermochemistry of Halogen-Substituted Methylbenzenes, *J. Chem. Eng. Data* **2015**, 60, 89–103; c) S. P. Verevkin, Experimental Thermodynamics, Volume 7 (Eds.: R. D. Weir, T. W. D. Loos), Elsevier, **2005**, pp. 5–30.

[21] E. C. W. Clarke, D. N. Glew, Evaluation of thermodynamic functions from equilibrium constants, *Trans. Faraday Soc.* **1966**, *62*, 539–547.

[22] R. Pilar, J. Pachman, R. Matyáš, P. Honcová, D. Honc, Comparison of heat capacity of solid explosives by DSC and group contribution methods, *J. Therm. Anal. Calorim.* **2015**, *121*, 683–689.

[23] J. E. Hurst, B. Keith Harrison, Estimation of Liquid and Solid Heat Capacities Using a Modified Kopps' Rule, *Chem. Eng. Commun.* **1992**, *112*, 21–30.

[24] W. Acree, J. S. Chickos, Phase Transition Enthalpy Measurements of Organic and Organometallic Compounds. Sublimation, Vaporization and Fusion Enthalpies From 1880 to 2010, *J. Phys. Chem. Ref. Data* **2010**, *39*, 043101.

[25] J. Mbah, D. Knott, S. Steward, D. Cornett, Vapor Pressure and Sublimation Enthalpy of Triacetone Triperoxide by a Gas Chromatography Headspace Approach, *Int. J. Energ. Mater. Chem. Propul.* **2015**, 14, 321–329.

[26] a) J. C. Oxley, J. L. Smith, W. Luo, J. Brady, Determining the Vapor Pressures of Diacetone Diperoxide (DADP) and Hexamethylene Triperoxide Diamine (HMTD), *Propellants, Explos., Pyrotech.* **2009**, *34*, 539–543. b) J. C. Oxley, J. L. Smith, K. Shinde, J. Moran, Determination of the vapor density of triacetone triperoxide (TATP) using a gas chromatography headspace technique, *Propellants, Explos., Pyrotech.* **2005**, *30*, 127–130.

[27] J. Mbah, D. Knott, S. Steward, Thermogravimetric study of vapor pressure of TATP synthesized without recrystallization, *Talanta* **2014**, *129*, 586–593.

[28] J. Oxley, J. L. Smith, J. Brady, S. Naik, Determination of Urea Nitrate and Guanidine Nitrate Vapor Pressures by Isothermal Thermogravimetry, *Propellants, Explos., Pyrotech.* **2010**, *35*, 278–283.

[29] M. L. Ramírez, L. C. Pacheco-Londoño, Á. J. Peña, S. P. Hernández-Rivera, *Characterization of peroxide-based explosives by thermal analysis, Proc. SPIE*, **2006**, *6201*, 62012B1–62012B10.

[30] V. Y. Egorshev, V. P. Sinditskii, S. P. Smirnov, A comparative study on two explosive acetone peroxides, *Thermochim. Acta* **2013**, *574*, 154–161.

[31] P. L. Damour, A. Freedman, J. Wormhoudt, Knudsen Effusion Measurement of Organic Peroxide Vapor Pressures, *Propellants, Explos., Pyrotech.* **2010**, *35*, 514–520.

[32] I. Dunayevskiy, A. Tsekoun, M. Prasanna, R. Go, C. K. N. Patel, High-sensitivity detection of triacetone triperoxide (TATP) and its precursor acetone, *Appl. Opt.* **2007**, *46*, 6397–6404.
[33] J. E. Brady, J. L. Smith, C. E. Hart, J. Oxley, Estimating Ambient Vapor Pressures of Low Volatility Explosives by Rising-Temperature Thermogravimetry, *Propellants, Explos., Pyrotech.* **2012**, *37*, 215–222.
[34] H. Félix-Rivera, M. L. Ramírez-Cedeño, R. A. Sánchez-Cuprill, S. P. Hernández-Rivera, Triacetone triperoxide thermogravimetric study of vapor pressure and enthalpy of sublimation in 303–338 K temperature range, *Thermochim. Acta* **2011**, *514*, 37–43.
[35] A. Dravnicks, R. Brabets, T. A. Stanley, Evaluating Sensitivity Requirements of Explosive Vapor Detector Systems, IIT Research Institute Technology Center, Chicago Illinois, **1972**.
[36] R. B. Bird, W. E. Stewart, E. N. Lightfoot, Transport Phenomena, Second Edition, John Wiley & Sons, Inc., New Jork, **2002**.
[37] C. Xue, J. Sun, B. Kang, Y. Liu, X. Liu, G. Song, Q. Xue, The β-δ-Phase Transition and Thermal Expansion of Octahydro-1,3,5,7-Tetranitro-1,3,5,7-Tetrazocine, *Propellants, Explos., Pyrotech.* **2010**, *35*, 333–338.
[38] G. R. Fulmer, A. J. M. Miller, N. H. Sherden, H. E. Gottlieb, A. Nudelman, B. M. Stoltz, J. E. Bercaw, K. I. Goldberg, NMR Chemical Shifts of Trace Impurities: Common Laboratory Solvents, Organics, and Gases in Deuterated Solvents Relevant to the Organometallic Chemist, *Organometallics* **2010**, *29*, 2176–2179.

Received: January 31, 2017
Revised: February 13, 2017
Published online: March 31, 2017

FULL PAPER

Determination of the gas phase concentration parameters of the notorious explosives triacetone triperoxide TATP **1** and diacetone diperoxide DADP **2** is essential for conception of detector devices. Vapor pressures and enthalpies of sublimation at the ambient temperature 298.15 K have been measured with the transpiration method. The results obtained were compared critically with literature values.

M. A. C. Härtel, T. M. Klapötke, B. Stiasny, J. Stierstorfer*

1 – 13

Gas-phase Concentration of Triacetone Triperoxide (TATP) and Diacetone Diperoxide (DADP)

7.3 Measurement of the Nitrate Esters EGDN 06, GTN 07 and ETN 08

This chapter deals with the measurement of the vapor pressure of the nitrate esters EGDN **06**, GTN **07** and ETN **08**:

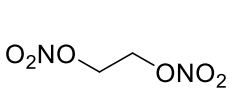

EGDN **06**

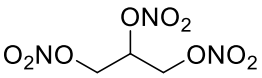

GTN **07**

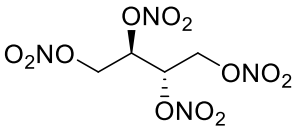

ETN **08**

The results were submitted to *Analytical Chemistry*. The original publication of the data follows.

Gas Phase Detectability by Vacuum Outlet GC/MS of Linear Nitrate Esters as Components in Improvised Explosive Devices

Martin A. C. Härtel, Thomas M. Klapötke*, Jörg Stierstorfer and Leopold Zehetner

Ludwig Maximilian University, Department of Chemistry, Butenandtstr. 9, D-81377 Munich

ABSTRACT: Gas phase detection of explosives is a new trend in the detection sciences. The conception of gas phase detection devices requires knowledge about gas phase concentration of the target analytes. Nitrate esters are well performing explosives with a high potential for misuse in improvised explosive devices that need to be detected at vulnerable infrastructures. With respect to this the six nitrate ester ethyl nitrate (**1**), ethylene glycol dinitrate (**2**), glycerol trinitrate (**3**), erythritol tetranitrate (4), mannitol hexanitrate (**5**) and pentaerythritol tetranitrate (**6**) were investigated in terms of detectability by vacuum outlet-GC/MS as potential components in improvised explosive devices. All compounds besides **5** could be detected using vacuum outlet GC/MS and their limits of detection were determined according to DIN 32645:2008. The vapor pressure of **2–4** was measured using the transpiration method. It was observed that the introduction of a $CHONO_2$ unit lowers the vapor pressure of the nitrate esters by about two orders of magnitude. For compound **4** the saturation concentration (73 ng L^{-1}) was compared with a vapor pressure based estimation of its concentration in diffusion equilibrium (0.385 pg L^{-1}).

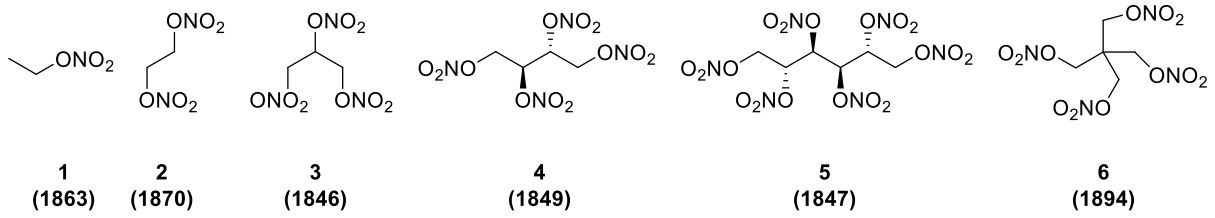

Figure 1. Chemical Structures of ethyl nitrate ($EtONO_2$, **1**), ethylene glycol dinitrate (EGDN, **2**), glyceryl trinitrate (GTN, **3**), meso-erythritol tetranitate (ETN, **4**), D-mannitol hexanitrate (MHN, **5**) and pentaerythritol tetranitrate (PETN, **6**) with the year of first publication given in brackets.

Nitrato compounds are the product of the esterificiation of (poly)-alcohols with nitric acid. Many molecules bearing this explosophore have been discovered in the 19th century. Figure 1 gives an overview of important representatives of this compound class with the year of first publication in scientific literature. Amongst these six representatives glyceryl trinitrate (GTN, **3**), more commonly known as nitroglycerine, is the compound that was published first in 1846 by *Sobrero* [1]. GTN (**3**) has been tamed by *Alfred Nobel* in 1866 by phlegmatization with Kieselgur as dynamite. Already *Sobrero* [1] knew about the tremendous toxicity of glyceryl trinitrate. The toxicity is caused by the vasodilative effect of nitrato compounds, which has been used in the pharmaceutical industry for the treatment of *Angina pectoris*. [2] Nitrato explosives still are widely distributed. Glyceryl trinitrate is used for mining explosives and double base propellants. Pentaerythritol tetranitrate (PETN **6**) is still in use as a booster explosive being appreciated for its readiness for detonation and high detonation pressure. Since the (poly-)alcohol starting materials for **1-5** are openly available to the public nitrato explosives are popular in the amateur chemist and terrorist scene. During the last years the increasing popularity and availability of the sweetening agents *meso*-erythritol and *D*-mannitol boosted the misuse of these food additives as an explosive precursor. With respect to this *Oxley at al.*[3,4] and *Matyas et al.*[5] investigated the analytical and energetic material properties of *meso*-erythritol tetranitrate (ETN, **4**). *Manner et al.* [6] published a crystallographic study of **4** in 2014. Within this work the gas phase detectability of the six nitrate esters ethyl nitrate ($EtONO_2$, **1**), ethylene glycol dinitrate (EGDN, **2**), glyceryl trinitrate (GTN, **3**), *meso*-erythritol tetranitrate (ETN, **4**), D-mannitol hexanitrate (MHN, **5**) and pentaerythritol tetranitrate (PETN, **6**) was investigated in terms of limits of detection and quantification using an improved method for vacuum outlet GC/MS (VO-GC/MS)[7] and vapor pressure measurements by the transpiration

method [8-10] for compounds **2–4** to provide reliable data considering the relatively new trend of gas phase explosive detection [11-17]. This work is the first experimental application of VO-GC/MS using the advantages of placing the necessary restriction inside the GC-injector using an improved setup with a *Siltite*® µ-union column connector. Compounds **1–5** are of special interest in the detection sciences since their potential precursors are available to the public in many countries including Germany. Therefore compounds **1–5** are potential candidates for the use in improvised explosive devices and their risk potential will be evaluated in this work in terms of energetic performance using the EXPLO5 computer code and their sensitivity toward impact, friction and electrostatic discharge. For each material a convenient method for small-scale synthesis resulting in high purity based on literature methods will be provided to facilitate the synthesis of reference materials for detection, training and instrument test purposes.

Experimental Section:

Synthesis and Characterization of Explosives

This work provides safe and reproducible procedures for the small scale synthesis of nitrate esters **1–6**. (see ESI pp. S-1–S-6) The syntheses of nitrato compounds **1–6** from their corresponding (poly-)alcohol starting materials were adapted from literature procedures which are stated in the experimental section. For safety reasons the purity of compounds **1–3** was assessed by ^{1}H NMR spectroscopy and VO-GC/MS. No impurities could be identified in compounds $EtONO_2$ **1** and EGDN **2.** The VO-GC/MS chromatogram of GTN **3** revealed a 1% impurity of glyceryl dinitrate based on signal area integration. The synthesis of ETN **4** and MHN **5** is carried out according to literature procedures with slight modifications. The protocol for the synthesis of PETN **6** was developed in our workgroup using *in situ* generated acetyl nitrate since initial attempts based on literature procedures were not satisfying in terms of product purity.

Within this work the crystal structure of MHN **5** at 100 K was elucidated for the first time and remeasurements of the crystal structure of ETN **4** at 100 K and 291 K were carried out. (see ESI pp. S-7–S-9) For all compounds **1-6** the friction and impact sensitivities were determined according to STANAG 4489 [18] and 4487 [19] with modified instructions [20,21] using a BAM impact and friction tester. [22,23] The sensitivity toward electrostatic discharge was determined using a testing device by OZM. [24] Melting and decomposition temperatures were determined with an OZM DTA device or a Linseis differential scanning calorimeter with a heating rate of 5 °C min^{-1}. The heat of formation of all analytes was calculated with Gaussian 09 [25] on a CBS-4M level. The room temperature densities of **4–6** were determined using a Quantachrome Ultrapyc 1200e gas pycnometer. Based on room temperature density and heat of formation the energetic performance of the explosives was calculated using the EXPLO5v6.03 computer code.

Vacuum Outlet GC/MS for Detection of Nitrate Esters

The gas-chromatography (GC) analysis of thermolabile analytes, which can be low-volatile, like nitrate esters is a delicate task since this analytical technique requires the transfer of the analyte into the gaseous state at elevated temperatures of operation in the typical range of 30 to 300 °C. The decomposition temperature of the analyte should be avoided throughout the analysis and its residence time in hotter zones like the injector minimized. The analytical GC column should be short enough to allow elution of the analyte without decomposition. In general two approaches for this problem exist. In case of atmospheric pressure detectors like the electron capture detector (ECD) the elution temperatures and retention times of the analytes can be reduced by increased carrier gas flow rates [26]. The beneficial use of analyte protectants for the GC/MS and GC/ECD-analysis of explosives has been demonstrated by *Kirchner et al.*.[27] Recently *Boeker et al.* [28] presented the application of flow field thermal gradient gas chromatography as a new technique for the analysis of explosives. In this work vacuum outlet gas-liquid-chromatography as established by *de Zeeuw et al.* [7] was chosen for the evaluation of the methods potential for the detection and quantification of nitrate esters **1–6**. The method uses a restriction capillary which is positioned inside the GC injector to limit the flow of carrier gas into a wide-bore analytical column (*Restek® RTX-TNT*, 6 m, 0.53 mm i.d., 1.5 µm film thickness). Placing the restriction in front of the analytical column results in a gradual expansion of the detector vacuum along the analytical column and increased optimum carrier gas velocities, which lowers the analyte elution temperatures. In the original literature [7] *Restek® press-tight* glass connectors and *Uniliner* were used for the connection of restriction and analytical column. Since both solutions are not compatible with the *Shimadzu® GCMS QP2010 SE* in combination with an *Atas® Optic 4* injector used in this work a *SGE SilTite®* µ-union column connector with an outer diameter of 3.5 mm was used in combination with a custom-made stainless steel liner (5 mm outer diameter, 0.5 mm wall thickness, split notches at bottom end). The numerous advantages of placing the restriction inside the injector were elucidated by *de Zeeuw et al.,*[7] but an important aspect was not mentioned: the GC-injector can be operated in constant pressure mode. Calculations that are based on the *Hagen-Poiseuille* equation [29] demonstrate that the flow-dynamics of the restriction-column assembly are dominated by the restriction in the isothermal injector and a change of the column oven temperature from 40 °C to 280 °C results in a negligible change of calculated column flow from 4.08 mL min^{-1} to 3.92 mL min^{-1} (see ESI p. S-10).

Transpiration Method Vapor Pressure Determination

For the transpiration experiment a carrier gas stream (nitrogen 5.0) is conducted over a P_4O_{10} drying tower to remove any traces of moisture before the gas flow rate is regulated with a mass flow controller (Natec Sensors MC-100 CCM) with flow rates from 1 to 5 L h^{-1}. The flow-

regulated gas stream then passes the saturator, which is a U-shaped glass tube (50 cm length, 8 mm i.d.) embedded in a cylindrical glass vessel (height: 25 cm, diameter: 10 cm). (see ESI Figure S-7) The temperature of the saturator is controlled by a circulation thermostat (Huber Ministat 230 with external class A PT-100 sensor pumping a thermofluid through the saturator. The analyte of choice is dispersed on 1 mm glass beads (Edmund Bühler GmbH #00001067) and filled into the saturator. As the carrier gas stream passes the saturator it reaches its saturation equilibrium with the analyte and is condensed in a cold trap at -30 °C. The vapor pressure of the analyte p_{sat} at the experimental temperature T_{exp} can be calculated according to the following equation based on the validity of the Ideal Gas Law and the Dalton's Law of partial pressures:

$$p_{sat}(T_{exp}) = \frac{m_a \mathrm{R} T_{amb}}{\mathrm{M} V_{amb}} \quad (1)$$

p_{sat}: vapor pressure of the analyte [Pa] , T_{exp}: temperature of the saturator [K], m_a: mass of analyte [kg], T_{amb}: ambient temperature [K], V_{amb}: volume of carrier gas at ambient conditions [m³], M: molecular weight of the analyte [kg mol⁻¹], R: universal gas constant: 8.314469 J mol⁻¹ K⁻¹

The volume of the carrier gas V_{amb} is measured at ambient conditions by measuring its flowrate with a soap film flowmeter at the ambient temperature T_{amb} with the assumption that the volume of carrier gas is significantly higher than the volume of the gaseous analyte. The mass of the analyte m_a is determined by VO-GC/MS quantification using *n*-alkanes (C-12, C-14 or C-16) as an internal standard, which is added to the trap as acetone solution of known concentration.

The p_{sat}-T_{exp} values obtained for each analyte are analyzed with a fitting function:

$$\ln {p_{\mathrm{sat}}}/{p^{\mathrm{o}}} - \frac{\Delta^{\mathrm{g}}_{\mathrm{l/cr}} C^{\circ}_{p,m}}{R} ln \frac{T}{T_0} = A - \frac{B}{T} \quad (2)$$

p^{o}: reference pressure (1 Pa), $\Delta^{\mathrm{g}}_{\mathrm{l/cr}} C^{\circ}_{p,m}$: difference between the heat capacity of the liquid (l, for vaporization) or crystalline (cr, for sublimation) and the gaseous state [J mol⁻¹ K⁻¹], T: temperature [K], T_0: reference temperature [K], A / B: fitting coefficients (A: [ ], B: [K]).

The enthalpy of vaporization or sublimation at the temperature T can be calculated by:

$$\Delta^{\mathrm{g}}_{\mathrm{l/cr}} H^{\mathrm{o}}_{\mathrm{m}}(T) = RB + \Delta^{\mathrm{g}}_{\mathrm{l/cr}} C^{\mathrm{o}}_{p,m} T \quad (3)$$

$\Delta^{\mathrm{g}}_{\mathrm{l/cr}} H^{\mathrm{o}}_{\mathrm{m}}(T)$: molar enthalpy of vaporization (l) or sublimation (cr)

The heat capacities $C^{\mathrm{o}}_{p,m}$ of the analytes **2–4** in liquid or crystalline state are either available in the literature or calculated according to the empirical element-increment approach by *Hurst et al.* [30]. (see ESI Table S-2) The corresponding heat capacity differences with the gaseous state are calculated according to the procedures by *Chickos et al.*[31].

Safety Considerations

All nitrate esters **1–6** are energetic materials with sensitivity to various stimuli. While we encountered no issues in the handling of these materials, proper protective measures (face shield, ear protection, body armor, Kevlar gloves, and earthed equipment) should be used during the handling of nitrate esters **1-6** including vapor pressure measurements.

Results and Discussion

Energetic Performance and Sensitivities

Table S-1 compiles the energetic performance and sensitivity parameters of nitrate esters **1–6**. The sensitivity classification in the following is carried out according to the UN Recommendations on the Transport of Dangerous Goods.[32] Compounds **1–3** are liquids at room temperature and insensitive toward friction (>360 N), yet very sensitive toward impact (1 J). The sensitivity toward electrostatic discharge cannot be measured for liquids with the used testing device. ETN (**4**), MHN (**5**) and PETN (**6**) are solids, which are very sensitive toward impact (3 J for **4** and **6**) and friction (60 N for **4** and **6**). MHN **5** is more sensitive toward impact (1 J) and friction (30 N) than ETN (**4**) and PETN (**6**). Compounds **2–6** have positive or equilibrated oxygen balances Ω_{CO_2} [33]. The exothermic heats of formation were calculated on a CBS-4M level using Gaussian 09.[25] The discrepancies between experimental and calculated enthalpy of formation are in the range of the accuracy of the CBS-4M method. For the reason of comparability the calculated values were used for the calculation of the energetic performance parameters. All nitrato compounds **1–6** are classical explosives that derive their energetic performance from the oxidation of their carbon backbone. The energetic performance parameters were calculated with the EXPLO5 (v6.03) computer code at the room temperature theoretical maximum density. Due to the low density **1** is the worst performing explosive. Compounds **2–5** are closely related in terms of their molecular structure since they only differ in the number of methylene nitrato (CH_2ONO_2) units. The introduction of these units increases the density of the molecule. According to the *Kamlet-Jacobs* equations [34] the detonation velocity is directly proportional to the density and the detonation pressure is proportional to the squared density. Compounds **4** (V_{det} 8540 m s⁻¹; $p_{C\text{-}J}$ 301 kbar) and **6** (V_{det} 8490 m s⁻¹; $p_{C\text{-}J}$ 296 kbar) outperform PETN **6** (V_{det} 7655 m s⁻¹; $p_{C\text{-}J}$ 298 kbar) in terms of detonation velocity with equal (**4**) or higher (**5**) sensitivity towards external stimuli, which is owed to the thermally stabilizing quarternary carbon unit in **6**. With respect to the high energetic performance and availability of the corresponding polyol starting materials **4** and **5** should be considered a seriously dangerous in the context of improvised explosive devices. All nitrate esters **1–6** melt prior to decomposition with increasing melting and decomposition temperatures from **1** to **6**.

Table 1. GC/MS retention times and elution temperatures, NIST match scores and relative intensities of mass fragments 30, 46 and 76.

cpd.[a]	t_{ret}[b]	$T_{elution}$[c]	NIST[d]	m/z 30[e]	m/z 46[e]	m/z 76[e]	R^2[f]	LOD/LOQ[g]
	[min]	[°C]	[%]	[%]	[%]	[%]		[pg]
1	0.24	30.0	88	17/9.5/12.8	100/100/100	17.5/38.5/35.2	0.9999	3/11
2	2.26	80.4	96	15.0/9.5/22.0	100/100/100	6.2/14.5/11.2	0.9999	24/85
3	4.11	121.5	94	4.4/82.9/16.4	100/100/100	12.2/99.1/55.2	0.9999	42/148
4	5.06	150.0	n.a.	13.3/12.1/n.a.	100/100/n.a.	3.0/8.2/n.a.	0.9938	424/1839
5	n.m.	n.m	n.m.	n.m/20.3/n.a.	n.m/100/n.a.	n.m/6.3/n.a.	n.m.	n.m.
6	6.27	150.0	76	9.7/7.6/0	100/100/88.4	8.6/19.9/100	0.9991	123/429

a Number of compound according to Figure 1 b retention time of compound in VO-GC/MS analysis c Elution temperature in VO-GC/MS analysis d NIST 08 Library search match score after background subtraction e Relative spectral intensity of corresponding mass channel (VO-GC/MS / DEI-MS / NIST 08). f R^2 of linear calibration for full range calibration , g Limit of Detection / Limit of Quantification according to DIN 32645:2008 with $\alpha = \beta = 0.01$ and $k = 3$. n.m.: not measured, n.a.: not available.

Table 2. Compilation of data on available on enthalpies of vaporization $\Delta_l^g H_m^\circ$ of **2**, **3** and **4**, enthalpy of sublimation $\Delta_{cr}^g H_m^\circ$ *of* **4** and vapor pressures of compounds **1–4** *at 298.15 K.*

Experiment[a]	M[b]	T-Range	T_{avg}	$\Delta_l^g H_m^\circ(T_{avg})$	$\Delta_l^g H_m^\circ$(298.2K)[c]	p_{sat}[d]
		K	K	kJ mol^{-1}	kJ mol^{-1}	mPa
2 (l) This Work	T	274.1–318.2	294.3	65.4±0.3	65.1±0.3	12.1×10^3
Pella 1977 [35,36]	T	254.7–298.2	272.5	65.2±0.1	63.7±0.3	10×10^3
St. John 1975 [37]	I	-/-	298.2	-/-	-/-	(3.7×10^3)
Brandner 1938 [38]	T	283.2–323.2	302.6	68.0±0.2	68.3±0.3	10.6×10^3
Crater 1929 [39]	T	288.2–328.2	307.5	72.8±1.7	73.4±1.7	9.5×10^3
Rinkenbach 1926 [40]	A	273.2–295.2	283.7	63.6	(62.9)	9.8×10^3
Average EGDN 2 (l)					**65.8±0.2[e]**	**10.4×10^3[f]**
3 (l) This Work	T	283.2–328.0	302.8	86.1±0.4	86.7±0.4	82.2
Tunnell 2015 [41]	T	290.2–308.6	299.9	70.2±4.8	(70.3±4.9)	(47.8)
Mirosh. 1988 [42]	C	-/-	298.2	92.0±2.1	92.0±2.1	
Dionne 1986 [43]	T	-/-	299.2	-/-	-/-	(41.4)
St. John 1975 [37]	I	-/-	298.2	-/-	-/-	(3.2)
Dravnicks 1972 [44]	T	-/-	298.2	-/-	-/-	66.7
Kemp 1957 [45]	T	293.2–313.2	303.5	107.3±2.9	107.8±2.9	58.7
Brandner 1938 [38]	T	283.2–323.2	302.6	80.3±0.4	80.7±0.5	88.4
Marshall 1916 [46]	T	293.2–366.6	332.2	85.9±0.4	89.1±0.5	60.4
Average GTN 3 (l)					**86.0±0.3[e]**	**71.3[f]**
4 (l) This Work	T	338.0–367.8	353.9	95.1±0.9[g]	101.6±1.0[g]	
Experiment[a]	M[b]	T-Range	T_{avg}	$\Delta_{cr}^g H_m^\circ(T_{avg})$	$\Delta_{cr}^g H_m^\circ$(298.2K)[c]	p_{sat}[d]
4 (cr) This Work	T	298.2–331.0	316.5	131.8±1.1[g]	129.1±1.1[g]	0.6[g]
Oxley 2012 [3,4]]	G,O	316.2–331.2	323.7	117.7	119	3.2

a First author and year of publication, b Methods: T: Transpiration, I: Isotope Dilution, A: Air Bubbling, G: Thermogravimetry, O: Equation Only c Enthalpies of vaporization or sublimation were adjusted according to *Chickos et al.* 31 with the heat capacity parameters stated in Table S-3 d Vapor pressure at 298.15 K, calculated according to equation (2) from the individual fitting parameters of each dataset. e Weighted average value, calculated using the uncertainty as the weighing factor.

f Average value. Values in brackets were excluded from average value calculation. g Value has to be regarded critically due to unavoidable slow decomposition of ETN **4**.

Thermolability of ETN 4

A sample of **4** which was repeatedly molten and resolidified did not show any significant signs of decomposition in the ^{1}H NMR spectrum. For the vapor pressure measurement of **4** the compound was subjected to temperatures ranging from 25 to 65 °C over a period of two weeks. This led to first products of decomposition (see ESI Figure S-8). Therefore ETN **4** should not be considered a high performance melt-cast explosive with long-term stability. Due to the close structural relation MHN **5** might show the same behavior. Long-term decomposition was not observed when compounds **1–5** were stored in an argon atmosphere at -30 °C.

VO-GC/MS

The VO-GC/MS setup and method in this work allows the successful detection and detection of nitrate esters **1-4** and PETN **6**, which is demonstrated by the measurement of a mixture of nitrate esters **1–6** in acetone. (see Figure **2**, **Table 1**). MHN **5** could not be detected using the VO-GC/MS setup, which is presumably caused by decreased volatility in comparison to the other analytes. The exact GC/MS measurement parameters used in this work can be found in ESI Table S-4.

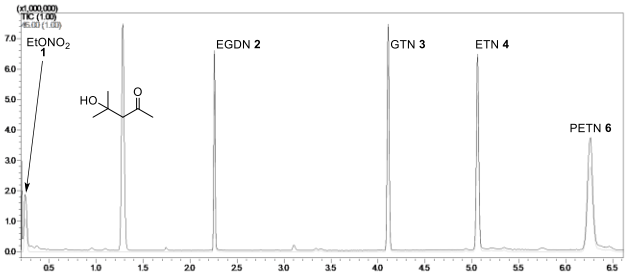

Figure 2. Vacuum Outlet GC/MS-Chromatogramm of a mixture containing nitrate esters **1–6** in acetone. Analyte concentration: 0.46 µmol mL^{-1} Black: Total Ion Count (TIC) chromatogram, grey: chromatogram of m/z 46 amu.

Table 1 is a compilation of GC/MS retention times and elution temperatures, NIST match scores and relative intensities of the selected fragment ions m/z 30, 46 and 76 amu. These mass fragments are the most intense peaks in the VO-GC/MS spectra of **2**, **3**, **4** and **6**. (see ESI p. S-16) Due to the high N,O content of the compounds the fragment ions m/z 30, 46 and 76 correspond potentially to the nitrosonium cation (NO^+, 29.9974 amu), nitronium cation (NO_2^+, 45.9924 amu) and the $N_2O_3^+$ cation (75.9903 amu). These predominant fragments are useful for the development of selective ion monitoring methods. The NIST match scores are in the range from 76% for PETN **6** to 96 % for EGDN **2**. In general the agreement of relative intensities of the fragment ions for VO-GC/MS, direct electron ionization MS and the NIST 08 library is poor for all compounds. It should be preferred to establish an internal mass spectra database for each instrument. The limits of detection (LOD) and quantification (LOQ) were calculated according to DIN 32645:2008. Both parameters increase with the molecular weight of the analyte. The LOD and LOQ of **6** are lower than that of **4**. This is presumably caused by the better thermostability of **6**. The details of calculation can be found in ESI pp. S-17–S-18.

Vapor Pressure Measurements

The detection of hazardous materials like explosives in the gaseous phase is a relatively new trend in the development of detection instruments. [11-17]. The knowledge of the vapor concentration of the analyte is essential for the definition of the air volume that needs to be sampled for exceeding the limit of detection of the applied detector system. The vapor pressure is the physico-chemical parameter that is linked to the saturation equilibrium concentration of the analytes to be detected. Therefore the vapor pressure at ambient temperatures of **2** (274–318 K), **3** (283–328 K) and **4** (298–338 K) was measured in this work with the transpiration method [8-10] and compared critically with the literature data available to establish vapor pressure and enthalpy of vaporization $\Delta_l^g H_m^\circ$ at the reference temperature 298.15 K for **2** and **3** and sublimation $\Delta_{cr}^g H_m^\circ$ (298.15 K) for the room temperature solid ETN **4**. The transpiration method is a well established [8-10] method method for the determination of vapor pressures for medium to low volatility analytes and therefore suitable for analytes **2–4**.

Experimental absolute vapor pressures measured by the transpiration method, coefficients A and B of Eq. (2), and vaporization enthalpies of analytes **2–4** derived from Eq. (3) are given in ESI pp. S-19–S-24. The procedure for calculation of the combined uncertainties of the vaporization enthalpy was described elsewhere [9]. They include uncertainties from the transpiration experimental conditions, uncertainties of vapor pressure and uncertainties from temperature adjustment to T = 298.15 K. We also collected available experimental literature data on vapor pressures of analytes **2–4**. Actually, authors not always derived vaporization enthalpies from their vapor pressures or performed it in different manner. We treated the literature vapor pressures using Eqs. (2) and (3) and calculated enthalpies of vaporization or sublimation at (298.15 K) for the sake of comparison with our results. Table 2 is a compilation of the results obtained in this work in comparison with literature values concerning the vaporization and sublimation enthalpies investigated at the average temperature of the measurement and the reference temperature 298.15 K. Additionally the vapor pressure at 298.15 K is stated. The absolute vapor pressures p_{sat} and thermodynamic properties of vaporization or sublimation obtained by the transpiration method in this work and *Clausius-Clapeyron* plots of own and literature data are available for all analytes in ESI pp. S-19–S-24.

The vaporization behavior of the analytes **2-4** was studied in this work in the temperature range from 274.1–318.2 K for **2**, 283.2 – 328.0 K for **3** and 338.0–367.8 K for **4**. The

enthalpies vaporization derived from the data obtained in this work and adjusted to 298.15 K are: 65.1±0.3 kJ mol⁻¹ for **2**, 86.7±0.4 kJ mol⁻¹ for **3** and 101.6±1.1 kJ mol⁻¹ for **4**. For compound **4** an enthalpy of sublimation at 298.15 K of 129.1±1.1 kJ mol⁻¹ was derived from the measurements. The vapor pressures at 298.15 K derived from the p-T-data obtained in this work are: 12.1 Pa for **2**, 82.2 mPa for **3** and 0.6 mPa for **4**. A Clausius-Clapeyron-plot of the data obtained in this work for compounds **2**–**4** is provided in Figure 3.

For EGDN **2**, available p-T literature data for comparison are three transpiration experiments by *Pella et al.* [35,36], *Brandner et al.* [38] and *Crater et al.* [39], an isotope dilution experiment by *St. John et al.* [37] and an air bubbling measurement by *Rinkenbach et al.* [40]. The isotope dilution data stated by *St. John et al.* [37] is considered erroneous in comparison with the other p-T-datasets available (cf. ESI Figure S-9) and is therefore disregarded. Isotope dilution measurements are not a well-established method of choice for vapor pressure measurements and may suffer from various error sources including isotope effects. *Rinkenbach et al.* [40] published solely two datapoints. This is insufficient for an error estimation – the data was therefore excluded from average value calculation.

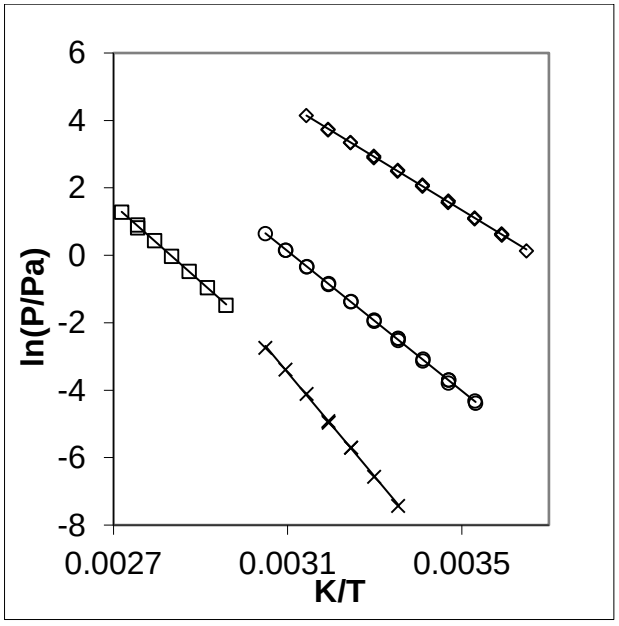

Figure 3. Clausius-Clapeyron (ln p vs 1/T) plot of the p-T-data obtained in this work for the vaporization of **2** (◊), GTN **3** (○),**4** (□) and the sublimation of **4** (×).

For GTN **3**, available p-T literature data for comparison are seven transpiration experiments by *Brandner et al.* [38], *Tunnell et al.* [41], *Dionne et al.* [43], *Dravnicks et al.* [44], *Kemp et al.* [45] and *Marshall et al.* [46] and one isotope dilution measurement by *St. John et al.* [37]. The isotope dilution data stated by *John et al.* [37] is disregarded for the reasons stated above. (cf. ESI Figure S-10) The enthalpy of vaporization at 298.15 K derived from the p-T-data of the most recent transpiration data reported by *Tunnell et al.* [41] is the lowest and most imprecise value available (cf. Table 2, 70.3 ± 4.9 kJ mol⁻¹). With respect to this their experiment is neglected in the calculation of recommended values. *Miroshnichenko et al.* [42] report calorimetric data for the enthalpy of vaporization of nitroglycerine at 298.15 K. Their value is higher than the one measured in this work. This might be caused by a dinitroglycerol sample impurity of 0.2 or 1.2 mass % stated by the authors. The enthalpy of vaporization at 298.15 K was derived from measurements in the temperature range from 40 – 120 °C, yet no statement about the sample purity after the measurements at relatively high temperatures was given. Considering this the value stated by *Miroshnichenko et al.* [42] should be regarded critically.

The sublimation behavior of the room temperature solid ETN **4** was studied in the temperature range of 298.2 – 331.0 K. The vapor pressure of ETN **4** at 298.15 K has been estimated via isothermal gravimetry by *Oxley et al.* [3,4]. This work is the first characterization of the sublimation and vaporization of ETN **4** with the well-established transpiration method, yet the values have be considered estimates due to the unavoidable slow decomposition of the analyte, which was elucidated before. (cf. ESI Figure S-8). The literature data provided by *Oxley et al.* [3,4] for ETN **4** is an Antoine equation in the temperature range of 43 °C to 58 °C and a vapor pressure at 298.15 K that was obtained by extrapolation in the original work. The values obtained in this work (101.6 ± 1.0 kJ mol⁻¹, 0.6 mPa) are not in agreement with the values published by *Oxley et al.* [3,4] (119.0 kJ mol⁻¹, 3.2 mPa), which are influenced presumably by the same decomposition problem observed in this work. Furthermore the pressure analog values obtained by thermogravimetric measurements were converted into vapor pressure values by reference material calibration with benzoic acid which is a suitable approximation for estimates but also an additional potential source of systematic error considering the absolute vapor pressures.

Oxley et al. [3,4] state an enthalpy of fusion for ETN **4** obtained by differential scanning calorimetry at heating rates from 1 to 20 K min⁻¹. The values spread from 29.9 kJ mol⁻¹ to 35.3 kJ mol⁻¹ at endotherm temperatures from 59 to 63 °C. After adjusting the values to 298.15 K according to *Chickos et al.* [31] using the heat capacity differences in ESI Table S-3 the values spread from 27.4 kJ mol⁻¹ to 32.9 kJ mol⁻¹ which results in an average value of 30.2±2.8 kJ mol for the enthalpy of fusion at 298.15 K.

Considering the relationship of the enthalpies of vaporization, sublimation and fusion at 298.15 K [31]:

$$\Delta_{\mathrm{l}}^{g} H_m^{\circ} = \Delta_{\mathrm{cr}}^{g} H_m^{\circ} - \Delta_{\mathrm{cr}}^{l} H_m^{\circ} \quad (4)$$

The enthalpy of vaporization can be derived from the enthalpy of sublimation obtained in this work: $\Delta_{\mathrm{l}}^{g} H_m^{\circ}$ = 129.1 kJ±1.1 kJ mol⁻¹ -30.2±2.8 kJ mol⁻¹ = 98.9±3.0 kJ mol

This approximated value is in fair agreement with the value for the enthalpy of vaporization at 298.15 K of 101.6±1.0 kJ mol⁻¹ measured in this work and proves the internal consistency of the data obtained despite the decomposition problem. For this reason the data published by Oxley et al. [3,4] should be regarded critically since their enthalpy of sublimation seems too low. The vapor pres-

sure at 298.15 K (0.6 mPa) estimated in this work is in rough agreement with that derived from the data by Oxley et al. (3.2 mPa) [3,4].

Based on the literature data available uncertainty weighted average values for the enthalpies of vaporization at 298.15 K and average values for the vapor pressure at 298.15 were calculated for **2** (65.8 ± 0.2 kJ mol^{-1}, 10.4 Pa) and **3** (86.0±0.3 kJ mol^{-1}, 71.3 mPa). These values are in fair agreement with the data obtained in this work. (**2**: 65.1±0.3 kJ mol^{-1}, 12.1 Pa; **3**: 86.7±0.4 kJ mol^{-1}, 82.2 mPa). Compounds **2–4** have similar structures but differ in the number of $CHONO_2$ units. With respect to the data recommended and obtained in this work the vapor pressure at 298.15 K is lowered by two orders of magnitude for each additional $CHONO_2$ unit. It is hard to measure the vapor pressure of **5**, yet it can be estimated that it should be lower than that of **4** (0.6 mPa at 298.15 K, measured in this work) by a factor of 10^4. This is a convenient explanation for its non-detectability by the VO-GC/MS method. Since **5** has the best energetic performance parameters (cf. Table S-2) but is the least volatile material with a high degree of precursor availability (as sweetening agent), it should be a benchmark analyte for the development of new explosive detection methods. Its sublimation behavior should be further investigated with low-temperature high precision methods like Knudsen-effusion and Quartz-crystal microbalances.

Conclusion

In this work the nitrate esters ethyl nitrate ($EtONO_2$, **1**), ethylene glycol dinitrate (EGDN, **2**), glyceryl trinitrate (GTN, **3**), meso-erythritol tetranitrate (ETN, **4**), D-mannitol hexanitrate (MHN, **5**) and pentaerythritol tetranitrate (PETN, **6**) were fully characterized in terms of classical chemical characterization, sensitivity toward external stimuli and energetic performance. It could be shown that compounds **1–5**, potential candidates in improvised explosive devices, are well-performing explosives with high sensitivity toward external stimuli. With respect to their gas-phase detectability the vapor pressure of compounds **2–4** was investigated. It could be demonstrated that the introduction of a $CHONO_2$ in linear nitrate esters lowers the vapor pressure by about two orders of magnitude. With respect to their vapor pressure p_{sat} at 298.2 K (**2**: 10.4 Pa, **3**: 0.071 Pa, **4**: 0.0032 Pa, **6**: 1.55×10^{-6} Pa[47]) the saturation concentration c_{sat} of the explosives can be calculated according to the ideal gas equation: c_{sat} [mg L^{-1}] $= p_{sat} \times M/(R \times 298.15\,K)$ The resulting values are: EGDN **2**: 637.9 µg L^{-1}, GTN **3**: 6.504 µg L^{-1} ETN **4**: ≈ 73 ng L^{-1} and PETN **6**: 0.198 ng L^{-1}. These values have to be considered as the maximum concentration observable. Calculations based on a mathematical model published by Dravnicks et al.[44] based on Fick's Law of diffusion (see ESI 10, exposed explosive surface 200 cm^2, 298.15 K) result in a non-equilibrium concentration for ETN **4** of 0.387 pg L^{-1}, which is lowered by about a factor of 1.9×10^5 in comparison to the saturation concentration. The limit of detection of **4** is 424 pg on column. For PETN **6** the detection limit is 123 pg on column and the non-equilibrium concentration 0.978 fg L^{-1} (same conditions). In case of an application of VO-GC/MS for gas phase detection of nitrate esters an air sampling unit needs to be constructed which collects the analytes of interest by adsorption followed by thermal desorption and lossless transfer to the analytical column. This concept was realized in Project SEDET[17]. For ETN **4** 1095 L of air need to be sampled for exceeding the limit of detection. For PETN **6** an air sampling volume of 126 m^3 would be necessary. This indicates that the gas-phase detectability of an explosive is dictated by the vapor pressure of the compound and its corresponding limit of detection. Although this calculation is just an estimate it demonstrates the feasibility of gas-phase detection of explosives since five of six nitrate esters can be detected using VO-GC/MS. The remaining challenge is the construction of a sampling unit which allows the sampling of high volumes of air and subsequent transfer to the detector system with high efficiency.

ASSOCIATED CONTENT

Supporting Information

The Supporting Information is available free of charge on the ACS Publications website:
Synthesis and Characterization of Nitrate Esters **1–6**, X-Ray Diffraction Analysis of **4** and **5**, Calculation of Column Flow at 40 and 280 °C for VO-GC/MS-Setup, Photo of the Saturator, Heat Capacities and Heat Capacity Differences of Compounds **2–4**, Long Term Stability NMR of ETN **4**, VO-GC/MS mass spectra and calculation of limits of detection of compounds **1–4** and **6**, detailed measurement results of vapor pressure measurements of compounds **2–4**, calculation of air concentration of **4** and **6**.

AUTHOR INFORMATION

Corresponding Author

*e-Mail: tmk@cup.uni-muenchen.de, tel.: +49-89-2180-77491 fax: +49-89-2180-77492, web: http://www.hedm.cup.uni-muenchen.de

Author Contributions

The manuscript was written through contributions of all authors. / All authors have given approval to the final version of the manuscript. / ‡These authors contributed equally.

ACKNOWLEDGMENT

Financial support of this work by the Ludwig-Maximilian University of Munich (LMU), the Office of Naval Research (ONR) under grant no. ONR.N00014-16-1-2062, and the Bundeswehr – Wehrtechnische Dienststelle für Waffen und Munition (WTD 91) under grant no. E/E91S/FC015/CF049 and the German Ministry of Education and Research (BMBF) under grant no. 13N12583 is gratefully acknowledged. Prof. Konstantin Karaghiosoff is thanked for help with the NMR experiments and crystallographic measurements. Miss Stefanie Schedlbauer is thanked for providing the synthetic protocol for the synthesis of PETN.

REFERENCES

(1) *Justus Liebigs Ann. Chem.* **1848**, 64, 396-398.

(2) Curry, S. H.; Aburawi, S. M. *Biopharm. Drug Dispos*. **1985**, 6, 235-280.

(3) Oxley, J. C.; Smith, J. L.; Brady, J. E.; Brown, A. C. *Propellants, Explos., Pyrotech.* **2012**, 37, 735-735.

(4) Oxley, J. C.; Smith, J. L.; Brady, J. E.; Brown, A. C. *Propellants, Explos., Pyrotech.* **2012**, 37, 24-39.

(5) Matyáš, R.; Lyčka, A.; Jirásko, R.; Jakový, Z.; Maixner, J.; Mišková, L.; Künzel, M. *J. Forensic Sci.* **2016**, 61, 759-764.

(6) Manner, V. W.; Tappan, B. C.; Scott, B. L.; Preston, D. N.; Brown, G. W. *Cryst. Growth Des.* **2014**, 14, 6154-6160.

(7)) de Zeeuw, J.; Reese, S.; Cochran, J.; Grossman, S.; Kane, T.; English, C. *J. Sep. Sci.* **2009**, 32, 1849-1857.

(8) Emel'yanenko, V. N.; Verevkin, S. P. *J. Chem. Thermodyn.* **2015**, 85, 111-119.

(9) Verevkin, S. P.; Sazonova, A. Y.; Emel'yanenko, V. N.; Zaitsau, D. H.; Varfolomeev, M. A.; Solomonov, B. N.; Zherikova, K. V. *J. Chem. Eng. Data* **2015**, 60, 89-103.

(10) Verevkin, S. P. In Experimental Thermodynamics, Weir, R. D.; Loos, T. W. D., Eds.; Elsevier, 2005, pp 5-30.

(11) Räsänen, R.-M.; Nousiainen, M.; Peräkorpi, K.; Sillanpää, M.; Polari, L.; Anttalainen, O.; Utriainen, M. Anal. Chim. Acta **2008**, 623, 59-65.

(12) Anderson, J. L.; Cantu, A. A.; Chow, A. W.; Fussell, P. S.; Nuzzo, R. G.; Parmeter, J. E.; Sayler, G. S.; Shreeve, J. n. M.; Slusher, R. E.; Story, M.; Trogler, W.; Venkatasubramaniam, V.; Waller, L. A.; Young, J.; Zukoski, C. F. Existing and Potential Standoff Explosives Detection Techniques; National Academies Press, 2004.

(13) Rhykerd, C. L.; Hannum, D. W.; Murray, D. W.; Parmeter, J. E., Guide for the Selection of Commercial Explosives Detection Systems for Law Enforcement Applications; National Institute of Justice Office of Science and Technology: Washington, DC, 1999.

(14) Cabalo, J.; Sausa, R. *Appl. Opt.* **2005**, 44, 1084-1091..

(15) Steinfeld, J. I.; Wormhoudt, *Annu. Rev. Phys. Chem.* **1998**, 49, 203-232.

(16) Bunte, G.; Hürttlen, J.; Pontius, H.; Hartlieb, K.; Krause, H. *Anal. Chimica Acta* **2007**, 591, 49-56.

(17) http://www.sedet.com/Technology.html

(18) Gatterman, L. Die Praxis des organischen Chemikers; Walter de Gruyter: Berlin / New York, 1982.

(19) NATO. Standardization Agreement (STANAG) on Explosives, Impact Sensitivity Tests, No. 4489, 1st ed.; NATO: Brussels, Belgium, 1999.

(20) NATO. Standardization Agreement (STANAG) on Explosive, Friction Sensitivity Tests, No. 4487, 1st ed.; NATO: Brussels, Belgium, 2002.

(21) WIWEB-Standardarbeitsanweisung, Nr. 4-5.1.03, Ermittlung der Explosionsgefährlichkeit oder der Reibeempfindlichkeit mit dem Reibeapparat; WIWEB: Erding, Germany, 2002.

(22) WIWEB-Standardarbeitsanweisung, Nr. 4-5.1.02, Ermittlung der Explosionsgefährlichkeit (Impact Sensitivity Tests with a Drophammer); WIWEB: Erding, Germany, 2002.

(23) http://www.reichel-partner.de

(24) http://www.bam.de

(25) http://www.ozm.cz/testing-instruments/small-scaleelectrostatic-discharge-tester.htm

(26) http://www.restek.com/images/cgram/gc_evo0406.pdf

(27) Kirchner, M.; Matisova, E.; Hrouzkova, S.; Huskova, R. *Pet. Coal* **2007**, 49, 72-79.

(28) Boeker, P.; Leppert, J. *Anal. Chem.* **2015**, 87, 9033-9041.

(29) Boeker, P.; Leppert, J.; Mysliwietz, B.; Lammers, P. S. Anal. Chem. **2013**, 85, 9021-9030.

(30) Hurst, J. E.; Keith Harrison, B. *Chem. Eng. Commun.* **1992**, 112, 21-30.

(31) Acree, W.; Chickos, J. S *J. Phys. Chem. Ref. Data* **2010**, 39, 043101.

(32) Impact: Insensitive > 40 J, less sensitive ≥ 35 J, sensitive ≥ 4 J, very sensitive ≤ 3 J; Friction: Insensitive > 360 N, less sensitive = 360 N, sensitive < 360 N and > 80 N, very sensitive ≤ 80 N, extremely sensitive ≤ 10 N. According to the UN Recommendations on the Transport of Dangerous Goods

(33) Ω [%] = (O – 2 C – H/2)·1600/M O: number of oxygen atoms, C: number of carbon atoms, H number of hydrogen atoms, M molecular mass of the compound.

(34) Kamlet, M. J.; Jacobs, S. J. *J. Chem. Phys.* **1968**, 48, 23-35.

(35) Pella, P. A. *J. Chem Thermodyn.* **1977**, 9, 301-305.

(36) Pella, P. A. *Anal. Chem.* **1976**, 48, 1632-1637.

(37)) John, G. A. S.; McReynolds, J. H.; Blucher, W. G.; Scott, A. C.; Anbar, M. *Forensic Sci.* **1975**, 6, 53-66.

(38) Brander, J. D. *Ind. Eng. Chem.* **1938**, 30, 681-684.

(39) Crater, W. D. *Ind. Eng. Chem.* **1929**, 21, 674-676.

(40) Rinkenbach, W. H. *Ind. Eng. Chem.* **1926**, 18, 1195-1197.

(41) Tunnell, R.; Tod, D. *Propellants, Explos., Pyrotech.* **2016**, 41, 173-178.

(42) Miroshnichenko, E. A.; Korchatova, L. I.; Shelaputina, V. P.; Zyuz'kevich, S. A.; Lebedev, Y. A. *Bull. Acad. Sci. USSR, Div. Chem. Sci. (Engl. Transl.)* **1988**, 37, 1778-1781.

(43) Dionne, B. C.; Rounbehler, D. P.; Achter, E. K.; Hobbs, J. R.; Fine, D. H. *J. Energ. Mater.* **1986**, 4, 447-472.

(44) Dravnicks, A.; Brabets, R.; Stanley, T. A., Evaluating Sensitivity Requirements of Explosive Vapor Detector Systems; IIT Research Institute Technology Center: Chicago Illinois, 1972.

(45) Kemp, M. D.; Goldhagen, S.; Zihlman, F. A. The Journal of Physical Chemistry **1957**, 61, 240-242.

(46) Marshall, A.; Peace, G. *J. Chem. Soc., Trans.* **1916**, 109, 298-302.

(47) Östmark, H.; Wallin, S.; Ang, H. G., *Propellants, Explos., Pyrotech.* **2012**, 37, 12-23.

Insert Table of Contents artwork here

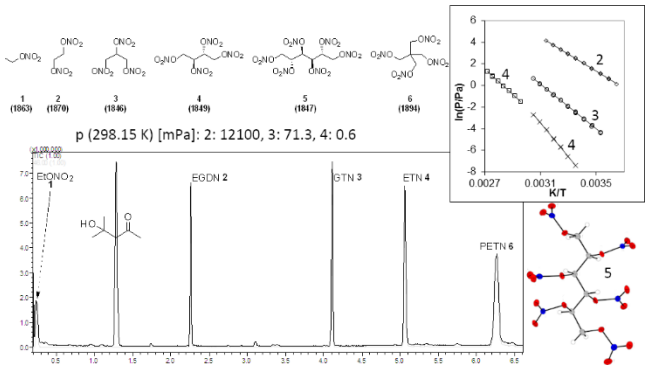

Supporting Information

Gas Phase Detectability of Linear Nitrate Esters as Components in Improvised Explosive Devices by Vacuum Outlet GC/MS

Martin A. C. Härtel, Thomas M. Klapötke*, Jörg Stierstorfer and Leopold Zehetner

Ludwig Maximilian University, Department of Chemistry, Butenandtstr. 9, 81377 Munich, Germany, *e-Mail: tmk@cup.uni-muenchen.de, tel.: +49-89-2180-77491 fax: +49-89-2180-77492, web: http://www.hedm.cup.uni-muenchen.de

1 Synthesis and Characterization of Nitrate Esters 1–6 195
1.1 Ethyl nitrate ($EtONO_2$, 1) 195
1.2 Ethylene glycol dinitrate (EGDN, 2) 196
1.3 Glyceryl trinitrate (GTN, 3) 196
1.4 meso-Erythritol tetranitrate (ETN, 4): 197
1.5 D-Mannitolhexanitrate (MHN, 5): 198
1.6 Pentaerythritoltetranitrate (PETN, 6): 198
2 X-ray Diffraction Analysis of ETN 4 and MHN 5 200
3 Calculations of Capillary Column Flows for used VO-GC/MS setup 203
3.1 Calculation of Column Flow at 40 °C Oven Temperature 203
3.2 Calculation of Column Flow at 280 °C Oven Temperature 203
4 Photo of the Saturator 204
5 Energetic Properties of Nitrate Esters 1-6 205
6 Heat Capacities and Heat Capacity Differences of compounds 2–4 206
7 Long-Term Instability of ETN 4 207
8 VO-GC/MS Parameters 208
9 VO-GC/MS mass spectra of compound 1–4 and 6 209
10 Limits of Detection LOD / Limits of Quantification LOQ 210
11 Vapor Pressure Measurements 212
11.1 p-T-data obtained in this work for EGDN 2 212
11.2 p-T-data obtained in this work for GTN 3 214
11.3 p-T-data obtained in this work for ETN 4 216
12 Calculation of Air Concentration according to Dravnicks 218
13 References 220

1 Synthesis and Characterization of Nitrate Esters 1–6

All reagents and solvents were used as received (Sigma-Aldrich, Fluka, Acros Organics, ACBR). NMR spectra were measured with a *JEOL* ECX-400 instrument. The chemical shift of the solvent peaks were adjusted according to literature values [1]. Multiplets are referred to as m (multiplet), s (singulet), d (doublet), t(triplet), q(quartett) and their combinations. Infrared spectra were measured with a Perkin-Elmer FT-IR Spektrum BXII instrument equipped with a Smith Dura SampIIR II ATR unit. Transmittance values are described as "strong" (s), "medium" (m), and "weak" (w). CI- mass spectra were measured with a JEOL MStation JMS 700 instrument. Elemental analyses (EA) were performed with a Netsch STA 429 simultaneous thermal analyzer. Sensitivity data were determined using a BAM drophammer and a BAM friction tester. The electrostatic sensitivity tests were carried out using an Electric Spark Tester ESD 2010 EN (OZM Research) operating with the "Winspark 1.15" software package. Melting and decomposition points were measured with an *Linseis PT-10 DSC* apparatus using heating rates of 5 °C min^{-1}. Temperatures are given in the order of beginning, onset, maximum, offset and end point. The literature reference for the original synthesis of the analytes 1-5 is stated at the end of each procedure.

*CAUTION! The majority of the described compounds are energetic materials with sensitivity to various stimuli. While we encountered no issues in the handling of these materials, proper protective measures (face shield, ear protection, body armor, Kevlar gloves, and earthened equipment) should be used during the handling of nitrate esters **1**-**6** including vapor pressure measurements.*

Important synthetical safety aspects will be elucidated in the following. For the synthesis of $EtONO_2$ **1** it is important to add uronium nitrate to the aqueous nitric acid before ethanol is added to prevent its oxidation to acetic acid which can result in dangerous runaway reactions. In the original literature [2] a riskful distillation is recommended but not necessary since the purity of the product before distillation is already satisfying. For EGDN **2** and GTN **3** a new workup method was established. It is important to stir the reaction strongly to avoid the dangerous build-up of a two-phase mixture. After the aqueous quenching of the mixed acid nitration the crude product is extracted and desensitized with dichloromethane, which is advantageous for the washing and drying steps that are normally carried out with the pure compound being the organic phase in the literature.

1.1 Ethyl nitrate ($EtONO_2$, 1)

Uronium nitrate **27** (5.00 g, 40.63 mmol, 0.1 eq.) was stirred with nitric acid (21 mL, 29.40 g, 466.59 mmol, 1.3 eq., 65 %) at room temperature. After 5 minutes of stirring absolute ethanol (21 mL 16.57 g, 359.66 mmol, 1.0 eq.) was added. The solution was then distilled from the reaction mixture at an oil bath temperature of 130 °C which was reached within one hour. The reaction is finished when the volume of the lower ethyl nitrate phase in the catching vessel remains constant. 34.50 g of the raw product, a colourless liquid, was washed with 3 x 20 mL of distilled water, sodium carbonate solution (0.50 g in 20 mL distilled water) and again with 2 x 20 mL distilled water. After drying over sodium sulphate 4.35 g (14 %) colourless liquid ethyl nitrate **10** were obtained and stored at -30 °C in a freezer under argon atmosphere.[2]

^{1}H NMR	(400.18 MHz, Acetone-d_6) δ 4.58 (q, *J* = 7.1 Hz, H-1), 1.34 (t, *J* = 7.1 Hz, H-2).
^{13}C{^{1}H} NMR	(100.53 MHz, Acetone-d_6) δ 70.7 (C-1), 12.4 (C-2)
^{15}N NMR	(40.51 MHz, Acetone-d_6) δ -40.8 (t, *J* = 3.0 Hz, ONO_2)
IR (ATR)	$\tilde{\nu}$ = 2992 (w), 2944 (w), 2889 (w), 1618 (s), 1477 (w), 1447 (w), 1383 (w), 1367 (m), 1277 (s), 1157 (w), 1118 (w), 1091 (w), 1009 (m), 902 (m), 853 (s), 760 (m), 703 (w) cm^{-1}.
Raman	$\tilde{\nu}$ = 2981 (36), 2948 (100), 2881 (16), 2732 (8), 1629 (8), 1459 (1), 1449 (14),

	1369 (8), 1281 (36), 1120 (13), 1093 (9), 1008 (1), 905 (3), 859 (27), 706 (4), 568 (23), 384 (27), 100 (56) cm^{-1}.
MS (CI)	m/z: 92.1 $[(C_2H_5NO_3 + H^+)^+]$.
IS	1 J (liquid).
FS [N]	> 360 N (liquid).
ESD [J]	not measurable with liquids.

1.2 Ethylene glycol dinitrate (EGDN, 2)

Nitric acid (10 mL, 15.13 g, 240.10 mmol, 12.0 eq., 100 %) was stirred and cooled by means of an ice-salt cooling bath and sulfuric acid (5 mL, 96 %) was added. Afterwards ethylene glycol (1.24 g, 19.99 mmol, 1.0 eq.) was added dropwise keeping the temperature below 10 °C. Cooling and stirring was continued for 1.5 hours and the solution was then poured in 100 mL of ice water. A white oily liquid occurred at the bottom of the beaker. Most of the water above the oil was decanted and the remaining phase mixture was extracted with dichloromethane (15 mL). The organic phase was washed with 2 x 20 mL distilled water, potassium bicarbonate solution (1.33 g in 20 mL distilled water), 2 x 20 mL distilled water and once with 20 mL brine. After drying over sodium sulfate the filtrate was separated through filtration and the solvent was removed with a rotary evaporator with a room temperature water bath. 0.88 g (29 %) of colourless liquid ethylene glycol dinitrate were obtained and stored at -30 °C in a freezer under argon atmosphere. [3]

^{1}H NMR	(400.18 MHz, dmso-d_6) δ 4.87 (s, H-1, H-2)
^{13}C{^{1}H} NMR	(100.53 MHz, dmso-d_6) δ 4.87 (s, H-1, H-2)
^{14}N NMR	(28.89 MHz, dmso-d_6) δ -43 (s, ONO_2)
IR (ATR)	$\tilde{\nu}$ = 2900 (w), 1624 (s), 1455 (w), 1427 (m), 1391 (w), 1289 (m), 1265 (s), 1038 (m), 885 (m), 831 (s), 754 (m), 710 (w) cm^{-1}.
Raman	$\tilde{\nu}$ = 3014 (4), 2975 (100), 2893 (6), 2768 (2), 2731 (3), 1639 (13), 1514 (3), 1457 (9), 1429 (13), 1396 (7), 1371 (3), 1290 (85), 1238 (4), 1115 (8), 858 (51), 754 (2), 695 (7), 647 (9), 580 (6), 562 (64), 477 (9), 386 (3), 353 (1), 280 (9), 239 (4) cm^{-1}.
MS (CI)	m/z: 153.1 $[(C_2H_4N_2O_6 + H^+)^+]$.
IS	1 J (liquid).
FS [N]	> 360 N (liquid).
ESD [J]	not measurable with liquids.

1.3 Glyceryl trinitrate (GTN, 3)

Sulfuric acid (6 mL, 96 %) and nitric acid (4 mL, 6.05 g, 96.04 mmol, 6.4 eq., 100 %) were stirred so that a swirl at the surface occurred and cooled below 0 °C by means of an ice-salt cooling bath. Glycerine (1.38 g, 14.99 mmol, 1.0 eq.) was added dropwise using a syringe without canula which was weighed before and after adding keeping the temperature below 10 °C. For three hours the temperature was kept beneath 10 °C under permanent stirring. The two phase mixture was poured into 150 mL ice water and dichloromethane (30 mL) was added. The organic phase was separated and washed with 3 x 30 mL distilled water, sodium bicarbonate solution (1.21 g in 30 mL distilled water), 2 x 30 mL distilled water and 30 mL brine. After drying over sodium sulphate the organic phase was filtered off and the solvent was evaporated with a rotary evaporator placing the flask in room temperature water. 2.56 g (75 %) colourless liquid nitroglycerine **13** were obtained and was stored at -30 °C in a freezer under argon atmosphere.[4],[3]

^{1}H NMR[5]	(400.18 MHz, Acetone-d_6) δ 5.89 (tt, J = 6.2, 3.4 Hz, H-2), 5.13 (dd, J = 13.0, 3.4 Hz, H-1,H-3), 4.95 (dd, J = 13.0, 6.2 Hz, H-1', H-3')

$^{13}C\{^1H\}$ NMR	(100.53 MHz, Acetone-d_6) δ 76.78 (C-2), 70.07 (C-1,C-3).
^{15}N NMR	(40.51 MHz, Acetone-d_6) δ -46.62 (dd, *J* = 3.8, 3.0 Hz, N-1, N3), -49.03 (d, *J* = 3.5 Hz N-2).
IR (ATR)	$\tilde{\nu}$ = 3024 (w), 1986 (w), 2911 (w), 2552 (w), 1630 (s), 1455 (w), 1427 (m), 1393 (w), 1352 (w), 1292 (m), 1264 (s), 1086 (w), 1052 (w), 1006 (m), 899 (m), 822 (s), 749 (m), 701 (w) cm^{-1}.
Raman	$\tilde{\nu}$ = 2976 (66), 2914 (3), 2899 (5), 2859 (7), 1655 (11), 1459 (7), 1431 (4), 1395 (4), 1353 (5), 1293 (53), 857 (32), 682 (5), 634 (3), 590 (6), 556 (9), 456 (1), 238 (8), 98 (100) cm^{-1}.
MS (CI)	m/z: 228.1 $[(C_3H_5N_3O_6 + H^+)^+]$.
DSC	Decompositon: 140/167/185/210/226 °C
IS	1 J (liquid).
FS [N]	> 360 N (liquid).
ESD [J]	not measurable with liquids.

1.4 meso-Erythritol tetranitrate (ETN, 4):

Nitric acid (19 mL, 28.75 g, 456.20 mmol, 13.9 eq. 100 %) was added to sulfuric acid (17 mL, 96 %) while being stirred and cooled to 0 °C by means of an ice-salt cooling bath. The temperature rose to 10 °C when D-erythritol (4.00 g, 32.75 mmol, 1.0 eq.) was added. Afterwards the solution was heated to 40 °C and stirred for one hour before it was poured on 200 mL ice water. The obtained white precipitate was washed with distilled water, sodium carbonate solution (0.70 g solved in 25 mL distilled water) and again with distilled water. After drying under suction for 20 minutes 8.17 g raw product was recrystallized from ethanol (20 mL) at 55 °C. The white crystalline product was filtered off and dried in high vacuum ($1x10^{-2}$ mbar) over night. 6.60 g (67 %) ETN **4** were obtained and stored at -30 °C in a freezer under argon atmosphere. [6]

^1H NMR	(400.18 MHz, Acetone-d_6) δ 6.03 – 5.97 (m, 2H, X-Part of $[ABX]_2$), 5.27 – 5.19 (m, 2H, A-Part of $[ABX]_2$), 5.04 – 4.95 (m, 2H, B-Part of $[ABX]_2$).
$^{13}C\{^1H\}$ NMR	(acetone-d_6, 100.53 MHz): δ 68.7 (2C, *C*-1, *C*-4), 76.5 (2C, *C*-2, *C*-3) ppm.
^{15}N NMR	(acetone-d_6, 40.51 MHz): δ -47.2 (dd, *J* = 3.9, 2.9 Hz, N-1, N-4), -51.1 (m, N-2, N-3, X-Part of AA'X).
EA	for $C_4H_6N_4O_{12}$ calculated: C 15.90, H 2.00, N 18.55 %; found: C 16.00, H 2.00, N 18.26 %.
IR (ATR)	$\tilde{\nu}$ = 3293 (w), 2978 (w), 2911 (w), 2555 (w), 1746 (w), 1656 (s), 1648 (s), 1631 (s), 1512 (w), 1488 (w), 1455 (m), 1375 (m), 1339 (w), 1294 (m), 1286 (m), 1277 (s), 1258 (s), 1228 (m), 1058 (m), 1032 (m), 982 (m), 918 (m), 872 (m), 827 (s), 754 (m), 740 (m), 696 (m) cm^{-1}.
Raman	$\tilde{\nu}$ = 3020 (19), 2980 (87), 2897 (9), 1673 (7), 1649 (17), 1632 (10), 1512 (2), 1488 (2), 1457 (25), 1386 (9), 1371 (5), 1358 (15), 1311 (15), 1297 (100), 1281 (5), 1270 (8), 1163 (9), 1085 (15), 1053 (5), 928 (3), 899 (6), 870 (71), 844 (5), 835 (15), 774 (8), 700 (45), 634 (17), 589 (20), 565 (58), 373 (5), 282 (16), 242 (18), 228 (82), 183 (22), 113 (7) cm^{-1}.
MS (DEI+)	m/z: 303.2 $[(C_4H_6N_4O_{12} + H^+)^+]$, 226.2 $[(C_4H_6N_4O_{12} - NO_2 - CH_2O)^+]$, 151.1 $[(C_4H_6N_4O_{12} + H^+ - 2\ NO_2 - 2\ CH_2O)^+]$, 118.1 $[(C_4H_6N_4O_{12} - 4\ NO_2)^+]$, 76.1 $[(CH_2NO_3)^+]$, 46.1 $[(NO_2)^+]$, 30.1 $[(CH_2O)^+]$.
DSC	Melting: 56/59/62/65/71 °C Decomposition: 144/170/182/191/210 °C
IS	3 J (100-500 µm).
FS [N]	60 N (100-500 µm).
ESD [J]	0.15 J (100-500 µm).

Density (pycnometer)	1.774 g cm^{-3}.

1.5 D-Mannitolhexanitrate (MHN, 5):

Nitric acid (15 mL, 22.69 g, 360.16 mmol, 21.9 eq., 100 %) was cooled below 0 °C by means of an acetone-ice cooling bath and D-mannitol (3.00 g, 16.47 mmol, 1.0 eq.) was added keeping the temperature below 0 °C. The obtained yellow suspension was stirred for 30 minutes while being cooled. This suspension was poured into a beaker and after adding sulfuric acid (16.5 mL, 96 %) a white viscous suspension was formed, which was poured into 300 mL ice water. A white precipitate was obtained and filtered off. It was washed with sodium carbonate solution (16.5 g in 300 mL distilled water) and with 300 mL of distilled water. 10.65 g of the wet product were recrystallized from boiling ethanol (35 mL). The fine white product was filtered off, washed with a small amount of ethanol (-30 °C cold) and dried in high vacuum (8 10^{-3} mbar) over night. 6.04 g (81 %) soft white needles of D-mannitolhexanitrate **5** were obtained and stored at -30 °C in a freezer under argon atmosphere. [7]

^{1}H NMR	(acetone-d_6, 399.78 MHz): δ = 6.33 – 6.23 (m, 1H, X-Part of $[ABMX]_2$), 6.12-6.04 (m, 1H, M-Part of $[ABMX]_2$), 5.29 (dd, *J* = 13.3, 3.3 Hz, 1H, H-1, H-6), 4.99 (dd, *J* = 13.3, 5.9 Hz, 1H, H-1, H-6).
^{13}C NMR	(acetone-d_6, 100.53 MHz): δ = 77.6 (C-2, C-5), 77.1 (C-3, C-4), 69.4 (C-1, C-6).
^{15}N NMR	(acetone-d_6, 40.51 MHz): δ = -47.8 (dd, *J* = 3.9, 3.0 Hz, N-1, N-6), -51.9 (d, *J* = 4.1 Hz, N-2, N-5), -53.2 – -54.6 (m, X-Part of AA'X, N-3, N-4).
EA	for $C_6H_8N_6O_{18}$ calculated: C 15.94, H 1.78, N 18.59 %; found: C 16.23, H 1.94, N 18.43 %.
IR (ATR)	$\tilde{\nu}$ = 3297 (w), 2981(m), 2916 (w), 2535 (w), 1677 (m), 1645 (s), 1637 (s), 1464 (m), 1378 (w), 1359 (w), 1340 (w), 1280 (s), 1271 (s), 1268 (s), 1224 (m), 1054 (w), 1042 (w), 1031 (m), 1001 (m), 963 (w), 930 (m), 860 (m), 826 (m), 749 (w), 733 (w), 701 (w), 681 (w) cm^{-1}.
Raman	$\tilde{\nu}$ = 3002 (16), 2976 (92), 2906 (14), 1681 (5), 1649 (31), 1467 (19), 1389 (7), 1356 (55), 1323 (13), 1302 (100), 1273 (4), 1235 (17), 1155 (12), 1092 (20), 1046 (5), 966 (5), 936 (8), 869 (99), 836 (8), 800 (4), 745 (9), 703 (31), 676 (16), 612 (18), 585 (8), 564 (7), 553 (10), 535 (27), 504 (6), 313 (22), 249 (5), 228 (96), 189 (34), 167 (5), 135 (34) cm^{-1}.
MS (CI)	m/z: 453.0 $[M+H^+]$
DSC	Melting: 107/109111/113/119 °C Decomposition: 162/179/200/212/230 °C
IS	1 J (100-500 µm).
FS [N]	30 N (100-500 µm).
ESD [J]	0.15 J (100-500 µm).
Density (pycnometer)	1.784 g cm^{-3}.

1.6 Pentaerythritoltetranitrate (PETN, 6):

Acetic anhydride (10.0 ml, 107 mmol) was cooled down to 0 °C. Afterwards nitric acid (2.00 ml, 44.1 mmol, 100%) and glacial acetic acid (2.00 ml, 33.1 mmol) were added slowly. The solution was stirred at 0 °C for 30 minutes. Pentaerythritol (1.00 g, 7.35 mmol) was dissolved in the nitrating medium and stirred for 4 hours at 0 °C. The mixture was brought to ambient temperature and stirred for 12 hours. Subsequently the suspension was diluted with ice-water (250 ml) and stirred for 30 minutes. A white precipitate was obtained. It was filtered off, washed

with water and $NaHCO_3$-solution (5.00 g $NaHCO_3$ in 200 ml water). After drying at ambient temperature the raw product (2.12 g) was recrystallized from ethanol (100 ml). The solution was stored in a fridge at 4 °C for 16 hours. Then the colorless needles were filtered off, washed with cold ethanol and dried in a desiccator *in vacuo* yielding 1.96 g (6.20 mmol, 84%) of white crystalline pentaerythritol tetranitrate **6**.

^{1}H NMR	(400.18 MHz, dmso-d_6) δ 4.70 (s, H-1, H-3, H-4, H-5)
^{13}C NMR	(100.53 MHz, dmso-d_6) δ 40.8 (C-2), 70.3 (C-1, C3, C-4, C-5)
^{14}N NMR	(28.89 MHz , dmso-d_6) δ -45 (s, N-1, N-3, N-4, N-5)
EA	for $C_5H_8N_4O_{12}$ calculated: C 19.00, H 2.55, N 17.72 %; found: C 19.18, H 2.49, N 17.54 %.
IR (ATR)	$\tilde{\nu}$ = 3273 (w), 3021 (w), 2983 (w), 2905 (w) 2551 (w), 1740 (w), 1638 (s), 1506 (w), 1471 (m), 1394 (w), 1383 (w), 1304 (m), 1282 (s), 1267 (s), 1193 (w), 1035 (m), 998 (m), 937 (w), 895 (w), 840 (m), 835 (m), 752 (m), 745 (m), 701 (m) cm^{-1}.
Raman	$\tilde{\nu}$ = 3024 (46), 2985 (100), 2917 (22), 2764 (3), 1671 (7), 1660 (23), 1628 (8), 1509 (4), 1469 (31), 1403 (13), 1292 (98), 1275 (8), 1251 (23), 1193 (7), 1043 (22), 1004 (5), 938 (10), 873 (52), 838 (2), 746 (6), 704 (5), 676 (12), 624 (61), 589 (24), 539 (23), 459 (9), 322 (4), 278 (12), 259 (7), 228 (43) cm^{-1}.
MS (CI)	m/z: 317.1 $[(C_5H_8N_4O_{12} + H^+)^+]$.
DSC	Melting: 132/138/140/144/150 °C Decomposition: 143/157/176/192/214 °C
IS	3 J.
FS [N]	60 N.
ESD [J]	0.19 J.
Density (pycnometer)	1.750 g cm^{-3}..

2 X-ray Diffraction Analysis of ETN 4 and MHN 5

For all measurements, an Oxford Xcalibur3 diffractometer with a CCD area detector was employed for data collection using Mo-*K*α radiation (*λ* = 0.71073 Å). By using the CRYSALISPRO software[8] the data collection and reduction were performed. The structures were solved by direct methods (SIR97[9] or SHELXS-97[10]) and refined by full-matrix least-squares on *F*2 (SHELXL [10]) and finally checked using the PLATON software [11] integrated in the WinGX software suite. The non-hydrogen atoms were refined anisotropically and the hydrogen atoms were located and freely refined. The absorptions were corrected by a SCALE3 ABSPACK multiscan method.[12] All DIAMOND2 plots are shown with thermal ellipsoids at the 50% probability level and hydrogen atoms are shown as small spheres of arbitrary radius.

*Table S-1. Crystallographic data and structure refinement details for MHN **6** and ETN **4**.*

	MHN 6 (100 K)	**ETN 4 (100K)**	**ETN 4 (291K)**
Chemical formula	$C_6H_8N_6O_{18}$	$C_4H_6N_4O_{12}$	$C_4H_6N_4O_{12}$
Molecular weight [g mol^{-1}]	452.18	302.13	302.13
Color, habit	colorless rod	colorless block	colorless block
Size [mm]	0.037x0.085x0.406	0.12 x 0.19 x 0.46	0.4x0.2x0.1
Crystal system	Orthorhombic	Monoclinic	Monoclinic
Space group	$P2_12_12_1$	$P2_1/c$	$P2_1/c$
a [Å]	4.8670(4)	15.9085(10)	16.131(4)
b [Å]	16.551(14)	5.1714(2)	5.3258(10)
c [Å]	19.6814(17)	14.7676(8)	14.849(4)
α [°]	90	90	90
β [°]	90	116.149(7)	116.56(3)
γ [°]	90	90	90
V [Å^3]	1585.8(2)	1090.57(12)	1141.5(2)
Z	4	4	4
ρ_{calc} [g cm^{-3}]	1.894	1.840	1.759
μ [mm^{-1}]	0.196	0.190	0.182
Irridiation [Å]	MoK_α 0.71069	MoK_α 0.71069	MoK_α 0.71073
F(000)	920	616	616
Q-Bereich [°]	4.23-25.68	4.2-27.5	4.6, 26.0
T [K]	100	100	291
Dataset h	-5 ≤ h ≤ 5	-20≤ h ≤ 20	-19 ≤ h ≤ 12
Dataset k	-18 ≤ k ≤ 20	-6≤ k ≤ 6	-6 ≤ k ≤ 6
Dataset l	-24 ≤ l ≤ 20	-19≤ l ≤ 19	-18 ≤ l ≤ 18
Reflecions coll.	10619	17110	7337
Independent refl.	2984	2505	2220
Observed refl.	2392	2117	1388
Parameters	272	205	205
R (int)	0.0546	0.029	0.039
GOOF	0.838	1.038	1.033
R_1, wR_2 (I>sI$_0$)	0.0393, 0.0672	0.0270, 0.0652	0.0402, 0.0918
R_1, wR_2 (all data)	0.0579, 0.0741	0.0350, 0.0701	0.0747, 0.1154
Remaining density [e Å^{-3}]	-0.271, 0.190	-0.21, 0.33	-0.18, 0.17
Device type	Oxford XCalibur3	Oxford XCalibur3	Oxford XCalibur3
Adsorption corr.	multi-scan	multi-scan	multi-scan
CCDC	1471378	1471379	1500841

[a] $wR_2 = [S[w(F_0^2-F_c^2)^2]/ S [w(F_0)^2]]^{1/2}$ where $w=[s_c^2(F_0^2)+(xP)^2+yP]$ and $P=(F_0^2+2F_c^2)/3$

Single crystals of ETN **4** were obtained by crystallization from ethanol. The structure was redetermined and corresponds to the description of *Manner et al.*.[13] It crystallizes in the monoclinic space group $P2_1/c$. Due to the high interest on compound ETN **4** two measurements were carried out at different temperatures (100 K and 291 K) to obtain a proper structural and density

parameter. At 100 K the density is 1.840 g cm^{-3}, at 291 K a value of 1.759 g cm^{-3} could be calculated. In comparison to the two polymorphs known for PETN **6**, which crystallizes tetragonal (1.778 g cm^{-3} at 283–303K [14]/ 1.845 g cm^{-3} at 100K [15]) and orthorhombic (1.72 g cm^{-3} at 283-303 K) [15] the obtained densities are very similar. The molecular structure at 100K is depicted in Figure 1. The molecular structure shows a centre of inversion at the middle of the C1–C1^{i} bond which has an expected length of 1.54 Å.

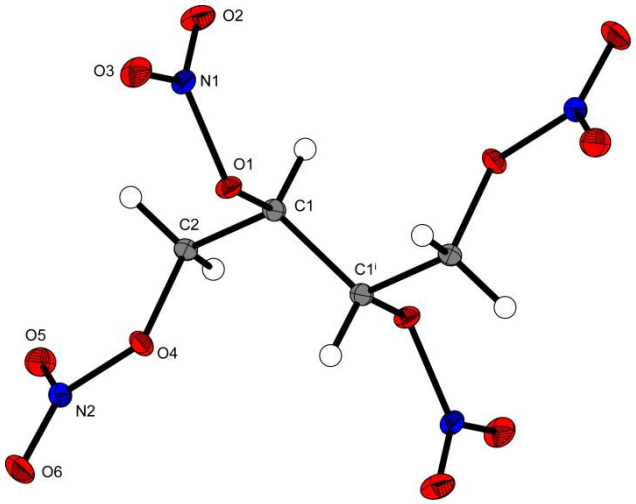

*Figure S-1. Molecular structure ETN **4** in the solid state at 100K. Thermal ellipsoids are drawn at the 50% probability level, and H atoms are shown as spheres of arbitrary radii*

Due to the absence of any NH and OH protons the structure is mainly dominated by nitro-nitro interactions and non-classical C-H···O hydrogen bonds which can be seen in Figure 2.

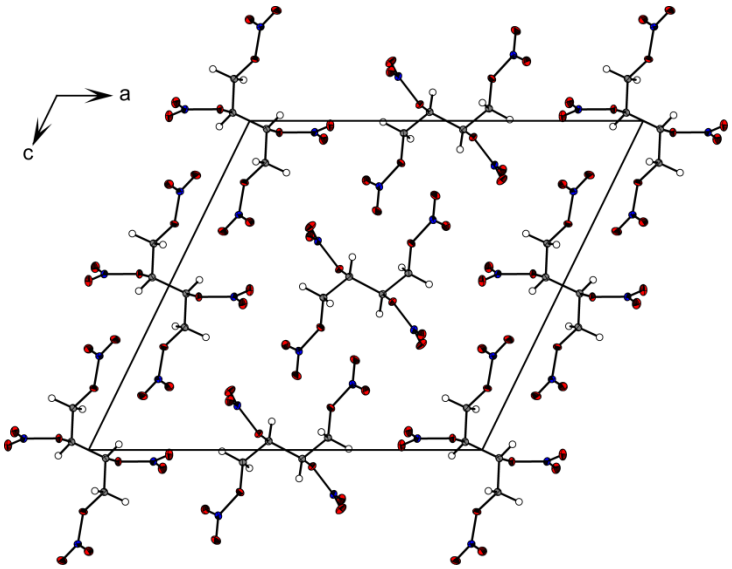

*Figure S-2 View on the unit cell of ETN **4** along the b axis*

Single crystals of MHN **6** were obtained by the vapor diffusion of n-pentane into a saturated solution of **6** in ethyl acetate. Mannitol hexanitrate (MHN, **6**) crystallizes in the orthorhombic space group $P2_12_12_1$ with a density of 1.894 g cm^{-3} at 100K. The bond length and angles of the molecular moiety are in the typical ranges and very similar to those observed for erythritol tetranitrate (see above) and also for glyceryl trinitrate (GTN **3**) (ρ = 1.842 g cm^{-3} at 153K) in the literature.[16]

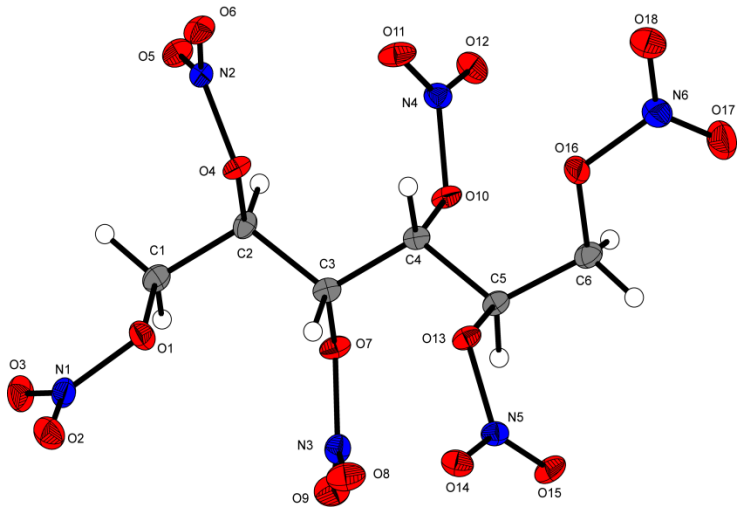

*Figure S-3. Molecular structure of mannitol hexanitrate (**6**) in the solid state at 100K. Thermal ellipsoids are drawn at the 50% probability level, and H atoms are shown as spheres of arbitrary radii.*

Again the intermolecular interactions (Figure S-4) are dominated by nitro-nitro interactions and C-H···O hydrogen bonds.

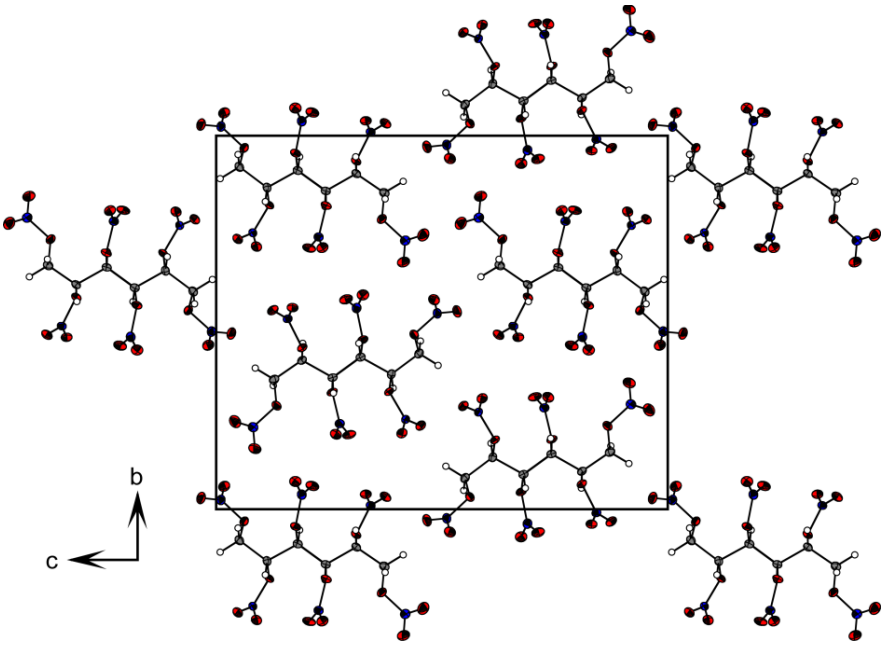

Figure S-4 - View on the unit cell of X along the a axes.

3 Calculations of Capillary Column Flows for used VO-GC/MS setup

The calculations in the following are based on the *Hagen-Poiseuille* equation [17], use the parameters of the VO-GC/MS setup in this work and demonstrate that the flow-dynamics of the restriction-column assembly are dominated by the restriction in the isothermal injector and a change of the column oven temperature from 40 °C to 280 °C results in a negligible change of calculated column flow from 4.08 mL/min to 3.92 mL/min, which corresponds to 3.9 %. Due to this it is possible to operate the GC carrier gas control unit in constant pressure mode.

3.1 Calculation of Column Flow at 40 °C Oven Temperature

Calculation of the flow through a series of capillaries

Input gauge pressures (above atmosphere as indicated by manometers)

Input pressure	kPa (g)	90
	bar (g)	0.9
	psi (gauge)	13.053

absolute pressure (needed for the calculation)

Input pressure abs.	Pa (abs.)	191300

Output pressure	Pa	0

101300=atmosphere
0=vacuum

Values from HP Flow Calculator, linear equation
Speed Optimized Flow from Blumberg (1999)

	Helium	Nitrogen	Hydrogen
C1	4.280E-08	3.500E-08	1.830E-08
C2	6.968E-06	7.994E-06	4.416E-06
SOF_100	0.8	0.25	1

Helium	C1	4.280E-08
	C2	6.968E-06
	SOF_100	0.8

capillary data		Injector	Transfer	Transfer	Column	Transfer	Transfer	Detector	Sum
i.D.	mm	0.05	0.53	0.53	0.1	0.1	0.1	0.1	
T	°C	175	40	200	240	300	300	290	
eta He	Pa s	2.615E-05	2.037E-05	2.722E-05	2.893E-05	3.150E-05	3.150E-05	3.107E-05	
lenght	m	0.0101	5.85	0.15	0	0	0	0	6.010
									K_tot
Factor K		1.89E+13	4.73E+11	2.45E+10	0	0	0	0	1.94E+13
Factor A		3.61E-05							
		Input press.	intermediate pressures						Output press.
p_middle	Pa	191300	30605	6790	0	0	0	0	0
hold-up time	s	0.00	3.79	0.01	0.00	0.00	0.00	0.00	3.80
med.lin.veloc.	m/s	40.46	1.55	10.95	0.00	0.00	0.00	0.00	
	cm/s	**4046**	**155**	**1095**	**0**	**0**	**0**	**0**	

s: 3.80 min: **0.06333**

flow @25°C,1,013 bar) ml/min: 4.08

Figure S-5. Calculation of Column Flow at 40 °C Oven Temperature

3.2 Calculation of Column Flow at 280 °C Oven Temperature

Calculation of the flow through a series of capillaries

Input gauge pressures (above atmosphere as indicated by manometers)

Input pressure	kPa (g)	90
	bar (g)	0.9
	psi (gauge)	13.053

absolute pressure (needed for the calculation)

Input pressure abs.	Pa (abs.)	191300

Output pressure	Pa	0

101300=atmosphere
0=vacuum

Values from HP Flow Calculator, linear equation
Speed Optimized Flow from Blumberg (1999)

	Helium	Nitrogen	Hydrogen
C1	4.280E-08	3.500E-08	1.830E-08
C2	6.968E-06	7.994E-06	4.416E-06
SOF_100	0.8	0.25	1

Helium	C1	4.280E-08
	C2	6.968E-06
	SOF_100	0.8

capillary data		Injector	Transfer	Transfer	Column	Transfer	Transfer	Detector	Sum
i.D.	mm	0.05	0.53	0.53	0.1	0.1	0.1	0.1	
T	°C	175	280	200	240	300	300	290	
eta He	Pa s	2.615E-05	3.064E-05	2.722E-05	2.893E-05	3.150E-05	3.150E-05	3.107E-05	
lenght	m	0.0101	5.85	0.15	0	0	0	0	6.010
									K_tot
Factor K		1.89E+13	1.26E+12	2.45E+10	0	0	0	0	2.02E+13
Factor A		3.61E-05							
		Input press.	intermediate pressures						Output press.
p_middle	Pa	191300	48155	6657	0	0	0	0	0
hold-up time	s	0.00	3.43	0.01	0.00	0.00	0.00	0.00	3.44
med.lin.veloc.	m/s	37.84	1.71	10.73	0.00	0.00	0.00	0.00	
	cm/s	**3784**	**171**	**1073**	**0**	**0**	**0**	**0**	

s: 3.44 min: **0.05738**

flow @25°C,1,013 bar) ml/min: 3.92

Figure S-6. Calculation of Column Flow at 40 °C Oven Temperature

4 Photo of the Saturator

Figure S-7. The Saturator (left) with attached cooling trap (right).

5 Energetic Properties of Nitrate Esters 1-6

*Table S-2 – Energetic Properties of Nitrate Esters **1**-**6***

	$EtONO_2$ **1**	EGDN **2**	GTN **3**	ETN **4**	MHN **5**	PETN **6**
Formula	$C_2H_5NO_3$	$C_2H_4N_2O_6$	$C_3H_5N_3O_9$	$C_4H_6N_4O_{12}$	$C_6H_8N_6O_{18}$	$C_5H_8N_4O_{12}$
MW / g mol^{-1}	91.0660	152.0620	227.0850	302.1080	452.1540	316.1350
IS[a] / J	1	1	1	3	1	3
FS[b] / N	>360	>360	>360	60	30	60
ESD[c] / *mJ*	n.m.	n.m.	n.m.	0.15	0.15	0.19
Grain Size / µm	Liquid	Liquid	Liquid	100 - 500	100 – 500	>1000
N+O[d] / %	68.09	81.55	81.91	82.10	82.28	78.45
Ω_{CO}; Ω_{CO2} / %	-26.4; -61.5	0.0; +21.0	+3.5; +24.7	+5.3; +26.5	+7.1; +28.3	-10.1; +15.2
T_{melt}[f] / °C	-95 [13]	-22 [14]	13 [15]	56 / 62 / 71	107 / 111 / 119	132 / 140 / 150
T_{dec}[g] / °C	n.m.	n.m.	140 / 185 / 226	144 / 182 / 210	143 / 176 / 214	162 / 200 /230
ρ[h] / g cm^{-3}	1.11(293 K)[16]	1.48(297 K)[14]	1.59(297 K)[14]	1.759(291 K)	1.894 (100 K)	1.845 (100 K)
	1.11*	1.48*	1.59*	1.76* (1.77)**	1.84* (1.78)**	1.79* (1.75)**
$\Delta_f H^{\circ}$[i] / kJ mol^{-1}	-190.4 ± 1.0	-233	-370 ± 2	n.a.	n.a.	-538.5 ± 0.8
$\Delta_f H$ [j] / kJ mol^{-1}	-174	-219	-311	-434	-622	-481
$\Delta_f U^{\circ}$[k] / kJ kg^{-1}	-1792	-1341	-1278	-1345	-1287	-1426
EXPLO6.03 values:						
$-\Delta_{ex}U^{\circ}$[l] / kJ kg^{-1}	4712	6563	6320	6105	5938	7797
P_{CJ}[m] / kbar	123	212	241	301	296	298
V_{det}[n] / m s^{-1}	6321	7576	7887	8540	8490	7655
V_0[o] / L kg^{-1}	976	811	782	767	755	502

[a] impact sensitivity, BAM drophammer (method 1 of 6); [b] friction sensitivity, BAM friction tester (method 1 of 6); [c] sensitivity towards electrostatic discharge; [d] summated nitrogen and oxygen content; [e] oxygen balance; [f] melting range according to DSC with 5 °C min^{-1} (start-/maximum-/end-temperature) [g] decomposition range according to DSC with 5 °C min^{-1} (start-/maximum-/end-temperature) [h] densities (*values at 298 K calculated using the equation ($\rho_{298K} = \rho_T$ / (1+α_V(298-T_0)); α_V = 1.5 10^{-4} K^{-1}; ** pycnometer density at 298 K); [i] experimental enthalpy of formation (data taken from [17]); [j] calculated condensed phase enthalpy of formation (CBS-4M) [k] calculated condensed phase energy of formation (CBS-4M; [l] heat of detonation; [m] detonation pressure; [n] detonation velocity; [o] volume of gases after detonation.

6 Heat Capacities and Heat Capacity Differences of compounds 2–4

Table S-3. Compilation of Heat Capacities and Heat Capacity Differences of Compounds 2–4

compound	$C^o_{p,m}$(l)	$C^o_{p,m}$(cr)	$C^o_{p,m}$(l)	$C^o_{p,m}$(cr)	$\Delta^g_l C^o_{p,m}$	$\Delta^g_{cr} C^o_{p,m}$
	calc.	calc.	lit.	lit.		
	[J mol^{-1} K^{-1}]	[J mol^{-1} K^{-1}]	[J mol^{-1} K^{-1}]	[J mol^{-1} K^{-1}]	[J mol^{-1} K^{-1}]	[J mol^{-1} K^{-1}]
EGDN **2**	219.3[a]	170.0[a]	(143.4) [18]	n.a.	-67.6	-26.3
GTN **3**	(319.8)[a]	247.5[a]	364.3 [19]	n.a.	-103.5	-37.9
ETN **4**	420.3	(324.9)	n.a.	334.1 [20]	-119.9	-50.9

Bracketed values not used for calculation of heat capacity differences. n.a.: not available a) calculated according to the increment method and data by *Hurst et al.* [21] b) calculated by $\Delta^g_l C^o_{p,m} = 10.58 + C^o_{p,m}(\mathrm{l}) \times 0.26$ according to [22] c) calculated by $\Delta^g_{cr} C^o_{p,m} = 0.75 + C^o_{p,m}(\mathrm{cr}) \times 0.15$ according to [22]

7 Long-Term Instability of ETN 4

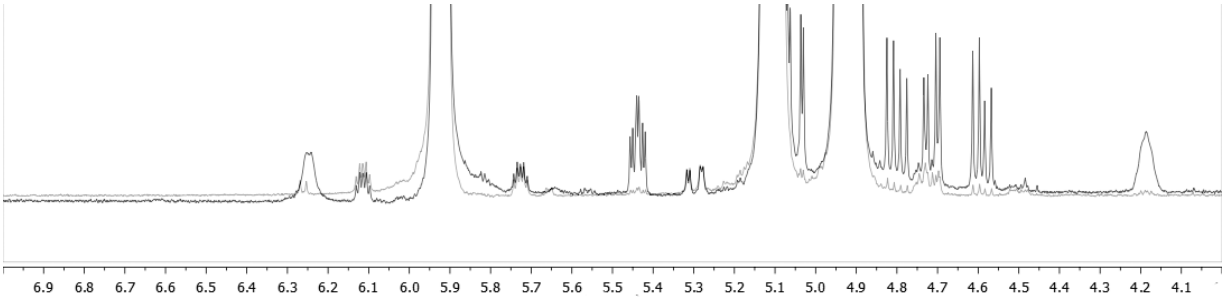

*Figure S-8. ^{1}H NMR spectra (400 MHz, DMSO-d_6, ppm-) of ETN **4** before (grey) and after (black) subjection to temperatures ranging from 25 to 58 °C over two weeks. Whilst the ^{13}C satellite signals at 5.73 and 6.13 ppm are scaled similarly the decomposition product signals are intensified significantly in the black spectrum. This demonstrates the lack of long-term stability for ETN **4**. Before: total integral of impurities <1 % of total integral. (After: 5%.)*

8 VO-GC/MS Parameters

Table S-4 – VO-GC/MS Parameters.

GC/MS	*Shimadzu QP2010SE®*
Injector	Atas Optic 4
Liner	10 mm V2A stainless steel tube, 5 mm wall thickness, equipped with silanized glass wool (2 mm injection needle penetration into wool)
Restriction	0.05 mm capillary, 10.10 mm length (Restek #10098)
Column connector	*SGE Siltite µ-Union®* (Restek #073562)
Analytical columns	*Restek RTX-TNT 1®* (6 m, 0.53 mm, 1.5 µm)
Oven program	30 °C (hold 1 min) → 100 °C (rate 40 °C min^{-1}) 100 °C (hold 1 min) → 150 °C (rate 60 °C min^{-1}) → hold 1 min **vapor pressure measurement quantification methods:** EGDN **2**/GTN **3:** 40 °C (hold 0.1 min) → 200 °C (rate 60 °C min^{-1}) ETN **4**: 40 °C (hold 0.1 min) → 200 °C (rate 33 °C min^{-1})
Injector head pressure	90 kPa
virtual column	100 m, 0.25 µm film thickness, 0.20 mm i.d.
column flow	3.92 – 4.08 mL min^{-1}
split ratio	150
split flow	25.37 mL/min (measured at split exit with soap film flow meter, corrected according to *Boeker et al.* [19]
purge flow	5 mL min^{-1}
injection volume	1 µL
Ion source	200 °C
MS interface	200 °C
MS	scan m/z 30-500, acquisition time 0.30 s SIM m/z 46 30 76, acquisition time 0.10 s **vapor pressure measurement quantification methods:** EGDN 2/ GTN 3: SIM 1.00 – 2.00 min m/z 46 30 76 2.00 – 2.77 min m/z 57 71 43 85 ETN 4: SIM 1.00 – 3.50 min m/z 71 57 43 85; 3.50 – 4.95 min 46 30 76 31 Acquisition time for SIM measurements: 0.10

9 VO-GC/MS mass spectra of compound 1–4 and 6

$Et(ONO_2)_2$ 1

# of Peaks 26
Raw Spectr 0.250 (scan : 11)
Backgroun 1.820 -> 2.080 (scan : 325 -> 377)
Base Peak m/z 46.00 (Inten : 985,530)

Event#	1	
m/z	Absolute Int	Relative Intensity
30	155091	15.74
31.05	6800	0.69
36.9	2545	0.26
38	3415	0.35
39	8320	0.84
39.9	2677	0.27
41.05	5345	0.54
42	22183	2.25
43	207101	21.01
44	11025	1.12
45.05	11808	1.2
46	985530	100
47	5122	0.52
48.05	4583	0.47
55.05	1586	0.16
58.05	31536	3.2
59	1996	0.2
59.85	1636	0.17
62	3466	0.35
72	1076	0.11
75.05	1426	0.14
76	178673	18.13
77	3490	0.35
83	1078	0.11
83.9	1914	0.19
90	3826	0.39

EGDN 2

# of Peaks 19
Raw Spectr 2.260 (scan : 413)
Backgroun 1.410 -> 1.655 (scan : 243 -> 292)
Base Peak m/z 46.00 (Inten : 5,258,290)

Event#	1	
m/z	Absolute Int	Relative Intensity
30	705581	13.42
31	110866	2.11
32	6428	0.12
38.95	653	0.01
39.85	425	0.01
41.05	3909	0.07
42	24503	0.47
43.05	45258	0.86
44	7477	0.14
45.05	46437	0.88
46	5258290	100
46.95	25467	0.48
48	17983	0.34
60	4263	0.08
75.05	2116	0.04
75.95	297427	5.66
76.9	4332	0.08
77.85	2270	0.04
89.95	3850	0.07

GTN 3

# of Peaks 27
Raw Spectr 4.110 (scan : 783)
Backgroun 3.585 -> 3.930 (scan : 678 -> 747)
Base Peak m/z 46.00 (Inten : 6,132,038)

Event#	1	
m/z	Absolute Int	Relative Intensity
30	539371	9.78
31.05	173319	2.83
32	6516	0.11
38	1089	0.02
39	2617	0.04
39.95	1019	0.02
41.05	5616	0.09
42	30663	0.5
43	56092	0.91
43.9	7964	0.13
45.05	53090	0.87
46	6132038	100
47	30791	0.5
47.95	24044	0.39
54.9	3606	0.06
55.9	2946	0.05
57.05	1081	0.02
58	2661	0.04
60	8252	0.13
70.8	1295	0.02
75.05	1481	0.02
76	274522	4.48
76.95	4715	0.08
78.05	1886	0.03
88.9	1318	0.02
119.05	2810	0.05
150.9	6281	0.1

ETN 4

# of Peaks 35
Raw Spectr 5.060 (scan : 973)
Backgroun 3.470 -> 3.925 (scan : 655 -> 746)
Base Peak m/z 46.00 (Inten : 5,223,388)

Event#	1	
m/z	Absolute Int	Relative Intensity
30	541118	10.36
31	174727	3.35
32	17918	0.34
37	1015	0.02
39	5048	0.1
40	237	0
41.05	7669	0.15
42	29826	0.57
43	73901	1.41
44.1	18475	0.35
45.05	46895	0.9
46	5223388	100
46.9	28417	0.54
48	19777	0.38
53.1	1599	0.03
54.05	1546	0.03
55.05	14856	0.28
56	4010	0.08
56.95	3460	0.07
58.05	4637	0.09
58.95	8552	0.16
60	12182	0.23
61	2962	0.06
69	3038	0.06
71.05	8052	0.15
72.05	4259	0.08
73.15	3698	0.07
75.05	1074	0.02
75.95	167390	3.2
76.9	3086	0.06
77.95	1082	0.02
89.15	1560	0.03
106	1932	0.04
118	3332	0.06
151	6446	0.12

PETN 6

# of Peaks 37
Raw Spectr 6.265 (scan : 1214)
Backgroun 6.635 -> 7.135 (scan : 1288 -> 1388)
Base Peak m/z 46.00 (Inten : 2,786,208)

Event#	1	
m/z	Absolute Int	Relative Intensity
30	230923	8.23
31.05	69094	2.48
32	2778	0.1
38.1	1570	0.06
39.05	20787	0.75
40.05	11524	0.41
41.05	24666	0.89
42	39470	1.42
43	40510	1.45
44	18480	0.66
45.05	30899	1.11
46	2786208	100
46.95	14848	0.53
48	8492	0.3
52.95	2581	0.09
53.95	5146	0.18
54.95	22481	0.81
56.05	15488	0.56
57.05	26699	0.96
58.05	5246	0.19
60.05	15806	0.57
68.15	1497	0.05
69.1	6018	0.22
69.95	3036	0.11
71.05	9448	0.34
72.05	2056	0.07
73	4630	0.17
75.05	1532	0.05
75.95	249015	8.94
77	4602	0.17
78.1	1839	0.07
82.9	1928	0.07
83.8	1063	0.04
84.9	5057	0.18
86.1	1521	0.05
87.15	1046	0.04
102.1	3873	0.14

10 Limits of Detection LOD / Limits of Quantification LOQ

A 1:1 dilution series mixture of the analytes **1**–**4** and **6** in acetone was created and measured in the GC/MS device. Each sample was measured three times and the average value of the peak area (automatic integration) calculated. The results for the dilution steps 1–6 are compiled in Table S-5 and can be regarded as an external standard quantification. Considering this the coefficient of determination R^2 by linear regression is given for each analyte.

Table S-5 – Results of LOD/LOQ measurement

$EtONO_2$ **1**		1	2	3	4	5	6
concentration	[µg/mL]	1.74	0.87	0.44	0.22	0.11	0.05
peak area	[counts]	58059	28711	14659	7198	3580	1842
σ	[counts]	1892	799	482	52	39	16
R^2	0.99995						
EGDN **2**							
concentration	[µg/mL]	6.57	3.29	1.64	0.82	0.41	0.21
peak area	[counts]	304428	154662	76294	36804	17310	5920
σ	[counts]	8567	1873	251	115	2073	109
R^2	0.99979						
GTN **3**							
concentration	[µg/mL]	4.85	2.42	1.21	0.61	0.30	0.15
peak area	[counts]	236295	111750	53592	27498	14530	8485
σ	[counts]	909	1395	642	710	687	375
R^2	0.99875						
ETN **4**							
concentration	[µg/mL]	13.21	6.60	3.30	1.65	0.83	0.41
peak area	[counts]	272349	102156	34764	12109	4408	1574
σ	[counts]	10803	2041	280	314	36	44
R^2	0.98347						
PETN **6**							
concentration	[µg/mL]	6.96	3.48	1.74	0.87	0.44	0.22
peak area	[counts]	242153	104134	42867	18749	8017	2494
σ	[counts]	8051	3606	894	560	378	1918
R^2	0.99493						

With the results from linear regression analysis for the external standard calibration in hands the Limit of Detection (LOD) and Quantification (LOQ) was calculated for the calibration method according to the German industry standard DIN 32645:2008 with $\alpha = \beta = 0.01$ and $k = 3$. A second boundary condition is the correct identification of the analyte by the absolute intensity ratio of quantification (m/z 46) and two reference ions (m/z 30, 76) with a default ion allowance of 30%. To generate values suitable for the comparison of different chromatographic setups the values obtained in µg mL^{-1} valid for the setup in the configuration stated above were calculated to the mass transferred into the analytical column [pg] considering the injection volume and the split proportion, which is the quotient of column flow to the sum of column and split flow. (4.08 mL min^{-1} / (4.08 + 25.37 mL min^{-1}) = 0.139) The results of the calculation are stated in Table S-6 in the publication.

Table S-6 – Limits of Detection and Quantification determined according to DIN 32645:2008 with α =°β = 0.01 and k = 3 using the values compiled in Table S-5.

	LOD [µg/mL]	LOQ [µg/mL]	LOD [pg]	LOQ [pg]
$EtONO_2$ **1**	0.022	0.079	3	11
EGDN **2**	0.172	0.615	24	85
GTN **3**	0.306	1.067	42	148
ETN **4**	3.059	13.272	424	1839
PETN **6**	0.888	3.098	123	429

11 Vapor Pressure Measurements

11.1 p-T-data obtained in this work for EGDN 2

*Table S-7. Ethylene glycol dinitrate **2**: absolute vapor pressures p_{sat} and thermodynamic properties of vaporization obtained by the transpiration method in this work*

Ethylene glycol dinitrate **2**: $\Delta_l^g H_m^\circ$ (298.15 K) = 65.1 ± 0.3 kJ mol^{-1}

$$\ln p_{sat}/p^\circ = \frac{306.8}{R} - \frac{85275.3}{RT} + \frac{67.6}{R} ln \frac{T}{298.15\mathrm{K}}$$

T_{exp}[a]	m[b]	V_{N2}[c]	T_{amb}[d]	Gasflow	p_{sat}[e]	$u(p_{sat})$[f]	$\Delta_l^g H_m^\circ$	$\Delta_l^g S_m^\circ$
[K]	[mg]	[dm³]	[K]	[dm³ h^{-1}]	[Pa]	[Pa]	[kJ mol^{-1}]	[J mol^{-1} K^{-1}]
274.1	0.55	8.160	302.3	3.06	1.15	0.03	66.75	148.9
278.4	0.90	7.915	297.2	4.75	1.89	0.05	66.45	148.2
278.4	0.77	6.803	297.2	5.75	1.87	0.05	66.46	148.2
278.4	0.31	2.835	299.1	3.04	1.82	0.05	66.45	148.0
283.3	1.06	5.693	297.3	4.74	3.05	0.08	66.12	146.9
283.3	0.31	1.720	299.7	3.04	2.95	0.08	66.12	146.6
288.3	0.85	2.770	297.6	4.75	5.05	0.15	65.79	146.0
288.3	0.96	3.318	302.9	3.06	4.80	0.13	65.79	145.5
293.3	0.82	1.651	297.9	4.72	8.09	0.23	65.45	144.9
293.3	1.03	2.195	302.7	3.06	7.77	0.22	65.45	144.5
298.2	1.39	1.810	297.9	4.72	12.53	0.34	65.11	143.6
298.3	0.86	1.175	303.3	3.07	12.14	0.33	65.11	143.3
303.2	0.89	0.766	297.9	2.87	18.95	0.50	64.78	142.4
303.2	0.83	0.765	303.2	3.06	18.11	0.48	64.78	142.0
308.2	2.77	1.575	297.5	4.73	28.60	0.74	64.44	141.3
308.2	0.86	0.503	301.3	2.01	28.23	0.73	64.44	141.1
313.2	3.06	1.180	297.6	4.72	42.24	1.08	64.11	140.1
313.2	0.86	0.342	301.9	1.03	41.47	1.06	64.10	139.9
318.2	6.42	1.651	297.4	4.72	63.22	1.61	63.77	139.2

[a] Saturation temperature ($u(T)$ = 0.1 K). [b] Mass of transferred sample condensed at T = 243 K [c] Volume of nitrogen ($u(V)$ = 0.005 dm^3) used to transfer m ($u(m)$ = 0.0001 g) of the sample. [d] T_a is the temperature of the soap bubble meter used for measurement of the gas flow. [e] Vapor pressure at temperature T, calculated from the m and the residual vapor pressure at the condensation temperature calculated by an iteration procedure; p°=1 Pa. [f] Standard uncertainty in p was calculated with $u(p/\mathrm{Pa})$ = 0.005+0.025(p/Pa) for p < 5 Pa and $u(p/\mathrm{Pa})$ = 0.025+0.025(p/Pa) for p > 5 to 3000 Pa.

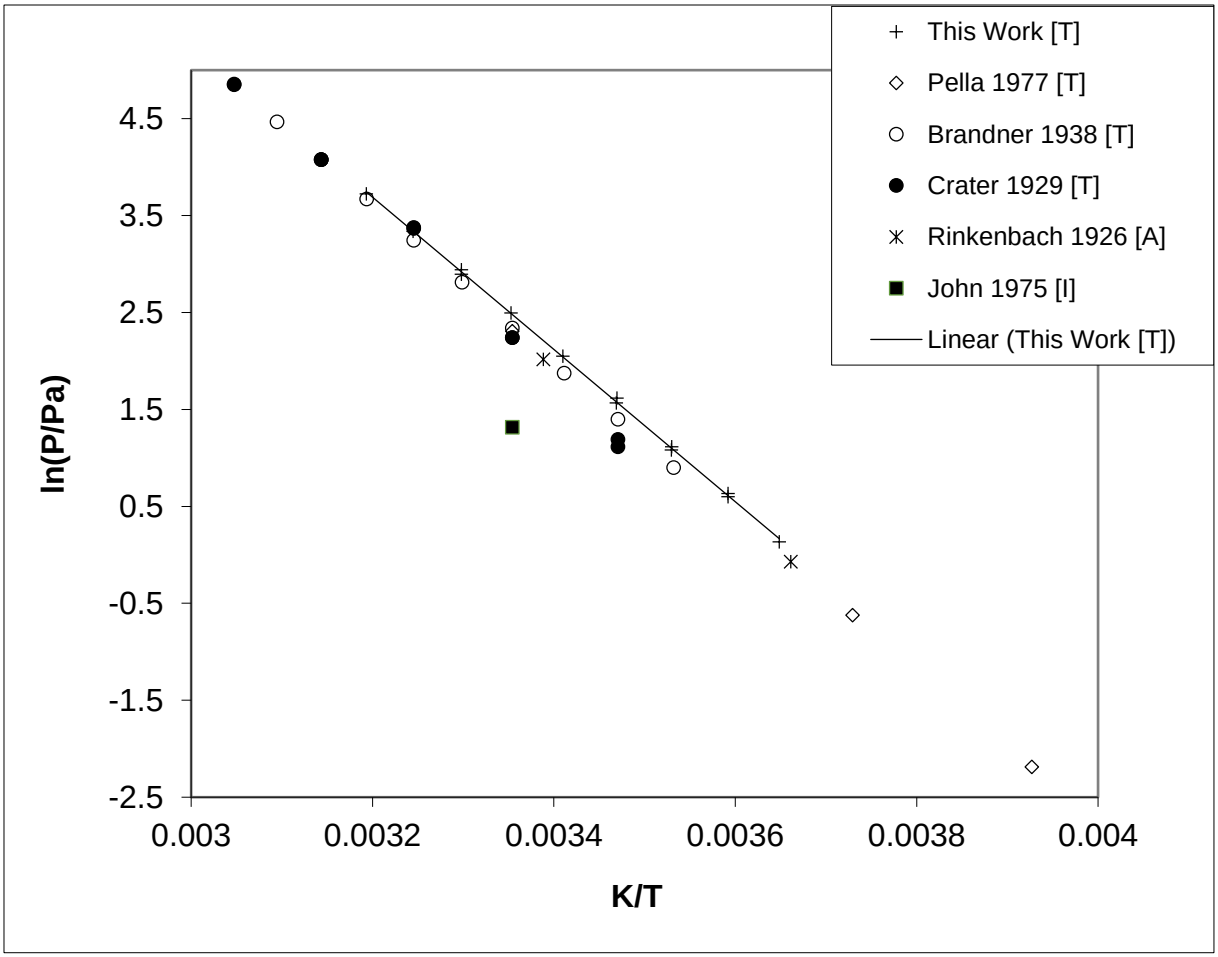

Figure S-9 – Experimental vapor pressure of EGDN 2 in comparison with literature values.

Table S-8 – Compilation of Data available on Enthalpies of vaporization $\Delta_l^g H_m^\circ$ for ethylene glycol dinitrate

Experiment[a]	Method[b]	T-Range	T_{avg}	$\Delta_l^g H_m^\circ(T_{avg})$	$\Delta_l^g H_m^\circ$(298.15K)[c]	p_{sat}[d]
		K	K	kJ mol^{-1}	kJ mol^{-1}	Pa
This Work	T	274.1 – 318.2	294.3	65.4±0.3	65.1±0.3	12.1
Pella 1977 [23]	T	254.7 – 298.2	272.5	65.2±0.1	63.7±0.3	10.0
John 1975 [24]	I		298.2			(3.7)
Brandner 1938 [25]	T	283.2 – 323.2	302.6	68.0±0.2	68.3±0.3	10.6
Crater 1929 [26]	T	288.2 – 328.2	307.5	72.8±1.7	73.4±1.7	9.5
Rinkenbach 1926 [27]	A	273.2 – 295.2	283.7	63.6	(62.9)	9.8
					65.8±0.2[e]	10.4[f]

[a] First author and year of publication, [b] Methods: T: Transpiration, I: Isotope Dilution, A: Air Bubbling [c] Enthalpies of vaporization were adjusted according to *Chickos et al.* [22] with $\Delta_{cr}^g C_{p,m}^\circ$= -47.9 J mol^{-1} K^{-1} and $C_{p,m}^\circ$(l)= 143.4 J mol^{-1} K^{-1} (see Table S-3) [d] Vapor pressure at 298.15 K, calculated according to equation 2 in the main paper. [e] Weighted average value, calculated using the uncertainty as the weighing factor. [f] Average value. Values in brackets were excluded from average value calculation.

11.2 p-T-data obtained in this work for GTN 3

Table S-9. Nitroglycerine: absolute vapor pressures p_{sat} and thermodynamic properties of vaporization obtained by the transpiration method in this work

Nitroglycerine : $\Delta_l^g H_m^\circ$ (298.15 K) = 86.7 ± 0.4 kJ mol^{-1}

$$\ln p_{sat}/p^\circ = \frac{375.4}{R} - \frac{118111.5}{RT} + \frac{105.3}{R} ln \frac{T}{298.15\text{K}}$$

T_{exp}[a]	m[b]	V_{N2}[c]	T_{amb}[d]	Gasflow	p_{sat}[e]	$u(p_{sat})$[f]	$\Delta_l^g H_m^\circ$	$\Delta_l^g S_m^\circ$
[K]	[mg]	[dm³]	[K]	[dm³ h^{-1}]	[Pa]	[Pa]	[kJ mol^{-1}]	[J mol^{-1} K^{-1}]
283.3	0.11	86.5	297.7	4.98	0.0134	0.0053	88.28	180.1
283.2	0.07	65.3	298.9	5.09	0.0125	0.0053	88.30	179.7
288.2	0.07	30.5	297.4	5.98	0.0249	0.0056	87.77	178.1
288.2	0.28	121	297.1	4.98	0.0248	0.0056	87.77	178.1
288.2	0.16	78.1	302.4	4.13	0.0227	0.0056	87.76	177.3
293.2	0.13	30.9	297.2	4.98	0.0464	0.0062	87.24	176.3
293.2	0.15	37.3	301.3	5.09	0.0437	0.0061	87.24	175.8
298.1	0.17	22.0	296.6	4.92	0.0857	0.0071	86.72	174.7
298.1	0.15	19.8	297.1	4.90	0.0847	0.0071	86.72	174.6
298.2	0.14	19.5	302.1	5.11	0.0802	0.0070	86.71	174.1
303.1	0.16	11.8	297.8	4.97	0.148	0.009	86.19	172.7
303.1	0.14	10.9	297.7	5.04	0.141	0.009	86.19	172.3
308.1	0.13	5.64	298.2	4.98	0.254	0.011	85.67	170.9
308.1	0.14	5.96	303.2	5.11	0.254	0.011	85.66	170.9
313.1	0.13	3.29	298.3	4.94	0.435	0.016	85.15	169.3
313.1	0.30	8.00	302.1	5.11	0.421	0.016	85.14	169.0
318.1	0.12	1.91	298.4	4.97	0.716	0.023	84.62	167.6
318.1	0.16	2.56	302.9	5.11	0.713	0.023	84.62	167.5
323.0	0.13	1.24	298.4	4.97	1.17	0.03	84.10	165.9
323.1	0.17	1.62	303.5	5.13	1.16	0.03	84.09	165.8
328.0	0.31	1.74	297.3	4.96	1.92	0.05	83.57	164.5

[a] Saturation temperature ($u(T)$ = 0.1 K). [b] Mass of transferred sample condensed at T = 243 K [c] Volume of nitrogen ($u(V)$ = 0.005 dm^3) used to transfer m ($u(m)$ = 0.0001 g) of the sample. [d] T_a is the temperature of the soap bubble meter used for measurement of the gas flow. [e] Vapor pressure at temperature T, calculated from the m and the residual vapor pressure at the condensation temperature calculated by an iteration procedure; p°=1 Pa. [f] Standard uncertainty in p was calculated with $u(p/\text{Pa})$ = 0.005+0.025(p/Pa) for p < 5 Pa and $u(p/\text{Pa})$ = 0.025+0.025(p/Pa) for p > 5 to 3000 Pa.

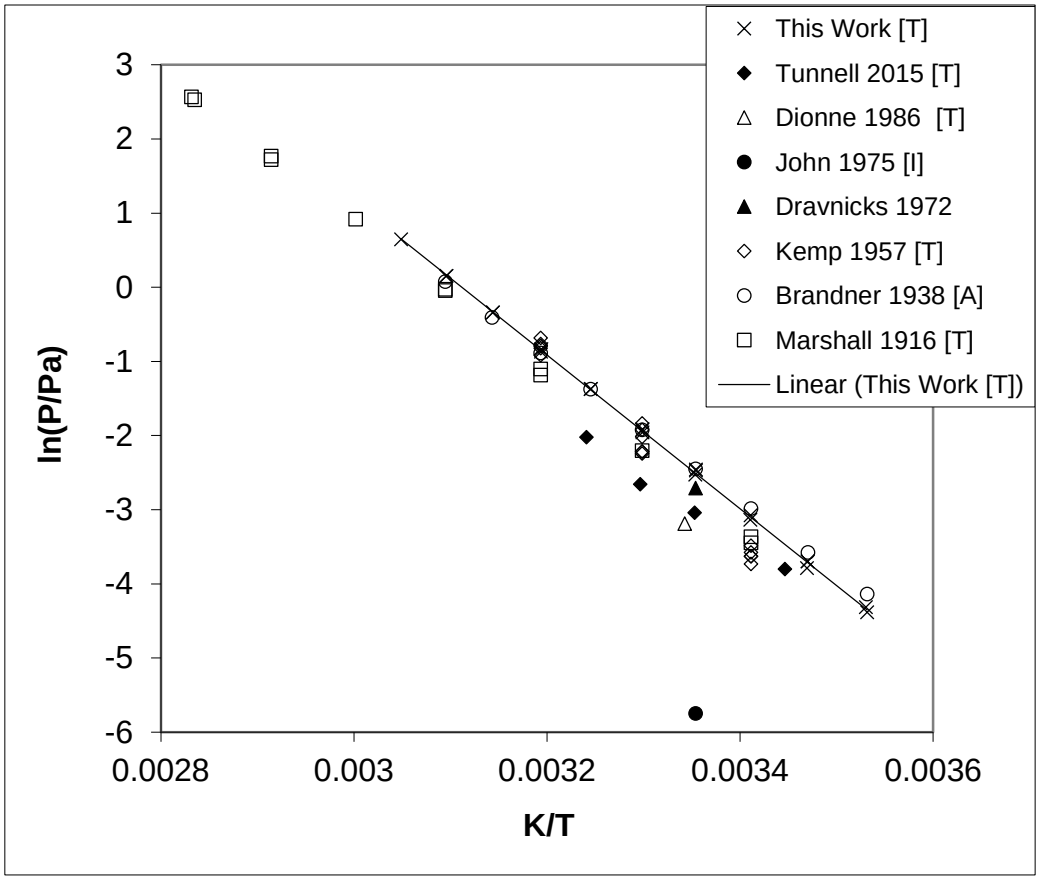

Figure S-10. Experimental vapor pressure of nitroglycerine in comparison with literature values.

Table S-10. Compilation of data available on enthalpies of vaporization $\Delta_l^g H_m^\circ$ for nitroglycerine

Experiment[a]	Method[b]	T-Range	T_{avg}	$\Delta_l^g H_m^\circ(T_{avg})$	$\Delta_l^g H_m^\circ$(298.15K)[c]	p_{sat}[d]
		K	K	kJ mol^{-1}	kJ mol^{-1}	mPa
This Work	T	283.2 – 328.0	302.8	86.1±0.4	86.7±0.4	82.2
Tunnell 2015 [28]	T	290.2 – 308.6	299.9	70.2±4.8	(70.3±4.9)	(47.8)
Mirosh. 1988 [29]	C		298.15	92.0±2.1	92.0±2.1	
Dionne 1986 [30]	T		299.2			(41.4)
John 1975 [24]	I		298.2			(3.2)
Dravnicks 1972 [31]	T		298.2			66.7
Kemp 1957 [32]	T	293.2 - 313.2	303.5	107.3±2.9	107.8±2.9	58.7
Brandner 1938 [25]	T	283.2 – 323.2	302.6	80.3±0.4	80.7±0.5	88.4
Marshall 1916 [33]	T	293.2 – 366.6	332.2	85.9±0.4	89.1±0.5	60.4
					86.0±0.3[e]	71.3[f]

[a] First author and year of publication, [b] Methods: T: Transpiration, C: Calorimetry, I: Isotope Dilution [c] Enthalpies of vaporization were adjusted according to *Chickos et al.* [22] with $\Delta_{cr}^g C_{p,m}^\circ$= -103.5 J mol^{-1} K^{-1} and $C_{p,m}^\circ$(l)= 364.3 J mol^{-1} K^{-1} (see Table S-3) [d] Vapor pressure at 298.15 K, calculated according to equation 2 in the main paper. [e] Weighted average value, calculated using the uncertainty as the weighing factor. [f] Average value. Values in brackets were excluded from average value calculation.

11.3 p-T-data obtained in this work for ETN 4

Table S-11. Erythritol tetranitrate: absolute vapor pressures p_{sat} and thermodynamic properties of sublimation obtained by the transpiration method in this work

Erythritol tetranitrate: $\Delta_{cr}^{g} H_m^{\circ}$ (298.15 K) = 129.1 ± 1.1 kJ mol^{-1}

$$\ln p_{sat}/p^{\circ} = \frac{422.2}{R} - \frac{144244.1}{RT} + \frac{50.9}{R} ln \frac{T}{298.15\mathrm{K}}$$

T_{exp}[a]	m[b]	V_{N2}[c]	T_{amb}[d]	Gasflow	p_{sat}[e]	$u(p_{sat})$[f]	$\Delta_{cr}^{g} H_m^{\circ}$	$\Delta_{cr}^{g} S_m^{\circ}$
[K]	[mg]	[dm³]	[K]	[dm³ h^{-1}]	[mPa]	[mPa]	[kJ mol^{-1}]	[J mol^{-1} K^{-1}]
298.2	0.02	329	296.5	4.92	0.6	5.0	129.07	275.4
303.1	0.02	90.4	296.4	5.00	1.4	5.0	128.82	274.7
308.1	0.04	109	296.6	4.99	3.3	5.1	128.56	274.1
308.1	0.14	351	296.6	5.17	3.3	5.1	128.56	274.1
313.1	0.19	211	296.7	4.88	7.4	5.2	128.31	273.3
313.1	0.10	122	297.3	5.01	7.0	5.2	128.31	272.9
318.1	0.24	120	296.7	5.05	16.4	5.4	128.05	272.7
323.0	0.47	114	296.9	5.05	33.7	5.8	127.80	271.7
328.0	0.30	38.4	296.8	5.05	64.4	6.6	127.55	270.3

Erythritol tetranitrate: $\Delta_{l}^{g} H_m^{\circ}$ (298.15 K) = 99.7 ± 2.5 kJ mol^{-1}

$$\ln p_{sat}/p^{\circ} = \frac{395.1}{R} - \frac{132411.2}{RT} + \frac{119.9}{R} ln \frac{T}{298.15\mathrm{K}}$$

T_{exp}[a]	m[b]	V_{N2}[c]	T_{amb}[d]	Gasflow	p_{sat}[e]	$u(p_{sat})$[f]	$\Delta_{l}^{g} H_m^{\circ}$	$\Delta_{l}^{g} S_m^{\circ}$
[K]	[mg]	[dm³]	[K]	[dm³ h^{-1}]	[Pa]	[Pa]	[kJ mol^{-1}]	[J mol^{-1} K^{-1}]
338.0	0.16	5.787	297.7	4.96	0.23	0.01	96.84	178.5
342.9	0.23	4.979	297.8	4.98	0.38	0.01	96.24	177.0
347.9	0.21	2.819	298.2	4.98	0.62	0.02	95.64	175.3
352.9	0.15	1.247	297.4	4.99	0.97	0.03	95.05	173.4
357.9	0.24	1.245	297.5	4.98	1.56	0.04	94.45	171.9
362.9	0.37	1.237	297.4	4.95	2.46	0.07	93.85	170.4
362.9	0.45	1.635	299.0	4.90	2.27	0.06	93.85	169.8
367.8	0.97	2.218	298.7	4.93	3.60	0.10	93.26	168.5

[a] Saturation temperature ($u(T)$ = 0.1 K). [b] Mass of transferred sample condensed at T = 243 K [c] Volume of nitrogen ($u(V)$ = 0.005 dm^3) used to transfer m ($u(m)$ = 0.0001 g) of the sample. [d] T_a is the temperature of the soap bubble meter used for measurement of the gas flow. [e] Vapor pressure at temperature T, calculated from the m and the residual vapor pressure at the condensation temperature calculated by an iteration procedure; p°=1 Pa. [f] Standard uncertainty in p was calculated with $u(p/\mathrm{Pa})$ = 0.005+0.025(p/Pa) for p < 5 Pa and $u(p/\mathrm{Pa})$ = 0.025+0.025(p/Pa) for p > 5 to 3000 Pa.

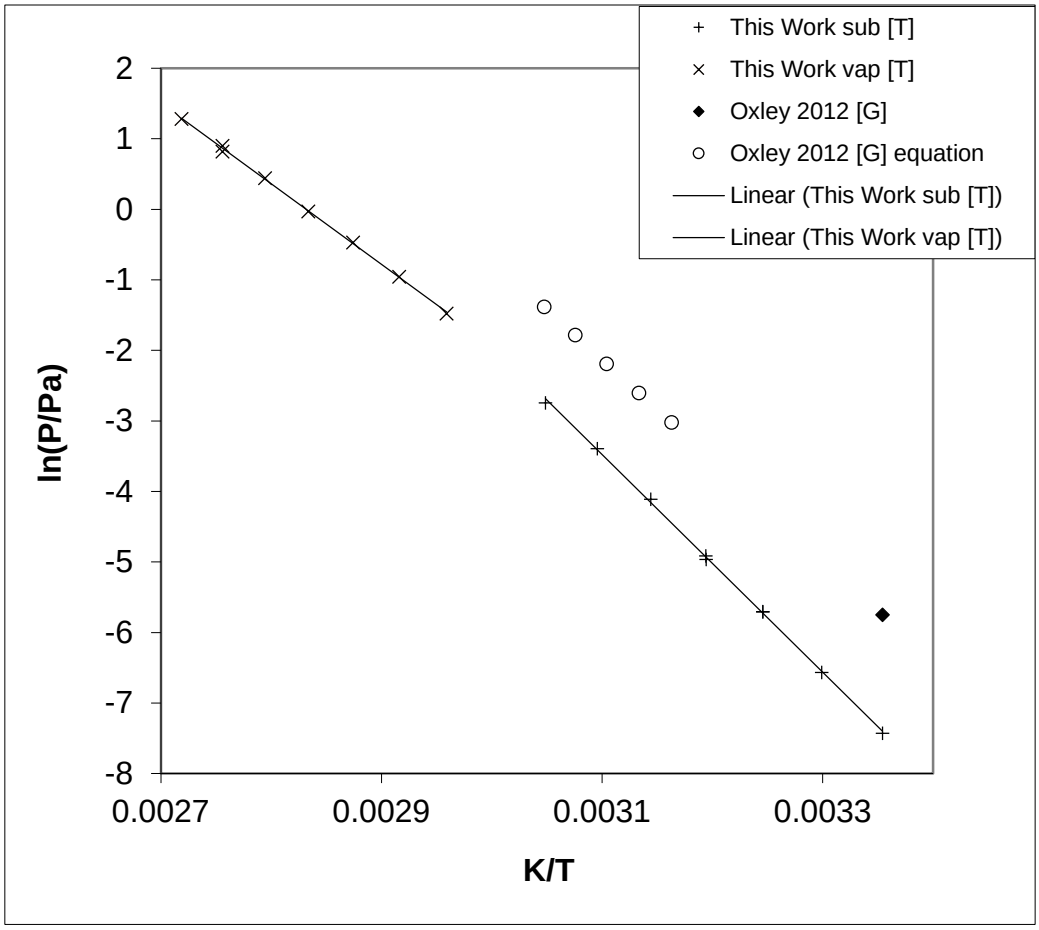

Figure S-11 – Experimental vapor pressure of erythritrol tetranitrate in comparison with literature values.

Table S-12 – Compilation of data available on enthalpies of vaporization $\Delta_l^g H_m^\circ$ erythritol tetranitrate

Experiment[a]	Method[b]	T-Range	T_{avg}	$\Delta_l^g H_m^\circ(T_{avg})$	$\Delta_l^g H_m^\circ$(298.15K)[c]
		K	K	kJ mol^{-1}	kJ mol^{-1}
This Work	T	338.0 – 367.8	353.9	95.1±0.9	101.6±1.0

[a] First author and year of publication, [b] Methods: T: Transpiration [c] Enthalpies of vaporization were adjusted according to *Chickos et al.* [22] with $\Delta_l^g C_{p,m}^\circ$= -119.9 J mol^{-1} K^{-1} and $C_{p,m}^\circ$(l)= 420.3 J mol^{-1} K^{-1} (see Table S-3) [d] Vapor pressure at 298.15 K, calculated according to equation 2 in the main paper. [e] Weighted average value, calculated using the uncertainty as the weighing factor. [f] Average value. Values in brackets were excluded from average value calculation.

Table S-13 – Compilation of data available on enthalpies of sublimation $\Delta_{cr}^g H_m^\circ$ for erythritol tetranitrate

Experiment[a]	Method[b]	T-Range	T_{avg}	$\Delta_l^g H_m^\circ(T_{avg})$	$\Delta_l^g H_m^\circ$(298.15K)[c]	p_{sat}[d]
		K	K	kJ mol^{-1}	kJ mol^{-1}	mPa
This Work	T	298.2 – 331.0	316.5	131.8±1.1	129.1±1.1[e]	0.6
Oxley 2012 [6, 34]	G	316.2 – 331.2	323.7	117.7	119.0	3.2

[a] First author and year of publication, [b] Methods: T: Transpiration, C: Calorimetry, I: Isotope Dilution [c] Enthalpies of vaporization were adjusted according to *Chickos et al.* [22] with $\Delta_{cr}^g C_{p,m}^\circ$= -50.9 J mol^{-1} K^{-1} and $C_{p,m}^\circ$(cr)= 334.1 J mol^{-1} K^{-1} (see Table S-3) [d] Vapor pressure at 298.15 K, calculated according to equation 2 in the main paper. [e] Weighted average value, calculated using the uncertainty as the weighing factor. [f] Average value. Values in brackets were excluded from average value calculation.

12 Calculation of Air Concentration according to Dravnicks

The following calculation is valid for a scenario in which a 200 cm² of ETN is in contact with air. The details of the calculation can be found in the literature given. [31, 35]

*Table S-14 results of calculation for c_{dif} of ETN **4** for an exposed surface of 200 cm²*

	ETN 4	PETN 6	Unit
$\boldsymbol{T_m}$	329.15	406.15	K
$\boldsymbol{\rho_{XRD}}$	1.746	1.845	g cm^{-3}
$\boldsymbol{T_{XRD}}$	291	100	K
$\boldsymbol{\rho_m}$	1.736	1.764	g cm^{-3}
$\boldsymbol{M}$	302.1080	316.135	g mol^{-1}
$\boldsymbol{V_m}$	174.029	179.216	cm^3 mol^{-1}
$\boldsymbol{\sigma_A}$	6.823	6.890	Å
$\boldsymbol{\varepsilon_B}$/κ	631.968	779.808	K
$\boldsymbol{\sigma_{AB}}$	5.220	5.253	Å
$\boldsymbol{\varepsilon_{AB}}$/κ	247.590	275.030	K
κT/$\boldsymbol{\varepsilon_{AB}}$	1.204	1.084	[]
$\boldsymbol{\Omega_{D,AB}}$	1.320	1.385	[]
$\boldsymbol{D_{AB}}$	0.052	0.049	cm^2 s^{-1}
$\boldsymbol{p_{sat}}$	0.0006	1.55 ×10^{-6}	Pa
$\boldsymbol{p_{sat}}$	4.50×10^{-6}	1.16×10^{-8}	mmHg
$\boldsymbol{Q}$	19.35	0.049	pg/cm² s
$\boldsymbol{c_{dif}}$	38	0.978	fg/L

$$J = A \times D_{AB} \times \frac{n_c - n_a}{d}$$

J:emission flux [molecules s^{-1}], A: area of explosive exposed to air [cm²], D_{AB}: diffusivity of explosive vapor in air [cm^2 s^{-1}], n_c: concentration of explosive under saturation conditions [molecules cm^{-3}], n_a: concentration of the explosive in air [molecules cm^{-3}], d: thickness of non-turbulent layer air [cm]

$$D_{AB} = 0.0018583 \sqrt{T^3 (\frac{1}{M_A} + \frac{1}{M_B})} \frac{1}{p \sigma_{AB}^2 \Omega_{D,AB}}$$

T: Temperature [K] (298.15 K), M_A: Molecular Mass of Explosive [g mol^{-1}], M_B: Molecular Mass of Air [g mol^{-1}] (28.97 g mol^{-1}), p: total pressure [atm] (1 atm), σ_{AB}: combined collision diameter [Å], $\Omega_{D,AB}$: collision integral for diffusion

$$\sigma_{AB} = 1/2(\sigma_A + \sigma_B)$$

σ_A: collision diameter of explosive [Å], σ_B: collision diameter of air [Å] (3.617 Å) [35]

$$\varepsilon_{AB} = \sqrt{\varepsilon_A \varepsilon_B}$$

ε_A: characteristic energy of explosive [J], ε_B: characteristic energy of air [J]

$$\varepsilon_B/\kappa = 1.92 T_m; \quad \sigma = 1.222 \sqrt[3]{V_m}$$

T_m: melting point [K], V_m: volume of the solid at the melting point [cm^3 mol^{-1}], p_c: critical pressue [atm], κ: Boltzmann's constant (1.38066 × 10^{-23} J K^{-1})

$$\Omega_{D,AB} = \frac{1.16145}{T^{*0.15610}} + \frac{0.19300}{\exp(0.47635 T^*)} + \frac{1.03587}{\exp(1.52996 T^*)} + \frac{1.76474}{\exp(3.89411 T^*)}$$

$$T^{*}=\kappa T/\varepsilon_{AB}$$

$$\rho_m = \rho_{XRD}/(1 + 0.00015(T_m - T_{XRD})$$

$$V_m = M/\rho_m$$

$$J = A \times D_{AB} \times \frac{n_c - n_a}{d}$$

$$J = \frac{D_{AB}}{0.2} \times n_c$$

$$Q = \frac{D_{AB}}{0.2} \times 3.3 \times 10^{16} p \times (\mathrm{M}/N_A)$$

Q: emission flux of explosive [g s^{-1}], N_A: Avogadro Constant (6.022 × 10^{23} mol^{-1})

$$c = S \times Q \times r$$

c: concentration of explosive in air, S: surface of explosive exposed to air, r: attenuation factor (10^{-4})

13 References

1. Fulmer, G. R.; Miller, A. J. M.; Sherden, N. H.; Gottlieb, H. E.; Nudelman, A.; Stoltz, B. M.; Bercaw, J. E.; Goldberg, K. I., NMR Chemical Shifts of Trace Impurities: Common Laboratory Solvents, Organics, and Gases in Deuterated Solvents Relevant to the Organometallic Chemist. *Organometallics* **2010,** *29* (9), 2176-2179.
2. Gatterman, L., *Die Praxis des organischen Chemikers*. Walter de Gruyter: Berlin / New York, 1982.
3. Urbanski, T.; Witanowski, M., Infra-red spectra of nitric esters. Part 1.-Influence of inductive effects of substituents. *Transactions of the Faraday Society* **1963,** *59* (0), 1039-1045.
4. Einwirkung der Mischung von Schwefelsäure und Salpetersäure auf einige organische Substanzen. *Justus Liebigs Annalen der Chemie* **1848,** *64* (3), 396-398.
5. Lemanceau, B.; Caire-Maurisier, M., Esters nitriques de polyols. Conformation de la nitroglycérine. Résonance magnétique nucléaire et moment dipolaire. *Propellants, Explosives, Pyrotechnics* **1980,** *5* (6), 147-150.
6. Oxley, J. C.; Smith, J. L.; Brady, J. E.; Brown, A. C., Characterization and Analysis of Tetranitrate Esters. *Propellants, Explosives, Pyrotechnics* **2012,** *37* (1), 24-39.
7. Patterson, T. S.; Todd, A. R., CCCXC.-The influence of solvents and of other factors on the rotation of optically active compounds. Part XXVIII. The rotation dispersion of mannitol and some of its derivatives. Note on rotation dispersion curves. *Journal of the Chemical Society (Resumed)* **1929,** (0), 2876-2889.
8. CrysAlisPro, Oxford Diffraction Ltd., version 171.33.41, **2009**.
9. (a) Altomare, A.; Burla, M. C.; Camalli, M.; Cascarano, G. L.; Giacovazzo, C.; Guagliardi, A.; Moliterni, A. G. G.; Polidori, G.; Spagna, R., SIR97: a new tool for crystal structure determination and refinement. *Journal of Applied Crystallography* **1999,** *32* (1), 115-119; (b) A. Altomare, G. Cascarano, C. Giacovazzo, A. Guagliardi, A. G. G. Moliterni, M. C. Burla, G. Polidori, M. Camalli, R. Spagna, SIR97, **1997**.
10. (a) G. M. Sheldrick, SHELX-97, University of Göttingen, Göttingen, Germany, **1997**; (b) Sheldrick, G., A short history of SHELX. *Acta Crystallographica Section A* **2008,** *64* (1), 112-122.
11. A. L. Spek, PLATON, A Multipurpose Crystallographic Tool, Utrecht University, The Netherlands, **1999**.
12. *SCALE3 ABSPACK – An Oxford Diffraction program* (1.0.4, gui: 1.0.3), Oxford Diffraction Ltd., **2005**.
13. Manner, V. W.; Tappan, B. C.; Scott, B. L.; Preston, D. N.; Brown, G. W., Crystal Structure, Packing Analysis, and Structural-Sensitivity Correlations of Erythritol Tetranitrate. *Crystal Growth & Design* **2014,** *14* (11), 6154-6160.
14. Cady, H. H.; Larson, A. C., Pentaerythritol tetranitrate II: its crystal structure and transformation to PETN I; an algorithm for refinement of crystal structures with poor data. *Acta Crystallographica Section B* **1975,** *31* (7), 1864-1869.
15. Zhurova, E. A.; Stash, A. I.; Tsirelson, V. G.; Zhurov, V. V.; Bartashevich, E. V.; Potemkin, V. A.; Pinkerton, A. A., Atoms-in-Molecules Study of Intra- and Intermolecular Bonding in the Pentaerythritol Tetranitrate Crystal. *Journal of the American Chemical Society* **2006,** *128* (45), 14728-14734.
16. Espenbetov, A. A.; Antipin, M. Y.; Struchkov, Y. T.; Philippov, V. A.; Tsirel'son, V. G.; Ozerov, R. P.; Svetlov, B. S., Structure of 1,2,3-propanetriol trinitrate ([beta] modification), C3H5N3O9. *Acta Crystallographica Section C* **1984,** *40* (12), 2096-2098.
17. Boeker, P.; Leppert, J.; Mysliwietz, B.; Lammers, P. S., Comprehensive Theory of the Deans' Switch As a Variable Flow Splitter: Fluid Mechanics, Mass Balance, and System Behavior. *Analytical Chemistry* **2013,** *85* (19), 9021-9030.
18. Li, M.; Guo, X.; Li, F.; Song, H., Theoretical Studies on the Structures, Thermodynamic Properties, Detonation Performance, and Pyrolysis Mechanisms for Six Dinitrate Esters. *Chinese Journal of Chemistry* **2009,** *27* (10), 1871-1878.

19. Ur'yash, V. F.; Mochalov, A. N.; Kupriyanov, V. F.; Smirnov, A. G.; Kuleshova, T. M.; Samoshkin, V. I., Heat capacity and thermodynamic functions of glycerol trinitrate. *Russ. J. Gen. Chem.* **1997,** *67* (4), 550-552.
20. Pilar, R.; Pachman, J.; Matyáš, R.; Honcová, P.; Honc, D., Comparison of heat capacity of solid explosives by DSC and group contribution methods. *Journal of Thermal Analysis and Calorimetry* **2015,** *121* (2), 683-689.
21. Hurst, J. E.; Keith Harrison, B., ESTIMATION OF LIQUID AND SOLID HEAT CAPACITIES USING A MODIFIED KOPP'S RULE. *Chemical Engineering Communications* **1992,** *112* (1), 21-30.
22. Acree, W.; Chickos, J. S., Phase Transition Enthalpy Measurementsof Organic and Organometallic Compounds. Sublimation, Vaporizationand Fusion Enthalpies From 1880 to 2010. *Journal of Physical and Chemical Reference Data* **2010,** *39* (4), 043101.
23. (a) Pella, P. A., Measurement of the vapor pressures of tnt, 2,4-dnt, 2,6-dnt, and egdn. *The Journal of Chemical Thermodynamics* **1977,** *9* (4), 301-305; (b) Pella, P. A., Generator for producing trace vapor concentrations of 2,4,6-trinitrotoluene, 2,4-dinitrotoluene, and ethylene glycol dinitrate for calibrating explosives vapor detectors. *Analytical Chemistry* **1976,** *48* (11), 1632-1637.
24. John, G. A. S.; McReynolds, J. H.; Blucher, W. G.; Scott, A. C.; Anbar, M., Determination of the concentration of explosives in air by isotope dilution analysis. *Forensic Science* **1975,** *6* (1), 53-66.
25. Brander, J. D., Nitroglycerin and Ethylene Glycol Dinitrate Vapor Pressures of Binary Solutions. *Industrial & Engineering Chemistry* **1938,** *30* (6), 681-684.
26. Crater, W. d., The Vapor Pressures of Glycerol Trinitrate and Certain Glycol Dinitrates. *Industrial & Engineering Chemistry* **1929,** *21* (7), 674-676.
27. Rinkenbach, W. H., The Properties of Glycol Dinitrate1. *Industrial & Engineering Chemistry* **1926,** *18* (11), 1195-1197.
28. Tunnell, R.; Tod, D., A New Method for Determining the Vapor Pressure of Nitroglycerine Above Solid Rocket Propellants. *Propellants, Explosives, Pyrotechnics* **2016,** *41* (1), 173-178.
29. Miroshnichenko, E. A.; Korchatova, L. I.; Shelaputina, V. P.; Zyuz'kevich, S. A.; Lebedev, Y. A., Thermochemistry of glyceryl trinitrate. *Bulletin of the Academy of Sciences of the USSR, Division of chemical science* **1988,** *37* (9), 1778-1781.
30. Dionne, B. C.; Rounbehler, D. P.; Achter, E. K.; Hobbs, J. R.; Fine, D. H., Vapor pressure of explosives. *Journal of Energetic Materials* **1986,** *4* (1-4), 447-472.
31. Dravnicks, A.; Brabets, R.; Stanley, T. A. *Evaluating Sensitivity Requirements of Explosive Vapor Detector Systems*; IIT Research Institute Technology Center: Chicago Illinois, 1972.
32. Kemp, M. D.; Goldhagen, S.; Zihlman, F. A., Vapor Pressures and Cryoscopic Data for Some Aliphatic Dinitroxy and Trinitroxy Compounds. *The Journal of Physical Chemistry* **1957,** *61* (2), 240-242.
33. Marshall, A.; Peace, G., XXXIII.-The vapour pressure of glyceryl trinitrate (nitroglycerin). *Journal of the Chemical Society, Transactions* **1916,** *109* (0), 298-302.
34. Oxley, J. C.; Smith, J. L.; Brady, J. E.; Brown, A. C., Erratum: Characterization and Analysis of Tetranitrate Esters. *Propellants, Explosives, Pyrotechnics* **2012,** *37* (6), 735-735.
35. Bird, R. B.; Stewart, W. E.; Lightfoot, E. N., *Transport Phenomena*. John Wiley & Sons, Inc. : New Jork, 2002.

7.4 Measurement of the Mononitrotoluenes 2-MNT 12, 3-MNT 13 and 4-MNT 14

This chapter deals with the measurement of the vapor pressure of the mononitrotoluenes 2-MNT **12**, 3-MNT **13** and 4-MNT **14**:

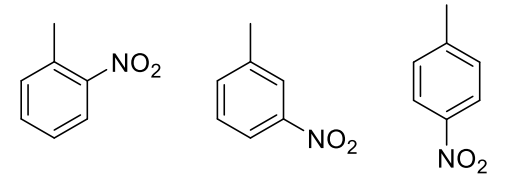

2-MNT **12** 3-MNT **13** 4-MNT **14**

The results were published in Journal of Chemical Thermodynamics [1] and are reprinted with permission. Copyright 2017 Elsevier Ltd.

DOI: 10.1016/j.jct.2017.03.029. The original publication of the data follows.

Since the publication does not include the vapor pressure at 298.15 K the values are stated separately in comparison with selected literature data-sets:

Table 1 – Compilation of Data available on Enthalpies of Vaporization $\Delta_l^g H_m^\circ$ for 2-Nitrotoluene 12

Experiment[a]	Method[b]	T-Range	T_{avg}	$\Delta_l^g H_m^\circ(T_{avg})$	$\Delta_l^g H_m^\circ$(298.15K)[c]	p_{sat}[d]
		K	K	kJ mol^{-1}	kJ mol^{-1}	Pa
This Work	T	278.3-323.0	298.9	58.8±0.3	58.9±0.3	18.0
Bruno 2010 [2]	T	283.2-313.2	297.7	59.4±0.8	59.4±0.9	19.7
Verevkin 2000 [3]	T	274.0-323.4	299.8	58.8±0.3	58.8±0.3	19.4
Aim 1994 [4]	E	388.96-447.86	419.81	51.4±0.1	59.2±0.7	17.8
					58.9±0.2[e]	18.7[f]

[a] First author and year of publication, [b] Methods: T: Transpiration, E: Ebulliometry [c] Enthalpies of vaporization were adjusted according to *Chickos et al.* [5] with $\Delta_l^g C_{p,m}^\circ$= -65.5 J mol^{-1} K^{-1} and $C_{p,m}^\circ$(liq)= 211.3 J mol^{-1} K^{-1} [d] Vapor pressure at 298.15 K [e] Weighted average value, calculated using the uncertainty as the weighing factor. [f] Average value.

Table 2 – Compilation of Data available on Enthalpies of Vaporization $\Delta_l^g H_m^\circ$ for 3-Nitrotoluene 13

Experiment[a]	Method[b]	T-Range	T_{avg}	$\Delta_l^g H_m^\circ(T_{avg})$	$\Delta_l^g H_m^\circ$(298.15 K)[c]	p_{sat}[d]
		K	K	kJ mol^{-1}	kJ mol^{-1}	Pa
Härtel 2015	T	298.2-338.0	313.5	58.3±0.2	59.4±0.3	11.8
Bruno 2010 [2]	T	283.2-313.2	298.2	59.5±1.6	59.5±1.7	12.6
Aim 1994 [4]	E	397.26-451.80	427.21	52.3±0.1	60.5±0.7	11.0
					58.7±0.3[e]	11.8[f]

[a] First author and year of publication, [b] Methods: T: Transpiration, E: Ebulliometry [c] Enthalpies of vaporization were adjusted according to *Chickos et al.* [5] with $\Delta_l^g C_{p,m}^\circ$= -65.5 J mol^{-1} K^{-1} and $C_{p,m}^\circ$(liq)= 211.3 J mol^{-1} K^{-1}. [d] Vapor pressure at 298.15 K [e] Weighted average value, calculated using the uncertainty as the weighing factor. [f] Average value.

Table 3 – Compilation of Data on Enthalpies of Sublimation $\Delta_{cr}^{g}H_{m}^{\circ}$ for 4-Nitrotoluene 14

Experiment[a]	Method[b]	T-Range	T_{avg}	$\Delta_{cr}^{g}H_{m}^{\circ}(T_{avg})$	$\Delta_{cr}^{g}H_{m}^{\circ}$(298.15 K)[c]	p_{sat}[d]
		K	K	kJ mol^{-1}	kJ mol^{-1}	Pa
Härtel 2015	T	288.3-323.1	304.9	74.8±0.3	74.9±0.5	5.6
Bruno 2010 [2]	T	283.2-313.2	297.7	74.8±0.4	74.8±0.7	6.3
Lenchitz 1970 [6]	K	297.0-309.5	303.6	80.1±3.0	(80.2±3.2)	(0.66)
					74.9±0.4[e]	6.0[f]

[a] First author and year of publication, [b] Methods: T: Transpiration, K: Knudsen Effusion [c] Enthalpies of Sublimation were adjusted according to *Chickos et al.* [5] with $\Delta_{cr}^{g}C_{p,m}^{\circ}$= -26.6 J mol^{-1} K^{-1} and $C_{p,m}^{\circ}$(cr)= 172.2 J mol^{-1} K^{-1} [d] Vapor pressure at 298.15 K [e] Weighted average value, calculated using uncertainty as the weighing factor. [f] Average value. Value in brackets was not used for calculation of the average value.

Literature References:

1. Bikelytė, G.; Härtel, M.; Stierstorfer, J.; Klapötke, T. M.; Pimerzin, A. A.; Verevkin, S. P., Benchmark properties of 2-, 3- and 4-nitrotoluene: Evaluation of thermochemical data with complementary experimental and computational methods. *The Journal of Chemical Thermodynamics* **2017,** *111* (Supplement C), 271-278.
2. Widegren, J. A.; Bruno, T. J., Gas Saturation Vapor Pressure Measurements of Mononitrotoluene Isomers from (283.15 to 313.15) K. *Journal of Chemical & Engineering Data* **2010,** *55* (1), 159-164.
3. Verevkin, S. P.; Heintz, A., Thermochemistry of substituted benzenes: quantification of ortho-, para-, meta-, and buttress interactions in alkyl-substituted nitrobenzenes. *The Journal of Chemical Thermodynamics* **2000,** *32* (9), 1169-1182.
4. Aim, K., Saturated Vapor Pressure Measurements on Isomeric Mononitrotoluenes at Temperatures between 380 and 460 K. *Journal of Chemical & Engineering Data* **1994,** *39* (3), 591-594.
5. Acree, W.; Chickos, J. S., Phase Transition Enthalpy Measurementsof Organic and Organometallic Compounds. Sublimation, Vaporizationand Fusion Enthalpies From 1880 to 2010. *Journal of Physical and Chemical Reference Data* **2010,** *39* (4), 043101.
6. Lenchitz, C.; Velicky, R. W., Vapor pressure and heat of sublimation of three nitrotoluenes. *Journal of Chemical & Engineering Data* **1970,** *15* (3), 401-403.

J. Chem. Thermodynamics 111 (2017) 271–278

Contents lists available at ScienceDirect

J. Chem. Thermodynamics

journal homepage: www.elsevier.com/locate/jct

Benchmark properties of 2-, 3- and 4-nitrotoluene: Evaluation of thermochemical data with complementary experimental and computational methods

Greta Bikelytė [a], Martin Härtel [a], Jörg Stierstorfer [a], Thomas M. Klapötke [a], Andrey A. Pimerzin [b], Sergey P. Verevkin [c,*]

[a] Department Chemie, Ludwig-Maximilians-Universität München, Butenandtstr. 5-13, 81377 München-Großhadern, Germany
[b] Chemical Department, Samara State Technical University, Molodogvardeyskaya 244, Samara 443100, Russia
[c] Department of Physical Chemistry and Department of "Science and Technology of Life, Light and Matter", University of Rostock, Dr-Lorenz-Weg 1, D-18059 Rostock, Germany

ARTICLE INFO

Article history:
Received 21 November 2016
Received in revised form 18 March 2017
Accepted 25 March 2017
Available online 27 March 2017

Keywords:
Nitrotoluenes
Enthalpy of vaporization
Vapour pressure measurements
Enthalpy of combustion
Enthalpy of formation
Quantum-chemical calculations

ABSTRACT

Thermochemical properties of nitrotoluenes are in disarray. New standard (p = 0.1 MPa) molar enthalpies of formation at the temperature T = 298.15 K of the liquid 3-nitrotoluene and crystalline 4-nitrotoluene were measured using high-precision combustion calorimetry. New molar enthalpies of vaporization of 2-, 3-, and 4-nitrotoluene were derived from the vapour pressure temperature dependence measured by the transpiration method. Thermodynamic data on nitrotoluenes available in the literature were collected, evaluated, and combined with own experimental results. This collection, together with the new experimental results reported here, has helped to resolve contradictions in the available enthalpies of formation data and to recommend the set of vaporization and formation enthalpies for 2-, 3-, and 4-nitrotoluene as the reliable benchmark properties for further thermochemical calculations. Gas phase molar enthalpies of formation of 2-, 3-, and 4-nitrotoluene, calculated by high-level quantum-chemical method G4, were found in a good agreement with the recommended experimental data.

1. Introduction

Nitrotoluenes are broadly used for the industrial synthesis of agricultural and dye chemicals as well as of explosives. The nitration of toluene typically yields a mixture of 55–60% 2-nitrotoluene, 3–4% of 3-nitrotoluene, and 35–40% of 4-nitrotoluene [1]. This mixture is an intermediate product of the further stepwise nitration of toluene, leading to the most well-known explosive 2,4,6-trinitrotoluene. Development of quick and reliable methods for detection of traces of explosives in air and on surfaces has gained importance during the last decade. According to the Montreal Convention on the Marking of Plastic Explosives for the Purpose of Detection [2], a certain amount of 2-nitrotoluene, 4-nitrotoluene or 2,3-dimethyl-2,3-dinitrobutane has to be integrated in the commercial explosive formulation as detection aid agents or so-called taggants. The gas-phase detection of trace amounts of explosives is a new trend in the development of a new generation of highly sensitive explosive detection devices [3,4]. Thus, nitrotoluenes are convenient model compounds for determination of detection limits of novel analytic methods.

The conception of novel analytic equipment for the gas phase detection of explosives must be based on reliable thermodynamic data of the model compounds since the air concentration is directly proportional to their vapour pressure. Surprisingly, the available thermochemical data for nitrotoluenes are in disarray [5]. New additional experiments with nitrotoluenes are intended to help with establishing consistency in the available data. This contribution complements and extends our previous studies of the thermochemistry of aliphatic [6] and aromatic nitro-compounds [7–11]. The aim of this study was an evaluation of thermochemical data available for 2-nitrotoluene, 3-nitrotoluene, and 4-nitrotoluene (see Fig. 1) with complementary experimental and computational methods in order to recommend benchmark thermochemical properties for these compounds.

2. Materials and methods

2.1. Materials

Samples of 2-, 3-, and 4-nitrotoluene were available from Sigma-Aldrich with the purity of 99%. The liquid samples were

* Corresponding author.
E-mail address: sergey.verevkin@uni-rostock.de (S.P. Verevkin).

http://dx.doi.org/10.1016/j.jct.2017.03.029
0021-9614/

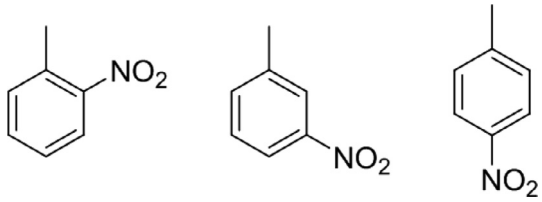

Fig. 1. Nitrotoluenes studied in this work: 2-nitrotoluene, 3-nitrotoluene, and 4-nitrotoluene.

further purified by fractional distillation with a spinning-band column in vacuum. The sample of 4-nitrotoluene was purified by fractional sublimation in vacuum. No impurities (>0.001 mass fraction) could be detected in the samples used for the thermochemical measurements. The degree of purity was determined using a GC equipped with an FID. A capillary column HP-5 was used with a column length of 30 m, an inside diameter of 0.32 mm, and a film thickness of 0.25 μm. Water mass fraction in the samples was determined using a Mettler Toledo DL38 Karl Fischer titrator using the HYDRANAL™ as the reagent. Provenance and purity of the compounds, prepared for thermochemical studies in this work, are given in Table 1.

2.2. Vapour pressure measurements. Transpiration method

Vapour pressures of nitrotoluenes were measured using the transpiration method [12–17]. About 0.5 g of a sample was mixed with small glass beads and placed in a thermostatted U-shaped saturator. A well-defined nitrogen stream was passed through the saturator at a constant temperature (±0.1 K), and the transported material was collected in a cold trap. The amount of condensed sample was determined by GC analysis using a suitable n-alkane as an external standard. The absolute vapour pressure p_i at each temperature T_i was calculated from the amount of the product, collected within a definite period. Assuming validity of the Dalton's law, applied to the nitrogen stream, which was saturated with the substance i, values of p_i were calculated with Eq. (1):

$$p_i = m_i R T_a / V M_i; \qquad V = V_{N2} + V_i; \quad (V_{N2} \gg V_i) \tag{1}$$

where $R = 8.314462\ \mathrm{J\cdot K^{-1}\cdot mol^{-1}}$; m_i is the mass of the transported compound, M_i is the molar mass of the compound, and V_i is its volume contribution to the gaseous phase. V_{N2} is the volume of the carrier gas and T_a is the temperature of the soap bubble meter used for the flow rate measurements. The volume of the carrier gas V_{N2} was determined from the flow rate and the time measurement.

Transpiration experiments with nitrotoluenes have been performed on the same highly purified samples independently in Rostock and in Munich. The experimental setup, used in Rostock, has been reported elsewhere [12]. For quantification of the transported sample mass, the capillary column HP-5 with a column length of 30 m × 0.32 mm × 0.25 μm was used.

An identical transpiration apparatus has been constructed for the first time in Munich and the results of parallel measurements on nitrotoluenes in Munich and in Rostock have been considered as a validation of the transpiration procedure transferred to the new lab. All parts of equipment in Munich have been identical to those in Rostock except for the GC analysis of the transported mass. A vacuum outlet GC/MS setup [18] with a restriction inside the injector was used. The restriction (8.11 mm, 0.025 mm i.d., Restek #10097) was connected with a Siltite μ-union (Restek #073562) to a Restek RTX-TNT 1 column with a column length of 6 m × 0.53 mm × 1.5 μm. More details on the GC experimental conditions are given in Table S1. The results measured by the transpiration (T) in Rostock were labeled in this work as TR and the results measured in Munich as TM.

2.3. Combustion calorimetry

The molar enthalpies of combustion of the 3- and 4-nitrotoluenes were measured with an self-made isoperibolic calorimeter with a static bomb and a stirred water bath. The liquid sample of 3-nitrotoluene was transferred into the polyethylene bulb (Fa. NeoLab, Heidelberg, Germany) with a syringe. The neck of the bulb was compressed with special tweezers and was sealed by heating the neck in a close proximity to a glowing wire. Then, the bulb was placed in the crucible and was burned in oxygen at a pressure of 3.04 MPa. The solid sample of 4-nitrotoluene was burned as a pellet. The detailed procedure has been described previously [16,17]. The combustion products were examined for carbon monoxide (Dräger tube) and unburned carbon, but neither was detected. The energy equivalent of the calorimeter $\varepsilon_{calor} = 15265.3\ \mathrm{J\cdot K^{-1}}$; $u(\varepsilon_{calor}) = 1.0\ \mathrm{J\cdot K^{-1}}$ was determined with a standard reference sample of benzoic acid (sample SRM 39*j*, NIST). Correction for nitric acid formation was based on titration with 0.1 $\mathrm{mol\cdot dm^{-3}}$ NaOH (aq). For the reduction of the data to standard conditions, conventional procedures [19] were used. Auxiliary data required for the reduction are collected in Table S2.

3. Results and discussion

3.1. Vapour pressures of nitrotoluenes

The temperature dependence of vapour pressure p_i measured for *nitrotoluenes* in this work was fit with the following equation [12]:

$$R \cdot \ln p_i = a + \frac{b}{T} + \Delta_l^g C_{p,m} \cdot \ln\left(\frac{T}{T_0}\right) \tag{2}$$

where a and b are adjustable parameters and $\Delta_l^g C_{p,m}$ is the difference of the molar heat capacities of the gaseous and the liquid phase respectively. T_0 appearing in Eq. (2) is an arbitrarily chosen reference temperature (which has been chosen to be 298.15 K) and R is the molar gas constant. Values of $\Delta_l^g C_{p,m}$ in Eq. (2) were calculated (see Table S3) according to the empirical procedure developed by Chickos and Acree [20]. Experimental vapour pressures measured by the transpiration method are given in Table S3. The Eq. (2) is also valid for the treatment of vapour pressures measured over the crystalline sample (4-nitrotoluene in this work). Values of

Table 1
Origin, purity and purification methods of chemicals used in this work.

Compound	CAS	Source	Initial purity	Purification method	Final purity[a]
2-Nitrotoluene (liq)	88-72-2	Sigma-Aldrich	0.99	Distillation	0.999
3-Nitrotoluene (liq)	99-08-1	Sigma-Aldrich	0.99	Distillation	0.999
4-Nitrotoluene (cr)	99-99-0	Sigma-Aldrich	0.99	Sublimation	0.999

[a] Final mass fraction of purity was determined by the gas chromatography. Not significant mass fraction of water at the level of 20–30 ppm was measured by the Karl Fisher titration.

$\Delta_{cr}^{g}C^{\circ}_{p,m}$ required for this case were also calculated (see Table S4) according to the procedure developed by Chickos and Acree [20].

Most of the vapour pressures of nitrotoluenes available in the literature were measured at elevated temperatures close to the normal boiling points [21–31]. As a rule, the primary experimental data are not reported in original papers and the coefficients of the linear approximation are given instead. Only few studies of low-temperature vapour pressures of nitrotoluenes were found in the literature [7,32–36] and they have been used for comparison with our new results, measured by the transpiration method (see Figs. 2–5).

2-Nitrotoluene. Three available low-temperature data sets of vapour pressures for 2-nitrotoluene, measured by the transpiration method, are in agreement within 10% (see Fig. 2). A reliable data set by Aim [26], measured by ebulliometry between 388.9 K and 447.9 K, makes a comparison with approximated results, reported in the earlier literature [21–25] in the high-temperature range redundant.

3-Nitrotoluene. The low-temperature absolute vapour pressures reported for 3-nitrotoluene in Ref. [32] are in good agreement with our new transpiration results (see Fig. 3), but results reported by Elias [35] are apparently in disagreement. It should be mentioned that experimental details in [35] are completely absent and it makes any speculations impossible. The ebulliometric data set of very good quality measured between 397.3 K and 451.8 K by Aim [26] can replace the available results of unknown quality, reported for the high-temperature range in the earlier literature [21–25,27,30].

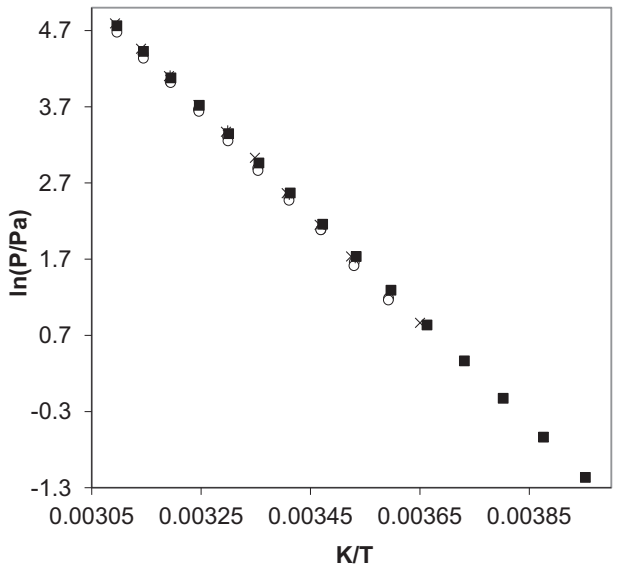

Fig. 2. Experimental vapour pressures of the 2-nitrotoluene: ○ – this work, TM; + – from [32]; × – from [7]; ■ – from [35].

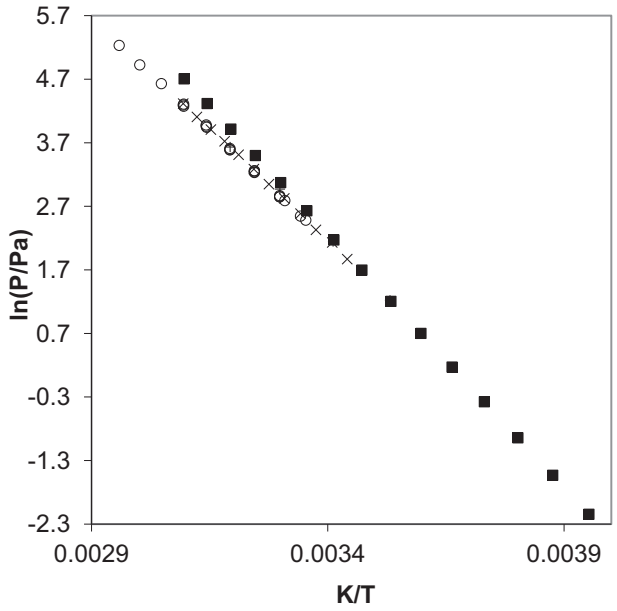

Fig. 3. Experimental vapour pressures of the 3-nitrotoluene: ○ – this work, TM; × – this work, TR; + – from [32]; ■ – from [35].

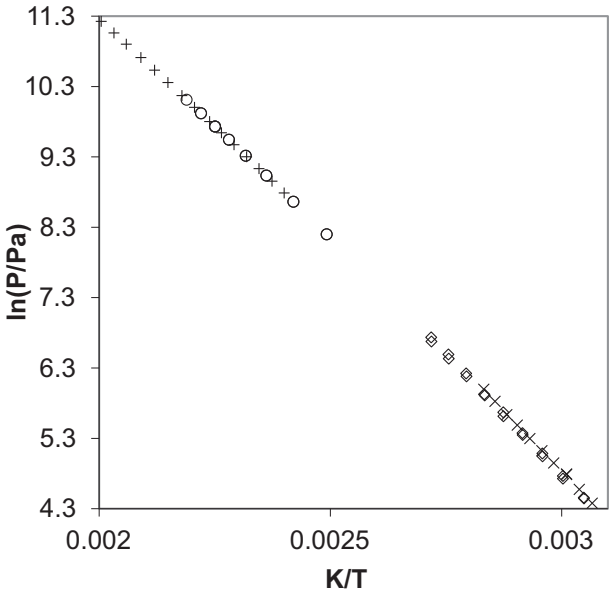

Fig. 4. Experimental vapour pressures over liquid sample of the 4-nitrotoluene: ◇ – this work, TM; × – this work, TR ○ – from [26]; + – from [31].

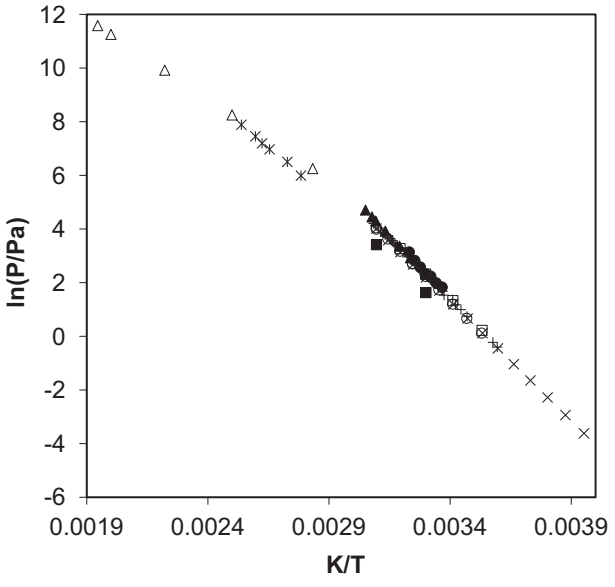

Fig. 5. Experimental vapour pressures over solid sample of the 4-nitrotoluene: ○ – this work, TM; + – this work, TR; ⁎ – from [21]; Δ – from [28]; ● – from [33]; □ – from [32]; ▲ – from [34]; × – from [35]; ■ – from [36].

4-Nitrotoluene. Consistent sets of absolute vapour pressures in a low-temperature range over the liquid sample of 4-nitrotoluene, measured in the current study by the transpiration method, are reported for the first time (see Fig. 4). A direct comparison of the transpiration results with the high-temperature results by Aim [26] and Ambrose and Gundry [31] is hardly possible due to the significantly different temperature ranges (see Fig. 4). Comparison of vapour pressures measured in a low-temperature range over the solid sample of 4-nitrotoluene is given in Fig. 5. New results, measured with the transpiration method in this work, are in a good agreement with the data, reported by Widegren and Bruno [32] and Smirnov et al. [33]. Lenchitz and Velicky [33] reported vapour pressures for 4-nitrotoluene, measured by the Knudsen effusion technique. However, the values reported in the original publication [33] contained a unit conversion error and we corrected their data for comparison (see Fig. 5).

The absolute vapour pressures measured by TGA by Felix-Rivera et al. [36] are significantly different from results measured by other techniques. This disagreement is most probably due to questionable calibration with vapour pressures of the benzoic acid commonly applied in TGA regardless of the structure of compounds under study.

3.2. Thermodynamics of vaporization and sublimation of nitrotoluenes

Vaporization enthalpies at temperature T were derived from the temperature dependence of vapour pressures using Eq. (3):

$$\Delta_{\mathrm{l}}^{\mathrm{g}}H^{\circ}{}_{m}(T) = -b + \Delta_{\mathrm{l}}^{\mathrm{g}}C^{\circ}{}_{p,m}\cdot T \tag{3}$$

Vaporization entropies at temperature T were also derived from the temperature dependence of vapour pressures using Eq. (4):

$$\Delta_{\mathrm{l}}^{\mathrm{g}}S^{\circ}{}_{m}(T) = \Delta_{\mathrm{l}}^{\mathrm{g}}H^{\circ}{}_{m}/T + R\ln(p_{\mathrm{i}}/p^{\circ}) \tag{4}$$

Experimental absolute vapour pressures measured by the transpiration method, coefficients a and b of Eq. (2), as well as values of $\Delta_{\mathrm{l}}^{\mathrm{g}}H^{\circ}{}_{m}$ (T) and $\Delta_{\mathrm{l}}^{\mathrm{g}}S^{\circ}{}_{m}$ (T) are given in Table S3. The procedure of calculation of the combined uncertainties of the vaporization enthalpy was described elsewhere [12–14]. It includes uncertainties from the transpiration experiment conditions, uncertainties in vapour pressure, and uncertainties in the temperature adjustment to T = 298.15 K.

In this study, we carefully collected available experimental literature data on vapour pressures of nitrotoluenes. Because authors not always derived vaporization enthalpies from their vapour pressures or performed it in different manner, we treated the literature vapour pressures using Eqs. (2) and (3) and calculated $\Delta_{\mathrm{l}}^{\mathrm{g}}H^{\circ}{}_{m}$ (298.15 K) for the purpose of comparison with our results (see Table 1).

It should be mentioned that vaporization enthalpies, derived from vapour pressures, collected in compilations by Dreisbach [30] and Stephenson and Malanowski [27], are of questionable quality, because the source of the primary data is not available, as well as specification of purity and experimental methods are not reported.

It has turned out that after uniform adjustment of all available data (new and from the literature) to the reference temperature T = 298.15 K with the $\Delta_{\mathrm{l}}^{\mathrm{g}}C_{p,m}$-values, given in Table S4, the vaporization enthalpies $\Delta_{\mathrm{l}}^{\mathrm{g}}H^{\circ}{}_{m}$ (298.15 K) of the nitrotoluenes were mostly close to a common level of 60 kJ·mol^{-1} regardless of the position of the methyl group on the benzene ring. Such a behaviour was already observed for $\Delta_{\mathrm{l}}^{\mathrm{g}}H^{\circ}{}_{m}$ (298.15 K) of methyl-substituted halobenzenes [13], where 2-, 3-, and 4-methyl isomers exhibited vaporization enthalpies indistinguishable within their boundaries of experimental uncertainties. This observation can be considered as an evidence of internal consistency of $\Delta_{\mathrm{l}}^{\mathrm{g}}H^{\circ}{}_{m}$ (298.15 K) results, evaluated in Table 2. The enthalpies of vaporization, derived from two available isoteniscope measurement data sets [23,28], are significantly larger in comparison to other results, but an absence of sufficient experimental details in the original papers makes it impossible to find an explanation for the disagreement observed. Taking into account the general agreement of data sets, measured by different methods and collected in Table 2, we calculated the weighted mean value $\Delta_{\mathrm{l}}^{\mathrm{g}}H^{\circ}{}_{m}$ (298.15 K) for each nitrotoluene (see Table 2) by using the experimental uncertainties as the weighting factor. These mean values are given in bold and they have been recommended for further thermochemical calculations.

The evaluation of the data on sublimation enthalpy of 4-nitrotoluene is troublesome (see Table 2). In fact, two values, reported by Lenchitz and Velicky [33] and by Lebedev et al. [40], are on the level of 80–81 kJ·mol^{-1} and they are significantly higher in comparison to the recent result $\Delta_{\mathrm{cr}}^{\mathrm{g}}H^{\circ}{}_{m}$ (298.15 K) = 74.8 ± 0.7 kJ·mol^{-1}, reported by Widegren and Bruno [32]. Even if the Knudsen results, reported by Lenchitz and Velicky [33], suffer from the unit conversion error as described in Section 3.1, the slope in the ln$p$ *vs* 1/T plot, responsible for the sublimation enthalpy, could be correct. In this context two new data sets, measured in the current study by the transpiration method, have helped to resolve the conflicting results and ascertain the recent result by Widegren and Bruno [32]. We calculated the weighted mean value $\Delta_{\mathrm{cr}}^{\mathrm{g}}H^{\circ}{}_{m}$ (298.15 K) = 75.3 ± 0.3 kJ·mol^{-1} for 4-nitrotoluene from the latest three data sets (see Table 1) by using experimental uncertainties as the weighting factor. This mean value is given in bold and it is recommended for further thermochemical calculations. However, an additional validation of the evaluated sublimation enthalpy has been performed with the help of standard molar enthalpy of fusion, $\Delta_{\mathrm{cr}}^{\mathrm{l}}H^{\circ}{}_{m}$, available for 4-nitrotoluene in the literature.

3.3. Enthalpy of fusion of 4-nitrotoluene

Generally, the experimental molar enthalpy of fusion $\Delta_{\mathrm{cr}}^{\mathrm{l}}H^{\circ}{}_{m}$ is referenced to the melting temperature T_{fus}. Compilation of available data on the fusion enthalpy for 4-nitrotoluene is presented in Table 3. For the thermochemical calculations the experimental enthalpy of fusion has to be adjusted to the reference temperature T = 298.15 K. The adjustment was calculated from the equation [20]:

$$\Delta_{\mathrm{cr}}^{\mathrm{l}}H^{\circ}{}_{m}(298.15\ \mathrm{K})/(\mathrm{J}\cdot\mathrm{mol}^{-1}) = \Delta_{\mathrm{cr}}^{\mathrm{l}}H^{\circ}{}_{m}(T_{\mathrm{fus}}/K) - (\Delta_{\mathrm{cr}}^{\mathrm{g}}C^{\circ}{}_{pm}\Delta_{\mathrm{cr}}^{\mathrm{l}}H^{\circ}{}_{p,m}) \times [(T_{\mathrm{fus}}/\mathrm{K}) - 298.15\ \mathrm{K}], \tag{5}$$

where $\Delta_{\mathrm{cr}}^{\mathrm{g}}C^{\circ}{}_{pm}$ and $\Delta_{\mathrm{cr}}^{\mathrm{l}}H^{\circ}{}_{p,m}$ are given in Table S4. With this adjustment, the molar enthalpy of fusion, $\Delta_{\mathrm{cr}}^{\mathrm{l}}H^{\circ}{}_{m}$ (298.15 K) = 15.7 ± 0.3 kJ·mol^{-1} was calculated (see Table 3) and used for consistency test of the phase change enthalpies for 4-nitrotoluene as it shown below.

3.4. Internal consistency of the phase change enthalpies of 4-nitrotoluene

The significant spread of values, reported for sublimation enthalpy, has prompted the additional efforts to validate the results, obtained in the current study. The internal consistency test of the experimental phase change data of the vaporization (Table 2), fusion (Table 3), and sublimation enthalpy (Table 2) of 4-nitrotoluene, can be performed according to the general relationship:

$$\Delta_{\mathrm{cr}}^{\mathrm{l}}H^{\circ}{}_{m} = \Delta_{\mathrm{cr}}^{\mathrm{g}}H^{\circ}{}_{m} - \Delta_{\mathrm{l}}^{\mathrm{g}}H^{\circ}{}_{m} \tag{6}$$

Table 2
Compilation of data on enthalpies of vaporization $\Delta_l^g H^\circ_m$ and enthalpies of sublimation $\Delta_{cr}^g H^\circ_m$ of nitrotoluenes.

Compound	Method[a]	T-range/K	$\Delta_l^g H^\circ_m$ (T_{av})/kJ·mol^{-1}	$\Delta_l^g H^\circ_m$ (298.15 K)[b]/kJ·mol^{-1}	Refs.
2-Nitrotoluene (liq)	S	323.0–493.6	47.1 ± 3.0	54.3 ± 3.1	[21]
	E	387.2–493.2	50.2 ± 2.0	59.5 ± 2.1	[22]
	E	402.5–495.3	50.1 ± 2.0	59.6 ± 2.1	[30]
	S	363.2–496.2	61.1 ± 2.0	(69.7 ± 2.1)	[23]
	DTA	411.2–495.2	51.5 ± 3.0	61.7 ± 3.1	[24]
	DSC	447.5	47.7 ± 3.0	57.5 ± 3.1	[25]
	GC/ECD	253–323	57.5 ± 1.0	56.7 ± 1.1	[35]
	E	388.9–447.8	51.4 ± 0.1	59.2 ± 0.7	[26]
	T	274.0-323.4	58.8 ± 0.3	58.8 ± 0.3	[7]
	T	283.2–313.2	59.4 ± 0.8	59.4 ± 0.9	[32]
	TM	278.3–323.0	58.8 ± 0.3	58.9 ± 0.3	This work
				58.8 ± 0.2[c]	Average
3-Nitrotoluene (liq)	S	363–505.1	50.2 ± 3.0	59.1 ± 3.1	[21]
	E	444.2–480.2	50.2 ± 2.0	60.9 ± 2.2	[22]
	S	363.2–505.2	61.5 ± 2.0	(70.4 ± 2.2)	[23]
	DTA	413.2–506.2	49.4 ± 3.0	60.0 ± 3.1	[24]
	N/A	353–505	49.5 ± 2.0	57.5 ± 2.1	[27]
	DSC	461.9	48.5 ± 3.0	59.2 ± 3.1	[25]
	GC/ECD	253–323	66.5 ± 1.0	(65.7 ± 1.1)	[35]
	E	397.3–451.8	52.3 ± 0.1	60.5 ± 0.7	[26]
	T	283.2–313.2	59.5 ± 1.6	59.5 ± 1.7	[32]
	TR	290.6–323.2	58.4 ± 0.3	58.9 ± 0.4	This work
	TM	298.2–338.0	58.3 ± 0.2	59.4 ± 0.3	This work
				59.4 ± 0.2[c]	Average
4-Nitrotoluene (liq)	S	353.0–511.4	50.0 ± 3.0	58.8 ± 3.1	[21]
	S	359.2–393.9	62.9 ± 1.7	(68.0 ± 1.8)	[28]
	E	387.2–493.2	51.9 ± 2.0	61.2 ± 2.1	[22]
	S	353–511	50.3 ± 3.0	59.1 ± 3.1	[29]
	N/A	420.9–506.4	50.6 ± 2.0	61.1 ± 2.1	[30]
	S	372.2–511.2	59.0 ± 2.0	(68.4 ± 2.1)	[23]
	DTA	411.2–511.2	51.0 ± 3.0	61.7 ± 3.1	[24]
	E	416.6–498.8	51.3 ± 0.3	61.5 ± 0.9	[31]
	N/A	423–512	50.1 ± 2.0	61.1 ± 2.1	[27]
	DSC	381.5	62.8 ± 3.0	(69.3 ± 3.1)	[25]
	E	401.3–456.8	52.5 ± 0.1	61.0 ± 0.7	[26]
	TR	326.2–353.2	56.6 ± 0.5	59.3 ± 0.6	This work
	TM	328.1–367.9	57.1 ± 0.4	60.3 ± 0.6	This work
				60.4 ± 0.3[c]	Average
4-Nitrotoluene (cr)[d]	K	297.0–309.5	80.1 ± 3.0	(80.2 ± 3.2)	[33]
	GC/ECD	253–323	74.1 ± 1.0	73.8 ± 1.1	[35]
	K	303–323	79.7 ± 0.8	(80.2 ± 1.2)	[34]
	C	296.15	77.5 ± 0.3	77.4 ± 0.3	[34]
	T	297–310	81.6 ± 1.3	(81.8 ± 1.5)	[40]
	T	283.2–313.2	74.8 ± 0.4	74.8 ± 0.7	[32]
	TGA	303–323	72.7 ± 2.0	73.0 ± 2.2	[36]
	TR	278.2–324.3	75.1 ± 0.2	75.7 ± 0.4	This work
	TM	283.3–323.1	74.8 ± 0.3	74.9 ± 0.5	This work
				76.2 ± 0.2[c]	Average

[a] Methods: E = ebulliometry; S = static method; T = transpiration (TR = measured in Rostock and TM = measured in Munich); DTA = differential thermal analysis; DSC = differential scanning calorimetry; K = Knudsen-effusion method; GC/ECD = gas-chromatography with the electron-capture detector; TGA = thermogravimetric analysis.
[b] Vapour pressures available in the literature were treated using Eqs. (2) and (3) in order to evaluate enthalpy of vaporization at 298.15 K in the same way as our own results in Table 2. Uncertainties in this table are expressed as the standard uncertainties and they derived according to the procedure reported in [13,14].
[c] Weighted mean value. Values in brackets were excluded from the calculation. Values in bold were recommended for further thermochemical calculations.
[d] Enthalpies of sublimation $\Delta_{cr}^g H^\circ_m$ measured over the crystalline sample.

Table 3
Compilation of experimental data on enthalpies of fusion available from DSC (in kJ·mol^{-1}).

Compound	T_{fus}, K	$\Delta_{cr}^l H^\circ_m$ at T_{fus}	$\Delta_{cr}^l H^\circ_m$ at 298.15 K[a]	References
4-Nitrotoluene	324.8	(13.3 ± 1.0)		[41]
	324.7	16.7 ± 1.0		[37]
	324.7	16.8 ± 0.1[b]		[37]
	–	15.4 ± 1.0		[38]
	321.8	(18.4 ± 1.0)		[25]
	324.8	16.5 ± 1.0		[42]
	324.8	16.8 ± 0.5		[43]
	322.6	16.0 ± 0.5		[39]
		16.7 ± 0.1[c]	**15.7 ± 0.3**	

[a] Uncertainties in this table are expressed as the standard uncertainties and they derived according to the procedure reported in [20]. The experimental enthalpies of fusion $\Delta_{cr}^l H^\circ_m$, measured at T_{fus} and adjusted to 298.15 K (see text). Values in parentheses were not considered in calculation of the average value.
[b] Measured by adiabatic calorimetry [37].
[c] Average value.

provided that all enthalpies in Eq. (6) are referenced to the same temperature (the reference temperature 298.15 K in this work). In this work the sample of 4-nitrotoluene was investigated by the transpiration method in both ranges, above and below its temperature of melting T_{fus} = 324.8 K. The value of $\Delta^{g}_{cr}H^{\circ}_{m}$ (298.15 K) = (75.3 ± 0.3) kJ·mol^{-1} for 4-nitrotoluene was obtained in this work from measurements in the temperature range 278.2 K–324.3 K and the vaporization enthalpy for 4-nitrotoluene $\Delta^{g}_{l}H^{\circ}_{m}$ (298.15 K) = (60.4 ± 0.3) kJ·mol^{-1} was derived from measurements in the temperature range 326.2 K–367.9 K. The standard molar enthalpy of fusion $\Delta^{l}_{cr}H^{\circ}_{m}$ (298.15 K) = (15.7 ± 0.3) kJ·mol^{-1} for 4-nitrotoluene was evaluated in Table 2. To test the consistency of the experimental data, measured in this work for 4-nitrotoluene, we have compared the enthalpy of fusion, calculated as the difference according to Eq. (6) $\Delta^{l}_{cr}H^{\circ}_{m}$ (298.15 K) = (75.3 ± 0.3) – (60.4 ± 0.3) kJ·mol^{-1} = (14.9 ± 0.4) kJ·mol^{-1} with the value $\Delta^{l}_{cr}H^{\circ}_{m}$ (298.15 K) = (15.7 ± 0.3) kJ·mol^{-1}, derived independently from calorimetric experiments (see Table 2). A good agreement (within the combined experimental uncertainties) of both results is an evidence of internal consistency of the of phase transition enthalpies data sets, evaluated for 4-nitrotoluene in Tables 2 and 3.

3.5. Calculation of the thermodynamic functions of vaporization in the broad temperature range

From our experiences, Eq. (2), used in Section 3.1 for fitting the temperature dependence of absolute vapour pressures p_i, is practical for the short temperature range of 30–50 K. As a rule, we use this equation in order to derive more precise enthalpies of vaporization in the temperature range, possibly close to the reference temperature 298.15 K (where transpiration experiments were performed). For the broader range (e.g. from ambient temperatures to the normal boiling point) we use the Clarke and Glew equation [44]:

$$R\ln\left(\frac{p}{p^{0}}\right) = -\frac{\Delta^{g}_{l}G^{\circ}_{m}(\theta)}{\theta} + \Delta^{g}_{l}H^{\circ}_{m}(\theta)\left(\frac{1}{\theta}-\frac{1}{T}\right) + \Delta^{g}_{l}C^{\circ}_{p,m}(\theta)\left[\frac{\theta}{T}-1+\ln\left(\frac{T}{\theta}\right)\right] \quad (7)$$

where p is the vapour pressure at the temperature T, p° is an arbitrary reference pressure (p° = 10^{5} Pa in this work), θ is an arbitrary reference temperature (in this work we use θ = 298.15 K), R is the molar gas constant (8.314462 J·K^{-1}·mol^{-1}), $\Delta^{g}_{l}G^{\circ}_{m}$ (θ) is the difference in the standard molar Gibbs energy between the gaseous and the liquid phases at the selected reference temperature, $\Delta^{g}_{l}H^{\circ}_{m}(\theta)$ is the difference in the standard molar enthalpy between the gas and the liquid phases, and $\Delta^{g}_{l}C^{\circ}_{p,m}$ (θ) is the difference in the molar heat capacity at constant pressure between the gaseous and the liquid phase. An advantage of the Clarke and Glew equation is that the fitting coefficients (in contrast to Eq. (2)) are directly related to the thermodynamic functions of vaporization.

Using consistent data sets the following thermodynamic functions of vaporization were derived for each nitrotoluene:

2-nitrotoluene in the range (274.0–447.9) K

$\Delta^{g}_{l}G^{\circ}_{m}$ (298.15 K) = (21.3 ± 0.2) kJ·mol^{-1}, $\Delta^{g}_{l}H^{\circ}_{m}$ (298.15 K) = (58.8 ± 0.3) kJ·mol^{-1}, and $\Delta^{g}_{l}C^{\circ}_{p,m}$ (298.15 K) = –(65 ± 5) J·K^{-1}·mol^{-1} using experimental vapour pressures from Ref. [7,26,32] and this work.

3-nitrotoluene in the range (283.2–451.8) K

$\Delta^{g}_{l}G^{\circ}_{m}$ (298.15 K) = (22.4 ± 0.1) kJ·mol^{-1}, $\Delta^{g}_{l}H^{\circ}_{m}$ (298.15 K) = (58.6 ± 0.3) kJ·mol^{-1}, and $\Delta^{g}_{l}C^{\circ}_{p,m}$ (298.15 K) = –(45 ± 4) J·K^{-1}·mol^{-1} using experimental vapour pressures from [26,32] and this work.

4-nitrotoluene in the range (326.2–498.9) K

$\Delta^{g}_{l}G^{\circ}_{m}$ (298.15 K) = (26.0 ± 0.1) kJ·mol^{-1}, $\Delta^{g}_{l}H^{\circ}_{m}$ (298.15 K) = (58.6 ± 0.4) kJ·mol^{-1}, and $\Delta^{g}_{l}C^{\circ}_{p,m}$ (298.15 K) = –(47 ± 4) J·K^{-1}·mol^{-1} using experimental vapour pressures from [26,31] and this work.

4-nitrotoluene in the range (253.2–324.3) K

$\Delta^{g}_{cr}G^{\circ}_{m}$ (298.15 K) = (24.2 ± 0.1) kJ·mol^{-1}, $\Delta^{g}_{cr}H^{\circ}_{m}$ (298.15 K) = (74.9 ± 0.3) kJ·mol^{-1}, and $\Delta^{g}_{cr}C^{\circ}_{p,m}$ (298.15 K) = –(5 ± 24) J·K^{-1}·mol^{-1} using experimental vapour pressures from [32,35] and this work.

Having established the values $\Delta^{g}_{l}G^{\circ}_{m}$, $\Delta^{g}_{l}H^{\circ}_{m}$, and $\Delta^{g}_{l}C^{\circ}_{p,m}$ as pure fitting parameters of Eq. (7) for each isomer of nitrotoluenes, it is important to compare them with values, obtained by other methods. As a rule, the empirical procedure, developed by Chickos and Acree [20], is used for estimation of $\Delta^{g}_{l}C^{\circ}_{p,m}$-values (see Table S4). The fitting parameter $\Delta^{g}_{l}C^{\circ}_{p,m}$ (298.15 K) of Eq. (7), derived from consistent vapour pressures in the broad temperature range, is a valuable tool to validate the empirical procedure by Chickos and Acree [20]. In this work for all three nitrotoluenes we used the same value $\Delta^{g}_{l}C^{\circ}_{p,m}$ (298.15 K) = –(65.5 ± 30) J·K^{-1}·mol^{-1}for calculations according to Eq. (2). This value matched exactly with the $\Delta^{g}_{l}C^{\circ}_{p,m}$ (298.15 K) = –(65 ± 5) J·K^{-1}·mol^{-1} for 2-nitrotoluene, but it is slightly higher than values $\Delta^{g}_{l}C^{\circ}_{p,m}$ (298.15 K) = –(45 ± 4) J·K^{-1}·mol^{-1} for 3-nitrotoluene and $\Delta^{g}_{l}C^{\circ}_{p,m}$ (298.15 K) = –(47 ± 4) J·K^{-1}·mol^{-1} for 4-nitrotoluene, as derived from the Clarke and Glew equation. The agreement of $\Delta^{g}_{l}C^{\circ}_{p,m}$-values for 3- and 4-nitrotoluene is satisfying, if taking into account the large uncertainties of the empirical estimate. Moreover, the values $\Delta^{g}_{l}H^{\circ}_{m}$ (298.15 K), derived as the fitting parameter of the Clarke and Glew equation, are close to our recommended values for all three nitrotoluenes, given in bold in Table 2.

The thermodynamic functions of vaporization, derived from the fitting of Eq. (7) to the evaluated vapour pressures in the broad temperature range up to the boiling temperature, are valuable guiding values. They can be applied for reliable calculation of vapour pressures at any required temperature, e.g. at ambient temperatures, where the vapour pressure is directly proportional to the concentration of the nitrotoluene taggants in air. Therefore, it is a valuable parameter for the conception of gas phase detection devices for explosives.

3.6. The enthalpies of formation from the combustion calorimetry

Results of typical combustion experiments on 3- and 4-nitrotoluenes are given in Tables 4 and 5. The relative atomic masses used for the elements C, H, N and O were the mean values recommended by the IUPAC commission in 2011 [45] for each of these elements. For 3-nitrotoluene the value of the standard specific energy of combustion $\Delta_{c}u^{\circ}$ = –27156.8 J·g^{-1} with ($\Delta_{c}u^{\circ}$) = 4.4) J·g^{-1} has been derived from six combustion experiments (see Table 4). For 4-nitrotoluene the value of the standard specific energy of combustion $\Delta_{c}u^{\circ}$ = –27034.4 J·g^{-1} with ($\Delta_{c}u^{\circ}$) = 4.2) J·g^{-1} has been derived from six combustion experiments (see Table 4). These values of the standard specific energy of combustion $\Delta_{c}u^{\circ}$ have been used to derive the standard molar enthalpies of combustion $\Delta_{c}H^{\circ}_{m}$ and the standard molar enthalpies of formation in the condensed state $\Delta_{f}H^{\circ}_{m}$ (liq or cr), given in Table 5. Values of $\Delta_{c}u^{\circ}$ and $\Delta_{c}H^{\circ}_{m}$ refer to reaction:

$$C_7H_7NO_2(\text{liq or cr}) + 8.75O_2(g) = 7CO_2(g) + 3.5H_2O(\text{liq}) + 0.5N_2(g) \quad (8)$$

The enthalpies of formation $\Delta_{f}H^{\circ}_{m}$ (liq or cr) of the nitrotoluenes were calculated from the enthalpic balance according to Eq. (8) using standard molar enthalpies of formation of H_2O (l) and CO_2 (g), recommended by CODATA [46]. Uncertainties related to combustion experiments, were calculated according to the

Table 4
Results for typical combustion experiments at T = 298.15 K (p° = 0.1 MPa) for 3-nitrotoluene.[a]

m(substance)/g	0.55291	0.54911	0.56922	0.56708	0.53222	0.52535
m'(cotton)/g	0.00440	0.00351	0.00382	0.00391	0.00356	0.00341
m''(polyethylene)/g	0.29251	0.28081	0.30209	0.30853	0.28706	0.30112
ΔT_c/K	1.87871	1.83456	1.93521	1.95122	1.82344	1.85371
$(\varepsilon_{calor})\cdot(-\Delta T_c)$/J	−28679.1	−28005.1	−29541.6	−29785.8	−27835.4	−28297.4
$(\varepsilon_{cont})\cdot(-\Delta T_c)$/J	−28.46	−27.61	−28.66	−28.83	28.33	−28.47
ΔU_{decomp} HNO_3/J	39.3	39.0	39.9	39.7	38.9	38.9
ΔU_{corr}/J	6.5	6.4	6.6	6.6	6.4	6.4
$-m'\cdot\Delta_c u'$/J	74.6	59.5	64.7	66.3	60.3	57.8
$-m''\cdot\Delta_c u''$/J	13559.9	13006.9	13990.2	14302.6	13298.5	13990.6
$\Delta_c u^\circ$ (liq)/(J·g^{-1})	−27178.4	−27153.5	−27151.0	−27155.7	−27151.4	−27150.9

[a] The definition of the symbols assigned according to ref [19] as follows: m(substance), m'(cotton) and m''(polyethylene) are, respectively, the mass of compound burnt, the mass of fuse (cotton) and auxiliary polyethylene used in each experiment, masses were corrected for buoyancy; V(bomb) = 0.32 dm^3 is the internal volume of the calorimetric bomb; p^i(gas) = 3.04 MPa is the initial oxygen pressure in the bomb; $m^i(H_2O)$ = 1.00 g is the mass of water added to the bomb for dissolution of combustion gases; $\Delta T_c = T^f - T^i + \Delta T_{corr}$ is the corrected temperature rise from initial temperature T^i to final temperature T^f, with the correction ΔT_{corr} for heat exchange during the experiment; ε_{cont} is the energy equivalents of the bomb contents in their initial ε^i_{cont} and final states ε^f_{cont}, the contribution for the bomb content is calculated with $(\varepsilon_{cont})\cdot(-\Delta T_c) = (\varepsilon^i_{cont})\cdot(T^i - 298.15) + (\varepsilon^f_{cont})\cdot(298.15 - T^f + \Delta T_{corr.})$. ΔU_{decomp} HNO_3 is the energy correction for the nitric acid formation. ΔU_{corr} is the correction to standard states.

Table 5
Results for typical combustion experiments at T = 298.15 K (p° = 0.1 MPa) for 4-nitrotoluene.[a]

m(substance)/g	0.66942	0.66531	0.58039	0.60999	0.62040	0.67506
m'(cotton)/g	0.00297	0.00310	0.00282	0.00291	0.00316	0.00391
ΔT_c/K	1.19041	1.18326	1.03168	1.08505	1.10284	1.20067
$(\varepsilon_{calor})\cdot(-\Delta T_c)$/J	−18172.0	−18062.8	−15748.9	−16563.6	−16835.2	−18328.6
$(\varepsilon_{cont})\cdot(-\Delta T_c)$/J	−26.4	−26.2	−25.8	−26.0	−26.1	−26.5
ΔU_{decomp} HNO_3/J	39.1	39.0	33.8	35.6	36.2	39.4
ΔU_{corr}/J	6.4	6.4	6.2	6.3	6.3	6.4
$-m'\cdot\Delta_c u'$/J	50.3	52.5	47.8	49.3	53.6	66.3
$\Delta_c u^\circ$ (liq)/(J·g^{-1})	−27042.1	−27041.7	−27028.2	−27047.0	−27023.3	−27024.3

[a] The definition of the symbols is the same as in Table 4.

guidelines presented in [19,47]. The uncertainties of the standard molar energies and enthalpies of combustion correspond to expanded uncertainties of the mean (0.95 level of confidence) and include the contribution from the calibration with benzoic acid and from the values of the auxiliary quantities used. The uncertainty, assigned to $\Delta_f H^\circ_m$ (liq or cr), is twice the overall standard deviation and includes the uncertainties from calibration, from the combustion energies of the auxiliary materials, and the uncertainties of the enthalpies of formation of the reaction products H_2O and CO_2 (see Table 6).

Standard molar enthalpies of formation of the nitrotoluenes collected in Table 5 were measured using the combustion calorimetry [7,34,40,48,49]. The first results, reported by Garner and Abernethy [48], were in significant disagreement with the values, reported later by Lenchitz et al. [49]. A combustion calorimetry study on 2-nitrotoluene, earlier performed in our lab [7], has established the reliable value $\Delta_f H^\circ_m$ (298.15 K, liq) for this compound. Our new combustion experiments on 3-nitro- and 4-nitrotoluene have generally supported the earlier results, reported by Lenchitz et al. [49] and Smirnov et al. [34], however, our new values

Table 6
Thermochemical data at T = 298.15 K (p° = 0.1 MPa) for nitrotoluenes (in kJ·mol^{-1}).[a]

Compound	$\Delta_c H^\circ_m$ (liq/cr)	$\Delta_f H^\circ_m$ (liq/cr)	$\Delta^g_l H^\circ_m$/[b] $\Delta^g_{cr} H^\circ_m$[b]	$\Delta_f H^\circ_m$ (g) exp	$\Delta_f H^\circ_m$ (g)[c] G4	Exp-G4[g]
1	2	3	4	5	6	7
2-Nitrotoluene (liq)	(−3753.9 ± 8.4) [48]	(−1.1 ± 8.4)				
	(−3745.3 ± 3.8) [49]	(−9.7 ± 3.9)				
	−3733.2 ± 0.4 [7]	**−21.7 ± 0.9**	**58.8 ± 0.4**	**37.1 ± 1.0**	40.5	−3.4
3-Nitrotoluene (liq)	(−3735.9 ± 8.4) [48]	(−19.1 ± 8.4)				
	−3723.5 ± 3.3 [49]	−31.5 ± 3.4				
	−3724.8 ± 1.4[d]	−30.2 ± 1.7				
		−30.4 ± 1.5[e]	**59.4 ± 0.4**	**29.0 ± 1.5**	30.2	−1.2
4-Nitrotoluene (cr)	(−3715.8 ± 8.4) [48]	(−37.1 ± 8.4)				
	−3706.9 ± 3.0 [49]	−48.1 ± 3.2				
	−3710.2 ± 1.7 [40]	−44.7 ± 2.0				
	−3709.8 ± 2.0 [34]	−45.2 ± 2.2				
	−3708.0 ± 1.3[d]	−47.0 ± 1.6				
		−46.3 ± 1.0[e]	**76.2 ± 0.4**	**29.9 ± 1.1**	29.5	0.4

[a] All uncertainties in this table are expressed as twice the standard deviation. Uncertainties of combustion enthalpies include uncertainty from calibration, benzoic acid and auxiliary materials. Values given in bold are recommended for thermochemical calculations.
[b] From Table 2.
[c] Calculated by G4 by using isodesmic reactions [50].
[d] This work.
[e] Weighted average value. Values given in brackets were excluded.
[g] Calculated as the difference between column 7 and 5 from this table.

$\Delta_f H^\circ_m$ (298.15 K) for both compounds possess smaller uncertainties (see Table 5). In order to establish more confidence, we calculated the weighted mean value $\Delta_f H^\circ_m$ (298.15, liq) for 3-nitrotoluene from own results and those from Lenchitz et al. [49]. Uncertainties in the enthalpies of formation were used as the weighting factor. For 4-nitrotoluene we calculated the weighted mean value $\Delta_f H^\circ_m$ (298.15, cr) from own results, those from Lenchitz et al. [49], and from the most recent studies by Smirnov et al. [34] and by Lebedev et al. [40]. These averaged results for $\Delta_f H^\circ_m$ (298.15 liq/cr) have been recommended for further thermochemical calculations, aiming to derive the gas-phase enthalpies of formation $\Delta_f H^\circ_m$ (298.15, g) and for comparison with results from quantum-chemical calculations.

3.7. Gas-phase standard molar enthalpies of formation of nitrotoluenes

The results from combustion calorimetry, evaluated in Section 3.4 (Table 5), and values of vaporization/sublimation enthalpies of nitrotoluenes, evaluated and averaged in this work (Table 2), can now be used together for further calculation of the gaseous standard enthalpies of formation, $\Delta_f H^\circ_m$ (g) at 298.15 K. The resulting values are given in Table 5, column 5. Since a significant discrepancy among available experimental enthalpies of formation for 2-nitrotoluene is apparent from Table 5, any additional arguments to support the reliability of the evaluated results are required. A valuable test of consistency of the experimental data is provided by high-level quantum-chemical composite method calculations at the G4 level, reported for nitrotoluenes quite recently [50] (see Table 5, column 6). As can be seen from Table 5, the G4 values for $\Delta_f H^\circ_m$ (g, 298.15 K) are in a good agreement with the experimental results, evaluated in this study, providing the additional confidence for the benchmark quality of thermochemical properties recommended in Table 5.

Acknowledgments

The work has been partly supported by the Federal Target Program "Research and development on priority directions of scientific-technological complex of Russia for 2014–2020", agreement no. 14.577.21.0140 of Nov 28, 2014 (unique applied research project identifier RFMEFI57714X0140). Financial support of this work by the Ludwig-Maximilian University of Munich (LMU), the Office of Naval Research (ONR) under grant no. ONR.N00014-16-1-2062 and the German Ministry of Education and Research (BMBF) under grant no. 13N12583 is gratefully acknowledged. Greta Bikelytė was provided an ERASMUS scholarship funding her research stay in the laboratories of Prof. Klapötke.

Appendix A. Supplementary data

Supplementary data associated with this article can be found, in the online version, at http://dx.doi.org/10.1016/j.jct.2017.03.029.

References

[1] IARC Working Group on the Evaluation of Carcinogenic Risks to Humans, Some chemicals present in industrial and consumer products, food and drinking-water, Iarc Monogr. Eval. Carcinogenic Risks Hum. 101 (2013) 9–549.
[2] http://www.mcgill.ca/iasl/files/iasl/montreal1991.pdf.
[3] G. Bunte, J. Hürttlen, H. Pontius, K. Hartlieb, H. Krause, Anal. Chim. Acta 591 (2007) 49–56.
[4] http://www.sedet.com/Technology.html.
[5] H. Östmark, S. Wallin, H.G. Ang, Propellants Explos. Pyrotech. 37 (2012) 12–23.
[6] S.P. Verevkin, Thermochim. Acta 307 (1997) 17–25.
[7] S.P. Verevkin, A. Heintz, J. Chem. Thermodyn. 32 (2000) 1169–1182.
[8] S.P. Verevkin, C. Schick, Fluid Phase Equilib. 211 (2003) 161–177.
[9] A. Heintz, S. Kapteina, S.P. Verevkin, J. Phys. Chem. A 111 (2007) 6552–6562.
[10] S.P. Verevkin, V.N. Emel'yanenko, V. Diky, O.V. Dorofeeva, J. Chem. Thermodyn. 73 (2014) 163–170.
[11] V.N. Emel'yanenko, M. Algarra, J.C.G. Esteves da Silva, J. Hierrezuelo, J.M. López-Romero, S.P. Verevkin, Thermochim. Acta 597 (2014) 78–84.
[12] S.P. Verevkin, V.N. Emel'yanenko, Fluid Phase Equilib. 266 (2008) 64–75.
[13] S.P. Verevkin, A.Y. Sazonova, V.N. Emel'yanenko, D.H. Zaitsau, M.A. Varfolomeev, B.N. Solomonov, K.V. Zherikova, J. Chem. Eng. Data 60 (2015) 89–103.
[14] V.N. Emel'yanenko, S.P. Verevkin, J. Chem. Thermodyn. 85 (2015) 111–119.
[15] S.P. Verevkin, Phase Changes in Pure Component Systems: Liquids and Gases, 1st ed., Elsevier B.V., Amsterdam, Netherlands, 2005.
[16] S.P. Verevkin, C. Schick, J. Chem. Eng. Data 45 (2000) 946–952.
[17] V.N. Emel'yanenko, S.P. Verevkin, A. Heintz, J. Am. Chem. Soc. 129 (2007) 3930–3937.
[18] J. de Zeeuw, S. Reese, J. Cochran, S. Grossman, T. Kane, C. English, J. Sep. Sci. 32 (2009) 1849–1857.
[19] W.N. Hubbard, D.W. Scott, G. Waddington, in: F.D. Rossini (Ed.), Experimental Thermochemistry, Interscience Publishers, New York, 1956, pp. 75–127.
[20] J.S. Chickos, W.E. Acree, J. Phys. Chem. Ref. Data 32 (2003) 519–878.
[21] J.F.T. Berliner, O.E. May, J. Am. Chem. Soc. 48 (1926) 2630–2634.
[22] E. Levin, I. Shtern, Zhurnal Prikladnoi Khimii (Sankt Petersburg, Russian Federation) 11 (1938) 426–440.
[23] V.M. Salachijev, G.P. Sharnin, Tr. Kazan. Khim. Technol. Inst. 52 (1973) 69–72.
[24] Y. Hara, H.J. Osada, J. Indus. Explos. Soc. (Kogyo Kagaku) 37 (1976) 233–236.
[25] D.-R. Hwang, M. Tamura, T. Yoshida, N. Tanaka, F. Hosoya, J. Energy Mater. 8 (1990) 85–98.
[26] K. Aim, J. Chem. Eng. Data 39 (1994) 591–594.
[27] R.M. Stephenson, S. Malanowski, D. Ambrose, Handbook of the Thermodynamics of Organic Compounds, Elsevier, New York, 1987.
[28] C.A. Mann, R.E. Montonna, M.G. Larian, Ind. Eng. Chem. 28 (1936) 598–601.
[29] K.A. Kobe, T.S. Okabe, M.T. Ramstad, P.M. Huemmer, J. Am. Chem. Soc. 63 (1941) 3251–3252.
[30] R.R. Dreisbach, S.A. Shrader, Ind. Eng. Chem. 41 (1949) 2879–2880.
[31] D. Ambrose, H.A. Gundry, J. Chem. Thermodyn. 12 (1980) 559–561.
[32] J.A. Widegren, T.J. Bruno, J. Chem. Eng. Data 55 (2010) 159–164.
[33] C. Lenchitz, R.W. Velicky, J. Chem. Eng. Data 15 (1970) 401–403.
[34] S.P. Smirnov, Y.N. Matiushin, I.Z. Akmetov, Conf. International Civil Aviation Organization, 14–18 February, paper No. AH-DE/8-WP/12, Montreal, Canada, 1994.
[35] L. Elias, AH-DE/5-WP/17, International Civil Aviation Organization, Montreal, Canada, 23–27 September 1991.
[36] H. Felix-Rivera, M.L. Ramirez-Cedeno, R.A. Sanchez-Cuprill, S.P. Hernandez-Rivera, Thermochim. Acta 514 (2011) 37–43.
[37] M.J. Richardson, N.G. Savill, Thermochim. Acta 30 (1979) 327–337.
[38] U.S. Tewari, M.K. Mathew, P. Vasudevan, J. Indian Chem. Soc. 56 (1979) 734–735.
[39] D.E.G. Jones, R.A. Augsten, K.K. Feng, J. Therm. Anal. 44 (1995) 533–546.
[40] Vyacheslav P. Lebedev, Valeriy V. Chironov, Yuriy N. Matyushin, Aleksei B. Vorobev, Yaroslav O. Inozemtsev. Enthalpy of formation of the radical 4-methylphenyl. 35th International Annual Conference of ICT, Karlsruhe, Germany, (2004), p. 94.
[41] R.P. Rastogi, R.K. Nigam, R.N. Sharma, H.L. Girdhar, J. Chem. Phys. 39 (1963) 3042–3044.
[42] A.A. Grigor'ev, G.G. Chernik, A.Y. Timoshkin, A.V. Suvorov, Russ. J. Gen. Chem. 64 (1994) 512–517.
[43] R.J.L. Andon, J.E. Connett, Thermochim. Acta 42 (1980) 241–247.
[44] E.C.W. Clarke, D.N. Glew, Trans. Faraday Soc. 62 (1966) 539–547.
[45] M.E. Wieser, N. Holden, T.B. Coplen, J.K. Böhlke, M. Berglund, W.A. Brand, P. De Bièvre, M. Gröning, R.D. Loss, J. Meija, T. Hirata, T. Prohaska, R. Schoenberg, G. O'Connor, T. Walczyk, S. Yoneda, X.C. Zhu, Pure Appl. Chem. 85 (2013) 1047–1078.
[46] J.D. Cox, D.D. Wagman, V.A. Medvedev, CODATA Key Values for Thermodynamics, Hemisphere, New York, 1989.
[47] G. Olofsson, in: S. Sunner, M. Mansson (Eds.), Combustion calorimetry, Pergamon, New York, 1979 (Chapter 6).
[48] W.E. Garner, C.L. Abernethy, Proc. R. Soc. London Ser. A 99 (1921) 213–235.
[49] C. Lenchitz, R.W. Velicky, G. Silvestro, L.P. Schlosberg, J. Chem. Thermodyn. 3 (1971) 689–692.
[50] M.A. Suntsova, O.V. Dorofeeva, J. Chem. Eng. Data 61 (2016) 313–329.

J. Chem. Thermodynamics. 2016

Electronic Supporting Information

Benchmark properties of 2-, 3- and 4-nitrotoluene: evaluation of thermochemical data with complementary experimental and computational methods

Greta Bikelytė,[a] Martin Härtel,[a] Jörg Stierstorfer[a], Thomas M. Klapötke, [a] Andrey A. Pimerzin,[b] Sergey P. Verevkin [c,]*

[a] *Department Chemie, Ludwig-Maximilians-Universität München, Butenandtstr. 5-13, 81377 München-Großhadern, Germany*

[b] *Chemical Department, Samara State Technical University, Molodogvardeyskaya 244, Samara 443100, Russia*

[c]*Department of Physical Chemistry and Department of „Science and Technology of Life, Light and Matter", University of Rostock, Dr-Lorenz-Weg 1, D-18059, Rostock, Germany*

Table S1

Compilation of VO-GC/MS parameters used for transpiration experiments in Munich

GC/MS	*Shimadzu QP2010SE®* with LabSolution GCMSsolution v4.11
Injector	Atas Optic 4 with Evolution Workstation v4.1
Liner	10 mm V2A stainless steel tube, 5 mm wall thickness, equipped with silanized glass wool (2 mm injection needle penetration into wool)
Restriction	0.025 mm capillary, 8.11 mm length (Restek #10097)
Column connector	*SGE Siltite µ-Union®* (Restek #073562)
Analytical columns	*Restek RTX-TNT 1®* (6 m, 0.53 mm, 1.5 µm)
Oven program	46 °C (hold 0.10 min) → 195 °C (rate 60 °C min^{-1})
Injector head pressure	472 kPa
virtual column	100 m, 0.25 µm film thickness, 0.20 mm i.d. (entry for GCMSsolution)
column flow	2.33 mL min^{-1}
split ratio	18.7 (entered in LabSolutions GCMSsolution)
purge flow	5 mL min^{-1}
injection volume	1 µL
Ion source	200 °C
MS interface	250 °C
MS	SIM mode (event Time 100 ms 2-NT: 1.00 – 1.60 min: m/z 120, 65, 92, 89, 77, 39. 3-NT: 1.00 – 1.60 min: m/z 137, 65, 39, 107, 63, 89. 4-NT: 1.00 – 1.60 min: m/z 91, 137, 65, 39, 107, 77. all: 1.60 – 2.58 min: m/z: 57 43 71 41 85 55 (C-16 standard) first: quantification Ion, 2nd-6th: reference ions

Table S2

Formula, density ρ (T = 293 K), massic heat capacity c_p (T = 298 K), and expansion coefficients $(\delta V/\delta T)_p$ of the materials used in the present study.

compounds	formula	ρ	c_p	$10^{-6}\cdot(\delta V/\delta T)_p$
		g·cm^{-3}	J·K^{-1}·g^{-1}	dm^3·K^{-1}
3-nitrotoluene (liq)	$C_7H_7NO_2$	1.15 [1]	1.54 [b]	1.0
4-nitrotoluene (cr)	$C_7H_7NO_2$	1.29 [2]	1.26 [b]	0.1
polyethylene [d]	$CH_{1.93}$	0.92	2.53	0.1
cotton [d]	$CH_{1.774}O_{0.887}$	1.50	1.67	0.1

[a] Literature values.

[b] Calculated according to the empirical procedure developed by Chickos and Acree [3].

[d] Data for density, specific heat capacity, and expansion coefficients of auxiliary materials are from our previous work [4]. Energy of combustion $\Delta_c u^\circ$(polyethylene) = -46357.3 J·g^{-1}; $u(\Delta_c u^\circ)$ = 3.6 J·g^{-1}. Energy of combustion $\Delta_c u°$ (cotton) = -16945.2 J·g^{-1}; $u(\Delta_c u^\circ)$ = 4.2 J·g^{-1} from [3].

Table S3

Results from transpiration method: absolute vapor pressures *p*, standard molar vaporization enthalpies and standard molar vaporization entropies.

2-Nitrotoluene (TM): $\Delta_l^g H_m^\circ$ (298.15 K) = 58.9 kJ mol^{-1}; $u(\Delta_l^g H_m^\circ)$ = 0.3 kJ mol^{-1}

$$\ln p/p^\circ = \frac{287.0}{R} - \frac{78395.6}{RT} + \frac{65.5}{R} ln \frac{T}{298.15\text{K}}$$

T_{exp}[a] [K]	m[b] [mg]	V_{N2}[c] [dm³]	T_{amb}[d] [K]	Gasflow [dm³ h^{-1}]	p[e] [Pa]	$u(p)$[f] [Pa]	$\Delta_l^g H_m^\circ$ [kJ mol^{-1}]	$\Delta_l^g S_m^\circ$ [J mol^{-1} K^{-1}]
278.3	0.88	10.1	296.5	5.04	3.28	0.09	60.17	130.3
278.4	1.04	6.00	296.8	2.00	3.20	0.09	60.16	130.0
283.3	1.03	7.39	296.8	5.04	5.26	0.16	59.84	129.3
283.3	1.85	6.74	297.3	5.06	5.02	0.15	59.84	128.9
288.3	0.88	4.05	297.3	5.06	8.06	0.23	59.51	128.1
288.3	1.86	4.21	297.7	5.05	8.04	0.23	59.51	128.0
293.2	0.89	2.69	297.2	5.04	12.4	0.3	59.19	127.1
293.2	2.28	3.49	296.7	3.04	11.9	0.3	59.19	126.7
298.2	0.87	1.77	297.0	5.05	18.1	0.5	58.86	125.8
298.2	1.97	2.03	295.9	5.07	17.5	0.5	58.86	125.5
303.1	1.95	1.37	297.1	4.55	25.9	0.7	58.54	124.5
303.2	0.9	1.22	297.0	4.56	27.3	0.7	58.54	124.8
308.1	1.97	0.941	298.7	2.02	38.1	1.0	58.22	123.5
308.2	0.56	0.502	297.4	2.01	39.1	1.0	58.21	123.6
313.1	0.77	0.501	297.0	2.01	56.3	1.4	57.89	122.7
313.1	1.55	0.505	298.4	2.02	55.5	1.4	57.89	122.6
318.0	2.13	0.503	298.2	2.01	76.5	1.9	57.57	121.4
318.1	0.87	0.398	297.2	1.49	81	2.1	57.56	121.8
323.0	2.27	0.382	298.0	1.53	108	3	57.24	120.4

3-Nitrotoluene (TM): $\Delta_l^g H_m^\circ$ (298.15 K) = 59.4 kJ mol^{-1}; $u(\Delta_l^g H_m^\circ)$ = 0.2 kJ mol^{-1}

$$\ln p/p^\circ = \frac{285.3}{R} - \frac{78945.5}{RT} + \frac{65.5}{R} ln \frac{T}{298.15\text{K}}$$

T_{exp}[a] [K]	m[b] [mg]	V_{N2}[c] [dm³]	T_{amb}[d] [K]	Gasflow [dm³ h^{-1}]	p[e] [Pa]	$u(p)$[f] [Pa]	$\Delta_l^g H_m^\circ$ [kJ mol^{-1}]	$\Delta_l^g S_m^\circ$ [J mol^{-1} K^{-1}]
298.2	1.22	1.85	297.0	5.04	12	0.3	59.41	124.1
299.2	2.69	3.81	296.5	3.34	12.7	0.3	59.35	123.8
302.2	2.51	2.78	296.5	3.34	16.3	0.4	59.15	123.2
303.2	2.96	3.04	296.8	4.92	17.6	0.5	59.09	123.0
303.2	2.57	2.69	297.6	5.04	17.3	0.5	59.09	122.8
303.2	1.92	2.01	296.9	5.01	17.3	0.5	59.09	122.8
308.2	2.73	1.90	298.0	2.59	26.0	0.7	58.76	122.0
308.2	2.63	1.83	296.6	3.32	25.9	0.7	58.76	122.0
308.2	2.25	1.59	296.3	5.02	25.5	0.7	58.76	121.9
308.2	2.59	1.85	297.3	5.03	25.3	0.7	58.76	121.8
313.2	2.08	1.01	296.5	4.05	37.0	0.9	58.43	120.9
313.2	2.84	1.41	297.7	4.70	36.3	0.9	58.43	120.7
313.2	2.58	1.29	297.3	4.07	36.1	0.9	58.43	120.7
318.2	2.93	0.989	297.5	1.86	53.5	1.4	58.10	120.0
318.2	1.98	0.680	296.4	2.72	52.4	1.3	58.10	119.8

318.1	2.60	0.910	297.4	2.73	51.6	1.3	58.11	119.7
323.1	2.89	0.703	297.5	2.72	74.3	1.9	57.78	118.9
323.2	2.03	0.499	296.6	1.99	73.2	1.9	57.78	118.7
323.1	2.65	0.665	297.4	2.00	71.8	1.8	57.78	118.7
328.1	2.14	0.376	296.7	1.50	103	3	57.45	117.9
333.1	2.06	0.269	296.4	1.01	138	3	57.13	116.7
338.0	2.8	0.271	298.0	1.02	187	5	56.81	115.8

3-Nitrotoluene (TR): $\Delta_l^g H_m^\circ$ (298.15 K) = 58.9 kJ mol^{-1}; $u(\Delta_l^g H_m^\circ)$ = 0.4 kJ mol^{-1}

$$\ln p/p^\circ = \frac{283.9}{R} - \frac{78450.5}{RT} + \frac{65.5}{R} ln \frac{T}{298.15\text{K}}$$

T_{exp}[a] [K]	m[b] [mg]	V_{N2}[c] [dm³]	T_{amb}[d] [K]	Gasflow [dm³ h^{-1}]	p[e] [Pa]	$u(p)$[f] [Pa]	$\Delta_l^g H_m^\circ$ [kJ mol^{-1}]	$\Delta_l^g S_m^\circ$ [J mol^{-1} K^{-1}]
290.6	2.43	6.84	293.4	3.32	6.48	0.19	59.42	124.3
293.3	1.92	4.15	293.4	3.32	8.42	0.24	59.24	124
296.3	1.72	3.04	293.4	3.32	10.3	0.3	59.04	122.9
299.2	2.77	3.79	293.4	3.32	13.3	0.4	58.85	122.5
302.3	2.57	2.77	293.4	3.32	16.8	0.4	58.65	121.8
305.3	2.48	2.13	293.4	3.32	21.1	0.6	58.45	121.1
308.3	2.69	1.83	293.4	3.32	26.7	0.7	58.26	120.6
311.4	3.17	1.72	293.4	3.32	33.5	0.9	58.05	119.9
314.3	2.85	1.25	293.4	3.32	41.4	1.1	57.86	119.3
317.2	2.82	1.02	293.4	3.32	49.8	1.3	57.67	118.6
320.2	2.79	0.83	293.4	3.32	60.7	1.5	57.48	117.9
323.2	2.29	0.553	293.4	3.32	74.9	1.9	57.28	117.4

4-Nitrotoluene (TM): $\Delta_l^g H_m^\circ$(298.15 K) = 60.3 kJ mol^{-1}; $u(\Delta_l^g H_m^\circ)$ = 0.6 kJ mol^{-1}

$$\ln p/p^\circ = \frac{286.6}{\text{R}} - \frac{79858.8}{\text{R}T} + \frac{65.5}{\text{R}} ln \frac{T}{298.15\text{K}}$$

T_{exp}[a] [K]	m[b] [mg]	V_{N2}[c] [dm³]	T_{amb}[d] [K]	Gasflow [dm³ h^{-1}]	p[e] [Pa]	$u(p)$[f] [Pa]	$\Delta_l^g H_m^\circ$ [kJ mol^{-1}]	$\Delta_l^g S_m^\circ$ [J mol^{-1} K^{-1}]
328.1	3.62	0.758	297.4	3.03	86.2	2.2	58.37	119.2
328.1	14.09	2.97	296.4	5.09	85.3	2.2	58.37	119.1
333.0	3.64	0.560	297.8	2.24	117	3	58.05	118.2
333.0	10.69	1.71	297.0	5.11	113	3	58.05	117.9
338.0	6.42	0.718	297.9	1.39	162	4	57.72	117.3
338.0	11.63	1.35	297.0	4.05	155	4	57.72	117.0
343.0	6.36	0.532	297.5	1.10	216	5	57.39	116.3
343.0	11.88	1.02	296.1	4.06	210	5	57.39	116.1
347.9	11.51	0.756	296.8	3.02	274	7	57.07	115.0
348.0	6.45	0.402	297.9	1.10	290	7	57.06	115.4
352.9	10.21	0.498	296.6	1.99	369	9	56.74	114.2
353.0	6.05	0.292	298.0	1.10	374	9	56.74	114.3
357.9	10.93	0.407	296.5	1.63	483	12	56.42	113.3
358.0	6.74	0.242	298.5	1.03	504	13	56.41	113.6
362.9	10.43	0.302	296.8	1.21	622	16	56.09	112.3
363.0	6.16	0.169	298.6	1.01	660	17	56.08	112.8
367.9	6.32	0.136	298.8	1.02	841	21	55.76	111.8
367.9	11.44	0.260	296.9	1.04	793	20	55.76	111.3

4-Nitrotoluene (TR): $\Delta_l^g H_m^\circ$(298.15 K) = 59.3 kJ·mol^{-1}; $u(\Delta_l^g H_m^\circ)$ = 0.6 kJ mol^{-1}

$$\ln p/p^\circ = \frac{284.1}{R} - \frac{78838.5}{RT} + \frac{65.5}{R} ln \frac{T}{298.15K}$$

T_{exp} [a] [K]	m [b] [mg]	V_{N2} [c] [dm³]	T_{amb} [d] [K]	Gasflow [dm³ h^{-1}]	p [e] [Pa]	$u(p)$ [f] [Pa]	$\Delta_l^g H_m^\circ$ [kJ mol^{-1}]	$\Delta_l^g S_m^\circ$ [J mol^{-1} K^{-1}]
326.2	3.40	0.765	293.2	3.01	79.7	2.0	57.48	116.9
329.2	3.93	0.727	293.2	3.01	97.0	2.4	57.28	116.3
332.2	4.05	0.602	293.2	3.01	120.7	3.0	57.08	116.0
332.2	3.66	0.548	293.2	3.01	119.8	3.0	57.08	115.9
335.3	4.34	0.552	293.2	3.01	141.1	3.6	56.88	115.1
338.2	4.23	0.452	293.2	3.01	168.0	4.2	56.69	114.5
341.2	5.02	0.452	293.2	3.01	199.5	5.0	56.49	113.9
344.4	4.73	0.351	293.2	3.01	241.7	6.1	56.28	113.4
347.1	3.92	0.251	293.2	3.01	280.2	7.0	56.11	112.8
350.2	5.21	0.276	293.2	3.01	338.8	8.5	55.90	112.4
353.2	5.63	0.251	293.2	3.01	402.4	10.1	55.71	111.9

4-Nitrotoluene (TM): $\Delta_{cr}^g H_m^\circ$ (298.15 K) = 74.9; $u(\Delta_l^g H_m^\circ)$ = 0.5 kJ mol^{-1} kJ mol^{-1}

$$\ln p/p^\circ = \frac{292.1}{R} - \frac{82822.3}{RT} + \frac{26.6}{R} ln \frac{T}{298.15K}$$

T_{exp} [a] [K]	m [b] [mg]	V_{N2} [c] [dm³]	T_{amb} [d] [K]	Gasflow [dm³ h^{-1}]	p [e] [Pa]	$u(p)$ [f] [Pa]	$\Delta_{cr}^g H_m^\circ$ [kJ mol^{-1}]	$\Delta_{cr}^g S_m^\circ$ [J mol^{-1} K^{-1}]
283.3	1.76	28.2	296.6	2.00	1.13	0.03	75.29	171.0
288.3	1.89	17.3	296.0	1.02	1.96	0.05	75.15	170.5
293.2	1.85	10.0	296.5	5.02	3.32	0.09	75.02	170.1
298.2	1.91	6.06	296.3	4.04	5.66	0.17	74.89	169.8
303.2	1.96	3.75	296.1	5.00	9.37	0.26	74.76	169.4
308.2	1.97	2.34	296.6	5.02	15.1	0.4	74.62	169.0
308.2	1.76	28.2	296.6	2.00	14.9	0.4	74.62	168.9
313.2	1.88	1.42	297.0	4.05	23.9	0.6	74.49	168.5
318.2	2.11	1.01	296.9	3.02	37.7	1.0	74.36	168.1
323.1	2.39	0.754	297.0	2.06	57.2	1.5	74.23	167.7
323.1	2.01	0.665	297.4	1.99	54.4	1.4	74.23	167.2

4-Nitrotoluene (TR): $\Delta_{cr}^g H_m^\circ$ (298.15 K) = 75.2; $u(\Delta_l^g H_m^\circ)$ = 0.4 kJ mol^{-1} kJ mol^{-1}

$$\ln p/p^\circ = \frac{293.7}{R} - \frac{83096.6}{RT} + \frac{26.6}{R} ln \frac{T}{298.15K}$$

T_{exp} [a] [K]	m [b] [mg]	V_{N2} [c] [dm³]	T_{amb} [d] [K]	Gasflow [dm³ h^{-1}]	p [e] [Pa]	$u(p)$ [f] [Pa]	$\Delta_{cr}^g H_m^\circ$ [kJ mol^{-1}]	$\Delta_{cr}^g S_m^\circ$ [J mol^{-1} K^{-1}]
278.2	1.86	50.4	293.6	2.72	0.67	0.07	75.70	173.0
279.6	1.70	38.7	293.6	2.72	0.80	0.07	75.66	173.0
288.2	1.37	11.7	293.6	2.72	2.11	0.10	75.43	172.2
290.3	1.46	9.76	293.6	2.72	2.71	0.12	75.37	172.2
292.2	2.10	11.6	293.6	3.25	3.26	0.13	75.32	171.9
296.8	1.67	5.61	293.6	3.25	5.39	0.18	75.20	171.7
298.3	1.76	5.31	293.6	3.25	5.99	0.20	75.16	171.1
301.4	1.88	4.09	293.6	3.25	8.33	0.23	75.08	171.0
304.3	2.03	3.33	293.6	3.25	11.0	0.3	75.00	170.7
307.4	2.38	2.87	293.6	3.25	15.0	0.4	74.92	170.5

310.3	2.58	2.41	293.6	3.25	19.3	0.5	74.84	170.1
313.2	6.13	4.39	293.6	3.25	25.2	0.7	74.77	169.8
314.3	2.29	1.42	293.6	3.25	29.2	0.8	74.74	170.1
314.3	2.29	1.42	293.6	3.25	29.2	0.8	74.74	170.1
315.2	2.47	1.44	293.6	3.25	30.9	0.8	74.71	169.8
315.7	2.56	1.40	293.6	3.25	33.0	0.8	74.70	170.0
316.2	2.74	1.40	293.6	3.25	35.4	0.9	74.69	170.1
316.7	3.23	1.63	293.6	3.25	35.9	0.9	74.67	169.8
317.2	2.75	1.29	293.6	3.25	38.3	1.0	74.66	170.0
318.2	2.43	1.10	293.6	3.25	40.0	1.0	74.63	169.5
319.3	2.66	1.10	293.6	3.25	43.8	1.1	74.60	169.3
320.3	2.66	0.996	293.6	3.25	48.3	1.2	74.58	169.3
321.2	2.75	0.948	293.6	3.25	52.3	1.3	74.55	169.3
322.2	2.51	0.798	293.6	3.25	56.9	1.4	74.53	169.2
323.3	2.59	0.748	293.6	3.25	62.6	1.6	74.50	169.1
324.3	3.28	0.879	293.6	3.25	67.3	1.7	74.47	168.9

[a] Saturation temperature ($u(T)$ = 0.1 K). [b] Mass of transferred sample condensed at T = 243 K. [c] Volume of nitrogen ($u(V)$ = 0.005 dm^3) used to transfer m ($u(m)$ = 0.0001 g) of the sample. [d] T_a is the temperature of the soap bubble meter used for measurement of the gas flow. [e] Vapor pressure at temperature T, calculated from the m and the residual vapor pressure at the condensation temperature calculated by an iteration procedure. [f] Uncertainties were calculated with $u(p/\text{Pa}) = 0.005 + 0.025(p/\text{Pa})$ for pressures below 5 Pa and with $u(p/\text{Pa}) = 0.025 + 0.025(p/\text{Pa})$ for pressure from 5 to 3000 Pa. Uncertainties of vaporization enthalpies are expressed as the standard uncertainties and they derived according to the procedure reported in [5,6]. The results measured by the transpiration (T) in Rostock were labeled in this work as TR, and the results measured in Munich as TM.

Table S4

Compilation of data on molar heat capacities (in J·mol^{-1}·K^{-1}) at 298.15 K of the nitrotoluenes

Compounds	$C^{\circ}_{p,m}$ (liq)[a]	$-\Delta^{g}_{l}C^{\circ}_{p,m}$ [b]	$C^{\circ}_{p,m}$ (cr)	$-\Delta^{g}_{cr}C^{\circ}_{p,m}$ [c]
2-nitrotoluene	211.3	65.5	-	
3-nitrotoluene	211.3	65.5	-	
4-nitrotoluene	214.0 [6]	65.6	172.2 [7]	-26.6

a) calculated according to the group-contribution method by Chickos and Acree [3].
b) calculated by $\Delta^{g}_{l}C^{o}_{p,m} = 10.58 + C^{o}_{p,m}(\text{l}) \times 0.26$ [3].
c) calculated by $\Delta^{g}_{cr}C^{o}_{p,m} = 0.75 + C^{o}_{p,m}(\text{cr}) \times 0.15$ [3].

[1] L. Venkatramana, R. L. Gardas, K. Sivakumar, K. D. Reddy, Fluid Phase Equilib., 367 (2014) 7-21
[2] J. V. Barve, L. M. Pant, Acta Cryst. B27 (1971) 1158-1162.
[3] J. S. Chickos, W. E. Acree, J. Phys. Chem. Ref. Data 31 (2002) 537-698.
[4] S .P. Verevkin, J. Chem. Thermodyn. 31 (1999) 559-585.
[5] S. P. Verevkin, A. Y. Sazonova, V. N. Emel'yanenko, D. H. Zaitsau, M. A. Varfolomeev, B. N. Solomonov, K. V. Zherikova, J. Chem. Eng. Data 60 (2015) 89-103.
[6] V. N. Emel'yanenko, S.P. Verevkin, J. Chem. Thermodyn. 85 (2015) 111-119.
[7] M. J. Richardson, N. G. Savill, Thermochim. Acta 30 (1979) 327-337.

7.5 Measurement of 2,4-Dinitrotoluene 15 and 2,6-Dinitrotoluene 16 and 2,4,6-Trinitrotoluene 17

This chapter deals with the measurement of the vapor pressure of the mononitrotoluenes 2,4-DNT **15**, 2,6-DNT **16** and TNT **17**:

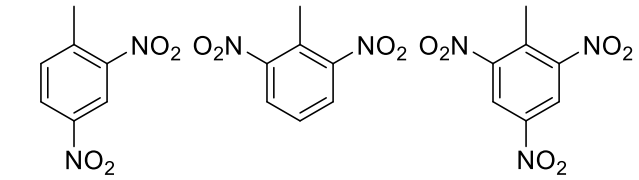

2,4-DNT **15** 2,6-DNT **16** TNT **17**

Table 1 – 2,4-Dinitrotoluene 15: absolute vapor pressures p_{sat} and thermodynamic properties of sublimation obtained by the transpiration method in this work

2,4-Dinitrotoluene **15** : $\Delta_{cr}^{g} H_m^{\circ}$ (298.15 K) = 93.9 ± 0.6 kJ mol^{-1}

$$\ln p_{sat}/p^{\circ} = \frac{323.1}{R} - \frac{78395.6}{RT} + \frac{34.8}{R} ln \frac{T}{298.15K}$$

T_{exp} [a]	m [b]	V_{N2} [c]	T_{amb} [d]	Gasflow	p_{sat} [e]	$u(p_{sat})$ [f]	$\Delta_{cr}^{g} H_m^{\circ}$	$\Delta_{cr}^{g} S_m^{\circ}$
[K]	[mg]	[dm³]	[K]	[dm³ h^{-1}]	[Pa]	[Pa]	[kJ mol^{-1}]	[J mol^{-1} K^{-1}]
298.2	0.34	112	296.3	2.55	0.04	0.01	93.91	192.7
303.2	0.33	58.6	297.8	2.55	0.08	0.01	93.74	192.1
308.2	0.32	32.1	298.0	1.82	0.14	0.01	93.56	191.4
313.2	0.26	14.2	298.4	5.00	0.25	0.01	93.39	190.8
318.2	0.28	9.00	295.9	5.00	0.42	0.02	93.22	190.1
323.1	0.30	5.50	296.2	5.00	0.73	0.02	93.04	189.7
328.1	0.31	3.34	297.0	5.01	1.26	0.04	92.87	189.2
333.2	0.30	1.92	297.1	5.02	2.11	0.06	92.69	188.7
338.0	0.30	1.15	297.5	4.07	3.49	0.09	92.53	188.4

[a] Saturation temperature ($u(T)$ = 0.1 K). [b] Mass of transferred sample condensed at T = 243 K [c] Volume of nitrogen ($u(V)$ = 0.005 dm^3) used to transfer m ($u(m)$ = 0.0001 g) of the sample. [d] T_a is the temperature of the s on procedure; p°=1 Pa. [f] Standard uncertainty in p was calculated with $u(p/\text{Pa})$ = 0.005+0.025(p/Pa) for p < 5 Pa and $u(p/\text{Pa})$ = 0.025+0.025(p/Pa) for p > 5 to 3000 Pa.

Table 2 – 2,4-Dinitrotoluene 15: absolute vapor pressures p_{sat} and thermodynamic properties of vaporization obtained by the transpiration method in this work

2,4-Dinitrotoluene **15**: $\Delta_{l}^{g} H_m^{\circ}$ (298.15 K) = 78.1 ± 0.6 kJ mol^{-1}

oap bubble meter used for measurement of the gas flow. [e] Vapor pressure at temperature T, calculated from the m and the residual vapor pressure at the condensation temperature calculated by an iteratiln $p_{sat}/p^{\circ} = \frac{321.4}{R} - \frac{101657.1}{RT} + \frac{79.1}{R} ln \frac{T}{298.15K}$

T_{exp} [a]	m [b]	V_{N2} [c]	T_{amb} [d]	Gasflow	p_{sat} [e]	$u(p_{sat})$ [f]	$\Delta_{l}^{g} H_m^{\circ}$	$\Delta_{l}^{g} S_m^{\circ}$
[K]	[mg]	[dm³]	[K]	[dm³ h^{-1}]	[Pa]	[Pa]	[kJ mol^{-1}]	[J mol^{-1} K^{-1}]
348.0	0.97	1.71	298.5	2.56	7.75	0.22	74.22	134.6
353.0	0.98	1.20	298.9	2.56	11.2	0.3	73.81	133.4
357.9	0.85	0.729	296.0	1.99	15.8	0.4	73.39	132.3
363.0	0.98	0.606	300.7	2.02	22.2	0.6	72.97	131.1
367.9	0.96	0.432	299.3	1.53	30.3	0.8	72.55	129.8
372.9	1.02	0.331	299.8	1.04	42.4	1.1	72.13	128.9
377.7	4.13	1.01	299.5	2.01	56.1	1.4	71.73	127.6
382.7	4.02	0.706	299.6	2.02	77.6	2.0	71.31	126.8
387.7	3.91	0.536	299.9	2.01	99.8	2.5	70.89	125.4

[a] Saturation temperature ($u(T)$ = 0.1 K). [b] Mass of transferred sample condensed at T = 243 K [c] Volume of nitrogen ($u(V)$ = 0.005 dm^3) used to transfer m ($u(m)$ = 0.0001 g) of the sample. [d] T_a is the temperature of the soap bubble meter used for measurement of the gas flow. [e] Vapor pressure at

temperature *T,* calculated from the *m* and the residual vapor pressure at the condensation temperature calculated by an iteration procedure; p°=1 Pa. [f] Standard uncertainty in *p* was calculated with *u*(*p*/Pa) = 0.005+0.025(*p*/Pa) for *p* < 5 Pa and *u*(*p*/Pa) = 0.025+0.025(*p*/Pa) for *p* > 5 to 3000 Pa.

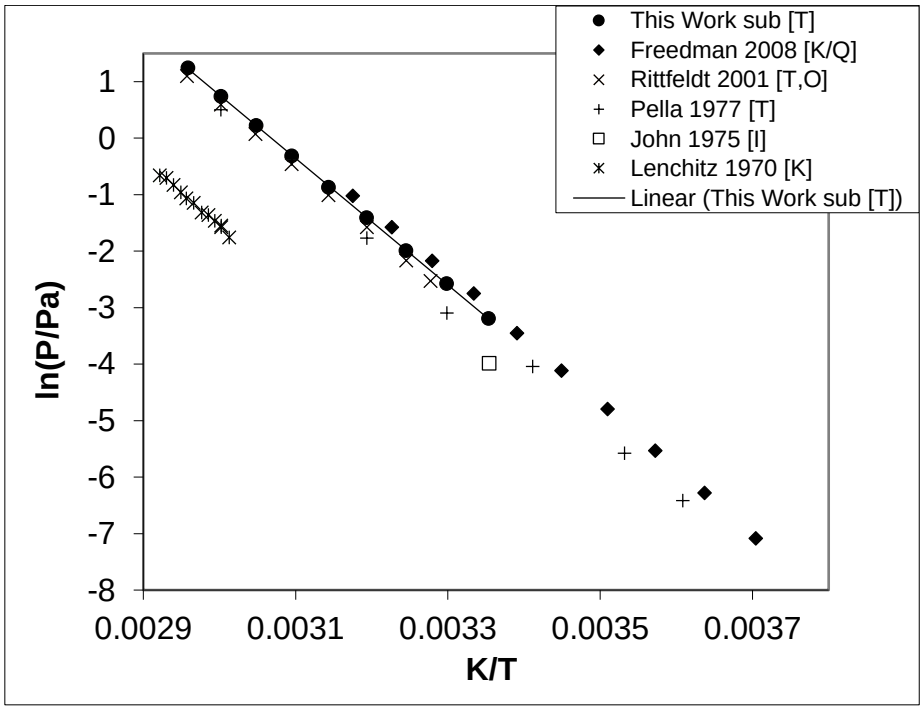

Figure 1 – Experimental vapor pressure of solid 2,4-Dinitrotoluene 15 in comparison with literature values.

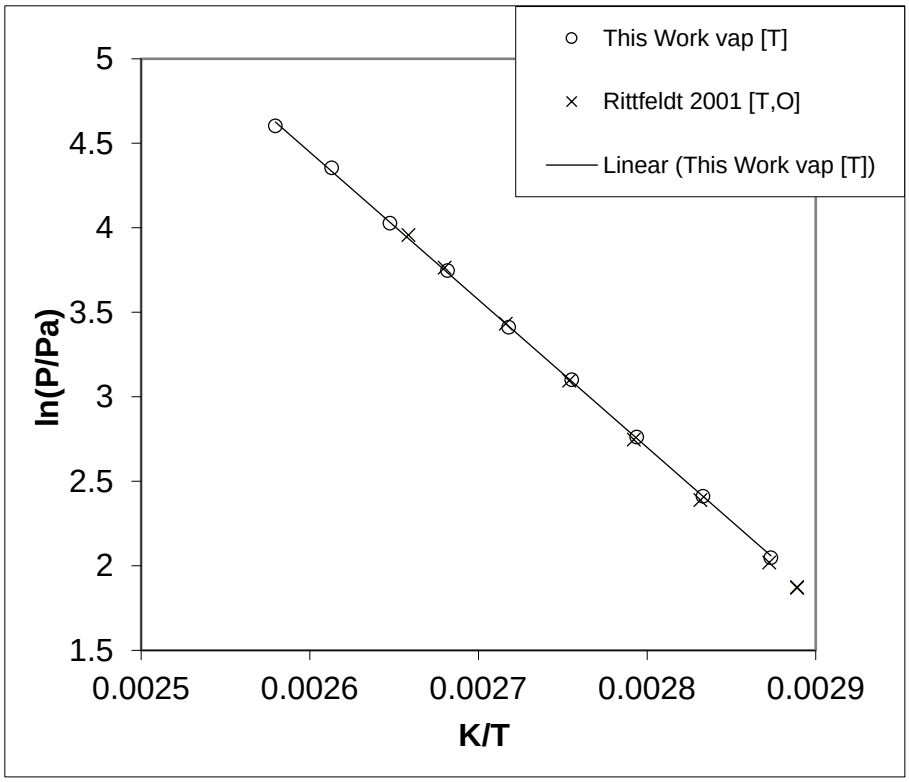

Figure 2 - Experimental vapor pressure of liquid 2,4-Dinitrotoluene 15 in comparison with literature values.

Table 3 – Compilation of Data available on Enthalpies of Sublimation $\Delta_{cr}^{g}H_m^{\circ}$ for 2,4-Dinitrotoluene 15

Experiment[a]	Method[b]	T-Range	T_{avg}	$\Delta_{cr}^{g}H_m^{\circ}(T_{avg})$	$\Delta_{cr}^{g}H_m^{\circ}$(298.15K)[c]	p_{sat}[d]
		K	K	kJ mol^{-1}	kJ mol^{-1}	Pa
This Work	T	298.2 – 338.0	317.6	93.3±0.4	93.9±0.6	0.04
Freedman 2008 [1]	K,Q	270.0 – 315.0	291.7	95.4±0.4	95.2±0.5	0.05
Rittfeldt 2001 [2]	T,O	305.2 – 346.2	325.1	94.2	(95.1)	0.03
Pella 1977 [3]	T	277.2 – 339.0	306.3	95.7±1.7	96.1±1.7	0.03
Lenchitz 1971 [4]	K	331.9 – 342.3	336.7	98.2±2.5	(99.6±3.1)	(0.003)
John 1975 [5]	I	298.2				0.02
					94.7±0.4[e]	0.03[f]

[a] First author and year of publication, [b] Methods: T: Transpiration, K: Knudsen-Effusion, Q: Quartz Crystal Microbalance, I: Isotope Dilution, O: Equation Only [c] Enthalpies of sublimation were adjusted according to *Chickos et al.* [6] with $\Delta_{cr}^{g}C_{p,m}^{\circ}$= -34.8 J mol^{-1} K^{-1} and $C_{p,m}^{\circ}$(cr)= 226.8 J mol^{-1} K^{-1} (see Table 12) [d] Vapor pressure at 298.15 K, calculated according to equation in Table 1 [e] Weighted average value, calculated using the uncertainty as the weighing factor. [f] Average value. Values in brackets were not used for calculation of average values.

Table 4 – Compilation of Data available on Enthalpies of Vaporization $\Delta_{l}^{g}H_m^{\circ}$ for 2,4-Dinitrotoluene 15

Experiment[a]	Method[b]	T-Range	T_{avg}	$\Delta_{l}^{g}H_m^{\circ}(T_{avg})$	$\Delta_{l}^{g}H_m^{\circ}$(298.15K)[c]
		K	K	kJ mol^{-1}	kJ mol^{-1}
This Work	T	348.0 – 387.7	367.4	72.6±0.4	78.1±0.6
Rittfeldt 2001 [2]	T,O	345.2 – 376.2	360.3	(75.3)	(80.2)
Maksimov 1964 [7]	S	493.2 – 572.2	530.3	59.0±1.2	77.4±1.7
					78.0±0.6[d]

[a] First author and year of publication, [b] Methods: T: Transpiration, S: Static Method, O: equation only [c] Enthalpies of vaporization were adjusted according to *Chickos et al.* [6] with $\Delta_{l}^{g}C_{p,m}^{\circ}$= -79.1 J mol^{-1} K^{-1} and $C_{p,m}^{\circ}$(liq) = 263.4 J mol^{-1} K^{-1} (see Table 12) [d] Weighted average value, calculated using the uncertainty as the weighing factor. Value in brackets was not used for calculation of average values.

Table 5 – Compilation of Data on Enthalpies of Fusion $\Delta_{cr}^{l}H_m^{\circ}$ for 2,4-Dinitrotoluene 15 (in kJ mol^{-1})

Author/Year	T_{fus}	$\Delta_{cr}^{l}H_m^{\circ}$ at T_{fus}	$\Delta_{cr}^{l}H_m^{\circ}$[a]	$\Delta_{cr}^{g}H_m^{\circ}$[b]	$\Delta_{l}^{g}H_m^{\circ}$[c]
	K			kJ mol^{-1}	
				at 298.15 K	
1	2	3	4	5	6
Ramirez 2010 [8]	70.2	22.6	20.6±0.6		
Acree 1991 [9]	70.1	20.1	18.1±0.6		
David 1964 [10]	70.1	21.4	19.4±0.6		
			19.4±0.4[d]	94.7±0.4	75.3±0.6

[a] Weighted average value of the experimental enthalpies of fusion $\Delta_{cr}^{l}H_m^{\circ}$ measured at T_{fus} and adjusted to 298.15 K according to [6]. [b] Recommended value taken from Table 3. [c] Calculated as the difference between column 5 and 4 in this table. [d] Weighted average value, calculated using the uncertainty as the weighing factor.

The sublimation behavior of 2,4-Dinitrotoluene (2,4-DNT, **15**) was studied in this work in the temperature range from 298.2 – 338.0 K. The absolute vapor pressures p_{sat} and thermodynamic properties of sublimation obtained by the transpiration method in this work for 2,4-DNT **15** are

compiled in Table 1. A comparison of own data with literature experiments regarding the enthalpies of sublimation is compiled in Table 3 and visualized in Figure 3. Figure 1 shows a *Clausius-Clapeyron* plot of the own and literature p-T data for the sublimation of 2,4-DNT **15**. Available p-T literature data for comparison is a Knudsen-effusion in combination with a quartz crystal microbalance experiment published by *Freedman et al.* [1], two transpiration experiments published by *Rittfeldt et al.* [2] and *Pella et al.* [3], a Knudsen-effusion measurement by *Lenchitz et al.* [4] and an isotope dilution ambient temperature vapor pressure determination published by *John et al.* [5]. The data published by *Lenchitz et al.* [4] is considered erroneous due to a raw data treatment error described by *Östmark et al.* [11] and therefore excluded from any average value calculation (cf. Table 3). For 2,4-DNT **15** an average uncertainty-weighted value for $\Delta_{cr}^{g}H_m^{\circ}$(298.15 K) of 94.7 ± 0.4 kJ mol^{-1} is recommended considering all available sets of data. This value is in agreement with the one obtained in this work (93.9 ± 0.4 kJ mol^{-1}). The vapor pressures of 2,4-DNT **15** at 298.15 K that were calculated from each individual complete dataset are compiled in Table 3. The mean value of 0.03 Pa can be considered as a recommendation for the ambient condition vapor pressure of 2,4-DNT **15**.

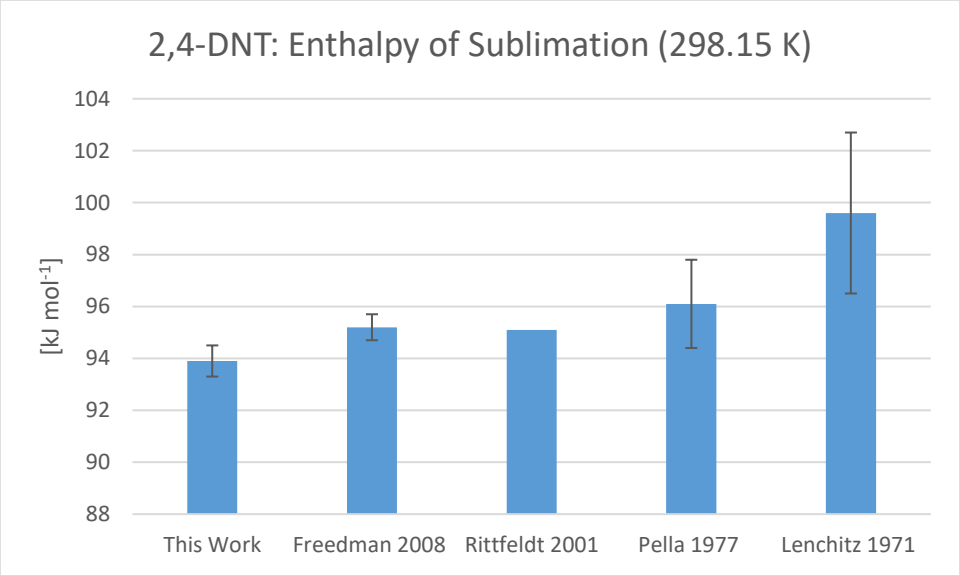

Figure 3 - Comparison of Enthalpies of Sublimation at 298.15 K for 2,4-Dinitrotoluene 15. (cf. Table 3)

The vaporization behavior of 2,4-Dinitrotoluene (2,4-DNT **15**) was studied in this work in the temperature range from 348.0 – 387.7 K. The absolute vapor pressures p_{sat} and thermodynamic properties of vaporization obtained by the transpiration method in this work for 2,4-DNT **15** are compiled in [a] Saturation temperature ($u(T)$ = 0.1 K). [b] Mass of transferred sample condensed at T = 243 K [c] Volume of nitrogen ($u(V)$ = 0.005 dm^3) used to transfer m ($u(m)$ = 0.0001 g) of the sample. [d] T_a is the temperature of the s on procedure; p°=1 Pa. [f] Standard uncertainty in p was calculated with $u(p/\text{Pa})$ = 0.005+0.025(p/Pa) for p < 5 Pa and $u(p/\text{Pa})$ = 0.025+0.025(p/Pa) for p > 5 to 3000 Pa.

Table 2 – 2,4-Dinitrotoluene 15: absolute vapor pressures p_{sat} and thermodynamic properties of vaporization obtained by the transpiration method in this work

2,4-Dinitrotoluene **15**: $\Delta_{l}^{g}H_m^{\circ}$ (298.15 K) = 78.1 ± 0.6 kJ mol^{-1}

oap bubble meter used for measurement of the gas flow. [e] Vapor pressure at temperature T, calculated from the m and the residual vapor pressure at the condensation temperature calculated by an iterati. A comparison of own data with literature experiments regarding the enthalpies of vaporization is compiled in Table 4. Figure 2 shows a *Clausius-Clapeyron* plot of the own and literature p-T data for the vaporization of 2,4-DNT **15**. Available p-T literature data for comparison is a transpiration experiment by *Rittfeldt et al.* [2] and a static method measurement by *Maksimov et al.* [7]. For 2,4-

DNT an average uncertainty-weighted value for $\Delta_l^g H_m^\circ$(298.15 K) of 78.0 ± 0.6 kJ mol^{-1} is recommended considering all available sets of data. This value is in agreement with the one obtained in this work (78.1 ± 0.6 kJ mol^{-1}).

For the enthalpy of fusion of 2,4-DNT three literature values by *Ramirez et al.* (22.6 kJ mol^{-1}, [8]), *Acree et al.* (20.1 kJ mol^{-1}, [9]) and *David et al.* (21.4 kJ mol^{-1}, [10]) exist. (cf. Table 5) The values were adjusted to 298.15 K according to the procedure provided by *Chickos et al.* [6]. The obtained average value $\Delta_{\mathrm{cr}}^l H_m^0$ (298.15 K) = 19.4 ± 0.6 kJ mol^{-1} was subtracted from the recommended weighted average sublimation enthalpy (94.7 ± 0.4 kJ mol^{-1}, cf. Table 3) to derive a calculated enthalpy of vaporization of 75.3 ± 0.6 kJ mol^{-1}. (cf. section 7.4 for the details of calculation). This value is not in agreement with the recommended weighted average vaporization enthalpy (78.0 ± 0.6 kJ mol^{-1}, cf. Table 4). A reason for this disagreement might be the inconsistency of the literature values for $\Delta_{\mathrm{cr}}^l H_m^0$ranging from 20.1 to 22.6 kJ mol^{-1}. In addition to that none of the literature sources for the enthalpy of fusion $\Delta_{\mathrm{cr}}^l H_m^0$ provide purity information of the analyte investigated. The possible presence of impurities is a potential explanation for the failure of this data consistency check using the relation between the enthalpies of fusion, sublimation and vaporization.

Table 6 – 2,6-Dinitrotoluene 16: absolute vapor pressures p_{sat} and thermodynamic properties of sublimation obtained by the transpiration method in this work

2,6-Dinitrotoluene **16**: $\Delta_{cr}^{g}H_m^{\circ}$ (298.15 K) = 94.7 ± 0.7 kJ mol^{-1}

$$\ln p_{sat}/p^{\circ} = \frac{332.6}{R} - \frac{105059.4}{RT} + \frac{34.8}{R} ln\frac{T}{298.15K}$$

T_{exp}[a]	m[b]	V_{N2}[c]	T_{amb}[d]	Gasflow	p_{sat}[e]	$u(p_{sat})$[f]	$\Delta_{cr}^{g}H_m^{\circ}$	$\Delta_{cr}^{g}S_m^{\circ}$
[K]	[mg]	[dm³]	[K]	[dm³ h^{-1}]	[Pa]	[Pa]	[kJ mol^{-1}]	[J mol^{-1} K^{-1}]
293.2	0.17	47.9	297.2	2.01	0.05	0.01	94.86	202.4
298.2	0.32	45.3	298.5	3.05	0.10	0.01	94.68	202.3
303.1	0.19	14.3	299.0	4.07	0.18	0.01	94.51	201.7
308.1	0.19	7.96	300.1	2.57	0.32	0.01	94.34	201.0
313.1	0.19	4.57	297.5	5.07	0.57	0.02	94.16	200.3
318.0	0.63	8.67	297.3	5.05	0.98	0.03	93.99	199.6
323.0	0.55	4.21	297.9	5.05	1.78	0.05	93.82	199.5
328.0	0.37	1.69	298.0	5.06	3.01	0.08	93.65	199.0
333.0	0.47	1.35	297.6	5.06	4.74	0.12	93.47	198.0

[a] Saturation temperature ($u(T)$ = 0.1 K). [b] Mass of transferred sample condensed at T = 243 K [c] Volume of nitrogen ($u(V)$ = 0.005 dm^3) used to transfer m ($u(m)$ = 0.0001 g) of the sample. [d] T_a is the temperature of the soap bubble meter used for measurement of the gas flow. [e] Vapor pressure at temperature T, calculated from the m and the residual vapor pressure at the condensation temperature calculated by an iteration procedure; p°=1 Pa. [f] Standard uncertainty in p was calculated with $u(p$/Pa) = 0.005+0.025(p/Pa) for p < 5 Pa and $u(p$/Pa) = 0.025+0.025(p/Pa) for p > 5 to 3000 Pa.

Table 7 – 2,6-Dinitrotoluene: absolute vapor pressures p_{sat} and thermodynamic properties of vaporization obtained by the transpiration method in this work

2,6-Dinitrotoluene **16**: $\Delta_{l}^{g}H_m^{\circ}$ (298.15 K) = 77.1 ± 0.6 kJ mol^{-1}

$$\ln p_{sat}/p^{\circ} = \frac{324.3}{R} - \frac{100667.2}{RT} + \frac{79.1}{R} ln\frac{T}{298.15K}$$

T_{exp}[a]	m[b]	V_{N2}[c]	T_{amb}[d]	Gasflow	p_{sat}[e]	$u(p_{sat})$[f]	$\Delta_{l}^{g}H_m^{\circ}$	$\Delta_{l}^{g}S_m^{\circ}$
[K]	[mg]	[dm³]	[K]	[dm³ h^{-1}]	[Pa]	[Pa]	[kJ mol^{-1}]	[J mol^{-1} K^{-1}]
343.0	0.61	0.770	297.2	2.01	10.7	0.3	73.54	138.4
347.9	1.13	0.972	298.0	2.01	15.8	0.4	73.15	137.5
352.9	1.37	0.846	299.8	2.03	22.1	0.6	72.76	136.2
357.8	1.45	0.645	301.8	2.04	31.0	0.8	72.36	135.0
362.8	5.43	1.71	301.1	2.03	43.7	1.1	71.97	134.0
362.8	1.66	0.541	300.3	2.03	42.0	1.1	71.97	133.7
367.8	5.47	1.26	300.9	2.04	59.9	1.5	71.58	132.9
372.8	5.05	0.845	300.4	2.03	81.9	2.1	71.18	131.9
377.7	5.28	0.645	301.0	2.04	112.6	2.8	70.79	130.9
382.7	5.23	0.488	300.7	1.54	147.1	3.7	70.40	129.7

[a] Saturation temperature ($u(T)$ = 0.1 K). [b] Mass of transferred sample condensed at T = 243 K [c] Volume of nitrogen ($u(V)$ = 0.005 dm^3) used to transfer m ($u(m)$ = 0.0001 g) of the sample. [d] T_a is the temperature of the soap bubble meter used for measurement of the gas flow. [e] Vapor pressure at

temperature *T,* calculated from the *m* and the residual vapor pressure at the condensation temperature calculated by an iteration procedure; p°=1 Pa. [f] Standard uncertainty in *p* was calculated with *u*(*p*/Pa) = 0.005+0.025(*p*/Pa) for *p* < 5 Pa and *u*(*p*/Pa) = 0.025+0.025(*p*/Pa) for *p* > 5 to 3000 Pa.

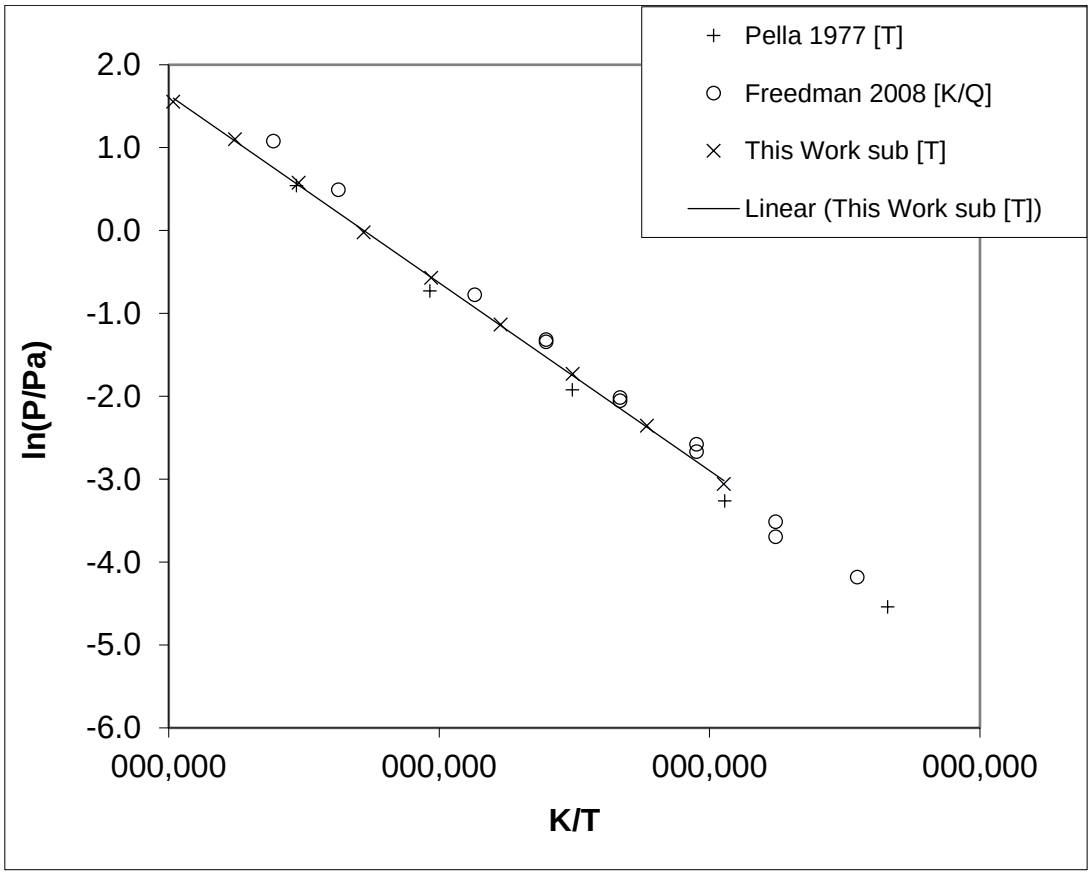

Figure 4 – Experimental vapor pressure of solid 2,6-Dinitrotoluene 16 in comparison with literature values.

Table 8 – Compilation of Data available on Enthalpies of Sublimation $\Delta_{cr}^{g}H_{m}^{\circ}$ for 2,6-Dinitrotoluene 16

Experiment[a]	**Method**[b]	**T-Range**	T_{avg}	$\Delta_{cr}^{g}H_{m}^{\circ}(T_{avg})$	$\Delta_{cr}^{g}H_{m}^{\circ}$**(298.15K)**[c]	p_{sat}[d]
		K	K	kJ mol^{-1}	kJ mol^{-1}	Pa
This Work	T	293.2 – 333.0	312.5	94.2±0.6	94.7±0.7	0.09
Freedman 2008 [1]	K	285.0 – 325.0	301.2	102.4±1.4	105.2±1.5	0.10
Pella 1977 [3]	T,O	278.2 – 323.2	300.0	98.5±1.7	98.6±1.8	0.08

[a] First author and year of publication, [b] Methods: T: Transpiration, K: Knudsen-Effusion, O: Equation Only [c] Enthalpies of sublimation were adjusted according to *Chickos et al.* [6] with $\Delta_{cr}^{g}C_{p,m}^{\circ}$= -34.8 J mol^{-1} K^{-1} and $C_{p,m}^{\circ}$(cr)= 226.8 J mol^{-1} K^{-1} (see Table 12) [d] Vapor pressure at 298.15 K, calculated according to equation in Table 6 [e] Weighted average value, calculated using the uncertainty as the weighing factor. [f] Average value

Table 9 – Compilation of Data available on Enthalpies of Vaporization $\Delta_l^g H_m^\circ$ for 2,6-Dinitrotoluene 16

Experiment[a]	Method[b]	T-Range	T_{avg}	$\Delta_l^g H_m^\circ(T_{avg})$	$\Delta_l^g H_m^\circ$(298.15K)[c]
		K	K	kJ mol^{-1}	kJ mol^{-1}
This Work	T	343.0 – 382.7	362.4	72.0±0.4	77.1±0.6
Maksimov [7]	S	423.2 – 533.2	470.8	57.0±1.3	70.7±1.5

[a] First author and year of publication, [b] Methods: T: Transpiration, S: Static Method [c] Enthalpies of sublimation were adjusted according to *Chickos et al.* [6] with $\Delta_l^g C_{p,m}^\circ$= -79.1 J mol^{-1} K^{-1} and $C_{p,m}^\circ$(liq)= 263.4 J mol^{-1} K^{-1} (see Table 12)

The evaluation of the measurement of 2,6-Dinitrotoluene (2,6-DNT **16**) is complicated due to its polymorphism. *Finch et al.* [12] report that 2,6-DNT which was recrystallized from benzene melts at 56.4 °C (polymorph A, enthalpy of fusion (DSC): 19.3 kJ mol^{-1}) whilst material that has been repeatedly resolidified from the melt melts at 66.0 °C (polymorph B, enthalpy of fusion (DSC): 16.1 kJ mol^{-1}). The different melting points and different enthalpies of fusion indicate that the enthalpy of sublimation and absolute vapor pressures of both polymorphs are different.

Within this work it is sure that polymorph B was measured since the sample was repeatedly resolidified from its melt for the coating of the glass beads inside the saturator.

The sublimation behavior of 2,6-dinitrotoluene (2,6-DNT **16**) was studied in this work in the temperature range from 293.2 – 333.0 K. The absolute vapor pressures p_{sat} and thermodynamic properties of sublimation obtained by the transpiration method in this work for 2,6-DNT **16** are compiled in Table 6. A comparison of own data with literature experiments regarding the enthalpies of sublimation is compiled in Table 8. Figure 1 shows a *Clausius-Clapeyron* plot of the own and literature p-T data for the sublimation of 2,6-DNT. Available p-T literature data for comparison is a Knudsen-effusion in combination with a quartz crystal microbalance experiment published by *Freedman et al.* [1] and a transpiration experiment by *Pella et al.* [3]. *Freedman et al.* [1] used 2,6-DNT **16** provided by Sigma Aldrich without further purification and no statement about the melting point. *Pella et al.* [3] used material that was recrystallized from benzene and reports a melting range of 57.3 – 57.8 °C which is in accordance with the value measured in this work (58 °C, cf. section 4.6.12) for the commercial product provided by Sigma Aldrich and indicates that polymorph A was used. No statement can be made about the identity of the polymorph investigated by Freedman. This work is the only measurement for polymorph B with a value for $\Delta_{cr}^g H_m^\circ$(298.15 K) of 94.7 ± 0.4 kJ mol^{-1}. Two values for $\Delta_{cr}^g H_m^\circ$(298.15 K) were derived from the p-T-data stated by *Freedman et al.* [1] (105.2 ± 1.4 kJ mol^{-1}, unknown polymorph) and *Pella et al.* [3] (98.6 ± 1.8 kJ mol^{-1}, polymorph A). In this work a vapor pressure of 2,6-DNT **16** at 298.15 K of 0.09 Pa was calculated for Polymorph B.

The vaporization behavior of 2,6-DNT was studied in this work in the temperature range from 348.0 – 387.7 K. The absolute vapor pressures p_{sat} and thermodynamic properties of vaporization obtained by the transpiration method in this work for 2,6-DNT are compiled in Table 7. A comparison of own data with literature experiments regarding the enthalpies of vaporization is compiled in Table 9.

Figure 4 shows a *Clausius-Clapeyron* plot of the own and literature p-T data for the vaporization of 2,6-DNT. Available p-T literature data for comparison is a static method measurement by *Maksimov et al.* [7]. The value for $\Delta_l^g H_m^\circ$(298.15 K) obtained in this work (77.1 ± 0.6 kJ mol^{-1}) is not in agreement with the value derived from the p-T-data by *Maksimov et al.* (70.7 ± 1.5 kJ mol^{-1}) [7].

Altogether more measurements of the sublimation characteristics of both polymorphs and the vaporization characteristics of 2,6-DNT **16** are necessary for a judgement of the quality of the data obtained in this work.

Table 10 – 2,4,6-Trinitrotoluene 17: absolute vapor pressures p_{sat} and thermodynamic properties of sublimation obtained by the transpiration method in this work

2,4,6-Trinitrotoluene **17**: $\Delta_{cr}^{g} H_m^{\circ}$ (298.15 K) = 111.6 ± 0.6 kJ mol^{-1}

$$\ln p_{sat}/p^{\circ} = \frac{355.5}{R} - \frac{123374.7}{RT} + \frac{39.6}{R} ln \frac{T}{298.15\mathrm{K}}$$

T_{exp}[a]	m[b]	V_{N2}[c]	T_{amb}[d]	Gasflow	p_{sat}[e]	$u(p_{sat})$[f]	$\Delta_{cr}^{g} H_m^{\circ}$	$\Delta_{cr}^{g} S_m^{\circ}$
[K]	[mg]	[dm³]	[K]	[dm³ h^{-1}]	[mPa]	[mPa]	[kJ mol^{-1}]	[J mol^{-1} K^{-1}]
308.2	0.09	245	298.9	5.05	3.92	5.10	111.17	218.9
313.1	0.09	120	298.8	2.62	7.91	5.20	110.97	218.4
313.2	0.24	342	299.8	5.07	7.67	5.19	110.97	218.2
318.2	0.16	118	300.7	5.07	14.8	5.4	110.78	217.4
323.2	0.20	75.0	299.0	5.06	29.2	5.7	110.58	217.1
328.1	0.34	68.3	295.9	3.54	53.4	6.3	110.38	216.3
333.1	0.47	52.4	299.0	3.05	98.2	7.5	110.18	215.8
338.1	0.44	26.7	295.9	5.00	176.8	9.4	109.99	215.2
343.1	0.39	13.9	300.9	5.10	307.6	12.7	109.79	214.5
348.0	0.40	8.02	299.8	5.07	552.5	18.8	109.59	214.3

[a] Saturation temperature ($u(T)$ = 0.1 K). [b] Mass of transferred sample condensed at T = 243 K [c] Volume of nitrogen ($u(V)$ = 0.005 dm^3) used to transfer m ($u(m)$ = 0.0001 g) of the sample. [d] T_a is the temperature of the soap bubble meter used for measurement of the gas flow. [e] Vapor pressure at temperature T, calculated from the m and the residual vapor pressure at the condensation temperature calculated by an iteration procedure; p°=1 Pa. [f] Standard uncertainty in p was calculated with $u(p/\mathrm{Pa})$ = 0.005+0.025(p/Pa) for p < 5 Pa and $u(p/\mathrm{Pa})$ = 0.025+0.025(p/Pa) for p > 5 to 3000 Pa.

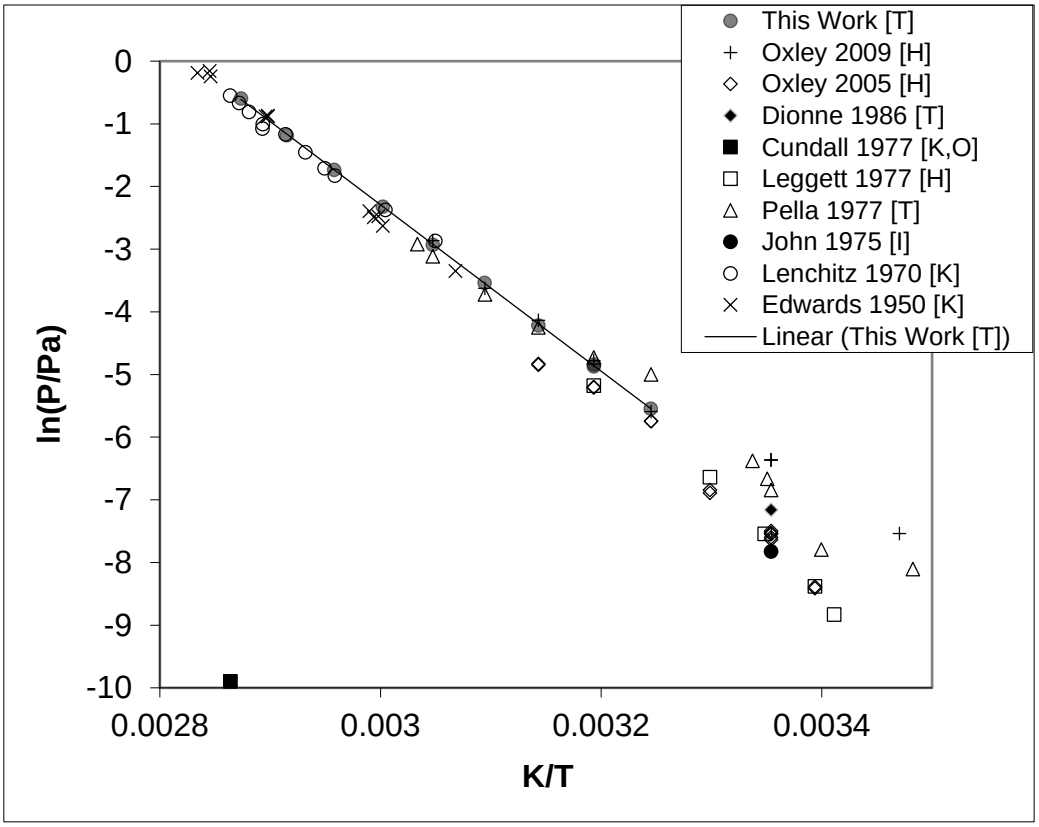

Figure 5 – Experimental vapor pressure of solid 2,4,6-Trinitrotoluene 17 in comparison with literature values.

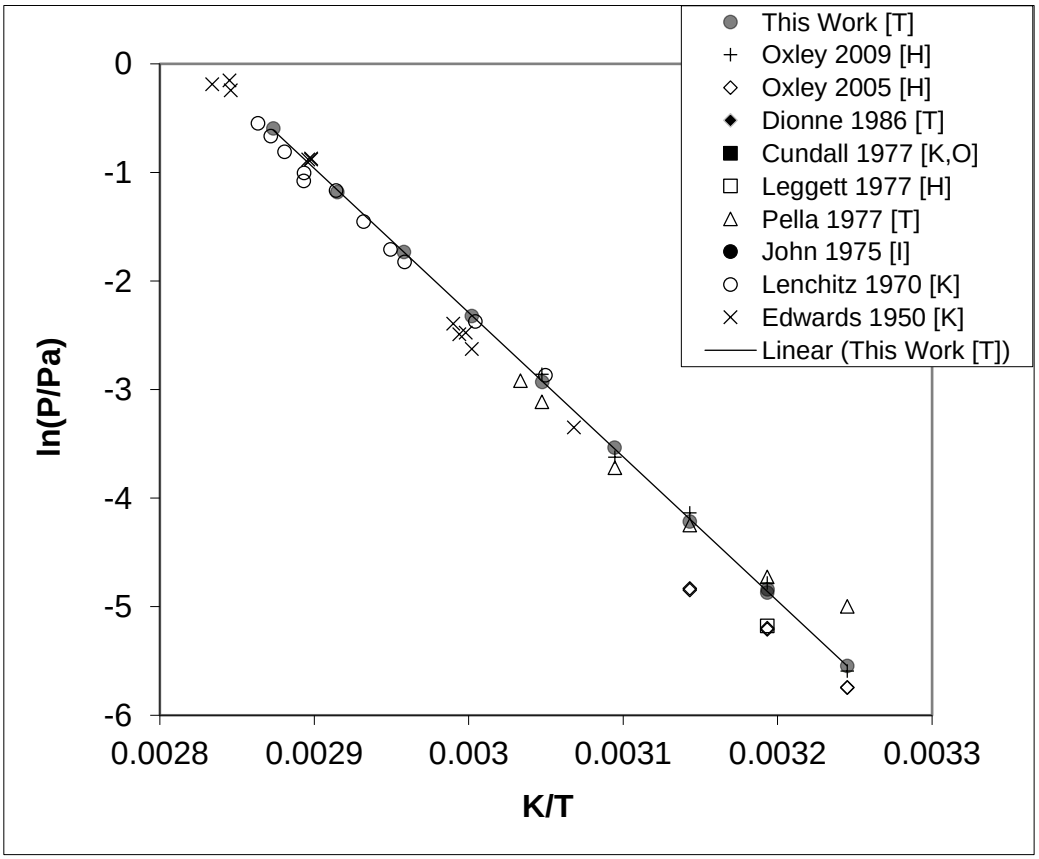

Figure 6 – Experimental vapor pressure of solid 2,4,6-Trinitrotoluene 17 in comparison with literature values. Zoom on values obtained in this work.

Table 11 – Compilation of Data available on Enthalpies of Sublimation $\Delta^{g}_{cr}H^{\circ}_{m}$ for 2,4,6-Trinitrotoluene 17

Experiment[a]	Method[b]	T-Range	T_{avg}	$\Delta^{g}_{cr}H^{\circ}_{m}(T_{avg})$	$\Delta^{g}_{cr}H^{\circ}_{m}$(298.15K)[c]	p_{sat}[d]
		K	K	kJ mol^{-1}	kJ mol^{-1}	mPa
This Work	T	308.2 – 348.0	326.1	110.4±0.4	111.6±0.6	0.9
Solomonov 2015 [13]	C				(117.7)	
Oxley 2009 [14]	H	288.2 – 328.2	307.6	89.5±3.7	89.9±3.8	1.7
Oxley 2005 [15]	H	285.2 – 318.2	301.6	137.7±6.3	137.8±6.3	0.4
Dionne 1986 [16]	T	298.2	298.2			0.8
Cundall 1977 [17]	K,O	301.5 – 349.2	322.3	113.0	(114.0)	-
Legget 1977 [18]	H	285.2 – 313.2	297.7	137.3±4.7	137.3±4.7	0.4
Pella 1977 [3]	T	287.2 – 329.7	308.3	99.8±4.2	100.2±4.2	1.2
John 1975 [5]	I		298.2			0.4
Lenchitz 1970 [19]	K	327.9 – 349.2	341.5	103.3±2.5	104.9±2.7	1.2
Edwards 1950 [20]	K	325.9 – 352.9	340.9	122.0±3.4	123.7±3.5	0.5
					111.6±0.6[e]	0.8[f]

[a] First author and year of publication, [b] Methods: T: Transpiration, C: Calorimenty, H: Headspace, K: Knudsen-Effusion, O: Equation Only, I: Isotope Dilution [c] Enthalpies of sublimation were adjusted according to *Chickos et al.* [6] with $\Delta^{g}_{cr}C^{\circ}_{p,m}$= -34.8 J mol^{-1} K^{-1} and $C^{\circ}_{p,m}$(liq)= 226.8 J mol^{-1} K^{-1} (see Table 12) [d] Vapor pressure at 298.15 K, calculated according to equation in Table 10 [e] Weighted average value, calculated using the uncertainty as the weighing factor. [f] Average value. Values in brackets were not used for calculation of average values.

The sublimation behavior of 2,4,6-Trinitrotoluene (2,4,6-TNT, **17**) was studied in this work in the temperature range from 308.2 – 348.0 K. The absolute vapor pressures p_{sat} and thermodynamic properties of sublimation obtained by the transpiration method in this work for 2,4,6-TNT **17** are compiled in Table 10. A comparison of own data with literature experiments regarding the enthalpies of sublimation is compiled in Table 11 and visualized in Figure 7. Figure 5 and Figure 6 show a *Clausius-Clapeyron* plot of the own and literature p-T data for the sublimation of 2,4,6-TNT **17**. Available p-T literature data for comparison are three headspace measurements by *Oxley et al.* [14-15] and *Legget et al.* [18], two transpiration method experiments by *Dionne et al.* [16] and *Pella et al.* [3], three Knudsen-effusion measurements by *Cundall et al.* [17], *Lenchitz et al.* [19] and *Edwards et al.* [20] and one isotope dilution determination of the ambient vapor pressure by *John et al.* [5]. The values for the enthalpy of sublimation spread from 89.9 ± 3.8 kJ mol^{-1} to 137.8 ± 6.3 kJ mol^{-1}. Both values were reported by *Oxley et al.* [14-15]. For 2,4,6-TNT an average uncertainty-weighted value for $\Delta^{g}_{cr}H^{\circ}_{m}$(298.15 K) of 111.6 ± 0.6 kJ mol^{-1} is recommended considering all available sets of data. This value is in absolute agreement with the one obtained in this work (111.6 ± 0.6 kJ mol^{-1}), yet incompatible with the value derived from solution calorimetry measurements by *Solomonov et al.* [13] (117.7 kJ mol^{-1}). This calorimetric value was reported without an error estimation and a GC-FID sample purity of 98 %.

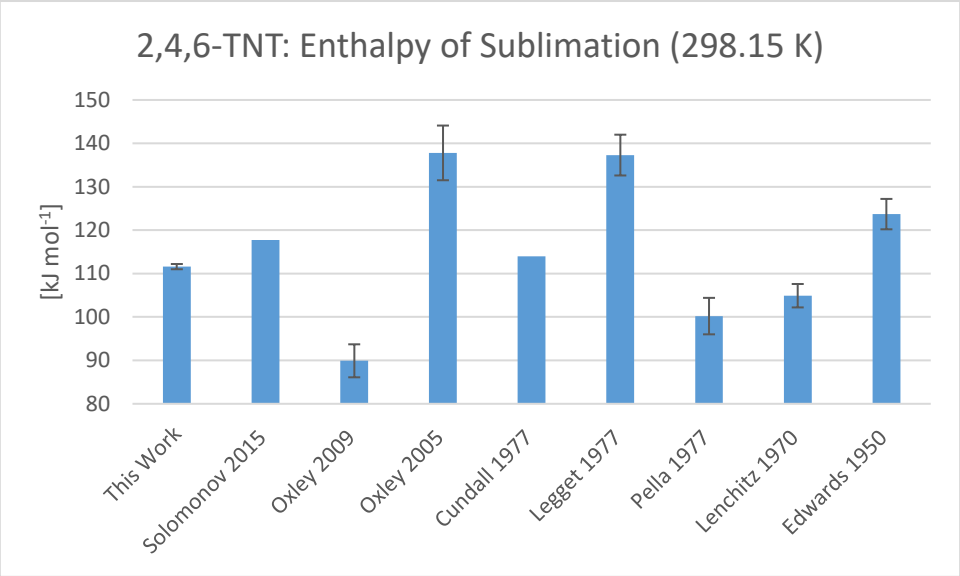

Figure 7 Comparison of Enthalpies of Sublimation at 298.15 K for 2,4-Dinitrotoluene. (cf. Table 11)

Considering the *Clausius-Clapeyron* plot depicted in Figure 6, it becomes obvious that the second measurement reported by *Oxley et al.* [14]reported in 2009 is in high agreement with the p-T-data reported in this work. Solely the low temperature data points below 308.2 K seem to be erroneous. If the temperature range of the dataset is cut to 308.2 – 328.2 K a value for $\Delta_{cr}^{g}H_{m}^{\circ}$(298.15 K) of 112.1 ± 4.4 kJ mol^{-1} can be derived from the p-T-data, which is in agreement with the value obtained in this work (111.6 ± 0.6 kJ mol^{-1}). In general vapor pressure measurements of 2,4,6-TNT **17** below 308.2 K seem to be unreliable due to the scattering of the p-T-data in the ambient temperature region. (cf. Figure 6)

The vapor pressures of 2,4,6-TNT **17** at 298.15 K that were calculated from each individual complete dataset are compiled in Table 11. The mean value of 0.08 mPa can be considered as a recommendation for the ambient condition vapor pressure of 2,4,6-TNT.

Table 12 - Calculation of Molar Heat Capacity Differences at T = 298.15 K

compound	$C_{p,m}^{o}$(l)	$C_{p,m}^{o}$(cr)	$C_{p,m}^{o}$(l)	$C_{p,m}^{o}$(cr)	$\Delta_{l}^{g}C_{p,m}^{o}$	$\Delta_{cr}^{g}C_{p,m}^{o}$
	exp.	exp.	calc.	calc.		
	[J mol^{-1} K^{-1}]	[J mol^{-1} K^{-1}]	[J mol^{-1} K^{-1}]	[J mol^{-1} K^{-1}]	[J mol^{-1} K^{-1}]	[J mol^{-1} K^{-1}]
2,4-Dinitrotoluene			263.4[a]	226.8[a]	-79.1[b]	-34.8[c]
2,6-Dinitrotoluene			263.4[a]	226.8[a]	-79.1[b]	-34.8[c]
2,4,6-Trinitrotoluene		258.7 [21]	315.5[a]	(273.9)[a]	-92.6[b]	-39.6[c]

Bracketed values not used for calculation of heat capacity differences. a) calculated according to the increment method and data by *Chickos et al.* [6] b) calculated by $\Delta_{l}^{g}C_{p,m}^{o} = 10.58 + C_{p,m}^{o}(\mathrm{l}) \times 0.26$ [6] c) calculated by $\Delta_{cr}^{g}C_{p,m}^{o} = 0.75 + C_{p,m}^{o}(\mathrm{cr}) \times 0.15$ [6]

Table 13 - Origin and Purity of the Compounds Investigated

compound	CAS#	Distributor	Product #	Lot #	purity	GC-MS-purity
2,4-Dinitrotoluene	121-14-2	Sigma Aldrich	101397	1354711 43607092	0.97	0.997
2,6-Dinitrotoluene	606-20-2	Sigma Aldrich	D200603	1358379 45107014	0.98	0.999
2,4,6-Trinitrotoluene	118-96-7	Fluka		6./122/00002	purum	0.999

Table 13 lists Name, CAS#, distributor, Product #, Lot #, manufacturer purity statement and GC-MS-purity. All purities were checked with a VO-GC/MS setup (cf. section 5) and the mass of analyte sample used for GC/MS quantification corrected by the purity obtained.

Literature References

1. Andrew, F.; Paul, L. K.; Ziman, L.; Wade, A. R.; Joda, C. W., Apparatus for determination of vapor pressures at ambient temperatures employing a Knudsen effusion cell and quartz crystal microbalance. *Measurement Science and Technology* **2008,** *19* (12), 125102.
2. Rittfeldt, L., Determination of Vapor Pressure of Low-Volatility Compounds Using a Method To Obtain Saturated Vapor with Coated Capillary Columns. *Analytical Chemistry* **2001,** *73* (11), 2405-2411.
3. Pella, P. A., Measurement of the vapor pressures of tnt, 2,4-dnt, 2,6-dnt, and egdn. *The Journal of Chemical Thermodynamics* **1977,** *9* (4), 301-305.
4. Lenchitz, C.; Velicky, R. W.; Silvestro, G.; Schlosberg, L. P., Thermodynamic properties of several nitrotoluenes. *The Journal of Chemical Thermodynamics* **1971,** *3* (5), 689-692.
5. John, G. A. S.; McReynolds, J. H.; Blucher, W. G.; Scott, A. C.; Anbar, M., Determination of the concentration of explosives in air by isotope dilution analysis. *Forensic Science* **1975,** *6* (1), 53-66.
6. Acree, W.; Chickos, J. S., Phase Transition Enthalpy Measurementsof Organic and Organometallic Compounds. Sublimation, Vaporizationand Fusion Enthalpies From 1880 to 2010. *Journal of Physical and Chemical Reference Data* **2010,** *39* (4), 043101.
7. Maksimov, Y. Y., Vapor pressures of aromatic nitro compounds at various temperatures. *Russian Journal of Physical Chemistry* **1968,** *42* (11), 1550-1552.
8. Ramírez, M. L.; Félix-Rivera, H.; Sánchez-Cuprill, R. A.; Hernández-Rivera, S. P., Thermal-spectroscopic characterization of acetone peroxide and acetone peroxide mixtures with nitrocompounds. *Journal of Thermal Analysis and Calorimetry* **2010,** *102* (2), 549-555.
9. Acree, W. E., Thermodynamic properties of organic compounds: enthalpy of fusion and melting point temperature compilation. *Thermochimica Acta* **1991,** *189* (1), 37-56.
10. David, D. J., Determination of Specific Heat and Heat of Fusion by Differential Thermal Analysis. Study of Theory and Operating Parameters. *Analytical Chemistry* **1964,** *36* (11), 2162-2166.
11. Östmark, H.; Wallin, S.; Ang, H. G., Vapor Pressure of Explosives: A Critical Review. *Propellants, Explosives, Pyrotechnics* **2012,** *37* (1), 12-23.
12. Finch, A.; Payne, J., Thermochemical study of 2,6-dinitrotoluene. *Thermochimica Acta* **1990,** *164*, 55-63.
13. Solomonov, B. N.; Varfolomeev, M. A.; Nagrimanov, R. N.; Novikov, V. B.; Buzyurov, A. V.; Fedorova, Y. V.; Mukhametzyanov, T. A., New method for determination of vaporization and sublimation enthalpy of aromatic compounds at 298.15 K using solution calorimetry technique and group-additivity scheme. *Thermochimica Acta* **2015,** *622*, 88-96.
14. Oxley, J. C.; Smith, J. L.; Luo, W.; Brady, J., Determining the Vapor Pressures of Diacetone Diperoxide (DADP) and Hexamethylene Triperoxide Diamine (HMTD). *Propellants, Explosives, Pyrotechnics* **2009,** *34* (6), 539-543.
15. Oxley, J. C.; Smith, J. L.; Shinde, K.; Moran, J., Determination of the Vapor Density of Triacetone Triperoxide (TATP) Using a Gas Chromatography Headspace Technique. *Propellants, Explosives, Pyrotechnics* **2005,** *30* (2), 127-130.
16. Dionne, B. C.; Rounbehler, D. P.; Achter, E. K.; Hobbs, J. R.; Fine, D. H., Vapor pressure of explosives. *Journal of Energetic Materials* **1986,** *4* (1-4), 447-472.

17. Cundall, R. B.; Frank Palmer, T.; Wood, C. E. C., Vapour pressure measurements on some organic high explosives. *Journal of the Chemical Society, Faraday Transactions 1: Physical Chemistry in Condensed Phases* **1978,** *74* (0), 1339-1345.
18. Leggett, D. C.; Jenkins, T. F.; Murrmann, R. P. *CRREL Special Report SR 77-16: COMPOSITION OF VAPORS EVOLVED FROM MILITARY TNT AS INFLUENCED BY TEMPERATURE, SOLID COMPOSITION, AGE, AND SOURCE*; Corps of Engineers, U.S. Army: Hanover, New Hampshire, 1977.
19. Lenchitz, C.; Velicky, R. W., Vapor pressure and heat of sublimation of three nitrotoluenes. *Journal of Chemical & Engineering Data* **1970,** *15* (3), 401-403.
20. Edwards, G., The vapour pressure of 2 : 4 : 6-trinitrotoluene. *Transactions of the Faraday Society* **1950,** *46* (0), 423-427.
21. Pilar, R.; Pachman, J.; Matyáš, R.; Honcová, P.; Honc, D., Comparison of heat capacity of solid explosives by DSC and group contribution methods. *Journal of Thermal Analysis and Calorimetry* **2015,** *121* (2), 683-689.

7.6 Measurement of 1-Nitronaphthalene and 2-Methyl-1-nitronaphthalene

This chapter deals with the measurement of the vapor pressure of 1-nitronaphthalene and 2-methyl-1-nitronaphthalene:

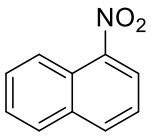

1-nitronaphthalene

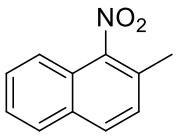

2-methyl-1-nitronaphthalene

Table 1 – 1-Nitronaphtalene: absolute vapor pressures p_{sat} and thermodynamic properties of sublimation obtained by the transpiration method in this work

1-Nitronaphthalene: $\Delta_{cr}^{g} H_m^{\circ}$ (298.15 K) = 92.5 ± 0.5 kJ mol^{-1}

$$\ln p_{sat}/p^{\circ} = \frac{320.2}{R} - \frac{101927.8}{RT} + \frac{31.5}{R} ln \frac{T}{298.15\text{K}}$$

T_{exp}[a]	m[b]	V_{N2}[c]	T_{amb}[d]	Gasflow	p_{sat}[e]	$u(p_{sat})$[f]	$\Delta_{cr}^{g} H_m^{\circ}$	$\Delta_{cr}^{g} S_m^{\circ}$
[K]	[mg]	[dm³]	[K]	[dm³ h^{-1}]	[Pa]	[Pa]	[kJ mol^{-1}]	[J mol^{-1} K^{-1}]
288.2	0.17	120.131	297.2	5.04	0.02	0.01	92.85	194.2
293.2	0.54	199.811	297.4	3.05	0.04	0.01	92.69	193.4
293.3	0.27	98.809	297.4	5.04	0.04	0.01	92.69	193.3
298.2	0.44	83.350	297.1	5.01	0.08	0.01	92.53	193.1
303.2	0.57	58.236	297.1	4.06	0.14	0.01	92.38	192.5
308.2	0.53	30.186	297.2	5.02	0.25	0.01	92.22	191.9
313.2	0.46	15.081	297.1	5.03	0.44	0.02	92.06	191.3
318.2	0.47	9.027	297.1	5.02	0.74	0.02	91.91	190.7
323.1	0.56	6.102	297.2	5.02	1.32	0.04	91.75	190.5
323.1	0.54	5.872	298.0	5.03	1.32	0.04	91.75	190.5
328.1	0.55	3.596	296.8	5.02	2.19	0.06	91.59	189.9
328.1	0.53	3.438	298.1	5.03	2.19	0.06	91.59	189.9

[a] Saturation temperature ($u(T)$ = 0.1 K). [b] Mass of transferred sample condensed at T = 243 K [c] Volume of nitrogen ($u(V)$ = 0.005 dm^3) used to transfer m ($u(m)$ = 0.0001 g) of the sample. [d] T_a is the temperature of the soap bubble meter used for measurement of the gas flow. [e] Vapor pressure at temperature T, calculated from the m and the residual vapor pressure at the condensation temperature calculated by an iteration procedure; p°=1 Pa. [f] Standard uncertainty in p was calculated with $u(p/\text{Pa})$ = 0.005+0.025(p/Pa) for p < 5 Pa and $u(p/\text{Pa})$ = 0.025+0.025(p/Pa) for p > 5 to 3000 Pa.

Table 2 – 1-Nitronaphthalene: absolute vapor pressures p_{sat} and thermodynamic properties of vaporization obtained by the transpiration method in this work

1-Nitronaphthalene: $\Delta_l^g H_m^\circ$ (298.15 K) = 75.8 ± 0.5 kJ mol^{-1}

$$\ln p_{\mathrm{sat}}/p^\circ = \frac{315.3}{R} - \frac{98954}{RT} + \frac{77.8}{R} ln \frac{T}{298.15\mathrm{K}}$$

T_{exp}[a]	m[b]	V_{N2}[c]	T_{amb}[d]	Gasflow	p_{sat}[e]	$u(p_{sat})$[f]	$\Delta_l^g H_m^\circ$	$\Delta_l^g S_m^\circ$
[K]	[mg]	[dm³]	[K]	[dm³ h^{-1}]	[Pa]	[Pa]	[kJ mol^{-1}]	[J mol^{-1} K^{-1}]
338.1	1.59	4.915	295.8	5.00	4.60	0.12	72.65	131.9
343.0	1.58	3.244	295.9	4.99	6.91	0.20	72.27	131.0
348.0	1.62	2.327	296.1	4.99	9.88	0.27	71.88	129.8
353.0	1.39	1.421	296.0	5.01	13.88	0.37	71.49	128.7
358.0	3.01	2.165	296.1	5.00	19.74	0.52	71.10	127.7
363.0	3.04	1.599	296.4	5.05	27.09	0.70	70.72	126.5
368.0	3.00	1.163	296.5	1.99	36.73	0.94	70.33	125.4
372.9	2.91	0.830	296.3	1.99	49.80	1.27	69.94	124.3
377.8	3.01	0.632	296.1	2.00	67.80	1.72	69.56	123.4

[a] Saturation temperature ($u(T)$ = 0.1 K). [b] Mass of transferred sample condensed at T = 243 K [c] Volume of nitrogen ($u(V)$ = 0.005 dm^3) used to transfer m ($u(m)$ = 0.0001 g) of the sample. [d] T_a is the temperature of the soap bubble meter used for measurement of the gas flow. [e] Vapor pressure at temperature T, calculated from the m and the residual vapor pressure at the condensation temperature calculated by an iteration procedure; p°=1 Pa. [f] Standard uncertainty in p was calculated with $u(p/\mathrm{Pa})$ = 0.005+0.025(p/Pa) for p < 5 Pa and $u(p/\mathrm{Pa})$ = 0.025+0.025(p/Pa) for p > 5 to 3000 Pa.

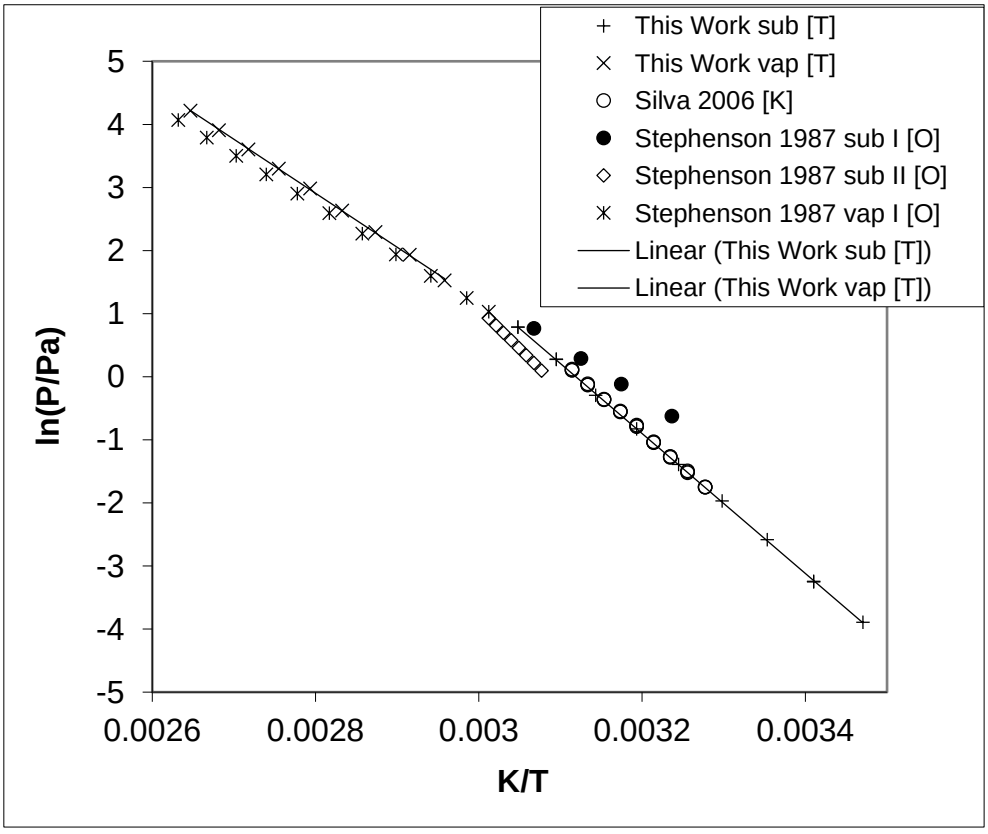

Figure 1 – Experimental vapor pressure of 1-nitronaphthalene in comparison with literature values.

Table 3 – Data obtained in this work on the Enthalpy of Sublimation $\Delta_{cr}^{g}H_{m}^{\circ}$ for 1-Nitronaphthalene

Experiment	Method[a]	T-Range	T_{avg}	$\Delta_{cr}^{g}H_{m}^{\circ}(T_{avg})$	$\Delta_{cr}^{g}H_{m}^{\circ}$(298.15K)[b]	p_{sat}[c]
		K	K	kJ mol^{-1}	kJ mol^{-1}	Pa
This Work	T	288.2 – 328.1	309.2	92.2±0.3	92.5±0.5	0.07
Silva 2006 [1]	K	305.1 – 321.1	313.1	94.4±0.4	94.9±1.1	0.07
Stephenson 1987 [2]	O	309.0 – 326.0	317.4	68.5	69.1	0.20
Stephenson 1987 [2]	O	325.0 – 332.0	328.5	106.9	107.9	0.03

[a] Methods: T: Transpiration, K: Knudsen-Effusion, O: Equation Only [b] Enthalpies of sublimation were adjusted according to *Chickos et al.* [3] with $\Delta_{cr}^{g}C_{p,m}^{\circ}$= -31.5 J mol^{-1} K^{-1} and $C_{p,m}^{\circ}$(cr)= 205.3 J mol^{-1} K^{-1} [c] Vapor pressure at 298.15 K

Table 4 – Compilation of Data available on Enthalpies of Vaporization $\Delta_l^g H_m^\circ$ for 1-Nitronaphthalene

Experiment[a]	Method[b]	T-Range	T_{avg}	$\Delta_l^g H_m^\circ(T_{avg})$	$\Delta_l^g H_m^\circ$(298.15K)[c]
		K	K	kJ mol^{-1}	kJ mol^{-1}
This Work	T	338.1 – 377.8	357.5	71.2±0.3	75.8±0.5
Stephenson 1987 [2]	O	332.0 – 580.0	442.9	66.4	77.1

[a] First author and year of publication, [b] Methods: T: Transpiration, O: Equation Only [c] Enthalpies of vaporization were adjusted according to *Chickos et al.* [3] with $\Delta_l^g C_{p,m}^\circ$= -77.8 J mol^{-1} K^{-1} and $C_{p,m}^\circ$(liq)= 258.5 J mol^{-1} K^{-1}

Table 5 – Compilation of Data on Enthalpies of Fusion $\Delta_{cr}^l H_m^\circ$ for 1-Nitronaphthalene (in kJ mol^{-1})

Author/Year	T_{fus}	$\Delta_{cr}^l H_m^\circ$ at T_{fus}	$\Delta_{cr}^l H_m^\circ$[a]	$\Delta_{cr}^g H_m^\circ$	$\Delta_l^g H_m^\circ$[b]
	K			kJ mol^{-1}	
				at 298.15 K	
1	2	3	4	5	6
Kestens 2009 [4]	328.9	17.3			
Acree 1991 [5]	329.9	18.4			
	329.4[c]	17.9±0.8[c]	16.5±0.8	92.5±0.5[d]	76.0±0.9
	329.4[c]	17.9±0.8[c]	16.5±0.8	94.9±1.1[e]	78.4±1.4

[a] Weighted average value of the experimental enthalpies of fusion $\Delta_{cr}^l H_m^\circ$ measured at T_{fus} and adjusted to 298.15 K according to [3]. [b] Calculated as the difference between column 5 and 4 in this table. [c] Average value. [d] Value from this work taken from Table 3. [e] Value from *Silva et al.* [1] taken from Table 3.

The sublimation behavior of 1-nitronaphthalene was studied in this work in the temperature range from 288.2 – 328.1 K. Figure 1 shows a *Clausius-Clapeyron* plot of the own and literature p-T data for the sublimation and vaporization of 1-nitronaphthalene. The absolute vapor pressures p_{sat} and thermodynamic properties of sublimation obtained by the transpiration method in this work for 1-nitronaphthalene are compiled in Table 1. Available p-T literature data for comparison is a Knudsen-effusion measurement by *Silva et al.* [1] and two p-T-equations that were published in the compendium by *Stephenson et al.* [2] with temperature ranges of 309 – 326 K and 325 – 332 K. The value for $\Delta_{cr}^g H_m^\circ$(298.15 K) of 92.5 ± 0.5 kJ mol^{-1} is not in agreement with the value derived from the p-T-data published by *Silva et al.* [1] (94.9 ± 1.1 kJ mol^{-1}) and those from the p-T equations by *Stephenson et al.* [2] (69.2 and 107.9 kJ mol^{-1}). The values stated by *Stephenson et al.* [2] are not in agreement with each other, the value from this work and *Silva et al.* [1]. Therefore they are not taken into account in the following. The vapor pressure at 298.15 K derived from this work is with a value of 0.07 Pa in agreement with the value derived from the p-T-data published by *Silva et al.* [1] and can be considered as a recommendation for the ambient condition vapor pressure of 1-nitronaphthalene.

The vaporization behavior of 1-nitronaphthalene was studied in this work in the temperature range from 338.1 – 377.8 K. The absolute vapor pressures p_{sat} and thermodynamic properties of vaporization obtained by the transpiration method in this work for 1-nitronaphtalene are compiled in Table 2. A comparison of own data with literature experiments regarding the enthalpies of vaporization is compiled in Table 4. Available p-T literature data for comparison is a p-T-equation that was published in the compendium by *Stephenson et al.* [2] with a temperature range of 332 – 580 K. The enthalpy of vaporization obtained in this work (75.8 ± 0.5 kJ mol^{-1}) is not in agreement with the value derived from the p-T-data stated by *Stephenson et al.* [2] (77.1 kJ mol^{-1}). Since *Stephenson et al.* [2] state no information about sample purity and method of measurement this value is not taken into consideration for the further discussion.

To judge the quality of the data obtained in this work in comparison with the literature values stated above the relationship between enthalpy of sublimation, vaporization and fusion is taken into account:

$$\Delta_{\mathrm{l}}^{g} H_m^{\circ}(298.15\ K) = \Delta_{\mathrm{cr}}^{g} H_m^{\circ}(298.15\ K) - \Delta_{\mathrm{cr}}^{l} H_m^{\circ}(298.15\ K) \quad (1)$$

For the enthalpy of fusion two literature values by *Kestens et al.* (17.3 ± 4.2 kJ mol^{-1}, [4]) and Acree (18.4 kJ mol^{-1}, [5]) exist. (cf. Table 5) The average value (17.9 ± 0.8 kJ mol^{-1}) was adjusted to 298.15 K according to the procedure provided by *Chickos et al.* [3]. The obtained average value $\Delta_{\mathrm{cr}}^{g} H_m^{0}$ (298.15 K) = 16.5 ± 0.8 kJ mol^{-1} was subtracted from the sublimation enthalpy at 298.15 K obtained in this work (92.5 ± 0.5 kJ mol^{-1}, cf. Table 3) to obtain a calculated enthalpy of vaporization of 76.0 ± 0.9 kJ mol^{-1}. (cf. equation 1) This value is in agreement with the vaporization enthalpy measured in this work (75.8 ± 0.5 kJ mol^{-1}). The agreement between enthalpies of sublimation, fusion and vaporization demonstrates that the enthalpy data evaluated in this work is internally consistent for 1-nitronaphthalene. If the same procedure is repeated with the enthalpy of sublimation at 298.15 K derived from the p-T-data stated by Silva et al. [1] an enthalpy of vaporization at 298.15 K of 78.4 ± 1.4 kJ mol^{-1} results. This value is not compatible with the data obtained in this work.

Table 6 – 2-Methyl-1-nitronaphtalene: absolute vapor pressures p_{sat} and thermodynamic properties of sublimation obtained by the transpiration method in this work

2-Methyl-1-nitronaphthalene: $\Delta_{\mathrm{cr}}^{\mathrm{g}} H_m^{\circ}$ (298.15 K) = 92.5 ± 0.6 kJ mol^{-1}

$$\ln p_{\mathrm{sat}}/p^{\circ} = \frac{320.6}{R} - \frac{103154.5}{RT} + \frac{35.7}{R} ln \frac{T}{298.15\mathrm{K}}$$

T_{exp}[a]	m[b]	V_{N2}[c]	T_{amb}[d]	Gasflow	p_{sat}[e]	$u(p_{sat})$[f]	$\Delta_{\mathrm{cr}}^{\mathrm{g}} H_m^{\circ}$	$\Delta_{cr}^{\mathrm{g}} S_m^{\circ}$
[K]	[mg]	[dm³]	[K]	[dm³ h^{-1}]	[Pa]	[Pa]	[kJ mol^{-1}]	[J mol^{-1} K^{-1}]
308.1	0.53	44.332	297.2	3.03	0.16	0.01	92.15	188.0
313.1	0.50	23.810	295.9	5.05	0.27	0.01	91.98	187.3
318.1	0.33	8.999	297.1	5.05	0.49	0.02	91.80	186.9
323.0	0.53	8.454	296.8	5.02	0.83	0.03	91.62	186.3
328.0	0.56	5.296	297.3	5.04	1.39	0.04	91.44	185.8
333.0	0.39	2.263	296.6	5.03	2.29	0.06	91.27	185.3
338.0	0.52	1.842	297.0	5.02	3.71	0.10	91.09	184.7
342.9	0.52	1.185	296.7	2.54	5.81	0.17	90.91	184.0
347.9	0.55	0.768	297.4	2.00	9.42	0.26	90.73	183.7

[a] Saturation temperature ($u(T)$ = 0.1 K). [b] Mass of transferred sample condensed at T = 243 K [c] Volume of nitrogen ($u(V)$ = 0.005 dm³) used to transfer m ($u(m)$ = 0.0001 g) of the sample. [d] T_a is the temperature of the soap bubble meter used for measurement of the gas flow. [e] Vapor pressure at temperature T, calculated from the m and the residual vapor pressure at the condensation temperature calculated by an iteration procedure; p°=1 Pa. [f] Standard uncertainty in p was calculated with $u(p/\mathrm{Pa})$ = 0.005+0.025(p/Pa) for p < 5 Pa and $u(p/\mathrm{Pa})$ = 0.025+0.025(p/Pa) for p > 5 to 3000 Pa.

Table 7 – 2-Methyl-1-nitronaphthalene: absolute vapor pressures p_{sat} and thermodynamic properties of vaporization obtained by the transpiration method in this work

2-Methyl-1-nitronaphthalene: $\Delta_l^g H_m^\circ$ (298.15 K) = 75.8 ± 0.5 kJ mol^{-1}

$$\ln p_{sat}/p^\circ = \frac{315.3}{R} - \frac{98954}{RT} + \frac{77.8}{R} ln \frac{T}{298.15\text{K}}$$

T_{exp}[a]	m[b]	V_{N2}[c]	T_{amb}[d]	Gasflow	p_{sat}[e]	$u(p_{sat})$[f]	$\Delta_l^g H_m^\circ$	$\Delta_l^g S_m^\circ$
[K]	[mg]	[dm³]	[K]	[dm³ h^{-1}]	[Pa]	[Pa]	[kJ mol^{-1}]	[J mol^{-1} K^{-1}]
357.1	1.27	2.190	297.1	5.05	13.98	0.37	70.82	124.5
362.1	1.30	1.620	297.7	3.04	19.37	0.51	70.40	123.3
368.0	1.31	1.118	298.0	3.53	28.35	0.73	69.89	122.0
373.0	1.29	0.804	298.2	2.01	38.92	1.00	69.47	121.0
378.0	1.28	0.603	298.2	2.01	51.66	1.32	69.05	119.8
382.9	2.63	0.938	297.4	2.01	67.85	1.72	68.63	118.6
387.8	2.61	0.705	298.3	2.02	89.89	2.27	68.21	117.5
393.3	3.17	0.637	297.5	2.01	120.45	3.04	67.74	116.3
398.3	3.20	0.502	297.9	2.01	154.57	3.89	67.32	115.2

[a] Saturation temperature ($u(T)$ = 0.1 K). [b] Mass of transferred sample condensed at T = 243 K [c] Volume of nitrogen ($u(V)$ = 0.005 dm^3) used to transfer m ($u(m)$ = 0.0001 g) of the sample. [d] T_a is the temperature of the soap bubble meter used for measurement of the gas flow. [e] Vapor pressure at temperature T, calculated from the m and the residual vapor pressure at the condensation temperature calculated by an iteration procedure; p°=1 Pa. [f] Standard uncertainty in p was calculated with $u(p/\text{Pa})$ = 0.005+0.025(p/Pa) for p < 5 Pa and $u(p/\text{Pa})$ = 0.025+0.025(p/Pa) for p > 5 to 3000 Pa.

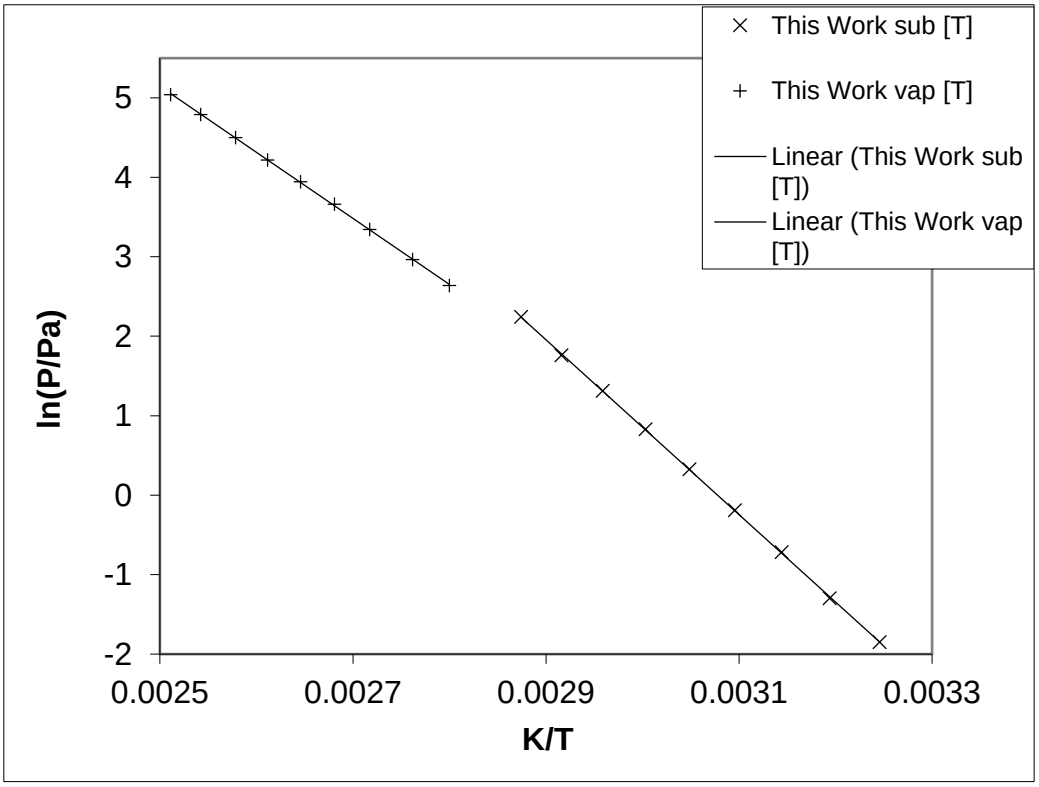

Figure 2 – Experimental vapor pressure of 2-methyl-1-nitronaphthalene in comparison with literature values.

Table 8 – Data obtained in this work on the Enthalpy of Sublimation $\Delta_{cr}^{g}H_{m}^{\circ}$ for 2-methyl-1-nitronaphthalene

Experiment	Method[a]	T-Range	T_{avg}	$\Delta_{cr}^{g}H_{m}^{\circ}(T_{avg})$	$\Delta_{cr}^{g}H_{m}^{\circ}$(298.15K)[b]	p_{sat}[c]
		K	K	kJ mol^{-1}	kJ mol^{-1}	Pa
This Work	T	308.1 – 347.9	327.5	91.5±0.3	92.5±0.6	0.05

[a] Methods: T: Transpiration [b] Enthalpies of sublimation were adjusted according to *Chickos et al.* [3] with $\Delta_{cr}^{g}C_{p,m}^{\circ}$= -35.7 J mol^{-1} K^{-1} and $C_{p,m}^{\circ}$(cr)= 232.9 J mol^{-1} K^{-1} [c] Vapor pressure at 298.15 K

Table 9 – Data obtained in this work on the Enthalpies of Vaporization $\Delta_{l}^{g}H_{m}^{\circ}$ for 2-methyl-1-nitronaphthalene

Experiment[a]	Method[b]	T-Range	T_{avg}	$\Delta_{l}^{g}H_{m}^{\circ}(T_{avg})$	$\Delta_{l}^{g}H_{m}^{\circ}$(298.15K)[c]
		K	K	kJ mol^{-1}	kJ mol^{-1}
This Work	T	357.1 – 398.3	377.4	69.1±0.2	75.9±0.5

[a] First author and year of publication, [b] Methods: T: Transpiration [c] Enthalpies of vaporization were adjusted according to *Chickos et al.* [3] with $\Delta_{l}^{g}C_{p,m}^{\circ}$= -77.8 J mol^{-1} K^{-1} and $C_{p,m}^{\circ}$(liq)= 258.5 J mol^{-1} K^{-1}

The sublimation behavior of 2-methyl-1-nitronaphthalene was studied in this work in the temperature range from 308.1 – 347.9 K. Figure 2 – Experimental vapor pressure of 2-methyl-1-nitronaphthalene in comparison with literature values. Figure 2 shows a *Clausius-Clapeyron* plot of p-T data for the sublimation and vaporization of 2-methyl-1-nitronaphthalene obtained in this work. The absolute vapor pressures p_{sat} and thermodynamic properties of sublimation obtained by the transpiration method in this work for 2-methyl-1-nitronaphthalene are compiled in Table 6. No p-T literature data is available for comparison. An enthalpy of sublimation $\Delta_{cr}^{g}H_{m}^{\circ}$(298.15 K) of 92.5 ± 0.6 kJ mol^{-1} was derived from the p-T-data obtained in this work. Extrapolation of the p-T-function stated in Table 6 to 298.15 K allows the calculation of a vapor pressure of 0.05 Pa under ambient conditions.

The vaporization behavior of 2-methyl-1-nitronaphthalene was studied in this work in the temperature range from 357.1 – 398.3 K. The absolute vapor pressures p_{sat} and thermodynamic properties of vaporization obtained by the transpiration method in this work for 2-methyl-1-nitronaphtalene are compiled in Table 9. No p-T literature data is available for comparison.

Literature References

1. Ribeiro da Silva, M. A. V.; Amaral, L. M. P. F.; Santos, A. F. L. O. M.; Gomes, J. R. B., Thermochemistry of nitronaphthalenes and nitroanthracenes. *The Journal of Chemical Thermodynamics* **2006,** *38* (6), 748-755.
2. Stephenson, R. M.; Malanowski, S.; Ambrose, D., *Handbook of the thermodynamics of organic compounds*. Elsevier: 1987.
3. Acree, W.; Chickos, J. S., Phase Transition Enthalpy Measurementsof Organic and Organometallic Compounds. Sublimation, Vaporizationand Fusion Enthalpies From 1880 to 2010. *Journal of Physical and Chemical Reference Data* **2010,** *39* (4), 043101.
4. Kestens, V.; Auclair, G.; Drozdzewska, K.; Held, A.; Roebben, G.; Linsinger, T., Thermodynamic property values of selected polycyclic aromatic hydrocarbons measured by differential scanning calorimetry. *Journal of Thermal Analysis and Calorimetry* **2010,** *99* (1), 245-261.
5. Acree, W. E., Thermodynamic properties of organic compounds: enthalpy of fusion and melting point temperature compilation. *Thermochimica Acta* **1991,** *189* (1), 37-56.

7.7 Measurement of 2-Nitropropane, 2-Methyl-2-nitropropane and DMDNB 26

This chapter deals with the measurement of the vapor pressure of the nitroalkanes 2-nitropropane, 2-methyl-2-nitropropane and 2,3-dimethyl-2,3-dinitrobutane (DMDNB **26**):

2-nitropropane

2-methyl-2-nitropropane

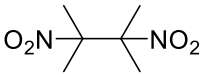

DMDNB **26**

The results were published in *Thermochimica Acta*. [1] and are reprinted with permission.

DOI: 10.1016/j.tca.2017.07.001

Since the publication does not include the vapor pressure at 298.15 K the values are stated separately in comparison with selected literature data-sets:

Table 1 – Compilation of Data available on Enthalpies of Sublimation $\Delta^g_{cr}H^\circ_m$ for 2,3-Dimethyl-2,3-dinitrobutane 26 (phase I)

Experiment[a]	Method[b]	T-Range	T_{avg}	$\Delta^{g}_{cr}H^\circ_m(T_{avg})$	$\Delta^{g}_{cr}H^\circ_m$(298.15K)[c]	p_{sat}[d]
		K	K	kJ mol^{-1}	kJ mol^{-1}	Pa
This Work (phase I)	T	278.4 – 318.2	299.4	87.0±0.5	87.1±0.6	0.2
Mirosh. 1999 [2]	C				79.5±1.3	
Elias 1991 [3]	T	253.2 – 323.2	286.5	93.5±0.1	93.0±0.3	0.3
Smirnov 1991 [4]	K	303.0 – 319.2	311.0	83.5±1.9	84.0±2.2	0.3
Smirnov 1991 [4]	C		303.2	84.5±1.4	85.4±1.4	
					91.4±0.3[e]	0.3[f]

[a] First author and year of publication, [b] Methods: T: Transpiration, C: Calorimetry, K: Knudsen-effusion [c] Enthalpies of sublimation were adjusted according to *Chickos et al.* [5] with $\Delta^g_{cr}C^\circ_{p,m}$= -38.0 J mol^{-1} K^{-1} and $C^\circ_{p,m}$(cr)= 248.6 J mol^{-1} K^{-1} [d] Vapor pressure at 298.15 K [e] Weighted average value, calculated using the uncertainty as weighing factor. [f] Average value.

Table 2 – Compilation of Data available on Enthalpies of Vaporization $\Delta^g_lH^\circ_m$ for 2-nitropropane

Experiment[a]	Method[b]	T-Range	T_{avg}	$\Delta^{g}_{cr}H^\circ_m(T_{avg})$	$\Delta^{g}_{cr}H^\circ_m$(298.15K)[c]	p_{sat}[d]
		K	K	kJ mol^{-1}	kJ mol^{-1}	Pa
This Work	T	274.7 – 314.1	291.5	41.5±0.2	41.2±0.3	2504
Mirosh. 1999 [2]	C				41.0±0.4	
Stephen. 1987 [6]	O	284.0 – 394.0	335.7	39.1	(40.9)	(2290)
Marsh 1979 [7]	S	318.2	318.2			(6388[e])
Lebedev 1970 [8]	C				(41.4)	
Saunders 1961 [9]	S	298.2	298.2			2379
v. Schickh 1950 [10]		293.2	293.2			(1720[e])
Holcomb 1949 [11]	S	283.2 – 383.2		39.5±0.1	41.0±0.2	2301
Stull 1947 [12]	O	254.4 – 393.5		39.7	(40.5)	(2302)
					41.1±0.2[f]	2395[g]

[a] First author and year of publication, [b] Methods: T: Transpiration, C: Calvet-Calorimetry, S: Static Method, O: Equation Only [c] Enthalpies of sublimation were adjusted according to *Chickos et al.* [5] with $\Delta^g_{cr}C^\circ_{p,m}$= -49.8 J mol^{-1} K^{-1} and $C^\circ_{p,m}$(l)= 150.8 J mol^{-1} K^{-1} [d] Vapor pressure at 298.15 K. [e] Vapor pressure at T_{avg} [f] Weighted average value, calculated using the uncertainty as the weighing factor. [g] Average value. Values in brackets were excluded from average value calculation.

Table 3 – Compilation of Data available on Enthalpies of Sublimation $\Delta_l^g H_m^\circ$ for 2-Methyl-2-nitropropane

Experiment[a]	**Method**[b]	**T-Range**	T_{avg}	$\Delta_l^g H_m^\circ(T_{avg})$	$\Delta_l^g H_m^\circ$**(298.15K)**[c]	p_{sat}[d]
		K	K	kJ mol^{-1}	kJ mol^{-1}	Pa
This Work	T	303.2 – 333.1	316.5	44.0±0.7	(45.1±0.8)	(1851)
Mirosh. 1999 [2]	C				41.8±0.8	
Stephenson 1987 [6]	O	334.0 – 401.0	366.4	38.4	(42.2)	(1716)
Toops 1956 [13]	O	334.0 – 401.0	366.4	38.4	(42.2)	1716
					41.8±0.8	1716

[a] First author and year of publication, [b] Methods: T: Transpiration [c] Enthalpies of sublimation were adjusted according to *Chickos et al.* [5] with $\Delta_l^g C_{p,m}^\circ$= -56.7 J mol^{-1} K^{-1} and $C_{p,m}^\circ$(liq)= 177.3 J mol^{-1} K^{-1} [d] Vapor pressure at 298.15 K.

Literature References

1. Härtel, M. A. C.; Klapötke, T. M.; Emel'yanenko, V. N.; Verevkin, S. P., Aliphatic nitroalkanes: Evaluation of thermochemical data with complementary experimental and computational methods. *Thermochimica Acta* **2017,** *656* (Supplement C), 151-160.
2. Miroshnichenko, E. O.; Vorob'eva, V. P., Thermochemical characteristics of nitroalkanes. *Zh. Fiz. Khim.* **1999,** *73* (3), 419-425.
3. L. Elias, AH–DE/5–WP/17, International Civil Aviation Organization, Montreal, Canada, 23–27 September 1991.
4. S.P. Smirnov, Y.N. Matiushin, I.Z. Akmetov, AH-DE/8-WP/12, International Civilian Aviation Organization, Montreal, Canada, 14-18 February 1994.
5. Acree, W.; Chickos, J. S., Phase Transition Enthalpy Measurementsof Organic and Organometallic Compounds. Sublimation, Vaporizationand Fusion Enthalpies From 1880 to 2010. *Journal of Physical and Chemical Reference Data* **2010,** *39* (4), 043101.
6. Stephenson, R. M.; Malanowski, S.; Ambrose, D., *Handbook of the thermodynamics of organic compounds*. Elsevier: 1987.
7. Marsh, K. N.; French, H. T.; Rogers, H. P., Excess Gibbs free energy for cyclohexane + nitromethane, + nitroethane, + 1-nitropropane, and + 2-nitropropane at 318.15 K. *The Journal of Chemical Thermodynamics* **1979,** *11* (9), 897-903.
8. Yu. A. Lebedev, E. A. Miroshnichenko, and Yu. K. Knobel', Thermochemistry of Nitrocompounds (Nauka, Moscow, 1970).
9. Saunders; Spaull, Total and Partial Vapour Pressures of a Series of Binary Liquid Mixtures of Organic Nitrocompounds. *Zeitschrift fuer Physikalische Chemie (Muenchen, Germany)* **1961,** *28*, 332-337.
10. von Schickh, O., Chemie und Technologie der Nitroalkane. *Angewandte Chemie* **1950,** *62* (23/24), 547-586.
11. Holcomb, D. E.; Dorsey, C. L., Thermodynamic Properties of Nitroparaffins. *Industrial & Engineering Chemistry* **1949,** *41* (12), 2788-2792.
12. Stull, D. R., Vapor Pressure of Pure Substances. Organic and Inorganic Compounds. *Industrial & Engineering Chemistry* **1947,** *39* (4), 517-540.
13. Toops, E. E., Physical Properties of Eight High-Purity Nitroparaffins. *The Journal of Physical Chemistry* **1956,** *60* (3), 304-306.

Thermochimica Acta 656 (2017) 151–160

Contents lists available at ScienceDirect

Thermochimica Acta

journal homepage: www.elsevier.com/locate/tca

Aliphatic nitroalkanes: Evaluation of thermochemical data with complementary experimental and computational methods

Martin A.C. Härtel[a], Thomas M. Klapötke[a], Vladimir N. Emel'yanenko[b,c], Sergey P. Verevkin[c,*]

[a] Department of Chemistry, Ludwig-Maximilians-Universität München, Butenandtstr. 5-13, 81377 München-Großhadern, Germany
[b] Department of Physical Chemistry, Kazan Federal University, Kremlevskaya Str. 18, 420008 Kazan, Russia
[c] Department of Physical Chemistry and Department of "Science and Technology of Life, Light and Matter", University of Rostock, Dr-Lorenz-Weg 2, D-18059, Rostock, Germany

ARTICLE INFO

Keywords:
Nitroalkanes
Enthalpy of vaporization
Vapor pressure measurements
Enthalpy of formation
Quantum-chemical calculations

ABSTRACT

Thermochemical properties of aliphatic nitroalkanes available in the literature are scarce and inconsistent. New standard molar enthalpies of vaporization and sublimation of 2-nitropropane, 2-methyl-2-nitropropane, and 2,3-dimethyl-2,3-dinitrobutane were derived from the vapor pressure temperature dependence measured by the transpiration method. Thermodynamic data on linear and branched aliphatic mono- and di-nitroalkanes available in the literature were combined with own experimental results and evaluated with help of empirical and theoretical methods aiming at recommendation of the sets of vaporization and formation enthalpies for aliphatic nitroalkanes as the reliable benchmark properties for further thermochemical calculations. Gas phase standard molar enthalpies of formation of aliphatic nitro-compounds derived by high-level quantum-chemical method G4 were found in a good agreement with the evaluated and recommended experimental data. Group-additivity procedure for calculation of vaporization and formation enthalpies have been developed and tested.

1. Introduction

Design and synthesis of new formulations of advanced propellants and explosives is a challenging task. Last decade, a computer aided screening of suitable hypothetical energetic materials is a popular endeavor [1–7]. However, it is reasonable to expend resources only on those molecules that show promise to provide enhanced performance, reduced sensitivity, or reduced environmental hazards. In order to assess potential performance of an energetic compound in explosive or propellant cases, the standard molar enthalpy of formation $\Delta_f H_m^\circ$, standard molar enthalpy of sublimation $\Delta_{cr}^g H_m^\circ$, standard molar enthalpy of vaporization $\Delta_l^g H_m^\circ$, and standard molar enthalpy of fusion $\Delta_{cr}^l H_m^\circ$, are considered as an important property [3,4,7]. They are used for the calculation of explosive and propellant properties such as detonation pressure, detonation velocity and specific impulse to investigate characteristics of energetic materials. The prediction of thermochemical properties of explosives to within 'chemical accuracy' (usually defined as theoretical values with mean absolute deviation within 4–5 kJ mol^{-1} from experimental data) using selected high-level methods from the G* family seems to be practicable [5] and these methods can be used to reduce experimental efforts to prepare promising compounds exhibiting required enhanced performance. However, the triumph of the modern quantum-chemical methods is aggravated with several issues thwarting a proper interpretation of the computational results. First of all converting of the enthalpic values H_{298} (directly available from the Gaussian output) to the standard molar enthalpy of formation is ambiguous. The conventionally used atomization and isodesmic reactions provide too different results even for simple compounds. For example, the most accurate Gaussian-4 (G4) method provides the $\Delta_f H_m^\circ(g)$ values calculated from the atomization reactions by 13 kJ mol^{-1} underestimated in comparison to the common isodesmic reaction procedure including 5–26 isodesmic reactions with different reference species that were constructed for each compound [8]. The second issue is that the thermochemical properties of reference species used for the construction of the isodesmic reactions are mostly of ill-defined quality. As a matter of fact, the most combustion experiments for simple aliphatic mono- and di-nitroalkanes were performed over 50 years ago [9–12] and at those times the methods for the purity attestation of the samples were not always sensitive enough. Moreover, in many cases the combustion results measured in different labs were significantly different [9–14] or for many nitro-alkanes only a single enthalpy of formation value was available. Experimental results on vaporization and sublimation enthalpies, required for calculation of $\Delta_f H_m^\circ(g)$, are practically absent in the literature in spite of the sufficient

* Corresponding author.
E-mail address: sergey.verevkin@uni-rostock.de (S.P. Verevkin).

http://dx.doi.org/10.1016/j.tca.2017.07.001
Received 3 January 2017; Received in revised form 30 June 2017; Accepted 4 July 2017
Available online 05 July 2017

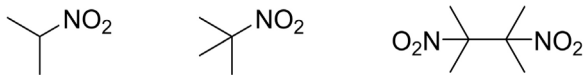

Fig. 1. Aliphatic nitroalkanes studied in this work: 2-nitropropane, 2-methyl-2-nitropropane, and 2,3-dimethyl-2,3-dinitrobutane.

amount of vapor pressure measurements published also more than 50 years ago [15–17] The reason for the absence of the vaporization/sublimation enthalpies is due to the fact that calculation of $\Delta_{cr}^{g} H_m^{\circ}/\Delta_{l}^{g} H_m^{\circ}$ from temperature dependence of vapor pressure is not a trivial task [18–21] and authors at those times were not experienced with this exercise. Critical analysis of the available thermochemical results for aliphatic mono- and di-nitroalkanes has revealed that the available thermochemical data for these compounds are in disarray. However, it should be mentioned that explicitly these species are most frequently used for the construction of the isodesmic reactions for recovering $\Delta_f H_m^{\circ}$(g)–values from quantum-chemical computations. For this reason the thermochemistry of the mono- and dinitroalkanes has to be evaluated carefully. New additional experiments with 2-nitropropane, 2-methyl-2-nitropropane, and 2,3-dimethyl-2,3-dinitrobutane (see Fig. 1) are intending to help with establishing consistency of available literature data. This contribution complements and extends our previous studies of the thermochemistry of aliphatic [22] and aromatic nitro-compounds [23–27]. The aim of this study was the evaluation of thermochemical data available for aliphatic mono- and di-nitro-alkanes with complementary experimental and computational methods in order to recommend benchmark thermochemical properties for these compounds.

2. Materials and methods

Samples of 2-nitropropane, 2-methyl-2-nitropropane and 2,3-dimethyl-2,3-dinitrobutane (DMDNB) were available from Sigma-Aldrich. The liquid samples were further purified by fractional distillation with a spinning-band column in vacuum. The solid sample of and 2,3-dimethyl-2,3-dinitrobutane was purified by fractional sublimation in vacuum. No impurities (greater than 0.001 mass fraction) could be detected in the samples used for the thermochemical measurements. The degree of purity was determined using a GC (see ESI). Provenance and purity of the compound prepared for thermochemical studies in this work are given in Table S1.

Vapor pressures of nitroalkanes were measured using the transpiration method [18–20,28]. Experimental details are given in *Electronic Supporting Information* (ESI). Transpiration experiments have been performed on the same highly purified samples independently in Rostock and in Munich. The results measured by the transpiration (T) in Rostock were labeled as the TR, and the results measured in Munich as the TM.

Quantum chemical calculations of the nitroalkanes were performed with the Gaussian 09 series software [29]. Energies of molecules involved in this study were calculated by using the G4 method [30]. Computational details for this approach were reported elsewhere [31,32]. We used the values of H_{298} directly available from the output, which were obtained according to the rigid rotor harmonic oscillator approach embedded in Gaussian.

3. Results and discussion

3.1. Vapor pressures of nitroalkanes

Experimental absolute vapor pressures for 2-nitropropane, 2-methyl-2-nitropropane and 2,3-dimethyl-2,3-dinitrobutane measured in this work by the transpiration method are given in Table S2. Experimental literature data on vapor pressure temperature dependence of nitroalkanes have been carefully collected from the literature. Because authors not derived vaporization/sublimation enthalpies from their vapor pressures or performed it in different manner, we treated the literature vapor pressures uniformly (see ESI) and calculated $\Delta_{l}^{g} H_m^{\circ}/\Delta_{cr}^{g} H_m^{\circ}$ values at the reference temperature $T = 298.15$ K for the sake of comparison with our results (see Tables 1 and 2). It should be mentioned that vaporization enthalpies derived from vapor pressures collected in compilations by Dreisbach and Shrader [16], Stull [17], and Stephenson and Malanowski [33] are of questionable quality, because the source of the primary data is not traceable, as well as specification of purity and experimental methods are not reported.

Most of the vapor pressures available in the literature for mono-nitroalkanes were measured over a broad temperature range and close to the normal boiling points [15,16,34,36]. As a rule the primary experimental data are not reported in original papers and the coefficients of the linear approximation are given instead. Only few studies of low-temperature vapor pressures of mono-nitroalkanes were found in the literature [10,35,37] and they have been taken for comparison with our new results measured by the transpiration method (see Figs. S1–S6). It has turned out that for each mono-nitroalkane the values of the available absolute vapor pressures are in agreement (see Fig. S1–S5) with exception for two studies [34,37]. In contrast, for the di-nitroalkanes the experimental vapor pressures are very scarce and contradictive. Comparison of vapor pressures available for the 2,3-dimethyl-2,3-dinitrobutane is given in Fig. S7. It is apparent from this figure that our new measurements have helped to reconcile the contradictive results from Smirnov et al. [14] and Elias [38].

3.2. Limits of vapor pressures measurements by the transpiration method

The careful experimental study of vapor pressures of nitroalkanes performed in two different labs simultaneously provides an opportunity to re-consider the limits of vapor pressures measurements by the transpiration method. As a matter of fact the validation of the transpiration method for relatively high vapor pressures have been reported in our previous work [18], where an extended investigation was undertaken to reveal the upper limit of vapor pressures which could be measured by using the transpiration method accurately. Molar enthalpies of vaporization of 10 esters of monocarboxylic acids were obtained from the temperature dependence of the vapor pressure measured by the transpiration method. The measured data sets were successfully checked for internal consistency. A large number of the primary experimental results on temperature dependences of vapor pressures have been collected from the literature and have been treated uniformly in order to derive vaporization enthalpies at the reference temperature 298.15 K. Comparing our experimental vapor pressures with those from literature we have assessed the pressure range of 5000–7000 Pa as the upper limit of vapor pressure, at which it is still possible to measure properly using the transpiration method. In this work we have also revealed that even somewhat higher vapor pressures up to approximately 9000 Pa are possible to obtain by the transpiration method without additional corrections for volume expansion. Indeed, the separate treatment of the experimental data for 2-nitropropane as well as for 2-methyl-2-nitropropane measured in the “low-pressure” as well as in the “high-pressure” range have provided the consistent results on vaporization enthalpy. Moreover, our vapor pressures in the “high pressure” are consistent with the results from Refs. [15] and [42] measured by the static and the ebulliometric methods. Nevertheless, it seems to be reasonable to apply the correction for the volume expansion for the transpiration studies in the extremal vapor pressure range of about 3000–9000 Pa. For these extremal for the transpiration method conditions the volume contribution from the compound under study to the total volume becomes not negligible, hence, for the measurements of 2-nitropropane and 2-methyl-2-nitropropane having the high-pressure range the equation for calculation of vapor pressure was modified in order to account for the additional volume expansion:

Table 1
Compilation of data on enthalpies of vaporization $\Delta_l^g H_m^\circ$ of mono-nitroalkanes.

Compound	Method[a]	T-range/K	$\Delta_l^g H_m^\circ$ (T_{av})/kJ·mol^{-1}	$\Delta_l^g H_m^\circ$ (298.15 K)[b]/kJ·mol^{-1}	Ref.
nitromethane (liq)				**38.4 ± 0.3**	[26]
nitroethane (liq)	S	298–383	38.8 ± 0.5	40.7 ± 0.6	[35]
	n/a	252–387	39.9 ± 0.5	40.5 ± 0.6	[17]
	S	283–383	39.5 ± 0.3	40.9 ± 0.4	[10]
	E	324–388	38.6 ± 1.0	41.2 ± 1.1	[15]
	E	390–459	30.3 ± 0.5	(36.1 ± 0.9)	[34]
	n/a			41.4 ± 0.4	[39,40]
	S	343.2–363.2	38.4 ± 0.2	40.9 ± 0.6	[36]
	S	298.2–318.2	34.8 ± 0.2	(35.3 ± 0.5)	[37]
				41.0 ± 0.2[c]	
1-nitropropane (liq)	S	313.1–403.1	40.1 ± 0.5	43.2 ± 0.6	[35]
	n/a	263.6–404.8	41.6 ± 0.5	43.1 ± 0.6	[17]
	S	283–403	41.2 ± 0.3	43.3 ± 0.4	[10]
	n/a	331.8–404.5	39.8 ± 0.5	43.4 ± 0.6	[16]
	E	349.3–404.3	39.3 ± 1.0	43.5 ± 1.1	[15]
	n/a	293–405	40.5 ± 1.0	43.2 ± 1.1	[33]
	n/a	298		43.1 ± 0.8	[39,40]
	CGC	298		43.9 ± 1.0	[41]
				43.3 ± 0.2[c]	
2-nitropropane (liq)	S	303–393	38.9 ± 0.5	41.0 ± 0.6	[35]
	n/a	254.3–393.5	39.7 ± 0.5	40.5 ± 0.6	[17]
	S	283–383	39.5 ± 0.3	41.1 ± 0.4	[10]
	E	284–394	39.1 ± 1.0	41.0 ± 1.1	[15]
	n/a	345–413	38.9 ± 1.0	41.0 ± 1.1	[33]
	CGC	298		(43.9 ± 1.0)	[41]
	n/a	298		41.0 ± 0.4	[39,40]
	TM	274.7–314.1	40.6 ± 0.2	40.3 ± 0.3	this work
				40.7 ± 0.2[c]	
2-methyl-2-nitropropane (liq)	E	334–401	38.4 ± 1.0	42.4 ± 1.2	[15]
	S	300–325	40.2 ± 0.4	41.0 ± 0.9	[42]
	C	298		41.8 ± 0.8	[39]
	TM	299.3–333.1	39.6 ± 0.4	40.5 ± 0.5	this work
				41.0 ± 0.4[c]	
1-nitrobutane (liq)	S	328–426	43.1 ± 0.5	47.8 ± 0.7	[35]
	S	283–423	45.1 ± 0.3	48.0 ± 0.6	[10]
	E	357–426	41.9 ± 1.0	47.6 ± 1.2	[15]
	CGC	298		47.0 ± 1.0	[41]
	n/a	298		47.3 ± 0.4	[39]
				47.5 ± 0.3[c]	
2-nitrobutane (liq)	S	318–413	40.8 ± 0.5	44.6 ± 0.7	[35]
	S	283–413	41.9 ± 0.3	44.4 ± 0.6	[10]
	E	343–413	39.7 ± 1.0	44.4 ± 1.2	[15]
	n/a	298		44.8 ± 0.8	[39]
				44.5 ± 0.4[c]	
2-methyl-1-nitropropane (liq)		347–415	40.3 ± 1.0	45.3 ± 1.2	[15]
1-nitropentane (liq)	T	278.5–318.6	50.4 ± 0.2	50.3 ± 0.2	[22]
	n/a	298		50.6 ± 0.8	[39]
				50.4 ± 0.5[c]	
nitro-cyclohexane (liq)	T	278.5–318.6	54.8 ± 0.6	54.8 ± 0.9	[22]
2,4,4-trimethyl-2-nitropentane (liq)	T	288.5–323.7	54.2 ± 0.8	54.7 ± 1.0	[22]
2-nitrodecane (liq)				73.4 ± 1.0[e]	this work
3-nitro-3-(4-nitrophenyl)-pentane (liq)	T	321.4–358.1	88.1 ± 0.8	92.8 ± 1.0	[22]
3-nitro-3-(4-nitrophenyl)-pentane (cr)				111.1 ± 1.2 [d]	[22]

[a] Methods: C = calorimetry; E = ebulliometry; S = static method; T = transpiration (TM = measured in Munich); CGC = correlation gas-chromatography; n/a = not available.
[b] Vapor pressures available in the literature were treated using Eqs. (S2) and (S3) given in ESI in order to evaluate enthalpy of vaporization at 298.15 K in the same way as our own results in Table S2. Uncertainties in this table are expressed as the standard uncertainties and they derived according to the procedure reported in [21].
[c] Weighted mean value. Values in brackets were excluded from the calculation. Values in bold are recommended for further thermochemical calculations.
[d] Enthalpies of sublimation $\Delta_{cr}^g H_m^\circ$ measured over the crystalline sample.
[e] Calculated with help of group additivity values given in Table 6.

$$p_i = m_i R \cdot T_a / V \cdot M_i;\ V = (n_{N2} + n_i) \cdot R \cdot T_a / P_a \quad (1)$$

where V is the volume of the gas phase consisting of the n_{N2} moles of the carrier gas and n_i mole of gaseous compound under study at the atmospheric pressure P_a and the ambient temperature T_a. The amount of the carrier gas n_{N2} was determined from the flow rate and the time measurement. The volume corrected calculations for the vapor pressures sets of the volatile 2-nitropropane and 2-methyl-2-nitropropane have been systematically conducted not only for pressures above 3000 Pa, but also for pressures above 600 Pa.

In contrast, by the transpiration study of 2,3-dimethyl-2,3-dinitrobutane the vapor pressures measured in the temperature range 278–318 K have been extremely low in the range between 0.02 and 2 Pa. The ability of the transpiration method to cope with the very low pressures measurements properly is apparent from good agreement between results from our study of the di-phenyl- and tri-phenyl benzenes by the transpiration method [19] with the results by the well-established Knudsen method reported in Ref. [20].

3.3. Thermodynamics of vaporization and sublimation of nitroalkanes

Having established good consistency of experimental vapor

Table 2
Compilation of data on enthalpies of vaporization $\Delta_l^g H_m^\circ$ and enthalpies of sublimation $\Delta_{cr}^g H_m^\circ$ of dinitroalkanes.

Compound	Method[a]	T-range/K	$\Delta_l^g H_m^\circ/\Delta_{cr}^g H_m^\circ$ (T_{av})/kJ mol^{-1}	$\Delta_l^g H_m^\circ/\Delta_{cr}^g H_m^\circ$ (298.15 K)[b]/kJ mol^{-1}	Refs.
Dinitromethane(liq)	E	n/a	46.0		[43]
	C	298		66.5 ± 0.8	[39]
1,2-Dinitroethane(cr)	n/a	298		81.6 ± 1.3	[39,40]
1,2-Dinitroethane(liq)				69.5 ± 1.4 [c]	this work
1,3-Dinitropropane(liq)	n/a	298		72.0 ± 0.8	[39]
	C	298		71.5 ± 0.4	[40]
				71.6 ± 0.4	average[d]
1,4-Dinitrobutane(cr)				93.6 ± 1.3 [c]	this work
1,4-Dinitrobutane(liq)	n/a	298		74.9 ± 1.7	[39]
	n/a	298		77.4 ± 0.8	[44]
				77.0 ± 0.7	average[d]
1,1-Dinitroethane (liq)	n/a	303–363	51.0 ± 1.0	53.1 ± 1.2	[33]
	n/a	298		61.1 ± 1.3	[39,40]
				56.8 ± 0.9	average[d]
2,2-Dinitropropane(liq)	S	343–453	47.9 ± 0.5	54.4 ± 0.7	[10]
	n/a	363–553	49.2 ± 1.0	(60.2 ± 1.2)	[33]
				55.7 ± 1.0[c]	this work
				54.8 ± 0.6	average[d]
2,2-Dinitropropane(cr)	n/a	298		57.3 ± 0.8	[39]
1,1-Dinitropropane(liq)	S	323–383	58.1 ± 0.6	61.8 ± 0.8	[10]
	n/a	298		59.8 ± 0.8	[39]
	C	298		59.4 ± 0.4	[40]
				59.9 ± 0.3	average[d]
1,1-Dinitrobutane(liq)	n/a	298		64.0 ± 1.3	[39]
	n/a	298		64.8 ± 0.8	[44]
				64.6 ± 0.7	average[d]
1,1-Dinitropentane(liq)	S	293–323	57.3 ± 1.3	(58.2 ± 1.5)	[45]
	n/a			(64.4 ± 1.3)	[39]
				69.1 ± 1.0[e]	this work
2,3-Dimethyl-	C	298		(79.5 ± 1.3)	[39]
2,3-Dinitrobutane (phase I)	GC/ECD	253–318	93.5 ± 0.1	(93.0 ± 0.3)	[38]
	n/a	298		(75.3 ± 0.8)	[44]
	C	303.2	84.5 ± 1.4	84.7 ± 1.4	[14]
	K	303.0 − 319.2	83.5 ± 1.9	84.0 ± 2.2	[14]
	RT	306.5–319.4	85.5 ± 2.2	86.1 ± 2.5	this work
	RM	278.4–318.2	87.0 ± 0.5	87.1 ± 0.6	this work
				86.5 ± 0.5	average[d]
2,3-Dimethyl-	IT	323.0–353.0	74.0 ± 1.0	(75.5 ± 1.2)	[46]
2,3-Dinitrobutane (phase II)	DT	340.0–380.0	74.0 ± 3.0	(76.3 ± 3.1)	[46]
	MS	253–323	93.4 ± 1.5	(92.9 ± 1.6)	[48]
	RT	328.0–352.6	83.6 ± 1.0	85.2 ± 1.3	this work
	RM	333.1–373.0	85.7 ± 0.3	87.8 ± 0.7	this work
				87.2 ± 0.6	average[d]
2,3-Dimethyl-				**70.1 ± 3.3** [f]	this work
2,3-Dinitrobutane (liq)					

[a] Methods: E = ebulliometry; S = static method; T = transpiration (TR = measured in Rostock and TM = measured in Munich); K = Knudsen-effusion method; IT = isothermal thermogravimetry; DT = dynamic thermogravimetry, GC/ECD – gas chromatography with the electron capture detector; MS- continuous flow desorption analysed by GC.
[b] Vapor pressure available in the literature were treated using Eqs. (S2) and (S3) in order to evaluate enthalpy of vaporization at 298.15 K in the same way as our own results in Table S2. Uncertainties in this table are expressed as the standard uncertainties and they derived according to the procedure reported in [21].
[c] Enthalpy of sublimation $\Delta_{cr}^g H_m^\circ$ was derived as a sum of vaporization enthalpy (this table) and enthalpy of fusion from Table 3.
[d] Weighted mean value. Values in brackets were excluded from the calculation. Values in bold were recommended for further thermochemical calculations.
[e] Calculated with help of group additivity values given in Table 6.
[f] Enthalpy of vaporization $\Delta_l^g H_m^\circ$ was derived as a difference between $\Delta_{cr}^g H_m^\circ$ (this table, phase II) and enthalpy of fusion from Table 3.

pressures for mono-nitroalkanes it has been easy to evaluate vaporization enthalpies for these compounds (see Table 1). We calculated the weighted mean value $\Delta_l^g H_m^\circ$(298.15 K) for each compound under study (see Table 1) by using experimental uncertainties as the weighting factor. These mean values are given in bold and they have been recommended for further thermochemical calculations. Nevertheless, an additional validation of the evaluated vaporization enthalpies has been performed with help of the structure-property correlations as described in Section 3.4.

Enthalpies of vaporization and enthalpies of sublimation at T = 298.15 K of the di-nitroalkanes are collected and evaluated in Table 2. The evaluation procedure for these compounds is extremely difficult because of the absence of the primary experimental information in the original sources stemming from the thermochemical lab in Moscow [40,44,45,52]. Moreover, from the reading of these original papers it is not quite apparent whether the number of the thermochemical property listed in the table was of the experimental origin or it was an estimate. Only in few cases we were able to identify the origin and the method corresponding to the vaporization/sublimation enthalpy value (see Table 2). Surprisingly, the most recent review articles [40,44,52] from the Moscow's working group contain quite different $\Delta_l^g H_m^\circ/\Delta_{cr}^g H_m^\circ$ values for the same compound. In such ambiguous situation, for each compound under study we calculated the weighted mean value of vaporization/sublimation enthalpy at 298.15 K (see Table 1) from all available data (by using experimental uncertainties as the weighting factor). These mean values are given in bold and they have been used for further validation with help of the group-additivity as described in Section 3.7.

The most striking results on sublimation enthalpies are reported for 2,3-Dimethyl-2,3-dinitrobutane. This compound is an important explosive taggant according to the Montreal Convention on the Marking of Plastic Explosives for the Purpose of Detection from 1991 [53]. Its

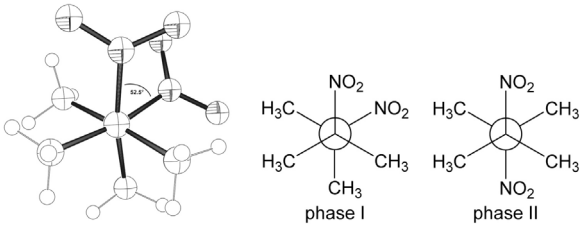

Fig. 2. Crystal structure of DMDNB phase I (view along C2-C3 axis, dihedral N-C-C-N angle: 52.5°) [54] and Newman-projection of the central C—C-bond conformation in phase I (gauche) and phase II (trans).

thermodynamics of phase transitions has been investigated and reviewed by *Jones* et al. [46,47]. DMDNB exhibits three polymorphs in the solid state with two solid–solid phase transitions in the range of 318–323 K (phase I/II, [46]) and 386–390 K (phase II/III, [46]). The phase I/II transition is a conformational change at the central C—C-bond from gauche to anti position (see Fig. 2) [46]. The gauche conformer of phase I has also been observed by X-ray diffraction crystal structure analysis with a measured dihedral angle of 52.5° between the nitro-groups [54]. Such a sophisticated phase behavior makes the study of the sublimation thermodynamics for DMDNB not easy.

The spread of available results for sublimation enthalpy for this compound is demonstrated in Table 2. For the phase I (which is important to derive the gas-phase enthalpy of formation), the value $\Delta^{g}_{cr}H^{\circ}_{m}(298.15\ K) = (93.0 \pm 0.3)\ kJ\ mol^{-1}$ was derived from the absolute vapor pressures reported by Elias [38] by using GC/ECD measurements. Any details on the method as well as on the sample purity are absent in this paper. In 1994 Smirnov et al. [14] from the Moscow lab reported results from the micro-calorimetry $\Delta^{g}_{cr}H^{\circ}_{m}(298.15\ K) = (84.7 \pm 1.4)\ kJ\ mol^{-1}$ and from the traditional Knudsen method $\Delta^{g}_{cr}H^{\circ}_{m}(298.15\ K) = (84.0 \pm 2.2)\ kJ\ mol^{-1}$. The latter two values are in close agreement but in the significant disagreement with the result by Elias [38]. To our surprise, in 1999 Miroshnichenko et al. [39] from the same lab in Moscow that published the value $\Delta^{g}_{cr}H^{\circ}_{m}(298.15\ K) = (79.5 \pm 1.3)\ kJ\ mol^{-1}$ [14] presumably from the micro-calorimetric measurements around room temperature, but the same authors in 2011 reported $\Delta^{g}_{cr}H^{\circ}_{m}(298.15\ K) = (75.3 \pm 0.8)\ kJ\ mol^{-1}$ [44].

In order to shed light to the apparent disagreement additional measurements are required. The sublimation behavior of DMDNB was studied in this work for the phase I in the temperature range of 278.4–318.2 K in Munich and 306.5–319.4 K in Rostock. For the phase II the transpiration method was used between 333.1 and 373.0 K in Munich and in the range 328.1–352.6 K in Rostock. Results are compiled in Table 2. Our new sublimation enthalpies for the phase I are in very good agreement with values from Smirnov et al. [14]. However, our new sublimation enthalpies for the phase II are in significant disagreement with values reported by Jones et al. [46] obtained from the thermogravimetry (TGA): $\Delta^{g}_{cr}H^{\circ}_{m}(298.15\ K) = (75.5 \pm 1.2)\ kJ\ mol^{-1}$ in the isothermal modus and $\Delta^{g}_{cr}H^{\circ}_{m}(298.15\ K) = (76.3 \pm 3.1)\ kJ\ mol^{-1}$ in the dynamic modus. Our recent experiences with the development of the TGA towards reliable determination of vaporization [55] has revealed that this method can be successfully applied for measurements of the liquid sample (having plain surface in the measuring cell) but it provides very often irreproducible results for the solid samples due to the apparent surface roughness in this case. This phenomenon could give the explanation for the disagreement observed between the TGA and the transpiration method used in this work. The acceptable agreement of sublimation enthalpies for the phase I measured by the direct calorimetric method [14] and indirectly by the Knudsen method [14] and the transpiration method (in this work) has allowed to calculate the weighted mean value $\Delta^{g}_{l}H^{\circ}_{m}(298.15\ K) = (86.5 \pm 0.5)\ kJ\ mol^{-1}$ for DMDNB (see Table 2) by using experimental uncertainties as the weighting factor. However, an additional validation of this evaluated sublimation enthalpy has to be performed with help of the data on the solid–solid phase transitions and on the standard molar enthalpy of fusion, $\Delta^{l}_{cr}H_{m}$, available for DMDNB in the literature (see Table 3).

Table 3
Compilation of experimental data on enthalpies of phase transitions of nitroalkanes (in kJ mol^{-1}).

Compound	T_{fus}, K	$\Delta^{l}_{cr}H_{m}$ at T_{fus}	References	$\Delta^{l}_{cr}H_{m}$ at 298.15 K[a]
2-Methyl-2-nitropropane	299.2	2.6 ± 0.5	[49]	2.6 ± 0.5
1,2-Dinitroethane	313.7	12.6 ± 0.4	[13]	12.1 ± 0.5
1,4-Dinitrobutane	306.7	16.6 ± 1.0[b]	[13]	16.2 ± 1.1
2,2-Dinitropropane	324.5	2.6 ± 0.5	[50]	1.6 ± 0.6
2,3-Dimethyl-2,3-dinitrobutane				
(phase I → II)	318	0.7 ± 0.2	[14]	
	318	0.6 ± 0.2	[46]	
		0.7 ± 0.1	average [c]	
(Phase II → III)	388	14.3 ± 2.2	[14]	
	388	18.0 ± 2.0	[46]	
		16.3 ± 1.5	average [c]	
(Phase III → liq)	476	6.1 ± 2.5	[14]	
	473	8.8 ± 0.5	[46]	
		8.7 ± 0.5	average [c]	16.4 ± 3.2 [d]
3-Nitro-3-(4-nitrophenyl)-pentane	325.6	20.3 ± 0.2	[22]	18.5 ± 0.6

[a] The experimental enthalpies of fusion $\Delta^{l}_{cr}H_{m}$ measured at T_{fus} and adjusted to 298.15 K (see text). Value in brackets was not considered by development of the average value. Uncertainties in this table are expressed as the standard uncertainties and they derived according to the procedure reported in [56].

[b] Calculated using the Walden rule $\Delta^{l}_{cr}H_{m} = 0.054 \times T_{fus}$.

[c] Weighted mean value with the uncertainty taken as the weighing factor.

[d] This value was derived from $\Delta^{T_{fus}}_{298}H^{\circ}_{m} = 25.7 \pm 1.6\ kJ{\cdot}mol^{-1}$which calculated as the sum of the enthalpy of fusion $\Delta^{l}_{cr}H^{\circ}_{m} = 8.7 \pm 0.5\ kJ\ mol^{-1}$ and enthalpies of the solid state phase transitions.$\Delta^{\beta}_{\alpha}H^{\circ}_{m} = 0.7 + 16.3 = 17.0\ kJ\ mol^{-1}$ and adjusted to the reference temperature according to Ref. [56].

3.4. Internal consistency of the phase change enthalpies of DMDNB

The significant spread of values reported for sublimation enthalpy of DMDNB has prompted the additional efforts for validation of the results obtained in the current study by the transpiration method. It makes oneself suspicious, that sublimation enthalpies $\Delta^{g}_{cr}H^{\circ}_{m}(298.15\ K)$ derived for phase I $\Delta^{g}_{cr}H^{\circ}_{m} = (86.5 \pm 0.5)\ kJ\ mol^{-1}$ and for phase II $\Delta^{g}_{cr}H^{\circ}_{m} = (87.2 \pm 0.6)\ kJ\ mol^{-1}$ are hardly distinguishable within their experimental uncertainties. But both these values have to be close to each other, because the solid-solid-phase transition enthalpy $\Delta^{II}_{I}H^{\circ}_{m} = (0.7 \pm 0.1)\ kJ\ mol^{-1}$ [46] between two polymorphs is very small. This finding strongly supports the consistency of the phase transition data on DMDNB and helps to recommend the sublimation enthalpy $\Delta^{g}_{cr}H^{\circ}_{m}(298.15\ K) = (86.5 \pm 0.5)\ kJ\ mol^{-1}$ obtained for phase I for further thermochemical calculations at the reference temperature 298.15 K (see Section 3.5). Also the enthalpies of the solid–solid and solid-liquid phase transition have to be adjusted to $T = 298.15$ K, because these enthalpies are usually referenced to the appropriate temperatures (e.g. the enthalpy of fusion $\Delta^{l}_{cr}H^{\circ}_{m}$ is referenced to the melting temperature). For compounds like DMDNB with numerous solid–solid phase transitions, $\Delta^{\beta}_{\alpha}H^{\circ}_{m}$, a total sum of solid state transition enthalpies, $\Delta^{T_{fus}}_{298}H^{\circ}_{m} = (25.7 \pm 1.6)\ kJ\ mol^{-1}$ was calculated as a sum of the enthalpy of fusion $\Delta^{l}_{cr}H^{\circ}_{m}$ and $\Sigma\Delta^{\beta}_{\alpha}H^{\circ}_{m}$ listed in Table 3. We adjusted $\Delta^{T_{fus}}_{298}H^{\circ}_{m} = (16.4 \pm 3.2)\ kJ\ mol^{-1}$ to the reference temperature $T = 298.15$ K (see Table 3, last column) according to recommendation by Chickos and Acree [54] in order to derive the vaporization enthalpy $\Delta^{g}_{l}H^{\circ}_{m}(298.15\ K) = \Delta^{g}_{cr}H^{\circ}_{m}(298.15\ K) = (86.5–16.4) = 70.1 \pm 3.3\ kJ\ mol^{-1}$ of DMDNB listed in Table 2. The latter value is required for testing of the group-additivity procedure discussed in Section 3.7.

Table 4
Thermochemical data at T = 298.15 K (p° = 0.1 MPa) for mono-nitroalkanes (in kJ mol^{-1}).[a]

Compound	$\Delta_f H^\circ_m$ (liq/cr)	$\Delta_l^g H^\circ_m/\Delta_{cr}^g H^\circ_m$[b]	$\Delta_f H^\circ_m$(g) exp	$\Delta_f H^\circ_m$(g)[c] G4	exp-G4
1	2	3	4	5	6
Nitromethane (liq)	**-109.9 ± 0.6** [26]	**38.4 ± 0.6** [26]	**-71.5 ± 0.8** [26]	−69.9	−1.6
Nitroethane (liq)	−140.1 ± 2.6 [10]				
	(−135.1 ± 1.3) [11]				
	−143.5 ± 1.1 [11]				
	−143.9 ± 1.0 [51]				
	−143.4 ± 0.7 [d]	41.0 ± 0.4	−102.4 ± 0.8	−99.9	−2.5
1-Nitropropane (liq)	−167.5 ± 3.5 [10]				
	−165.9 ± 2.9 [11]				
	−168.8 ± 1.3 [11]				
	−167.2 ± 1.0 [51]				
	−167.7 ± 0.8 [d]	43.3 ± 0.4	−124.4 ± 0.9	−121.7	−2.7
2-Nitropropane (liq)	−183.3 ± 2.6 [10]				
	−181.0 ± 1.3 [11]				
	−180.2 ± 0.9 [11]				
	−180.7 ± 0.7 [d]	40.7 ± 0.4	−140.0 ± 0.8	−137.5	−2.5
2-Me-2-nitropropane(cr)	−229.7 ± 2.5 [42]	43.6 ± 1. [e]	−186.1 ± 2.9	−173.9	−12.2
1-Nitrobutane (liq)	−192.5 ± 2.8 [10]	47.5 ± 0.6	−145.0 ± 2.9	−142.6	−2.4
2-Nitrobutane (liq)	−207.5 ± 3.0 [10]	44.5 ± 0.8	−163.0 ± 3.1	−160.8	−2.2
1-Nitropentane (liq)	−215.4 ± 1.5 [51]	50.4 ± 1.0	−165.0 ± 1.8	−165.8	0.8
Nitro-cyclohexane (liq)	−214.0 ± 0.4 [22]	54.8 ± 1.8	−159.2 ± 1.8	−157.0	−2.2
2,4,4-Trimethyl-2-nitropentane (liq)	−304.1 ± 1.1[22]	54.7 ± 2.0	−249.4 ± 2.3	−266.6	17.2
3-Nitro-3-(4-nitrophenyl)-pentane (cr)	−201.9 ± 0.7[22]	111.3 ± 2.4	−90.6 ± 2.5	–	–
2-Nitrodecane (liq)	−351.5 ± 1.3 [51]	73.4 ± 3.0	−278.1 ± 3.3	–	–

[a] All uncertainties in this table are expressed as twice the standard deviation. Uncertainties of the standard enthalpies of formation in the condensed state are given as reported in the original work. Values given in bold are recommended for thermochemical calculations.
[b] From Table 1.
[c] Calculated by G4 by using isodesmic reactions [66].
[d] Weighted average value. Values given in brackets were excluded.
[e] Calculated a sum of vaporization enthalpy from Table 1 and fusion enthalpy from Table 3.

3.5. Structure-property relationships: validation of vaporization enthalpies of mono-nitroalkanes

The correlation of vaporization enthalpies $\Delta_l^g H^\circ_m$(298.15 K) of the functional substituted alkanes with the number of C atoms in the alkyl chain is a valuable test for the consistency of the experimental data. The $\Delta_l^g H^\circ_m$(298.15 K)-values appear to be a linear function of the number of carbon atoms in homologous series of alkenes [57], aldehydes [58], halogenoalkanes [59], aliphatic esters [60], nitriles [61], ethers [62], alkylimidazoles [63], and alkylbenzenes [64]. We have used the evaluated results for nitroalkanes with the chain length C_1-C_5 (see Table 2) in order to test their consistency. The data for $\Delta_l^g H^\circ_m$(298.15 K) fit very well in the linear correlation:

$$\Delta_l^g H^\circ_m\ (298\ \mathrm{K})/\mathrm{kJ\cdot mol^{-1}} = 35.0 + 3.0 \times N_C \text{ with } (R^2 = 0.990), \quad (2)$$

where N_C is the number of C-atoms in the nitroalkane and R^2 is correlation coefficient. This relationship can be used at least as an indication of the internal consistency of the evaluated experimental results, but also for a quick assessment of $\Delta_l^g H^\circ_m$(298.15 K)-values for the representatives of this homologous series with the longer chain length, e.g. for the 1-nitrohexane the estimate $\Delta_l^g H^\circ_m$(298.15 K) = 53.2 ± 0.5 kJ mol^{-1} can be derived.

The correlation of the enthalpies of vaporization $\Delta_l^g H^\circ_m$(298.15 K) with the retention indices measured by gas-chromatography in the series of homologues is another valuable test to check the internal consistency of the experimental results [64]. From the plotting of $\Delta_l^g H^\circ_m$(298.15 K) against Kovaťs indices for these molecules (see Table S4) the following linear trend was observed:

$$\Delta_l^g H^\circ_m\ (298\ \mathrm{K})/\mathrm{kJ\cdot mol^{-1}}) = 24.1 + 0.0297 \times J_x \text{ with } (R^2 = 0.990), \quad (3)$$

where J_x is the experimental isothermal Kovaťs index [64]. The good correlation coefficient and R^2 is an evidence of the internal consistency of the correlated experimental results, moreover the value $\Delta_l^g H^\circ_m$(298.15 K) = 53.2 ± 0.5 kJ mol^{-1} has been derived for 1-nitrohexane using Eq. (3) and it is indistinguishable from the estimate according to Eq. (2), thus this value can reliably fill the gap in the available enthalpy of vaporization of 1-nitrohexane.

Structure-property correlations according to Eqs. (2) and (3) involved only linear mono-nitroalkanes. In order to check consistency also for the branched species we decided to perform correlation of vaporization enthalpies $\Delta_l^g H^\circ_m$(298.15 K) of the linear and branched mono-nitroalkanes with the vaporization enthalpies $\Delta_l^g H^\circ_m$(298.15 K) of the linear and branched mono-alkanols, where reliable experimental data are available from the literature [63] (see Table S5). From the plotting of $\Delta_l^g H^\circ_m$(298.15 K) of the mono-nitroalkane (R-NO_2) against $\Delta_l^g H^\circ_m$(298.15 K) of alkanols (R-OH) a following linear trend was observed:

$$\Delta_l^g H^\circ_m(298\,\mathrm{K},\ \text{R-NO}_2)/\mathrm{kJ\cdot mol^{-1}} = 3.7 + 0.82 \times \Delta_l^g H^\circ_m(298\,\mathrm{K},\ \text{R-OH}) \text{ with } (R^2 = 0.994), \quad (4)$$

The very high correlation coefficient R^2 is first of all a clear evidence of the mutual consistency of both data sets involved in the correlation according to Eq. (4), moreover, having the remarkable correlation even for the branched species (e.g. *tert*-butanol and nitro-*tert*-butane), we can suggest to use Eq. (4) for the reliable assessment of vaporization enthalpies of the broad range of mono-nitroalkanes which are similarly in the shape to alkanols evaluated in our previous study [65].

Evaluation and validation of the data set on $\Delta_l^g H^\circ_m$(298.15 K)-values available for the di-nitroalkanes (see Table 2) with the structure-property relationships (as described for the mono-nitro-alkanes above) failed due to absence of thermochemical data for suitable parent structures. Nevertheless, we shall perform validation of this data set with help of a group-additivity procedure as described in Section 3.7.

3.6. Enthalpies of formation of aliphatic mono- and di-nitroalkanes

Standard molar enthalpies of formation of nitroethane, 1-nitropropane, and 2-nitropropane were reported three times [10,11,51].

Details on the combustion calorimetry measurements and purity of samples used has allowed to consider all three sources as reliable. Moreover, in the paper by Cass et al. [11] combustion results "available in personal communication from the National Bureau of Standards, Washington" were listed. Unfortunately, these results have never been published in details later, but they are in good agreement with the earlier work by Holocomb et al. [10], as well as with the later results by Lebedeva et al. [51]. In order to establish more confidence, we calculated the weighted mean values $\Delta_f H_m^\circ$(298.15 K, liq) for nitroethane, 1-nitropropane, and 2-nitropropane (see Table 4). Uncertainties of the enthalpies of formation were used as the weighting factor. These averaged results for $\Delta_f H_m^\circ$(298.15 K, liq) have been recommended for further thermochemical calculations aiming to derive the gas-phase enthalpies of formation $\Delta_f H_m^\circ$(298.15 K, g) and to compare the latter values with results from quantum-chemical calculations. For other mono-nitroalkanes listed in Table 4 only single experimental studies were found in the literature and these values require careful validation before recommendation for thermochemical calculations.

The data set on $\Delta_f H_m^\circ$(298.15 K, liq or cr)-values for the di-nitroalkanes (see Table 5) is also troublesome. In spite of the few experimental results mostly available for each compound, the discrepancy among available values are inacceptable (e.g. the discrepancy of 17 kJ mol^{-1} was observed for 1,3-dinitropropane or the discrepancy even of 100 kJ mol^{-1} was observed for 2,3-dimethyl-2,3-dinitrobutane). Thus, also for this series of nitro-alkanes a careful validation is required.

Unfortunately, the proper evaluation of the condensed state enthalpies of formation $\Delta_f H_m^\circ$(298.15 K, liq or cr) for both series of nitroalkanes is difficult because these enthalpy values have included a large portion of the intermolecular interactions. In contrast, the gas-phase enthalpies of formation $\Delta_f H_m^\circ$(298.15 K, g), lend themselves for easier interpretation, because in this case the energetics of a single molecule in the gas-phase can be rationalised with any empirical (e.g. group-additivity) or theoretical (e.g. quantum-chemistry) procedure.

We used the common thermochemical equations:

$$\Delta_f H_m^\circ\ (298.15\ \mathrm{K},\ \mathrm{g}) = \Delta_f H_m^\circ\ (298.15\ \mathrm{K},\ \mathrm{liq}) + \Delta_l^g H_m^\circ(298.15\,\mathrm{K}) \quad (5)$$

$$\Delta_f H_m^\circ\ (298.15\ \mathrm{K},\ \mathrm{g}) = \Delta_f H_m^\circ\ (298.15\ \mathrm{K},\ \mathrm{cr}) + \Delta_{cr}^g H_m^\circ\ (298.15\ \mathrm{K}) \quad (6)$$

in order to derive the gas-phase enthalpies of formation aiming at the validation of the experimental data sets on nitro-alkanes collected in Tables 1–5. Values of vaporization and sublimation enthalpies (Tables 1–2) can now be used together with the combustion calorimetry data (Tables 4 and 5) to yield the gas phase standard enthalpies of formation, $\Delta_f H_m^\circ$(g) at 298.15 K. The resulting values are given in Tables 4 and 5 (column 5). These values can now be compared to results from the high-level quantum-chemical calculations (see Tables 4 and 5, column 6). The composite method G4 [30,32] has been used in this work for estimation of the theoretical gas-phase enthalpies of formation for comparison with the experimental data. An agreement between the experimental and theoretical results could provide a desired mutual validation for both results.

In this work we have mostly used the G4 results from a comprehensive study of different nitro-compounds published by Suntsova and Dorofeeva [66] recently. However, for three compounds showing a conspicuous disagreement with the experiment (2-methyl-2-nitropropane, 2,4,4-trimethyl-2-nitropentane, and 2,3-dimethyl-2,3-dinitrobutane) an additional structure optimization and G4 re-calculations have been performed in this work. However the results by Suntsova and Dorofeeva [66] have been reconfirmed. For three compounds 3-nitro-3-(4-nitrophenyl)-pentane, 2-nitrodecane and 1,1-dinitropentane the G4 calculations have been conducted for the first time.

The enthalpies H_{298} estimated by Suntsova and Dorofeeva [66] were converted to enthalpies of formation $\Delta_f H_m^\circ$(g, 298.15 K) with help of 4–9 isodesmic reactions. As can be seen from Tables 4 and 5, the G4 values for $\Delta_f H_m^\circ$(g, 298.15 K)$_{theor}$ are mostly in a good agreement with

Table 5
Thermochemical data at T = 298.15 K (p° = 0.1 MPa) for di-nitroalkanes (in kJ mol^{-1}).[a]

Compound	$\Delta_f H_m^\circ$ (liq/cr)	$\Delta_l^g H_m^\circ$/[b] $\Delta_{cr}^g H_m^\circ$ [b]	$\Delta_f H_m^\circ$(g) exp	$\Delta_f H_m^\circ$(g) [c] G4	exp-G4
1	2	3	4	5	6
Dinitromethane(liq)	−104.9 ± 0.8 [43]	66.5 ± 1.6	−38.4 ± 1.8	−40.4	2.0
1,2-Dinitroethane(cr)	−175.7 ± 2.4 [12]				
	−178.7 ± 0.9 [13]				
	−178.3 ± 0.8 [d]	81.6 ± 2.6	−96.7 ± 2.7	−96.8	0.1
1,3-Dinitropropane(liq)	(-223.9 ± 2.8)[10]				
	−207.1 ± 0.9 [13]	71.6 ± 1.6	−135.5 ± 1.8	−137.3	1.8
1,4-Dinitrobutane(cr)	−249.2 ± 1.3 [13]	93.6 ± 2.6	−155.6 ± 2.9	−161.7	6.1
1,1-Dinitroethane(liq)	−148.2 ± 0.9 [13]				
	−149.4 ± 4.2 [45]				
	−148.3 ± 0.9 [d]	61.1 ± 2.6	−87.2 ± 2.7	−89.5	2.3
2,2-Dinitropropane(cr)	−187.7 ± 5.4 [10]				
	−192.5 ± 1.3 [45]				
	−191.2 ± 1.3 [40]				
	−192.3 ± 0.4 [d]	57.3 ± 1.6	−135.0 ± 1.6	−139.0	4.0
1,1-Dinitropropane(liq)	−170.6 ± 2.8 [10]				
	(−163.2 ± 1.3) [13]				
	−168.2 ± 0.4 [40]				
	−169.4 ± 0.6 [d]	59.9 ± 0.6	−109.5 ± 0.8	−111.6	2.1
1,1-Dinitrobutane(liq)	−196.7 ± 1.3 [45]	64.6 ± 1.4	−132.1 ± 1.9	−134.3	2.2
1,1-Dinitropentane(liq)	−216.9 ± 1.3 [13]	69.1 ± 3.0	−147.8 ± 3.3	−152.4[e]	4.6
2,3-Dimethyl-2,3-dinitrobutane(cr)	(−220.9 ± 6.7) [9]				
	−311.5 ± 1.3 [13]				
	(−320.1 ± 2.9)[14]				
	−313.8 ± 1.3 [52]				
	−312.7 ± 0.9 [d]	86.5 ± 1.0	−226.2 ± 1.3	−240.6	14.4

[a] All uncertainties in this table are expressed as twice the standard deviation. Uncertainties of the standard enthalpies of formation in the condensed state are given as reported in the original work. Values given in bold are recommended for thermochemical calculations.
[b] From Table 2.
[c] Calculated by G4 by using isodesmic reactions [66].
[d] Weighted average value. Values given in brackets were excluded.
[e] Calculated by using Eq. (8).

the experimental results evaluated in this study, providing the additional confidence for the benchmark quality of properties recommended in Tables 4 and 5 for thermochemical calculations. There are only three striking outliers 2-methyl-2-nitropropane (-11.1 kJ mol^{-1}), 2,4,4-trimethyl-2-nitropentane ($+17.2$ kJ mol^{-1}), and 2,3-dimethyl-2,3-dinitrobutane ($+14.4$ kJ mol^{-1}), that have been observed among series of mono- and di-nitroalkanes. The outlying of 2-methyl-2-nitropropane could be possibly be attributed to the "amorphous" state of the sample used for combustion calorimetry [42]. However, the deviation observed by 2,3-dimethyl-2,3-dinitrobutane could be hardly ascribed to the ambiguity of experiment (see evaluation of the sublimation enthalpy and the solid state enthalpy of formation given in Tables 2 and 5). In our opinion, the most probable reason for such a disagreement between the experimental and G4 calculated $\Delta_f H_m^\circ$(g, 298.15 K) could be attributed to the "rigid rotor and harmonic oscillator" approximations incorporated in the G4 composite method. Indeed, the outlying molecules 2,4,4-trimethyl-2-nitropentane and 2,3-dimethyl-2,3-dinitrobutane are not only strained, but also possess numerous free (or hindered?) rotating groups. These rotations are dominated by vibrational terms and, in particular, by low frequencies, where hindered rotors are usually to be found. Thus a proper addition of anharmonic vibrational modes as well as a proper approach to rotors, hindered or free, is generally required. Nevertheless, except for two highly branched and strained nitroalkanes 2,4,4-trimethyl-2-nitropentane and 2,3-dimethyl-2,3-dinitrobutane, the results from the G4 procedure combined with isodesmic reactions are apparently in good agreement with the evaluated data for both sets of mono- and di-nitroalkanes, proving validity of our recommendations.

The procedure used by Suntsova and Dorofeeva [66] to derive enthalpies of formation $\Delta_f H_m^\circ$(g, 298.15 K) with help of isodesmic reactions is reliable, but tedious and restricted by a number of reaction participants with reliable thermochemical properties. In contrast, the commonly used atomization procedure is simple, but for nitro-compounds it underestimates enthalpies of formation by 10–13 kJ mol^{-1} [8,66]. Nevertheless, it is interesting to analyse the systematics of the deviations observed, having well established experimental data sets evaluated in this work given in Tables 4 and 5. We have correlated the experimental and G4 for $\Delta_f H_m^\circ$(g, 298.15 K) results separately for mono-nitroalkanes (Table 4, columns 4 and 5):

$$\Delta_f H_m^\circ(\mathrm{g})(298.15\,\mathrm{K},\ \text{mono-NO}_2)_{exp}/\mathrm{kJ\cdot mol^{-1}} = 5.0 + 0.99 \times \Delta_f H_m^\circ(\mathrm{g})(298.15\,\mathrm{K},\ \text{mono-NO}_2)_{ther} \text{ with } (R^2 = 0.999), \quad (7)$$

as well as those for di-nitroalkanes (Table 5, columns 4 and 5):

$$\Delta_f H_m^\circ(\mathrm{g})(298.15\,\mathrm{K},\ \text{di-NO}_2)_{exp}/\mathrm{kJ\cdot mol^{-1}} = 11.5 + 0.97 \times \Delta_f H_m^\circ(\mathrm{g})(298.15\,\mathrm{K},\ \text{di-NO}_2)_{ther} \text{ with } (R^2 = 0.998). \quad (8)$$

We have deliberately omitted by both correlations the results for the three highly branched and strained nitroalkanes criticized above. It has turned out, that both series have significantly different bias, but Eqs. (6) and (7) exhibit very high correlation coefficients R^2. The latter fact could be considered as the additional prove for the consistency of the experimental and theoretical results on $\Delta_f H_m^\circ$(g) evaluated in this study. Moreover, it is reasonable to apply both Eqs. (7) and (8) for a reliable assessment of unknown formation enthalpies of compounds within the families of mono- or di-substituted nitroalkanes.

Structure-property correlations according to Eqs. (2) and (3) observed for vaporization enthalpies of mono-nitroalkanes and mono-alkanols can also be applied for correlation of formation enthalpies $\Delta_f H_m^\circ$(g) (298.15 K) of the linear and branched mono-nitroalkanes with those of the linear and branched mono-alkanols, where reliable experimental data are available from the literature (see Table S5). From the plotting of $\Delta_f H_m^\circ$(g) (298.15 K) of mono-nitroalkane (R-NO$_2$) against $\Delta_f H_m^\circ$(g) (298.15 K) of alkanols (R-OH) a following linear trend was observed:

$$\Delta_f H_m^\circ(\mathrm{g})(298.15\,\mathrm{K},\ \text{R-NO}_2)/\mathrm{kJ\cdot mol^{-1}} = 142.7 + 1.05 \times \Delta_f H_m^\circ(\mathrm{g})(298.15\,\mathrm{K},\ \text{R-OH}) \text{ with } (R^2 = 0.998), \quad (9)$$

The very high correlation coefficient R^2 is an apparent evidence of the mutual consistency of both data sets involved in the correlation according to Eq. (9). To our surprise, the highly branched species (e.g. *tert*-butanol and nitro-*tert*-butane) fit the same trend as the linear species and we suppose that Eq. (9) can be used for the quick, but reliable assessment of $\Delta_f H_m^\circ$(g, 298.15 K) of the broad range of mono-nitroalkanes which are similarly in the shape to alkanols evaluated in our previous study [65]

3.7. Group-additivity: validation of the vaporization enthalpies and gas-phase enthalpies of formation

Admittedly, a group-additivity (GA) procedure is a valuable tool for validation as well as for prediction of thermochemical properties of organic compounds [22,65,67–69]. The use of group additivity is straightforward and easy. It does not require the computing resource as ab initio calculations do. Another advantage of using GA is convenience of predicting thermodynamic properties for large molecules [65]. In this work we endorse and follow Benson [22,65,67–69]. We used the evaluated data sets for vaporization enthalpies (Tables 1 and 2) and formation enthalpies (Table 4 and 5) in order to develop collection of the GAVs for nitroalkanes given in Table 6. The detailed procedure is described elsewhere [22,69].

Enthalpies of vaporization and the gas phase enthalpies of formation of the nitroalkanes estimated by using GAV are given in Table 7.

As can be seen from this table, the estimated vaporization enthalpies are in agreement with the experimental values mostly within $\pm$ 1 kJ mol^{-1} for the mono-nitroalkanes. Even for the highly branched 2,4,4-trimethyl-2-nitropentane the theoretical vaporization enthalpy is overestimated by only 1.8 kJ mol^{-1}. Agreement between additive and experimental vaporization enthalpies for di-nitroalkanes is somewhat larger $\pm$ (1–2) kJ mol^{-1} but is still acceptable taking into account the ambiguities related to the primary sources of the data. The only exceptionally large discrepancy of -4.7 kJ mol^{-1} was observed for the vaporization enthalpy of 1,1-dinitropentane. But taking into account that two available experimental values for this compound differ by 6.2 kJ mol^{-1} we would prefer the additive value 69.1 $\pm$ 1.5 kJ mol^{-1} for thermochemical calculations with this compound instead of the uncertain experimental values.

The gas phase enthalpies of formation estimated by GA are in agreement with the experiment within the boundaries of experimental

Table 6
Group-additivity values for calculation of enthalpies of vaporization and enthalpies of formation of nitroalkanes at 298.15 K K (in kJ·mol^{-1}).

GAV	$\Delta_l^g H_m^\circ$	$\Delta_f H_m^\circ$(g)
NO_2(C)	32.1	−29.45
C-(C)(H)$_3$	6.33 [65]	−42.05 [22]
C-(C)$_2$(H)$_2$	4.52 [65]	−21.46 [22]
C-(C)$_3$(H)	1.24 [65]	−9.04 [22]
C-(C)$_4$	−2.69 [65]	−1.26 [22]
(C-C)$_{1-4}$	0.26[65]	2.92 [22]
(C-C)$_{1-5}$	−0.42[65]	10.7 [65]
C-(NO$_2$)(C)(H)$_2$	−0.8	−30.5
C-(NO$_2$)(C)$_2$(H)	−3.8	−26.2
C-(NO$_2$)(C)$_3$	−9.0	−29.7
C-(NO$_2$)$_2$(H)$_2$	2.6	20.5
C-(NO$_2$)$_2$(C)(H)	−14.9	11.8
C-(NO$_2$)$_2$(C)$_2$	−22.1	8.1

Table 7
Estimation of the vaporization enthalpies and the gas phase enthalpies of formation by using GA at 298 K (in kJ mol^{-1}).

Compounds	$\Delta_l^g H_m^\circ$ [a] exp	GA	exp-GA	$\Delta_f H_m^\circ(g)$ [b] exp	GA	exp-GA
1-Nitropropane	43.3 ± 0.2	42.2	1.1	−124.4 ± 0.9	−123.5	−0.9
2-Nitropropane	41.0 ± 0.2	41.0	0.0	−139.7 ± 0.8	−139.7	0.0
2-Methyl-2-nitropropane	42.1 ± 0.3	42.1	0.0	−186.1 ± 2.9	−185.3	−0.8
1-Nitrobutane	47.5 ± 0.3	46.7	0.8	−145.0 ± 2.9	−144.9	−0.1
2-Nitrobutane	44.5 ± 0.4	45.5	−1.0	−163.0 ± 3.1	−161.2	−1.8
2-Methyl-1-nitropropane	45.3 ± 1.2	45.2	0.1	–	−153.1	–
1-Nitropentane	50.4 ± 0.5	51.2	−0.8	−165.0 ± 1.8	−166.4	1.4
2,4,4-Trimethyl-2-nitropentane	54.7 ± 1.0	56.5	−1.8	−249.4 ± 2.3	−248.4	−1.0
2-Nitrodecane	–	73.4	–	−278.1 ± 3.3	−275.5	−2.6
1,2-Dinitroethane	69.5 ± 1.4	69.4	0.1	−96.7 ± 1.8	−119.9	23.2
1,3-Dinitropropane	71.6 ± 0.4	73.9	−2.3	−135.5 ± 2.7	135.6	0.1
1,4-Dinitrobutane	77.0 ± 0.7	78.4	−1.4	−155.6 ± 2.9	154.1	−1.5
1,1-Dinitroethane	56.8 ± 0.9	55.6	1.2	−87.2 ± 2.7	−89.2	2.0
1,1-dinitropropane	59.9 ± 0.3	60.1	−0.2	−109.5 ± 0.8	−110.6	−1.1
1,1-Dinitrobutane	64.6 ± 0.7	64.6	0.0	−132.1 ± 1.9	−132.1	0.0
1,1-Dinitropentane	(64.4 ± 1.3)	69.1	−4.7	−147.8 ± 3.3	−150.7	2.9
2,3-Dimethyl-2,3-dinitrobutane	70.1 ± 3.3	71.5	−1.4	−226.2 ± 1.3	−274.9	48.7

[a] Recommended values from Tables 1 and 2.
[b] Recommended values from Tables 4 and 5.

uncertainties of ± (2–3) kJ mol^{-1}, except for 1,2-dinitroethane (see Table 7), where the larger disagreement of 23.2 kJ mol^{-1} is probably caused by vicinal strained interactions of groups which are in close proximity to each other. Also the large disagreement of 48.7 kJ mol^{-1} observed for the 2,3-dimethyl-2,3-dinitrobutane is apparently of the same nature. The strained interactions in this di-nitroalkane are comparable to those in similarly shaped strain pattern present in 2,2,3,3-tetramethylbutane ($\Delta_f H_m^\circ$ (g, 298.15 K) = −177.8 ± 1.0 kJ mol^{-1} [70]). Strain interactions of the two *tert*-butyl moieties in the 2,2,3,3-tetramethylbutane of 28.6 kJ mol^{-1} (calculated with GAVs from Table 6) indicates that larger NO_2 substituents in 2,3-dimethyl-2,3-dinitrobutane should cause a more profound extent of the strain. Good agreement between experiment and results from GA calculations observed for the most species listed in Table 7 can serve as a valuable test for internal consistency of the vaporization and formation enthalpies measured in this work.

4. Conclusions

In the recent decade, the modern quantum chemical methods have reached the "chemical accuracy" for prediction of the gas-phase enthalpies of formation, provided that the proper procedure is used to convert H_{298} values to $\Delta_f H_m^\circ$(g, 298.15 K). The most promising procedure for this purpose seems to be the construction of the well balanced isodesmic reactions with the "anchoring" reaction participants with thermochemical properties of the benchmark quality. The "anchoring" $\Delta_f H_m^\circ$(g, 298.15 K-values for the expansion of current databases must be validated comprehensively so they can be relied on. The establishment of the database of accurate thermochemical data is also important for the testing of new high-level quantum methods capable of dealing with a wide range of chemical compounds. In this work thermodynamic data on linear and branched aliphatic mono- and di-nitroalkanes available in the literature were combined with own experimental results and evaluated with help of empirical and theoretical methods aiming at recommendation of the sets of vaporization and formation enthalpies for aliphatic nitroalkanes as the reliable benchmark properties for further thermochemical calculations. Evaluated data sets on vaporization and formation enthalpies have been used for development of the group-additivity values required for reliable prediction of these thermochemical properties. Using of reasonable combination of the group-additivity and the quantum-chemical methods is a valuable tool for validation of available experimental results as well as for assessment of thermochemical properties for species for which advanced quantum methods are currently too expensive from a computational viewpoint or for which the experiment is much too difficult.

Acknowledgments

Financial support of this work by the Ludwig-Maximilian University of Munich (LMU), the Office of Naval Research (ONR) under grant no. ONR.N00014-16-1-2062, and the Bundeswehr – Wehrtechnische Dienststelle für Waffen und Munition (WTD 91) under grant no. E/E91S/FC015/CF049 and the German Ministry of Education and Research (BMBF) under grant no. 13N12583 is gratefully acknowledged. The authors acknowledge collaborations with Dr. Mila Krupka (OZM Research, Czech Republic) in the development of new testing and evaluation methods for energetic materials and with Dr. Muhamed Suceska (Brodarski Institute, Croatia) in the development of new computational codes to predict the detonation and propulsion parameters of novel explosives. We are indebted to and thank Drs. Betsy M. Rice, Jesse Sabatini and Brad Forch (ARL, Aberdeen, Proving Ground, MD) for many inspired discussions." This work has been also partly supported by the Russian Government Program of Competitive Growth of Kazan Federal University.

Appendix A. Supplementary data

Supplementary data associated with this article can be found, in the online version, at http://dx.doi.org/10.1016/j.tca.2017.07.001.

References

[1] E.F.C. Byrd, B.M. Rice, A comparison of methods to predict solid phase heats of formation of molecular energetic salts, J. Phys. Chem. A 113 (2009) 345–352.
[2] A.K. Sikder, G. Maddala, J.P. Agrawal, H. Singh, Important aspects of behavior of organic energetic compounds: a review, J. Hazard. Mater. A 84 (2001) 1–26.
[3] M.H. Keshavarz, Improved prediction of heats of sublimation of energetic compounds using their molecular structure, J. Hazard. Mater. 177 (2010) 648–659.
[4] M.H. Keshavarz, H. Sadeghi, A new approach to predict the condensed phase heat of formation in acyclic and cyclic nitramines, nitrate esters and nitroaliphatic energetic compounds, J. Hazard. Mater. 171 (2009) 140–146.
[5] K.R. Jorgensen, G.A. Oyedepo, A.K. Wilson, Highly energetic nitrogen species: reliable energetics via the correlation consistent composite approach (ccCA), J. Hazard. Mater. 186 (2011) 583–589.
[6] M.H. Keshavarz, B.E. Saatluoa, A. Hassanzadeh, A new method for predicting the heats of combustion of polynitro arene polynitro heteroarene, acyclic and cyclic nitramine, nitrate ester and nitroaliphatic compounds, J. Hazard. Mater. 185 (2011) 1086–1106.
[7] M. Kamalvand, M.H. Keshavarz, M. Jafari, Prediction of the strength of energetic materials using the condensed and gas phase heats of formation, Propellants Explos. Pyrotech. 40 (2015) 551–557.
[8] M.A. Suntsova, O.V. Dorofeeva, Use of G4 theory for the assessment of inaccuracies

in experimental enthalpies of formation of aromatic nitro compounds, J. Chem. Eng. Data 61 (2016) 313–329.
[9] A.J. Miller, H. Hunt, Heats of combustion. III The heats of combustion of some polynitroparaffins, J. Phys. Chem. 49 (1945) 20–21.
[10] D.E. Holcomb, C.L. Dorsey Jr., Thermodynamic properties of nitroparaffins, Ind. Eng. Chem. 41 (1949) 2788–2792.
[11] R.C. Cass, S.E. Fletcher, C.T. Mortimer, P.G. Quincey, H.D. Springall, Heats of combustion and molecular structure, Part IV. Aliphatic nitroalkanes and nitric esters, J. Chem. Soc. (1958) 958–962.
[12] L. Medard, M. Thomas, Chaleurs de combustion de vingt-quatre substances explosives ou apparentees a des explosifs, Mem. Poudres 36 (1954) 97–127.
[13] N.D. Lebedeva, V.L. Ryadnenko, Heats of combustion and formation of polynitroalkanes, Russ. J. Phys. Chem. (Engl. Transl.) 42 (1968) 1225–1227.
[14] S.P. Smirnov, Y.N. Matiushin, I.Z. Akmetov, Conf International Civil Aviation Organization, 14–18 February, paper No. AH-DE/8-WP/12, Montreal, Canada, 1994.
[15] E.E. Toops, Physical properties of eight high-purity nitroparaffins, J. Phys. Chem. 60 (1956) 304–306.
[16] R.R. Dreisbach, S.A. Shrader, Vapor pressure-temperature data on some organic compounds, Ind. Eng. Chem. 41 (1949) 2879–2880.
[17] D.R. Stull, Vapor pressure of pure substances. Organic and inorganic compounds, Ind. Eng. Chem. 39 (1947) 517–540.
[18] S.P. Verevkin, V.N. Emel'yanenko, Transpiration method: vapor pressures and enthalpies of vaporization of some low-boiling esters, Fluid Phase Equilib. 266 (2008) 64–75.
[19] S.P. Verevkin, Thermochemistry of substituted benzenes. Experimental standard molar enthalpies of formation of o-,m-, and p-terphenyls and 1,3, 5-triphenylbenzene, J. Chem. Thermodyn. 29 (1997) 1495–1501.
[20] M.A.V. Ribeiro da Silva, L.M.N.B.F. Santos, L.M. Spencer, S. Lima, Thermodynamic study of 1,2,3-triphenylbenzene and 1,3,5-triphenylbenzene, J. Chem. Thermodyn. 42 (2010) 134–139.
[21] S.P. Verevkin, A.Y. Sazonova, V.N. Emel'yanenko, D.H. Zaitsau, M.A. Varfolomeev, B.N. Solomonov, K.V. Zherikova, Thermochemistry of halogen-substituted methylbenzenes, J. Chem. Eng. Data 60 (2015) 89–103.
[22] S.P. Verevkin, Thermochemistry of nitro compounds. Experimental standard enthalpies of formation and improved group-additivity values, Thermochim. Acta 307 (1997) 17–25.
[23] S.P. Verevkin, A. Heintz, Thermochemistry of substituted benzenes: quantification of ortho-, para-, meta-, and buttress interactions in alkyl-substituted nitrobenzenes, J. Chem. Thermodyn. 32 (2000) 1169–1182.
[24] S.P. Verevkin, C. Schick, Determination of vapor pressures enthalpies of sublimation, enthalpies of vaporization and enthalpies of fusion of a series of chloro-aminobenzenes and chloro-nitrobenzenes, Fluid Phase Equilib. 211 (2003) 161–177.
[25] A. Heintz, S. Kapteina, S.P. Verevkin, Pairwise-substitution effects and intramolecular hydrogen bonds in nitrophenols and methylnitrophenols. Thermochemical measurements and ab initio calculations, J. Phys. Chem. A 111 (2007) 6552–6562.
[26] S.P. Verevkin, V.N. Emel'yanenko, V. Diky, O.V. Dorofeeva, Enthalpies of formation of nitromethane and nitrobenzene: new experiments vs quantum chemical calculations, J. Chem. Thermodyn. 73 (2014) 163–170.
[27] V.N. Emel'yanenko, M. Algarra, J.C.G. Esteves da Silva, J. Hierrezuelo, J.M. López-Romero, S.P. Verevkin, Thermochemistry of organic azides revisited, Thermochim. Acta 597 (2014) 78–84.
[28] V.N. Emel'yanenko, S.P. Verevkin, Benchmark thermodynamic properties of 1,3-propanediol: comprehensive experimental and theoretical study, J. Chem. Thermodyn. 85 (2015) 111–119.
[29] M.J. Frisch, G.W. Trucks, H.B. Schlegel, G.E. Scuseria, M.A. Robb, J.R. Cheeseman, G. Scalmani, V. Barone, B. Mennucci, G.A. Petersson, et al., Gaussian 09. Revision A.02, Gaussian Inc., Wallingford CT, 2009.
[30] L.A. Curtiss, P.C. Redfern, K. Raghavachari, Gaussian-4 theory, J. Chem. Phys. 126 (2007) 084108.
[31] S.P. Verevkin, V.N. Emel'yanenko, R. Notario, M.V. Roux, J.S. Chickos, J.F. Liebman, Rediscovering the wheel. Thermochemical analysis of energetics of the aromatic diazines, J. Phys. Chem. Lett. 3 (2012) 3454–3459.
[32] S. Rayne, K. Forest, Estimated gas-phase standard state enthalpies of formation for organic compounds using the Gaussian-4 (G4) and W1BD theoretical methods, J. Chem. Eng. Data 55 (2010) 5359–5364.
[33] R.M. Stephenson, S. Malanowski, Handbook of the Thermodynamics of Organic Compounds, Elsevier, New York, 1987.
[34] T.S. Tolstova, V.B. Kogan, V.L. Skorokhodova, Equilibrium liquid-steam in systems nitrobensol-nitromethane, nitrobensol-nitroethane, Zh. Prikl. Khim. (Leningrad) 38 (1965) 2617–2618.
[35] E.B. Hodge, Vapor pressures for six aliphatic nitro compounds, Ind. Eng. Chem. 32 (1940) 748.
[36] M. Teodorescu, D. Dragoescu, D. Gheorghe, Isothermal (vapour + liquid) equilibria for (nitromethane or nitroethane + 1, 4-dichlorobutane) binary systems at temperatures between (343.15 and 363.15) K, J. Chem. Thermodyn. 56 (2013) 32–37.
37] D. Dragoescu, M. Teodorescu, D. Gheorghe, Isothermal vapor–liquid equilibria and excess Gibbs free energies in some binary nitroalkane + chloroalkane mixtures at temperatures from 298. 15 K to 318. 15 K, Fluid Phase Equilib. 338 (2013) 16–22.
[38] L. Elias, AH-DE/5-WP/17, International Civil Aviation Organization, Montreal, Canada, 2017 23–27 September 1991.
[39] E.A. Miroshnichenko, V.P. Vorob'eva, Thermochemical characteristics of nitroalkanes, Zh. Fiz. Khim. 73 (1999) 419–425.
[40] E.A. Miroshnichenko, T.S. Kon'kova, Y.O. Inozemtsev, Y.N. Matyushin, Bond energies and the enthalpies of formation of mono- and polyradicals in nitroalkanes. 2. Nitro derivatives of ethane and propane, Russ. Chem. Bull. 59 (2010) 890–895.
[41] J.S. Chickos, S. James, S. Hosseini, D.G. Hesse, Determination of vaporization enthalpies of simple organic molecules by correlations of changes in gas chromatographic net retention times, Thermochim. Acta 249 (1995) 41–62.
[42] Y.K. Knobel, E.A. Miroshnichenko, Y.A. Lebedev, Heat of combustion of 2-methyl-2-nitropropane and dissociation of CN bond in mononitro derivatives of propane and butane, Dokl. Phys. Chem. (Engl. Transl.) 190 (1970) 45–47.
[43] Y.K. Knobel, E.A. Miroshnichenko, Y.A. Lebedev, Heats of combustion of nitromethane and dinitromethane: enthalpies of formation of nitromethyl radicals and energies of dissociation of bonds in nitro derivatives of methane, Bull. Acad. Sci. USSR Div. Chem. Sci. 20 (1971) 425–428.
[44] E.A. Miroshnichenko, T.S. Kon'kova, Y.O. Inozemtsev, V.P. Vorob'eva, Y.N. Matyushin, S.A. Shevelev, Bond energies and formation enthalpies of mono- and polyradicals in nitroalkanes. 1. Nitromethanes, Russ. Chem. Bull. 58 (2009) 772–776.
[45] Y.A. Lebedev, E.A. Miroshnichenko, Y.K. Knobel, Thermochemistry of Nitrocompounds, Nauka, Moscow, 1970, pp. 1–176.
[46] D.E.G. Jones, P.D. Lightfoot, R.C. Fouchard, Q.S.M. Kwok, Thermal properties of DMNB, a detection agent for explosives, Thermochim. Acta 388 (2002) 159–173.
[47] D.E.G. Jones, R.A. Augsten, K.K. Feng, Detection agents for explosives, J. Therm. Anal. 44 (1995) 533–546.
[48] A.H. Lawrence, P. Neudorfl, J.A. Stone, The formation of chloride adducts in the detection of dinitro-compounds by ion mobility spectrometry, Int. J. Mass Spectrom. 209 (2001) 185–195.
[49] J. Reuter, D. Büsing, J.L. Tamarit, A. Würflinger, High-pressure differential thermal analysis study of the phase behaviour in sometert-butyl compounds: pivalic acid, 2-methylpropane-2-thiol and tert-butylamine, J. Mater. Chem. 7 (1997) 41–46.
[50] M. Godlewska, M. Rachwalska, An adiabatic calorimetric study of the phase situation in 2,2-dinitropropane, Phys. Status Solidi A 47 (1978) 661–665.
[51] N.D. Lebedeva, V.L.R. Ryadenko, Enthalpies of formation of nitroalkanes, Russ. J. Phys. Chem. (Engl. Transl.) 47 (1973) 1382.
[52] E.A. Miroshnichenko, T.S. Kon'kova, Y.O. Inozemtsev, Y.N. Matyushin, Bond energies and the enthalpies of formation of mono- and polyradicals in nitroakanes. 3. Nitroalkanes C4-C7, Russ. Chem. Bull. 60 (2011) 36–41.
[53] http://www.mcgill.ca/iasl/files/iasl/montreal1991.pdf.
[54] Y. Kai, P. Knochel, S. Kwiatkowski, J.D. Dunitz, J.F.M. Oth, D. Seebach, H.-O. Kalinowski, Structure synthesis, and properties of some persubstituted 1,2-dinitroethanes in quest of nitrocyclopropyl-anion derivatives, Helv. Chim. Acta 65 (1982) 137–161.
[55] S.P. Verevkin, R.V. Ralys, D.H. Zaitsau, V.N. Emel'yanenko, C. Schick, Express thermo-gravimetric method for the vaporization enthalpies appraisal for very low volatile molecular and ionic compounds, Thermochim. Acta 238 (2012) 55–62.
[56] J.S. Chickos, W.E. Acree, Total phase change entropies and enthalpies: an update on their estimation and applications to the estimations of amphiphillic fluorocarbon-hydrocarbon molecules, Thermochim. Acta 395 (2003) 59–113.
[57] S.P. Verevkin, D. Wandschneider, A. Heintz, Determination of vaporization enthalpies of selected linear and branched C7, C8 C9, C11 and C12 monoolefin hydrocarbons from transpiration and correlation gas-chromatography method, J. Chem. Eng. Data 45 (2000) 618–625.
[58] S.P. Verevkin, E.L. Krasnykh, T.V. Vasiltsova, B. Koutek, J. Doubsky, A. Heintz, Vapor pressures and enthalpies of vaporization of a series of the linear aliphatic aldehydes, Fluid Phase Equilib. 206 (2003) 331–339.
[59] M. Mansson, P. Sellers, G. Stridh, S. Sunner, Enthalpies of vaporization of some 1-substituted *n*-alkanes, J. Chem. Thermodyn. 9 (1977) 91–97.
[60] E.L. Krasnykh, S.P. Verevkin, B. Koutek, J. Doubsky, Vapour pressures and enthalpies of vaporization of a series of the linear n-alkyl acetates, J. Chem. Thermodyn. 38 (2006) 717–723.
[61] V.N. Emel'yanenko, S.P. Verevkin, B. Koutek, J. Doubsky, Vapour pressures and enthalpies of vaporization of a series of the linear aliphatic nitriles, J. Chem. Thermodyn. 37 (2005) 73–81.
[62] S.P. Verevkin, E.L. Krasnykh, T.V. Vasiltsova, A. Heintz, Determination of ambient temperature vapor pressures and vaporization enthalpies of branched ethers, J. Chem. Eng. Data 48 (2003) 591–599.
[63] V.N. Emel'yanenko, S.V. Portnova, S.P. Verevkin, A. Skrzypczak, T. Schubert, Building blocks for ionic liquids: vapor pressures and vaporization enthalpies of 1-(n-alkyl)-imidazoles, J. Chem. Thermodyn. 43 (2011) 1500–1505.
[64] S.P. Verevkin, vapour pressures and enthalpies of vaporization of a series of the linear n-alkyl-benzenes, J. Chem. Thermodyn. 38 (2006) 1111–1123.
[65] G.N. Roganov, P.N. Pisarev, V.N. Emel'yanenko, S.P. Verevkin, Measurement and prediction of thermochemical properties. Improved Benson-type increments for the estimation of enthalpies of vaporization and standard enthalpies of formation of aliphatic alcohols, J. Chem. Eng. Data 50 (2005) 1114–1124.
[66] M.A. Suntsova, O.V. Dorofeeva, Use of G4 theory for the assessment of inaccuracies in experimental enthalpies of formation of aliphatic nitro compounds and nitramines, J. Chem. Eng. Data 59 (2014) 2813–2826.
[67] S.W. Benson, Thermochemical Kinetics, Wiley, New York, 1976.
[68] N. Cohen, Revised group additivity values for enthalpies of formation (at 298 K) of carbon-hydrogen and carbon-hydrogen-oxygen compounds, J. Phys. Chem. Ref. Data 25 (1996) 1411–1481.
[69] S.P. Verevkin, V.N. Emel'yanenko, V. Diky, C.D. Muzny, R.D. Chirico, M. Frenkel, New group contribution approach to thermochemical properties of organic compounds: hydrocarbons and oxygen containing compounds, J. Phys. Chem. Ref. Data 42 (2013) 033102.
[70] W.D. Good, The enthalpies of combustion and formation of n-octane and 2,2,3,3-tetramethylbutane, J. Chem. Thermodyn. 4 (1972) 709–714.

Electronic supporting information

Thermochimica Acta, 2017

Aliphatic nitroalkanes: evaluation of thermochemical data with complementary experimental and computational methods

Martin Härtel,[a] Thomas M. Klapötke,[a] Vladimir N. Emel´yanenko,[b,c] Sergey P. Verevkin[c,]*

[a] *Department of Chemistry, Ludwig-Maximilians-Universität München, Butenandtstr. 5-13, 81377 München-Großhadern, Germany*
[b]*Department of Physical Chemistry, Kazan Federal University, Kremlevskaya str. 18, 420008 Kazan, Russia*
[c]*Department of Physical Chemistry and Department of „Science and Technology of Life, Light and Matter", University of Rostock, Dr-Lorenz-Weg 1, D-18059, Rostock, Germany*

Transpiration method: Vapor pressures of nitroalkanes were measured using the transpiration method [1-4]. About 0.8 g of a sample was mixed with small glass beads and placed in a thermostatted U-shaped saturator. A well-defined nitrogen stream was passed through the saturator at a constant temperature (± 0.1 K), and the transported material was collected in a cold trap. The amount of condensed sample was determined by GC analysis using a suitable n-alkane as an external standard. The absolute vapor pressure p_i at each temperature T_i was calculated from the amount of the product collected within a definite period. Assuming validity of the Dalton`s law and the Ideal Gas Law applied to the nitrogen stream saturated with the substance *i*, values of p_i were calculated with Eq. (1):

$$p_i = m_i \cdot R \cdot T_a / V \cdot M_i \; ; \qquad V = V_{N2} + V_i ; \qquad (V_{N2} \gg V_i) \qquad \text{(S1)}$$

where R = 8.314462 J·K^{-1}·mol^{-1}; m_i is the mass of the transported compound, M_i is the molar mass of the compound, and V_i is its volume contribution to the gaseous phase. V_{N2} is the volume of the carrier gas and T_a is the temperature of the soap bubble meter used for measurement of the gas flow. The volume of the carrier gas V_{N2} was determined from the flow rate and the time measurement.

Transpiration experiments have been performed on the same highly purified samples independently in Rostock and in Munich. The experimental set up used in Rostock have been reported elsewhere [1]. For quantification of the transported sample mass the capillary column HP-5 was used with a column length of 30 m × 0.32 mm × 0.25 μm was used. A twin transpiration apparatus has been established for the first time in Munich and the parallel measurements on nitroalkanes have been considered as a validation of the transpiration procedure transferred to the new lab. All parts of equipment in Munich have been identical to those in Rostock except for the GC analysis of the transported mass. A vacuum outlet GC/MS

setup [5] with a restriction inside the injector was used. The restriction (8.11 mm, 0.025 mm i.d., Restek# 10097) was connected with a Siltite µ-union (Restek #073562) to a Restek RTX-TNT 1 column with a column length of 6 m × 0.53 mm × 1.5 µm. The results measured by the transpiration (T) in Rostock were labeled as the TR, and the results measured in Munich as the TM.

Temperature dependence of vapor pressures p_i measured for *nitroalkanes* in this work were fitted with the following equation [1]:

$$R \cdot \ln p_i = a + \frac{b}{T} + \Delta_l^g C_{p,m} \cdot \ln\left(\frac{T}{T_0}\right) \qquad \text{(S2)},$$

where a and b are adjustable parameters and $\Delta_l^g C_{p,m}$ is the difference of the molar heat capacities of the gaseous and the liquid phase respectively. T_0 appearing in Eq. (S2) is an arbitrarily chosen reference temperature (which has been chosen to be 298.15 K) and R is the molar gas constant. Values of $\Delta_l^g C_{p,m}$ in Eq. (2) were calculated (see Table S3) according to the empirical procedure developed by Chickos and Acree [6]. Experimental vapor pressures measured by the transpiration method are given in Table S2. The Eq. (S2) is also valid for the treatment of vapour pressures measured over the crystalline sample. Values of $\Delta_{cr}^g C_{p,m}^{\circ}$ required for this case were also calculated (see Table S3) according to the procedure developed by Chickos and Acree [6].

By the transpiration studies of the volatile 2-nitropropane and 2-methyl-2-nitropropane a relatively high vapor pressures (3000 – 9000 Pa) have been observed at elevated temperatures. For these extremal for the transpiration method conditions the volume contribution from the compound under study to the total volume becomes not negligible, hence, equation S1 for the measurements of 2-nitropropane and 2-methyl-2-nitropropane having the high-pressure range was modified in order to account for the additional volume expansion:

$$p_i = m_i \cdot R \cdot T_a / V \cdot M_i \; ; \qquad V = (n_{N2} + n_i) \cdot R \cdot T_a / P_a \qquad \text{(S3)}$$

where V is the volume of the gas phase consisting of the n_{N2} moles of the carrier gas and n_i mole of gaseous compound under study at the atmospheric pressure P_a and the ambient temperature T_a. The amount of the carrier gas n_{N2} was determined from the flow rate and the time measurement. The volume corrected calculations for the vapor pressures sets of the volatile 2-nitropropane and 2-methyl-2-nitropropane have been systematically conducted not only for pressures above 3000 Pa, but also for pressures above 600 Pa.

Vaporization enthalpies at temperature *T* were derived from the temperature dependence of vapor pressures using Eq. (S3):

$$\Delta_l^g H_m^\circ(T) = -b + \Delta_l^g C_{p,m}^\circ \cdot T \quad \text{(S4)}$$

Vaporization entropies at temperature *T* were also derived from the temperature dependence of vapor pressures using Eq. (S5):

$$\Delta_l^g S_m^\circ(T) = \Delta_l^g H_m^\circ / T + R \ln(p_i / p^\circ) \quad \text{(S5)}$$

Experimental absolute vapor pressures measured by the transpiration method, coefficients *a* and *b* of Eq. (S2), as well as values of $\Delta_l^g H_m^\circ(T)$ and $\Delta_l^g S_m^\circ(T)$ are given in Table S2. Procedure for calculation of the combined uncertainties of the vaporization enthalpy was described elsewhere [2-3]. It includes uncertainties from the transpiration experiment conditions, uncertainties in vapor pressure, and uncertainties in the temperature adjustment to *T* = 298.15 K.

Table S1

Origin, purity, methods of purification of chemicals used in this work

Compound	CAS	Source	Initial purity	Purification method	Final purity[a]
2-nitropropane (liq)	79-46-9	Aldrich	0.99	distillation	0.999
2-methyl-2-nitropane (liq)	594-70-7	Aldrich	0.96	distillation	0.999
2,3-dimethyl-2,3-dinitrobutane (cr)	3964-18-9	Aldrich	0.98	sublimation	0.999

[a] Mass fraction purity obtained by the gas chromatography.

Table S2

Absolute vapor pressures *p*, vaporization enthalpies, $\Delta_l^g H_m^\circ$, and vaporization entropies, $\Delta_l^g S_m$, obtained by the transpiration method.

2-Nitropropane (TM): $\Delta_l^g H_m^\circ$ (298.15 K) = 40.3 ± 0.3 kJ mol^{-1}

$$\ln p/p^\circ = \frac{255.7}{R} - \frac{56819.2}{RT} + \frac{52.6}{R} ln \frac{T}{298.15\text{K}}$$

T_{exp}[a] [K]	m[b] [mg]	V_{N2}[c] [dm³]	T_{amb}[d] [K]	Gasflow [dm³ h^{-1}]	p[e] [Pa]	$u(p)$[f] [Pa]	$\Delta_l^g H_m^\circ$ [kJ mol^{-1}]	$\Delta_l^g S_m^\circ$ [J mol^{-1} K^{-1}]
274.7	1.65	0.082	297.7	0.99	609	15	41.54	108.8
274.8	1.63	0.082	297.6	0.98	604	15	41.53	108.7
274.8	1.63	0.083	297.7	1.00	597	15	41.53	108.6
279.6	2.29	0.082	297.9	0.99	827	21	41.28	107.8
279.5	2.25	0.083	297.8	1.00	799	20	41.29	107.6
284.4	3.09	0.082	297.6	0.98	1092	27	41.03	106.7
284.4	3.08	0.082	297.6	0.98	1091	27	41.03	106.7
289.3	4.27	0.083	297.8	1.00	1459	37	40.77	105.8
294.2	5.68	0.082	297.5	0.98	1953	49	40.51	105.0
294.3	5.57	0.083	298.5	0.99	1900	48	40.51	104.7

299.2	7.59	0.082	297.9	0.98	2574	64	40.25	104.1
304.1	10.06	0.082	297.9	0.99	3344	84	39.99	103.3
304.2	10.07	0.082	297.5	0.99	3336	83	39.99	103.2
309.1	13.27	0.083	297.7	1.00	4299	107	39.73	102.4
314.1	17.24	0.081	297.7	0.98	5612	140	39.47	101.7
314.1	17.04	0.081	298.0	0.98	5563	139	39.47	101.6

2-Methyl-2-nitropropane: $\Delta_{\mathrm{l}}^{\mathrm{g}}H_m^{\circ}$ (298.15 K) = 40.5 ± 0.5 kJ mol^{-1}

$$\ln p/p^{\circ} = \frac{264.7}{R} - \frac{60132.7}{RT} + \frac{59.5}{R} ln \frac{T}{298.15\mathrm{K}}$$

T_{exp}[a]	m[b]	V_{N2}[c]	T_{amb}[d]	Gasflow	p[e]	$u(p)$[f]	$\Delta_l^{\mathrm{g}}H_m^{\circ}$	$\Delta_l^{\mathrm{g}}S_m^{\circ}$
[K]	[mg]	[dm³]	[K]	[dm³ h^{-1}]	[Pa]	[Pa]	[kJ mol^{-1}]	[J mol^{-1} K^{-1}]
299.3	7.74	0.091	297.2	1.10	2054	51	40.39	102.6
303.2	9.81	0.091	297.2	1.10	2553	64	40.16	101.9
304.2	10.32	0.091	297.2	1.09	2705	68	40.10	101.8
308.2	12.65	0.091	297.4	1.10	3261	82	39.86	100.9
309.2	13.64	0.091	297.1	1.09	3527	88	39.80	100.9
313.2	16.50	0.091	297.1	1.09	4205	105	39.56	100.0
314.2	17.26	0.091	297.0	1.09	4410	110	39.50	99.8
318.2	20.90	0.091	297.3	1.09	5269	132	39.26	98.9
323.2	26.71	0.091	297.2	1.09	6650	166	38.97	98.0
328.1	35.03	0.091	297.1	1.09	8479	212	38.67	97.4

2,3-Dimethyl-2,3-dinitrobutane (phase I): $\Delta_{\mathrm{cr}}^{\mathrm{g}}H_m^{\circ}$ (298.15 K) = 87.0 ± 0.6 kJ mol^{-1} (TM)

$$\ln p/p^{\circ} = \frac{317.5}{R} - \frac{98400.4}{RT} + \frac{38.0}{R} ln \frac{T}{298.15\mathrm{K}}$$

T_{exp}[a]	m[b]	V_{N2}[c]	T_{amb}[d]	Gasflow	p[e]	$u(p)$[f]	$\Delta_{\mathrm{cr}}^{\mathrm{g}}H_m^{\circ}$	$\Delta_{\mathrm{cr}}^{\mathrm{g}}S_m^{\circ}$
[K]	[mg]	[dm³]	[K]	[dm³ h^{-1}]	[Pa]	[Pa]	[kJ mol^{-1}]	[J mol^{-1} K^{-1}]
278.4	0.18	145	297.2	3.03	0.02	0.01	87.82	186.1
283.3	0.12	46.0	297.4	2.79	0.04	0.01	87.63	186.4
283.3	0.31	125	297.4	1.86	0.03	0.01	87.63	185.7
283.3	0.12	49.2	297.9	3.31	0.04	0.01	87.63	185.9
283.3	0.17	71.8	296.6	3.03	0.03	0.01	87.63	185.5
288.3	0.18	36.4	299.8	2.80	0.07	0.01	87.45	185.4
288.3	0.40	88.1	297.6	2.25	0.06	0.01	87.45	184.8
293.2	0.19	22.8	298.0	3.04	0.12	0.01	87.26	184.2
293.3	0.09	9.52	298.8	2.82	0.13	0.01	87.26	184.7
293.4	0.31	36.0	296.8	2.42	0.12	0.01	87.25	184.1
298.2	0.19	12.1	296.9	3.03	0.22	0.01	87.07	183.7
298.2	0.16	9.68	298.6	2.82	0.23	0.01	87.07	184.0
303.2	0.38	13.8	296.8	5.02	0.38	0.01	86.88	182.8
303.2	0.12	3.91	297.9	2.86	0.42	0.02	86.88	183.6
308.1	0.41	8.75	298.0	2.43	0.66	0.02	86.69	182.2
308.2	0.12	2.30	298.1	2.87	0.71	0.02	86.69	182.6
313.0	0.36	4.46	298.0	2.43	1.13	0.03	86.50	181.6

313.0	0.44	5.50	296.7	5.00	1.13	0.03	86.50	181.6
313.2	0.13	1.45	297.1	2.90	1.25	0.04	86.50	182.3
318.0	0.40	2.83	297.9	2.43	1.99	0.05	86.32	181.5
318.0	0.53	3.59	296.9	5.00	2.06	0.06	86.32	181.7
318.2	0.47	3.44	297.0	3.03	1.90	0.05	86.31	180.9
318.2	0.13	0.871	297.8	2.90	2.05	0.06	86.31	181.5

2,3-Dimethyl-2,3-dinitrobutane (phase I): $\Delta_{\mathrm{cr}}^{\mathrm{g}} H_m^{\circ}$ (298.15 K) = 86.1 ± 2.5 kJ mol^{-1} (TR)

$$\ln p/p^{\circ} = \frac{315.1}{R} - \frac{97379.3}{RT} + \frac{38.0}{R} ln \frac{T}{298.15\mathrm{K}}$$

T_{exp}[a]	m[b]	V_{N2}[c]	T_{amb}[d]	Gasflow	p[e]	$u(p)$[f]	$\Delta_{cr}^{g} H_m^{\circ}$	$\Delta_{cr}^{g} S_m^{\circ}$
[K]	[mg]	[dm³]	[K]	[dm³ h^{-1}]	[Pa]	[Pa]	[kJ mol^{-1}]	[J mol^{-1} K^{-1}]
306.5	2.89	62.4	293.2	3.74	0.64	0.02	85.73	180.3
311.1	1.30	17.2	293.2	3.69	1.04	0.03	85.56	179.7
315.3	1.55	12.7	293.2	3.69	1.70	0.05	85.40	179.5
319.4	1.28	7.23	293.2	3.74	2.45	0.07	85.24	178.6

2,3-Dimethyl-2,3-dinitrobutane (phase II): $\Delta_{\mathrm{cr}}^{\mathrm{g}} H_m^{\circ}$ (298.15 K) = 87.8 ± 0.7 kJ mol^{-1} (TM)

$$\ln p/p^{\circ} = \frac{310.8}{R} - \frac{96052.3}{RT} + \frac{38.0}{R} ln \frac{T}{298.15\mathrm{K}}$$

T_{exp}[a]	m[b]	V_{N2}[c]	T_{amb}[d]	Gasflow	p[e]	$u(p)$[f]	$\Delta_{cr}^{g} H_m^{\circ}$	$\Delta_{cr}^{g} S_m^{\circ}$
[K]	[mg]	[dm³]	[K]	[dm³ h^{-1}]	[Pa]	[Pa]	[kJ mol^{-1}]	[J mol^{-1} K^{-1}]
333.1	0.35	0.600	295.9	2.00	8.18	0.23	86.45	181.3
338.1	0.76	0.831	295.9	1.99	12.82	0.35	86.26	180.6
343.1	0.72	0.499	296.0	1.99	20.18	0.53	86.07	180.1
348.1	1.57	0.698	296.0	2.00	31.45	0.81	85.88	179.7
353.1	3.20	0.933	296.1	2.00	47.99	1.22	85.69	179.2
358.0	3.19	0.633	296.1	2.00	70.47	1.79	85.50	178.5
363.0	7.62	1.033	295.9	2.00	103.08	2.60	85.31	177.8
368.0	7.73	0.698	296.0	2.00	154.60	3.89	85.12	177.5
373.0	8.00	0.500	296.3	2.00	223.89	5.62	84.93	177.0

2,3-Dimethyl-2,3-dinitrobutane (phase II): $\Delta_{\mathrm{cr}}^{\mathrm{g}} H_m^{\circ}$ (298.15 K) = 85.2 ± 1.3 kJ mol^{-1} (TR)

$$\ln p/p^{\circ} = \frac{312.2}{R} - \frac{96514.1}{RT} + \frac{38.0}{R} ln \frac{T}{298.15\mathrm{K}}$$

T_{exp}[a]	m[b]	V_{N2}[c]	T_{amb}[d]	Gasflow	p[e]	$u(p)$[f]	$\Delta_{cr}^{g} H_m^{\circ}$	$\Delta_{cr}^{g} S_m^{\circ}$
[K]	[mg]	[dm³]	[K]	[dm³ h^{-1}]	[Pa]	[Pa]	[kJ mol^{-1}]	[J mol^{-1} K^{-1}]
328.0	1.02	2.49	293.2	3.74	5.66	0.15	84.05	175.0
332.9	1.57	2.55	293.2	3.82	8.51	0.22	83.87	174.0
337.5	2.31	2.36	293.2	3.82	13.55	0.36	83.69	173.9

342.3	3.50	2.42	293.2	3.82	19.98	0.52	83.51	173.2
347.9	3.37	1.47	293.2	3.82	31.79	0.82	83.30	172.5
352.6	2.87	0.83	293.2	3.82	47.91	1.22	83.12	172.2

[a] Saturation temperature ($u(T)$ = 0.1 K). [b] Mass of transferred sample condensed at T = 243 K [c] Volume of nitrogen ($u(V)$ = 0.005 dm^3) used to transfer m ($u(m)$ = 0.0001 g) of the sample. [d] T_a is the temperature of the soap bubble meter used for measurement of the gas flow. [e] Vapor pressure at temperature T, calculated from the m and the residual vapor pressure at the condensation temperature calculated by an iteration procedure; p°=1 Pa. [f] Standard uncertainty in p was calculated with $u(p/\text{Pa}) = 0.005+0.025(p/\text{Pa})$ for $p < 5$ Pa and $u(p/\text{Pa}) = 0.025+0.025(p/\text{Pa})$ for $p > 5$ to 3000 Pa. Uncertainties of vaporisation/sublimation enthalpies in this table are expressed as the standard uncertainties and they derived according to the procedure reported in [19] (citations in main document)

Table S3

Compilation of data on molar heat capacities (in J·mol^{-1}·K^{-1}) at 298.15 K of the nitroalkanes.

Compounds	$C^{\circ}_{p,m}$(liq)[a]	$-\Delta^{g}_{l}C^{\circ}_{p,m}$ [b]	$C^{\circ}_{p,m}$(cr) [a]	$-\Delta^{g}_{cr}C^{\circ}_{p,m}$ [c]
Nitroethane	134.2[11]	45.5	-	-
1-nitropropane	168.0	54.3		
2-nitropropane	161.5	52.6		
1-nitrobutane	199.9	62.6		
2-nitrobutane	193.4	60.9		
2-methyl-nitropropane	193.4	60.9		
2-methyl-2-nitropropane	188.0	59.5	160.9	24.9
1-nitropropentane	231.8	70.8		
1-nitrocyclohexane	219.4	67.6		
2,2,4,4-tetramethyl-nitrobutane	303.7	89.5		
1,1-dinitromethane	170.5	54.9		
1,2-dinitroethane	202.4	63.2	166.0	25.7
1,3-dinitropropane	234.3	71,5		
1,4-dinitrobutane	266.2	79.8	219.8	33.7
1,1-dinitroethane	195.9	61.5	157.8	24.4
2,2-dinitropropane	222.4	68.4	180.4	27.8
1,1-dinitroethane	227.8	69.8		
1,1-dinitropentane	291.6	86.4		
2,3-dimethyl-2,3-dinitrobutane	306.2	90.2	248.6	38.0

a) calculated according to the group-contribution method by Chickos and Acree [6]
b) calculated by $\Delta^{g}_{l}C^{o}_{p,m} = 10.58 + C^{o}_{p,m}(\mathrm{l}) \times 0.26$ [6]
c) calculated by $\Delta^{g}_{cr}C^{o}_{p,m} = 0.75 + C^{o}_{p,m}(\mathrm{cr}) \times 0.15$ [6]

Generally, the experimental molar enthalpy of fusion $\Delta^{l}_{cr}H_{m}$ is referenced to the melting temperature T_{fus}. Compilation of available data on the fusion enthalpy for solid nitroalkanes is presented in Table 3. For the thermochemical calculations the experimental enthalpy of fusion have to be adjusted to the reference temperature T = 298.15 K. The adjustment was calculated from the equation [6]:

$$\Delta^{l}_{cr}H_{m}(298.15\ \mathrm{K})/(\mathrm{J\cdot mol^{-1}}) = \Delta^{l}_{cr}H_{m}(T_{fus}/\mathrm{K}) - (\Delta^{g}_{cr}C^{\circ}_{p,m} - \Delta^{g}_{l}C^{\circ}_{p,m})\times[(T_{fus}/\mathrm{K}) - 298.15\ \mathrm{K}] \quad (5),$$

where $\Delta^{g}_{cr}C^{\circ}_{p,m}$ and $\Delta^{g}_{l}C^{\circ}_{p,m}$ are given in Table S3. With this adjustment, the molar enthalpy of fusion, $\Delta^{l}_{cr}H_{m}(298.15\ \mathrm{K})$ was calculated (see Table 3) and used for consistency test of the phase change enthalpies for nitroalkanes.

Table S4
Compilation of the experimental Kovat´s indices of nitroalkanes used for correlation with enthalpies of vaporization.

Compound	J_x [a]	$\Delta_l^g H_m^\circ$ (298.15 K)[b] kJ·mol^{-1}
nitromethane	467.3	38.4±0.3
nitroethane	577.2	41.0±0.2
1-nitropropane	672.0	43.3±0.2
1-nitrobutane	777.2	47.5±0.3
1-nitropentane	877.3	50.3±0.5
1-nitrohexane	978.6	53.2±0.5[c]

[a] Data for retention indicies J_x at 403 K from [7]
[b] From Table 1. Uncertainties of vaporisation are expressed as the standard deviation.
[c] Calculated by Eq. 2 (see main text)

Table S5
Compilation of the experimental vaporization and formation enthalpies, of alkanols used for correlation with enthalpies of mono-nitroalkanes (in kJ·mol^{-1}).

compound	$\Delta_l^g H_m^\circ$ (298.15 K)[a]	$\Delta_f H_m^\circ$ (g, 298.15 K) [b]
methanol	37.8±0.1 [8]	-201.5±0.3 [9]
ethanol	42.5±0.1 [8]	-235.2±0.4 [9]
1-propanol	47.5±0.1 [8]	-255.1±0.5 [9]
2-propanol	45.5±0.1 [8]	-272.8±0.5 [9]
1-butanol	52.4±0.1 [8]	-274.9±0.4 [10]
2-butanol	49.8±0.1 [8]	-293.0±1.0 [10]
2-methylpropanol-1	50.9±0.1 [8]	-282.4±0.8 [10]
2-methyl-2-propanol	46.7±0.1 [8]	-312.6±0.8 [10]
1-pentanol	56.9±0.2 [8]	-294.7±0.8 [10]
1-hexanol	61.6±0.2 [8]	-315.8±0.6 [10]
1-cyclohexanol	62.0±0.2 [8]	-286.2±2.1 [9]

[a] Uncertainties of vaporisation, $\Delta_l^g H_m^\circ$ (298.15 K), are expressed as the standard deviation.

[b] Uncertainties of enthalpies of fprmation, $\Delta_f H_m^\circ$ (g, 298.15 K), are expressed as the twice standard deviation.

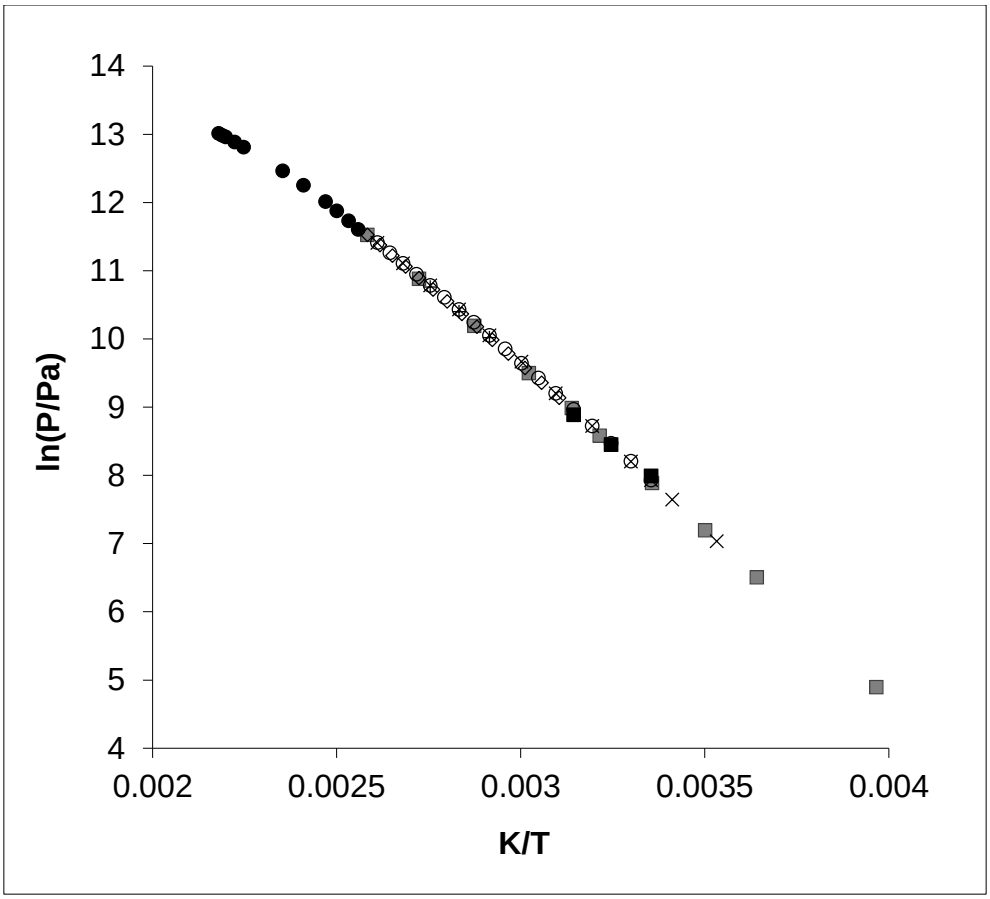

Fig. S1. Experimental vapor pressures over liquid sample of the nitroethane: ■ - [17]; ● - [34]; × - [10]; ◊ - [15]; ○ - [35]; + - [36]; ■ - [37]. (citations in main document)

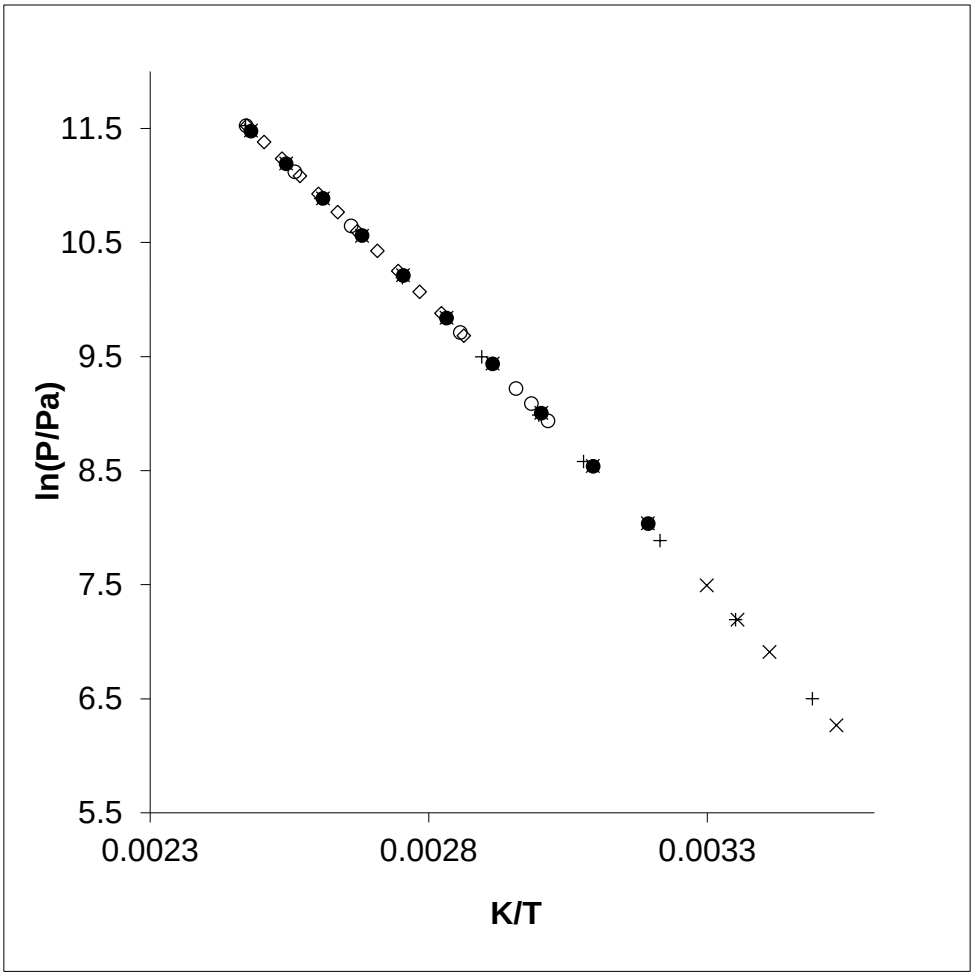

Fig. S2. Experimental vapor pressures over liquid sample of the 1-nitropropane:

× - [10]; ◊ - [15]; ○ - [16]; + - [17]; ● - [35]. (citations in main document)

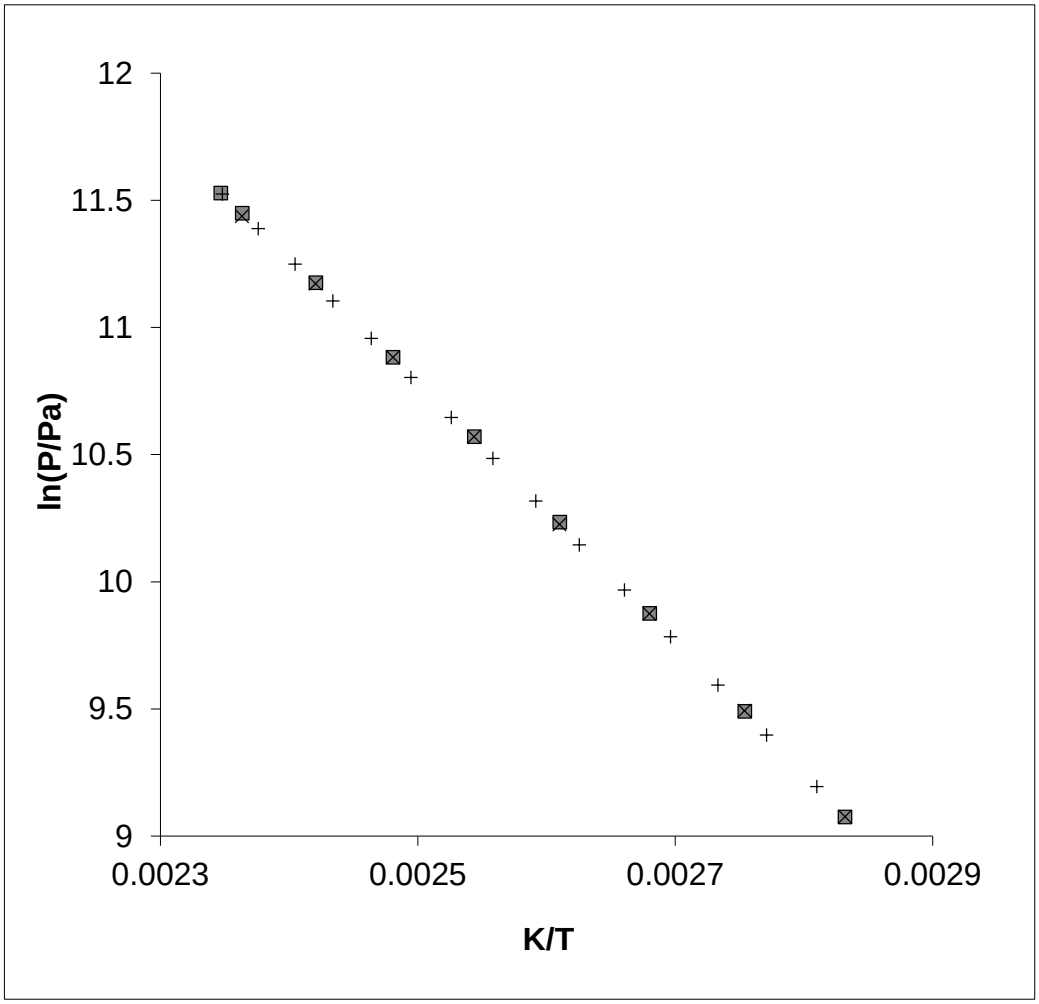

Fig. S3. Experimental vapor pressures over liquid sample of the 1-nitrobutane:
× - [10]; + - [15]; ▪ - [35]. (citations in main document)

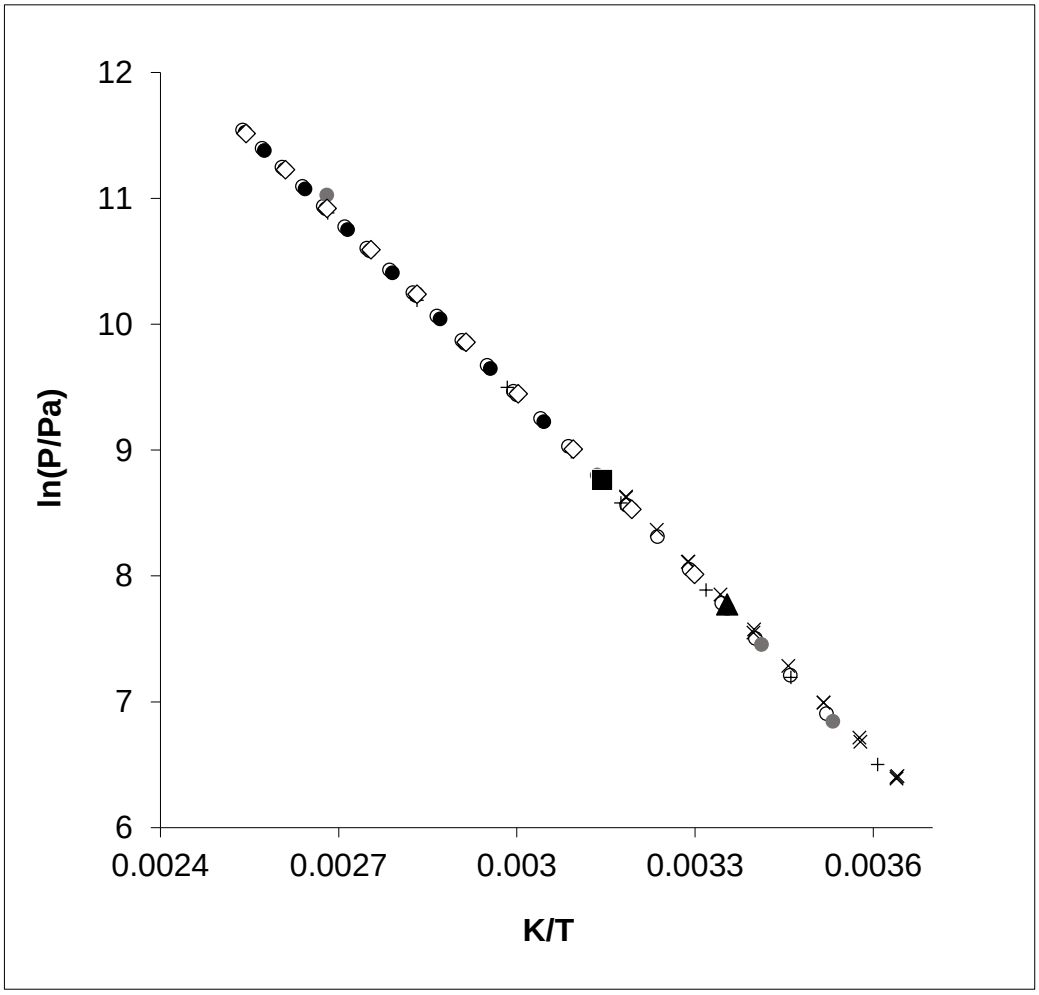

Fig. S4. Experimental vapor pressures over liquid sample of the 2-nitropropane:
× this work (Munich); ● - [10]; ● - [15];+ - [17];○ - [33]; ◊ - [35]. (citations in main document);
▲ – from ref [12] in supporting materials; ■ – from ref [13] in supporting materials.

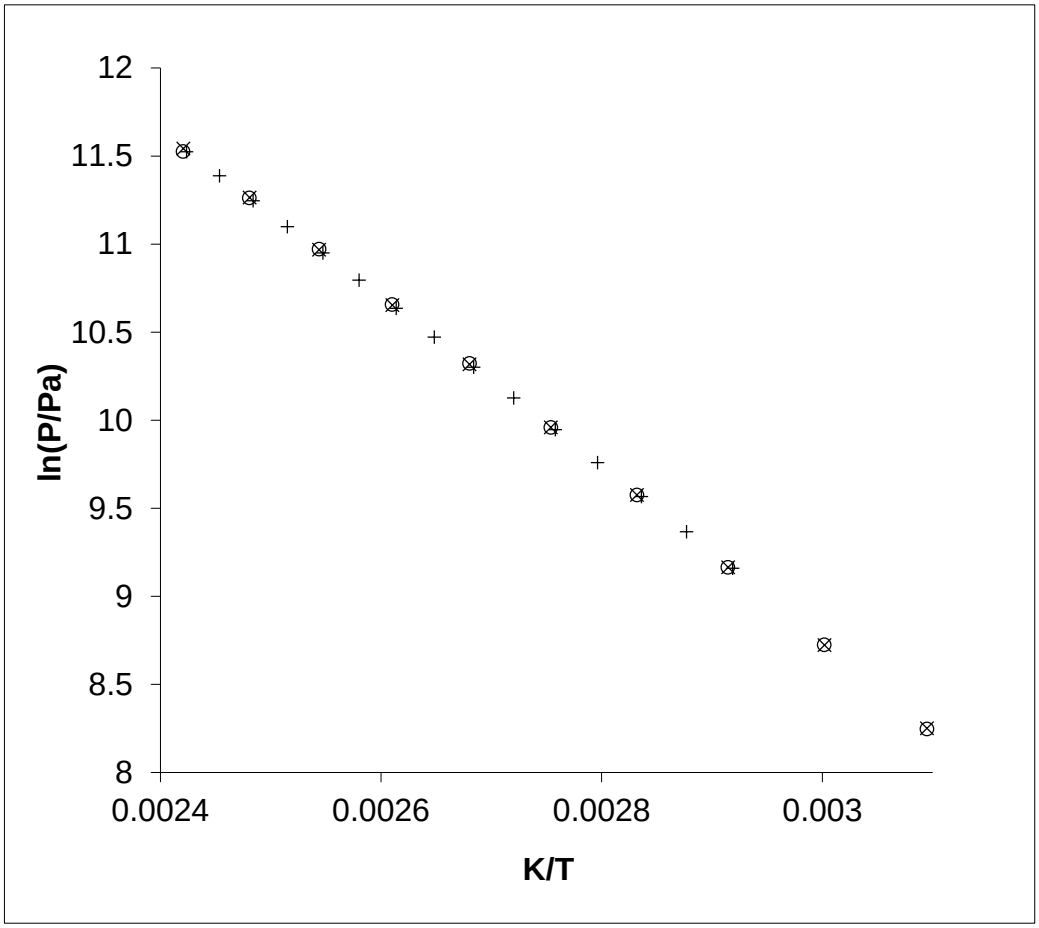

Fig. S5. Experimental vapor pressures over liquid sample of the 2-nitrobutane:

○ - [10]; + - [15]; × - [35]. (citations in main document)

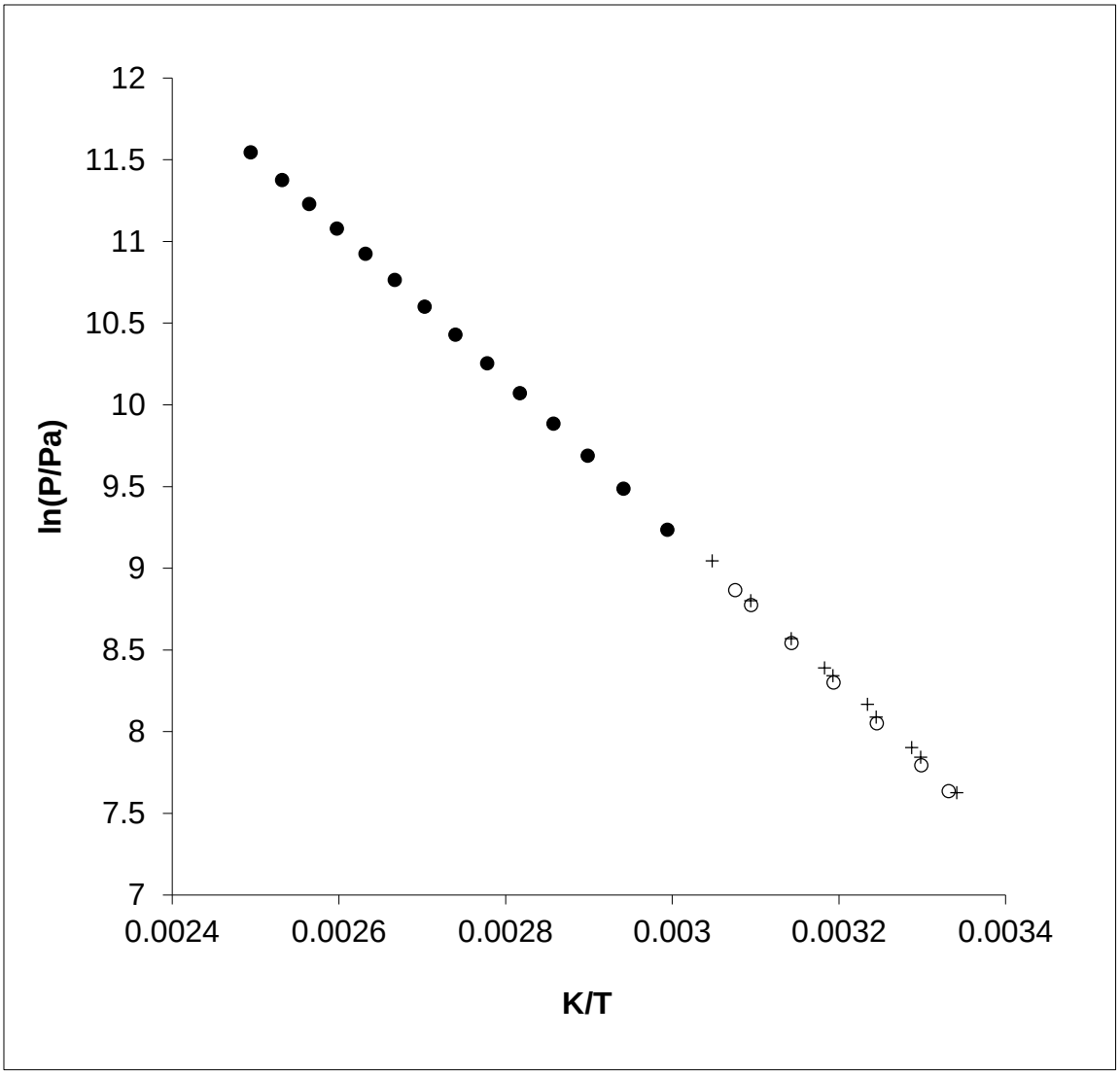

Fig. S6. Experimental vapor pressures over 2-methyl-2-nitropropane:
+ this work (Munich); ● - [15]; ○ - [42] (citations in main document).

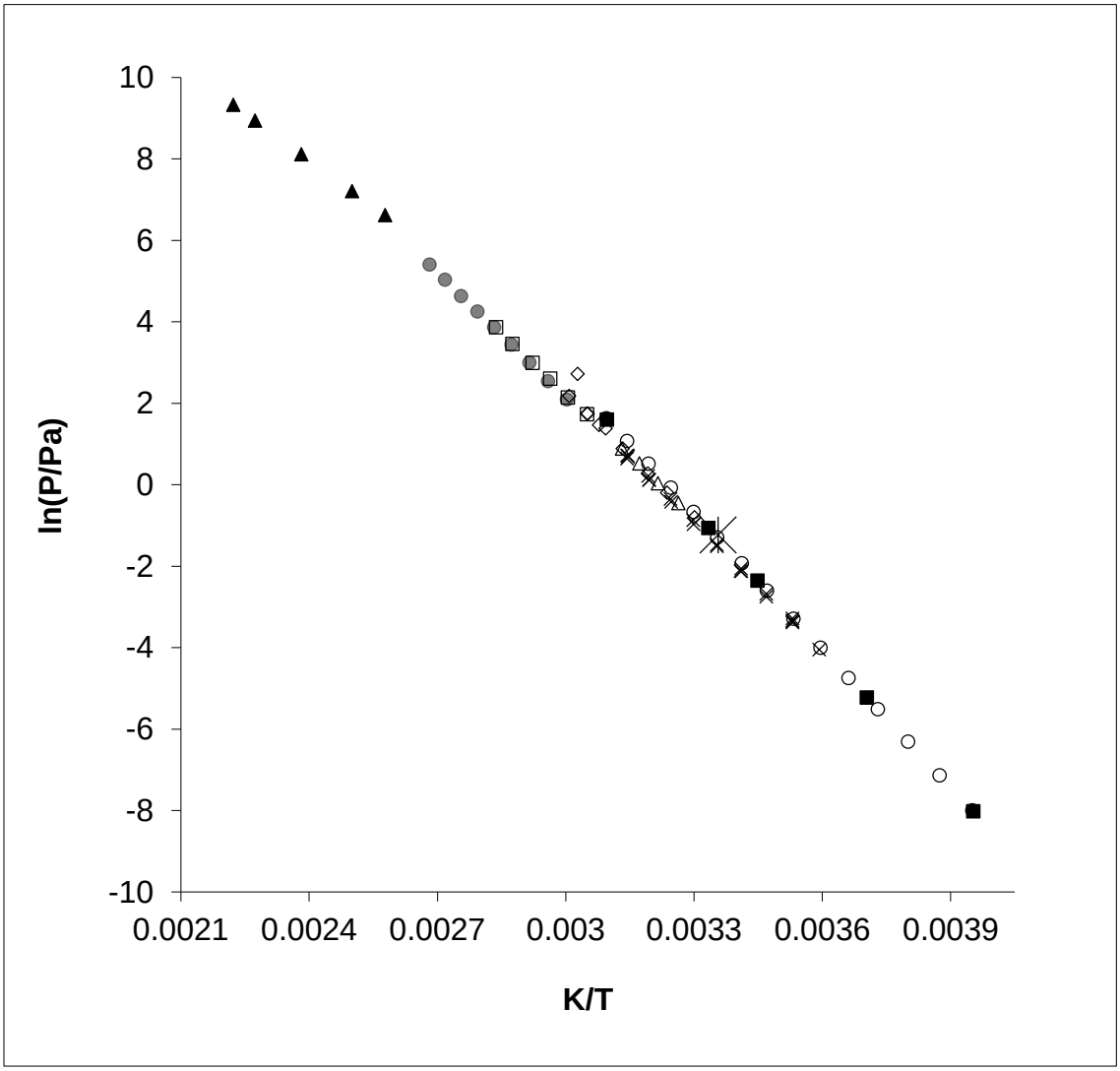

Fig. S7. Experimental vapor pressures over the solid sample of 2,3-dimethyl-2,3-dinitrobutane:

× this work (Munich, phase I); ● this work (Munich, phase II); Δ this work (Rostock, phase I); □ this work (Rostock phase II), ◊ - [14]; ○ - [38]; ▲ - [46]; ж - [47]; ■ - [48]. (citations are given in main document).

References

[1] S.P. Verevkin, V.N. Emel'yanenko, Transpiration method: vapor pressures and enthalpies of vaporization of some low-boiling esters, Fluid Phase Equilib. 266 (2008) 64-75.
[2] S.P. Verevkin, A.Y. Sazonova, V.N. Emel'yanenko, D.H. Zaitsau, M.A. Varfolomeev, B.N. Solomonov, K.V. Zherikova, Thermochemistry of halogen-substituted methylbenzenes, J. Chem. Eng. Data 60 (2015) 89-103.
[3] V.N. Emel'yanenko, S.P. Verevkin, Benchmark thermodynamic properties of 1,3-propanediol: Comprehensive experimental and theoretical study, J. Chem. Thermodyn. 85 (2015) 111-119.
[4] S.P. Verevkin, Pure component phase changes liquid and gas in Experimental thermodynamics: measurement of the thermodynamic properties of multiple phases. (Editors: R.D. Weir; Th.W. De Loos), Vol 7, Elsevier, 2005, 6-30.
[5] J. de Zeeuw, S. Reese, J. Cochran, S. Grossman, T. Kane, C. English, Simplifying the setup for vacuum outlet GC: using a restriction inside the injection port, J. Sep. Sci. 32 (2009) 1849-1857.
[6] J. S. Chickos, W. E. Acree, Enthalpies of sublimation of organic and organometallic compounds. 1910-2001, J. Phys. Chem. Ref. Data 31 (2002) 537–698.
[7] G. Defayes, D.F. Fritz, T. Görner, G. Huber, C.D. Reyff, E. sz. Kovats. Organic solutes in paraffin solvents: influence of the size of the solvent molecule on solution data, J. Chromatogr. 500 (1990) 139-184.
[8] V. Majer, V. Svoboda, Enthalpies of vaporization of organic compounds: a critical review and data compilation, Blackwell Scientific Publications, Oxford, 1985, 300.
[9] J.P. Pedley, R.D. Naylor, S.P. Kirby, Thermochemical data of organic compounds, 2nd ed.; Chapman and Hall: London, 1986.
[10] G. N. Roganov, P. N. Pisarev, V. N. Emel'yanenko, S. P. Verevkin, Measurement and prediction of thermochemical properties. Improved Benson-type increments for the estimation of enthalpies of vaporization and standard enthalpies of formation of aliphatic alcohols, J. Chem. Eng. Data 50 (2005) 1114-1124.
[11] K. F. Liu, W. T. Ziegler, Heat capacity from 80° to 300°K, melting point and heat of fusion of nitroethane, J. Chem. Eng. Data 11 (1966) 187-189.
[12]. Saunders, D. F.; Spaull, A. J. B. Total and Partial Vapour Pressures of a Series of Binary Liquid Mixtures of Organic Nitrocompounds. Z. Phys. Chem. (Munich), 1961, 28, 332- 343
[13] Marsh, K. N.; French, H. T.; Rogers, H. P. D. Excess Gibbs free energy for cyclohexane + nitromethane, + nitroethane, + 1-nitropropane, and + 2-nitropropane at 318.15 K. J. Chem. Thermodyn., 1979, 11, 897-903

7.8 Measurement of Amitone and Seven Related Derivatives

This chapter deals with the measurement of the vapor pressure of Amitone **I** and seven related derivatives (**II** – **VIII**):

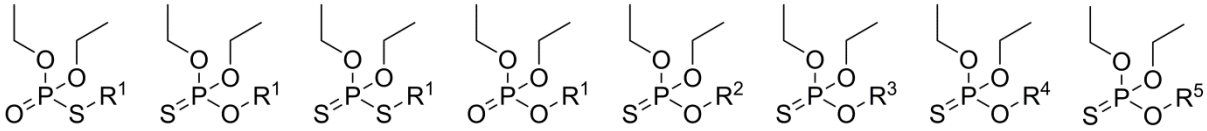

I **II** **III** **IV** **V** **VI** **VII** **VIII**

R[1]: $(CH_2)_2N(Et)_2$ **R[2]**: $(CH_2)_3N(Et)_2$ **R[3]**: $(CH_2)_2N(Me)_2$ **R[4]**: $(CH_2)_3N(Me)_2$ **R[5]**: $CH(CH_3)CH_2N(Me_2)$

The results were published in Journal of Physical Chemistry A. [1]

DOI: 10.1021/acs.jpca.7b01177

The original publication of the data follows.

1. Althoff, M. A.; Grieger, K.; Härtel, M. A. C.; Karaghiosoff, K. L.; Klapötke, T. M.; Metzulat, M., Application of the Transpiration Method To Determine the Vapor Pressure and Related Physico-Chemical Data of Low Volatile, Thermolabile, and Toxic Organo(thio)phosphates. *The Journal of Physical Chemistry A* **2017,** *121* (13), 2603-2609.

THE JOURNAL OF PHYSICAL CHEMISTRY A

Article

pubs.acs.org/JPCA

Application of the Transpiration Method To Determine the Vapor Pressure and Related Physico-Chemical Data of Low Volatile, Thermolabile, and Toxic Organo(thio)phosphates

Marc A. Althoff,[†,‡] Kathrin Grieger,[†] Martin A. C. Härtel,[†] Konstantin L. Karaghiosoff,[†] Thomas M. Klapötke,*[,†] and Manfred Metzulat[†,‡]

[†]Department of Chemistry, Ludwig Maximilian University, Butenandtstraße 9, D-81377 Munich, Germany

[‡]Chemistry Section, Science Department, CBRN Defence, Safety and Environmental Protection School, Mühlenweg 12, 87527 Sonthofen, Germany

Supporting Information

ABSTRACT: The present work represents the most recent study on the physico-chemical properties of the organophosphate compound class being directly related to the Chemical Weapons Convention (CWC). This compound class is of great importance in the ongoing conflict in Syria. Here, the vapor pressure of the deadly organo(thio)phosphate Amiton and seven of its derivatives was investigated. These medium to low volatile analytes pose a potential threat toward human life by inhalation or direct contact with the skin at very low doses. Therefore, the vapor pressures in ambient temperature regimes were measured by utilizing the transpiration method to determine the saturation vapor pressure p_{sat} and the enthalpy of vaporization $\Delta_l^g H_m^\circ$ at 298.15 K. We also successfully applied the transpiration method for the examination of thermolabile compounds. In particular, five of the molecules can undergo a thiono−thiolo rearrangement at elevated temperatures within a couple of hours and thus could possibly alter in the course of the experiment. In addition we demonstrate that the concentration under diffusion conditions, c_{dif}, is a useful parameter for the choice of suitable gas phase detection equipment for Amiton and its derivatives, because it can be directly compared with the limit of detection LOD [ng L^{-1}] of the device used. Finally, we proved the transpiration method to be applicable for the investigation of toxic and also high boiling and even thermolabile chemicals in general.

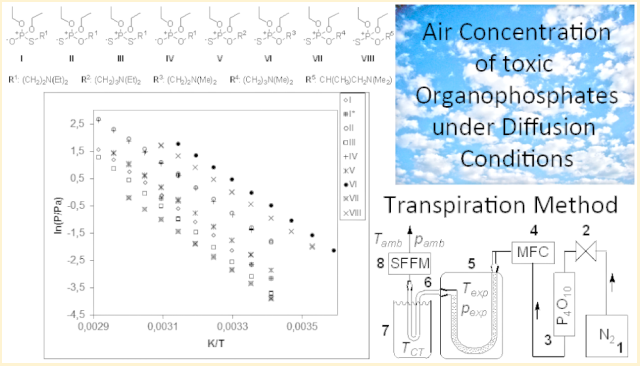

1. INTRODUCTION

The vapor pressure is the physico-chemical parameter that is linked to the saturation equilibrium concentration of the analytes to be detected from the gas phase. The knowledge of the gas phase concentration of the analyte is essential for the definition of the air volume that needs to be sampled for exceeding the limit of detection (LOD) of the applied detector system. In the case of substances being toxic or harmful by inhalation or direct contact with the skin, early detection is of great importance for obvious reasons. Such substances are primarily those listed as nerve agents or choking agents in the annexes of the Chemical Weapon Convention (CWC).[1] The molecule Amiton (I) belongs to the class of very toxic compounds which cause severe injury and even death.[2,3] Organophosphates themselves are a well-known compound class that is readily available in nature, e.g., in RNA and DNA.[4] Besides this, they have several industrial applications ranging from plasticizers and flame retardants to pesticides and chemical warfare agents.[1,5−7] Especially organo(thio)-phosphates, which are less toxic than organophosphates, can undergo a so-called thiono−thiolo rearrangement at elevated temperatures and are thus thermolabile (Figure 1).[8−10]

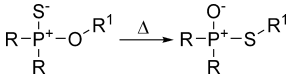

Figure 1. Minimum structural prerequisites for an organothiophosphate molecule capable of undergoing a thiono−thiolo rearrangement. R can be O-alkyl/O-aryl or O-alkyl/S-aryl; R^1 has to be alkyl.[11,12]

However, this feature of organo(thio)phosphates can have an impact on the determination of the vapor pressure data because the isomers have different vapor pressure values. Thus, measurements with isomer mixtures will result in mixed vapor pressures weighted by the molar ratio of the isomers

Received: February 6, 2017
Revised: March 9, 2017
Published: March 10, 2017

DOI: 10.1021/acs.jpca.7b01177
J. Phys. Chem. A 2017, 121, 2603−2609

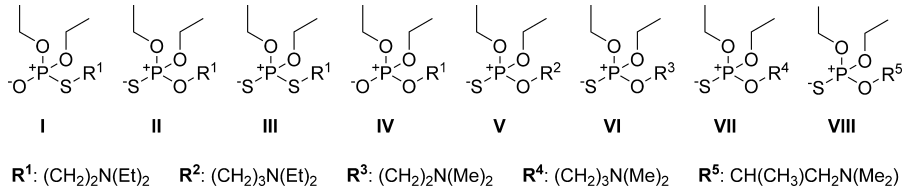

Figure 2. Chemical structures of Amiton (I) and its derivatives II–VIII. They differ from each other by (i) the variation of the configuration of the position of the chalcogens (O, S) attached to the phosphorus atom, (ii) the variation in the amino side chain by altering the spacing between the oxygen and the nitrogen atom, and (iii) the variation of the alkyl substituent of the nitrogen atom.

according to Dalton's Law of partial pressures for a binary mixture.

Today's standard mobile detection instruments of civilian and military action forces are based on, e.g., ion mobility spectroscopy or gas chromatography coupled to mass spectrometry and can thus only detect airborne substances without laborious sampling and sample pretreatment procedures.[13,14] Moreover, if the vapor pressure of a substance is very low, the compound poses only a little threat to living beings by inhalation but is therefore more persistent in the environment and causes a severe threat upon direct contact.

However, the vapor pressure data can also help to estimate a hazardous area and time frame after the release of such substances. Organo(thio)phosphates were chosen in this study because only a small number of values on the vapor pressure of pesticides and especially chemical warfare agents are reported in literature so far[15,16] and their detectability is thus hard to predict. With the ideal gas equation, the saturation concentration c_{sat} of an analyte can be calculated from its vapor pressure:

$$c_{sat} = \frac{p_{sat} \times M}{R \times T} \quad (1)$$

with c_{sat} the saturation concentration [mg L^{-1}], R the ideal gas constant (8.31446 J mol^{-1} K^{-1}), T the temperature [K], and M the molecular mass [g mol^{-1}]

The vapor pressure is an essential parameter in a multitude of models for the evaporation of droplets.[17−19] To overcome this lack of information on vapor pressure data and other physico-chemical values for Amiton, we synthesized a set of eight different molecules (Figure 2), which are structurally closely related to each other, and determined the (i) vapor pressure, p_{sat}, and (ii) and enthalpy of vaporization $\Delta_l^g H_m^\circ$(298.15 K).

Therefore, the vapor pressure in ambient temperature regimes of I (298−343 K), II (293−343 K), III (293−343 K), IV (298−343 K), V (293−338 K), VI (279−318 K), VII (293−333 K), and VIII (283−323 K) was measured with the transpiration method, which is a well-established method for the determination of vapor pressures for medium to low volatility analytes.[20−22]

This transpiration experiment has been newly established in the research group of Prof. Klapötke at the University of Munich. The method was adapted from the existing experimental setup of Prof. S. Verevkin from the University of Rostock.[20−22] The basic principle of the transpiration experiment is to saturate a well-defined carrier gas stream at a temperature T_{exp} and to measure the concentration of the analyte within. Additionally, we wanted to prove the general applicability of this method for the investigation of highly toxic and thermolabile compounds.

2. EXPERIMENTAL SECTION

2.1. Safety Aspects. Organophosphates are known to be (strong) acetylcholine esterase inhibitors and thus pose a threat toward human health and life. While handling the substances under consideration, proper PPE has to be worn, which is at least butyl rubber gloves, lab coat and safety goggles or preferably a face shield. All work has to be done in a fume cupboard. Moreover, all glassware and equipment in contact with the organo(thio)phosphates was thoroughly decontaminated by cleaning with reactive skin decontamination lotion. During the preparational part of this work an emergency medical assistant was available in the lab and a toxicological trained emergency physician was available on short notice.

2.2. Synthesis. The molecules investigated in this study were synthesized on a 40 mmol scale according to literature-known procedures[23,24] at the Chemistry Section of the CBRN Defense, Safety, and Environmental Protection School of the German Army. All reagents were of *purum* grade, and solvents were of analytical grade and were used without further purification prior to use.

The general reaction pathway is shown in Figure 3. The synthesis and isolation of the Amiton analogs follows a one-pot

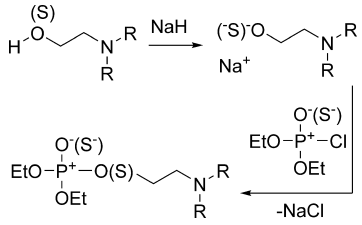

Figure 3. General schema of the one-pot two-step syntheses with R = Me, Et, according to Gupalo et al.[24]

two-step procedure: step I, formation of the (thio)alcoholate anion; step II, coupling with the chloro(thio)phosphate.

The purities and degree of isomerization were determined by either a GC-FID or HPLC−MS measurement. Because the focus of this work is the determination of the physico-chemical properties of the molecules no further details on synthetic aspects are given here. Additional information regarding the synthesis will be published separately soon or can be requested from the corresponding author in the meantime. However, it has to be noted that some of the compounds are regulated under the CWC and restrictions may be applicable.

2.3. Transpiration Method Setup. The basic concept of the transpiration method has already been established[20−22] and is realized in this work as follows: From a nitrogen tank 1 (Figure 4) the carrier gas (nitrogen, Air Liquide, Stickstoff HG flüssig, ≥99.999 vol %) is conducted through a pressure reduction valve 2 and a phosphorus pentoxide (Sicapent) drying tower. The flow rate of the carrier gas is adjusted and

DOI: 10.1021/acs.jpca.7b01177
J. Phys. Chem. A 2017, 121, 2603−2609

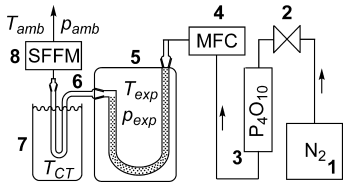

Figure 4. Transpiration method experimental setup: 1, nitrogen reservoir; 2, pressure reduction valve; 3, P_4O_{10} drying tower; 4, mass flow controller; 5, saturator; 6, condenser pipe; 7, cooling trap; 8, soap film flowmeter.

kept constant by a mass flow controller 4 (Natec Sensors MC-100 CCM) before it reaches the saturator 5, which is a cylindrical glass vessel (height 25 cm, diameter 10 cm) containing a U-shaped tube (length 50 cm, diameter 0.8 cm) filled with glass beads (diameter 1 mm). The glass beads are coated with the analyte (0.6 g) of choice by mixing of the liquid and beads in a beaker. The saturator is thermostated by a circulation thermostat (Huber Ministat 230) pumping a thermofluid (ethylene glycol (50% aqueous)) through it. At the end of the saturator the carrier gas stream reaches its saturation equilibrium with the analyte and then passes a cooling trap with the temperature T_{CT} (−30 °C). The flow rate of the carrier gas stream is measured under ambient conditions (T_{amb}, p_{amb}) with a soap film flowmeter (HP #0101−0113). The experimental time to generate one data point ranges from 15 min to 24 h. This time is needed to collect a sufficient amount of analyte (Table S5−S12) in the cooling trap to meet the requirements of the analytical instruments used for quantification.

At the end of the experiment the condenser pipe is separated from the saturator and *tert*-butyl methyl ether solvent is added together with a solution of the internal standard (*n*-alkanes C-12, C-14, or C-16) of known concentration (≈1 mg/mL). The solution of analyte and standard is then used for internal standard quantification using either a Thermo Fisher Scientific GC/FID system equipped with a TriPlus RSH autosampler or a Shimadzu VO-GC/MS[25] system equipped with an AOC-20i autosampler. The exact chromatographic setup and operational modes can be found in Supporting Information Tables S2 and S3, respectively. For an initial validation of the experimental setup the following reference compounds were chosen: naphthalene, anthracene, isoamyl acetate, *n*-hexanol, and *n*-octanol. The obtained results were compared to a large number of literature values. Detailed information on the results of this study can be found in the Supporting Information.

The transpiration method setup is suitable for the purification of the analytes during the experiment. Prior to the experiment, the analyte is conditioned by subjection to the carrier gas stream at elevated temperatures for the removal of impurities. The weight of the substance sample for the internal standard calibration was corrected by the purities stated in Table 1.

3. RESULTS AND DISCUSSION

3.1. Synthesis. All but one (VII) of the synthesized compounds have been reported in the literature before by different authors.[15,26−29] Compound V was synthesized and recently published by us for the first time among other molecules (I−IV) of this study with the basic IR, GC−MS, HPLC−MS, and ^{31}P NMR data of compounds I−V.[10] Thus, a detailed discussion can be omitted at this point. Additional information on spectroscopic and spectrometric properties of the molecules will be published soon. The purities, which are important for the vapor pressure experiment, are given in Table 1 and range from 95.07 to 99.71%. Because compounds II, III, and V−VIII have the structural prerequisites to undergo the described thiono−thiolo rearrangement at elevated temperatures (Figure 1), the degree of isomerization was checked at the beginning and end of the transpiration experiment by means of HPLC−MS (Supporting Information Table S4). In all cases the observed conversion was less than 0.5% and thus no correction of the obtained data necessary.

Table 1. Calculation of Molar Heat Capacity Differences c_{dif} at T = 298.15 K

compd	$C^{\circ}_{p,m}(l)$[a] [J mol^{-1} K^{-1}]	$\Delta^{g}_{l}C^{\circ}_{p,m}$[b] [J mol^{-1} K^{-1}]	purity[c]	T_{boil}[d]	ρ[e] [g cm^{-3}]
I	488.03	137.47	97.38	364	1.044
II	488.03	137.47	98.54	338	1.010
III	504.08	141.64	97.42	363	1.035
IV	471.98	133.29	95.07	326	1.061[33]
V	519.51	145.65	99.07	405	1.015
VI	425.07	121.10	97.88	301	1.059
VII	456.55	129.28	99.71	312[f]	1.021
VIII	456.55	129.28	96.28	387	1.034

[a]Calculated with elemental increments by Hurst et al.[34] [b]Calculated by $\Delta^{g}_{l}C^{\circ}_{p,m}$ = 10.58 + $C^{\circ}_{p,m}(l)$ × 0.26.[32] [c]Purity according to GC-FID analysis. [d]Boiling point at 101325 Pa = 1 atm. [e]Density at 293.15 K (gravimetric determination with calibrated Eppendorf pipet (100 μL)). [f]Linear estimation with $\Delta^{g}_{l}C^{\circ}_{p,m}$ = 0 due to nonconvergence of iteration process.

3.2. Determination of Vapor Pressure and Enthalpy of Vaporization. The vapor pressure of the analyte $p_{sat}(T_{exp})$ can be calculated using the Ideal Gas Law and Dalton's Law of partial pressures under the assumption that the volume of the carrier gas stream is significantly higher than that of the gaseous analyte.[20,22]

$$p_{sat}(T_{exp}) = \frac{m_a R T_{amb}}{M V_{amb}} \quad (2)$$

with p_{sat} the vapor pressure of the analyte [Pa], T_{exp} the temperature of the saturator [K], m_a the mass of analyte [kg], T_{amb} the ambient temperature [K], V_{amb} the volume of carrier gas at ambient conditions [m^3], M the molecular weight of the analyte [kg mol^{-1}], and R the universal gas constant: 8.31446 [J mol^{-1} K^{-1}].

The p_{sat}−T_{exp} values obtained for each analyte are analyzed with a fitting function based on the Clarke−Glew equation:[30]

$$\ln p_{sat}/p^{\circ} - \frac{\Delta^{g}_{l}C^{\circ}_{p,m}}{R} \ln \frac{T}{T_0} = A - \frac{B}{T} \quad (3)$$

with p° the reference pressure being 1 [Pa], $\Delta^{g}_{l}C^{\circ}_{p,m}$ the molar heat capacity difference from liquid to gaseous state [J K^{-1} mol^{-1}], T the temperature [K], T_0 the reference temperature [K], and A and B fitting coefficients (A [−], B [K]).

The enthalpy of vaporization at temperature T can be calculated by

$$\Delta^{g}_{l}H^{\circ}_{m}(T) = RB + \Delta^{g}_{l}C^{\circ}_{p,m}T \quad (4)$$

with $\Delta^{g}_{l}H^{\circ}_{m}(T)$ the molar enthalpy of vaporization [J mol^{-1}].

The heat capacities $C^{\circ}_{p,m}$ at 298.15 K of the analytes I−VIII in liquid state are calculated according to the empirical element-increment approach by Hurst et al.[34] (cf. Table 1). The

DOI: 10.1021/acs.jpca.7b01177
J. Phys. Chem. A 2017, 121, 2603−2609

Table 2. Compilation of Obtained Data on Enthalpies of Vaporization, $\Delta_l^g H_m^\circ$, and Saturation Vapor Pressures, p_{sat},[d] for Compounds I−VIII

compd[a]	method[b]	T range [K]	T_{avg} [K]	$\Delta_l^g H_m^\circ(T_{avg})$ [kJ mol^{-1}]	$\Delta_l^g H_m^\circ$(298.15 K)[c] [kJ mol^{-1}]	p_{sat}(298.15 K)[d] [Pa]	M [g mol^{-1}]
I	T	298.2−342.9	318.6	80.9 ± 0.2	83.6 ± 0.3	0.070	269.34
I[31]	na	293.2−323.2	304.3	77.0 ± 0.5	78.4 ± 0.6	0.073	269.34
I[16]	na, O	358.0−407.0	382.3	94.5	106.0	0.005	269.34
II	T	293.3−343.0	314.2	76.2 ± 0.4	78.5 ± 0.5	0.278	269.34
III	T	293.2−342.9	315.7	83.8 ± 0.2	86.3 ± 0.3	0.045	285.40
IV	T	298.2−342.9	318.4	76.5 ± 0.2	79.0 ± 0.3	0.258	253.28
V	T	293.3−338.1	318.0	78.9 ± 0.2	81.4 ± 0.3	0.100	283.37
VI	T	278.5−318.1	297.7	72.7 ± 0.2	72.7 ± 0.3	0.988	241.29
VII	T	293.3−333.1	310.9	75.2 ± 0.2	76.9 ± 0.3	0.035	255.31
VIII	T	283.4−323.1	302.5	70.9 ± 0.2	71.5 ± 0.3	0.636	255.31

[a]Citation given for literature values. [b]Methods: T, transpiration; O, equation only. [c]Enthalpies of sublimation were adjusted according to Chickos et al.[32] with $\Delta_l^g C_{p,m}^\circ$ and $C_{p,m}^\circ$(liq) according to Table 1. [d]Vapor pressure at 298.15 K, calculated according to eq 3. na: not available.

corresponding heat capacity differences with the gaseous state are calculated according to the procedures by Chickos et al.,[32] which were also used for the adjustment of the obtained enthalpies of vaporization to 298.15 K for the reason for comparability. The detailed error estimation and error calculation, which is valid for this work and its experiments was elucidated before[21] for a nearly identical experimental setup that was adapted in this work. Table 2 is a compilation of the results obtained in this work in comparison with the few available literature values of Amiton (I) concerning the vaporization enthalpies investigated at the average temperature of the measurement and the reference temperature 298.15 K.[15,16] Additionally, the vapor pressure at 298.15 K is stated. For all analytes the results obtained by the transpiration method for the absolute vapor pressures p_{sat} and thermodynamic properties of vaporization are available in Supporting Information Tables S5−S12. A condensation of the data can be achieved by a Clausius−Clapeyron plot (Figure 5) for each

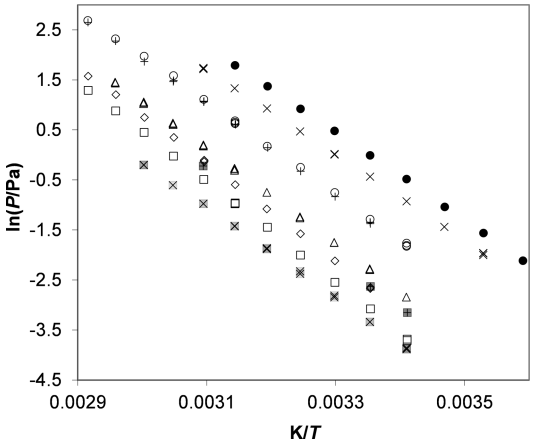

Figure 5. Clausius−Clapeyron plot of p−T data of compounds I−VIII: (◇) I + I*; (○) II; (□) III + IV; (△) V; (●) VI × VII × VIII. *Literature data were provided by Baldit.[31]

analyte and also allows a visual comparison of the results with literature data. Actually, the authors did not always derive vaporization enthalpies from their determined vapor pressures or they performed that calculation in a different manner. The literature vapor pressures were thus treated using eqs 3 and 4 and the calculated enthalpies of vaporization adjusted[32] to 298.15 K for the sake of comparison with our results (Table 2).

In terms of vapor pressure, the following observations can be made for Amiton (I) (P═O, P—S), II (P═S, P—O), III (P═S, P—S), and IV (P═O, P—O), which have different chalcogen coordinations at the phosphorus atom but the same carbon backbone. I and II only differ in the position of the sulfur atom, which is located in the P−S single bond in one and in the formal P═S double bond in II.

With respect to the octet rule, the formal P═S and P═O double bonds should be regarded as more polar P^+—S^- and P^+—O^- single bonds. II (p_{sat}(298.15 K), 0.278 Pa; $\Delta_l^g H_m^\circ$(298.15 K), 78.5 ± 0.5 kJ mol^{-1}) is more volatile than I (p_{sat}(298.15 K), 0.070 Pa; $\Delta_l^g H_m^\circ$(298.15 K), 83.6 ± 0.3 kJ mol^{-1}). This can be justified by the increased polarity of the P^+−0^- bond in I compared to that of the P^+—S^- bond in II. Increased bond polarity generally results in stronger intermolecular dipole−dipole interactions. Interestingly, compound IV (p_{sat}(298.15 K), 0.258 Pa; $\Delta_l^g H_m^\circ$(298.15 K), 79.0 ± 0.3 kJ mol^{-1}) has a vaporization behavior very similar to that of the more toxic[35] compound II. Therefore, II might be used as a precise simulant for compound IV in terms of gas phase detectability. Compound III (p_{sat}(298.15 K), 0.045 Pa; $\Delta_l^g H_m^\circ$(298.15 K), 86.3 ± 0.3 kJ mol^{-1}) has the highest molecular weight and is therefore the least volatile compound among Amiton (I) and its derivatives II−IV.

Compounds V−VIII are derivatives of compound II with identical chalcogen coordinations of the phosphorus atom (P═S, P—O). In compound V (p_{sat}(298.15 K), 0.100 Pa; $\Delta_l^g H_m^\circ$(298.15 K), 81.4 ± 0.3 kJ mol^{-1}) the alkyl bridge between the thiophosphate unit and amine functionality is extended by a CH_2 unit, which results in a lower vapor pressure and a higher (+2.9 ± 0.6 kJ mol^{-1}) enthalpy of vaporization. In compound VI (p_{sat}(298.15 K), 0.988 Pa; $\Delta_l^g H_m^\circ$(298.15 K), 72.7 ± 0.3 kJ mol^{-1}) the terminal *N*-ethyl chains are substituted with *N*-methyl substituents, which results in a higher vapor pressure and lower (−5.8 ± 0.6 kJ mol^{-1}) enthalpy of vaporization.

The difference of compound VII (p_{sat}(298.15 K), 0.035; $\Delta_l^g H_m^\circ$(298.15 K), 76.9 ± 0.3 kJ mol^{-1}) and compound VI is the length of the alkyl chain between thiophosphate and amine functionality. In compound VII it is extended by a CH_2 unit. With respect to this, the vapor pressure and enthalpy of vaporization of VII are increased (+4.2 ± 0.4 kJ mol^{-1}) in comparison to that of VI. Compound VIII (p_{sat}(298.15 K), 0.636 Pa; $\Delta_l^g H_m^\circ$(298.15 K), 71.5 ± 0.3 kJ mol^{-1}) is a branched constitutional isomer of compound VII. With respect to the reduced contact surface for van der Waals interactions of the alkyl functionalities, the vapor pressure of VIII is increased and

DOI: 10.1021/acs.jpca.7b01177
J. Phys. Chem. A 2017, 121, 2603−2609

the enthalpy of vaporization is decreased (-5.4 ± 0.4 kJ mol^{-1}) in comparison to that of VII.

For Amiton (I) one $p-T$ data set (20, 25, and 50 °C) published by Baldit[31] and one $p-T$ equation published by Stephenson et al.[16] (358–407 K) are available. In both publications the purity of the sample and the method of measurement are not stated. The data derived from the $p-T$ data published by Baldit[31] (p_{sat}(298.15 K), 0.073 Pa; $\Delta_f^g H_m^\circ$(298.15 K), 78.4 ± 0.6 kJ mol^{-1}) are in fair agreement with the values obtained in this work. Especially the literature value reported by Baldit[31] at 298.2 K (0.072 Pa) is in good agreement with the two values obtained in this work (0.071 ± 0.007 and 0.069 ± 0.007 Pa; cf. Supporting Information Table S5). The vapor pressure of I at 323.2 K (0.800 Pa) reported by Baldit[31] does not match the three values obtained in this work at 323.0 K (0.90 ± 0.03, 0.90 ± 0.03, 0.87 ± 0.03 Pa; cf. Supporting Information Table S5). Therefore, the value reported by Baldit[31] at 323.2 K is considered to be imperfect, which explains the discrepancy regarding the enthalpies of vaporization. The data derived from the $p-T$ equation published by Stephenson et al.[16] (p_{sat}(298.15 K), 0.005 Pa; $\Delta_f^g H_m^\circ$(298.15 K), 106.0 kJ mol^{-1}) do not agree with the data obtained in this work and those published by Baldit.[31]

3.3. Calculation of Concentration c_{dif} under Diffusion Conditions of Amiton Derivatives in Air. Vapor pressures are measured under ideal saturation conditions. In a real case scenario the saturation equilibrium of the analyte will not be reached and diffusion processes will dictate the air concentration of the analyte. Dravnieks et al.[36] have stated a mathematical model for the estimation of the nonequilibrium air concentration of an explosive, which is applied to compounds I–VIII in the following using the equations and values provided by Bird et al.[37]

Fick's Law of Diffusion provides a suitable approximation for the rate of molecular vapor emission J:

$$J = A \times D_{AB} \times \frac{n_c - n_a}{d} \tag{5}$$

with J the emission flux [molecules s^{-1}], A the area of analyte exposed to air [cm^2], D_{AB} the diffusivity of analyte vapor in air [cm^2 s^{-1}], n_c the concentration of analyte under saturation conditions [molecules cm^{-3}], n_a the concentration of the analyte in air [molecules cm^{-3}], and d the thickness of nonturbulent layer air [cm].

The concentration of the analyte in the air is considered to be negligibly small ($n_c - n_a \sim n_c$), and the thickness of the nonturbulent layer of air surrounding the analyte is considered to be 0.2 cm.[36]

The diffusivity D_{AB} can be calculated by the following formula:[39−41]

$$D_{AB} = 0.0018583 \frac{1}{p\sigma_{AB}^{\ 2}\Omega_{D,AB}} \sqrt{T^3\left(\frac{1}{M_A} + \frac{1}{M_B}\right)} \tag{6}$$

with T the temperature [K] (298.15 K), M_A the molecular mass of the analyte [g mol^{-1}], M_B the molecular mass of air [g mol^{-1}] (28.97 g mol^{-1}), p the total pressure [atm] (1 atm), σ_{AB} the combined collision diameter [Å], and $\Omega_{D,AB}$ the collision integral for diffusion.

$$\sigma_{AB} = (\sigma_A + \sigma_B)/2 \tag{7}$$

with σ_A the collision diameter of analyte [Å] and σ_B the collision diameter of air [Å] (3.617 Å).[37]

$$\varepsilon_{AB} = \sqrt{\varepsilon_A \varepsilon_B} \tag{8}$$

with ε_A the characteristic energy of analyte [J] and ε_B the characteristic energy of air [J].

Though the collision diameter σ_B (3.617 Å)[37] and the characteristic energy ε_B (ε_B/κ = 97.0 K)[37] of air are known, the collision diameter of the analyte σ_A and its characteristic energy ε_A have to be estimated. These values may be estimated from the liquid at the boiling point (b):

$$\varepsilon/\kappa = 1.15 T_b \qquad \sigma = 1.166 \sqrt[3]{V_b} \tag{9}$$

with T_b the boiling point [K], V_b the molar volume of the liquid at the boiling point [cm^3 mol^{-1}], and κ the Boltzmann constant (1.38065×10^{-23} J K^{-1}).

With ε_{AB} the collision integral for diffusion $\Omega_{D,AB}$ can be calculated according to

$$\Omega_{D,AB} = \frac{1.16145}{T^{*0.15610}} + \frac{0.19300}{\exp(0.47635T^*)} + \frac{1.03587}{\exp(1.52996T^*)} + \frac{1.76474}{\exp(3.89411T^*)} \tag{10}$$

where

$$T^* = \kappa T/\varepsilon_{AB}$$

with T the temperature [K].

In the case of compounds I–VIII the diffusion coefficient can be calculated from their boiling point, which is calculated by extrapolation of the $p-T$ data obtained in this work with eq 3 to the atmospheric pressure (101 325 Pa) (cf. Table 1). The molar volume V_b at the boiling point can be approximated from the density at 20 °C (cf. Table 1) using an equation that was derived from the thermal expansion of the model compound triethylphosphate[38] by linear regression of the temperature-dependent density data provided:

$$\rho_b = \rho_{20°C} - 0.0009943(T_b - 293.15) \tag{11}$$

with ρ_b the density at boiling point [g cm^{-3}] and $\rho_{20°C}$ the density at 20 °C.

The molar volume at the boiling point can be calculated by

$$V_b = M/\rho_b \tag{12}$$

With eqs 5–12 the diffusion coefficient of a liquid analyte in air can be approximated when solely its melting point and a density are known and eq 5 can be used to calculate the mass flux of material from the analyte to the air. With A = 1 cm^2, $n_a \sim$ 0, and d = 0.2 cm it can be written

$$J = \frac{D_{AB}}{0.2\ \text{cm}} \times n_c \tag{13}$$

If the concentration n_c is converted to partial pressure ($n_c = 2.47520 \times 10^{14} p$, p is the vapor pressure [Pa]) and the emission flux is converted into a mass flux (unit conversion factor: M/N_A), the mass flux can be calculated:

$$Q = 2.47520 \times 10^{14} \times D_{AB} \times p \times (M/N_A) \tag{14}$$

with Q the emission flux of analyte [g s^{-1} cm^{-2}] and N_A the Avogadro constant (6.022×10^{23} mol^{-1}).

An example of this calculation for Amiton (I) can be found in Supporing Information Table S1. With the emission flux Q in hand, the concentration of the analyte in air can be calculated:

$$c_{dif} = S \times Q \times r \tag{15}$$

DOI: 10.1021/acs.jpca.7b01177
J. Phys. Chem. A 2017, 121, 2603−2609

Table 3. Condensed Summary of the Calculated Saturation Concentration c_{sat} and Concentration under Diffusion Conditions c_{dif} for the Molecules of This Study

	compound[a]							
	I	II	III	IV	V	VI	VII	VIII
M [g mol^{-1}][b]	269.34	269.34	285.40	253.28	283.37	241.29	255.31	255.31
ρ [g cm^{-3}][c]	1.044	1.011	1.035	1.061	1.015	1.059	1.021	1.034
p_{sat} [Pa][d]	0.070	0.278	0.045	0.258	0.100	0.988	0.035	0.636
c_{sat} [ng L^{-1}][e]	7606	30205	5181	26360	11431	96166	3605	65503
c_{dif} [ng L^{-1}][f]	1.5	5.8	1.0	5.5	2.0	20.9	0.7	12.5
c_{sat}/c_{dif}	5232	5208	5424	4828	5730	4597	4899	5255

[a]Compound according to Figure 2. [b]Molar weight. [c]Density at 20 °C. [d]Vapor pressure at 25 °C. [e]Saturation concentration at 25 °C calculated according to eq 1. [f]Concentration under diffusion conditions at 25 °C calculated according to eq 15 for an exposed surface of 1 m^2.

with c_{dif} the concentration of analyte in air [g L^{-1}], S the surface of analyte exposed to air [cm^2], and r the attenuation factor (10^{-4}) [s^{-1}]. The attenuation factor r has been established in the study by Dravnieks et al.[36]

For a surface area of 1 m^2 the values for c_{dif} stated in Table 3 were obtained. These values can serve as a kind of standardized surface density if 1 m^2 is used as a reference area for the analyte under investigation. However, this value must be regarded as the maximum concentrations of analyte that can be present for detection in air in an open-exposure scenario under the given environmental conditions, e.g., temperature.

From the calculated values for the concentration under diffusion conditions, it is possible to estimate the sampling volume necessary to meet the analytical requirements of the detection instrument used. Moreover, it is possible to predict under which environmental conditions (e.g., operating temperature) it is possible to detect the analyte in the gas phase or not. Knowing this is crucial for first responders who are threatened by evaporating toxic gases. On the contrary, if the detection device is not giving an alert, one could easily be lulled into a false sense of security because the molecules investigated in this study still pose a threat to human life by being also active as a contact poison.

4. CONCLUSIONS

As a main finding of this work, the transpiration method approach was successfully applied for the determination of the vapor pressure of Amiton (I) and seven derivatives (II–VIII). Furthermore, this approach proved viable for both thermolabile and highly toxic compounds. Additionally, the concentration c_{dif} of freshly synthesized compounds I–VIII, of which compound VII has not yet been reported in the literature, was calculated on the basis of a diffusion model stated by Dravnieks et al.[36] With equations and values published by Bird et al.[37] it was possible to determine values for the concentrations c_{sat} and c_{dif}. They range from 3605 (VII) to 96 166 ng L^{-1} (VI) for c_{sat} and from 0.7 (VII) to 20.9 ng L^{-1} (VI) for c_{dif}, respectively. The ratio of c_{sat}/c_{dif} is in the range 4597–5730. A condensed summary of the values obtained is given in Table 3.

For a quick conservative estimation of c_{dif} for Amiton derivatives it is recommended to divide c_{sat} by 6000.

The concentration c_{dif} is a useful parameter for the choice of suitable gas phase detection equipment for Amiton and its derivatives because it can be directly compared with the limit of detection LOD [ng L^{-1}] of the device used.

Our results, for example, allow us now to easily estimate the necessary sampling volume, in the case of analyte enrichment from the gas phase, by dividing the limit of detection by the concentration under diffusion conditions.

■ ASSOCIATED CONTENT

Supporting Information

The Supporting Information is available free of charge on the ACS Publications website at DOI: 10.1021/acs.jpca.7b01177.

Calculation of the emission flux of Amiton, compilation of VO-GC/MS, GC-FID, and HPCL-ESI-MS parameters, detailed measurement results of the transpiration method for compounds I–VIII, reference compound measurements with the transpiration method (PDF)

■ AUTHOR INFORMATION

Corresponding Author

*T. M. Klapötke. E-mail: tmk@cup.uni-muenchen.de. Tel: +49-89-2180-77491. Fax: +49-89-2180-77492. Web: http://www.hedm.cup.uni-muenchen.de.

ORCID

Martin A. C. Härtel: 0000-0001-8247-5314

Thomas M. Klapötke: 0000-0003-3276-1157

Author Contributions

The manuscript was written through contributions of all authors.

Notes

The authors declare no competing financial interest.

■ ACKNOWLEDGMENTS

We acknowledge the collaboration between the German Armed Forces (Bundeswehr) and the Ludwig-Maximilian University (LMU) according to the official collaboration agreement between the two institutions. Financial support of this work by the LMU, the German Armed Forces, the Office of Naval Research (ONR) under grant no. ONR.N00014-16-1-2062 and the German Ministry of Education and Research (BMBF) under grant no. 13N12583 is gratefully acknowledged. We thank Prof. Sergey Verevkin (University of Rostock) for tremendous help with establishing the transpiration method at our laboratory.

■ REFERENCES

(1) OPCW. *Convention on the prohibition of the development, production, stockpiling and use of chemical weapons and on their destruction*; OPCW: The Hague, 1997.

(2) Ghosh, R. New basic esters of phosphorus-containing acids. GB738839 (A), 19/11/1952, 1952.

(3) Pirila, L. Toxicity of organophosphorus compounds. *Kem. - Kemi* **1978**, *5* (9), 374–376.

(4) Ghosh, A.; Bansal, M. A glossary of DNA structures from A to Z. *Acta Crystallogr., Sect. D: Biol. Crystallogr.* **2003**, *59* (4), 620–626.

(5) Levchik, S. V.; Weil, E. D. A Review of Recent Progress in Phosphorus-based Flame Retardants. *J. Fire Sci.* **2006**, *24*, 345−364.
(6) Wypych, G. *Handbook of Plasticizers*; ChemTec Publishing: Norwich, NY, 2004.
(7) Fest, C.; Schmidt, K. J. *The Chemistry of Organophosphorus Pesticides*; Springer: Berlin, Heidelberg, 2012.
(8) Kuntsivich, A. D.; Golovkov, V. F.; Kusnetsova, N. B.; Kuznetsov, P. E.; Ivanov, K. N.; Kozyreva, A. V. Thion-thiol izomerization mechanism investigation of thion-derivatives of phosphoric acids. *Dokl. Akad. Nauk* **1996**, *346* (3), 350−352.
(9) Paudyal, B. P. Organophosphorus Poisoning. *J. Nepal Med. Assoc.* **2008**, *47* (4), 251−258.
(10) Althoff, M. A.; Bertsch, A.; Metzulat, M.; Kalthoff, O.; Karaghiosoff, K. *Phosphorus, Sulfur Silicon Relat. Elem.* **2017**, *192*, 149−156.
(11) Schaumann, E.; Akai, S. *Sulfur-Mediated Rearrangements I*; Springer: Berlin, 2007.
(12) Schaumann, E. *Sulfur-Mediated Rearrangements II*; Springer: Berlin, 2007.
(13) Giannoukos, S.; Brkic, B.; Taylor, S.; Marshall, A.; Verbeck, G. F. Chemical Sniffing Instrumentation for Security Applications. *Chem. Rev.* **2016**, *116* (14), 8146−8172.
(14) Gałuszka, A.; Migaszewski, Z. M.; Namieśnik, J. Moving your laboratories to the field − Advantages and limitations of the use of field portable instruments in environmental sample analysis. *Environ. Res.* **2015**, *140*, 593−603.
(15) Baldit, G. L. Amiton - a New Acaricide and Scalicide. *J. Sci. Food Agric.* **1958**, *9* (8), 516−524.
(16) Stephenson, R. M.; Malanowski, S.; Ambrose, D. *Handbook of the thermodynamics of organic compounds*; Elsevier: Amsterdam, 1987.
(17) Birdi, K. S.; Vu, D. T.; Winter, A. A study of the evaporation rates of small water drops placed on a solid surface. *J. Phys. Chem.* **1989**, *93* (9), 3702−3703.
(18) Charlesworth, D. H.; Marshall, W. R. Evaporation from drops containing dissolved solids. *AIChE J.* **1960**, *6* (1), 9−23.
(19) Melnikov, N. N. *Residue reviews: residues of pesticides and other foreign chemicals in foods and feeds*; With cumulative table of subjects covered, detailed subject-matter index, and author index of volumes *31−40*; Springer: Berlin, 1971; Vol. 40.
(20) Emel'yanenko, V. N.; Verevkin, S. P. Benchmark thermodynamic properties of 1,3-propanediol: Comprehensive experimental and theoretical study. *J. Chem. Thermodyn.* **2015**, *85*, 111−119.
(21) Verevkin, S. P.; Sazonova, A. Y.; Emel'yanenko, V. N.; Zaitsau, D. H.; Varfolomeev, M. A.; Solomonov, B. N.; Zherikova, K. V. Thermochemistry of Halogen-Substituted Methylbenzenes. *J. Chem. Eng. Data* **2015**, *60* (1), 89−103.
(22) Verevkin, S. P. 2 Phase changes in purecomponent systems: Liquids and gases. In *Experimental Thermodynamics*; Weir, R. D., Loos, T. W. D., Eds.; Elsevier: Amsterdam, 2005; Vol. 7, pp 5−30.
(23) Timperley, C. *Best Synthetic Methods: Organophosphorus (V) Chemistry*; Elsevier Science: Amsterdam, 2014.
(24) Gupalo, A. P.; Khmilevskaya, M. I.; Tsepukh, N. E. Thiophosphoric Acid Amino Esters 0.6. Reaction of Monoethanolamine with Thiophosphoric Acid-Chlorides. *Zh. Obshch. Khim.* **1979**, *49* (1), 93−97.
(25) de Zeeuw, J.; Reese, S.; Cochran, J.; Grossman, S.; Kane, T.; English, C. Simplifying the setup for vacuum-outlet GC: Using a restriction inside the injection port. *J. Sep. Sci.* **2009**, *32* (11), 1849−1857.
(26) Cadogan, J. I. G.; Thomas, L. C. the Reactivity of Organophosphorus Compounds 0.3. The Decomposition of 2-Diethylaminoethyl Diethyl Phosphate and of S-2-Diethylaminoethyl Diethyl Phosphorothioate (Amiton). *J. Chem. Soc.* **1960**, *0*, 2248−2252.
(27) Schrader, G. Verfahren zur Herstellung von Thiono-thiolphosphorsaeuretriestern. DE951717 C 1956.
(28) Tammelin, L. E. ISOMERISATION OF OMEGA-DIMETHYLAMINOETHYL-DIETHYL-THINOPHOSPHATE. *Acta Chem. Scand.* **1957**, *11* (10), 1738−1744.
(29) Fitch, H. M. Quaternary ammonium salts of dialkylaminoalkyl thiophosphate esters. GB819735, 1959.
(30) Clarke, E. C. W.; Glew, D. N. Evaluation of thermodynamic functions from equilibrium constants. *Trans. Faraday Soc.* **1966**, *62* (0), 539−547.
(31) Baldit, G. L. Amiton—a new acaricide and scalicide. *J. Sci. Food Agric.* **1958**, *9* (8), 516−524.
(32) Acree, W.; Chickos, J. S. Phase Transition Enthalpy Measurementsof Organic and Organometallic Compounds. Sublimation, Vaporizationand Fusion Enthalpies From 1880 to 2010. *J. Phys. Chem. Ref. Data* **2010**, *39* (4), 043101.
(33) Malinovskii, M. S.; Solomko, Z. F.; Yurilina, L. M. Reaction of dialkylaminoethanols with esters of phosphoric and thiophosphoric acids. *Zh. Obshch. Khim.* **1960**, *30*, 3454−6.
(34) Hurst, J. E.; Harrison, B. K. ESTIMATION OF LIQUID AND SOLID HEAT CAPACITIES USING A MODIFIED KOPP'S RULE. *Chem. Eng. Commun.* **1992**, *112* (1), 21−30.
(35) Zhuang, X.-M.; Wei, X.; Tan, Y.; Xiao, W.-B.; Yang, H.-Y.; Xie, J.-W.; Lu, C.; Li, H. Contribution of Carboxylesterase and Cytochrome P450 to the Bioactivation and Detoxification of Isocarbophos and Its Enantiomers in Human Liver Microsomes. *Toxicol. Sci.* **2014**, *140* (1), 40−48.
(36) Dravnieks, A.; Brabets, R.; Stanley, T. A. *Evaluating Sensitivity Requirements of Explosive Vapor Detector Systems*; IIT Research Institute Technology Center: Chicago, IL, 1972.
(37) Bird, R. B.; Stewart, W. E.; Lightfoot, E. N. *Transport Phenomena*; John Wiley & Sons, Inc.: New York, 2002.
(38) Vogel, A. I.; Cowan, D. M. 8. Physical properties and chemical constitution. Part VII. Alkyl sulphides, disulphides, sulphites, sulphates, and orthophosphates. *J. Chem. Soc.* **1943**, *0*, 16−24.
(39) Chapman, S.; Cowling, T. G. *The MathematicaI Theory of Non-Uniform Gases*, 3rd ed.; Cambridge University Press: Cambridge, U.K., 1970; Chapters 10 and 14.
(40) Hirschfelder, J. O.; Curtiss, C. F.; Bird, R. B. *Molecular Theory of Gases and Liquids*, 2nd corrected printing; Wiley, New York, 1964; p 539.
(41) Cussler, E. L. *Diffusion − Mass Transfer in Fluid Systems*; Cambridge University Press: Cambridge/New York, 1997.

DOI: 10.1021/acs.jpca.7b01177
J. Phys. Chem. A 2017, 121, 2603−2609

Supporting Information

Application of the Transpiration Method to Determine the Vapor Pressure and Related Physico-Chemical Data of Low Volatile, Thermolabile and Toxic Organo(thio)phosphates

Marc A. Althoff[a,b], Kathrin Grieger[a], Martin A. C. Härtel[a], Konstantin L. Karaghiosoff[a], Thomas M. Klapötke*[,a], Manfred Metzulat[a,b]

[a]Ludwig Maximilian University, Department of Chemistry, Butenandtstr. 9, D-81377 Munich

[b]Chemistry Section, Science Department, CBRN Defence, Safety and Environmental Protection School, Mühlenweg 12, 87527 Sonthofen, Germany

Contents

1 Calculation of the emission flux of Amiton I 2

2 Compilation of VO-GC/MS parameters 3

3 Compilation of GC-FID parameters 4

4 Compilation of HPLC-ESI-MS parameters 5

5 Detailed Measurement Results of the Transpiration Method 6

5.1 Compound I 6

5.2 Compound II 7

5.3 Compound III 8

5.4 Compound IV 9

5.5 Compound V 10

5.6 Compound VI 11

5.7 Compound VII 12

5.8 Compound VIII 13

6 Reference Compound Measurements 14

6.1 Naphthalene 17

6.2 Anthracene 20

6.3 *iso*-amyl acetate 24

6.4 n-Hexanol 27

6.5 n-Octanol 31

6.6 Purity of used Chemicals 34

6.7 Compilation of Heat Capacities and Heat Capacity Differences 35

7 Literature References 36

1 Calculation of the emission flux of Amiton I

Table S1: Example of calculation for the emission flux of Amiton I at STP conditions (298.2 K, 1 atm).

	Amiton I	**Unit**
T_b	636.98[a]	K
ρ_{20}	1.044[a]	g cm^{-3}
ρ_m	0.702	g cm^{-3}
M	222.237	g mol^{-1}
V_m	383.444	cm^3 mol^{-1}
σ_A	8.470	Å
ε_B/κ	732.527	K
σ_{AB}	6.044	Å
ε_{AB}/κ	266.561	K
$\kappa T/\varepsilon_{AB}$	1.118	[]
$\Omega_{D,AB}$	1.365	[]
D_{AB}	0.038	cm^2 s^{-1}
p_{sat}	0.070	Pa
Q	1.454	ng/cm² s

[a] value obtained in this work

2 Compilation of VO-GC/MS parameters

Table S2: Compilation of VO-GC/MS parameters

GC/MS	*Shimadzu QP2010SE*® with LabSolution GCMSsolution v4.11
injector	Atas Optic 4 with Evolution Workstation v4.1
liner	10 mm V2A stainless steel tube, 5 mm wall thickness, equipped with silanized glass wool (2 mm injection needle penetration into wool)
restriction	0.025 mm capillary, 8.11 mm length (Restek #10097)
column connector	*SGE Siltite µ-Union*® (Restek #073562)
analytical column	*Restek RTX-TNT 1*® (6 m, 0.53 mm, 1.5 µm)
oven program	40 °C (hold 0.10 min) → 280 °C (rate 60 °C min^{-1})
injector head pressure	472 kPa
virtual column	100 m, 0.25 µm film thickness, 0.20 mm i.d. (entry for GCMSsolution)
column flow	2.33 mL min^{-1} (calculated according to [1])
split ratio	18.7 (entered in LabSolutions GCMSsolution)
purge flow	5 mL min^{-1}
injection volume	1 µL
ion source	250 °C
MS interface	250 °C
MS	SCAN (for purity check): 30-500 amu event-time 300 ms SIM (for quantification): 1 quantification (strongest relative intensity) + 3 reference ion channels, event time 100 ms, time-dependent program for analyte and internal standard

3 Compilation of GC-FID parameters

Table S3: Compilation of GC-FID parameters

GC/FID	*Thermo Fisher Scientific Trace 1310* operated via *Chromeleon* Data Handling Software V. 7.2 SR 4
autosampler	TriPlus RSH with syringe tool, tray holder, and standard wash station
injector	PTV, temperature 200 °C
liner	4 mm V2A stainless steel tube
analytical column	*Agilent* J&W GC columns, CP-Sil 8, low bleed/MS (30m, 0,25mm, 0,25µm)
oven program	40 °C (hold 1 min) → 260 °C (rate 20 °C / min)
column flow	1 mL / min
split ratio	1/20
purge flow	5.0 mL / min
injection volume	1 µL
detector temperature	280 °C

4 Compilation of HPLC-ESI-MS parameters

Table S4: Compilation of HPLC-ESI-MS parameters

HPLC-ESI-MS	*Thermo Fisher Scientific* DIONEX UltiMate™ 3000HPLC System equipped with a SRD-3400 (4-channel degasser) Solvent Racks, HPG-3400SD gradient pump, WPS-3000TSL (Analytical) Autosampler, TCC-3000SD column oven, DAD-3000 Photometer , MSQ-Plus mass detector operated via *Chromeleon* Data Handling Software V. 7.2 SR 4
mobile Phase	Gradient A: H_2O/MeOH 95/5 + 0.4mM ammonium acetate Gradient B: H_2O/MeOH 5/95 + 0.4mM ammonium acetate
gradient	0 Min 100% A, 8-12 Min 25% A, 12-20 Min 100% A
flow	0.3 mL/min
sample temperature	20 °C
analysis time	20 min
Column type	Accucore RP-MS column (3.0 x 150.0 mm, particle size 2.6 µm Thermo Scientific Part.No.17626-153030)
column temperature	30 °C
ionization mode	ESI
temperature	400 °C
MS	Full Scans: 50-350m/z +ve ConeVoltage: 30/50/80 V

5 Detailed Measurement Results of the Transpiration Method

For all following tables a common footnote has to be applied:

[a] Saturation temperature ($u(T)$ = 0.1 K). [b] Mass of transferred sample condensed at T = 243 K [c] Volume of nitrogen ($u(V)$ = 0.005 dm^3) used to transfer m ($u(m)$ = 0.0001 g) of the sample. [d] T_a is the temperature of the soap bubble meter used for measurement of the gas flow. [e] Vapor pressure at temperature T, calculated from the m and the residual vapor pressure at the condensation temperature calculated by an iteration procedure; p°=1 Pa. [f] Standard uncertainty in p was calculated with $u(p/\text{Pa}) = 0.025+0.025(p/\text{Pa})$ for p > 5 to 3000 Pa and $u(p/\text{Pa}) = 0.005+0.025(p/\text{Pa})$ for p < 5 Pa.

5.1 Compound I

Table S5 Compound I: absolute vapor pressures $\boldsymbol{p_{sat}}$ and thermodynamic properties of vaporization obtained by the transpiration method in this work.

Compound I: $\Delta_l^g H_m^\circ$ (298.15 K) = 83.6 ± 0.3 kJ mol^{-1}

$$\ln p_{sat}/p^\circ = \frac{395.8}{R} - \frac{124623.0}{RT} + \frac{137.5}{R} ln \frac{T}{298.15\text{K}}$$

T_{exp} [a]	m [b]	V_{N2} [c]	T_{amb} [d]	Gasflow	p_{sat} [e]	$u(p_{sat})$ [f]	$\Delta_l^g H_m^\circ$	$\Delta_l^g S_m^\circ$
[K]	[mg]	[dm³]	[K]	[dm³ h^{-1}]	[Pa]	[Pa]	[kJ mol^{-1}]	[J mol^{-1} K^{-1}]
298.2	0.33	43.4	300.3	2.98	0.071	0.007	83.64	162.8
298.2	0.28	37.0	300.1	2.65	0.069	0.007	83.63	162.6
303.1	0.19	14.4	300.9	4.81	0.12	0.01	82.95	160.3
308.1	0.26	11.9	301.5	4.84	0.21	0.01	82.27	158.2
313.2	0.19	5.18	301.1	5.18	0.34	0.01	81.57	155.8
318.0	0.17	2.84	299.9	4.87	0.55	0.02	80.90	153.7
323.0	0.17	1.78	299.9	4.86	0.90	0.03	80.22	151.7
323.0	0.29	3.01	300.6	4.02	0.90	0.03	80.22	151.7
323.0	0.25	2.67	300.7	4.01	0.87	0.03	80.22	151.5
328.0	0.17	1.13	299.8	4.86	1.42	0.04	79.54	149.7
332.9	0.18	0.786	300.3	3.14	2.11	0.06	78.85	147.3
337.9	0.41	1.15	301.7	3.14	3.33	0.09	78.17	145.6
342.9	0.46	0.889	302.3	3.14	4.83	0.13	77.48	143.3

5.2 Compound II

Table S6: Compound II: absolute vapor pressures p_{sat} and thermodynamic properties of vaporization obtained by the transpiration method in this work.

Compound II: $\Delta_l^g H_m^\circ$ (298.15 K) = 78.5 ± 0.5 kJ mol^{-1}

$$\ln p_{sat}/p^\circ = \frac{390.0}{R} - \frac{119442.7}{RT} + \frac{137.5}{R} ln \frac{T}{298.15K}$$

T_{exp} [a]	m [b]	V_{N2} [c]	T_{amb} [d]	Gasflow	p_{sat} [e]	$u(p_{sat})$ [f]	$\Delta_l^g H_m^\circ$	$\Delta_l^g S_m^\circ$
[K]	[mg]	[dm³]	[K]	[dm³ h^{-1}]	[Pa]	[Pa]	[kJ mol^{-1}]	[J mol^{-1} K^{-1}]
293.3	0.15	8.20	296.1	2.86	0.171	0.009	79.13	159.4
293.3	0.12	6.78	296.2	3.60	0.164	0.009	79.13	159.0
293.3	0.15	8.38	295.9	2.86	0.161	0.009	79.13	158.9
298.2	0.14	4.71	296.1	2.88	0.276	0.012	78.45	156.6
303.2	0.15	2.87	296.5	2.87	0.470	0.017	77.77	154.5
308.1	0.29	3.35	297.0	2.88	0.780	0.025	77.08	152.4
313.1	0.25	1.92	297.4	2.88	1.19	0.03	76.40	149.7
318.1	0.25	1.15	297.0	2.86	1.97	0.05	75.72	148.0
318.1	0.24	1.15	297.1	2.87	1.92	0.05	75.72	147.7
318.1	0.23	1.15	296.9	2.86	1.88	0.05	75.72	147.6
318.1	0.24	1.20	297.1	2.87	1.87	0.05	75.72	147.5
323.1	0.35	1.05	296.5	2.86	3.03	0.08	75.03	145.8
328.0	0.63	1.18	296.4	2.83	4.88	0.13	74.35	144.1
333.0	1.23	1.56	296.5	2.84	7.19	0.20	73.66	141.9
338.0	1.06	0.950	296.6	2.85	10.2	0.3	72.98	139.5
343.0	1.14	0.711	296.7	2.84	14.7	0.4	72.29	137.4

5.3 Compound III

Table S7: Compound III: absolute vapor pressures p_{sat} and thermodynamic properties of vaporization obtained by the transpiration method in this work.

Compound III: $\Delta_l^g H_m^\circ$ (298.15 K) = 86.3 ± 0.3 kJ mol^{-1}

$$\ln p_{sat}/p^\circ = \frac{405.1}{R} - \frac{128482.1}{RT} + \frac{141.6}{R} ln \frac{T}{298.15K}$$

T_{exp} [a] [K]	m [b] [mg]	V_{N2} [c] [dm³]	T_{amb} [d] [K]	Gasflow [dm³ h^{-1}]	p_{sat} [e] [Pa]	$u(p_{sat})$ [f] [Pa]	$\Delta_l^g H_m^\circ$ [kJ mol^{-1}]	$\Delta_l^g S_m^\circ$ [J mol^{-1} K^{-1}]
293.2	0.023	7.75	296.9	3.87	0.025	0.006	86.96	170.3
293.2	0.024	8.59	296.6	3.12	0.024	0.006	86.96	170.0
298.1	0.025	4.65	296.5	3.10	0.046	0.006	86.25	168.0
303.1	0.048	5.29	297.2	3.11	0.078	0.007	85.55	165.3
308.1	0.024	1.56	297.3	3.12	0.13	0.01	84.84	163.0
313.1	0.28	10.4	295.9	3.10	0.24	0.01	84.14	161.0
318.1	0.23	5.23	297.1	3.11	0.38	0.01	83.43	158.6
318.1	0.051	1.16	297.7	3.88	0.38	0.01	83.43	158.5
318.1	0.051	1.17	297.6	3.89	0.38	0.01	83.43	158.5
318.1	0.050	1.16	297.6	3.87	0.38	0.01	83.43	158.5
323.0	0.26	3.64	297.5	3.12	0.61	0.02	82.73	156.3
328.0	0.23	2.08	297.5	3.12	0.98	0.03	82.02	154.1
333.0	0.35	1.91	296.6	3.10	1.57	0.04	81.32	152.2
338.0	0.33	1.19	297.0	3.10	2.41	0.07	80.61	150.1
342.9	0.48	1.14	295.9	3.10	3.62	0.10	79.91	148.0

5.4 Compound IV

Table S8: Compound IV: absolute vapor pressures p_{sat} and thermodynamic properties of vaporization obtained by the transpiration method in this work.

IV: $\Delta_l^g H_m^\circ$ (298.15 K) = 79.0 ± 0.3 kJ mol^{-1}

$$\ln p_{sat}/p^\circ = \frac{387.0}{R} - \frac{118746.4}{RT} + \frac{133.3}{R} ln \frac{T}{298.15\text{K}}$$

T_{exp}[a]	m[b]	V_{N2}[c]	T_{amb}[d]	Gasflow	p_{sat}[e]	$u(p_{sat})$[f]	$\Delta_l^g H_m^\circ$	$\Delta_l^g S_m^\circ$
[K]	[mg]	[dm³]	[K]	[dm³ h^{-1}]	[Pa]	[Pa]	[kJ mol^{-1}]	[J mol^{-1} K^{-1}]
298.2	1.30	49.1	296.4	3.00	0.26	0.01	79.00	158.0
298.2	1.17	45.2	297.4	2.98	0.25	0.01	79.00	157.8
298.2	0.52	19.3	297.4	3.95	0.26	0.01	79.00	158.0
303.1	0.23	5.16	297.2	3.01	0.43	0.02	78.34	155.8
308.1	0.38	5.19	296.5	2.99	0.72	0.02	77.68	153.7
313.0	0.24	2.00	296.8	3.01	1.15	0.03	77.02	151.5
318.0	0.49	2.61	298.0	3.02	1.84	0.05	76.36	149.5
318.1	0.53	2.79	298.4	5.08	1.85	0.05	76.35	149.5
323.0	0.58	1.95	298.9	5.08	2.92	0.08	75.69	147.5
323.0	0.47	1.61	298.9	4.02	2.89	0.08	75.69	147.4
323.0	0.47	1.61	298.9	4.02	2.89	0.08	75.69	147.4
323.1	0.50	1.68	298.4	4.02	2.89	0.08	75.69	147.4
323.1	0.57	1.93	298.3	3.04	2.88	0.08	75.69	147.4
328.0	1.14	2.54	299.5	5.07	4.43	0.12	75.03	145.4
328.1	1.01	2.28	298.4	3.04	4.32	0.11	75.02	145.1
333.0	1.17	1.79	299.8	3.06	6.45	0.19	74.36	143.1
338.0	1.16	1.17	299.8	3.05	9.73	0.27	73.70	141.2
342.9	1.09	0.755	298.8	3.02	14.12	0.38	73.04	139.3

5.5 Compound V

Table S9: Compound V: absolute vapor pressures p_{sat} and thermodynamic properties of vaporization obtained by the transpiration method in this work.

V: $\Delta_l^g H_m^\circ$ (298.15 K) = 81.4 ± 0.3 kJ mol^{-1}

$$\ln p_{sat}/p^\circ = \frac{399.6}{R} - \frac{124860.5}{RT} + \frac{145.7}{R} ln \frac{T}{298.15K}$$

T_{exp} [a]	m [b]	V_{N2} [c]	T_{amb} [d]	Gasflow	p_{sat} [e]	$u(p_{sat})$ [f]	$\Delta_l^g H_m^\circ$	$\Delta_l^g S_m^\circ$
[K]	[mg]	[dm³]	[K]	[dm³ h^{-1}]	[Pa]	[Pa]	[kJ mol^{-1}]	[J mol^{-1} K^{-1}]
293.3	0.041	6.23	299.8	3.06	0.058	0.006	82.15	160.7
298.2	0.040	3.43	299.2	2.39	0.10	0.01	81.42	158.4
298.2	0.043	3.75	298.0	3.63	0.10	0.01	81.42	158.3
298.2	0.041	3.57	299.5	3.06	0.10	0.01	81.42	158.2
303.2	0.041	2.10	300.4	3.07	0.17	0.01	80.70	155.8
303.2	0.041	2.10	300.1	3.07	0.17	0.01	80.70	155.8
308.2	0.042	1.28	300.2	3.08	0.29	0.01	79.97	153.5
308.2	0.041	1.28	300.3	3.08	0.28	0.01	79.97	153.3
313.2	0.041	0.770	300.5	3.08	0.47	0.02	79.25	151.1
318.1	0.11	1.20	296.3	3.00	0.76	0.02	78.53	148.9
318.2	0.14	1.62	298.4	3.04	0.76	0.02	78.52	148.8
318.2	0.067	0.771	300.7	3.08	0.76	0.02	78.52	148.8
318.2	0.067	0.772	300.5	3.09	0.76	0.02	78.52	148.8
318.1	0.064	0.763	298.3	3.05	0.74	0.02	78.52	148.6
318.2	0.064	0.772	300.4	3.09	0.73	0.02	78.52	148.5
323.1	0.11	0.801	297.0	3.00	1.22	0.04	77.80	146.7
323.1	0.14	1.016	299.1	3.05	1.21	0.04	77.80	146.6
323.1	0.10	0.764	299.1	3.06	1.19	0.03	77.80	146.5
328.1	0.16	0.762	299.6	3.05	1.89	0.05	77.07	144.4
328.1	0.17	0.800	296.7	3.00	1.87	0.05	77.07	144.4
328.1	0.16	0.768	299.5	3.07	1.83	0.05	77.07	144.2
333.1	0.25	0.750	296.9	3.00	2.88	0.08	76.35	142.3
333.1	0.25	0.765	300.1	3.06	2.85	0.08	76.35	142.2
333.1	0.24	0.770	300.3	3.08	2.78	0.07	76.35	142.0
338.1	0.37	0.771	300.2	3.08	4.28	0.11	75.62	140.1
338.1	0.37	0.775	300.8	3.10	4.24	0.11	75.62	140.0
338.1	0.37	0.770	300.4	3.08	4.20	0.11	75.62	139.9

5.6 Compound VI

Table S10: Compound VI: absolute vapor pressures p_{sat} and thermodynamic properties of vaporization obtained by the transpiration method in this work.

Compound VI: $\Delta_l^g H_m^\circ$ (298.15 K) = 72.7 ± 0.3 kJ mol^{-1}

$$\ln p_{sat}/p^\circ = \frac{364.7}{R} - \frac{108756.3}{RT} + \frac{121.1}{R} ln \frac{T}{298.15K}$$

T_{exp} [a]	m [b]	V_{N2} [c]	T_{amb} [d]	Gasflow	p_{sat} [e]	$u(p_{sat})$ [f]	$\Delta_l^g H_m^\circ$	$\Delta_l^g S_m^\circ$
[K]	[mg]	[dm³]	[K]	[dm³ h^{-1}]	[Pa]	[Pa]	[kJ mol^{-1}]	[J mol^{-1} K^{-1}]
278.5	0.18	15.4	300.4	2.64	0.12	0.01	75.03	156.1
283.3	0.28	14.0	301.3	4.01	0.21	0.01	74.44	154.0
288.3	0.26	7.72	300.4	3.62	0.35	0.01	73.85	151.8
293.3	0.72	12.1	300.1	3.96	0.62	0.02	73.24	150.0
298.2	0.52	5.41	300.8	4.01	0.99	0.03	72.64	147.8
303.2	0.57	3.63	299.5	3.97	1.62	0.05	72.04	145.9
308.1	0.49	2.00	298.4	3.99	2.50	0.07	71.44	143.8
313.1	0.51	1.34	300.4	4.01	3.94	0.10	70.85	142.0
318.1	0.58	0.995	299.3	3.98	5.98	0.17	70.24	140.0

5.7 Compound VII

Table S11: Compound VII: absolute vapor pressures p_{sat} and thermodynamic properties of vaporization obtained by the transpiration method in this work.

VII: $\Delta_l^g H_m^\circ$ (298.15 K) = 76.9 ± 0.3 kJ mol^{-1}

$$\ln p_{sat}/p^\circ = \frac{359.5}{R} - \frac{115475.8}{RT} + \frac{129.3}{R} ln \frac{T}{298.15K}$$

T_{exp} [a]	m [b]	V_{N2} [c]	T_{amb} [d]	Gasflow	p_{sat} [e]	$u(p_{sat})$ [f]	$\Delta_l^g H_m^\circ$	$\Delta_l^g S_m^\circ$
[K]	[mg]	[dm³]	[K]	[dm³ h^{-1}]	[Pa]	[Pa]	[kJ mol^{-1}]	[J mol^{-1} K^{-1}]
293.3	0.0066	3.01	296.8	3.01	0.021	0.006	77.56	136.7
293.3	0.0064	3.00	297.0	3.60	0.021	0.006	77.56	136.5
293.3	0.0090	4.25	299.3	3.64	0.021	0.006	77.56	136.5
293.3	0.0066	3.12	297.0	4.16	0.021	0.006	77.56	136.5
298.2	0.011	3.03	299.3	3.64	0.035	0.006	76.92	134.4
298.2	0.0070	1.92	296.8	3.59	0.035	0.006	76.92	134.4
303.2	0.011	1.80	296.6	3.60	0.060	0.006	76.28	132.5
303.2	0.0072	1.20	297.0	3.59	0.058	0.006	76.28	132.2
308.2	0.012	1.20	298.0	3.60	0.10	0.01	75.64	130.4
308.2	0.0086	0.901	297.4	3.60	0.09	0.01	75.63	129.9
313.2	0.014	0.904	298.3	3.62	0.15	0.01	74.99	128.2
313.2	0.014	0.905	298.4	3.62	0.15	0.01	74.99	128.2
313.2	0.014	0.903	298.0	3.61	0.15	0.01	74.99	128.1
318.1	0.022	0.905	299.1	3.62	0.24	0.01	74.35	126.2
318.1	0.022	0.909	299.2	3.63	0.24	0.01	74.35	126.1
323.1	0.035	0.906	299.2	3.62	0.38	0.01	73.70	124.3
323.1	0.035	0.913	299.2	3.65	0.38	0.01	73.70	124.3
328.1	0.051	0.912	299.6	3.65	0.55	0.02	73.06	121.9
333.1	0.077	0.915	300.2	3.66	0.82	0.03	72.42	120.0
333.1	0.076	0.913	300.2	3.65	0.82	0.03	72.42	120.0
333.1	0.077	0.919	300.4	3.67	0.82	0.03	72.42	120.0

5.8 Compound VIII

Table S12: Compound VIII: absolute vapor pressures p_{sat} and thermodynamic properties of vaporization obtained by the transpiration method in this work.

Compound VIII: $\Delta_l^g H_m^\circ$ (298.15 K) = 71.5 ± 0.3 kJ mol^{-1}

$$\ln p_{sat}/p^\circ = \frac{365.2}{R} - \frac{110006.2}{RT} + \frac{129.3}{R} ln \frac{T}{298.15K}$$

T_{exp} [a]	m [b]	V_{N2} [c]	T_{amb} [d]	Gasflow	p_{sat} [e]	$u(p_{sat})$ [f]	$\Delta_l^g H_m^\circ$	$\Delta_l^g S_m^\circ$
[K]	[mg]	[dm³]	[K]	[dm³ h^{-1}]	[Pa]	[Pa]	[kJ mol^{-1}]	[J mol^{-1} K^{-1}]
283.4	0.020	1.40	295.0	2.81	0.13	0.01	73.37	146.6
283.4	0.022	1.50	295.4	3.34	0.14	0.01	73.37	146.9
283.4	0.020	1.36	295.6	2.20	0.14	0.01	73.37	146.8
288.3	0.022	0.885	295.5	2.80	0.24	0.01	72.73	144.6
293.3	0.029	0.698	295.6	2.79	0.39	0.01	72.09	142.4
298.2	0.047	0.699	295.5	2.79	0.65	0.02	71.45	140.3
303.2	0.074	0.698	295.6	2.79	1.02	0.03	70.81	138.0
303.2	0.074	0.699	295.6	2.80	1.02	0.03	70.81	138.0
303.2	0.073	0.698	295.6	2.79	1.00	0.03	70.81	137.9
308.2	0.11	0.694	295.8	2.78	1.60	0.04	70.17	135.8
313.1	0.18	0.692	295.7	2.77	2.53	0.07	69.52	134.0
318.1	0.27	0.691	295.9	2.76	3.79	0.10	68.88	131.9
323.1	0.40	0.687	295.7	2.75	5.61	0.17	68.23	129.8
323.1	0.40	0.687	295.8	2.75	5.68	0.17	68.23	129.9
323.1	0.40	0.689	295.9	2.76	5.56	0.16	68.23	129.7

6 Reference Compound Measurements

As stated in the main document an initial validation of the experimental setup the following reference compounds were chosen: naphthalene, anthracene, *iso*-amyl acetate, n-hexanol and n-octanol. (see Figure S1)

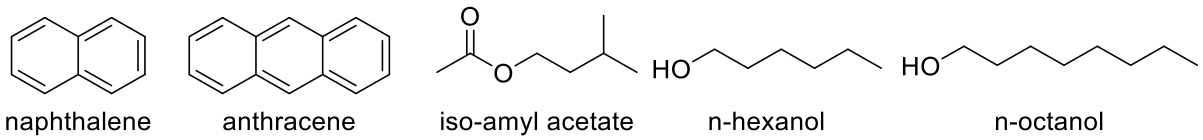

Figure S1 – Chemical structures of the reference compounds investigated in this work: naphthalene, anthracene, iso-amyl acetate, n-hexanol and n –octanol.

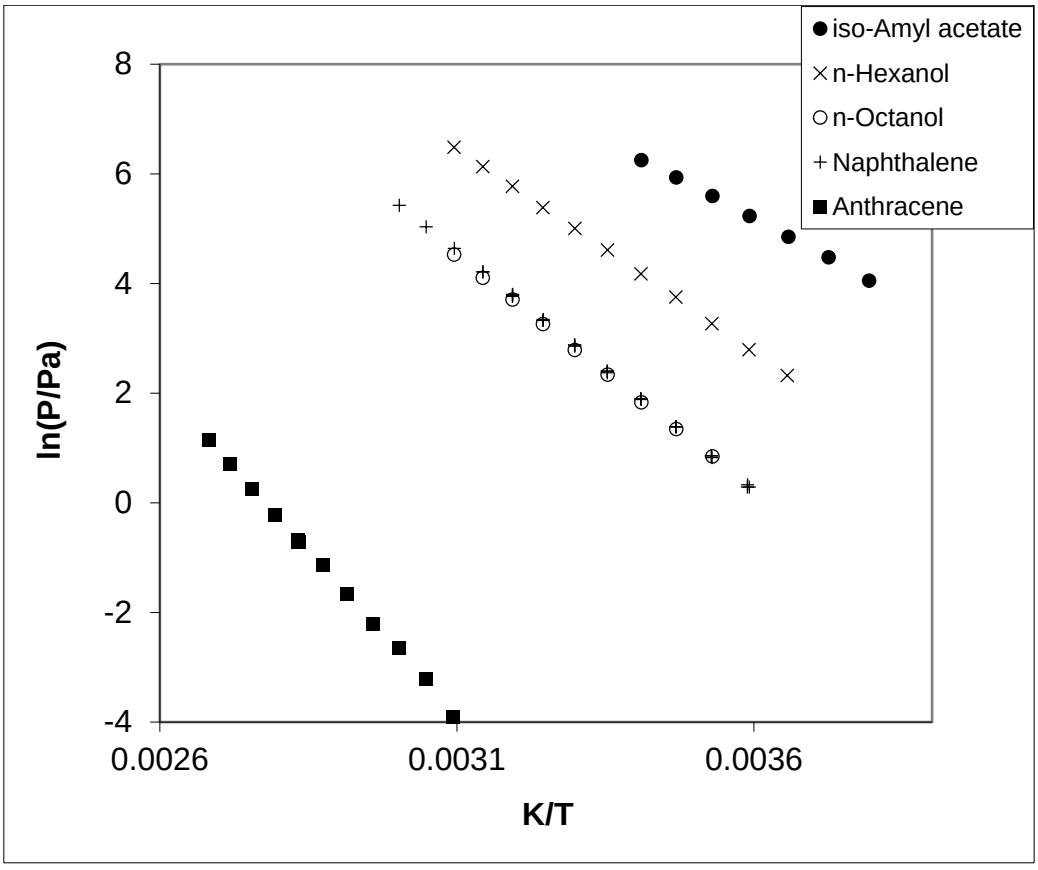

Figure S2- Experimental vapor pressures of iso-amyl acetate, n-hexonal, n-octanol, naphthalene and anthracene obtained in this work.

A *Clausius-Clapeyron* plot of all reference compound p-T datasets measured in this work is compiled in Figure S2. The reference compounds cover measurement scenarios for compounds with high volatility (*iso*-amyl acetate), medium volatility (*n*-hexanol, *n*-octanol, naphthalene) and low volatility (anthracene). In the following the measurement of each reference compound will be discussed in detail including the p-T-data measured in this work

in comparison with literature p-T-datasets. All p-T sets of data discussed were analyzed with the Fit-Function (equation (1) and (2)) using the heat capacity differences stated in Table S24.

$$\ln {}^{p_{sat}}/_{p^o} - \frac{\Delta_l^g C_{p,m}^{\circ}}{R} ln \frac{T}{T_0} = A - \frac{B}{T} \quad (1)$$

$$\ln {}^{p_{sat}}/_{p^o} - \frac{\Delta_{cr}^g C_{p,m}^{\circ}}{R} ln \frac{T}{T_0} = A - \frac{B}{T} \quad (2)$$

with: p^o: reference pressure being 1[Pa],

$\Delta_l^g C_{p,m}^{\circ}$: molar heat capacity difference from liquid to gaseous state [J K^{-1} mol^{-1}],

$\Delta_{cr}^g C_{p,m}^{\circ}$: molar heat capacity difference from solid to gaseous state [J K^{-1} mol^{-1}]

T: temperature [K],

T_0: reference temperature [K],

A, B: fitting coefficients (A: [ ], B: [K]).

In this way the fitting coefficients A and B can be obtained for each individual set of data, which allows the calculation of enthalpies of vaporization and sublimation at the average temperature of the measurement:

$$\Delta_l^g H_m^o(T) = RB + \Delta_l^g C_{p,m}^{\circ} T \quad (3)$$

$$\Delta_{cr}^g H_m^o(T) = RB + \Delta_{cr}^g C_{p,m}^{\circ} T \quad (4)$$

with: $\Delta_l^g H_m^o(T)$: molar enthalpy of vaporization [J mol^{-1}]

$\Delta_{cr}^g H_m^o(T)$ molar enthalpy of sublimation [J mol^{-1}]

The obtained enthalpies of vaporization (eq. (3)) or sublimation (eq. (4)) are adjusted for comparison to T = 298.15 K according to the method provided by *Chickos et al.* [2] using the heat capacity differences and heat capacities stated in Table S24. Furthermore p_{sat} at T = 298.15 K can be evaluated from each individual complete *p*-*T*-dataset using equation (1) or (2). The commercial source and purity of each reference compound is detailed in Table S23.

In the following each measurement of the reference compounds will be discussed presenting the absolute vapor pressures p_{sat} and thermodynamic properties of sublimation or vaporization obtained by the transpiration method in this work. All *p*-*T*-datasets discussed will be visualized for comparison using Clausius-Clapeyron plots. The enthalpies of sublimation and vaporization at 298.15 K will be compared with literature values that were derived from the literature *p*-*T*-data by identical data treatment using equations (1) to (4) and the error estimation stated

elsewhere [3] for the sake of comparability. For each compound an average uncertainty-weighted average value of own and literature data will be calculated from own and literature *p*-*T*-data, which is used as a benchmark for the precision of the own transpiration method experiments. Furthermore an average value for the vapor pressure at 298.15 K derived by equation (1) or (2) from the *p*-*T*-dataset will be stated for each reference compound.

With this it will be demonstrated in the following for each individual reference compound that the experimental *p*-*T*-data measured in this work are in agreement with literature data and that the transpiration method experiment has been established successfully at the research group of Prof. Klapötke. This successful and precise measurement of five reference compounds covering low, medium and high volatility enables the credible measurement of *p*-*T*-data for analytes with no or insufficient literature data for comparison.

6.1 Naphthalene

Table S13 - Naphthalene: absolute vapor pressures p_{sat} and thermodynamic properties of sublimation obtained by the transpiration method in this work

Naphthalene: $\Delta_{cr}^{g} H_m^{\circ}$ (298.15 K) = 72.76 ± 0.32 kJ mol^{-1}

$$\ln p_{sat}/p^{\circ} = \frac{289.5}{R} - \frac{80397.1}{RT} + \frac{25.6}{R} ln \frac{T}{298.15\text{K}}$$

T_{exp} [a]	m [b]	V_{N2} [c]	T_{amb} [d]	Gasflow	p_{sat} [e]	$u(p_{sat})$ [f]	$\Delta_{cr}^{g} H_m^{\circ}$	$\Delta_{cr}^{g} S_m^{\circ}$
[K]	[mg]	[dm³]	[K]	[dm³ h^{-1}]	[Pa]	[Pa]	[kJ mol^{-1}]	[J mol^{-1} K^{-1}]
278.6	0.28	3.95	297.8	1.98	1.39	0.04	73.27	170.0
278.4	1.02	14.8	296.0	4.94	1.33	0.04	73.27	169.9
278.6	0.25	3.58	297.7	1.96	1.34	0.04	73.27	169.6
283.4	0.26	2.13	297.4	1.94	2.36	0.06	73.14	169.5
283.4	0.26	2.16	297.7	1.96	2.36	0.06	73.14	169.5
283.3	1.02	8.65	295.9	1.97	2.28	0.06	73.14	169.3
288.3	1.15	5.54	297.0	1.98	4.01	0.11	73.02	169.1
288.3	0.52	2.51	297.6	1.93	4.01	0.11	73.02	169.1
288.3	0.52	2.54	298.2	1.95	3.98	0.10	73.02	169.0
293.3	0.22	0.652	299.0	1.96	6.70	0.19	72.89	168.6
293.3	0.44	1.28	297.6	1.92	6.64	0.19	72.89	168.6
293.2	1.21	3.57	297.5	1.98	6.58	0.19	72.89	168.5
298.2	0.32	0.56	299.9	1.96	11.1	0.3	72.76	168.3
298.2	0.54	0.96	297.7	1.91	11.0	0.3	72.76	168.2
298.2	0.98	1.75	295.9	1.99	10.7	0.3	72.76	168.0
303.2	0.53	0.57	297.8	1.91	17.8	0.5	72.64	167.8
303.2	0.50	0.55	300.3	1.95	17.8	0.5	72.64	167.8
303.2	1.97	2.18	296.4	1.98	17.4	0.5	72.64	167.7
308.1	1.53	1.04	298.0	1.90	28.4	0.7	72.51	167.4
308.2	0.75	0.520	300.2	1.95	28.0	0.7	72.51	167.3
308.2	0.91	0.628	297.0	1.98	27.9	0.7	72.51	167.2
313.1	1.06	0.453	297.3	1.01	44.9	1.2	72.38	167.1
313.1	1.48	0.643	298.4	1.93	44.5	1.1	72.38	167.0
313.1	1.44	0.632	297.8	1.90	44.1	1.1	72.38	166.9
313.1	1.44	0.649	300.1	1.95	43.2	1.1	72.38	166.7
318.1	1.68	0.482	298.6	1.93	67.7	1.7	72.25	166.5
318.1	1.17	0.334	296.5	1.00	67.4	1.7	72.25	166.4
323.0	2.54	0.474	297.5	1.90	104	3	72.13	166.1
328.0	3.75	0.471	297.6	1.88	154	4	72.00	165.6
333.0	5.65	0.480	297.9	1.92	228	6	71.87	165.2

[a] Saturation temperature ($u(T)$ = 0.1 K). [b] Mass of transferred sample condensed at T = 243 K [c] Volume of nitrogen ($u(V)$ = 0.005 dm^3) used to transfer m ($u(m)$ = 0.0001 g) of the sample. [d] T_a is the temperature of the soap bubble meter used for measurement of the gas flow. [e] Vapor pressure at temperature T, calculated from the m and the residual vapor pressure at the condensation temperature calculated by an iteration procedure; p° = 1 Pa. [f] Standard uncertainty in p was calculated with $u(p/\text{Pa})$ = 0.005+0.025(p/Pa) for p < 5 Pa and $u(p/\text{Pa})$ = 0.025+0.025(p/Pa) for p > 5 to 3000 Pa.

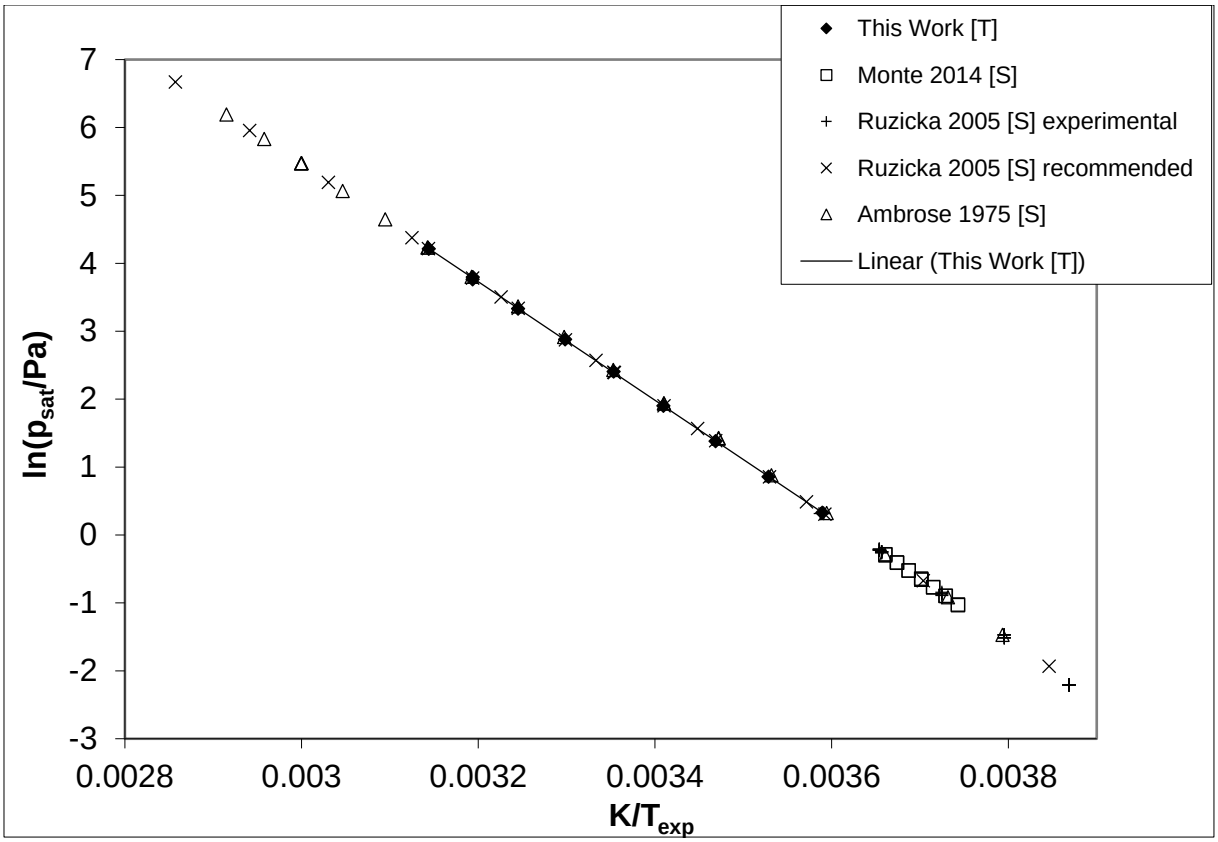

Figure S3 – Experimental vapor pressure of naphthalene in comparison with literature values.

Table S14 – Compilation of data on enthalpies of sublimation $\Delta_{cr}^{g}H_{m}^{\circ}$ of naphthalene

Experiment[a]	**Method**[b]	**T-Range**	T_{avg}	$\Delta_{cr}^{g}H_{m}^{\circ}(T_{avg})$	$\Delta_{cr}^{g}H_{m}^{\circ}$**(298.15K)**[c]	p_{sat}[d]
		K	K	kJ mol^{-1}	kJ mol^{-1}	
This work	T	278.4-333.0	300.3	72.7±0.1	72.8±0.2	10.8
Monte 2006 [4]	S	267.2-273.2	270.2	74.6±0.4	73.8±2.1	11.6
Ruzicka 2005 [5]	S	258.5-278.8	268.1	75.7±0.3	74.9±0.7	12.0
Ambrose 1975 [6]	S	263.6-343.1	303.6	72.2±0.1	72.3±0.3	11.2
					72.8±0.2[e]	11.4[f]

[a] First author and year of publication, [b] Methods: T: Transpiration Method, S: Static Method [c] Enthalpies of Sublimation were adjusted according to *Chickos et al.* [2] with $\Delta_{cr}^{g}C_{p,m}^{\circ}$= -25.6 J mol^{-1} K^{-1} and $C_{p,m}^{\circ}$(cr)= 165.7 J mol^{-1} K^{-1} (see Table S24). [d] Weighted average value, calculated using uncertainty as the weighing factor. [e] Vapor pressure at 298.15 K [f] Average value.

Naphthalene is the common reference compound for validation of vapor pressure measurements since reliable experimental data exists. (cf. Table S14) The sublimation behavior of naphthalene was measured with the transpiration method in this work. The results obtained are compared with three static method datasets by *Monte et al*. [4], *Ruzicka et al*. [5] and *Ambrose et al.* [6]. *Ruzicka et al*. [5] provide for the temperature range 150 – 350 K a set of recommended vapor pressures of naphtalene that was developed by a multi-property simultaneous correlation of vapor pressures and related thermal data. The excellent agreement of the *p-T*-data obtained by the transpiration experiment with the literature values

can be visualized by graphical comparison in a *Clausius-Clapeyron* plot (cf. Figure S3). It reveals the high agreement of all sets of data.

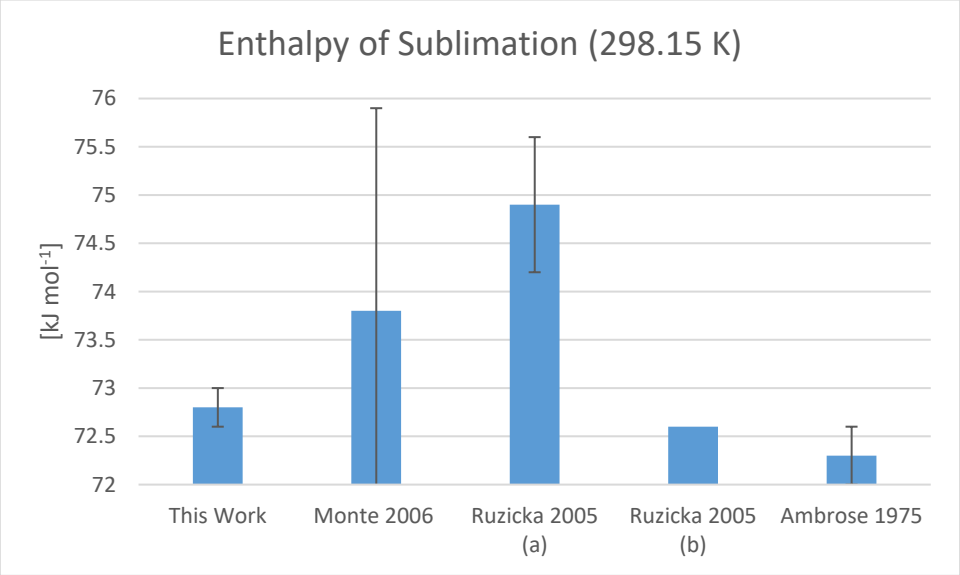

Figure S4 - Comparison of enthalpies of sublimation at 298.15 K for naphthalene. (cf. Table S14) a) experimental values, b) recommended, compiled literature data

The enthalpies of sublimation at 298.15 K obtained by this work in comparison with literature values are compiled in Table S14 and visualized in Figure S4. The value measured in this work (72.8 ± 0.2 kJ mol^{-1}) is in agreement the static method measurements by *Ambrose et al.* [6] and *Monte et al.* [4] and the compiled data recommended by *Ruzicka et al.* [5]. Based on the data available a weighted average sublimation enthalpy of 72.8 ± 0.2 kJ mol^{-1} was calculated using the uncertainty as the weighing factor. The vapor pressures of naphthalene at 298.15 K that were calculated from each individual complete dataset are compiled in Table S14. The mean value of 11.4 Pa can be considered as a recommendation for the ambient condition vapor pressure of naphthalene. *Ruzicka et al*. [5] provide a dataset of recommended vapor pressures of naphtalene that was developed by a multi-property simultaneous correlation of vapor pressures and related thermal data. For the temperature T = 298.15 K an enthalpy of sublimation of 72.44 kJ mol^{-1} and a vapor pressure of 10.92 Pa are recommended. The values recommended by *Ruzicka et al*. [5] are in fair agreement with the enthalpy of sublimation and absolute vapor pressures evaluated in this work (72.8 ± 0.2 kJ mol^{-1}; 11.4 Pa) considering the fact that *Ruzicka et al*. used the highly sophisticated SimCor Method for the temperature correlation of vapor pressures and related thermal data. This method outperforms the two parameter *p*-*T*-data fitting approach (equation (1)) in this work, yet the results are in sufficient agreement.

6.2 Anthracene

Table S15 - Anthracene: absolute vapor pressures p_{sat} and thermodynamic properties of sublimation obtained by the transpiration method in this work

Anthracene: $\Delta_{cr}^{g} H_m^{\circ}$(298.15 K) = 101.50 ± 0.59 kJ mol^{-1}

$$\ln p_{sat}/p^{\circ} = \frac{314.9}{R} - \frac{111194.6}{RT} + \frac{32.5}{R} ln \frac{T}{298.15K}$$

T_{exp} [a]	m [b]	V_{N2} [c]	T_{amb} [d]	Gasflow	p_{sat} [e]	$u(p_{sat})$ [f]	$\Delta_{cr}^{g} H_m^{\circ}$	$\Delta_{cr}^{g} S_m^{\circ}$
[K]	[mg]	[dm³]	[K]	[dm³ h^{-1}]	[Pa]	[Pa]	[kJ mol^{-1}]	[J mol^{-1} K^{-1}]
323.2	0.34	223	297	5.03	0.02	0.01	100.69	183.9
328.0	0.30	111	297.1	5.05	0.04	0.01	100.53	183.4
333.0	0.32	65.5	297.1	5.04	0.07	0.01	100.37	183.4
333.0	0.34	73.0	297.3	5.05	0.07	0.01	100.37	182.9
338.0	0.28	35.4	296.7	5.03	0.11	0.01	100.21	182.4
338.0	0.30	36.8	296.6	2.55	0.11	0.01	100.21	182.6
343.0	0.29	21.1	296.8	5.04	0.19	0.01	100.05	182.2
347.9	0.30	13.3	296.6	5.03	0.32	0.01	99.89	181.7
352.9	0.28	7.96	295.9	5.03	0.49	0.02	99.72	180.9
352.9	0.27	7.54	297.1	5.03	0.49	0.02	99.72	180.9
352.9	0.29	7.92	298.0	2.56	0.51	0.02	99.72	181.1
357.9	0.29	5.02	296.5	5.02	0.80	0.02	99.56	180.6
362.9	0.28	3.12	296.3	5.05	1.28	0.04	99.40	180.2
367.8	0.24	1.67	296.3	5.02	2.03	0.06	99.24	179.9
372.8	0.28	1.25	296.3	5.01	3.12	0.08	99.08	179.5

[a] Saturation temperature ($u(T)$ = 0.1 K). [b] Mass of transferred sample condensed at T = 243 K [c] Volume of nitrogen ($u(V)$ = 0.005 dm^3) used to transfer m ($u(m)$ = 0.0001 g) of the sample. [d] T_a is the temperature of the soap bubble meter used for measurement of the gas flow. [e] Vapor pressure at temperature T, calculated from the m and the residual vapor pressure at the condensation temperature calculated by an iteration procedure; p° = 1 Pa. [f] Standard uncertainty in p was calculated with $u(p/\text{Pa})$ = 0.005+0.025(p/Pa) for p < 5 Pa and $u(p/\text{Pa})$ = 0.025+0.025(p/Pa) for p > 5 to 3000 Pa.

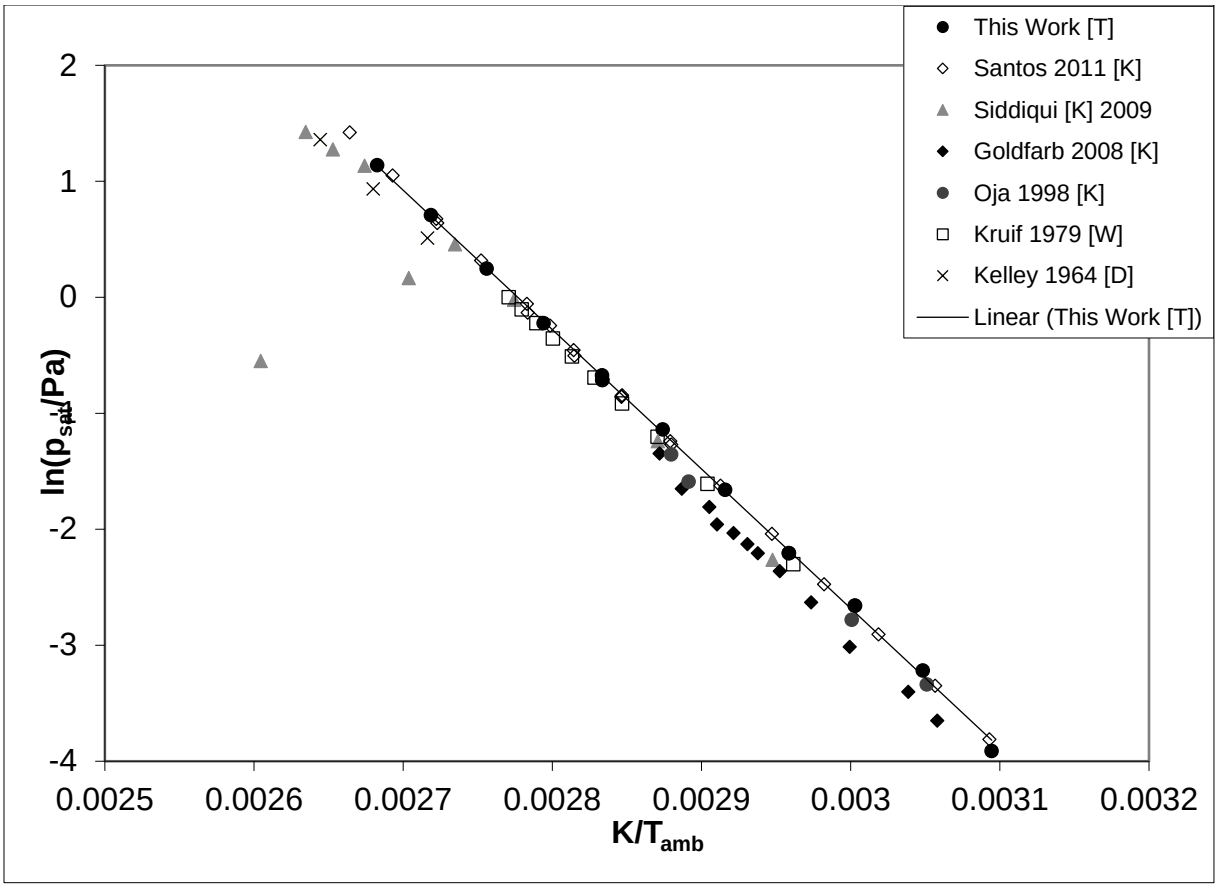

Figure S5 – Experimental vapor pressure of anthracene in comparison with literature values.

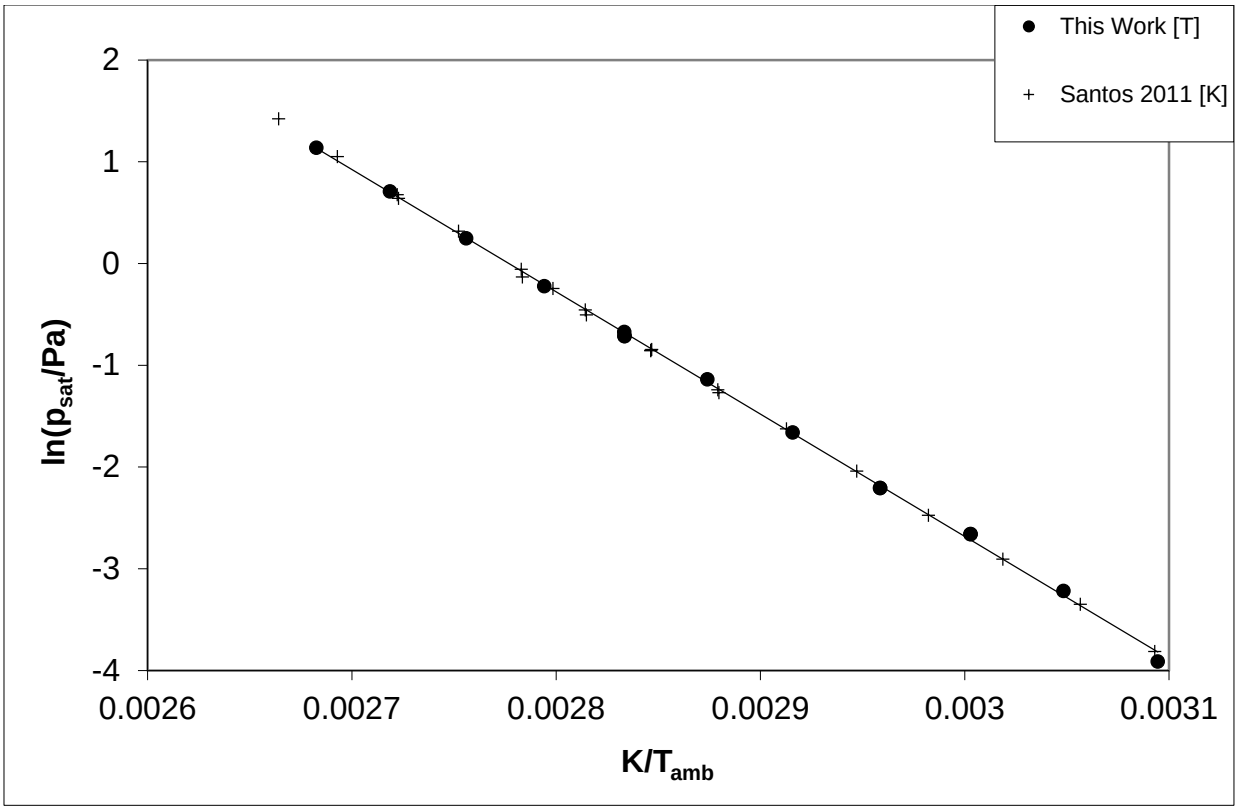

Figure S6 – Experimental vapor pressure of anthracene. Internal comparison of own experimental results with the literature data from Santos et al. [7].

Table S16 – Compilation of data on enthalpies of sublimation $\Delta_{cr}^{g}H_{m}^{\circ}$ of anthracene

Experiment[a]	**Method**[b]	**T-Range**	T_{avg}	$\Delta_{\mathbf{cr}}^{\mathbf{g}}H_{m}^{\circ}(T_{avg})$	$\Delta_{\mathbf{cr}}^{\mathbf{g}}H_{m}^{\circ}$**(298.15K)**[c]	p_{sat}[d]
		K	K	kJ mol^{-1}	kJ mol^{-1}	mPa
This Work	T	323.2-372.8	346.4	99.9±0.4	101.5±0.6	0.93
Santos 2011 [7]	K	323.3-375.4	350.8	100.5±0.5	102.2±0.7	0.89
Siddiqi 2009 [8]	K	339.3-398.6	379.1	96.2±1.4	98.5±1.5[e]	0.99[e]
Goldfarb 2008 [9]	K	322.2-348.2	337.8	98.4±1.6	99.6±1.7	0.77
Bender 2008 [10]	T	353.6-398.6	374.8	94.7±0.6	97.2±0.9	1.29
Chen 2006 [11]	K	320.2-354.1	337.9	93.4±2.5	94.6±2.6	1.44
R. da Silva 2006 [12]	K	340.4-360.4	349.8	107.0±0.6	108.6±1.2	0.56
Oja 1998 [13]	K	300.9-347.3	326.2	100.1±1.6	100.9±1.6	0.85
Hansen 1986 [14]	T	313.2-363.2	337.4	102.6±1.3	103.9±1.4	0.78
Macknick 1979 [15]	T	358.4-393.1	375.9	94.7±0.1	97.3±0.8	1.29
De Kruif 1979 [16]	W	337.7-360.9	352.6	100.4±0.0	102.1±0.9	0.83
Kelley 1964 [17]	D	368.2-378.2	373.1	98.2±0.8	100.6±2.5	0.80
					100.9±0.3[f]	0.95[g]

[a] Author and year of publication [b] Methods: T: Transpiration Method, K: Knudsen Effusion, W: Torsion-and Weighing-Effusion, D: dynamic method, [c] Enthalpies of Sublimation were adjusted according to *Chickos et al.* [2] with $\Delta_{cr}^{g}C_{p,m}^{\circ}$ = 32.5 J mol^{-1} K^{-1} and $C_{p,m}^{\circ}$(cr) = 211.7 J mol^{-1} K^{-1} (see Table S24) [d] Vapor pressure at 298.15 K. [e] For data analysis the apparently erroneous data points (p_{sat}/T_{exp}): 1.18 Pa / 369.85 K and 0.577 Pa / 383.95 K were disregarded. [f] Weighted average value, calculated using uncertainty as the weighing factor. [g] Average value.

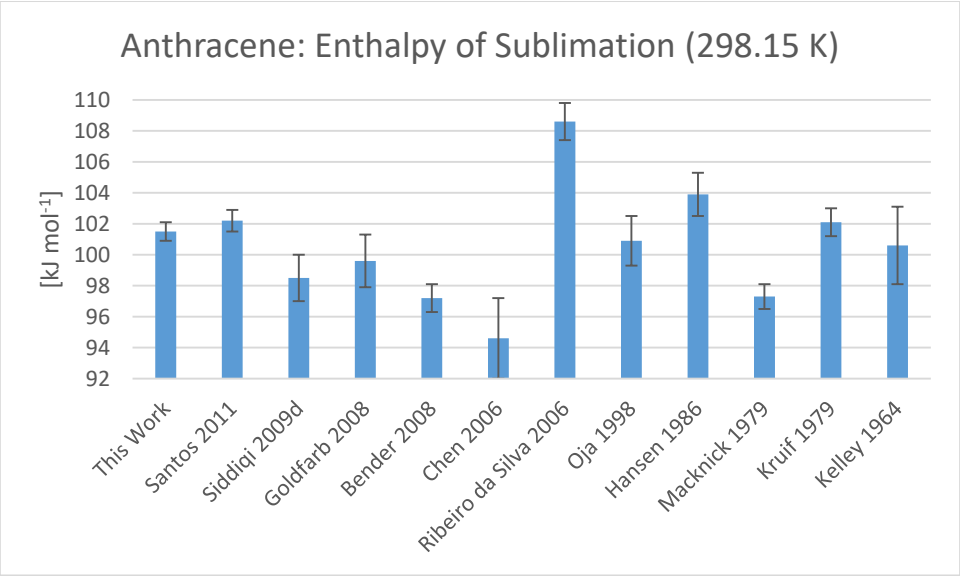

Figure S7 - Comparison of Enthalpies of Sublimation at 298.15 K for Anthracene. (cf. Table S16)

Anthracene is the reference compound with the lowest volatility analyzed within this work. The literature data compiled in Table S16 includes six Knudsen-effusion measurements, four transpiration method experiments, one torsion- and weighing-effusion experiment and one dynamic method measurement. (cf. Table S16) The enthalpies of sublimation $\Delta_{cr}^{g}H_m^{\circ}$(298.15 K) available in the literature spread from 94.6 ± 2.6 kJ mol^{-1} reported by *Chen et al.* [11] to 108.6 ± 1.2 kJ mol^{-1} reported by *Ribeiro da Silva et al.* [12]. A graphic visualization of all sublimation enthalpies $\Delta_{cr}^{g}H_m^{\circ}$(298.15 K) compiled in Table S16 for anthracene can be found in Figure S7. The value obtained in this work (101.5 ± 0.6 kJ mol^{-1}) is in very good agreement with the uncertainty-weighted average value 100.9±0.3 kJ mol^{-1} derived from all available $\Delta_{cr}^{g}H_m^{\circ}$(298.15 K)-values. (cf. Table 4) A Clausius-Clapeyron plot of selected datasets can be found in Figure S5. The data from this work was plotted together with the set of data from *Santos et al.* [7] in Figure S6. The absolute vapor pressures measured in this work are in a good agreement with this most recent measurement. Few points from the dataset reported by *Siddiqi et al.* [8] (p_{sat}/T_{exp}): 1.18 Pa/369.85 K and 0.577 Pa / 383.95 K. (cf. Figure S5) seem to be erroneous. They were excluded from data treatment (see Table S16).

The vapor pressures of anthracene at 298.15 K that were calculated from each individual complete dataset are compiled in Table S16. The mean value of 0.95 mPa can be considered as a recommendation for the ambient condition vapor pressure of anthracene.

6.3 *iso*-amyl acetate

Table S17 iso-Amyl acetate: absolute vapor pressures p_{sat} and thermodynamic properties of vaporization obtained by the transpiration method in this work

Isoamyl acetate : $\Delta_l^g H_m^\circ$ (298.15 K) = 46.28 ± 0.40 kJ mol^{-1}

$$\ln p_{sat}/p^\circ = \frac{285.8}{R} - \frac{68908.5}{RT} + \frac{75.9}{R} ln \frac{T}{298.15K}$$

T_{exp} [a]	m [b]	V_{N2} [c]	T_{amb} [d]	Gasflow	p_{sat} [e]	$u(p_{sat})$ [f]	$\Delta_l^g H_m^\circ$	$\Delta_l^g S_m^\circ$
[K]	[mg]	[dm³]	[K]	[dm³ h^{-1}]	[Pa]	[Pa]	[kJ mol^{-1}]	[J mol^{-1} K^{-1}]
263.6	2.69	1.07	296.0	2.00	56.9	1.5	48.90	123.4
268.4	3.03	0.730	295.9	1.99	87.6	2.2	48.54	122.3
273.4	2.95	0.471	296.0	1.01	127	3	48.16	120.8
278.3	3.31	0.353	296.0	1.01	187	5	47.78	119.4
283.3	4.64	0.337	295.6	1.01	269	7	47.41	118.2
288.2	6.57	0.337	295.7	1.01	378	9	47.03	116.8
293.2	6.78	0.252	295.8	1.01	517	13	46.66	115.4

[a] Saturation temperature ($u(T)$ = 0.1 K). [b] Mass of transferred sample condensed at T = 243 K [c] Volume of nitrogen ($u(V)$ = 0.005 dm^3) used to transfer m ($u(m)$ = 0.0001 g) of the sample. [d] T_a is the temperature of the soap bubble meter used for measurement of the gas flow. [e] Vapor pressure at temperature T, calculated from the m and the residual vapor pressure at the condensation temperature calculated by an iteration procedure; p° = 1 Pa. [f] Standard uncertainty in p was calculated with $u(p/\text{Pa})$ = 0.005+0.025(p/Pa) for p < 5 Pa and $u(p/\text{Pa})$ = 0.025+0.025(p/Pa) for p > 5 to 3000 Pa.

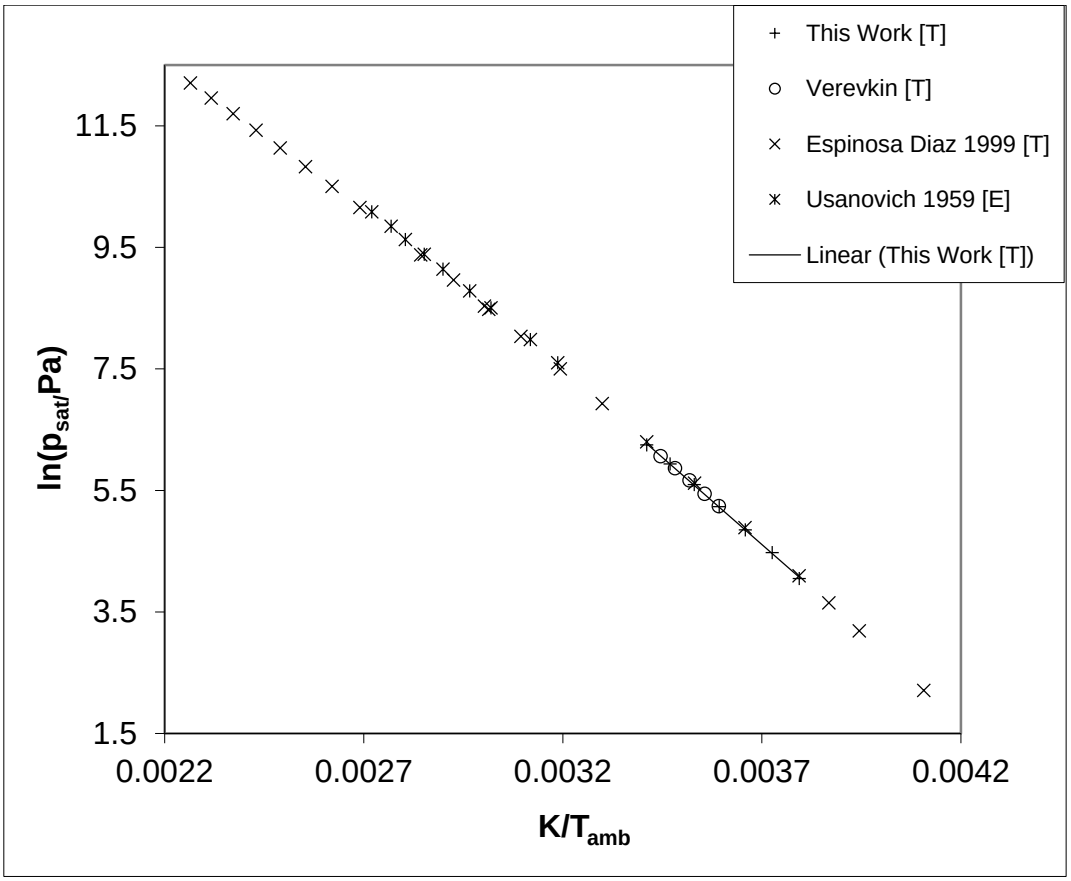

Figure S8 – Experimental vapor pressure of iso-amyl acetate in comparison with literature values.

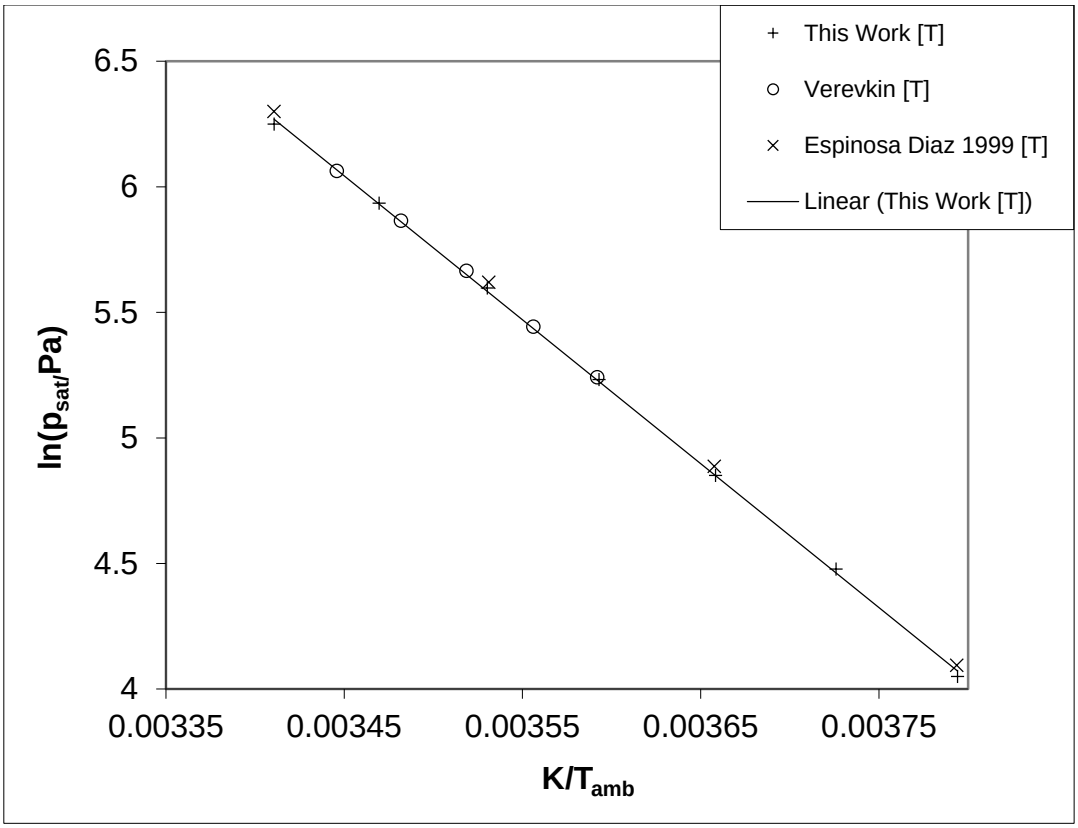

Figure S9 – Experimental vapor pressure of iso-amyl acetate. Zoom on datapoints measured within this work.

Table S18 – Compilation of Data on Enthalpies of Vaporisation $\Delta_c^g H_m$ of iso-amyl acetate

Experiment[a]	**Method**[b]	**T-Range**	T_{avg}	$\Delta_l^g H_m^\circ(T_{avg})$	$\Delta_l^g H_m^\circ$**(298.15K)**[c]	p_{sat}[d]
		K	K	kJ mol^{-1}	kJ mol^{-1}	Pa
This Work	T	263.6-293.2	278.0	48.0±0.3	46.3±0.4	720
Verevkin 1999 [18]	T	278.4-290.2	284.2	46.9±0.4	45.8±0.7	718
Espinosa D. 1999 [19]	S	225-442	315.2	45.7±0.6	46.8±0.2	763
Usanovich 1959 [20]	E	313.8-367.7	341.74	44.2±0.3	47.3±0.4	779
					46.7±0.2[e]	745[f]

[a] Author and year of publication, [b] Methods: T: Transpiration Method, S: Static Method, E: Ebulliometry [c] Enthalpies of vaporization were adjusted according to *Chickos et al.* [2] with $\Delta_l^g C_{p,m}^\circ$= 75.9 J mol^{-1} K^{-1} and $C_{p,m}^\circ$(liq) = 251.4 J mol^{-1} K^{-1} (see Table S24) [d] Vapor pressure at 298.15 K. [e] Weighted average value, calculated using uncertainty as the weighing factor. [f] Average value.

Iso-amyl acetate is the most volatile reference compound whose vaporization characteristics were analyzed. Literature data for comparison was reported by *Verevkin et al*. [18] with a transpiration method dataset, *Espinosa Díaz et al.* [19] with a static method dataset and *Usanovich et al.* [20] with a high temperature ebulliometry dataset. The high precision static method measurement by *Espinosa Díaz et al.* [19] is ideal for benchmarking of the data obtained with the transpiration method since it was generated by a highly reliable direct measurement of the vapor pressure.

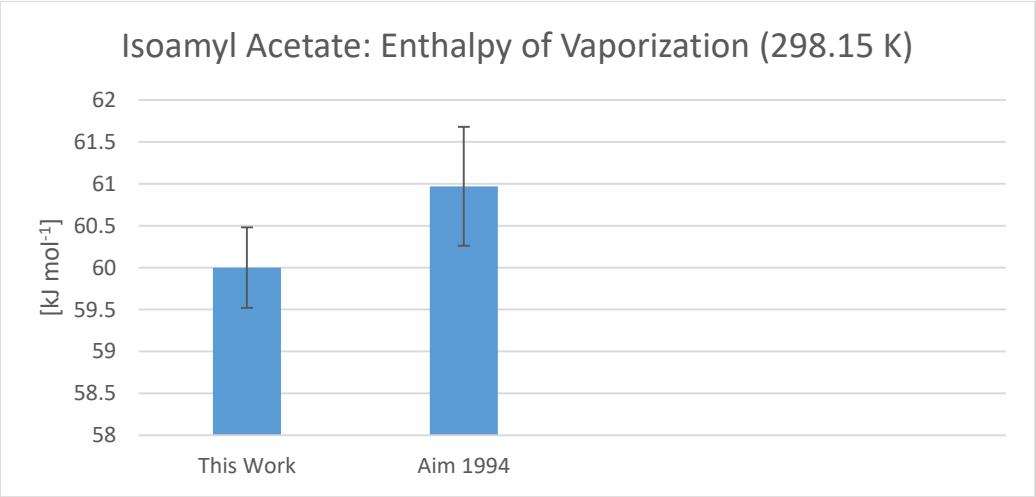

Figure S10 - Comparison of enthalpies of sublimation at 298.15 K for iso-amyl acetate. (cf. Table S18)

The enthalpies of vaporization of *iso*-amyl acetate at 298.15 K are compiled in Table S18 and visualized in Figure S10. The value measured in this work (46.3 ± 0.4 kJ mol^{-1}) is in agreement with the measurements by *Verevkin et al*. [18], *Espinosa Díaz et al.* [19] and *Usanovich et al.* [20]. A weighted average value of 46.7 ± 0.2 kJ mol^{-1} was calculated from all available data using the uncertainty of the values as the weighing factor.

The vapor pressures of *iso*-amyl acetate at 298.15 K that were calculated from each individual complete dataset are compiled in Table S18. The mean value of 745 Pa can be considered as a recommendation for the ambient condition vapor pressure of *iso*-amyl acetate.

6.4 n-Hexanol

Table S19 – n-Hexanol: absolute vapor pressures p_{sat} and thermodynamic properties of vaporization obtained by the transpiration method in this work

n-Hexanol: $\Delta_l^g H_m^\circ$ (298.15 K) = 61.70 ± 0.23 kJ mol^{-1}

$$\ln p_{sat}/p^\circ = \frac{329.4}{R} - \frac{86832.2}{RT} + \frac{84.3}{R} ln \frac{T}{298.15K}$$

T_{exp} [a]	m [b]	V_{N2} [c]	T_{amb} [d]	Gasflow	p_{sat} [e]	$u(p_{sat})$ [f]	$\Delta_l^g H_m^\circ$	$\Delta_l^g S_m^\circ$
[K]	[mg]	[dm^3]	[K]	[dm^3 h^{-1}]	[Pa]	[Pa]	[kJ mol^{-1}]	[J mol^{-1} K^{-1}]
273.5	1.07	2.61	297.3	2.00	10.2	0.3	63.78	156.8
278.4	1.12	1.69	295.9	2.01	16.3	0.4	63.36	155.1
283.3	0.99	0.929	298.0	1.99	26.3	0.7	62.95	153.6
288.3	3.08	1.75	295.9	1.98	42.7	1.1	62.53	152.4
293.3	3.11	1.16	295.9	1.98	65.2	1.7	62.11	150.8
298.2	3.01	0.729	298.5	1.99	101	3	61.7	149.5
303.2	3.06	0.497	298.1	1.99	149	4	61.28	148.0
308.2	5.70	0.633	297.6	2.00	218	5	60.85	146.5
313.1	6.02	0.454	298.0	1.01	322	8	60.44	145.3
318.1	5.74	0.302	298.0	1.01	461	12	60.02	144.0
323.1	5.45	0.202	298.1	1.01	656	16	59.60	142.7

[a] Saturation temperature ($u(T)$ = 0.1 K). [b] Mass of transferred sample condensed at T = 243 K [c] Volume of nitrogen ($u(V)$ = 0.005 dm^3) used to transfer m ($u(m)$ = 0.0001 g) of the sample. [d] T_a is the temperature of the soap bubble meter used for measurement of the gas flow. [e] Vapor pressure at temperature T, calculated from the m and the residual vapor pressure at the condensation temperature calculated by an iteration procedure; p° = 1 Pa. [f] Standard uncertainty in p was calculated with $u(p/\text{Pa})$ = 0.005+0.025(p/Pa) for p < 5 Pa and $u(p/\text{Pa})$ = 0.025+0.025(p/Pa) for p > 5 to 3000 Pa.

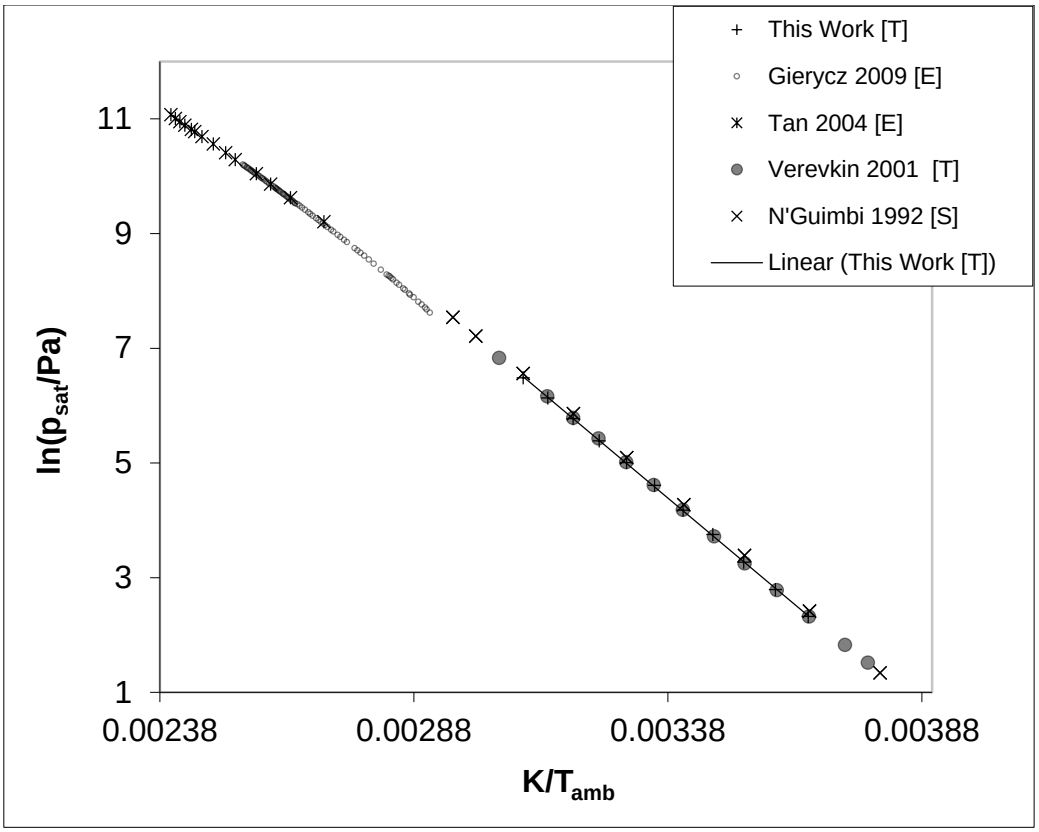

Figure S11 – Experimental vapor pressure of n-hexanol in comparison with literature values.

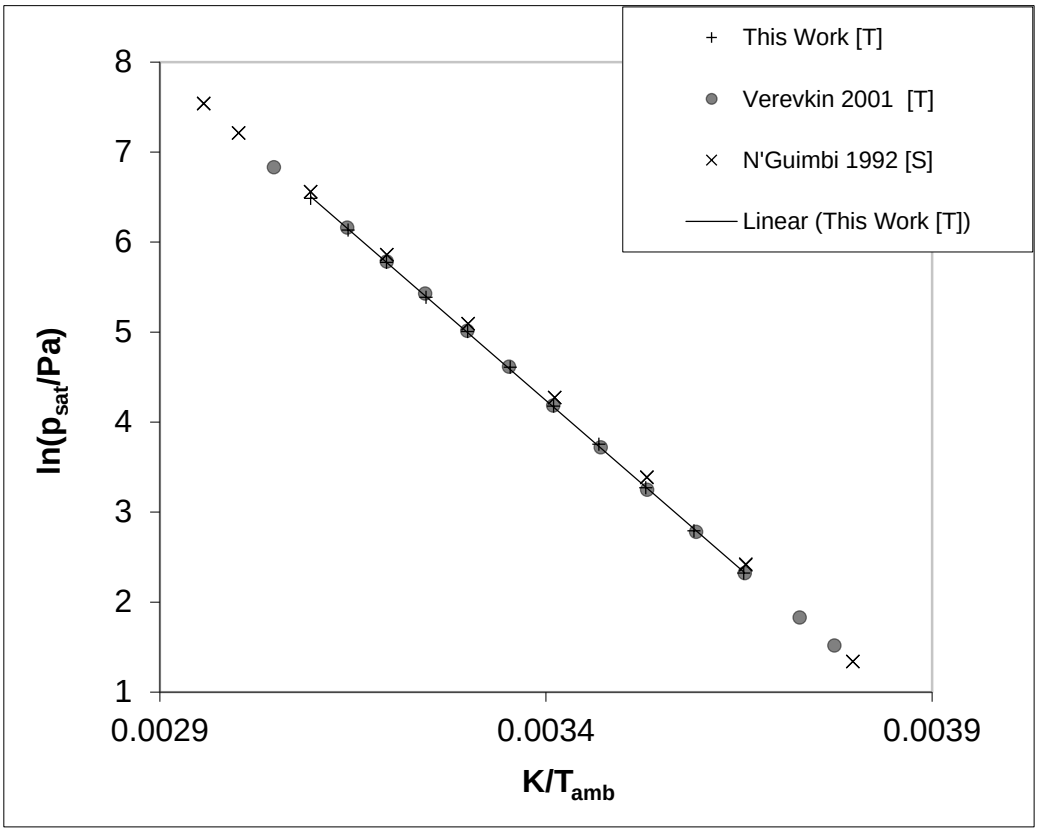

Figure S12 – Experimental vapor pressure of n-hexanol. Zoom on datapoints measured within this work.

Table S20 – Compilation of Data on Enthalpies of Vaporization $\Delta_l^g H_m^\circ$ of n-Hexanol

Experiment[a]	**Method**[b]	**T-Range**	T_{avg}	$\Delta_l^g H_m^\circ(T_{avg})$	$\Delta_l^g H_m^\circ$**(298.15K)**[c]	p_{sat}[d]
		K	K	kJ mol^{-1}	kJ mol^{-1}	Pa
This Work	T	273.5-323.1	297.4	61.8±0.15	61.7±0.2	99
Gierycz 2009 [21]	E	343.46-393.15	371.84	57.5±0.14	63.4±0.5	81
Tan 2004 [22]	E	369.95-416.39	399.47	51.0±0.14	59.1±0.6	121
Verevkin 2001 [23]	T	265.0-328.1	292.5	61.5±0.31	61.1±0.4	100
N'Guimbi 1992 [24]	S	253.4-338.2	297.6	61.4±0.06	61.1±0.1	109
Mansson 1977 [25]	C				61.85±0.20	
Wadsö 1966 [26-27]	C				61.63±0.17	
Green 1960 [28]	C				62.8±1.3	
					61.4±0.1[e]	102[f]

[a] First author and year of publication, [b] Methods: T: Transpiration, E: Ebulliometry, S: Static Method C: Calorimetry [c] Enthalpies of vaporization were adjusted according to *Chickos et al.* [2] with $\Delta_l^g C_{p,m}^\circ$= -84.3 J mol^{-1} K^{-1} and $C_{p,m}^\circ$(liq)= 240.1 J mol^{-1} K^{-1} (see Table S24) [d] Vapor pressure at 298.15 K. [e] Weighted average value, calculated using uncertainty as the weighing factor. [f] Average value

n-Hexanol is a medium volatility reference compound. The literature data compiled in Table S20 includes direct calorimetric vaporization enthalpy measurements by *Mansson et al.* [25], *Wadsö et al.* [26] and *Green et al.* [28], a static method measurement by *N'Guimbi* [24], two recent high temperature ebuliometric measurements by *Tan et al.* [22] and *Gierycz et al.* [21] and a transpiration experiment *by Verevkin et al.* [23]. In this work the vapor pressure of the medium volatility compound n-hexanol was measured in the temperature range from 273.5 K to 323.1 K. The enthalpies of vaporization of n-hexanol at 298.15 K are compiled in Table S20 and visualized in Figure S13. The value measured in this work (61.7 ± 0.2 kJ mol^{-1}) is in a good agreement with all literature data values besides the high temperature ebuliometry measurements by *Tan et al.* [22] and *Gierycz et al.* [22] and the static method data measured by *N'Guimbi et al.* [24]. The best agreement can be found by comparing the data obtained in this work with the direct calorimetric measurements.

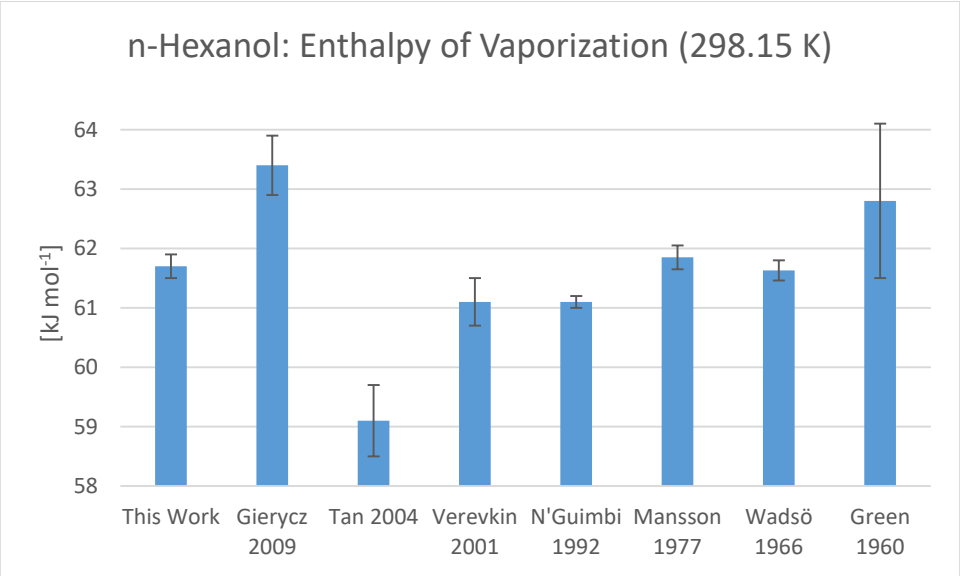

Figure S13 - Comparison of Enthalpies of Vaporization at 298.15 K for n-hexanol. (cf. Table S20)

Based on the data available a weighted average value of 61.4 ± 0.1 kJ mol^{-1} was calculated using the uncertainty of the values as the weighing factor.

The *p*-*T*-data of this work was plotted together with that of the literature in Figure S11 and Figure S12. The vapor pressures of n-hexanol at 298.15 K that were calculated from each individual complete dataset are compiled in Table S20. The mean value of 102 Pa can be considered as a recommendation for the ambient condition vapor pressure of n-hexanol.

6.5 n-Octanol

Table S21 – n-Octanol: absolute vapor pressures p_{sat} and thermodynamic properties of vaporization obtained by the transpiration method in this work

n-Octanol: $\Delta_l^g H_m^\circ$ (298.15 K) = 71.02 ± 0.43 kJ mol^{-1}

$$\ln p_{sat}/p^\circ = \frac{361.4}{R} - \frac{101940.0}{RT} + \frac{103.7}{R} ln \frac{T}{298.15K}$$

T_{exp} [a]	m [b]	V_{N2} [c]	T_{amb} [d]	Gasflow	p_{sat} [e]	$u(p_{sat})$ [f]	$\Delta_l^g H_m^\circ$	$\Delta_l^g S_m^\circ$
[K]	[mg]	[dm³]	[K]	[dm³ h^{-1}]	[Pa]	[Pa]	[kJ mol^{-1}]	[J mol^{-1} K^{-1}]
283.3	1.10	8.99	295.7	1.99	2.33	0.06	72.57	167.5
288.2	1.17	5.79	296.1	2.00	3.84	0.10	72.05	165.4
293.2	0.99	3.00	296.1	2.00	6.24	0.18	71.54	163.5
298.2	1.15	2.10	295.8	2.00	10.4	0.3	71.02	161.9
303.2	1.00	1.17	296.1	2.00	16.2	0.4	70.5	160.0
308.2	1.03	0.745	295.9	1.02	26.0	0.7	69.98	158.5
313.1	1.02	0.475	297.4	1.02	40.7	1.0	69.47	157.0
318.1	2.03	0.635	297.5	1.00	60.6	1.5	68.95	155.2
323.1	2.06	0.422	296.4	1.01	92.5	2.3	68.44	153.8

[a] Saturation temperature ($u(T)$ = 0.1 K). [b] Mass of transferred sample condensed at T = 243 K [c] Volume of nitrogen ($u(V)$ = 0.005 dm^3) used to transfer m ($u(m)$ = 0.0001 g) of the sample. [d] T_a is the temperature of the soap bubble meter used for measurement of the gas flow. [e] Vapor pressure at temperature T, calculated from the m and the residual vapor pressure at the condensation temperature calculated by an iteration procedure; p° = 1 Pa. [f] Standard uncertainty in p was calculated with $u(p/\text{Pa})$ = 0.005+0.025(p/Pa) for p < 5 Pa and $u(p/\text{Pa})$ = 0.025+0.025(p/Pa) for p > 5 to 3000 Pa.

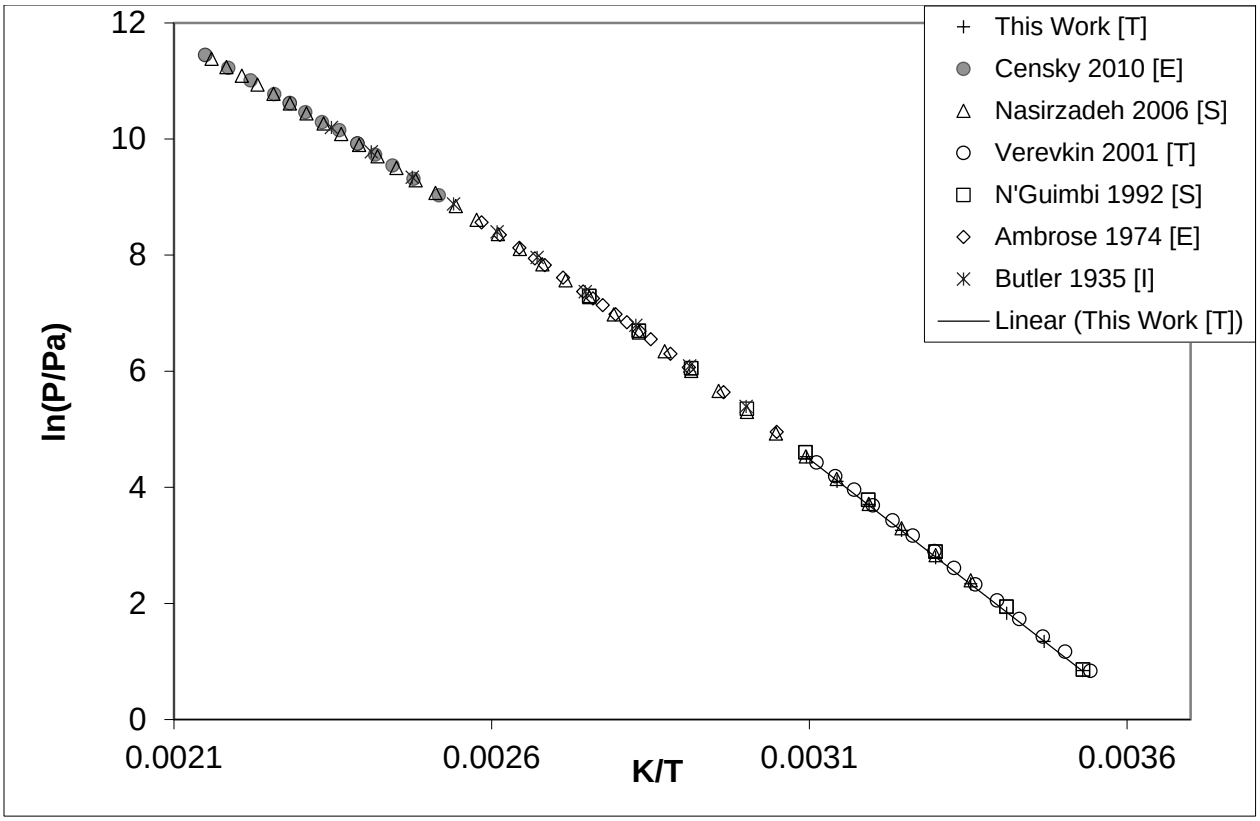

Figure S14 – Experimental vapor pressure of n-octanol in comparison with literature values.

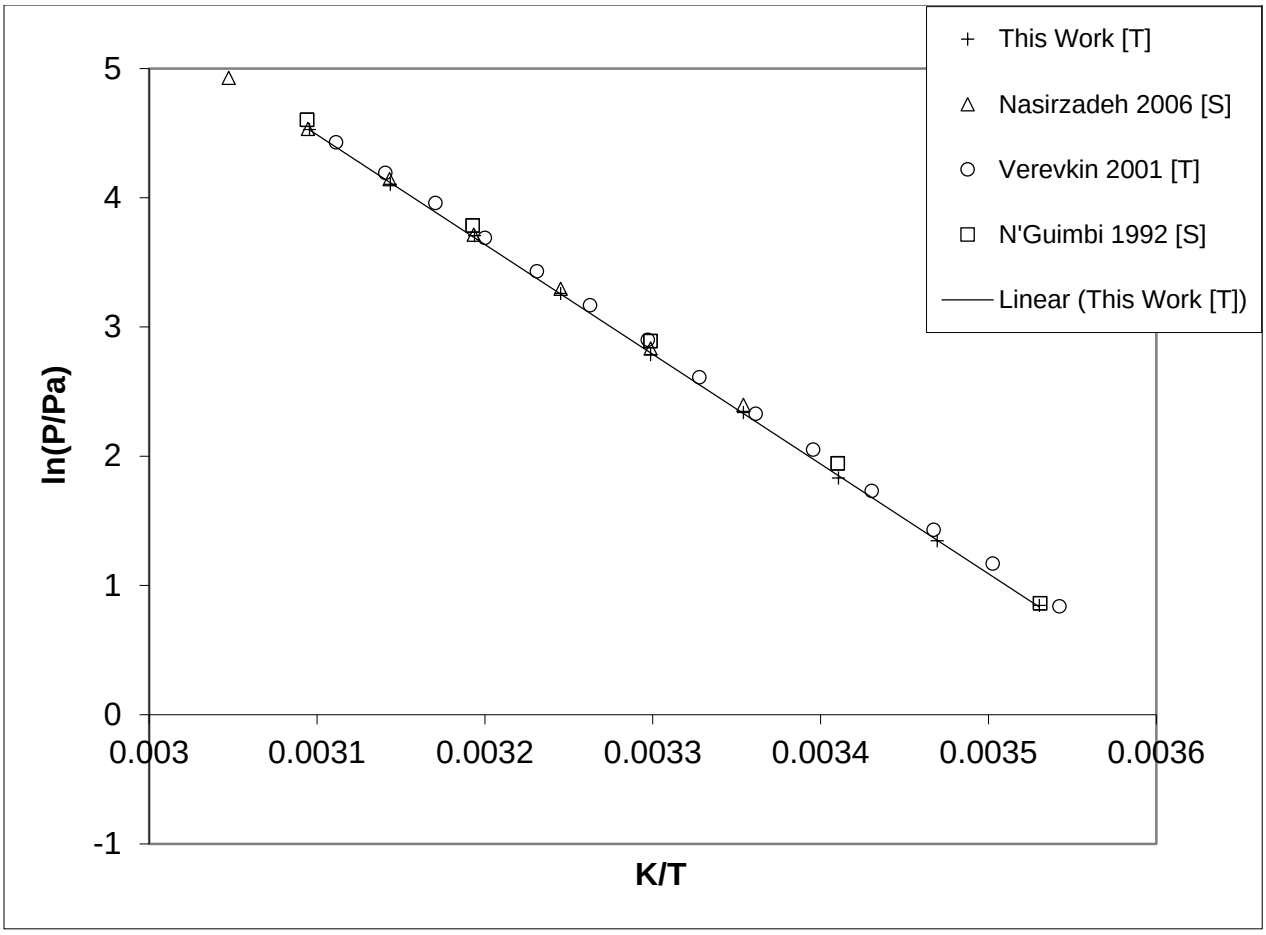

Figure S15 – Experimental vapor pressure of n-octanol. Zoom on datapoints measured within this work.

Table S22 – Compilation of data on enthalpies of vaporization $\Delta_l^g H_m^\circ$ of n-octanol

Experiment[a]	**Method**[b]	**T-Range**	T_{avg}	$\Delta_l^g H_m^\circ(T_{avg})$	$\Delta_l^g H_m^\circ$**(298.15K)**[c]	p_{sat}[d]
		K	K	kJ mol^{-1}	kJ mol^{-1}	
This Work	T	283.3-323.1	302.61	70.6±0.4	71.0±0.4	10.4
Censky 2010 [29]	E	397.31-465.29	429.85	54.2±0.2	(68.0±0.7)	(14.4)
Nasirzadeh 2006 [30]	S	298.2-463.2	374.24	62.6±0.1	70.1±0.5	11.1
Verevkin 2001 [23]	T	282.3-321.4	301.46	69.8±0.3	70.1±0.4	11.1
N'Guimbi 1992 [24]	S	273.3-363.2	314.72	69.5±0.2	71.2±0.2	11.1
Ambrose 1974 [31]	E	328.03-386.96	359.56	64.4±0.1	70.5±0.4	11.4
Butler 1935 [32]	I	333.3-425.9	376.79	61.1±0.3	(69.2±0.3)	(12.8)
Mansson 1977 [25]	C				71.98±0.42	
Green 1960 [28]	C				72.8±1.7	
					71.0±0.1[e]	11.0[f]

[a] First author and year of publication, [b] Methods: T: Transpiration, E: Ebulliometry, S: Static Method, I: Isoteniscope, C: Compiled Data [c] Enthalpies of vaporization were adjusted according to *Chickos et al.* [2] with $\Delta_l^g C_{p,m}^\circ$= -103.7 J mol^{-1} K^{-1} and $C_{p,m}^\circ$(liq) = 305.2 J mol^{-1} K^{-1} (see Table S24) [d] Vapor pressure at 298.15 K. [e] Weighted average value, calculated using uncertainty as the weighing factor. [f] Average value. Values in brackets were not used for calculation of average value.

The vapor pressure of the medium volatility compound n-octanol was measured in this work in the temperature range from 283.3 K to 323.1 K. An enthalpy of vaporization $\Delta_l^g H_m^\circ$(298.15 K) of 71.0 ± 0.4 kJ mol^{-1} was derived from the transpiration experiment in this work. (cf. Table S21) Literature data is compiled for comparison in Table S22 and illustrated in Figure S16.

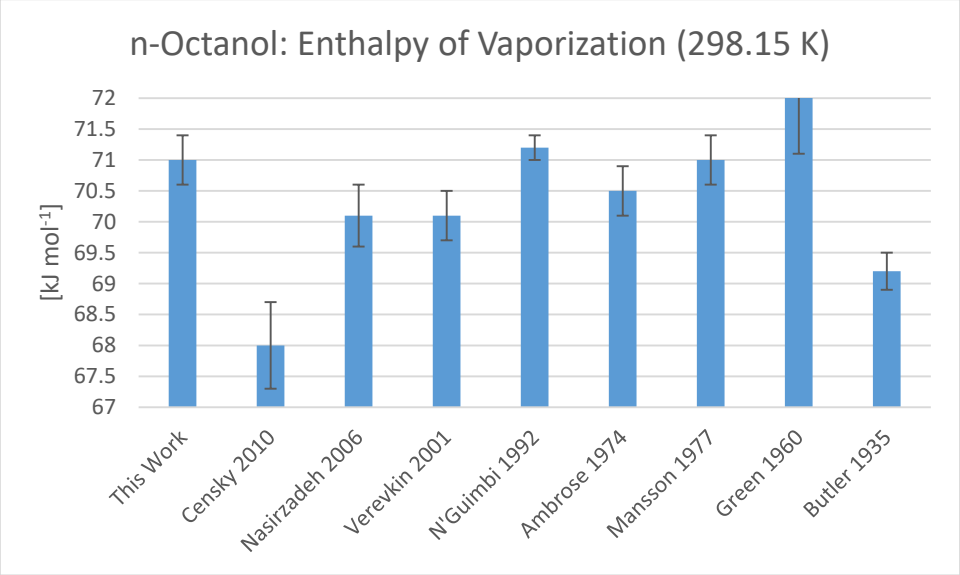

Figure S16 Comparison of enthalpies of vaporization at 298.15 K for n-octanol. (cf. Table S22)

The vaporization enthalpy measured in this work is in very good agreement with those derived from the static method measurement by *N'Guimbi et al.* [24], the Ebuliometry measurement by Ambrose and the calorimetric measurements. Based on the data available a weighted average value of 71.0 ± 0.1 kJ mol^{-1} was calculated using the uncertainty of the literature values as the weighing factor. Our value value (71.0 ± 0.4 kJ mol^{-1}) is in agreement with the averaged result. Vaporization enthalpies derived from *Censky et al.* [29] and *Butler et al*. [32] are in poor agreement with other results and they were excluded from the average value calculation. The *p*-*T*-data for n-octanol (cf. Figure S14, Figure S15) available in the literature are in very good agreement.

Regarding the p-T-data all measurements agree excellently based on graphical comparison. The vapor pressures of n-octanol at 298.15 K (see Table S22) that were calculated from each individual complete dataset are compiled in Table S18. The arithmetic mean value of 11.0 Pa can be considered as a recommendation for the ambient condition vapor pressure of *n*-octanol.

6.6 Purity of used Chemicals

Table S23 - Origin and Purity of the Compounds Investigated

compound	CAS#	Distributor	Product #	Lot #	purity	GC-FID-purity

iso-Amyl acetate	123-92-2	Fisher Chemicals	A/6880/08	1378565	>0.98	0.999
Naphthalene	91-20-2	Bayer	LLB LEV-C703	5H531	„pure“	0.999
Anthracene	120-12-7	Acros Organics	104861000	A0345887	0.99	0.999
n-Hexanol	111-27-3	Sigma-Aldrich	471402	SHBF4653V	≥0.99	0.999
n-Octanol	111-87-5	Sigma-Aldrich	297887	STBD7196V	≥0.99	0.999

Table 11 lists Name, CAS#, distributer, Product #, Lot #, manufacturer purity statement and GC-FID-purity. All purities were checked with a GC-FID setup and the mass of analyte sample used for GC/MS quantification corrected by the purity obtained.

6.7 Compilation of Heat Capacities and Heat Capacity Differences

Table S24 - Calculation of Molar Heat Capacity Differences at T = 298.15 K

compound	$C^o_{p,m}$(l)	$C^o_{p,m}$(cr)	$C^o_{p,m}$(l)	$C^o_{p,m}$(cr)	$\Delta^g_l C^o_{p,m}$	$\Delta^g_{cr} C^o_{p,m}$
	exp.	exp.	calc.	calc.		
	[J mol^{-1} K^{-1}]	[J mol^{-1} K^{-1}]	[J mol^{-1} K^{-1}]	[J mol^{-1} K^{-1}]	[J mol^{-1} K^{-1}]	[J mol^{-1} K^{-1}]
iso-Amyl acetate	251.4[33]		(254.1)		-75.9[a]	
Naphthalene		165.7[34-35]		(158.2)		-25.6[a]
Anthracene		211.7[35]		(211.4)		-32.5[a]
n-Hexanol	240.1[23]		(247.5)		-84.3[b]	
n-Octanol	305.2[23]		(311.3)		-103.7[b]	

Bracketed values not used for calculation of heat capacity differences. a) calculated by $\Delta^g_l C^o_{p,m} = 10.58 + C^o_{p,m}(\mathrm{l}) \times 0.26$ [2] b) calculated with experimental values for $C^o_{p,m}$(g) [36] c) calculated by $\Delta^g_{cr} C^o_{p,m} = 0.75 + C^o_{p,m}(\mathrm{cr}) \times 0.15$ [2]

7 Literature References

1. Boeker, P.; Haas, T.; Schulze Lammers, P., Theory and practice of a variable dome splitter for gas chromatography-olfactometry. *J. Chromatogr. A* **2013,** *1286*, 200-207.
2. Acree, W.; Chickos, J. S., Phase Transition Enthalpy Measurementsof Organic and Organometallic Compounds. Sublimation, Vaporizationand Fusion Enthalpies From 1880 to 2010. *J. Phys. Chem. Ref. Data* **2010,** *39*, 043101.
3. Verevkin, S. P.; Sazonova, A. Y.; Emel'yanenko, V. N.; Zaitsau, D. H.; Varfolomeev, M. A.; Solomonov, B. N.; Zherikova, K. V., Thermochemistry of Halogen-Substituted Methylbenzenes. *J. Chem. Eng. Data* **2015,** *60*, 89-103.
4. Monte, M. J. S.; Santos, L. M. N. B. F.; Fulem, M.; Fonseca, J. M. S.; Sousa, C. A. D., New Static Apparatus and Vapor Pressure of Reference Materials: Naphthalene, Benzoic Acid, Benzophenone, and Ferrocene. *J.Chem. Eng. Data* **2006,** *51*, 757-766.
5. Růžička, K.; Fulem, M.; Růžička, V., Recommended Vapor Pressure of Solid Naphthalene. *J. Chem. Eng. Data* **2005,** *50*, 1956-1970.
6. Ambrose, D.; Lawrenson, I. J.; Sprake, C. H. S., The vapour pressure of naphthalene. *J. Chem. Thermodyn.* **1975,** *7*, 1173-1176.
7. Santos, L. M. N. B. F.; Lima, L. M. S. S.; Lima, C. F. R. A. C.; Magalhães, F. D.; Torres, M. C.; Schröder, B.; Ribeiro da Silva, M. A. V., New Knudsen effusion apparatus with simultaneous gravimetric and quartz crystal microbalance mass loss detection. *J. Chem. Thermodyn.* **2011,** *43*, 834-843.
8. Siddiqi, M. A.; Siddiqui, R. A.; Atakan, B., Thermal Stability, Sublimation Pressures, and Diffusion Coefficients of Anthracene, Pyrene, and Some Metal β-Diketonates. *J. Chem. Eng. Data* **2009,** *54*, 2795-2802.
9. Goldfarb, J. L.; Suuberg, E. M., Vapor Pressures and Enthalpies of Sublimation of Ten Polycyclic Aromatic Hydrocarbons Determined via the Knudsen Effusion Method. *J. Chem. Eng. Data* **2008,** *53*, 670-676.
10. Bender, R.; Bieling, V.; Maurer, G., The vapour pressures of solids: anthracene, hydroquinone, and resorcinol. *J. Chem. Thermodyn*. **1983,** *15*, 585-594.
11. Chen, X.; Oja, V.; Chan, W. G.; Hajaligol, M. R., Vapor Pressure Characterization of Several Phenolics and Polyhydric Compounds by Knudsen Effusion Method. *J. Chem. Eng. Data* **2006,** *51*, 386-391.
12. Ribeiro da Silva, M. A. V.; Monte, M. J. S.; Santos, L. M. N. B. F., Vapor Pressure Characterization of Several Phenolics and Polyhydric Compounds by Knudsen Effusion Method. *J. Chem. Thermodyn.* **2006,** *38*, 778-787.
13. Oja, V.; Suuberg, E. M., Vapor Pressures and Enthalpies of Sublimation of Polycyclic Aromatic Hydrocarbons and Their Derivatives. *J. Chem. Eng. Data* **1998,** *43*, 486-492.
14. Hansen, P. C.; Eckert, C. A., An improved transpiration method for the measurement of very low vapor pressures. *J. Chem. Eng. Data* **1986,** *31*, 1-3.
15. Macknick, A. B.; Prausnitz, J. M., Vapor pressures of high-molecular-weight hydrocarbons. *J. Chem. Eng. Data* **1979,** *24*, 175-178.
16. De Kruif, C. G., Enthalpies of sublimation and vapour pressures of 11 polycyclic hydrocarbons. *J. Chem. Thermodyn*. **1980,** *12*, 243-248.
17. Kelley, J. D.; Rice, F. O., The Vapor Pressures of Some Polynuclear Aromatic Hydrocarbons. *J. Phys. Chem.* **1964,** *68*, 3794-3796.
18. Verevkin, S. P.; Heintz, A., Determination of Vaporization Enthalpies of the Branched Esters from Correlation Gas Chromatography and Transpiration Methods. *J. Chem. Eng. Data* **1999,** *44*, 1240-1244.
19. Espinosa Díaz, M. A.; Guetachew, T.; Landy, P.; Jose, J.; Voilley, A., Experimental and estimated saturated vapour pressures of aroma compounds. *Fluid Phase Equilib.* **1999,** *157*, 257-270.

20. Usanovich, M.; Dembitskii A., Vapor Pressure of Systems Formed by Stannic Chloride with Esters. *Zh. Obshch. Khim.* **1959,** *29*, 1744-1753.
21. Gierycz, P.; Kosowski, A.; Swietlik, R., Vapor−Liquid Equilibria in Binary Systems Formed by Cyclohexane with Alcohols. *J. Chem. Eng. Data* **2009,** *54*, 2996-3001.
22. Tan, T.; Li, H.; Wang, C.; Jiang, H.; Han, S., Isothermal and isobaric vapor–liquid equilibria for the binary system trimethylbenzoquinone + n-hexanol. *Fluid Phase Equilib.* **2004,** *224*, 279-283.
23. Kulikov, D.; Verevkin, S. P.; Heintz, A., Enthalpies of vaporization of a series of aliphatic alcohols: Experimental results and values predicted by the ERAS-model. *Fluid Phase Equilib.* **2001,** *192*, 187-207.
24. N'Guimbi, J.; Kasehgari, H.; Mokbel, I.; Jose, J., Tensions de vapeur d'alcools primaires dans le domaine 0,3 Pa à 1,5 kPa. *Thermochim. Acta* **1992,** *196*, 367-377.
25. Månsson, M.; Sellers, P.; Stridh, G.; Sunner, S., Enthalpies of vaporization of some 1-substituted n-alkanes. *J. Chem. Thermodyn*. **1977,** *9*, 91-97.
26. Wadsö, I., A Heat of Vaporization Calorimeter for Work at 25 °C and for Small Amounts of Substances. *Acta Chem. Scand.* **1966,** *20*, 536-543.
27. Wadsö, I., Heats of Vaporization for a Number of Organic Compounds at 25 degrees C. *Acta Chem. Scand.* **1966,** *20*, 554-552.
28. Green, J. H. S., Revision of the values of the heats of formation of normal alcohols. *Chem. Ind. (London, U. K.)* **1960**, 1215-16.
29. Čenský, M.; Roháč, V.; Růžička, K.; Fulem, M.; Aim, K., Vapor pressure of selected aliphatic alcohols by ebulliometry. Part 1. *Fluid Phase Equilib.* **2010,** *298*, 192-198.
30. Nasirzadeh, K.; Neueder, R.; Kunz, W., Vapor Pressure Determination of the Aliphatic C5 to C8 1-Alcohols. *J. Chem. Eng. Data* **2006,** *51*, 7-10.
31. Ambrose, D.; Ellender, J. H.; Sprake, C. H. S., Thermodynamic properties of organic oxygen compounds XXXV. Vapour pressures of aliphatic alcohols. *J. Chem. Thermodyn*. **1974,** *6*, 909-914.
32. Butler, J. A. V.; Ramchandani, C. N.; Thomson, D. W., The solubility of non-electrolytes. Part I. The free energy of hydration of some aliphatic alcohols. *J. Chem. Soc. (Resumed)* **1935**, 280-285.
33. Becker, L.; Gmehling, J., Measurement of Heat Capacities for 12 Organic Substances by Tian−Calvet Calorimetry. The Low-Temperature Thermodynamic Properties of Naphthalene, l-Methylnaphthalene, 2-Methylnaphthalene, 1,2,3,4-Tetrahydronaphthalene,trans-Decahydronaphthalene and cis-Decahydronaphthalene. *J. Chem. Eng. Data* **2001,** *46*, 1638-1642.
34. McCullough, J. P.; Finke, H. L.; Messerly, J. F.; Todd, S. S.; Kincheloe, T. C.; Waddington, G., *J. Phys. Chem.* **1957,** *61*, 1105-1116.
35. Radomska, M.; Radomski, R., Calorimetric studies of binary systems of 1,3,5-trinitrobenzene with naphthalene, anthracene and carbazole. I. Phase transitions and heat capacities of the pure components and charge-transfer complexes. *Thermochim. Acta* **1980,** *40*, 405-414.
36. Domalski, E. S.; Hearing, E. D., Estimation of the Thermodynamic Properties of C-H-N-O-S-Halogen Compounds at 298.15 K. *J. Phys. Chem. Ref. Data* **1993,** *22*, 805-1159.

7.9 Measurement of Vapor Pressures with the Transpiration Method: Facit

The transpiration method has been used in this work for the precise characterization of the vapor pressure of 5 reference compounds and 19 analytes. The precise results for the measurements of the reference compounds enhance the credibility of measurements for compounds with disagreeing literature values. For the peroxide TATP **03** it could be demonstrated that the polymorphism of the compound may not be neglected in the discussion of its vapor pressure. For the nitrate esters EGDN **06**, GTN **07** and ETN **08** it was demonstrated that the vapor pressure of a linear nitrate ester is lowered by two orders of magnitudes by the addition of a methylene nitrato unit. The measurement of the important potential home-made explosive ETN **08** is the first measurement of its sublimation and vaporization characteristics with a well-established method despite its unavoidable long-term decomposition. For the mononitrotoluenes **12**-**14** and the nitroalkanes DMDNB **26** reliable benchmark data for their vapor pressure could be established. For the organo(thio)phosphate compounds **I**-**VIII** it could be demonstrated that the transpiration method is suitable for thermolabile compounds that can undergo a thiono-thiolo-rearrangement. Besides for Amiton **I**, for which good agreement with a literature dataset could be established, the vapor pressure of the other derivatives **II**-**VIII** has been characterized for the first time. All measurements were evaluated by comparison of the enthalpy of vaporization or sublimation at 298.15 K. Additionally the vapor pressure at 298.15 K has been calculated from each dataset. As already stated before (cf. section 7.0) the community of physico-chemists avoids the discussion of absolute vapor pressures for various reasons. Since the absolute vapor pressure is an important parameter for the detection of explosives and various models for the estimation of room temperature concentrations of explosives the results obtained with the transpiration method in this work are compared with the results of the literature analysis by Östmark et al. and Ewing et al. (cf. Table 1)

Table 1 – Comparison of vapor pressures at $\boldsymbol{p_{sat}}$ at T = 298.15 K of values stated in the reviews by Östmark and Ewing with the values obtained by the transpiration method in this work.

	I	II	III		
analyte	p_{sat}**(298 K) Ewing et al.**	p_{sat}**(298 K) Östmark et al.** [1]	p_{sat}**(298 K) this work**	p_{sat}**(298 K) I/III**	p_{sat}**(298 K) II/III**
	[Pa]	[Pa]	[Pa]	%	%
TATP **02**	6,39E+00	6,20E+00	6,73E+00	5,00	7,86
DADP **03**	2,47E+01	1,77E+01	2,66E+01	7,06	33,34
EGDN **06**	1,03E+01	1,01E+01	1,21E+01	14,59	16,26
GTN **07**	6,54E-02	6,41E-02	8,22E-02	20,49	21,97
4-MNT **14**	6,56E+00	6,52E+00	5,57E+00	-17,70	-16,97
2,4-DNT **15**	4,16E-02	3,51E-02	4,03E-02	-3,34	13,01
2,6-DNT **16**	9,05E-02	8,27E-02	9,29E-02	2,60	11,00
TNT **17**	9,27E-04	7,34E-04	9,03E-04	-2,67	18,76

The deviation of the results measured in this work for p_{sat}(298 K) in comparison with the results by *Östmark et al.* [1] ranges from -16.97 % to 33.34 %, whilst for the results by *Ewing et al.* [2] it ranges from -17.70 % to 20.49 %. *Ewing et al.* [2] selected less sets of data for his recommended values at 298.15 K more carefully than *Östmark et al.* [1]. It can be concluded that the precision of the vapor pressure at 298.15 K by comparison of literature values with own experimental results is about ± 20%.

This is sufficient for the estimation of the air concentration of hazardous materials, which might be influenced by numerous other parameters like confinement, air humidity, surface, etc. (cf. section)

In this work the vapor pressures of the complete ChemAir substance repertoire could not be measured. Ethyl nitrate **04** and nitromethane **27** are too volatile for the transpiration method. The main-reason for this is either non-detectability or non-quantifiability by VO-GC/MS (cf. section 5). Whilst HMTD **01**, PETN **09**, RDX **19**, TETRYL **22** can be detected with VO-GC/MS they cannot be quantified using the external standard quantification method used in this work. For the transpiration method it is necessary that the analyte can be quantified with ±1 % reproducibility without concentration-dependency in a suitable working range. No method could be optimized for the measurement of the analytes **01, 09**, **19** and **22**. This is elucidated with possible reasons in section 5.

HMTD **01** is not stable in the gas-phase. In 2015 Aernecke et al. [3] estimated the vapor pressure of HMTD **01** using Secondary Electrospray Ionization Mass Spectroscopy using heroine and cocaine as calibrants. At 20 °C a HMTD vapor pressure of 6.1×10^{-6}Pa (cocaine) and 4.5×10^{-6}Pa (heroine) was reported with enthalpies of sublimation of 92 ± 3 kJ mol^{-1} (cocaine) and 116 ± 4 kJ mol^{-1} (heroine).

One of the advantages of the transpiration method experiment is that the quantification of the analyte can be carried out using various methods including high performance liquid chromatography (HPLC) with UV-detection (diode array detector, DAD). This method is advantageous for the quantification of explosives since it does not require the transfer of the analytes in the gaseous state. In cooperation with the Shimadzu Deutschland GmbH test measurements of six analytes were performed.

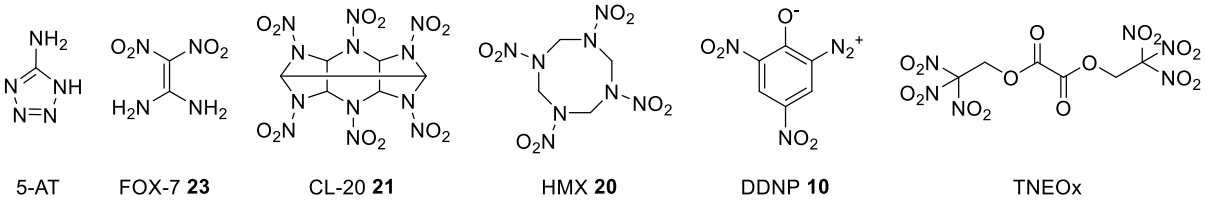

Figure 1 – The repertoire of substances tested for quantifiability with HPLC-DAD.

All compounds could be quantified successfully using a biphenyl stationary phase column (Restek cat. # 9309A65) with an isocratic mobile phase (85 % methanol, 15 % water) using internal standard and external standard quantification for concentrations in the µg/mL regime which is suitable for the transpiration method experiment (cf. Table 2)

Table 2 – Coefficients of determination of HPLC-DAD calibration of six explosives. ISTD: internal standard (naphthalene), ESTD: external standard

Substance	**5-AT**	**FOX-7**	**CL-20**	**HMX**	**DDNP**	**TNEO**
R^2 (ISTD)	0.9933	0.9997	0.9985	0.9949	0.9999	0.9987
R^2 (ESTD)	0.9990	0.9999	0.9999	0.9993	0.9999	0.9998

Especially the results for the external standard calibration ($R^2 > 0.999$) are promising for all analytes and will enable the measurement of their vapor pressure with the transpiration method. The work with the transpiration method will be continued using HPLC quantification of the analytes. With this work the transpiration method has been successfully established in the research group of Prof. Klapötke and can be used to measure the vapor pressure of further analytes of the ChemAir substance repertoire and new explosives that were developed in our laboratories.

Literature References

1. Östmark, H.; Wallin, S.; Ang, H. G., Vapor Pressure of Explosives: A Critical Review. *Propellants, Explosives, Pyrotechnics* **2012,** *37* (1), 12-23.

2. Ewing, R. G.; Waltman, M. J.; Atkinson, D. A.; Grate, J. W.; Hotchkiss, P. J., The vapor pressures of explosives. *TrAC Trends in Analytical Chemistry* **2013,** *42*, 35-48.

3. Aernecke, M. J.; Mendum, T.; Geurtsen, G.; Ostrinskaya, A.; Kunz, R. R., Vapor Pressure of Hexamethylene Triperoxide Diamine (HMTD) Estimated Using Secondary Electrospray Ionization Mass Spectrometry. *The Journal of Physical Chemistry A* **2015,** *119* (47), 11514-11522.

8 Evaluation of the Suitability of Isothermal Thermogravimetric Analysis for the Measurement of Vapor Pressures

In 1974 *Gückel et al.*[1] carried out the first experiment which applied thermogravimetric analysis (TGA) for estimating the volatility of organic compounds. They investigated the vaporization behaviour of pesticides. It was demonstrated that the mass loss of pure pesticides is linear over time when the temperature is held constant. Moreover, they were able to show that multicomponent formulations of pesticides show no linear behaviour at the same conditions.

Knowing the vaporization behaviour, especially the vapour pressure, of substances is important for many industrial applications and processes like chemical vapour deposition (CVD). *Siddiqi and Atakan*[2] measured for this reason the vapor pressure of organometallic compounds using a one-dimensional diffusion theory.

Verevkin et al.[3] showed that TGA can be used as an express method for the determination of vaporization enthalpies of ionic liquids which are extremely low-volatile.

This work explores the suitability of isothermal TGA measurements for the determination of vaporization enthalpies of liquids and sublimation of solids and whether the obtained results can be converted to vapor pressures by calibration with a compound that is different to the analyte but is well-characterized in terms of temperature-dependent vapor pressure.

The isothermal TGA experiment has several advantages. Especially the simple, commercially available, experimental setup that is operated at ambient pressure. About 40-100 mg of substance are placed into a crucible which is placed on a microbalance within a dry nitrogen flushed chamber that can be heated.[3] The mass loss over several isothermal steps is recorded and evaluated using the *Langmuir equation*[4] for evaporation in vacuum which was adjusted for TGA measurements by *Price and Hawkins*[5],[6]:

$$\frac{dm}{dt} = p \cdot \alpha \cdot S \sqrt{\frac{M}{2 \cdot \pi \cdot R \cdot T}} \qquad (1)$$

m: mass [kg], *t*: time [s], **p**: vapor pressure [Pa], ***α***: vaporization coefficient, ***M***: molar weight of the analyte [kg·mol^{-1}]*, ***R***: universal gas constant (8.3144598 (48) J·mol^{-1}·K^{-1}), ***T***: temperature of the isothermal experiment [K];

When the analyte is volatilizing into a purge gas stream at ambient pressure, ***α*** cannot assumed to be 1, which would be the case for vacuum conditions.

Equation (1) can be rearranged[5],[6]:

$$p = k \cdot \frac{dm}{dt} \cdot \sqrt{\frac{T}{M}} \qquad (2)$$

$$k = \frac{\sqrt{2 \cdot \pi \cdot R}}{\alpha} \qquad (3)$$

k: calibration constant

Price and Hawkins[5] claimed that the calibration constant *k* does not depend on the sample and can be identified by the use of calibrants with well-known vapor pressure. *Verevkin et al.*[3] remarked that the assumption that the calibration constant can be derived from some reference substances and the independence of calibrant and analyte structure needs to be studied carefully. For example it is

questionable if benzoic acid is a suitable calibrant for ionic compounds[7]. The vaporization coefficient α could additionally depend on the experimental temperature range. The *Clausius-Clapeyron* equation describes the temperature dependence of the vapour pressure[5],[6]:

$$\frac{d(\ln(p))}{dT} = \frac{\Delta^{\mathrm{g}}_{\mathrm{l/cr}} H^0_m}{R \cdot T^2} \qquad (4)$$

$\Delta^{\mathrm{g}}_{\mathrm{l/cr}} H^0_m$: molar heat of sublimation or vaporisation [kJ mol^{-1}]

$\Delta^{\mathrm{g}}_{\mathrm{l/cr}} H^0_m$ is the molar heat of sublimation ($\Delta^{\mathrm{g}}_{\mathrm{cr}} H^0_m$) for solids and the molar heat of vaporisation ($\Delta^{\mathrm{g}}_{\mathrm{l}} H^0_m$) for liquids. For limited temperature ranges and for practical purposes $\Delta^{\mathrm{g}}_{\mathrm{l/cr}} H^0_m$ can be assumed to be constant and equation (4) can be written as:

$$\ln(p) = B - \frac{\Delta^{\mathrm{g}}_{\mathrm{l/cr}} H^0_m}{R \cdot T} \qquad (5)$$

Equation (5) and equation (2) can be combined:

$$\ln\left(\frac{dm}{dt} \cdot \sqrt{T}\right) = B' - \frac{\Delta^{\mathrm{g}}_{\mathrm{l/cr}} H^0_m}{R \cdot T} \qquad (6)$$

$$B' = B - \ln(k) + ln\sqrt{M} \qquad (7)$$

Linear regression analysis of equation (6) (cf. Figure 3) results in a slope u, which can be used for the calculation of the enthalpy of sublimation or vaporization (valid for: *m* [mg], *t*[min] as in the output files of the TGA device used):

$$\Delta^{\mathrm{g}}_{\mathrm{l/cr}} H^0_m(T_{avg}) = \frac{u \cdot R}{1000} \qquad (8)$$

Ashcroft[8] state that a constant surface during the thermogravimetric experiment is needed to calculate enthalpies of sublimation or vaporisation directly from the mass loss. *Price and Hawkins*[5] suggested for this reason the melting of the substance to obtain a flat and constant surface.

The analyte repertoire in this study (cf. Figure 1) includes three low-volatile reference substances (phenanthrene, hexadecane, dibutyl phthalate), the nitrotoluenes 2-MNT **12**, 3-MNT **13**, 4-MNT **14**, 2,4-DNT **15**, 2,6-DNT **16**, the explosive TNT **17** and the explosive taggant DMDNB **26**.

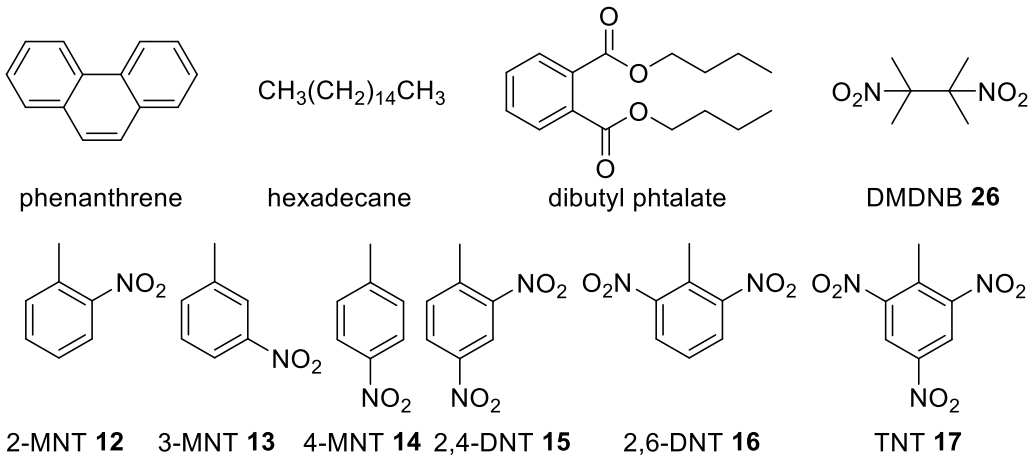

Figure 1 – The repertoire of analytes investigated in this study.

8.1 The isothermal TGA Experiment

All experiments were performed using a *PerkinElmer TGA 4000* device with dry nitrogen as purge gas. Different temperature programs were used and will be explained in detail for each substance. Heating rates for temperature changes in all temperature programs were 5 °C·min^{-1} and the temperature increment was 5 °C per minute. Temperatures were held isothermal for 15 minutes as shown in *Figure 2* in every experiment. The temperature stabilizes after 3-4 minutes after the temperature change.

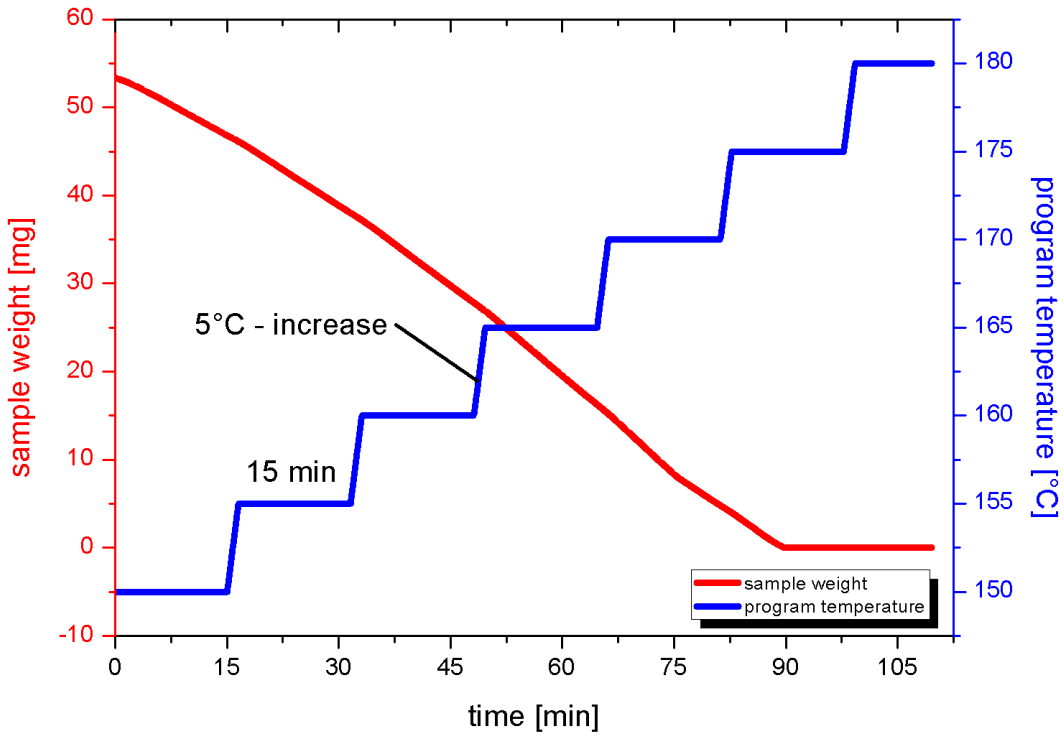

Figure 2: Typical temperature program for TGA-experiments where the red line shows the change of mass over time and the blue line shows the change of temperature that is intended by the program

Previous to all experiments a temperature range starting above of the melting point of the substance was investigated to find the best temperature range regarding the linear regression analysis of the results obtained using equation (6). In the case of energetic materials it must be kept in mind that the decomposition temperature may not be reached. According to *Verevkin et al.*[3] it was intended to measure over a temperature range of at least 60 K. In some cases the temperature range was decreased to 50 K or even 30 K due to the high vaporisation rate of the substance.

The purge gas stream of nitrogen was set to 200 mL per minute for every experiment. The TGA crucible was filled to its edge, so that, depending on the substance, 40-100 mg of it were used. The best results were obtained when the vaporization rate *dm/dt* of the substance was in the range of 0.1 to 2.5 mg per 10 minutes.

As it can be seen in *Figure 3* the first run differs from the others regarding to the sample temperatures and is therefore not taken into account. This results probably from the fact that the sample needs to be preconditioned prior to the measurement to remove sample impurities. All literature values and enthalpies of vaporization and sublimation obtained for the average temperature of the experiment were adjusted to 298.15 K according to *Chickos et al.* [9] using their heat capacity increments for each analyte. The uncertainties stated for individual experimental runs are derived from the standard uncertainty of the slope of the linear regression analysis using equation (6). They were treated as enthalpy values for the adjustment to 298.15 K according to *Chickos et al.* [9]. For each experiment an

average value was calculated and assigned a conservative 2.0 kJ mol^{-1} error, estimated by *Verevkin et al.*[3] for low-volatile liquids.

8.1.1 Measurement of Phenanthrene

Phenanthrene was used as a calibration substance by *Price*[6] as well as by *Siddiqi and Atakan*[2]. It was used as received by *Sigma-Aldrich*. The experiment was performed in the temperature range from 103 °C to 156 °C. The mass loss rate was between 0.1 to 1.5 mg per 10 minutes. For experiment run #2, #3 and #4 the results are compared with the recommended literature values by *Roux et al.[10]* in *Table 1*.

Table 1: Selected results of the TGA-experiment for the determination of the enthalpy of vaporization of Phenanthrene.

run#[a]	T_{avg} [°C][b]	$\Delta_l^g H_m^\circ(T_{avg})$[kJ mol^{-1}][c]	$\Delta_l^g H_m^\circ(298.15\ K)$[kJ mol^{-1}][d]	R^2 [e]
1	129.6	69.7 ± 0.8	78.4 ± 0.9	0.99877
2	130.2	70.3 ± 0.2	79.0 ± 0.3	0.99988
3	130.2	68.3 ± 0.9	77.0 ± 1.0	0.99829
4	(130.2)	(64.7 ± 1.4)	(73.5 ± 1.6)	(0.99512)
(2-4)[f]			**78.1 ± 2.0**	
lit.[10]	/	/	78.3 ± 1.8	/

[a] number of TGA experiment run [b] average temperature of experiment [c] enthalpy of vaporization at average temperature of the experiment [c] enthalpy of vaporization at 298.15 K (adjusted according to *Chickos et al.* [9] using their heat capacity increments) [e] coefficient of determination of ln((dm/dt)T$^{0.5}$) vs. 1/T-plot. [f] average value with 2.0 kJ mol^{-1} uncertainty according to *Verevkin et al.*[3]

In terms of $\Delta_l^g H_m^\circ$(298.15 K) the results of run #1 (79.0 ± 0.3 kJ mol^{-1}), run #2 (79.0 ± 0.3 kJ mol^{-1}) and run #3 (77.0 ± 1.0 kJ mol^{-1}) as well as the average value (78.1 ± 2.0 kJ mol^{-1}) are in agreement with the literature value of 78.3 ± 1.8 kJ mol^{-1} recommended by *Roux et al.[10]*. Figure 3 is a plot of the analog pressure versus reciprocal temperature. It becomes apparent that for run #3 and especially run #4 the linear relation is lost at higher temperatures. For this reason the results from run #4 are considered erroneous.

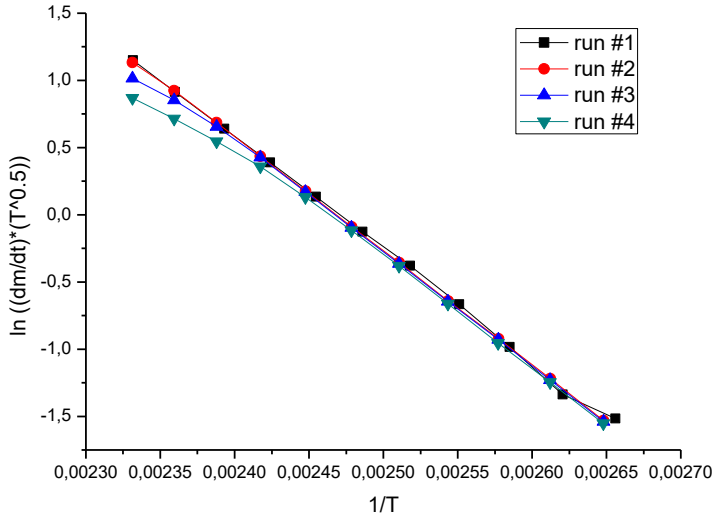

Figure 3: Plot of ln((dm/dt)√T) vs. 1/T of the experimental results obtained for phenanthrene.

8.1.2 Measurement of Hexadecane

Hexadecane was obtained from Sigma Aldrich and distilled under reduced pressure (0.26 mbar, 115-116 °C). The measurement was carried out in the temperature range from 68 to 149 °C. The obtained sets of data were cut to the temperature range from 68 to 134 °C with respect to the non-linear behavior of the data points at higher temperatures. (cf. *Figure 4*).

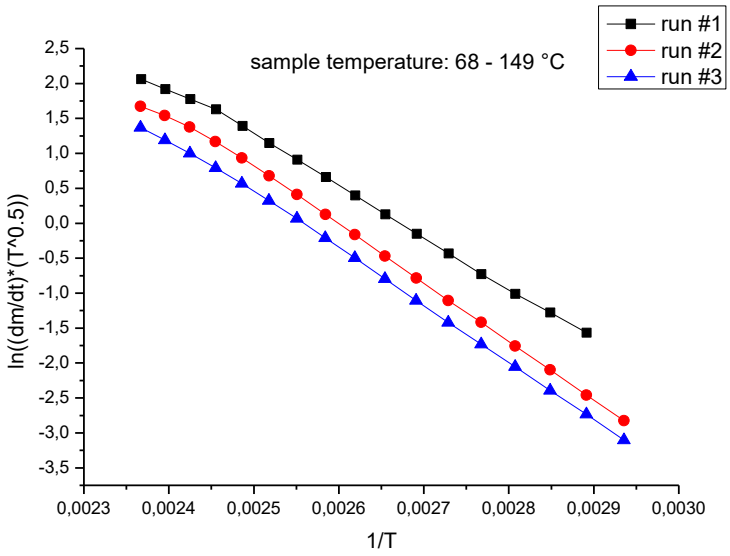

Figure 4: Plot of ln((dm/dt)√T) vs. 1/T of the experimental results obtained for hexadecane.

The literature value stated by *Verevkin et al.*[3] ($\Delta_l^g H_m^\circ$(298.15 K) = 80.7 ± 0.4 kJ mol^{-1}) was derived from transpiration method measurements. It is in excellent agreement with the results from run #2 (80.6 ± 0.2 kJ mol^{-1}) and the average value (79.8 ± 2.0 kJ mol^{-1}) and in sufficient agreement with the results from run #3 (78.9 ± 0.3 kJ mol). (cf. Table 2)

Table 2: Selected results of the TGA-experiment for the determination of the enthalpy of vaporization of Hexadecane.

run#[a]	T_{avg} [°C][b]	$\Delta_l^g H_m^\circ(T_{avg})$[kJ mol^{-1}][c]	$\Delta_l^g H_m^\circ$(298.15 K)[kJ mol^{-1}][d]	R^2 [e]
2	100.9	69.6 ± 0.2	80.6 ± 0.2	0.99992
3	100.9	68.0 ± 0.2	78.9 ± 0.3	0.99986
(2-3)[f]			**79.8 ± 2.0**	
lit.[3]	/	/	80.7 ± 0.4	/

[a] number of TGA experiment run [b] average temperature of experiment [c] enthalpy of vaporization at average temperature of the experiment [c] enthalpy of vaporization at 298.15 K (adjusted according to *Chickos et al.* [9] using their heat capacity increments) [e] coefficient of determination of ln((dm/dt)$T^{0.5}$) vs. 1/T-plot. [f] Average value with 2.0 kJ mol^{-1} uncertainty according to *Verevkin et al.*[3]

8.1.3 Measurement of Dibutyl Phthalate

Dibutyl phthalate was obtained from *Sigma-Aldrich* and distilled at reduced pressure (0.07 mbar, 141-142 °C). The measurement was performed in temperature range from 119 °C to 184 °C. The obtained sets of data were cut to the temperature range from 119 to 169 °C with respect to the non-linear behavior of the data points at higher temperatures. (cf. Figure 5). Within this range the mass loss was between 0.2 to 2.4 mg per 10 minutes.

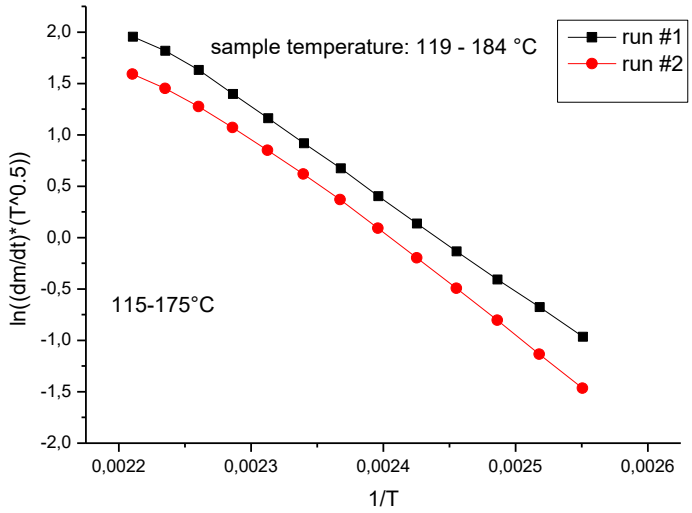

Figure 5: Plot of ln((dm/dt)√T) vs. 1/T of the experimental results obtained for dibutylphtalate.

The literature value stated by *Verevkin et al.*[3] ($\Delta_{cr}^{g}H_{m}^{\circ}$(298.15 K) = 95.8 ± 0.3 kJ mol^{-1}) was derived from transpiration method measurements. It is in good agreement with the results derived from run #2 in this work. (cf. Table 3)

Table 3: Selected results of the TGA-experiment for the determination of the enthalpy of vaporization of dibutylphtalate.

run#[a]	T_{avg} [°C][b]	$\Delta_{l}^{g}H_{m}^{\circ}(T_{avg})$[kJ mol^{-1}][c]	$\Delta_{l}^{g}H_{m}^{\circ}$(298.15 K)[kJ mol^{-1}][d]	R^2 [e]
2	144.1	74.6 ± 1.1	95.9 ± 1.4	0.99822
lit.[3]	/	/	95.8 ± 0.3	/

[a] number of TGA experiment run [b] average temperature of experiment [c] enthalpy of vaporization at average temperature of the experiment [c] enthalpy of vaporization at 298.15 K (adjusted according to *Chickos et al.* [9] using their heat capacity increments) [e] coefficient of determination of ln((dm/dt)$T^{0.5}$) vs. 1/T-plot.

8.1.4 Measurement of DMDNB 26

The explosives taggant DMDNB **26** was used as received from *Sigma-Aldrich*. The best measurement conditions could be found in the temperature regime from 70 – 100 °C. In this temperature range DMDNB **26** exists in the polymorph phase II (cf. chapter 7.7).

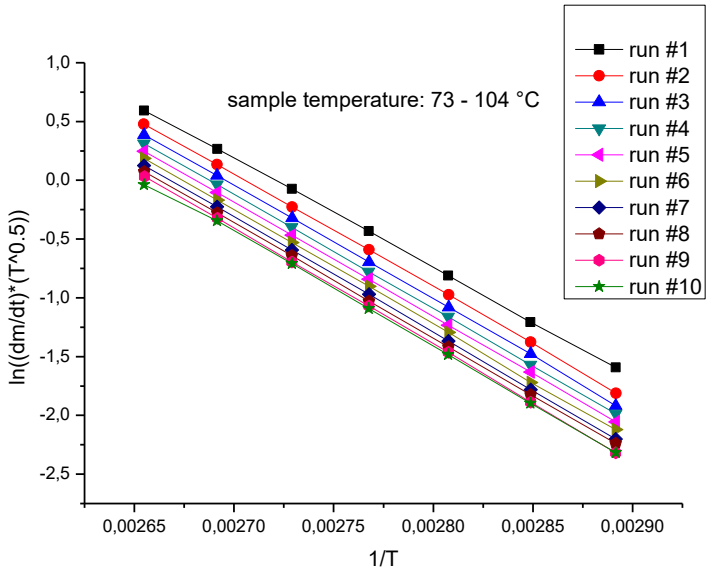

Figure 6: Plot of ln((dm/dt)√T) vs. 1/T of the experimental results obtained for DMDNB 26

The results obtained from run #2 – run #9 (average value: 86.6 ± 2.0 kJ mol^{-1}**)** are in good agreement with the values for phase II of DMDNB **26** measured with the transpiration method in this work. ($\Delta_l^g H_m^\circ$(298.15 K): experiment from Rostock: 85.2 ± 1.3 kJ mol^{-1}, experiment from Munich: 87.8 ± 0.7 kJ mol^{-1}). (cf. chapter 7.7, Table 2) (cf. Table 4)

Table 4: Selected results of the TGA-experiment for the determination of the enthalpy of sublimation of DMDNB 26.

run#[a]	T_{avg} [°C][b]	$\Delta_{cr}^g H_m^\circ(T_{avg})$[kJ mol^{-1}][c]	$\Delta_{cr}^g H_m^\circ$(298.15 K)[kJ mol^{-1}][d]	R^2 [e]
2	88.2	80.1 ± 0.2	85.4 ± 0.2	0.99979
3	88.2	80.7 ± 0.3	86.0 ± 0.3	0.99984
4	88.2	80.8 ± 0.2	86.2 ± 0.2	0.99998
5	88.2	80.8 ± 0.2	86.2 ± 0.3	0.99998
6	88.1	81.3 ± 0.3	86.7 ± 0.3	0.99987
7	88.2	81.9 ± 0.1	87.2 ± 0.1	0.99994
8	88.1	81.5 ± 0.4	86.8 ± 0.4	0.99997
9	88.1	82.6 ± 0.3	88.0 ± 0.4	0.99989
(2-9)[f]			**86.6 ± 2.0**	
this work[g]			87.8 ± 0.7	

[a] number of TGA experiment run [b] average temperature of experiment [c] enthalpy of sublimation at average temperature of the experiment [c] enthalpy of sublimation at 298.15 K (adjusted according to *Chickos et al.* [9] using their heat capacity increments) [e] coefficient of determination of ln((dm/dt)$T^{0.5}$) vs. 1/T-plot. [f] Average value with 2.0 kJ mol^{-1} uncertainty according to *Verevkin et al.*[3] [g] value measured with the transpiration method in this work (cf. chapter 7.7, table 2)

This demonstrates that TGA measurements can also be applied for the determination of enthalpies of sublimation of solids without melting the sample in advance.

8.1.5 Measurement of 2-MNT 12

2-MNT **12** was obtained from *Sigma-Aldrich* and used as received. The measurement was performed in temperature range from 35 °C to 67 °C. Within this range the mass loss was between 0.3 to 1.8 mg per 10 minutes. (cf. Figure 7) The enthalpies of vaporization derived from the results obtained (cf. Table 5) (average value: 53.0 ± 2.0 kJ mol^{-1}) are not in agreement with the values recommended in this work ($\Delta_l^g H_m^\circ$(298.15 K) = 59.8 ± 0.2 kJ mol^{-1}) (cf. section 7.4, Table 2 (publication)) despite the high linearity of the results.

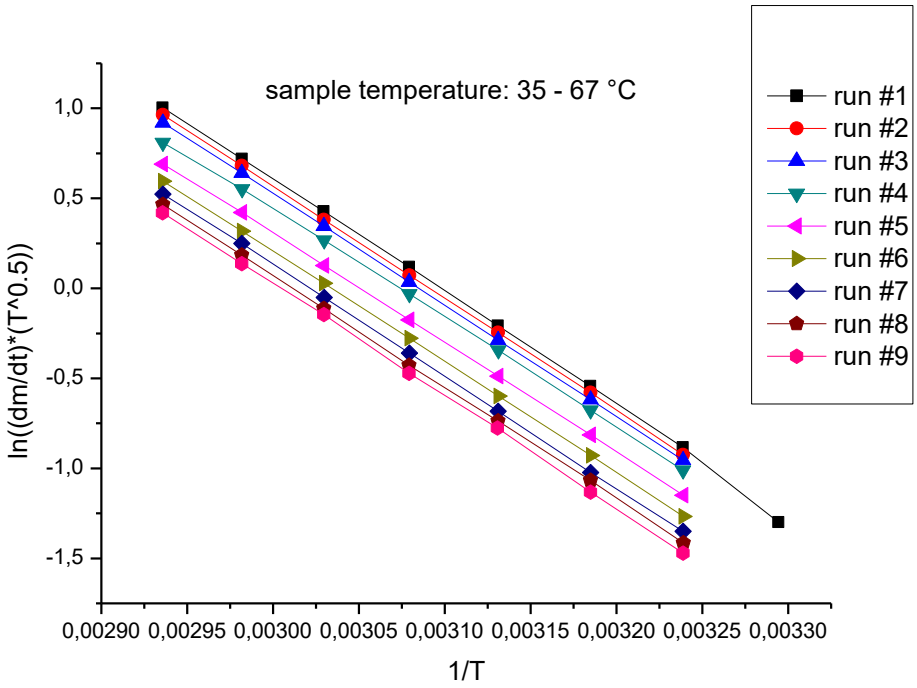

Figure 7 - Plot of ln((dm/dt)√T) vs. 1/T of the experimental results obtained for 2-MNT 12.

Table 5 - Selected results of the TGA-experiment for the determination of the enthalpy of vaporization of 2-MNT 12.

run#[a]	T_{avg} [°C][b]	$\Delta_{cr}^g H_m^\circ(T_{avg})$[kJ mol^{-1}][c]	$\Delta_{cr}^g H_m^\circ$(298.15 K)[kJ mol^{-1}][d]	R^2 [e]
1	322.1	(52.8 ± 0.6)	(54.4 ± 0.6)	0.99916
2	324.7	51.7 ± 0.1	53.5 ± 0.1	0.99996
3	324.7	51.5 ± 0.1	53.2 ± 0.1	0.99998
4	324.7	50.1 ± 0.3	51.8 ± 0.3	0.99974
5	324.7	50.5 ± 0.1	52.2 ± 0.2	0.99995
6	324.7	51.1 ± 0.1	52.8 ± 0.1	0.99996
7	324.7	51.6 ± 0.2	53.4 ± 0.2	0.99995
8	324.7	51.5 ± 0.2	53.2 ± 0.2	0.99991
9	324.7	51.9 ± 0.3	53.6 ± 0.3	0.99979
(2-9)[f]			**53.0 ± 2.0**	
rec.[g]			59.8 ± 0.2	

[a] number of TGA experiment run [b] average temperature of experiment [c] enthalpy of sublimation at average temperature of the experiment [c] enthalpy of sublimation at 298.15 K (adjusted according to *Chickos et al.* [9] using their heat capacity increments) [e] coefficient of determination of ln((dm/dt)T$^{0.5}$) vs. 1/T-plot. [f] Average value with 2.0 kJ mol^{-1} uncertainty according to *Verevkin et al.*[3] [g] value recommended in this work (cf. section 7.4, Table 2 (publication))

8.1.6 Measurement of 3-MNT 13

3-MNT **13** was obtained from *Sigma-Aldrich* and used as received. The measurement was performed in temperature range from 30 °C to 78 °C. Within this range the mass loss was between 0.5 to 2.0 mg per 10 minutes. (cf. Figure 8)

The enthalpies of vaporization derived from the results obtained (cf. Table 6) (average value: 50.1 ± 2.0 kJ mol^{-1}) are not in agreement with the values recommended in this work ($\Delta_l^g H_m^\circ$(298.15 K) = 59.4 ± 0.2 kJ mol^{-1}) (cf. section 7.4, Table 2 (publication)) despite the high linearity of the results.

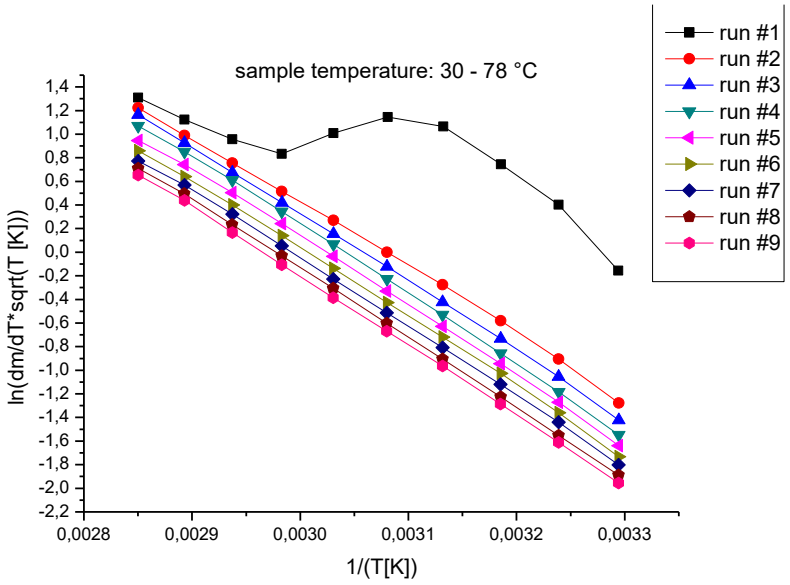

Figure 8 - Plot of ln((dm/dt)√T) vs. 1/T of the experimental results obtained for 3-MNT 13

Table 6 - Selected results of the TGA-experiment for the determination of the enthalpy of vaporization of 3-MNT 13.

run#[a]	T_{avg} [°C][b]	$\Delta_l^g H_m^\circ(T_{avg})$[kJ mol^{-1}][c]	$\Delta_l^g H_m^\circ$(298.15 K)[kJ mol^{-1}][d]	R^2 [e]
2	327.2	46.0 ± 0.6	47.9 ± 0.6	0.99847
3	327.2	47.9 ± 0.4	49.9 ± 0.4	0.99940
4	327.2	49.0 ± 0.5	50.9 ± 0.5	0.99923
5	327.2	48.5 ± 0.5	50.4 ± 0.6	0.99894
6	327.2	48.3 ± 0.5	50.2 ± 0.5	0.99911
7	327.2	48.3 ± 0.4	50.2 ± 0.4	0.99939
8	327.2	48.9 ± 0.3	50.8 ± 0.3	0.99971
9	327.2	48.9 ± 0.2	50.8 ± 0.3	0.99978
(2-9)[f]			**50.1 ± 2.0**	
rec.[g]			59.4 ± 0.2	

[a] number of TGA experiment run [b] average temperature of experiment [c] enthalpy of vaporization at average temperature of the experiment [c] enthalpy of vaporization at 298.15 K (adjusted according to *Chickos et al.* [9] using their heat capacity increments) [e] coefficient of determination of ln((dm/dt)$T^{0.5}$) vs. 1/T-plot. [f] Average value with 2.0 kJ mol^{-1} uncertainty according to *Verevkin et al.*[3] [g] value recommended in this work (cf. section 7.4, Table 2 (publication))

8.1.7 Measurement of 4-MNT 14

4-MNT **14** was obtained from *Sigma-Aldrich* and used as received. The measurement was performed in temperature range from 30 °C to 52 °C for the measurement of the enthalpy of sublimation and from 67 – 103 °C for the enthalpy of vaporization. For the sublimation experiment the mass loss was between 0.1 to 0.3 mg per 10 minutes (cf. Figure 10). For the vaporization experiment the mass loss was between 0.4 to 2.5 mg per 10 minutes. (cf. Figure 9)

The enthalpies of sublimation derived from the results obtained (cf. Table 8) (average value: 66.4 ± 2.0 kJ mol^{-1}) are not in agreement with the value recommended in this work ($\Delta_{cr}^{g}H_{m}^{\circ}$(298.15 K) = 75.3 ± 0.3 kJ mol^{-1}) (cf. section 7.4, Table 2 (publication)) despite the high linearity of the results obtained.

The enthalpies of vaporization derived from the results obtained (cf. Table 7) (average value: 57.3 ± 2.0 kJ mol^{-1}) are not in agreement with the value recommended in this work ($\Delta_{l}^{g}H_{m}^{\circ}$(298.15 K) = 60.4 ± 0.3 kJ mol^{-1}) (cf. section 7.4, Table 2 (publication)) despite the high linearity of the results obtained.

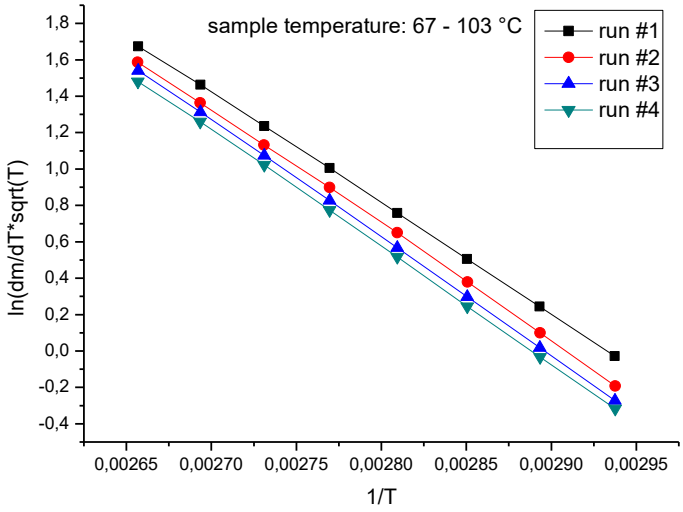

Figure 9 Plot of ln((dm/dt)√T) vs. 1/T of the experimental results obtained 4-MNT 14. (vaporization)

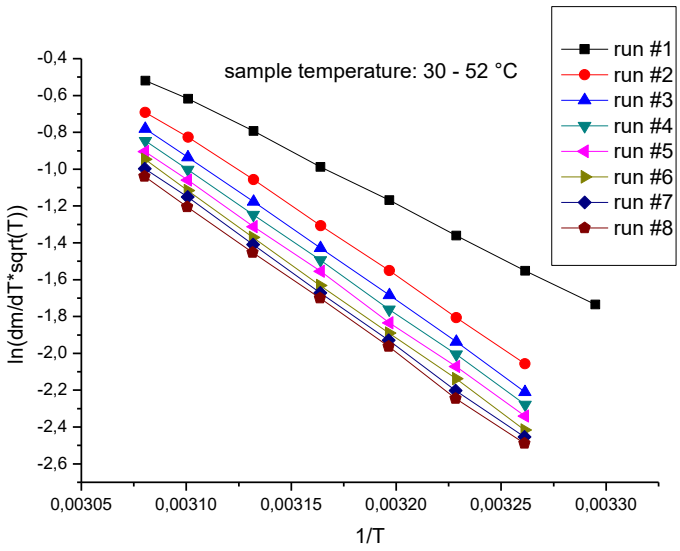

Figure 10 Plot of ln((dm/dt)√T) vs. 1/T of the experimental results obtained for 4-MNT 14. (sublimation)

Table 7 Selected results of the TGA-experiment for the determination of the enthalpy of vaporization of 4-MNT 14.

run#[a]	T_{avg} [°C][b]	$\Delta_l^g H_m^\circ(T_{avg})$[kJ mol^{-1}][c]	$\Delta_l^g H_m^\circ(298.15\ K)$[kJ mol^{-1}][d]	R^2 [e]
2	358.4	52.6 ± 0.4	56.6 ± 0.4	0.99961
3	358.4	53.8 ± 0.2	57.8 ± 0.2	0.99992
4	358.4	53.5 ± 0.2	57.5 ± 0.3	0.99986
2-4			57.3 ± 2.0	
rec.[g]			75.3 ± 0.3	

[a] number of TGA experiment run [b] average temperature of experiment [c] enthalpy of vaporization at average temperature of the experiment [c] enthalpy of vaporization at 298.15 K (adjusted according to *Chickos et al.* [9] using their heat capacity increments) [e] coefficient of determination of $\ln((dm/dt)T^{0.5})$ vs. 1/T-plot. [f] Average value with 2.0 kJ mol^{-1} uncertainty according to *Verevkin et al.*[3] [g] value recommended in this work (cf. section 7.4, Table 2 (publication)).

Table 8 Selected results of the TGA-experiment for the determination of the enthalpy of sublimation of 4-MNT 14.

run#[a]	T_{avg} [°C][b]	$\Delta_l^g H_m^\circ(T_{avg})$[kJ mol^{-1}][c]	$\Delta_l^g H_m^\circ(298.15\ K)$[kJ mol^{-1}][d]	R^2 [e]
2	315.6	63.2 ± 0.5	63.6 ± 0.6	0.99956
3	315.6	65.5 ± 0.4	66.0 ± 0.4	0.99980
4	315.6	65.7 ± 0.3	66.1 ± 0.3	0.99987
5	315.6	66.0 ± 0.4	66.5 ± 0.4	0.99981
6	315.6	67.1 ± 0.3	67.6 ± 0.3	0.99986
7	315.6	67.4 ± 0.3	67.9 ± 0.4	0.99984
8	315.7	66.8 ± 0.5	67.3 ± 0.5	0.99969
2-8			66.4 ± 2.0	
rec.[g]			60.4 ± 0.3	

[a] number of TGA experiment run [b] average temperature of experiment [c] enthalpy of sublimation at average temperature of the experiment [c] enthalpy of sublimation at 298.15 K (adjusted according to *Chickos et al.* [9] using their heat capacity increments) [e] coefficient of determination of $\ln((dm/dt)T^{0.5})$ vs. 1/T-plot. [f] Average value with 2.0 kJ mol^{-1} uncertainty according to *Verevkin et al.*[3] [g] value recommended in this work (cf. section 7.4, Table 2 (publication)).

8.1.8 Measurement of 2,4-DNT 15

2,4-Dinitrotoluene was obtained from *Sigma-Aldrich* and used as received. The measurement was performed in temperature range from 83 °C to 118 °C for the measurement of the enthalpy of vaporization. The rate of mass loss was between 0.03 to 0.23 mg per 10 minutes. (cf. Figure 11)

The enthalpies of vaporization derived from the results obtained (cf. Table 9) (average value: 77.3 ± 2.0 kJ mol^{-1}) are in agreement with the value recommended in this work ($\Delta_l^g H_m^\circ$(298.15 K) = 78.0 ± 0.6 kJ mol^{-1}) (cf. section 7.5, Table 5).

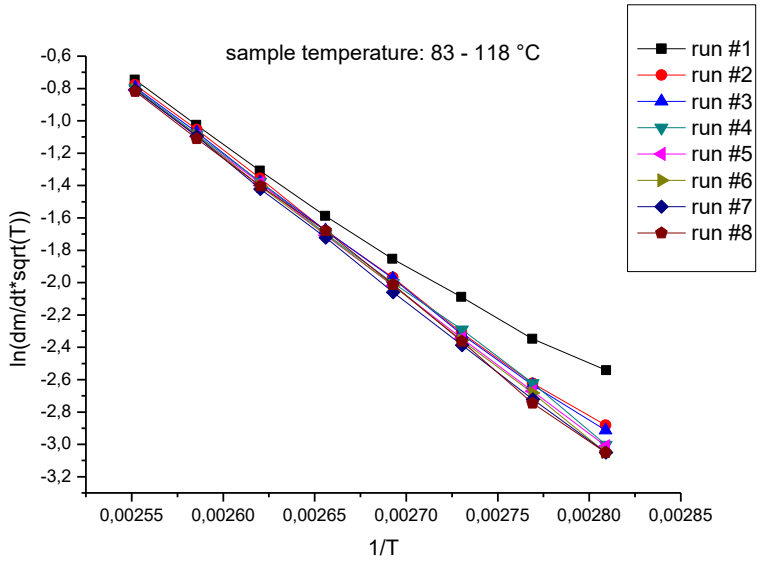

Figure 11 - Plot of ln((dm/dt)√T) vs. 1/T of the experimental results obtained for 2,4-DNT 15.

Table 9 Selected results of the TGA-experiment for the determination of the enthalpy of vaporization of 2,4-DNT 15.

run#[a]	T_{avg} [°C][b]	$\Delta_l^g H_m^\circ(T_{avg})$[kJ mol^{-1}][c]	$\Delta_l^g H_m^\circ$(298.15 K)[kJ mol^{-1}][d]	R^2 [e]
2	373.94	69.3 ± 1.0	75.3 ± 1.1	0.99847
3	373.93	69.4 ± 0.7	75.4 ± 0.8	0.99920
4	373.93	70.5 ± 0.6	76.5 ± 0.6	0.99951
5	373.92	71.4 ± 0.2	77.4 ± 0.2	0.99995
6	373.93	72.4 ± 0.3	78.4 ± 0.3	0.99989
7	373.92	72.9 ± 0.4	78.9 ± 0.5	0.99978
8	373.93	72.9 ± 0.9	78.9 ± 1.0	0.99896
(2-8)[f]			77.3 ± 2.0	
this work[g]			78.0 ± 0.6	

[a] number of TGA experiment run [b] average temperature of experiment [c] enthalpy of vaporization at average temperature of the experiment [c] enthalpy of vaporization at 298.15 K (adjusted according to *Chickos et al.* [9] using their heat capacity increments) [e] coefficient of determination of ln((dm/dt)$T^{0.5}$) vs. 1/T-plot. [f] Average value with 2.0 kJ mol^{-1} uncertainty according to *Verevkin et al.*[3] [g] value measured in this work (cf. chapter 7.5, table 5)

8.1.9 Measurement of 2,6-DNT 16

2,6-Dinitrotoluene **16** was obtained from *Sigma-Aldrich* and used as received. The measurement was performed in temperature range from 73 °C to 114 °C for the measurement of the enthalpy of vaporization. The rate of mass loss was between 0.03 to 0.35 mg per 10 minutes. (cf. Figure 12)

The enthalpies of vaporization derived from the results obtained (cf. Table 10) (average value: 75.1 ± 2.0 kJ mol^{-1}) are in agreement with the value measured with the transpiration method in this work ($\Delta_l^g H_m^\circ$(298.15 K) = 77.1 ± 0.6 kJ mol^{-1}) (cf. section 7.5, Table 9).

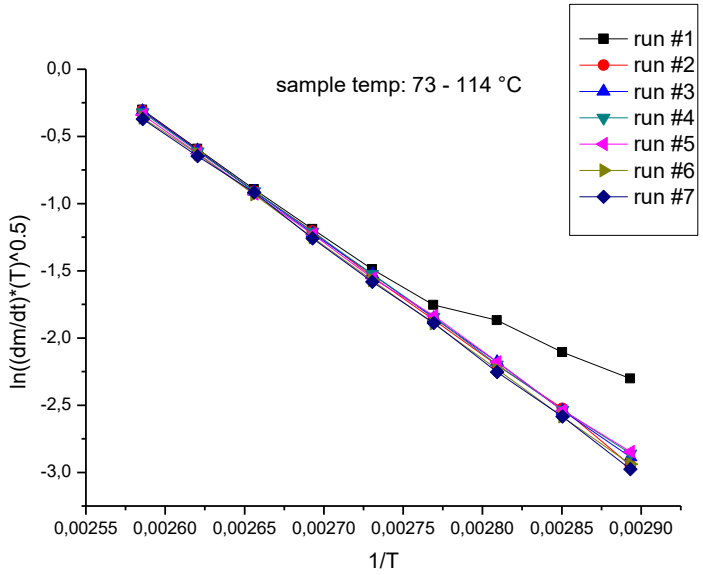

Figure 12 - Plot of ln((dm/dt)√T) vs. 1/T of the experimental results obtained for 2,6-DNT 15.

Table 10 Selected results of the TGA-experiment for the determination of the enthalpy of vaporization of 2,6-DNT 15.

run#[a]	T_{avg} [°C][b]	$\Delta_l^g H_m^\circ(T_{avg})$[kJ mol^{-1}][c]	$\Delta_l^g H_m^\circ$(298.15 K)[kJ mol^{-1}][d]	R^2 [e]
2	366.2	70.7 ± 0.5	76.1 ± 0.5	0.99962
3	366.2	69.6 ± 0.2	75.0 ±0.2	0.99994
4	366.2	69.1 ± 0.3	74.4 ±0.3	0.99983
5	366.2	68.1 ± 0.4	73.5 ± 0.5	0.99967
6	366.2	70.1 ± 0.2	75.5 ± 0.2	0.99992
7	366.2	70.6 ± 0.5	76.0 ±0.5	0.99959
(2-9)[f]			**75.1 ± 2.0**	
this work[g]			77.1 ± 0.6	

[a] number of TGA experiment run [b] average temperature of experiment [c] enthalpy of vaporization at average temperature of the experiment [c] enthalpy of vaporization at 298.15 K (adjusted according to Chickos et al. using their heat capacity increments) [e] coefficient of determination of ln((dm/dt)$T^{0.5}$) vs. 1/T-plot. [f] Average value with 2.0 kJ mol^{-1} uncertainty according to *Verevkin et al.*[3] [g] value measured in this work (cf. chapter 7.5, table 9)

8.1.10 Measurement of TNT 17

TNT **17** was obtained from Fluka and used as first energetic substance. The melting point of TNT **17** is 81 °C and its decomposition temperature 306 °C. (cf. section 4 table 3). The temperature range from 80 °C to 200 °C was monitored to find the optimum temperature range. The final measurements were carried out in the temperature range from 109 °C to 139 °C. The mass loss rate within this temperature interval ranged between 0.03 to 0.19 mg per 10 minutes. Prior to the measurement the sample was conditioned in the TGA device at 110 °C for 2 hours. After the experiment a ^{1}H-NMR spectrum was recorded to ensure that the sample did not decompose during the measurement. No decomposition products could be observed.

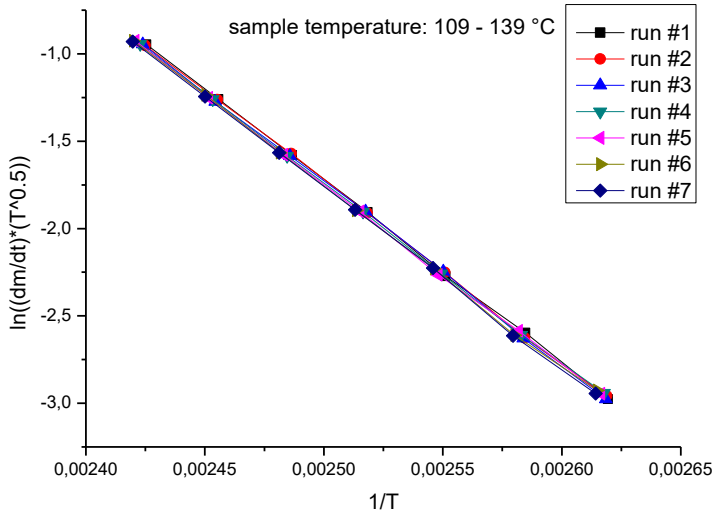

Figure 13: Plot of ln((dm/dt)√T) vs. 1/T of the experimental results obtained for TNT 17.

The literature value ($\Delta_l^g H_m^\circ$(298.15 K) = 97.6 ± 1.3 kJ mol^{-1}) was derived from Knudsen-effusion measurements of liquid TNT stated by Edwards.[11] The results derived from run #2 – #7 ((average value: 95.5 ± 2.0 kJ mol^{-1}) are in agreement with this literature value.

Table 11: Selected results of the TGA-experiment for the determination of the enthalpy of vaporization of TNT 17.

run#[a]	T_{avg} [°C][b]	$\Delta_l^g H_m^\circ(T_{avg})$[kJ mol^{-1}][c]	$\Delta_l^g H_m^\circ$(298.15 K)[kJ mol^{-1}][d]	R^2 [e]
2	124.0	86.6 ± 0.6	95.8 ± 0.7	0.99971
3	124.1	86.8 ± 0.7	95.9 ± 0.8	0.9996
4	124.3	85.7 ± 0.5	94.8 ± 0.5	0.99983
5	124.5	85.8 ± 0.5	95.0 ± 0.6	0.99979
6	124.7	86.1 ± 0.7	95.4 ± 0.8	0.99959
7	124.8	86.6 ± 0.6	95.8 ± 0.7	0.99967
(2-7)[f]			**95.5 ± 2.0**	
lit.[11]	111.4	89.8 ± 1.2	97.6 ± 1.3	0.99897

[a] number of TGA experiment run [b] average temperature of experiment [c] enthalpy of vaporization at average temperature of the experiment [c] enthalpy of vaporization at 298.15 K (adjusted according to *Chickos et al.* [9] using their heat capacity increments) [e] coefficient of determination of ln((dm/dt)T$^{0.5}$) vs. 1/T-plot. [f] Average value with 2.0 kJ mol^{-1} uncertainty according to *Verevkin et al.*[3]

In addition to the measurement of the enthalpy of vaporisation it was tried to perform experiments to receive the enthalpy of sublimation of TNT **17**. The experiments were performed in a temperature

range of 40-70 °C due to the melting point of TNT **17** at 80 °C. The first screening run showed no linearity of the results obtained and mass losses were extremely low, so a second experiment was executed with elongated isothermal times, which were 60 minutes instead of 15 minutes. No linear relationship of $\ln(dm/dt \cdot (T)^{0.5})$ versus 1/T could be obtained. The mass loss rates ranged 0.2 to 1.0 µg per 10 minutes.

8.2 Facit

The enthalpies of vaporization and sublimation obtained by the TGA experiments in this work are summarized and compared with reference values in Table 12. For all compounds besides the mono-nitrotoluenes **12**-**14** a sufficient agreement between TGA result and reference value could be established. The uncertainty of the TGA results was estimated to be 2.0 kJ mol^{-1} according to the results for low-volatile liquids from *Verevkin et al.*[3]. The reason for the failure of the experiment with the mononitrotoluene compounds **12**-**14** is probably linked to their increased volatility since their enthalpies of vaporization and sublimation and vapor pressures at room temperature (cf. Table 12) are higher than those of the other compounds. Regarding the results obtained in this work the isothermal TGA experiment for the determination of vaporization and sublimation enthalpies is suitable for compounds with an enthalpy of vaporization above 75 kJ mol^{-1} (298.15 K) and a vapor pressure below 1 Pa (298.15 K). The method and TGA device used in this work could not be applied to the low-volatile solid TNT **17** ($\Delta^{g}_{cr}H^{\circ}_{m}$(298.15K) = 111.6 ± 0.6 kJ mol^{-1}, p_{sat}(298.15 K): 0.9 mPa) with respect to the low mass loss rates ranging from 0.2 to 1.0 µg per 10 minutes in the temperature range from 40 to 70 °C. The measured mass loss rates should be above 0.1 mg per 10 minutes. With DMDNB **26** it could be demonstrated that reasonable results can also be obtained for solid compounds despite the more complex surface in comparison to liquids.

Table 12 – Summary of results obtained by TGA in comparion with reference values.

Compound	$\Delta^{g}_{l/cr}H^{\circ}_{m}$(298.15 K) (TGA)[a]	$\Delta^{g}_{l/cr}H^{\circ}_{m}$(298.15 K) (REF)[b]	Agreement[c]	p_{sat}(298.15 K)[d]
	[kJ mol^{-1}]	[kJ mol^{-1}]		[Pa]
Phenanthrene (l)	78.1 ± 2.0	78.3 ± 1.8	yes	24.2 [12]
Hexadecane (l)	79.8 ± 2.0	80.7 ± 0.4	yes	< 1 [13]
DBP (l)	95.9 ± 2.0	95.8 ± 0.3	yes	0.002 [14]
DMDNB (cr)	86.6 ± 2.0	87.8 ± 0.7	yes	0.2[e]
2-MNT (l)	53.0 ± 2.0	59.8 ± 0.2	no	18.0[e]
3-MNT (l)	50.1 ± 2.0	59.4 ± 0.2	no	11.7[e]
4-MNT (l)	57.3 ± 2.0	75.3 ± 0.3	no	9.5[e]
4-MNT (cr)	66.4 ± 2.0	60.4 ± 0.3	no	5.4[e]
2,4-DNT (l)	77.3 ± 2.0	78.0 ± 0.6	yes	0.1[e]
2,6-DNT (l)	75.1 ± 2.0	77.1 ± 0.6	yes	0.2[e]
2,4,6-TNT (l)	95.5 ± 2.0	97.6 ± 1.3	yes	<0.001[14]

[a] enthalpy of vaporization/sublimation at 298.15 K measured by TGA method (cf. Table 1 – 11), [b] reference value for enthalpy of vaporization/sublimation at 298.15 K (cf. Table 1 – 11), [c] agreement of TGA and reference value, [d] vapor pressure at 298.15 K [e] results obtained in this work

A major disadvantage of the TGA experiments in this work is that the coefficient of determination R^2 is not a reliable parameter for the correctness of the results obtained. For the experiments with the mono-nitrotoluenes **12**-**14** all obtained R^2 values are >0.998. Despite that the derived enthalpies of vaporization and sublimation were proven to be wrong.

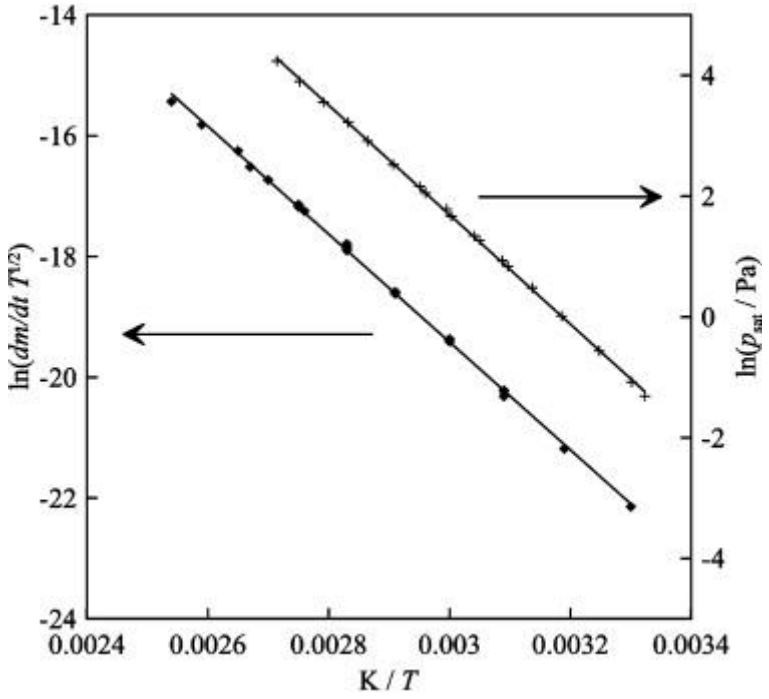

Figure 14 Comparison of the results from the transpiration method and TGA for hexadecane; + – the transpiration data, ♦ – the TGA data. Reprinted with permission from [3] Copyright 2012 Elsevier B.V.

Figure 14 demonstrates that the pressure analog values ($\ln((dm/dt)T^{0.5})$) obtained from the TGA experiment need to be converted to real pressure values by calibration with a reference substance with well-known vapor pressure or a measurement of the compound with a well-established measurement method for vapor pressure. (cf. Figure 14) Despite the numerous literature examples for calibration with a compound different to the analyte [1-2, 5, 7, 15-17] the use of a calibrant for the determination of the vaporization coefficient α (cf. equation (1)) different to the analyte should be avoided for various reasons:

- It has not been proven that α is independent of the analyte and the measurement temperature. This needs to be investigated carefully. [3]
- The results obtained in this work have demonstrated that α drifts for each experimental run. (cf. Figure 2 – 12) This problem is more severe for volatile compounds in comparison to low-volatile compounds.
- The results presented in this work are the best results obtained. It was observed that for other individual experiments of the same analyte results with good coefficients of determination but wrong enthalpies of vaporization (in comparison with values from well-established methods) were obtained.

With respect to this it is recommended to use the isothermal TGA method for the determination of vaporization and sublimation enthalpies exclusively for analytes that have been characterized with a well-established method like the transpiration method used in this work. If the results of both methods are in agreement the TGA experiment is a useful supplement for the validation of experiments with well-established methods. This is the case for DMDNB **26**. The TGA experiment supports the results obtained with the transpiration method in this work that are in conflict with literature values. The isothermal TGA experiment for the determination of the enthalpies of vaporization and sublimation is a quick (<24 h), fully automated method. Yet it should not be used without additional well-established method for the validation of the results obtained. If both methods are in agreement the vaporization coefficient α can be determined for the conversion of the pressure analog values to real vapor pressure values and extend the temperature range of known vapor pressures for an analyte.

Literature References

1. Gücke, W.; Rittig, F. R.; Synnatschke, G., A method for determining the volatility of active ingredients used in plant protection II. Applications to formulated products. *Pesticide Science* **1974,** *5* (4), 393-400.
2. Siddiqi, M. A.; Atakan, B., Combined experiments to measure low sublimation pressures and diffusion coefficients of organometallic compounds. *Thermochimica Acta* **2007,** *452* (2), 128-134.
3. Verevkin, S. P.; Ralys, R. V.; Zaitsau, D. H.; Emel'yanenko, V. N.; Schick, C., Express thermogravimetric method for the vaporization enthalpies appraisal for very low volatile molecular and ionic compounds. *Thermochimica Acta* **2012,** *538*, 55-62.
4. Langmuir, I., The Vapor Pressure of Metallic Tungsten. *Physical Review* **1913,** *2* (5), 329-342.
5. Price, D. M.; Hawkins, M., Calorimetry of two disperse dyes using thermogravimetry. *Thermochimica Acta* **1998,** *315* (1), 19-24.
6. Price, D. M., Vapor pressure determination by thermogravimetry. *Thermochimica Acta* **2001,** *367–368* (0), 253-262.
7. Oxley, J.; Smith, J. L.; Brady, J.; Naik, S., Determination of Urea Nitrate and Guanidine Nitrate Vapor Pressures by Isothermal Thermogravimetry. *Propellants, Explosives, Pyrotechnics* **2010,** *35* (3), 278-283.
8. Ashcroft, S. J., The measurement of enthalpies of sublimation by thermogravimetry. *Thermochimica Acta* **1971,** *2* (6), 512-514.
9. Acree, W.; Chickos, J. S., Phase Transition Enthalpy Measurementsof Organic and Organometallic Compounds. Sublimation, Vaporizationand Fusion Enthalpies From 1880 to 2010. *Journal of Physical and Chemical Reference Data* **2010,** *39* (4), 043101.
10. Roux, M. V.; Temprado, M.; Chickos, J. S.; Nagano, Y., Critically Evaluated Thermochemical Properties of Polycyclic Aromatic Hydrocarbons. *Journal of Physical and Chemical Reference Data* **2008,** *37* (4), 1855-1996.
11. Edwards, G., The vapour pressure of 2 : 4 : 6-trinitrotoluene. *Transactions of the Faraday Society* **1950,** *46* (0), 423-427.
12. Macknick, A. B.; Prausnitz, J. M., Vapor pressures of high-molecular-weight hydrocarbons. *Journal of Chemical & Engineering Data* **1979,** *24* (3), 175-178.
13. López, J. A.; Pérez, P.; Gracia, M.; Gutiérrez Losa, C., GmE(298.15 K) of mixtures containing 1,2-dichloroethane. *The Journal of Chemical Thermodynamics* **1988,** *20* (4), 447-451.
14. Hammer, E.; Lydersen, A. L., The vapour pressure of di-n-butylphthalate, di-n-butylsebacate, lauric acid and myristic acid. *Chemical Engineering Science* **1957,** *7* (1), 66-72.
15. Oxley, J. C.; Smith, J. L.; Brady, J. E.; Brown, A. C., Characterization and Analysis of Tetranitrate Esters. *Propellants, Explosives, Pyrotechnics* **2012,** *37* (1), 24-39.
16. Brady, J. E.; Smith, J. L.; Hart, C. E.; Oxley, J., Estimating Ambient Vapor Pressures of Low Volatility Explosives by Rising-Temperature Thermogravimetry. *Propellants, Explosives, Pyrotechnics* **2012,** *37* (2), 215-222.
17. Mbah, J.; Knott, D.; Steward, S., Thermogravimetric study of vapor pressure of TATP synthesized without recrystallization. *Talanta* **2014,** *129*, 586-593.

9 Investigation on the Sodium and Potassium Tetrasalts of 1,1,2,2-Tetranitraminoethane

This chapter deals with the Investigation on the Sodium and Potassium Tetrasalts of 1,1,2,2-Tetranitraminoethane.

The results were published in Zeitschrift für anorganische und allgemeine Chemie [1] and are reprinted with permission.

DOI: 10.1002/zaac.201600339

The original publication of the data follows.

1. Born, M.; Härtel, M. A. C.; Klapötke, T. M.; Mallmann, M.; Stierstorfer, J., Investigation on the Sodium and Potassium Tetrasalts of 1,1,2,2-Tetranitraminoethane. *Zeitschrift für anorganische und allgemeine Chemie* **2016,** *642* (24), 1412-1418.

Journal of Inorganic and General Chemistry
ZAAC
Zeitschrift für anorganische und allgemeine Chemie
www.zaac.wiley-vch.de
ARTICLE

DOI: 10.1002/zaac.201600339

Investigation on the Sodium and Potassium Tetrasalts of 1,1,2,2-Tetranitraminoethane

Maximilian Born,[a] Martin A. C. Härtel,[a] Thomas M. Klapötke,*[a] Mathias Mallmann,[a] and Jörg Stierstorfer[a]

Keywords: High energy density materials; Nitramines; Alkali metals; Polyanions; Structure elucidation

Abstract. With respect to high-energy dense materials with high oxygen-content, the tetrasodium salt of 1,1,2,2-tetranitraminoethane as monohydrate $Na_4TNAE{\cdot}H_2O$ (**4**) and the tetrapotassium salt as dihydrate $K_4TNAE{\cdot}2H_2O$ (**5**) were synthesized and reported for the first time together with their crystal structures at 173 K. Whilst **4** cannot be dehydrated the crystal water content of **5** can be removed irreversibly at 160 °C to obtain K_4TNAE (**6**) as demonstrated by DTA and TGA measurements. K_4TNAE (**6**) was demonstrated using the small scale reactivity test to be a inferior explosive to RDX and CL-20. However the anionic nitramine compound was measured to be less toxic against *Vibrio fischeri* than RDX (EC_{50}: 240 mg·L^{-1}) with respect to its EC_{50} value above 15070 mg·L^{-1}. This demonstrates that the introduction of anionic nitramine moieties is a promising concept for the stabilization of energetic materials with lower toxicity.

Introduction

1,1,2,2-Tetranitraminoethane (TNAE) (**3**) has been first published in 1980 by *Lee* et al. in China.[1] In western literature the synthesis of TNAE (**3**) appears first in a military report from 1982.[2] The scientists from Lawrence Livermore National Laboratory intended to use it as a building block for the synthesis of novel cycloaliphatic explosives containing the secondary nitramine explosophore. The excellent acid-base reactivity of TNAE (**3**) has been reported by *Daozheng* in 1991.[3] A special focus was set on the tetrasodium salt Na_4TNAE, which was reported with a crystal density of 2.11 g·cm^{-3} and a detonation velocity of 8995 m·s^{-1} at a density of 1.89 g·cm^{-3}. Despite that an X-ray structure elucidation of Na_4TNAE has not been published. It was stated that the salt is hygroscopic, which supposedly could be overcome by the coating with TNT. In 2005 *Lee* et al.[4] published the tetrapotassium salt K_4TNAE (**6**) amongst the nitrogen-rich ammonium and guanidinium derivatives. In 2011 *Szala* et al.[5] reported a synthesis of TNAE (**3**) from glycoluril (**1**) without the use of nitronium nitrate N_2O_5 and reported for the tetrasodium salt Na_4TNAE a detonation velocity of 10900 m·s^{-1} in combination with a detonation pressure of 42.7 GPa for the theoretical maximum density of 2.11 g·cm^{-3} based on calculations with the CHEETAH code.

* Prof. Dr. T. M. Klapötke
Fax: +49-89-2180-77492
www.hedm.cup.uni-muenchen.de
E-Mail: tmk@cup.uni-muenchen.de
[a] Department of Chemistry
University of Munich (LMU)
Butenandtstr. 5–13 (D)
81377 München, Germany
Supporting information for this article is available on the WWW under **http://dx.doi.org/10.1002/zaac.201600339** or from the author.

In 2016 *Fischer* et al.[6] reported the synthesis of 1,1,2,2-tetranitratoethane (TNE), which is a powerful solid C,H,N,O oxidizer with a high oxygen balance $\Omega(CO_2)$ of 40.9 %. The isoelectronicity of the corresponding TNAE (**3**) tetraanion with TNE and the lack of structure elucidation by X-ray diffraction was the motivation to synthesize the sodium and potassium salt of TNAE. The outstanding energetic properties of the TNAE salts that were reported in the literature should be verified. Anionic nitramines are proposed structural motifs for the stabilization of energetic materials by ionic interactions.[7] Despite that the toxicity of the nitramine moieties in RDX (1,3,5-trinitroperhydro-1,3,5-triazine) is the essential motivation for the search of replacement compounds for this important ubiquitious military explosive.[8] Bearing four anionic nitramines the TNAE (**3**) tetraanion is an excellent model compound for the aquatic toxicity of anionic nitramines.

Results and Discussion

Synthesis

The synthetic route employed is based on the work of *Szala* et al.[5] since it does not require the use of nitronium nitrate N_2O_5 for the synthesis of tetranitroglycoluril (**2**). It was optimized in several aspects, which shall be elucidated in the following. The fundamental principle of synthetic optimization in the frame of this work is the abdication of purification steps of the unstable synthetic intermediates tetranitroglycoluril (TNGU) (**2**) and TNAE (**3**). TNGU (**2**) is known to be hydrolytically unstable[9] and TNAE (**3**) can only be properly stored at –30 °C. The NMR spectra of **3** must be recorded instantaneously due to its slow decomposition in solution. Therefore TNGU (**2**) and TNAE (**3**) were directly used as crude products without purification for further synthesis and only the stable

salts $Na_4TNAE{\cdot}H_2O$ (**4**) and $K_4TNAE{\cdot}2H_2O$ (**5**) were purified by vapor diffusion recrystallization.

The synthesis starts from commercially available glycoluril (**1**), which can also be easily prepared by the acid-catalyzed condensation of urea and glyoxal.[10] **1** can be nitrated four times by the use of *in situ* generated acetyl nitrate in fuming nitric acid. For the aqueous, alkaline hydrolysis and decarboxylation of TNGU (**2**) *Szala* et al.[5] suggest the use of sodium hydroxide (3 M, aq.). Under these conditions the reaction of TNGU (**2**) is strongly exothermic and led twice to the autoignition of reactant **2** during the addition. Therefore a lower base concentration (1 M, aq.) was applied facilitating the addition of TNGU (**2**). With TNAE (**3**) in hands the synthesis of the salts could be started. For $Na_4TNAE{\cdot}H_2O$ (**4**) the literature procedure[5a] was applied using methanol as solvent. The synthesis of $K_4TNAE{\cdot}2H_2O$ (**5**) was carried out in water. For both salts the crude product was purified by gas-phase diffusion of methanol in a highly concentrated aqueous solution of the corresponding crude product. This cleanup step results in crystals that are suitable for X-ray structure elucidation. $K_4TNAE{\cdot}2H_2O$ (**5**) can be dehydrated to K_4TNAE (**6**) at 160 °C in nearly quantitative yield (Figure 1). K_4TNAE (**6**) is not hygroscopic since the subjection of a sample to ambient conditions for two weeks did not alter the results of elemental analysis.

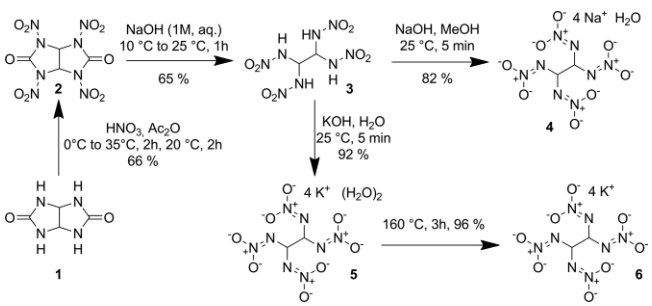

Figure 1. Synthetic route for the synthesis of the target compounds $Na_4TNAE{\cdot}H_2O$ (**4**), $K_4TNAE{\cdot}2H_2O$ (**5**), and K_4TNAE (**6**).

Vibrational and NMR Spectroscopy

The crystal water absorptions in the IR spectra of **4** (3476, 3246 cm^{-1}) and **5** (3486 cm^{-1}) are absent in the case of anhydrous K_4TNAE (**6**). The N–H functionality in TNAE (**3**) causes a strong IR absorption at 3236 and 3146 cm^{-1}, which is absent in the IR spectra of compounds **4**–**6**. All compounds show the characteristic absorptions of the TNAE (**3**) tetraanion. Furthermore strong absorption bands associated with the nitramine functionality can be observed at 1433/1388/1332 cm^{-1} (**4**/**5**/**6**), 1392/1332/1372 cm^{-1} and 1289/1270/1298 cm^{-1}. The NMR spectra in D_2O of **4** and **5** are almost identical with a singlet at 5.97 (**4**) and 5.95 ppm (**5**) corresponding to the C–H functionality in the proton NMR spectrum, a ^{13}C signal at $\delta = 74.6$ ppm, and a ^{14}N signal at –25 ppm corresponding to the nitro group.

X-ray Diffraction

The solid-state structures of $Na_4TNAE{\cdot}H_2O$ (**4**) and $K_4TNAE{\cdot}2H_2O$ (**5**) were determined by low temperature (173 K) single-crystal X-ray diffraction. Details on the measurements and refinements are given in the Supplementary Information. Cif files were deposited with the CCDC database.[11] Single crystals containing crystal water of both compounds were grown by slow diffusion of methanol into a saturated aqueous solution of the corresponding compound. The sodium salt crystallizes as a monohydrate (**4**) in the monoclinic space group $P2_1/n$, the potassium salt as a dihydrate (**5**) in the alternative space group $P2_1/c$. The densities at 173 K follow the expected trend increasing within the group of alkali metal salts (**4**: 2.060 g·cm^{-3}, **5**: 2.195 g·cm^{-3}). The molecular moieties are shown in Figure 2 and Figure 3. Both tetranitraminoethane tetraanions show very similar structures. The molecular structures are also comparable to that of 1,1,2,2-tetranitratoethane.[5] The bond lengths and angles (given in the figure captions) agree nearly perfectly with literature values. The hydrogen atoms in both structures are arranged *trans* to each other with a planar H–C–C–H torsion angle in the case of **5** (180°) and almost planar in the case of **4** (177.8°). The middle C–C bond in the tetraanions is a typical single bond (1.54 Å). Both sp^3 carbon atoms show expected tetrahedral surroundings with C–N single bonds (1.46–1.47 Å). The adjacent N–N bonds (1.27–1.28 Å) are closer to N=N double bonds (1.20 Å) which supports the nitramine Lewis structure with both negative charges on the outer oxygen atoms as depicted in Figure 1.

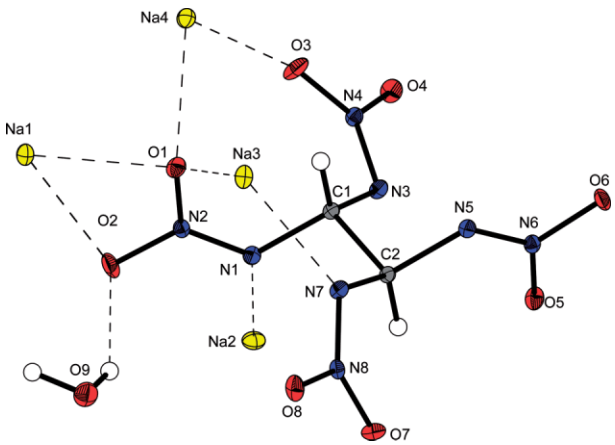

Figure 2. Molecular moiety of **4** in the crystalline state. Ellipsoids in both crystal structures drawn with Diamond2 represent the 50% probability level. Selected bond lengths /Å: C1–C2 1.5366(15), N1–C1 1.4649(15), C1–N3 1.4599(15), N1–N2 1.2721(14), N4–N3 1.2786(14), O1–N2 1.2869(13), O2–N2 1.2842(13), N4–O3 1.2688(13), N4–O4 1.2862(13). Selected bond angles /°: N3–C1–N1 107.04(9), N4–N3–C1 112.13(9). Selected torsion angles /°: N1–C1–C2–N5 178.78(8).

Both structures form 3D networks, which are strongly dominated by the following interactions: (i) electrostatic ion interactions, (ii) classical O–H···X hydrogen bonds, (iii) non-classical O–H···X hydrogen bonds, and (iv) nitro–nitro interactions. In both structures the different alkaline metal salts do not form regular coordination polyhedrons, e.g. the octahedral coordina-

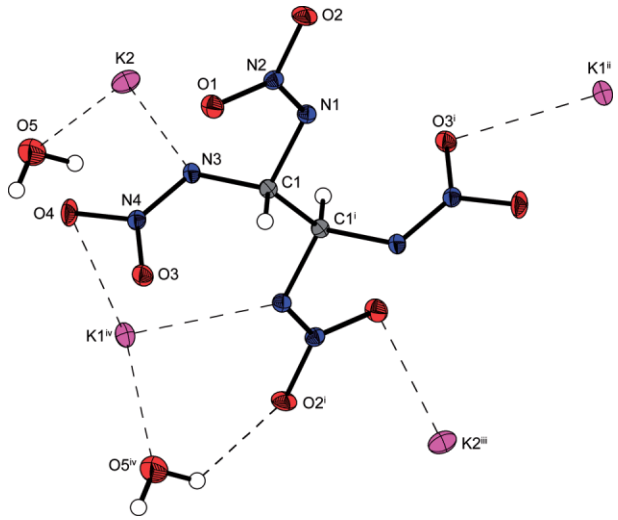

Figure 3. Molecular moiety of **5** in the crystalline state. Symmetry codes: (i) –*x*, –*y*, 1–*z*; (ii) 1–*x*, –0.5+*y*, 0.5–*z*; (iii) –*x*, –*y*, –*z*; (iv) –1+*x*, *y*, *z*. Selected bond lengths /Å: C1–C1^{i} 1.542(3), N1–C1 1.4628(17), N3–C1 1.4622(18), N1–N2 1.2864(16), N3–N4 1.2722(17), O1–N2 1.2709(15), O2–N2 1.2832(15), O3–N4 1.2837(16), O4–N4 1.2938(16). Selected bond angles /°: N3–C1–N1 109.78(11), N2–N1–C1 112.13(11).

tion sphere, which is oftentimes observed for sodium salts. Selected depictions on larger excerpts of the packing of $Na_4TNAE{\cdot}H_2O$ (**4**) and $K_4TNAE{\cdot}2H_2O$ (**5**) are shown in Figure 4.

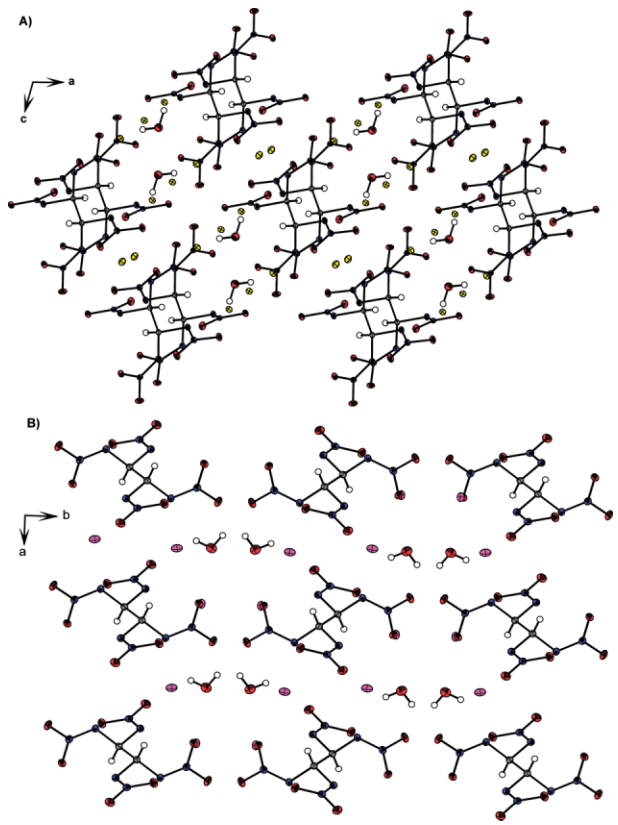

Figure 4. View on the 3D crystal structure packing: (A) along the *b* axis in $Na_4TNAE\ H_2O$ (**4**) and (B) along the *c* axis in $K_4TNAE{\cdot}2H_2O$ (**5**).

Thermogravimetric and Differential Thermal Analysis

The hydrated species $Na_4TNAE{\cdot}H_2O$ (**4**) and $K_4TNAE{\cdot}2H_2O$ (**5**) have never been described in the literature. Differential thermal analysis (DTA, see Figure 5) shows that $K_4TNAE{\cdot}2H_2O$ (**5**) loses its crystal water content at 142 °C and the unhydrated K_4TNAE (**6**) decomposes at 225 °C. (lit. value 284 °C)[4] $Na_4TNAE{\cdot}H_2O$ (**4**) decomposes without loss of water at 197 °C. (lit. value 192 °C for unhydrated species).[5a]

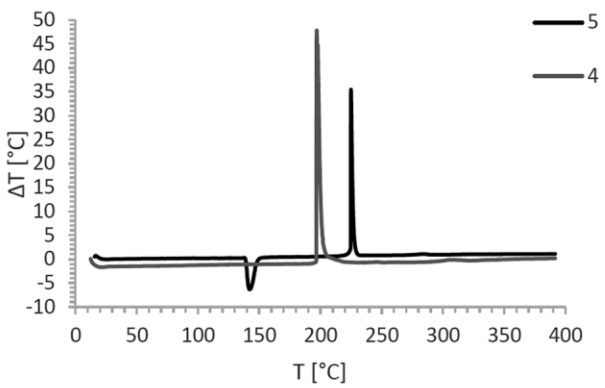

Figure 5. DTA thermogram of $Na_4TNAE{\cdot}H_2O$ (**4**) (grey line) and $K_4TNAE{\cdot}2H_2O$ (**5**) (black line). Endothermic loss of water for compound **5** at 142 °C Temperature of decomposition T_{dec}: 197 °C (**4**), 225 °C (**5**) (5 K·min^{-1} in glass vessel, T_{max} values).

$K_4TNAE{\cdot}2H_2O$ (**5**) was analyzed by thermogravimetric analysis (TGA, see Figure 6). Two water molecules (36.03 g·mol^{-1}) represent 7.87 % the molecular weight of the compound (458.51 g·mol^{-1}). The temperature-mass plot resulting from thermogravimetric analysis (2 K·min^{-1}) shows that from 50 °C to 152 °C one molecule of water is evaporated continuously with a weight loss of 3.90 %. The second molecule of water is lost with a high mass loss rate from 152 °C to 156 °C with a total weight loss of 8.38 %, which is in agreement with the vaporization of two equivalents of water. The discrepancy of 0.51 % to the theoretical loss can be explained by sublimation of the salt in the temperature regime investi-

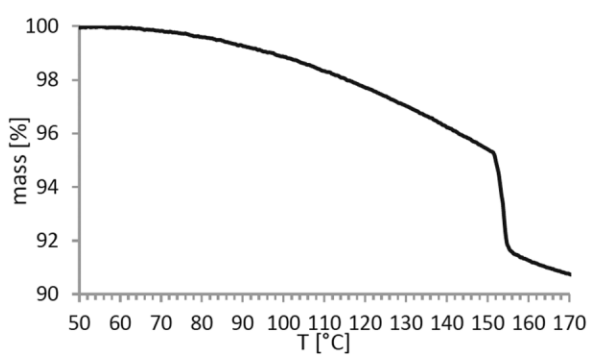

Figure 6. Thermogravimetric analysis (2 °C min^{-1}) of $K_4TNAE{\cdot}2H_2O$ (**5**). Plot of temperature /°C vs. sample weight /%. Continuous loss of mass from 50 to 152 °C, which corresponds to one equivalent of crystal water. The second crystal water equivalent is lost with a high mass loss rate in the temperature range from 152 °C to 156 °C.

gated. The sublimation of K_4TNAE (**6**) also causes the mass loss during the dehydration of **5**, which indicates a solid-gaseous phase transition without decomposition. The temperature range for water loss from TGA (142–156 °C, 2 K·min^{-1}) is in agreement with the endothermic peak area in the DTA (138–152, 5 K·min^{-1}).

Sensitivities

The sensitivities toward external stimuli and selected other parameters of compounds **4**–**6** are compiled in Table 1. Sodium salt **4** can be classified as very sensitive toward impact and sensitive toward friction. The potassium compounds **5** and **6** can be classified as sensitive toward impact and insensitive toward friction.[12] The sensitivity toward electrical discharge of all salts **4**–**6** is above the 50 mJ discharge that can be generated by human interaction. Compounds **4**–**6** possess a positive oxygen balance Ω ranging from 3.49 % to 4.25 % with the postulated combustion products CO_2, H_2O, N_2, Na_2O, and K_2O. Alternatively the same Ω values can be obtained with the metal carbonates Na_2CO_3 and K_2CO_3 as a combination of the metal oxide M_2O with CO_2. For K_4TNAE (**6**) an enthalpy of formation of –1554 kJ·mol^{-1} was calculated on a CBS-4M level using the Gaussian 09 software.[13] The strong exothermicity of the compound is predominantly caused by the high lattice enthalpy of the tetraanion salt and the high oxidation state of all non-oxygen atoms. The densities of all compounds are in the typical range for alkali metal salts of energetic C,H,N,O compounds.

Small Scale Reactivity Test (SSRT)

The calculation of detonation parameters relies extensively on the detonation products formed during the detonation process. In case of alkali metal salts it is hard to state, which products are formed since the presence of these metal cations might lead to the formation of metal oxides (Na_2O, Na_2O_2, K_2O), metal carbonates (Na_2CO_3, K_2CO_3) or other compounds. With this unknown detonation behavior the theoretical calculation of detonation parameters is an unreliable estimation and was not used for compounds **4**–**6**. Instead the Small Scale Reactivity Test (SSRT)[14] was carried out to obtain a reliable experimental benchmark parameter for the energetic performance of the water-free compound K_4TNAE (**6**). For this test a steel block with a drill hole is placed on top of an aluminum block. The drill hole is filled with the explosive and a detonator is positioned over the explosive. After the detonation a dent has been formed in the aluminum block. The dent is filled with standardized SiO_2, which is weighed. The mass ratio $\varepsilon = m(SiO_2)/m(EXP)$ is a parameter for the energetic performance of the explosive. It can be clearly stated that K_4TNAE (**6**) (ε: 0.76) is outperformed by the military explosive RDX (ε: 1.17, V_{DET}: 8983 m·s^{-1}, p_{CJ}: 380 kbar)[8] and high-performance explosive CL-20 (2,4,6,8,10,12-hexanitro-2,4,6,8,10,12-hexaazaisowurtzitane) (ε: 1.72, V_{DET}: 9455 m·s^{-1}, p_{CJ}: 467 kbar)[8]. The calculated detonation performance of Na_4TNAE (V_{DET}: 10900 m·s^{-1}, p_{CJ}: 427 kbar) reported by *Szala* et al.,[5] which would be in the range of CL-20 should be regarded critically in comparison with the experimental performance of K_4TNAE (**6**) and CL-20 in the SSRT test. (cf. Table 2) K_4TNAE (**6**) was preferred over Na_4TNAE·H_2O (**4**) for the SSRT test since it does not contain crystal water.

Table 2. Results of the SSRT test.

	K_4TNAE (**6**)	RDX[8]	CL-20[8]
m(EXP)[a)]	586	504	550
$m(SiO_2)$[b)]	445	589	947
$\varepsilon = m(SiO_2)/m$(EXP)	0.76	1.17	1.72

a) Mass of explosive /mg. b) Mass of SiO_2 /mg.

Aquatic Toxicity: EC_{50}

K_4TNAE (**6**) can be considered as an aliphatic C_2H_2 unit connected to four anionic nitramines, which is highly water soluble (>662 g·L^{-1}). Regarding the toxicity problem of RDX,[8] a cycloaliphatic triazinane containing three secondary nitramines, it is interesting to investigate the toxicity of the compound. The commercially available bioassay system LUMIStox® analyzes the toxicity of a compound towards the marine, bioluminescent bacterium *Vibrio fischeri*. For toxicological analysis the concentration which inhibits 50 % of the

Table 1. Sensitivity toward external stimuli and other selected parameters of compounds **4**–**6**.

	Na_4TNAE·H_2O (**4**)	K_4TNAE·$2H_2O$ (**5**)	K_4TNAE·(**6**)
Formula	$C_2H_4Na_4N_8O_9$	$C_2H_6K_4N_8O_{10}$	$C_2H_2K_4N_8O_8$
IS[a)] /J	2	10	4
FS[b)] /N	240	>360	>360
ESD[c)] /mJ	300	1500	1500
Grain size /µm	100–500	100–500	<100
N[d)] /%	29.80	24.44	26.52
Ω[e)] /%	+4.25	+3.49	+3.79
T_{dec}[f)] /°C	197	142	225
ρ[g)] /g cm^{-3}	2.060[i]	2.159[i]	2.152[j]
$\Delta_f H^{0h)}$ /kJ·mol^{-1}	–	–	–1554

a) Impact sensitivity (BAM drophammer 1 of 6). b) Friction sensitivity (BAM friction tester 1 of 6). c) Sensitivity towards electrostatic discharge (OZM research testing device). d) Nitrogen content. e) Oxygen balance [$\Omega = w$O – 2C – 0.5yH – '0.5M (M: Na or K)]. f) Decomposition temperature (T_{max} from DTA /5 K·min). g) Density. h) Calculated (CBS-4M method) enthalpy of formation. i) Density from X-ray diffraction at 173 K. j) Density from pycnometer at 298 K.

bioluminescence activity, the EC_{50} value, is determined after an incubation period of 30 min. For RDX an EC_{50} value of 240 mg·L^{-1} was observed. For K_4TNAE (**6**) a first sign of inhibition (26.7 %) could be observed at a concentration of 15070 mg·L^{-1}. The final EC_{50} value will be higher than this concentration, yet it can already be stated that the toxicity of K_4TNAE (**6**) towards *Vibrio fischeri* is significantly lower by a factor >60 than RDX. This result demonstrates that anionic nitramines can be explosophores for future explosives with high biocompatibility. The introduction of anionic nitramine moieties to energetic materials has been proposed as a concept for the stabilization of novel energetic materials by ionic interactions.[7] Despite that it should be kept in mind that the bacterial strain *Vibrio fischeri* is a relatively simple organism. The environmental degradation products and toxicity towards higher life forms of this attractive model compound **6** should be further investigated.

Conclusions

The sodium salt Na_4TNAE·H_2O (**4**) and K_4TNAE·2 H_2O (**5**) were synthesized and reported with their crystal structures at 173 K for the first time. Whereas sodium salt **4** cannot be dehydrated, the dihydrated potassium salt **5** can be dehydrated at 160 °C to K_4TNAE (**6**). This in accordance with the results of differential thermal analysis as an endotherm corresponding to a loss of water was absent in the thermogram of **4** but present in that of **5**. The loss of two equivalents of water could be demonstrated by thermogravimetric analysis of **5**. Anhydrous K_4TNAE (**6**) was outperformed by the military explosive RDX and high performance explosive CL-20 in the SSRT test. The EC_{50} value aquatic bacteria of K_4TNAE (**6**) (>15.07 g·L^{-1}) is more than 60 times higher than that of RDX (0.24 g·L^{-1}). Because of these results anionic nitramines were demonstrated to be a useful tool for the stabilization of energetic materials and might be suitable explosophores for high energy density materials with decreased toxicity in comparison to the widely used military explosive RDX.

Experimental Section

All reagents and solvents were used as received (Sigma-Aldrich, Fluka, Acros Organics, ACBR). NMR spectra were measured with a JEOL ECX-400 and a Bruker AVANCE 400 MHz NMR instrument. The chemical shifts of the solvent peaks were adjusted according to literature values [15]. Infrared spectra were measured with a Perkin-Elmer FT-IR Spektrum BXII instrument equipped with a Smith Dura SampIIR II ATR unit. Transmittance values are described as "strong" (s), "medium" (m), and "weak" (w). Raman spectra were recorded with a Bruker RAM II device (1064 nm, 300 mW). Relative peak intensities are given in brackets. Elemental analyses (EA) were performed with a Netsch STA 429 simultaneous thermal analyzer. Sensitivity data were determined using a BAM drophammer and a BAM friction tester. The electrostatic sensitivity tests were carried out using an Electric Spark Tester ESD 2010 EN (OZM Research) operating with the "Winspark 1.15" software package. The particle sizes stated are valid for all sensitivity measurements. Melting and decomposition points were measured with an OZM DTA 551-EX DTA apparatus using heating rates of 5 K·min^{-1}. Thermogravimetric measurements were performed with a Perkin-Elmer TGA 4000 apparatus using a heating rate of 2 K·min^{-1}. Pycnometric measurements were carried out with a Quantachrome Ultrapyc 1200 e pycnometer using the large measurement cell. The EC_{50} values were determined with a Dr. Lange LUMIStox 300 luminometer.

CAUTION! All of the described compounds are energetic materials with sensitivity to various stimuli. While we encountered no issues in the handling of these materials, proper protective measures (face shield, ear protection, body armor, Kevlar gloves, and earthened equipment) should be used during the handling of compounds **2**–**5** at all times.

Tetranitroglycoluril (2): Glycoluril (**1**) (4.59 g, 32.30 mmol) was added whilst stirring to fuming nitric acid (81 mL, 100 %) in a 250 mL round-bottomed flask at 0 °C. The dissolution is slightly exothermic. After reaching 0 °C again, acetic anhydride (40.5 mL) was added dropwise over a period of 10 min. The temperature was lowered to 0 °C and the ice bath was removed. The reaction mixture was stirred for 2 h letting the temperature rise to 35 °C. The mixture was cooled using a water bath and was stirred for another 2 h, while keeping the temperature at 20 °C. The crude product was filtered off, washed with ice water (200 mL) and dispersed in a 3:1 mixture of chloroform and ethanol (90 mL) applying ultrasound. The colorless product was filtered off and dried in a desiccator to yield 6.83 g (65.7 %) of colorless tetranitroglycoluril **2** as crude product for further synthesis. **^{1}H NMR** (400.18 MHz, [D_6]acetone): δ = 7.77 (s, C–H). **^{13}C NMR** (100.64 MHz, [D_6]acetone): δ = 65.9 (C-H), 142.4 (C=O). **^{14}N NMR** (28.89 MHz, [D_6]acetone), δ = –57 (NO_2). **IR** (ATR): $\tilde{\nu}$ = 3735 (w), 2997 (w), 2360 (m), 2341 (m), 1825 (s), 1797 (s), 1654 (m), 1621(s), 1595(s), 1369 (w), 1298 (m), 1258 (s), 1230 (m), 1212 (m), 1182 (m), 1147 (m), 1094 (s), 957 (w), 938 (w), 848 (w), 828 (w), 810 (m), 770 (w), 742 (m), 698 (m) cm^{-1}. **RAMAN**: $\tilde{\nu}$ = 3010 (1), 2999 (22), 1827 (6), 1799 (13), 1663 (3), 1639 (7), 1598 (4), 1386 (3), 1359 (7), 1314 (48), 1271 (5), 1214 (2), 1186 (5), 1043 (4), 960 (3), 850 (7), 834 (70), 771 (3), 723 (10), 699 (6), 521 (5), 471 (3), 440 (3), 420 (10), 340 (2), 312 (45), 220 (5), 174 (4), 93 (100) cm^{-1}. **$C_4H_2N_8O_{10}$** (322.11) C 15.37 (calcd. 14.92), H 0.89 (calcd. 0.63), N 34.27 (calcd. 34.79) %. **MS** (DEI+): 322 (M^+). **IS:** >5 J, **FS:** 80 N. **ESD:** 0.2 J [<100 µm]. **DTA:** T_{begin}: 190 °C, T_{onset}: 208 °C, T_{max} 215 °C, T_{offset}: 222 °C (decomposition).

1,1,2,2-Tetranitraminoethane (TNAE) (3): A 250 mL round-bottomed flask was placed in an ice bath and sodium hydroxide (74.40 mL, 74.40 mmol, 4 equiv., aq., 1 M) solution were added. TNGU (**2**) (6.00 g, 18.63 mmol) was added in small portions whilst stirring, keeping the temperature below 10 °C. Having completed the addition, the ice bath was removed and the reaction mixture was allowed to stir for 1 h at room temperature. The reaction was quenched by the slow addition of hydrochloric acid (37.2 mL, 74.40 mmol, 4 equiv., aq., 2 M). The aqueous phase was extracted with diethyl ether (5 × 30 mL) and the combined organic phases were dried with anhydrous sodium sulfate. The drying agent was filtered off and the organic phase was removed using a rotary evaporator (0 mbar, 40 °C, 15 min). TNAE (**3**) was obtained as colorless solid with a yield of 3.25 g (65 %) as crude product for further synthesis. **^{1}H NMR** (400.18 MHz, [D_6]DMSO): δ = 6.07 (s, C–H). **^{13}C NMR** (100.64 MHz, [D_6]DMSO): δ = 63.3 (C–H). **IR** (ATR): $\tilde{\nu}$ = 3626 (w), 3480 (w), 3236 (s), 3146 (s), 3004 (m), 2361 (m), 2341 (w), 1768 (w), 1573 (s), 1448 (m), 1423 (m), 1323 (s), 1232 (s), 1162 (m), 1094 (m), 1061 (s), 930 (w), 835 (w), 774 (w), 695 (w), 667 (w) cm^{-1}. **RAMAN**: $\tilde{\nu}$ = 2997 (6), 1595 (6), 1404 (5), 1333 (18), 1162 (6), 1109 (4), 1020 (22), 934 (20), 840 (3), 828 (1), 739 (4), 677 (3), 661 (1), 601 (1), 435 (5), 344 (4), 323

(1), 296 (2), 271 (1), 245 (7), 212 (4), 96 (100) cm^{-1}. **$C_2H_6N_8O_8$** (270.12): C 9.59 (calcd. 8.89), H 2.46 (calcd. 2.24), N 40.65 (calcd. 41.48)%. **MS** (FAB-) 269 ($(M–H)^-$). **IS:** 2 J, **FS:** 30 N. **ESD:** 0.1 J [<100 µm]. **DTA:** T_{begin}: 115 °C, T_{onset}: 131 °C, T_{max} 136 °C, T_{offset}: 139 °C (decomposition).

Tetrasodium 1,1,2,2-Tetranitramidoethane Monohydrate ($Na_4TNAE{\cdot}H_2O$) (4): To methanol (250 mL) in a 500 mL round-bottomed flask was added sodium hydroxide (1.4814 g, 37.04 mmol, 4 equiv.) and mechanical stirring was applied. The obtained solution was cooled to 0 °C and TNAE (**3**) (2.5012 g, 9.26 mmol) was added in one portion. The reaction mixture was stirred for 5 min at 0 °C and methanol was removed using a rotary evaporator (30 mbar, 60 °C). The colorless residue was dried in a desiccator under high vacuum to yield 3.4012 g of crude product. For purification the crude product (2.50 g) was dissolved in distilled water (3.56 mL). The solution was filled in a 10 mL test tube, which was positioned in a vessel filled with methanol. The vessel was closed to allow vapor diffusion of methanol into the solution. After two weeks the formed crystals were collected by filtration, washed with methanol and dried in high vacuum over silica gel. 2.85 g (82%) $Na_4TNAE{\cdot}H_2O$ **4** was obtained as colorless crystals suitable for X-ray diffraction. **^{1}H NMR** (400.13 MHz, D_2O): δ = 5.97 (s, C–H). **^{13}C NMR** (100.62 MHz, D_2O): δ = 74.6 (C–H). **^{14}N NMR** (28.91 MHz, D_2O), δ = –25 (NO_2). **IR** (ATR): $\tilde{\nu}$ = 3626 (w), 3480 (w), 3236 (s), 3146 (s), 3004 (m), 2361 (m), 2341 (w), 1768 (w), 1573 (s), 1448 (m), 1423 (m), 1323 (s), 1232 (s), 1162 (m), 1094 (m), 1061 (s), 930 (w), 835 (w), 774 (w), 695 (w), 667 (w) cm^{-1}. **RAMAN** $\tilde{\nu}$ = 2997 (6), 1595 (6), 1404 (5), 1333 (18), 1162 (6), 1109 (4), 1020 (22), 934 (20), 840 (3), 828 (1), 739 (4), 677 (3), 661 (1), 601 (1), 435 (5), 344 (4), 323 (1), 296 (2), 271 (1), 245 (7), 212 (4), 96 (100) cm^{-1}. **$C_2H_4N_8Na_4O_9$** (376.06) C 6.65 (calcd. 6.39), H 1.11 (calcd. 1.07), N 29.50 (calcd. 29.80)%. **IS:** 2 J, **FS:** 240 N. **ESD:** 0.3 J [100–500 µm]. **DTA:** T_{begin}: 190 °C, T_{onset} 195 °C, T_{max}: 197 °C (decomposition).

Tetrapotassium 1,1,2,2-Tetranitramidoethane Dihydrate ($K_4TNAE{\cdot}2H_2O$) (5): To water (120 mL) in a 250 mL round-bottomed flask was added potassium hydroxide (85 wt-%, 1.21 g, 18.19 mmol, 4 equiv.) and mechanical stirring was applied. TNAE (**3**) (1.2277 g, 4.55 mmol) was added to the obtained solution all at once. The reaction mixture was stirred for 5 min and water was removed using a rotary evaporator (30 mbar, 60 °C). The colorless crude product (1.85 g, 97%) was dried in a desiccator. For purification the crude product (1.38 g) was dissolved in distilled water (1.92 mL). The solution was filled in a 10 mL test tube, which was positioned in a vessel filled with methanol. The vessel was closed to allow vapor diffusion of methanol into the solution. After two weeks the crystals were collected by filtration, washed with methanol and dried in high vacuum over silica gel. 1.34 g (94%) $K_4TNAE{\cdot}2H_2O$ (**5**) was obtained as colorless crystals suitable for X-ray diffraction. **^{1}H NMR** (400.13 MHz, D_2O): δ = 5.95 (s, C–H). **^{13}C NMR** (100.62 MHz, D_2O): δ = 74.6 (C–H). **^{14}N NMR** (28.91 MHz, D_2O), δ = –25 (NO_2). **IR** (ATR): $\tilde{\nu}$ = 3746 (w), 3486 (m), 2955 (w), 2361 (m), 2337(m), 1617(w), 1388 (s), 1332 (s), 1270 (s), 1240 (s), 1124 (m), 1100 (m), 976 (m), 968 (m), 779 (m), 765 (m), 718 (w), 657 (w) cm^{-1}. **RAMAN**: $\tilde{\nu}$ = 84 (15), 110 (9), 164 (37), 194 (6), 232 (8), 281 (5), 338 (5), 390 (6), 433 (7), 538 (12), 674 (7), 713 (6), 758 (5), 1002 (16), 1018 (41), 1096 (5), 1109 (19), 1128 (5), 1292 (7), 1341 (21), 1393 (10), 1454 (27), 2028 (10), 2083 (20), 2858 (100), 2953 (25) cm^{-1}. **$C_2H_6K_4N_8O_{10}$** (458.51) C 5.46 (calcd. 5.24), H 1.26 (calcd. 1.32), N 24.47 (calcd. 24.44)%. **IS:** 10 J, **FS:** >360 N, **ESD:** 1.5 J [100–500 µm], **DTA:** T_{begin}: 137 °C, T_{onset} 139 °C, T_{max}: 142 °C (loss of water).

Tetrapotassium 1,1,2,2-Tetranitramidoethane (K_4TNAE) (6): $K_4TNAE{\cdot}2H_2O$ **5** (1.25 g, 2.73 mmol) was filled in a glass vessel, which was placed in an oven and heated from room temperature to 160 °C for 4 h. After cooling to room temperature K_4TNAE **6** (1.11 g, 96%) was obtained as a colorless powder. **IR** (ATR): $\tilde{\nu}$ = 2956 (w), 2920 (w), 2361 (m), 2337(m), 1398 (s), 1372 (s), 1339(s), 1298 (s), 1247 (s),1129 (w), 1104 (m), 1016 (w), 1000 (w), 971(w), 958 (m), 771 (w), 743 (w), 721 (w), 657 (m) cm^{-1}. **RAMAN**: $\tilde{\nu}$ = 143 (22), 225 (3), 280 (4), 334 (3), 364 (5), 430 (4), 538 (11), 666 (4), 715 (3), 961 (6), 1004 (3), 1018 (42), 1107 (13), 1281 (3), 1340 (11), 1385 (9), 1400 (4), 1433 (13), 2028 (10), 2083 (19), 2228 (4), 2858 (100), 2925 (11), 2951 (4), 2962 (5) cm^{-1}. **$C_2H_2K_4N_8O_8$** (422.48): C 5.89 (calcd. 5.69), H 0.57 (calcd. 0.48), N 26.22 (calcd. 26.52)%. **IS:** 4 J, **FS:** >360 N. **ESD:** 1.5 J [<100 µm]. ρ_{298K} (pycnometer): 2.152 g cm^{-3}. **DTA:** T_{begin}: 208 °C, T_{onset} 224 °C, T_{max}: 225 °C (decomposition).

Crystallographic data (excluding structure factors) for the structures in this paper have been deposited with the Cambridge Crystallographic Data Centre, CCDC, 12 Union Road, Cambridge CB21EZ, UK. Copies of the data can be obtained free of charge on quoting the depository numbers CCDC-1408630 (**4**) and CCDC-1408628 (**5**)[11] (Fax: +44-1223-336-033; E-Mail: deposit@ccdc.cam.ac.uk, http://www.ccdc.cam.ac.uk).

Supporting Information (see footnote on the first page of this article): Details on the X-Ray diffraction measurements and refinements of compounds **4** and **5**.

Acknowledgements

Financial support of this work by the Ludwig-Maximilian University of Munich (LMU), the Office of Naval Research (ONR) under grant no. ONR.N00014-16-1-2062, and the Bundeswehr – Wehrtechnische Dienststelle für Waffen und Munition (WTD 91) under grant no. E/E91S/FC015/CF049 and the Bundesministerium für Bildung und Forschung (BMBF) under grant no. 13N12583 is gratefully acknowledged. *Ms. Regina Scharf* is thanked for the measurement of the EC_{50} values in this work. The authors acknowledge collaborations with *Dr. Mila Krupka* (OZM Research, Czech Republic) in the development of new testing and evaluation methods for energetic materials and with *Dr. Muhamed Suceska* (Brodarski Institute, Croatia) in the development of new computational codes to predict the detonation and propulsion parameters of novel explosives. We are indebted to and thank *Drs. Betsy M. Rice*, *Jesse Sabatini* and *Brad Forch* (ARL, Aberdeen, Proving Ground, MD) for many inspired discussions.

References

[1] Y. Lee, P. Zhongij, W. Daozheng, *Acta Armamentarii* **1980**, 23.
[2] C. Coon, *Synthesis of Dense Energetic Materials, Annual Report*; Lawrence Livermore National Laboratory, Livermore, CA, USA, **1982**.
[3] D. Wan, Proc. Int. 17th Pyrotech. Semin. **1991**, 231–234.
[4] Y. Lee, P. Goede, N. Latypov, H. Oestmark, *36th Int. Annu. Conf. ICT* **2005**, 124/121–124/129.
[5] a) M. Szala, L. Szymanczyk, *36th Int. Annu. Conf. ICT* **2011**, 40/41–40/46; b) M. Szala, L. Szymanczyk, *Biul. Wojsk. Akad. Technol.* **2012**, *61*, 257–267.
[6] D. Fischer, T. M. Klapötke, J. Stierstorfer, *Chem. Commun.* **2016**, *52*, 916–918.
[7] a) D. Fischer, T. M. Klapötke, J. Stierstorfer, *Angew. Chem. Int. Ed.* **2014**, *53*, 8172–8175; b) Y. Tang, J. Zhang, L. A. Mitchell, D. A. Parrish, J. n. M. Shreeve, *J. Am. Chem. Soc.* **2015**, *137*, 15984–15987.

[8] N. Fischer, D. Fischer, T. M. Klapötke, D. G. Piercey, J. Stierstorfer, *J. Mater. Chem.* **2012**, *22*, 20418–20422.
[9] R. Meyer, J. Köhler, A. Homburg, *Explosives*, Wiley-VCH, Weinheim, **2016**.
[10] L. A. Wingard, E. C. Johnson, J. J. Sabatini, *Tetrahedron Lett.* **2016**, *57*, 1681–1682.
[11] C. R. Groom, I. J. Bruno, M. P. Lightfoot, S. C. Ward, *Acta Crystallogr., Sect. B* **2016**, *72*, 171–179.
[12] Impact: Insensitive > 40 J, less sensitive ≥ 35 J, sensitive ≥ 4 J, very sensitive ≤ 3 J; Friction: Insensitive > 360 N, less sensitive = 360 N, sensitive < 360 N and >80 N, very sensitive ≤ 80 N, extremely sensitive ≤ 10 N. According to the UN Recommendations on the Transport of Dangerous Goods.
[13] M. J. Frisch, G. W. Trucks, H. B. Schlegel, G. E. Scuseria, M. A. Robb, J. R. Cheeseman, G. Scalmani, V. Barone, B. Mennucci, G. A. Petersson, H. Nakatsuji, M. Caricato, X. Li, H. P. Hratchian, A. F. Izmaylov, J. Bloino, G. Zheng, J. L. Sonnenberg, M. Hada, M. Ehara, K. Toyota, R. Fukuda, J. Hasegawa, M. Ishida, T. Nakajima, Y. Honda, O. Kitao, H. Nakai, T. Vreven, J. A. Montgomery Jr., J. E. Peralta, F. Ogliaro, M. J. Bearpark, J. Heyd, E. N. Brothers, K. N. Kudin, V. N. Staroverov, R. Kobayashi, J. Normand, K. Raghavachari, A. P. Rendell, J. C. Burant, S. S. Iyengar, J. Tomasi, M. Cossi, N. Rega, N. J. Millam, M. Klene, J. E. Knox, J. B. Cross, V. Bakken, C. Adamo, J. Jaramillo, R. Gomperts, R. E. Stratmann, O. Yazyev, A. J. Austin, R. Cammi, C. Pomelli, J. W. Ochterski, R. L. Martin, K. Morokuma, V. G. Zakrzewski, G. A. Voth, P. Salvador, J. J. Dannenberg, S. Dapprich, A. D. Daniels, Ö. Farkas, J. B. Foresman, J. V. Ortiz, J. Cioslowski, D. J. Fox, *Gaussian*, Gaussian Inc., Wallingford, CT, USA, **2009**.
[14] a) J. E. Felts, H. W. Sandusky, R. H. Granholm, *AIP Conf. Proc.* **2009**, *1195*, 233–236; b) H. W. Sandusky, R. H. Granholm, D. G. Bohl, *IHTR 2701*, Naval Surface Warfare Center, Indian Head Division, MD, USA, August 12, **2005**.
[15] G. R. Fulmer, A. J. M. Miller, N. H. Sherden, H. E. Gottlieb, A. Nudelman, B. M. Stoltz, J. E. Bercaw, K. I. Goldberg, *Organometallics* **2010**, *29*, 2176–2179.

Received: September 16, 2016
Published Online: October 11, 2016

Persönliche Daten

Name	Martin Andreas Christian Härtel
e-Mail	dr.martin.haertel@gmail.com

Beruflicher Werdegang

04/2017 - heute	**Anstellung als Wissenschaftlicher Mitarbeiter** Referat 65 (Forschung und Erprobung) des Bundespolizeipräsidiums
01/2013 – 06/2017	**Promotion als Wissenschaftlicher Mitarbeiter** Department Chemie, Ludwig-Maximilians-Universität München Lehrstuhl für Anorganische Molekülchemie Prof. Dr. Thomas M. Klapötke
03/2013 - 05/2016	**Teilnahme am BMBF Projekt ChemAir** zur Gasphasen-Detektion luftübertragener Gefahrstoffe mittels GC/MS
05/2016	Installation eines VO-GC/MS Setup bei der Bundespolizei in Lübeck im Auftrag der Shimadzu Deutschland GmbH
04/2016	Teilnahme mit Vortrag am 4. interdisziplinären Doktorandenseminar des Deutschen Arbeitskreises für Analytische Spektroskopie der GdCh
10/2015-12/2015	Forschungsaufenthalt an der Schule für ABC-Abwehr und gesetzliche Schutzaufgaben Sonthofen
05/2014	Teilnahme am Seminar „GC-Methodenentwicklung, Optimierung und Troubleshooting“ der Firma Phenomenex

Ausbildung

02/2010 – 09/2012	**M.Sc. in Chemie,** Abschlussnote 1.33 (sehr gut) Anorganische und Organische Chemie, Materialwissenschaften
10/2006 – 02/2010	**B.Sc. in Chemie & Biochemie,** Abschlussnote 2.42 (gut)
09/1996-06/2006	**Abitur**, Gymnasium Bad Aibling, Abschlussnote 2.3 (gut)

Kenntnisse

Synthese von Explosivstoffen	4 Jahre Erfahrung in der Synthese, Handhabung und energetischen Charakterisierung von hochempfindlichen Explosivstoffen
GC/MS	Anschaffung, Betrieb und Wartung eines Shimadzu GC/MS mit exklusiver Allein-Nutzung für das Promotionsprojekt
Gas-Sättigungs-Methode	Dampfdruckmessungen von mittel- bis schwerflüchtigen Gefahrstoffen
Chemische Analytik	NMR, IR, Raman, EA, MS, DTA, DSC, TGA
EDV-Kenntnisse	Microsoft Office, Adobe Creative Suite, Chemdraw, Mestrenova, LabSolutions GCMSsolution, Gaussian 09, EXPLO5
Betreuung von Studenten	2 Bachelorarbeiten und 1 F-Praktikum (je 2 Monate), 1 Erasmus Forschungspraktikum und 1 Masterarbeit (je 6 Monate)
Führerschein	Klasse B
Sprachkenntnisse	Englisch (verhandlungssicher), Französisch (gute Grundkenntnisse)

Weitere Publikationen

2015: *Härtel et al.*, Milde Analytikmethode für Explosivstoffe
URL: http://tinyurl.com/VOGCMS
2012: *Härtel et al.*, Synthesis and Characterization of Alkaline and Alkaline Earth Salts of the Nitrotetrazolate-2N-oxide Anion.
URL: http://dx.doi.org/10.1002/zaac.201200049

Mitgliedschaften
Gesellschaft Deutscher Chemiker

Presseauftritte
Interview bei ntv.de http://tinyurl.com/NTVDEXPLO und Weitere